ESA PSS-03-108 Issue 1
November 1989

Spacecraft thermal control design data

Volume 2

Prepared by:
Thermal Control & Life Support Division
European Space Research and Technology Centre
Noordwijk, The Netherlands

Approved by:
The Inspector General, ESA

european space agency / agence spatiale européenne
8-10, rue Mario-Nikis, 75738 PARIS 15, France

Published by ESA Publications Division,
ESTEC, Noordwijk, The Netherlands

Printed in The Netherlands

ESA price code: E4

ISSN 0379 - 4059

ABSTRACT

The aim of the present handbook is to assist the thermal design engineer by presenting him in a single document with all the information relevant to spacecraft thermal-control design.

This handbook has been compiled by the School of Aeronautics of the Polytechnic University of Madrid (ETSI-A) under several ESA contracts.

REVISION PROCEDURE

It is intended to issue revisions and additions to this handbook as they become available. It is hoped that in this way it will remain up-to-date as regards state-of-the-art information and recent developments in the field of spacecraft thermal control.

VOLUME 2
CONTENTS

PAGE INTENTIONALLY LEFT BLANK

DISCLAIMER

The description in this handbook of thermal-control components and systems is intended to be purely illustrative, and the use of tradenames of specific products, which is essential to a proper understanding of the data presented herein, in no way implies any approval, endorsement or recommendation of these products by the European Space Agency.

PAGE INTENTIONALLY LEFT BLANK

THERMAL CONTROL SURFACES

1 COATINGS

2 ADHESIVE TAPES

THERMAL CONTROL SURFACES

Table of Contents

INTENTIONALLY BLANK PAGE

THERMAL CONTROL SURFACES

List of Symbols

LIST OF SYMBOLS

A , Area of the Sensor. [m^2].

C , Conductive Thermal Coupling Constant between Sensor and Tray. [$W.K^{-1}$].

D , Irradiation Dose. [GY/particle].

F , View Factor from the Sun.

F , Adhesive Force. [N].

F_a , View Factor for Albedo.

F_{sp} , View Factor for Earth Infrared Radiation.

K , Radiative Thermal Coupling Constant between Sensor and Tray. [$W.K^{-4}$].

P , Earth Infrared Radiation. [$W.m^{-2}$].

Q , Heat Transfer Rate through Sensor Insulation from External Sources. [W].

Q_i , Internal Dissipated Power or Heat Load. [W].

R , Sheet Electrical Resistance. [Ω per square, Ω/□].

S , Solar Flux. [$W.m^{-4}$].

T , Temperature. [K].

T_R , Equilibrium Temperature for an Isothermal Sphere at 1 AU. [K].

T_c , Tray or Sample-Housing Temperature. [K].

T_s , Equivalent Surrounding Temperature. [K].

Tmax , Maximum Temperature. [K].

Tmin , Minimum Temperature. [K].

X_d , Irradiation Penetration Range. [$kg.m^{-2}$].

X_u , Photon Absorption and Scattering Range. [$kg.m^{-2}$].

Rev. 1. 1981

THERMAL CONTROLSURFACES

List of Symbols

a , Mean Albedo of the Earth.

c , Specific Heat of a Sample. [$J.kg^{-1}.K^{-1}$].

c , Resin Concentration in an Adhesive.

p , Pressure. [Pa].

t , Thickness. [m].

t_c , Coating Thickness. [m].

t , Time. [h] or [ESH].

n , Number of Experimental Data Points.

w , Width. [m].

α , Hemispherical Total Absorptance.

α_p , Earth Infrared Radiation Absorptance.

α_s , Solar Absorptance.

$\alpha'_\lambda(\lambda,\beta,\theta)$, Directional-Hemispherical Spectral Absorptance.

β , Angle between Surface Normal and Direction of Incident Flux. [Angular Degrees].

β' , Angle between Surface Normal and Direction of Emitted, Reflected or Transmitted Flux. [Angular Degrees].

ε , Hemispherical Total Emittance.

$\varepsilon'(\beta',\theta')$, Directional Total Emittance.

θ , Azimuthal Angle of Incident Flux. [Angular Degrees].

θ' , Azimuthal Angle of Emitted, Reflected or Transmitted Flux. [Angular Degrees].

λ , Wavelength. [m].

ρ , Electrical Resistivity. [$\Omega.m$].

ρ_c , Specific Electrical Cross Resistance. [$\Omega.m^2$].

Rev. 1. 1981

THERMAL CONTROL SURFACES

List of Symbols

ρ_s , Solar Reflectance.

$\rho_{s_{IR}}$, Solar Reflectance in the Infrared Range.

$\rho_{s_{UV}}$, Solar Reflectance in the UV Range.

ρ_{s_V} , Solar Reflectance in the Visible Range.

$\rho'_\lambda(\lambda,\beta,\theta)$, Directional-Hemispherical Spectral Reflectance.

σ , Stefan-Boltzmann Constant. $\sigma=5.6697\times10^{-8}$ $W.m^{-2}.K^{-4}$.

σ , Standard Deviation.

ω , Solid Angle of Incident Radiation Beam. [Steradians].

ω' , Solid Angle of Emitted, Reflected or Transmitted Radiation Beam. [Steradians].

Subscripts

o , Refers to Initial Values.

f , Refers to After-Exposure Values.

Superscripts

$\bar{}$, Mean Value.

Angles used to define directional emittance.

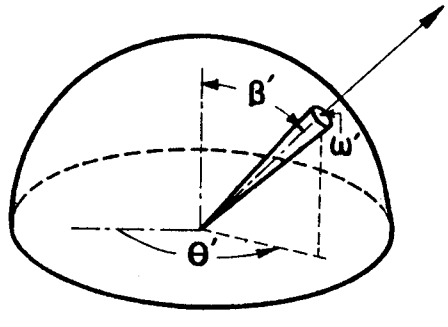

Angles used to define bidirectional reflectance.

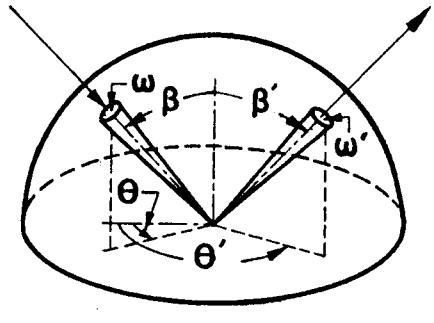

Rev. 1. 1981

THERMAL CONTROL SURFACES

List of Symbols

Acronyms

AU , Astronomical Unit. 1 AU = 1.495×10^{11} m.

CC , Conductive Coated.

COP , Coprecipitation.

CVCM , Collected Volatile Condensable Materials.

ESH , Equivalent Sun Hours.

EWH , Equivalent (Solar) Wind Hours.

GY , Gray. 1 GY = 1 $J.kg^{-1}$.

IR , Infrared.

ITO , Indium-Tin Oxide.

LDEF , Long Duration Exposure Facility.

MLI , Multilayer Insulation.

MOX , Mixed Oxalate Process.

OSR , Optical Solar Reflector.

PBR , Pigment to Binder Ratio by Weight.

RML , Remainder Mass Loss.

RMS , Root Mean Square.

RTV , Room Temperature Vulcanizing.

SCATHA , Spacecraft Charging at High Altitudes.

SSM , Second Surface Mirror.

SSR , Solid State Reaction.

TML , Total Mass Loss.

TWL , Total Weight Loss.

UV , Ultra-Violet.

VCM , Volatile Condensable Materials.

Other symbols are introduced when used.

THERMAL CONTROL SURFACES

General Introduction

GENERAL INTRODUCTION

A coating consists of a layer (or layers) of any substance (s) upon a substrate.

Optical coatings have been used to control the temperature of satellites since the first successful orbital flight in 1958. Since then coating materials have been developed to the point where reasonably stable coatings are available that give any desired value of the hemispherical total emittance, ε, between .1 and .9 for any desired value of the solar absorptance, α_s, between .1 and .9 .

According to Touloukian, DeWitt & Hernicz (1972) three types of coatings can be identified:

1) Pigmented coatings which are mixtures of a pigment and a vehicle.

2) Contact coatings, formed by layers of a substance coated on a substrate without chemical reaction occurring between the coating material and the substrate.

3) Conversion coatings which are layers of compounds formed by the chemical reaction of the substrate with another material.

Fig 0-1, from Touloukian et al. (1972) is a plot of solar absorptance, α_s, vs. hemispherical total emittance, ε. For each ray from the origin two values are given. The first one, T_R, is the equilibrium temperature for an isothermal sphere at 1 AU; the second value is the ratio α_s/ε.

Fig 0-2, from the same source, indicates how to obtain the various types of surfaces exhibiting the characteristics shown in the previous figure.

THERMAL CONTROL SURFACES

General Introduction

The basic requirement for a coating to be used in spacecraft is long-term space stability for periods of months and even of years. This objective, however, has not yet been achieved in many instances.

The problem of selecting the specific coating for a given α_s/ε is somewhat circumvented by the use of mosaics or coating patterns, normally combining white and black paints. Nevertheless, the possibility of using a single paint should not be lay aside; for example, Triolo (1973) reports that encouraging results have been obtained by using green paints to take the place of white and black paint patterns.

This data item, which is intended to give information on several pigmented and contact coatings, has two clearly different parts. In the first one data concerning several coating materials are gathered. These coatings are classified according to their thermal radiation characteristics.

The second part deals with coated foils and tapes. The main characteristic of these coatings is that they are flexible and can be applied to a surface by mere pressure, although a double-faced adhesive tape must be used in several case. Since ease of application and removal is the peculiar feature of these coatings, particular emphasis has been placed on their adhesive characteristics.

No attempt has been made to classify foils and tapes according to their thermal radiation properties. On the other hand,

THERMAL CONTROL SURFACES

General Introduction

this classification is by no means obvious in several cases. For example: Series Emittance Tapes are coatings whose emittance is controlled by the thickness of a Teflon Type A film, and their solar absorptance by a metallic second surface. By choosing the proper Teflon thickness and the appropriate metal it is possible to specify a thermal control surface within a wide range of α_s/ε values.

In addition to the data collected here, information concerning aluminium coatings can be found in G, Section 1.2.

THERMAL CONTROL SURFACES

General Introduction

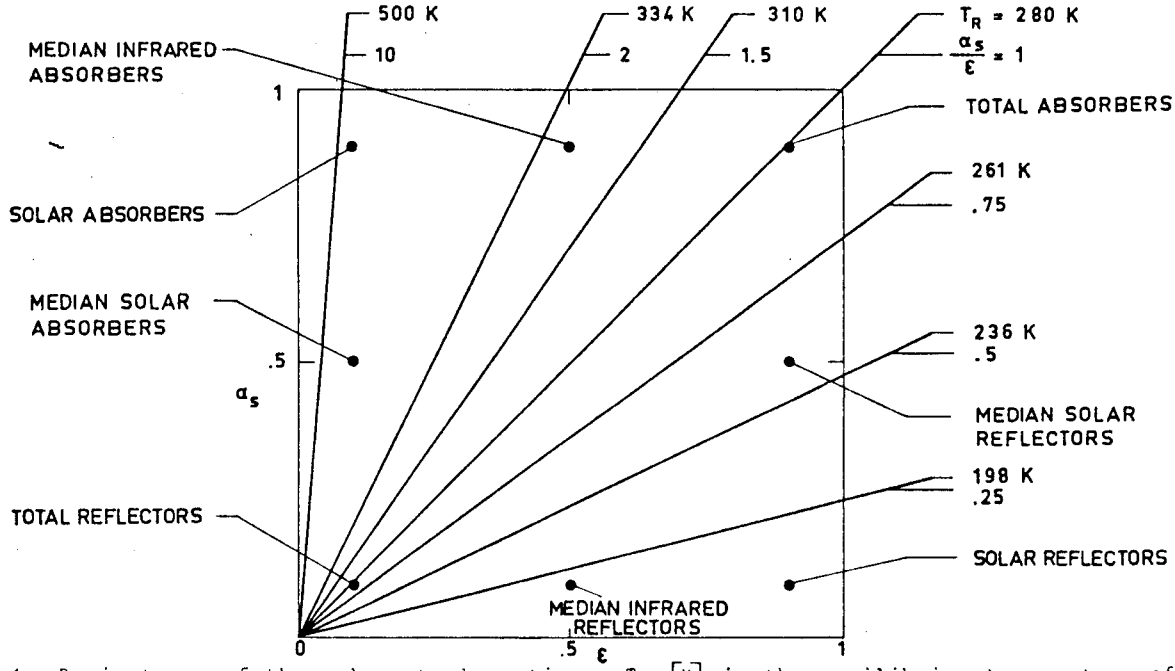

Fig 0-1. Basic types of thermal control coatings. T_p [K] is the equilibrium temperature of a coated isothermal sphere at 1 AU. From Touloukian, DeWitt & Hernicz (1972).

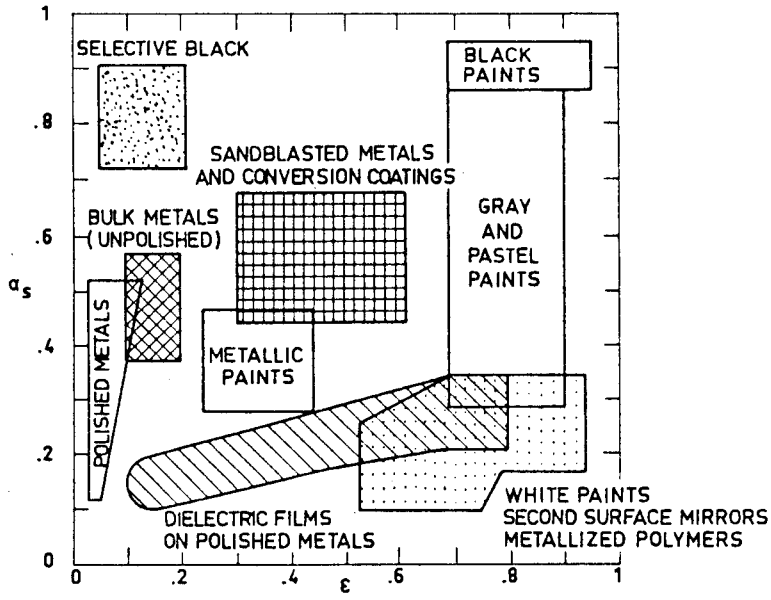

Fig 0-2. Range of solar absorptance, α_s, and hemispherical total emittance, ε, covered by available thermal control coatings. From Touloukian, DeWitt & Hernicz (1972).

Rev. 1. 1981

COATINGS

General

1. COATINGS

1.1 GENERAL

The data concerning each coating have been arranged, whenever possible and meaningful, as indicated below. When no data on a given property are available the corresponding heading has been normally omitted.

1. COMPOSITION
2. FORMULATION
3. USUAL DESIGNATION
4. SUBSTRATE
5. METHOD OF APPLICATION
   - 5.1. Preparation of paint for application
   - 5.2. Preparation of surfaces for painting
   - 5.3. Application of paint
   - 5.4. Coating thickness
   - 5.5. Curing process
6. SOLVENTS RESISTANCE
7. PHYSICAL PROPERTIES
   - 7.1. Density
   - 7.2. Outgassing
   - 7.3. Thermal radiation properties
     - 7.3.1. Emittance
       - 7.3.1.1. Hemispherical total emittance
       - 7.3.1.2. Variation of hemispherical total emittance whith coating thickness

7.3.1.3. Effects of the Space Environment on hemispherical total emittance

7.3.1.3.1. Ultra-Violet Radiation

7.3.2. Absorptance

7.3.2.1. Solar absorptance

7.3.2.2. Variation of solar absorptance with coating thickness

7.3.2.3. Variation of solar absorptance with incidence angle

7.3.2.4. Earth Albedo normal absorptance

7.3.2.5. Effects of Space Environment on absorptance

7.3.2.5.1. Ultra-Violet Radiation

7.3.2.5.2. Gamma Radiation

7.3.2.5.3. Protons only exposure

7.3.2.5.4 Electrons only exposure

7.3.2.5.5. Contamination

7.3.2.5.6. Combined exposure

7.3.2.6. Effects of the Space Environment on solar absorptance to emittance ratio

7.3.3. Reflectance

7.3.3.1. Normal-hemispherical spectral reflectance

7.3.3.2. Effects of the Space Environment on reflectance

7.3.3.2.1. Ultra-Violet Radiation

7.3.3.2.2. Gamma Radiation

7.3.3.2.3. Protons only exposure

7.3.3.2.4. Electrons only exposure

7.3.3.2.5. Contamination

7.3.3.2.6. Combined exposure

Rev. 1. 1981

COATINGS

General

7.4. Electrical resistance

7.4.1. Effects of Temperature on electrical resistance

7.4.2. Effects of the Space Environment on electrical resistance

7.4.2.1. Ultra-Violet Radiation

7.4.2.2. Gamma Radiation

7.4.2.3. Protons only exposure

7.4.2.4. Electrons only exposure

7.4.2.5. Contamination

7.4.2.6. Combined exposure

7.4.3. Charging

8. ENVIRONMENTAL BEHAVIOR

8.1. Prelaunch

8.2. Postlaunch

8.2.1. Ascent

8.2.2. Orbital

9. THERMAL CYCLING

10. SOURCE

11. COST

12. PAST SPATIAL USE

INTENTIONALLY BLANK PAGE

COATINGS

Solar Reflectors

1.2. SOLAR REFLECTORS

1.2.1. TITANIUM DIOXIDE-POLYMETHYL VINYL SILOXANE

1. COMPOSITION

Pigment: Titanox Ra-NC, Titanium Pigment Corp. propietary, calcined rutile TiO_2, 93% TiO_2.

Vehicle: Dow-Corning propietary, Q 92-007. 33% nonvolatile content by weight after 24 h at 343 K.

From Cunnington, Grammer & Smith (1969), Cunnington (1974).

2. FORMULATION

1:1 by weight of pigment and vehicle (Cunnington et al. (1969)).

3. USUAL DESIGNATION

LMSC/Dow-Corning Thermatrol 2A-100.

4. SUBSTRATE

Any clean substrate, either rigid or non-rigid (Breuch (1967)).

5. METHOD OF APPLICATION

5.2. Preparation of surfaces for painting. The entire surface is primed with one coat of silicone primer, Dow Corning Corp. A-4094 or equivalent, to a thickness of approximately 5×10^{-6} m. The primer is air cured 30 min minimum prior to application of top coats.

5.3. Application of paint. By spray techniques.

5.4. Coating thickness. For internal application, where emittance is of primary interest, a minimum thickness of 2.54×10^{-5} m should be maintained. For external surfaces, where both α_s and ε are

COATINGS

Solar Reflectors

important, the minimum thickness for opacity is .9 x 10^{-4} to 1.3 x 10^{-4} m.

5.5. Curing process. 24 h minimum at room temperature and normal pressure, after final coat.

From Breuch (1967), Cunnington, Grammer & Smith (1969).

6. SOLVENTS RESISTANCE

The following data, concerning resistance of elastomeric silicones to chemical attack, have been reported by the producer of the vehicle.

Solvents and Fuels (after 7 d at room temperature)	Volume Variation (per cent)
Acetone	15 to 25
Carbon tetrachloride	above 150
Ethyl alcohol	0 to 20
Isooctane	above 150
Xylene	above 150
B type fuel	above 150
JP-4 jet fuel	above 150
Oils (after 70 h at T=423 K)	
ASTM No. 1 Oil	5 to 10
ASTM No. 3 Oil	35 to 60
Hydraulic fluid Mil-0-5606 (Univis J-43)	above 150
Oronite 8200 (silicate ester)	above 150

From DOW-CORNING (1970).

7. PHYSICAL PROPERTIES

7.1. Density. 1 500 kg.m^{-3} after curing (Cunnington et al. (1969)).

COATINGS

Solar Reflectors

7.2. Outgassing. Negligible after coating has been fully cured (Cunnington, Grammer & Smith (1969)).

7.3. Thermal radiation properties

7.3.1. Emittance.

7.3.1.1. Hemispherical total emittance.

T [K]	ε [a]	ε [b]
295	.86 ± .03	.84
395	.86 ± .02	.84

[a] Determined calorimetrically. Chamber pressure: 1.33×10^{-5} Pa.

[b] From spectral reflectance data in the range 2×10^{-6} to 2.5×10^{-5} m and the blackbody function corresponding to the temperatures quoted.

From Cunnington et al. (1969).

7.3.1.3. Effects of the Space Environment on hemispherical total emittance.

7.3.1.3.1. Ultra-Violet Radiation.

t [h]	.25	5	69	117	168	250	360	410	457	486	550
ε	.87	.87	.87	.85	.88	.88	.87	.85	.86	.85	.85

Degrading Source: 2×10^{-7} to 4×10^{-7} Xenon Lamp, 1 Sun level.

Method of obtaining data: Calorimetric. Chamber pressure: 1.33×10^{-5} Pa.

Probe temperature 395 K.

t, exposure time.

From Cunnington et al. (1969).

7.3.2. Absorptance.

Rev. 1. 1981

COATINGS

Solar Reflectors

7.3.2.1. Solar Absorptance.

T [K]	α_s
278	.16 ± .03 [a]
295	.15 ± .02 [b]
389	.16 ± .03 [a]
395	.18 ± .01 [b]

[a] From Breuch (1967).

[b] From Cunnington, Grammer & Smith (1969).

7.3.2.5. Effects of the Space Environment on absorptance.

7.3.2.5.1. Ultra-Violet Radiation. Laboratory data concerning the effects of UV radiation on spectral absorptance are given in Table 1-1. Calculated values of α_s are also included.

Table 1-1

Ultra-Violet Radiation Effects on Spectral Absorptance of Thermatrol 2A-100

T [K]	t [h]	α for Xenon Lamp Range of λ x 10^7 [m]					α_s
		2-4.1	4.1-6	6-8.5	8.5 -	Total	
395	.25	.70	.12	.07	.13	.18	.18
395	5	.70	.17	.07	.19	.21	.21
395	69	.85	.25	.16	.22	.29	.29
395	117	.85	.24	.18	.26	.30	.31
395	168	.85	.25	.18	.28	.31	.32
395	360	.80	.24	.17	.27	.29	.31
395	410	.85	.25	.18	.26	.30	.31
395	457	.85	.24	.18	.26	.30	.31
395	486	.90	.25	.18	.27	.31	.32
395	550	.90	.25	.19	.27	.31	.32
Before Exposure[a]		.69	.08	.06	.07	.14	.15
After Exposure[a]		.79	.27	.15	.13	.24	.26

[a] Values deduced from spectral reflectance data.

(Continued onto next page)

COATINGS

Solar Reflectors

Degrading Source: 2×10^{-7} to 4×10^{-7} m Xenon lamp, 1 Sun level.

Method of obtaining data: Calorimetric in situ absorptance.

Chamber pressure: 1.33×10^{-5} Pa.

From Cunnington, Grammer & Smith (1969).

Similar laboratory data are compared with those corresponding to orbital flight in Fig 1-1.

The influence of different radiation conditions on the degradation of solar absorptance is represented in Fig 1-2. It can be deduced from this figure that the intensity of the radiating source does not affect significantly the results, since the difference between the curves labeled 5 Suns and 10 Suns seems to be smaller than the experimental error.

7.3.3. Reflectance.

7.3.3.1. Normal-hemispherical spectral reflectance: Fig 1-3.

7.3.3.2. Effects of the Space Environment on reflectance.

7.3.3.2.1. Ultra-Violet Radiation: Fig 1-4.

8. ENVIRONMENTAL BEHAVIOR

8.1. Prelaunch. The surface is soft and rubbery and should be protected from abrasion or scratches. Since this paint is electrostatic, contamination must be avoided.

8.2. Postlaunch. In order to avoid blistering during ascent heating, the paint must be cured, at room temperature, at least for 24 h. In this manner, volatile materials are removed.

COATINGS

Solar Reflectors

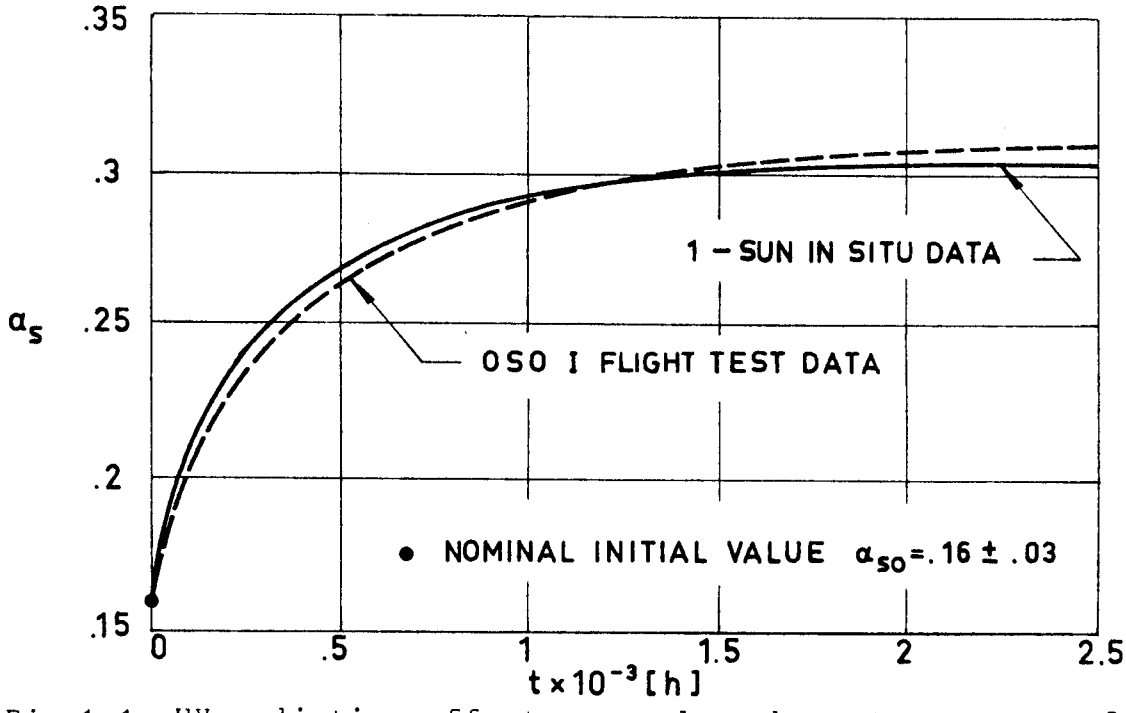

Fig 1-1. UV radiation effects on solar absorptance, α_s, of Thermatrol 2A-100 vs. exposure time, t. From Breuch (1967).

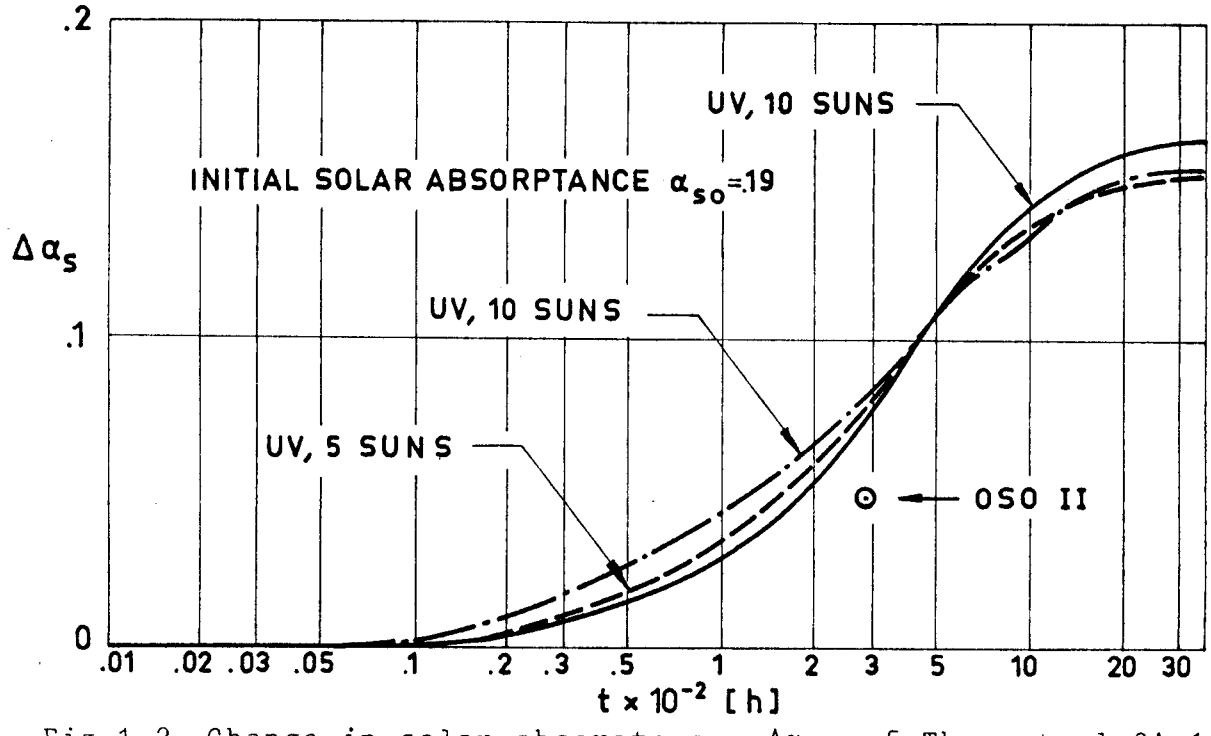

Fig 1-2. Change in solar absorptance, $\Delta\alpha_s$, of Thermatrol 2A-100, under various radiation conditions, vs. exposure time, t. From McCargo et al. (1971).

COATINGS

Solar Reflectors

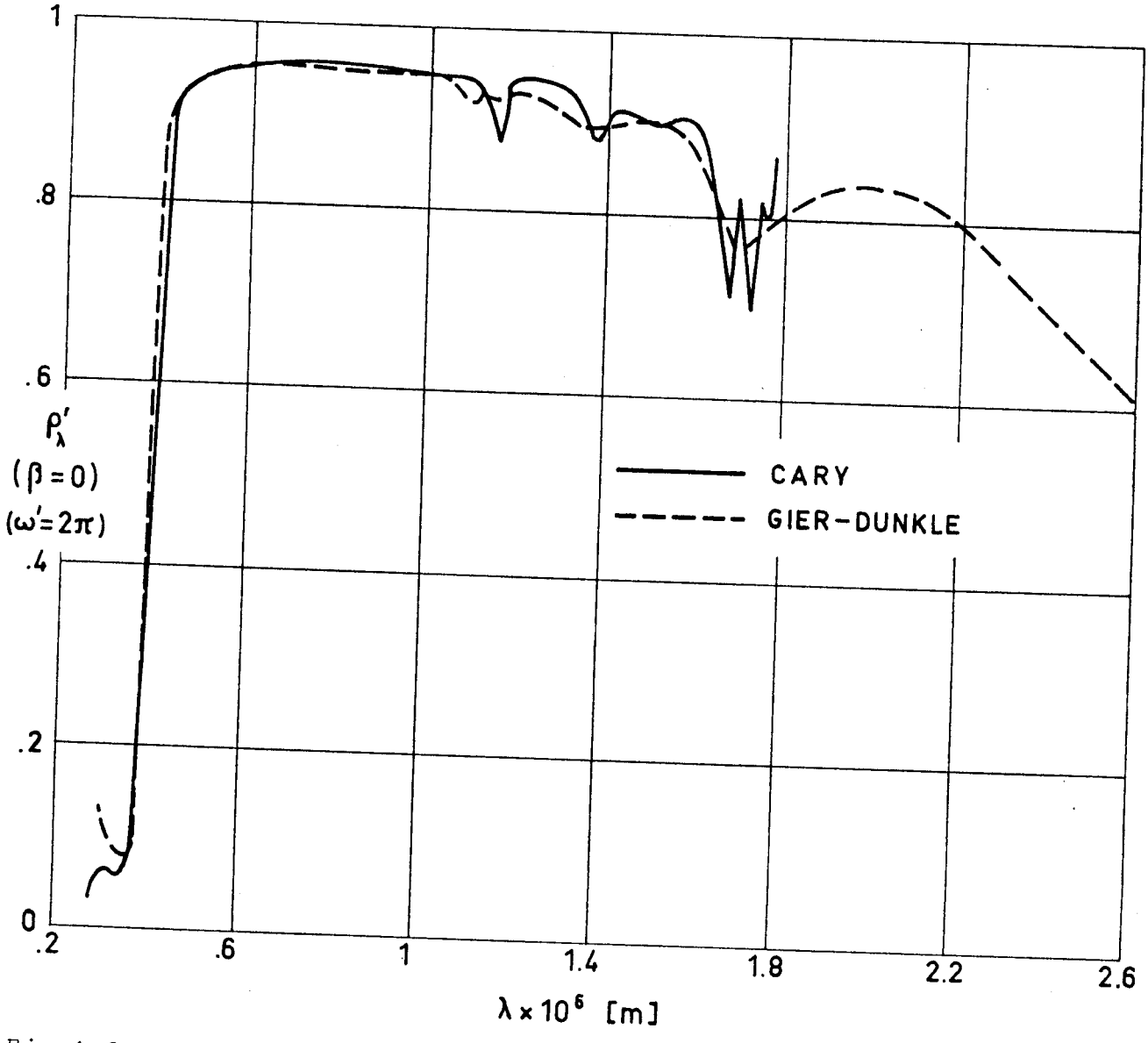

Fig 1-3. Normal-hemispherical spectral reflectance, ρ'_λ, of Thermatrol 2A-100, measured by two different methods, vs. wavelength, λ. From Cunnington, Grammer & Smith (1969).

Rev. 1. 1981

COATINGS

Solar Reflectors

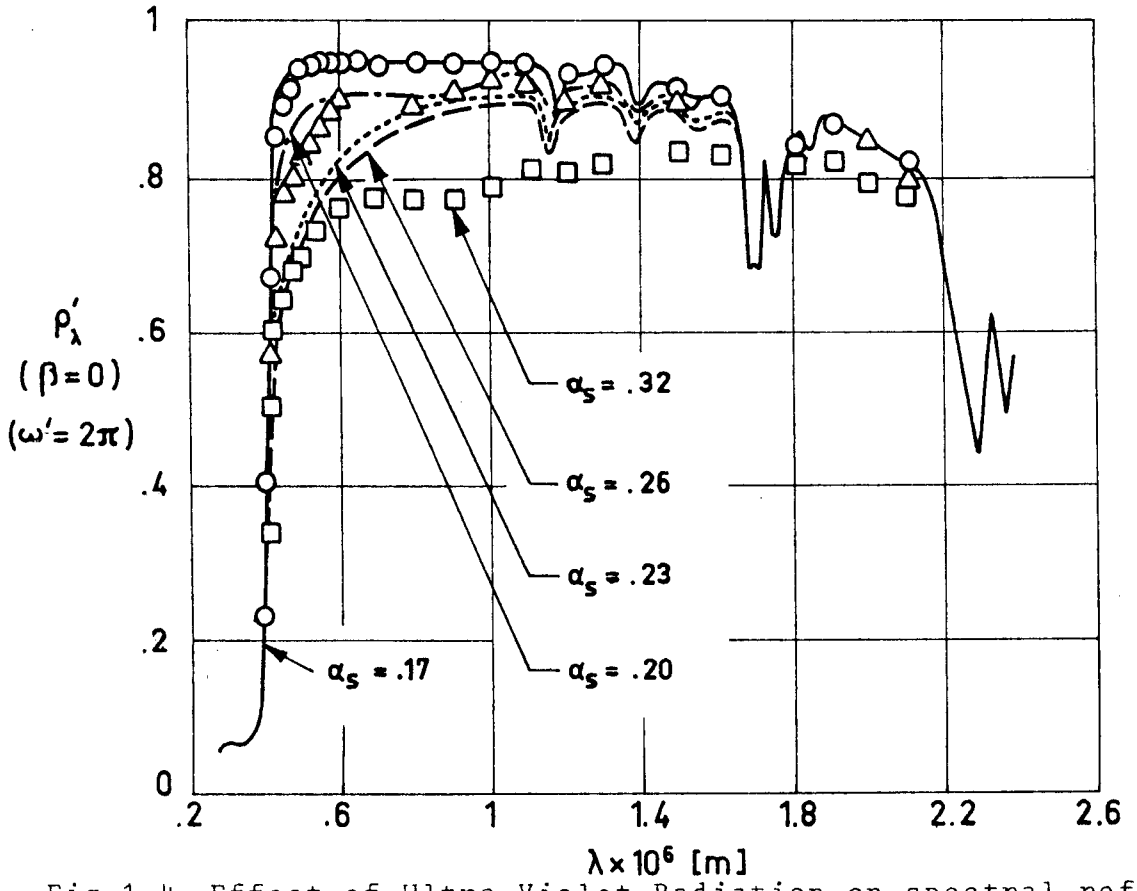

Fig 1-4. Effect of Ultra-Violet Radiation on spectral reflectance, ρ'_λ, of Thermatrol 2A-100 vs. wavelength, λ. Most of the data, concerning bidirectional reflectance, are from Rittenhouse & Singletary (1969), while ——— and ·····, normal-hemispherical reflectance, are from Cunnington, Grammer & Smith (1969).

Explanation

Key	Description	Comments
———		T=313 K. Near-normal reflectance (Cary).
O		T=313 K. Measured in vacuum (6.65×10^{-5} Pa).
□		Same as O except exposed to UV radiation (PEK Type C(A-H6) lamp, 20 Suns). ESH 1330. During exposure $p=9.3\times10^{-5}$Pa.
△		Same as □ except sample in air at 40 Pa for 24 h after exposure.
——·——		Same as ——— except exposed to the same radiation as □ .
– – –	6061-T6 Al substrate polished and then machined to a $(30\pm3)\times$ $\times10^{-6}$ m RMS finish.	T=395 K. Exposed to UV radiation (900 W Hanovia, Xenon lamp, 1 Sun) ESH 550. Sample in air for 5 min after exposure.
·····	Same as – – – .	Same as – – – . Sample in air for 30 min.

COATINGS

Solar Reflectors

8.2.1. Ascent. Ascent heating histories with peak temperatures below 615 K cause an increase in α_s of .03 or less, while ε is unaffected.

8.2.2. Orbital. The primary source of degradation appears to be the near-ultra-violet portion of incident solar and albedo radiation.

From Breuch (1967).

9. THERMAL CYCLING

The maximum and minimum temperatures at which the paint has been tested without major changes in properties were:

Tmin = 211 K
Tmax = 366 K

(Rittenhouse & Singletary (1969)).

10. SOURCE

Lockheed Missiles and Space Company Inc. 3251 Hanover Street. Palo Alto, California 94304.

11. COST

Varies depending on quantity; Cunnington et al. (1969) indicate that the nominal price is 16 US $ per litre.

12. PAST SPATIAL USE

Thermatrol 2A-100 has been used for thermal control in Explorer 33 (launched July 1, 1966), Rittenhouse & Singletary (1969). According to Neel (1967), this paint has been tested on board OSO I (launched March 7, 1962) and OSO II (Feb. 3, 1965). The results obtained have been presented in Figs 1-1 and 1-2.

INTENTIONALLY BLANK PAGE

COATINGS

Solar Reflectors

1.2.2. ZINC OXIDE-POTASSIUM SILICATE

1. COMPOSITION

Pigment: New Jersey Zinc Co., SP500 zinc oxide; calcined at 873 to 973 K for 16 h. (Heating and cooling rates are not critical).

Binder: Sylvania Electric Products Corp., PS7 potassium silicate.

From Cunnington, Grammer & Smith (1969).

2. FORMULATION

4.3:1 by weight of pigment and binder (Cunnington et al. (1969)).

3. USUAL DESIGNATION

Z-93. IIT Research Institute.

4. SUBSTRATE

All metals except noble; Aluminium is preferred (IITRI (1974)).

5. METHOD OF APPLICATION

5.1. Preparation of paint for application. The components are mixed in a pigment to binder ratio of 4.3 with a solids content of 56.9%. A typical batch may be .1 kg of ZnO, 50 cm^3 of PS7 (35% solution), and 50 cm^3 distilled water.

The paint should be prepared just before use. Shelf life is limited. Actual shelf life should exceed 24 h. The mixture should be shaken to maintain the pigment in suspension (Cunnington et al. (1969)).

5.2. Preparation of surfaces for painting. The substrate should be abraded and thoroughly washed with detergent and water.

Rev. 1. 1981

COATINGS

Solar Reflectors

According to the supplier, chromate treatments are not permissable.

5.3. Application of paint. By spray-painting. Because of the porous nature of the cured coating, heavy spraying upon application of a second coat is required to achieve a satisfactory finished texture (Breuch (1967)).

For process specification see Stevens (1971).

5.4. Coating thickness. A thickness of about 2.54×10^{-5} m is achieved per cycle. Total thickness should be of the order of 1.1×10^{-4} to 1.5×10^{-4} m.

5.5. Curing process. Satisfactory physical properties are obtained by an air-drying cure for 4 h. The supplier recommends, as optional, a cure at 366 K for 16 h, while Cunnington at al (1969) indicate that improved hardness is obtained by heat curing at 413 K.

6. SOLVENTS RESISTANCE

Not attacked by the solvents.

7. PHYSICAL PROPERTIES

7.2. Outgassing. Initial weight loss in 20 h: 8.0×10^{-4} kg.m^{-2}.

Stationary loss rate: 5.6×10^{-10} kg.m^{-2}.s^{-1} (McCargo, Spradley, Greenberg & McDonald (1971)).

7.3. Thermal radiation properties

7.3.1. Emittance.

7.3.1.1. Hemispherical total emittance.

COATINGS

Solar Reflectors

T [K]	ε^a	ε^b	Ref.
295	.90±.05	.87	c
310	.96		d
394		.88	c
533		.88	c

a Determined calorimetrically. Chamber pressure: 1.33×10^{-5} Pa.

b From spectral reflectance data in the range 2×10^{-6} m to 2.5×10^{-5} m and the blackbody function corresponding to the temperatures quoted.

c From Cunnington, Grammer & Smith (1969).

d From Westcott (1968).

7.3.1.3. Effects of the Space Environment on hemispherical total emittance.

7.3.1.3.1. Ultra-Violet Radiation. The following table has been prepared using data given by Cunnington et al. (1969).

T[K]	t[h]	n	ε_o	ε_f	$\bar{\varepsilon}$	σ
300	2001	28	.90	.88	.882	.012
366	2024	33	.89	.88	.887	.007
422	10517	140	.88	.87	.878	.010
450	1004	19	.87	.87	.871	.004
534	502	12	.81	.81	.811	.009

Degrading Source: 2×10^{-7} to 4×10^{-7} m Xenon Lamp, 1 Sun level.

Method of obtaining data: Calorimetric. Chamber pressure: 1.33×10^{-5} Pa.

t, total exposure time. [h].

n, number of data points given in the source.

ε_o, ε_f, initial and after-exposure values of the hemispherical total emittance.

$\bar{\varepsilon}$, mean value. $\bar{\varepsilon} = \dfrac{\sum_1^n \varepsilon_i \, \Delta t_i}{t}$

σ, standard deviation. $\sigma = \sqrt{\dfrac{\sum_1^n (\varepsilon_i - \bar{\varepsilon})^2 \, \Delta t_i}{t-1}}$

7.3.2. Absorptance.

7.3.2.1. Solar absorptance: Table 1-2.

Rev. 1. 1981

COATINGS

Solar Reflectors

Table 1-2

Solar Absorptance of Zinc Oxide-Potassium Silicate Paint

No	T [K]	α_s	Comments
1	278	.114	Measured in vacuum (1.2×10^{-4} Pa).
2	278	.112	Similar to above specimen and conditions.
3	279	.153	Air dried at 100% relative humidity; measured in vacuum (1.3×10^{-4} Pa).
4	279	.168	Similar to above specimen and conditions except air dried at 0% relative humidity.
5	279	.161	Similar to No. 3 specimen and conditions except air dried at 35% relative humidity.
6	279	.147	Spray application; measured in vacuum (1.3×10^{-4} Pa); fresh preparation.
7	279	.150	Similar to above specimen and conditions except measured in vacuum (6.7×10^{-4} Pa).
8	279	.150	Similar to No. 6 specimen and conditions except measured in vacuum (4.7×10^{-4} Pa).
9	279	.138	Spray application; measured in vacuum (1.3×10^{-4} Pa); preparation aged 120 d.
10	279	.119	Above specimen and conditions except heat-treated at 773 K for 2 h.
11	279	.131	Similar to No. 9 except measured at pressure of 6.7×10^{-4} Pa.
12	279	.126	Above specimen and conditions except heat-treated at 773 K for 2 h.
13	279	.140	Similar to No. 9 specimen and conditions except measured at pressure of 4.7×10^{-4} Pa.
14	279	.119	Above specimen and conditions except heat-treated at 773 K for 2 h.
15	279	.120	Spray application; measured in vacuum (1.3×10^{-4} Pa); preparation aged 120 d.
16	279	.133	Similar to above specimen and conditions except measured in vacuum (6.7×10^{-4} Pa).
17	279	.124	Similar to No. 15 specimen and conditions except measured at pressure of 4.7×10^{-4} Pa.
18	298	.164	Substrate abraded with No. 60 Aloxite cloth. Sample cured at 413 K for 18 h.
19	298	.158	Above specimen and conditions except heat-treated (418 K for 16 h); time lapse, 1 d.
20	298	.149	Similar to No. 18 specimen and conditions except heat-treated (773 K for 2 h); time lapse, 6 h.
21	298	.160	Similar to No. 18 specimen and conditions except after time lapse of 90 d.
22	298	.165	Abraded magnesium silicate substrate.
23	298	.158	Similar to above specimen and conditions except heat-treated (418 K for 16 h); time lapse, 1 d.
24	298	.158	Similar to No. 22 specimen and conditions except heat-treated (973 K for 2 h); time lapse, 1 d.
25	298	.159	Similar to No. 22 specimen and conditions except heat-treated (1073 K for 2 h); time lapse,6 h.
26	298	.161	Similar to No. 22 specimen and conditions except after time lapse of 90 d.
27	298	.168	Abraded alumina substrate.
28	298	.159	Similar to above specimen and conditions except heat-treated (418 K for 16 h); time lapse, 1 d.
29	298	.160	Similar to No. 27 specimen and conditions except heat-treated (973 K for 2 h); time lapse, 1 d.
30	298	.160	Similar to No. 27 specimen and conditions except heat-treated (1073 K for 2 h); time lapse, 6 h.
31	298	.165	Similar to No. 27 specimen and conditions except after time lapse of 90 d.
32	298	.153	Measured in vacuum (4×10^{-3} Pa).
33	298	.120	Aluminium substrate; supplied by IITRI.
34	298	.220	Similar to above specimen and conditions except supplied by ESRO I Project Group; coating thickness 8.9×10^{-5} m.
35	298	.260	Similar to above specimen and conditions except soiled.
36	298	.184	Property calculated from reflectance; lab data taken on sample to be tested on Lunar Orbiter V.
37	293	.14±.02	Substrate abraded with No. 60 Aloxite cloth. [a]
38	289	.14±.02	Same as above [a].
39	533	.14±.02	Same as above [a].

[a] From Breuch (1967).

All data, unless otherwise stated, are from Touloukian, DeWitt & Hernicz (1972).

COATINGS

Solar Reflectors

7.3.2.2. Variation of solar absorptance with coating thickness: Fig 1-5

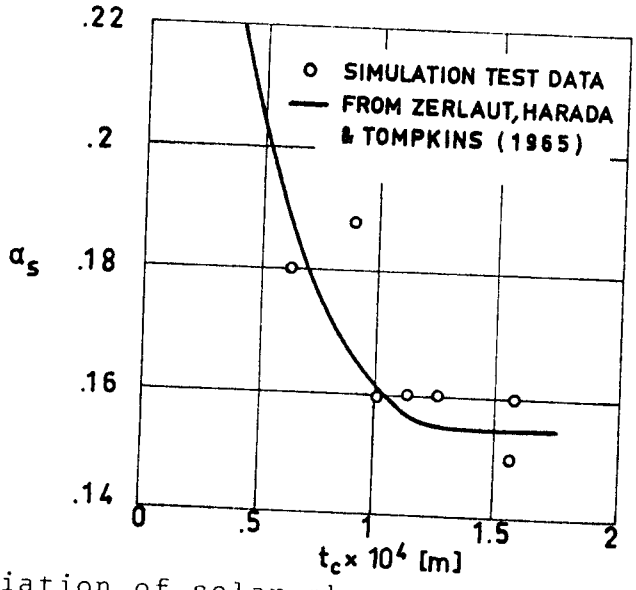

Fig 1-5. Variation of solar absorptance, α_s, with thickness, t_c. From Stevens (1971).

7.3.2.4. Earth Albedo normal absorptance. The value α=.26 has been obtained by Westcott (1968) from spectral data. Albedo radiation is approximated by the solar spectrum truncated below 3.5×10^{-7} m. Aluminium substrate.

7.3.2.5. Effects of the Space Environment on absorptance.

7.3.2.5.1. Ultra-Violet Radiation. Fairly detailed laboratory data on the effects of UV radiation on spectral absorptance are given in Table 1-3. Table 1-4 has a broader scope, it is intended to illustrate how the experimental conditions influence the results.

Changes in solar absorptance during the total mission profile for a near-Earth orbit, as estimated by McCargo, Spradley, Greenberg & McDonald (1971) are shown in Fig 1-6.

COATINGS

Solar Reflectors

Table 1-3

Ultra-Violet Radiation Effects on Spectral Absorptance of Zinc Oxide-Potassium Silicate Paint

T[K]	t[h]	α for Xenon Lamp, Range of λ x 10^7 [m]					α_s
		2-4.1	4.1-6	6-8.5	8.5 -	Total	
300	0	.72	.10	.05	.08	.14	.14
300	43	.70	.09	.05	.09	.14	.14
300	293	.67	.11	.06	.08	.15	.14
300	365	.67	.15	.04	.09	.14	.15
300	461	.66	.15	.05	.09	.15	.15
300	509	.65	.14	.06	.09	.15	.15
300	605	.69	.14	.06	.09	.15	.16
300	701	.70	.16	.07	.09	.15	.16
300	773	.67	.19	.09	.08	.16	.16
300	821	.71	.18	.05	.09	.15	.17
300	869	.70	.19	.08	.09	.16	.17
300	941	.65	.19	.08	.09	.15	.17
300	989	.70	.15	.09	.08	.16	.17
300	1039	.65	.19	.09	.08	.15	.17
300	1109	.66	.20	.08	.08	.16	.17
300	1157	.73	.19	.10	.08	.16	.17
300	1205	.69	.20	.09	.08	.16	.18
300	1277	.68	.20	.07	.09	.16	.17
300	1325	.63	.23	.07	.09	.16	.18
300	1373	.65	.22	.10	.08	.16	.17
300	1445	.66	.23	.10	.08	.16	.18
300	1545	.65	.22	.08	.09	.16	.18
300	1617	.68	.22	.10	.08	.16	.19
300	1665	.67	.24	.08	.08	.16	.18
300	1713	.67	.22	.08	.09	.16	.18
300	1785	.69	.22	.09	.09	.17	.18
300	1953	.69	.21	.09	.08	.17	.18
300	2001	.68	.21	.09	.09	.17	.18
After Exposure[a]		.75	.17	.06	.08	.16	.17
366	0	.84	.05	.04	.08	.14	.14
366	17	.88	.10	.06	.08	.16	.16
366	70	.89	.14	.08	.08	.17	.18
366	93	.89	.16	.06	.08	.17	.18
366	161	.90	.14	.09	.08	.17	.18
366	233	.90	.16	.07	.08	.18	.18
366	329	.91	.16	.10	.08	.18	.19
366	377	.90	.16	.10	.08	.18	.19
366	425	.90	.16	.09	.08	.18	.19
366	497	.89	.16	.09	.09	.18	.19
366	545	.85	.17	.10	.09	.17	.19
366	593	.85	.20	.09	.09	.18	.20
366	665	.82	.18	.08	.09	.18	.18
366	713	.87	.18	.10	.09	.19	.20
366	761	.87	.19	.10	.09	.19	.20
366	833	.85	.19	.11	.09	.18	.20
366	881	.85	.18	.11	.09	.18	.19
366	939	.80	.20	.12	.09	.19	.20
366	1011	.80	.19	.10	.09	.17	.20
366	1059	.83	.19	.10	.09	.18	.19
366	1179	.84	.18	.09	.09	.17	.19
366	1227	.85	.19	.13	.09	.19	.20
366	1275	.82	.21	.12	.08	.181	.19
366	1347	.84	.21	.11	.09	.183	.20
366	1395	.84	.19	.13	.09	.187	.20
366	1443	.85	.18	.11	.09	.173	.19
366	1575	.85	.18	.10	.09	.173	.19
366	1621	.82	.19	.12	.09	.183	.20
366	1693	.82	.19	.12	.09	.183	.20
366	1741	.81	.22	.11	.09	.187	.20
366	1909	.80	.22	.11	.09	.183	.20
366	1957	.80	.22	.12	.085	.183	.20
366	2024	.80	.22	.11	.085	.185	.20
After Exposure[a]		.75	.25	.12	.10	.18	.21

T[K]	t[h]	α for Xenon Lamp, Range of λ x 10^7 [m]					α_s
		2-4.1	4.1-6	6-8.5	8.5 -	Total	
422	0	.75	.11	.05	.05	.126	.137
422	22	.90	.16	.05	.05	.15	.16
422	96	.92	.16	.07	.07	.17	.18
422	144	.87	.17	.07	.07	.16	.18
422	192	.80	.20	.07	.07	.16	.18
422	264	.80	.18	.10	.07	.16	.19
422	312	.78	.20	.07	.08	.16	.18
422	360	.80	.17	.08	.09	.16	.18
422	432	.76	.19	.07	.08	.16	.18
422	480	.76	.20	.09	.08	.16	.18
422	528	.76	.19	.08	.08	.16	.18
422	600	.80	.17	.10	.08	.16	.19
422	648	.80	.19	.09	.08	.16	.19
422	768	.77	.18	.07	.08	.15	.18
422	816	.80	.17	.08	.08	.15	.19
422	864	.75	.18	.07	.08	.14	.17
422	936	.78	.16	.08	.08	.14	.17
422	984	.78	.18	.08	.08	.15	.18
422	1032	.78	.18	.08	.08	.14	.18
422	1152	.70	.16	.08	.08	.14	.17
422	1200	.72	.17	.09	.08	.15	.17
422	1272	.73	.17	.08	.08	.14	.17
422	1320	.72	.18	.08	.08	.14	.17
422	1488	.70	.19	.08	.08	.14	.17
422	1536	.68	.21	.09	.09	.15	.18
422	1608	.66	.18	.09	.09	.15	.17
422	1656	.65	.18	.10	.08	.15	.17
422	1704	.67	.18	.10	.08	.15	.17
422	1776	.68	.20	.09	.08	.15	.18
422	1824	.70	.18	.11	.08	.16	.18
422	1872	.70	.19	.09	.09	.16	.18
422	1944	.70	.18	.09	.09	.16	.18
422	2016	.68	.19	.10	.08	.16	.18
422	2256	.69	.19	.09	.08	.16	.17
422	2424	.69	.17	.11	.08	.15	.17
422	2472	.66	.19	.10	.08	.15	.17
422	2560	.68	.17	.11	.08	.15	.18
422	2644	.67	.18	.10	.09	.15	.17
422	2736	.68	.18	.10	.08	.15	.17
422	2784	.68	.18	.11	.09	.15	.18
Xenon Lamp off 2832 to 3335 h.							
422	3336	.66	.17	.10	.09	.16	.17
422	3408	.64	.16	.11	.09	.15	.17
422	3508	.64	.18	.10	.09	.15	.17
422	3580	.64	.18	.11	.09	.15	.17
422	3678	.62	.16	.12	.09	.16	.17
422	3676	.64	.20	.11	.09	.16	.18
422	3798	.63	.17	.12	.09	.16	.18
422	3866	.66	.17	.11	.09	.16	.18
422	3914	.64	.20	.12	.09	.16	.18
422	3962	.61	.17	.13	.09	.16	.17
422	4034	.65	.20	.12	.09	.17	.18
422	4082	.66	.21	.12	.09	.17	.18
422	4202	.65	.20	.13	.09	.16	.19
422	4298	.66	.20	.12	.09	.17	.19
422	4370	.65	.20	.12	.09	.17	.18
422	4466	.63	.20	.13	.09	.17	.18
422	4530	.62	.21	.13	.09	.17	.19
422	4634	.61	.20	.13	.10	.17	.19
422	4706	.61	.25	.12	.09	.17	.19
422	4754	.66	.22	.12	.09	.17	.19
422	4802	.65	.23	.12	.09	.17	.19
422	4874	.62	.21	.12	.10	.17	.20
422	4921	.63	.22	.11	.10	.17	.19

(Continued onto next page)

COATINGS

Solar Reflectors

Table 1-3 (Continued)

Ultra-Violet Radiation Effects on Spectral Absorptance of Zinc Oxide-Potassium Silicate Paint

T[K]	t[h]	α for Xenon Lamp, Range of λ x 10^7 [m]					α_s
		2-4.1	4.1-6	6-8.5	8.5 -	Total	
422	4969	.66	.20	.11	.10	.17	.19
422	5089	.62	.22	.10	.11	.17	.18
422	5137	.59	.24	.11	.09	.17	.18
422	5209	.63	.24	.10	.10	.17	.19
422	5329	.60	.25	.11	.10	.17	.19
422	5401	.61	.25	.11	.11	.17	.19
422	5449	.64	.25	.13	.09	.17	.20
422	5497	.59	.26	.12	.09	.17	.20
422	5617	.62	.25	.12	.10	.18	.20
422	5665	.58	.25	.11	.10	.17	.19
422	5737	.59	.26	.12	.09	.17	.19
422	5785	.58	.26	.14	.09	.17	.20
422	5833	.59	.25	.11	.10	.17	.19
422	5905	.58	.22	.14	.10	.17	.19
422	5953	.58	.25	.11	.10	.17	.19
422	6001	.61	.25	.11	.10	.17	.19
422	6073	.62	.22	.11	.10	.17	.19
422	6121	.60	.26	.09	.10	.17	.19
422	6169	.63	.22	.11	.09	.17	.19
422	6241	.64	.23	.09	.10	.17	.19
422	6289	.64	.22	.08	.10	.16	.19
422	6457	.68	.20	.10	.10	.17	.19
422	6505	.64	.23	.08	.10	.17	.19
422	6577	.63	.22	.11	.09	.17	.19
422	6625	.65	.20	.11	.10	.17	.19
422	6673	.62	.24	.10	.09	.17	.19
422	6745	.62	.22	.11	.10	.16	.19
422	6793	.62	.22	.10	.09	.16	.19
422	6913	.62	.23	.10	.09	.17	.19
422	6961	.62	.23	.10	.10	.16	.19
422	7009	.62	.20	.10	.10	.16	.19
422	7081	.66	.19	.10	.10	.16	.18
422	7129	.63	.19	.09	.10	.16	.19
422	7177	.65	.21	.09	.10	.16	.18
422	7249	.65	.18	.10	.10	.16	.18
422	7345	.60	.18	.11	.10	.16	.18
422	7417	.62	.18	.10	.10	.16	.18
422	7465	.63	.19	.09	.10	.16	.18
422	7513	.65	.20	.11	.10	.16	.19
422	7585	.62	.22	.10	.10	.16	.19
422	7633	.65	.20	.10	.10	.17	.19
422	7681	.63	.17	.10	.10	.16	.18
422	7753	.64	.18	.12	.10	.16	.18
422	7801	.60	.19	.10	.10	.16	.18
422	7849	.62	.20	.11	.09	.17	.18
422	7921	.63	.20	.09	.09	.17	.18
422	8017	.62	.21	.09	.10	.16	.18
422	8029	.62	.20	.10	.10	.16	.18
422	8125	.62	.20	.10	.10	.16	.18
422	8251	.57	.17	.12	.10	.16	.18
422	8301	.56	.17	.12	.10	.16	.18
422	8349	.57	.18	.11	.10	.16	.18
422	8421	.55	.17	.13	.10	.16	.18
422	8517	.54	.17	.12	.10	.16	.18
422	8589	.57	.17	.12	.10	.16	.18
422	8781	.59	.19	.13	.10	.16	.18
422	9021	.54	.21	.11	.11	.17	.18
422	9093	.57	.19	.11	.10	.16	.17
422	9189	.50	.20	.09	.10	.15	.17
422	9285	.53	.21	.11	.10	.16	.18
422	9357	.54	.23	.14	.10	.17	.19
422	9424	.54	.21	.12	.10	.17	.18
422	9501	.52	.20	.09	.10	.16	.17
422	9597	.54	.19	.13	.10	.16	.18
422	9645	.52	.21	.11	.10	.15	.18
422	9693	.52	.19	.11	.10	.16	.18
422	9789	.54	.19	.09	.11	.16	.18
422	9861	.50	.19	.11	.11	.15	.17
422	9885	.53	.20	.12	.10	.15	.18
422	9975	.50	.18	.11	.11	.16	.17
422	10071	.48	.19	.10	.11	.15	.17
422	10143	.50	.17	.13	.10	.14	.17
422	10239	.49	.19	.12	.10	.15	.17
422	10431	.49	.21	.11	.10	.15	.17
422	10454	.49	.19	.12	.10	.14	.17
422	10517	.45	.19	.13	.10	.15	.17
422	10517	.62	.22	.14	.12	.17	.19
Before Exposure[a]		.60	.06	.06	.07	.13	.15
After Exposure[a]		.66	.23	.14	.10	.20	.21
450	0	.50	.10	.04	.08	.12	.12
450	20	.75	.15	.07	.08	.16	.16
450	58	.80	.17	.08	.08	.18	.18
450	106	.84	.23	.09	.09	.18	.20
450	154	.85	.23	.10	.10	.19	.20
450	226	.91	.23	.12	.10	.20	.22
450	274	.90	.23	.11	.11	.21	.22
450	322	.94	.29	.10	.11	.21	.24
450	394	.95	.27	.10	.11	.20	.24
450	488	.87	.28	.13	.11	.22	.24
450	560	.87	.24	.14	.12	.20	.23
450	608	.85	.30	.14	.13	.22	.24
450	656	.88	.28	.18	.13	.22	.24
450	728	.85	.31	.16	.13	.24	.26
450	776	.80	.31	.16	.14	.25	.25
450	824	.75	.35	.20	.14	.25	.26
450	896	.80	.30	.20	.14	.25	.26
450	944	.80	.30	.19	.14	.25	.25
450	1004	.85	.30	.20	.14	.25	.26
Before Exposure[a]		.60	.05	.05	.07	.12	.14
After Exposure[a]		.90	.25	.15	.10	.21	.23
534	0	-	-	-	-	.11	-
534	0	.60	.03	.05	.08	.11	.12
534	12	.55	.20	.08	.09	.16	.16
534	60	.55	.27	.10	.12	.20	.20
534	140	.55	.28	.13	.16	.21	.22
534	181	.55	.27	.15	.17	.22	.23
534	256	.55	.25	.20	.16	.23	.24
534	304	.55	.25	.20	.18	.23	.24
534	356	.50	.25	.20	.18	.23	.24
534	404	.50	.25	.23	.19	.24	.25
534	426	.55	.26	.22	.19	.24	.25
534	502	.55	.26	.23	.19	.24	.25
Before Exposure[a]		.64	.05	.05	.07	.13	.14
After Exposure[a]		.70	.28	.19	.16	.25	.26

[a] Values deduced from spectral reflectance data.

Degrading Source: 2x10-7 to 4x10-7 m Xenon Lamp, 1 Sun level.
Method of obtaining data: Calorimetric in situ absorptance. Chamber pressure: 1.33x10-5 Pa.
From Cunnington, Grammer & Smith (1969).

COATINGS

Solar Reflectors

Table 1-4

Ultra-Violet Radiation Effects on Solar Absorptance of Zinc Oxide-Potassium Silicate Paint

T [K]	Intensity Suns	Exp. Time ESH	$\Delta\alpha_s$	Comments
258-280		0	.003	Calculated from sample temperature; flight data of Lunar Orbiter I. Data from smooth curve.
		310	.022	
		444	.029	
		661	.038	
		881	.047	
		1194	.058	
		1629	.071	
		1995	.081	
278	3.9	1020	.010	Sample No. 1 of Table 1-2
279	10	2160	.006	Sample No. 3
279	10	2160	.006	Sample No. 4
279	10	2160	.004	Sample No. 5
279	4.8	300	.003	Sample No. 6
279	6.1	4500	.024	Sample No. 7
279	5.8	7900	.049	Sample No. 8
279	4.8	300	.005	Sample No. 10
279	6.1	4500	.026	Sample No. 12
279	5.8	7900	.053	Sample No. 14
279	4.8	300	.005	Sample No. 15
279	6.1	4500	.024	Sample No. 16
279	5.8	7900	-.004	Sample No. 17
293	11.7	1000	.006	Sample No. 32
298		800	.010	UV from a G.E.AH-6 lamp in vacuum. Absorptance calculated from reflectance measured in situ.
~298	6	100	.000	UV from a AH-6 lamp in vacuum; property measured in situ. Data from smooth curve.
		500	.005	
		1000	.009	
		3000	.019	
~298	1	100	.083	UV from Xenon lamp in vacuum at 460 K, property measured in situ. Data from smooth curve.
		500	.129	
		1000	.152	
		1800	.155	
~298	1	100	.000	UV from Xenon lamp in vacuum; property measured in situ. Data from smooth curve.
		500	.012	
		1000	.024	
		2100	.041	
unknown		100	.010	Calculated from flight data of Mariner IV.
		500	.046	
		650	.050	
		1000	.068	
		2650	.118	
unknown		.46	.002	Calculated from temperature of substrate from flight data of OSO III.
		1.1	-.001	
		3.9	-.004	
		4.0	-.001	
		4.3	-.001	
		4.9	-.001	
		5.2	.002	
		7.1	-.003	
		7.4	.001	
		7.7	-.001	
		8.1	.000	
		8.5	-.004	

(Continued onto next page)

COATINGS

Solar Reflectors

Table 1-4 (Continued)

Ultra-Violet Radiation Effects on Solar Absorptance of Zinc Oxide-Potassium Silicate Paint

T [K]	Intensity Suns	Exp. Time ESH	$\Delta\alpha_s$	Comments
unknown		8.7	.001	Calculated from temperature of substrate from flight data of OSO III.
		721	-.004	
		717	.000	
		727	.002	
		751	.000	
		1336	-.004	
		1336	-.001	
		1336	.000	
		1336	.003	
		1513	.005	
		1577	.002	
		1577	.003	
		1577	.005	
unknown		.1	.000	Calculated from temperature of substrate from flight data of Pegasus II. Data from smooth curve.
		1.0	.000	
		10	.000	
		100	.000	
		1000	.000	
		2500	.000	
unknown		.1	.000	Calculated from temperature of substrate from flight data of OSO III. Data from smooth curve.
		1.0	.000	
		10	.000	
		100	.000	
		1000	.000	
		2500	.000	

From Touloukian, DeWitt & Hernicz (1972).

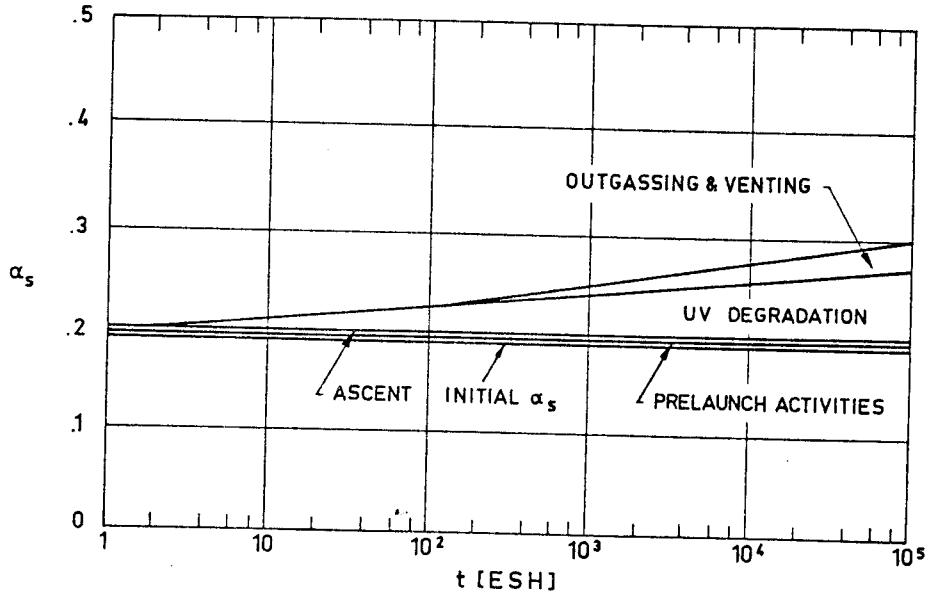

Fig 1-6. Estimated changes in the solar absorptance, α_s, of Z-93 during the total mission profile for a near-Earth orbit. From McCargo, Spradley, Greenberg & McDonald (1971).

COATINGS

Solar Reflectors

7.3.2.5.3. Protons only exposure. The available data are given in the following table.

Radiation Exposure		α_{so}	$\Delta\alpha_s$	Comments
Intensity [keV]	Integrated Flux [protons.m^{-2}]	Initial		
150	1×10^{18}	.17	.02	
20	1×10^{20}	.17	.13	
2	5×10^{20}		.26	Protons in situ
1	4.2×10^{21}	.15	.35	Solar wind protons
1	1.9×10^{22}	.15	.67	Solar wind protons

From Rittenhouse & Singletary (1969).

7.3.2.5.4. Electrons only exposure.

Radiation Exposure		α_{so}	$\Delta\alpha_s$	Comments
Intensity [keV]	Integrated Flux [electrons.m^{-2}]	Initial		
2×10^{3}	1×10^{20}	.17	.03	

From Rittenhouse & Singletary (1969).

7.3.2.5.6. Combined exposure.

Near UV ESH	Lyman ESH	Protons		T [K]	α_{so} Initial	$\Delta\alpha_s$
		[keV]	[protons.m^{-2}]			
375-450	750	10	1.4×10^{19}	304	.139	.019
375-450	750	-	-	304	.139	.004
-	-	-	-	304	.139	.002
375-450	750	10	1×10^{19}	301	.143	.023
375-450	750	-	-	301	.144	.005
-	-	10	1×10^{19}	290	.147	.020
-	-	10	1×10^{19}	291	.142	.026
750	750	10	2×10^{19}	300	.145	.030
750	750	-	-	300	.145	.007
-	-	-	-	300	.148	.001
750	750	10	2×10^{19}	304	.144	.035
750	750	-	-	304	.146	.014
750	750	10	2×10^{19}	295	.144	.029
750	750	-	-	295	.144	.011

From Stevens (1971).

Rev. 1. 1981

COATINGS

Solar Reflectors

7.3.2.6. Effects of the Space Environment on solar absorptance to emittance ratio.

T [K]	ESH	α_s/ε	Comments
∿298	1160	.183	Data taken from flight of Pegasus II. Values deduced from the temperature of the substrate.
	1169	.226	
	1178	.199	
	1198	.231	
	1258	.212	
	1291	.240	
	1308	.208	
	1537	.259	
	2048	.188	
	2070	.200	
	2089	.221	
	2100	.200	
	2110	.173	
	2133	.254	
	2141	.282	
	2243	.245	
	2246	.229	
	2260	.243	
	2291	.173	
	2300	.234	
	2300	.279	
	2423	.173	
	2431	.240	
	2431	.270	
	2442	.216	
258-280	0	.185	Data taken from flight of Lunar Orbiter V. Values deduced from the temperature of the substrate. Data stracted from smooth curve.
	54	.226	
	120	.251	
	214	.285	
	346	.309	
	783	.336	
	2038	.416	

From Touloukian, DeWitt & Hernicz (1972).

COATINGS

Solar Reflectors

7.3.3. Reflectance.

7.3.3.1. Normal-hemispherical spectral reflectance: Fig 1-7.

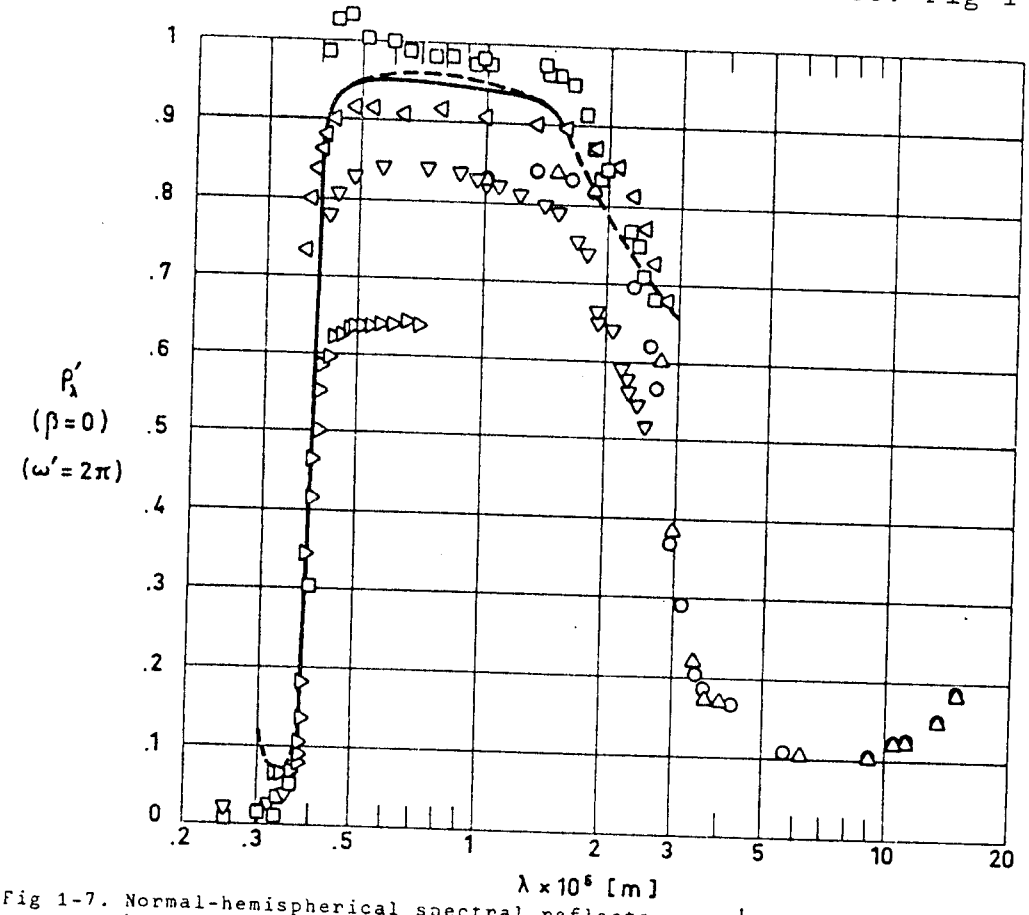

Fig 1-7. Normal-hemispherical spectral reflectance, ρ'_λ, of Z-93 vs. wavelength, λ. All data are from Touloukian, DeWitt & Hernicz (1972) except ——— and – – – – which are from Cunnington, Grammer & Smith (1969).

Explanation

Key	Description	Comments
○	Sprayed onto a 1.27×10^{-3} m thick aluminium substrate.	T∿300 K. Measured in vacuum (1.33×10^{-4} Pa). Data from smooth curve.
□	Sprayed on an aluminium substrate.	T∿298 K. Measured relative to MgO. Data from smooth curve.
△	Same as □.	Same as □. Not referenced to MgO.
▽		T∿298 K. Data from smooth curve.
▷		T∿298 K. Measured in vacuum. Data from smooth curve.
◁		T∿298 K. Exposed to vacuum. Measured in situ.
———	Applied to disc substrates of 6061-T6 aluminium. The discs, 2.54×10^{-2} m diameter by 1.27×10^{-3} m thick, were polished on one side and edge. The surface to be coated was machined to a $(30\pm3)\times10^{-6}$ m RMS finish.	T∿298 K. Measured in vacuum (1.33×10^{-5} Pa) by using an integrating sphere attached to a Cary Model 14 spectrophotometer. Reported error 2%.
– – –	Same as ———.	Same as ——— except measured using a Gier-Dunkle reflectometer. Reported error ±1%.

Rev. 1. 1981

COATINGS

Solar Reflectors

7.3.3.2. Effects of the Space Environment on reflectance.

7.3.3.2.1. Ultra-Violet Radiation: Fig 1-8.

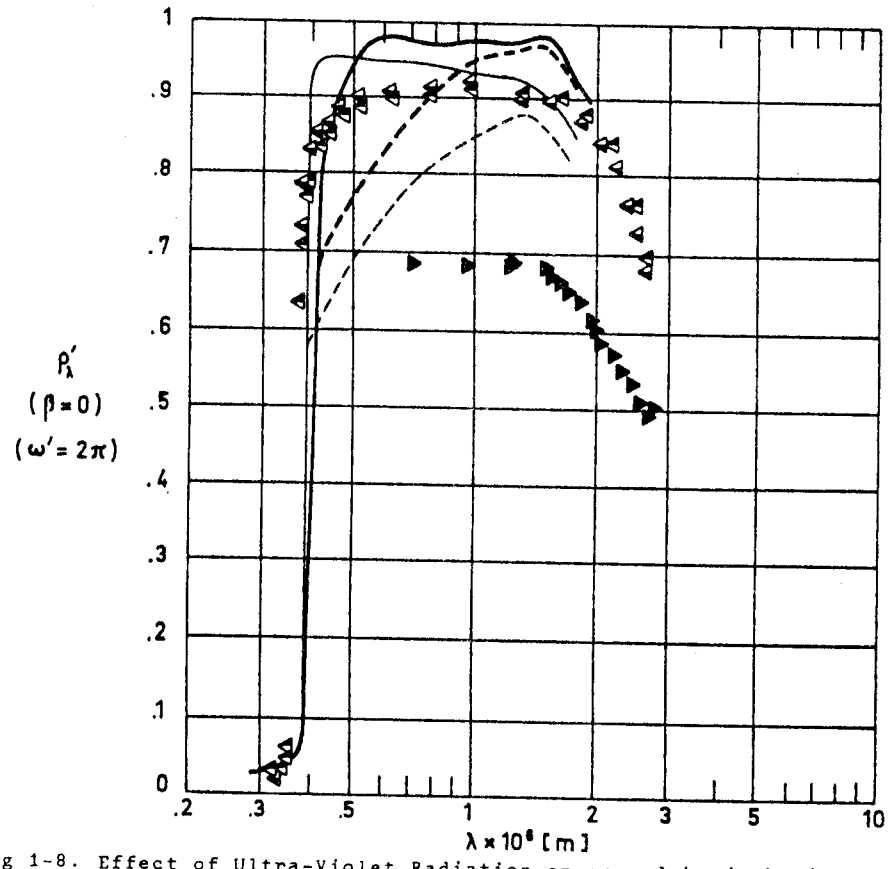

Fig 1-8. Effect of Ultra-Violet Radiation on normal-hemispherical spectral reflectance, ρ'_λ, of Z-93 vs. wavelength, λ. Data points are from Touloukian, DeWitt & Hernicz (1972), while smooth curves are from Cunnington, Grammer & Smith (1969).

Explanation

Key	Description	Comments
▶		T∿298 K. Exposed in vacuum to 200 ESH. Measured in situ. Data from smooth curve.
◀		T∿298 K. Exposed to UV radiation (from a GE AH-6 lamp) in vacuum. ESH 800. Measured in situ.
◁		Same as ◀ except measured in air after UV exposure.
———	Applied to disc substrates of 6061--T6 Aluminium. The discs, 2.54×10^{-2} m diameter by 1.27×10^{-3} m thick, were polished on one side and edge. The surface to be coated was machined to a $(30\pm3)\times10^{-6}$ m RMS finish.	T∿422 K. Measured in vacuum (1.33×10^{-5} Pa) by using an integrating sphere attached to a Cary Model 14 spectrophotometer. Reported error 2% (Calibrations made using a Gier--Dunkle reflectometer).
- - -	Same as ———.	Same as ——— except exposed to UV radiation (from a 900 W Hanovia xenon lamp, 1 Sun level). ESH 10014.
——	Same as ———.	Same as ——— except T∿534 K.
— —	Same as ———.	Same as ——— except exposed to UV radiation (from a 900 W Hanovia xenon lamp, 1 Sun level). ESH 502.

COATINGS

Solar Reflectors

7.3.3.2.3. Protons only exposure: Fig 1-9.

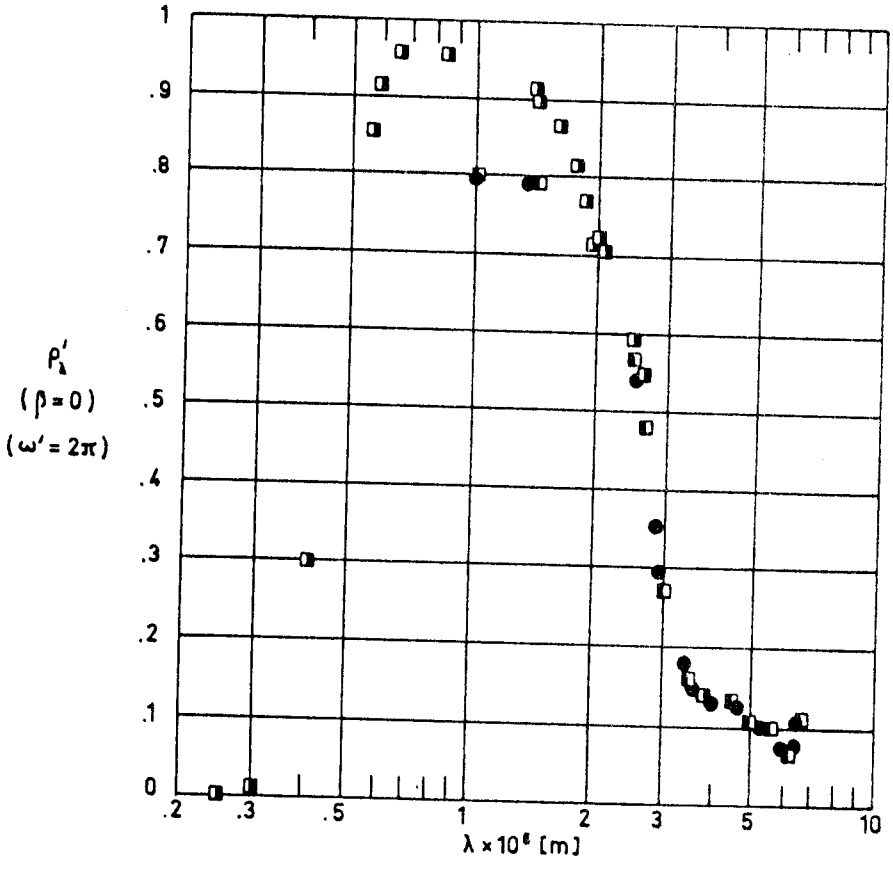

Fig 1-9. Effect of Protons Radiation on normal-hemispherical spectral reflectance, ρ'_λ, of Z-93 vs. wavelength, λ. From Touloukian, DeWitt & Hernicz (1972).

Explanation

Key	Description	Comments
●	Sprayed onto a 1.27×10^{-3} m thick aluminium substrate.	T∿298 K. Exposed to 10^{20} p.m^{-2}.
◘	Sprayed on an aluminium substrate.	T∿298 K. Irradiated in vacuum at 300 K with 7.7×10^3 eV protons to a total dose of 10^{20} p.m^{-2}. Measured in vacuum (1.33×10^{-4} Pa). Measured relative to MgO. Data from smooth curve.
◘	Same as ◘.	Same as ◘ except not referenced to MgO.

Rev. 1. 1981

COATINGS

Solar Reflectors

8. ENVIRONMENTAL BEHAVIOR

8.1. Prelaunch. The coating is brittle, hard to apply and maintain (Scollon & Carpitella (1970)).

8.2. Postlaunch. Blistering during ascent heating can be avoided by curing appropriately the paint (Stevens (1971)).

8.2.1. Ascent. Ascent heating histories with peak temperatures below 645 K do not cause increase in α_s and ε (Rittenhouse & Singletary (1969)).

8.2.2. Orbital. The primary source of degradation appears to be the near ultraviolet portion of incident solar and albedo radiation.

The presence of impurities can greatly decrease the stability to the space environment of this coating (Cunnington, Grammer & Smith (1969)).

9. THERMAL CYCLING

The maximum and minimum temperatures at which the paint has been tested without major changes in properties were:

Tmin = 211 K
Tmax = 366 K

(Rittenhouse & Singletary (1969)).

10. SOURCE

IIT Research Institute. 10 West 35 Street, Chicago, Illinois 60616.

11. COST

Pigment: 165 US $.kg^{-1} (Minimum order 2 lb).

Potassium Silicate: 22 US $.kg^{-1}.

COATINGS

Solar Reflectors

These prices are FOB Chicago. 35 US $ per shipment for prepaid should be added.

Effective July 1, 1974

(IITRI 1974).

12. PAST SPATIAL USE

This coating has been widely tested and used in spacecraft. The table below gives several precedents.

Spacecraft	Launching Date	Used or Tested	References
Mariner IV	Nov. 28, 1964	Tested	Lewis & Thostesen (1965).
Pegasus II	May 25, 1965	Tested	Schafer & Bannister (1967).
Pegasus III	July 30, 1965		
Lunar Orbiter V	Aug. 1, 1967	Tested	Caldwell y Nelson (1968).
SERT II (Space Electric Rocket Test)	Feb. 3, 1970	Used	Stevens (1971), Stevens & Smolak (1971).
OSO III (Orbiting Solar Observatory)	March 8, 1967	Tested	Millard & Pearson (1973).

COATINGS

Solar Reflectors

1.2.3. ZINC ORTHOTITANATE - POTASSIUM SILICATE

1. COMPOSITION

Pigment: IIT Research Institute, Zn_2TiO_4.

Binder: GTE Sylvania Incorporated, PS7 potassium silicate.

Distilled water.

From Harada & Wilkes (1979).

Details on pigment preparation are given overleaf. These details, which are not very relevant to the user of the coating, could be essential to the proper understanding of this data item.

2. FORMULATION

As given in the following table. PBR is the pigment to binder ratio by weight.

PBR	Components		
	Zn_2TiO_4 [kg]	PS7 [m^3]	H_2O [m^3]
4.3	.1	50×10^{-6}	30×10^{-6}
5.3	.1	40×10^{-6}	35×10^{-6}
6.1	.1	35×10^{-6}	40×10^{-6}
7.1	.1	30×10^{-6}	45×10^{-6}
8.5	.1	25×10^{-6}	50×10^{-6}
10.6	.1	20×10^{-6}	55×10^{-6}

From Harada & Wilkes (1979).

High PBR values provide both higher reflectance and greater stability.

COATINGS

Solar Reflectors

PREPARATION OF THE PIGMENT

Three processes have been considered at IITRI for the synthesis of Zn_2TiO_4. All of them involve calcination and reaction of zinc and titanium precursors.

Solid State Reaction (SSR)

New Jersey Zinc Co., SP500 zinc oxide, ZnO, and E.I. DuPont de Nemours Co., R900 anatase, TiO_2, are grinded and mixed at low temperature for a total of 4 h of wet grinding and .5 h of dry grinding. The aim of these grinding and mixing operations is to assure good particle to particle contact, and hence, reactivity of the two oxides.

Zn_2TiO_4 pigment is formed by firing at 1 200 K for 18 h, additional 12 h to 24 h of grinding followed by reactive encapsulation and/or induction plasma calcining to obtain a stable product.

Reactive encapsulation aims at stabilizing pigments against ultra-violet space damage. Encapsulating a pigment also avoids the possibility of a radiation-induced change in surface state. A number of reactive encapsulants can be used as, sodium acid phosphate, potassium hexafluorosilicate, ferro-ferricyanide, PS7 potassium silicate,... The last is the most widely used.

Plasma heat treatment basically consists in passing an Ar/O_2 aerosol of the pigment through a plasma reactor with temperature jumps across the boundary layer close to 2 000 K. This annealing of the reactively encapsulated pigment results in enhanced ultra-violet behavior of both pigment alone and coating.

The solid state reaction process is time consuming, presents the danger of introducing degradable contaminants and does not allow an appropriate control of the pigment size. Because of these limitations, studies on the use of salt precursors for Zn and Ti were conducted in order to improve the pigment.

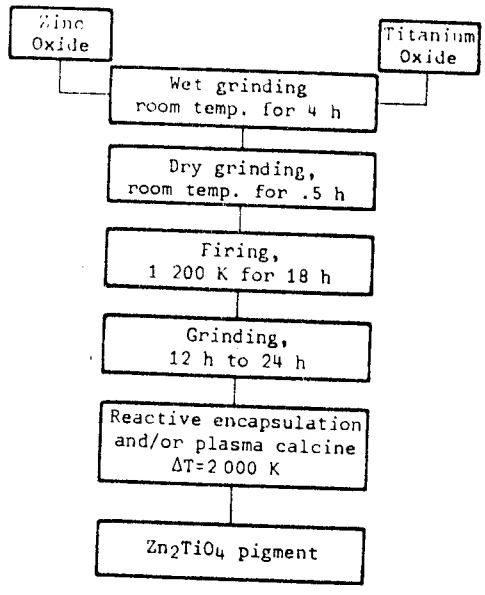

Coprecipitation (COP)

A mixed solution of zinc and titanium chlorides is added to a solution of oxalic acid. The resulting solution is then heated to 873 K and held at this temperature during 2 h, being continuously stirred while the Zn_2TiO_4 precipitate is formed.

Calcination and firing at 1 473 K are performed in standard atmospheric Globar furnaces (bonded silicon carbide resistance elements).

No grinding is required for obtaining pigment particles amenable to incorporation to a paint. Ultra-violet irradiation in vacuum of these powders resulted in minimal change in reflectance after 1 000 ESH, although damage resulted when the powders, incorporated in a silicone binder, were irradiated as coating. The particles showed a tendency toward agglomeration which can be avoided by use of the third process, below.

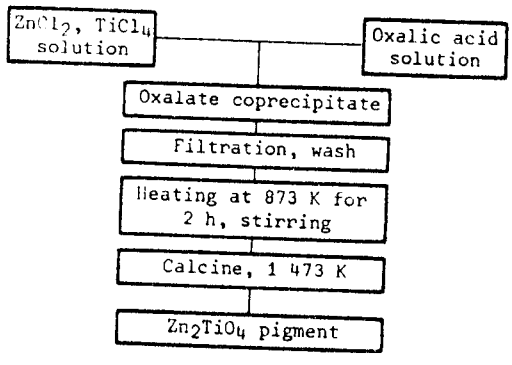

Mixed Oxalate Process (MOX)

Zinc and titanium oxalates are produced from the corresponding chlorides through two independent steps which can be separately established and controlled to produce an optimum precipitated product.

The resulting titanium and zinc oxalates are mixed and ball milled for 4 h, pre-calcined at 873 K for 2 h and, finally, calcined at 1 173 K for 4 h.

Fine particle size zinc orthotitanate is achieved using very fine precursors.

The product obtained by this method can be utilized as a pigment with no grinding.

This is the most current state of the art pigment preparation process. Most of the information given below refers to a coating based on MOX prepared pigment.

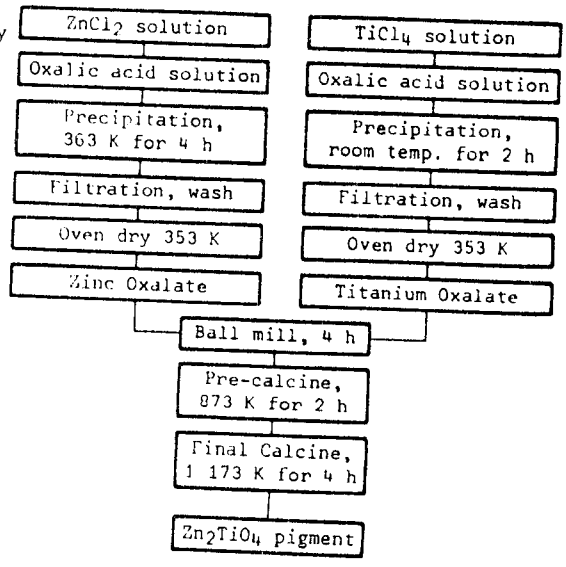

References: Zerlaut, Gilligan & Ashford (1972), Gilligan & Zerlaut (1973), Gilligan, Harada & Gates (1974), Harada & Wilkes (1979).

COATINGS

Solar Reflectors

3. USUAL DESIGNATION

Zinc Orthotitanate (ZOT). IIT Research Institute.

Coating corresponding to PBR=7.1, which is the most current, is known as YB-71 (Harada (1981)).

4. SUBSTRATE

Most surfaces (IITRI (1974)).

5. METHOD OF APPLICATION

5.1. Preparation of paint for application. The components are mixed in a porcelain ball mill with porcelain balls for 4 h.

5.2. Preparation of surfaces for painting. The surface should be chemically etched or abraded and then cleaned with an alkaline detergent and rinsed with distilled water.
The complete surface must be water-break free after the abrasion and cleaning process. By observing the above practices, excellent adhesion on metal surfaces is achieved.

5.3. Application of paint. By spray-painting, using standard paint spray guns. The coating is applied as a continuous, wet film. This film is permitted to dry until the gloss has almost disappeared and then the next coat is sprayed on. The process is repeated until the desired thickness is achieved.

5.4. Coating thickness. A thickness of .004" to .006" (10^{-4} m to 1.5×10^{-4} m) is recommended by the supplier (IITRI (1974), which concerns a silicone binded coating). Minimum solar absorptance is achieved with a coating thickness close to .010" (2.5×10^{-4} m), Fig 1-11.

COATINGS

Solar Reflectors

5.5. Curing process. According to Harada & Wilkes (1979) the YB-71 coating can be air-dried, or can be baked at 390 K for complete water removal.

The curing process indicated in IITRI (1974), also given in Gilligan, Harada & Gates (1974), is for a silicone binded coating.

6. SOLVENTS RESISTANCE

Not attacked by the solvents.

7. PHYSICAL PROPERTIES

7.1. Density. 2 460 $kg.m^{-3}$ for the YB-71 formulation. This value has been deduced by Harada & Wilkes (1979) from a plot of coating mass vs. coating thickness for several samples.

7.2. Outgassing. No data available. Water is the only volatile component of these inorganic coatings.

7.3. Thermal radiation properties. The optical properties of these coatings depend upon pigment purity, stoichiometry, particle size and ZnO content. Stability also relates to the last three mentioned variables. In addition, the influence of the binder on the ultra-violet damage of the coating has been noted by Zerlaut, Gilligan & Ashford (1972), Gilligan & Zerlaut (1973), and Gilligan, Harada & Gates (1974). Since these coatings are evolving from many years of research effort and apparently conflicting data have been reported, emphasis should be placed on the correct identification of both pigment preparation process and binder used. Table 1-5 has been devised to this aim.

COATINGS

Solar Reflectors

Table 1-5

Literature Search for Thermal Radiation Properties of ZOT Coatings

Reference	Pigment		Binder	Available Data	Data in this Item
	Process	Encapsulation			
Zerlaut, Gilligan & Harada (1964) quoted by Touloukian, DeWitt & Hernicz (1972).	Solid State Reaction (SSR).	Not given. Pigment calcined at 973 K for 16 h.	PS7 Potassium Silicate. Silvania, Inc.	α_s and $\Delta\alpha_s$ after 690 ESH, UV radiation.	Tables 1-6 and 1-7.
		Not given.		α_s.	
		Not given. Pigment calcined at 973 K for 4 h.		α_s and $\Delta\alpha_s$ after 170 ESH, UV radiation.	
		Not given.			
Zerlaut, Noble & Rogers (1968).	SSR.	None. Phosphated. Phosphated and recalcined at 925 K for 18 h. None but recalcined at 925 K for 18 h.	OI-650 Polymonomethyl-siloxane, Owens Illinois, Inc.	α_s and $\Delta\alpha_s$ after 300, 550, 1 200 ESH, UV radiation and after Air exposure. ρ'_λ vs. λ before and after the above exposures.	Not given.
Gilligan & Zerlaut (1971).	SSR.	None. Plasma calcined.	None.	ρ'_λ vs. λ before and after proton exposure.	Not given.
		Ferro-ferricyanide treated.	OI-650.	ρ'_λ vs. λ before and after the following exposures: proton, UV radiation (600, 1 300 ESH), combined UV and proton (1 300 ESH + 972 EWH) and O_2 bleach. $\Delta\alpha_s$ after the above exposures.	
		Phosphated.	PS7.	ρ'_λ vs. λ before and after 1 300 ESH and O_2 bleach.	Fig 1-14.
				ρ'_λ vs. λ before and after proton exposure.	Fig 1-15.
				$\Delta\alpha_s$ after UV radiation (600, 1 300 ESH), combined UV and proton (1 300 ESH + 972 EWH) and O_2 bleach.	p. 1-41.
Zerlaut, Gilligan & Ashford (1972).	SSR.	Several treatments with soluble alkali salts were tested, among them: Potassium silicate, Lithium silicofluoride, Potassium silicofluoride.	None.	UV effect on ρ'_λ after 970 or 1 010 ESH (depending on the case) at selected values of λ. ρ'_λ vs. λ for the mentioned encapsulants, before and after 970 or 1 010 ESH (depending on the case), UV radiation.	Not given.
		Untreated, plasma calcined (several plasma temperatures).	None.	UV effect on ρ'_λ after 1 010 or 2 500 ESH (depending on the case) at selected values of λ. α_s and $\Delta\alpha_s$ after 1 010 or 2 500 ESH (depending on the case), UV radiation. ρ'_λ vs. λ before and after 2 500 ESH, UV radiation. $\Delta\alpha_s$ after proton exposure.	
		Phosphated and silicated, plasma calcined (several plasma temperatures).	None.	UV effect on ρ'_λ after 2 500 ESH, UV radiation at selected values of λ. α_s and $\Delta\alpha_s$ after 2 500 ESH, UV radiation. ρ'_λ vs. λ before and after 2 500 ESH, UV radiation.	

(Continued onto next page)

COATINGS

Solar Reflectors

Table 1-5 (Continued)

Literature Search for Thermal Radiation Properties of ZOT Coatings

Reference	Pigment		Binder	Available Data	Data in this Item
	Process	Encapsulation			
Zerlaut, Gilligan & Ashford (1972).	Solid State Reaction (SSR).	Potassium silicated. Phosphated. Ferro-ferricyanide treated. Potassium hexafluorosilicate treated.	PS7 Potassium Silicate.	UV effect on ρ'_λ after 1 200, 2 000 or 2 400 ESH (depending on the case) at selected values of λ.	p. 1-43.
				α_s and $\Delta\alpha_s$ after 1 200, 2 000 or 2 400 ESH (depending on the case), UV radiation.	Tables 1-6 and 1-7.
		Potassium hexafluorosilicate treated.	PS7.	ρ'_λ vs. λ before and after 1 200 ESH, UV radiation.	Fig 1-14.
		Phosphated.	PS7.	$\Delta\alpha_s$ after proton exposure.	p. 1-41.
		Untreated. Phosphated and silicated. Ferro-ferricyanide treated. Potassium hexafluorosilicate treated.	OI-650.	UV effect on ρ'_λ after 970, 1 000, 1 200 or 2 000 ESH (depending on the case) at selected values of λ. α_s and $\Delta\alpha_s$ after 1 200 or 2 000 ESH (depending on the case), UV radiation. ρ'_λ vs. λ before and after 970 or 2 000 ESH (depending on the case), UV radiation (Phosphated and Silicated). $\Delta\alpha_s$ after proton exposure (Ferro-ferricyanide treated).	Not given.
		Untreated.	RTV-602 Silicone General Electric Co.		
Triolo (1975).	SSR.	Phosphated (Zerlaut et al. (1972)), plasma calcined.	PS7.	α_s/ε initial and after 20, 780 and 8 225 OSO-H orbits (~8 000 ESH).	p. 1-39.
			OI-650.	ε. α_s initial. $\Delta\alpha_s$ vs. ESH, UV radiation.	Not given.
Triolo Heaney & Hass (1978).	SSR.	Phosphated (Zerlaut et al. (1972)), plasma calcined.	PS7.	α_s/ε initial and after 20, 780 and 8 225 OSO-H orbits (~8 000 ESH).	p. 1-39.
Keyte (1975).	SSR.	Phosphated.	PS7.	ε at room temperature.	Fig 1-10.
				ρ'_λ vs. λ.	Fig 1-13.
				α_s and $\Delta\alpha_s$ after 700 ESH, UV radiation.	Tables 1-6 and 1-7.
				α_s vs. incidence angle, β.	Fig 1-12.
				$\Delta\alpha_s$ after 15 and 330 d, Prospero satellite.	p. 1-40.
Gilligan & Zerlaut (1973).	Coprecipitation (COP).	None.	None.	ρ'_λ vs. λ before and after 1 000 ESH, UV radiation.	Not given.
Gilligan, Harada & Gates (1974).	COP.	None.	None.	ρ'_λ vs. λ before and after 1 650 ESH, UV radiation. O_2 bleach effect also considered.	Not given.
		None.	OI-650.		
		Potassium silicated.	OI-650 G (modified by IITRI).		
Harada & Wilkes (1979).	Mixed Oxalate (MOX).	None.	PS7.	ε vs. T.	Fig 1-10.
				ρ'_λ vs. λ for different values of t_c.	Fig 1-13.
				α_s and $\Delta\alpha_s$ after 1 000 ESH, UV radiation, several PBRs.	Tables 1-6 and 1-7.
				α_s vs. t_c.	Fig 1-11. Fig 1-13 (Caption).

COATINGS

Solar Reflectors

7.3.1. Emittance.

7.3.1.1. Hemispherical total emittance. Fig 1-10.

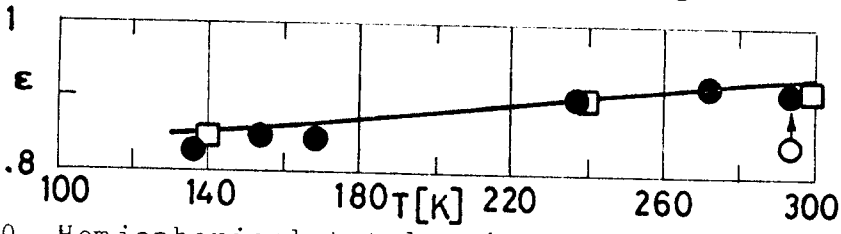

Fig 1-10. Hemispherical total emittance, ε, of Zinc Orthotitanate-Potassium Silicate Coatings vs. temperature, T.
○ SSR pigment, phosphated. From Keyte (1975).
● MOX pigment, YB-71. From Harada & Wilkes (1979).
□ YB-71. AESC. From Ahern & Karperos (1983).

7.3.2. Absorptance.

7.3.2.1. Solar absorptance. Table 1-6. See also p. 1-40.2.

7.3.2.2. Variation of solar absorptance with coating thickness.

Fig 1-11. Differently prepared coatings. Partial removal of ZnO from the pigment decreases α_s.

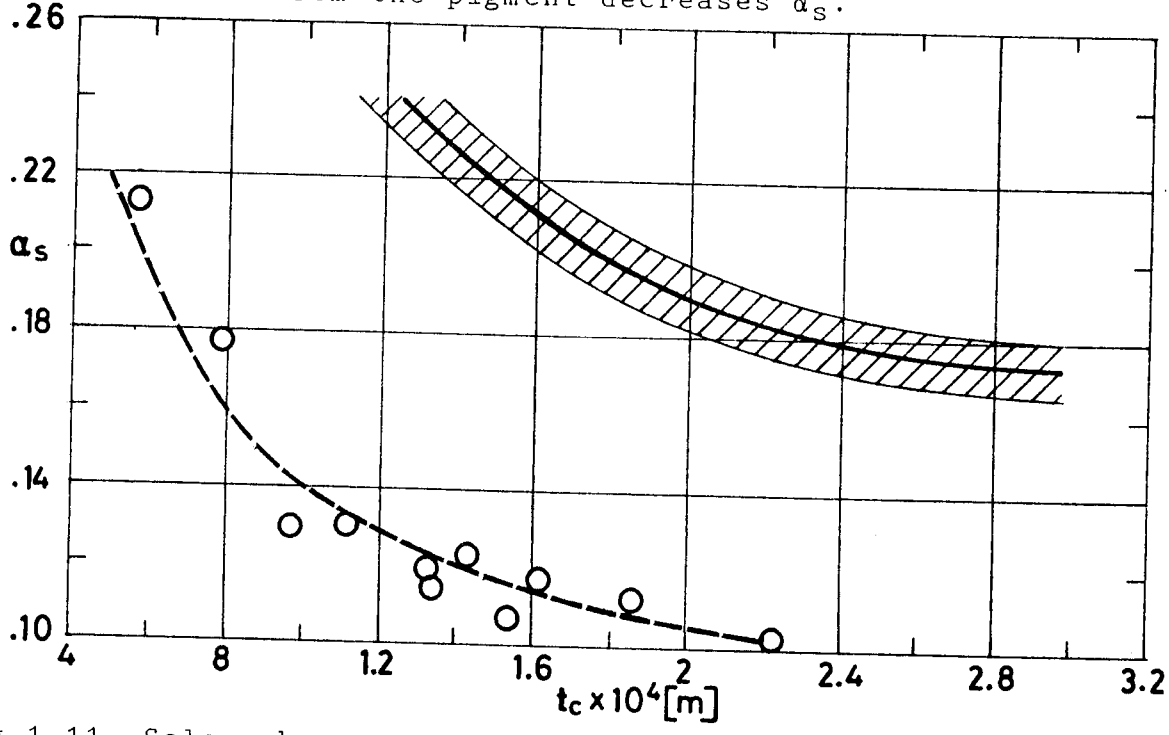

Fig 1-11. Solar absorptance, α_s, of YB-71 vs. thickness, t_c.
○ From Harada & Wilkes (1979).
▨ From measurements on 16 panels by AESC. Scatter is due to t_c variation. From Ahern & Karperos (1983).

COATINGS

Solar Reflectors

Table 1-6

Solar Absorptance of Zinc Orthotitanate-Potassium Silicate Coatings [a]

No.	SAMPLE: PIGMENT: Process	Zn/Ti Stoichiometric Ratio	Encapsulation	Calcination: Temp. [K]	Calcination: Time [h]	PBR	Coating Curing Process	Author's Designation	TEST CONDITIONS	α_s	References
1	Solid State Reaction (SSR).			973	16	4.30	Air dried	Sample No. 7008	T≈298 K β≈0°	.122	Zerlaut, Gilligan & Harada (1964), quoted by Touloukian, DeWitt & Hernicz (1972).
2				773	2			Sample No. 7009		.118	
3				973	4		Air dried	Sample No. H-19-53		.139	
4				773	2					.128	
5			Silicated					Batch No. B-419	$p=1.3\times10^{-4}$-1.3×10^{-5} Pa β=7°	.136	Zerlaut, Gilligan & Ashford (1972). Test Conditions, Zerlaut & Courtney (1967).
6			Phosphated					Batch No. B-421		.122	
7			Ferro-ferricyanide treated.					Batch No. B-424		.154	
8			Potassium hexa-fluorosilicate treated.	773	7			Batch No. B-563		.120	
9			Phosphated					Surface No. 9 white paint B-303	$p=10^5$ Pa β=0°	.109	Keyte (1975).
10	Mixed Oxalate (MOX).	1.95		1 173		4.26				.192	Harada & Wilkes (1979).
11						5.32				.169	
12						7.09				.153	
13				1 323		4.26				.228	
14						5.32				.203	
15						7.09				.205	
16		2.00		1 173		4.26				.190	
17						5.32				.183	
18						7.09				.154	
19				1 323		4.26				.230	
20						5.32				.225	
21						7.09				.198	

[a] Values deduced from spectral reflectance data.

COATINGS

Solar Reflectors

7.3.2.3. Variation of solar absorptance with incidence angle.

Fig 1-12. Solar absorptance deduced from spectral reflectance measured in air. Two different sample sizes were used to assure full sample illumination at all incidence angles. Thence, a discontinuity appears in the curve plotted in Fig 1-12 at $\beta=60°$.

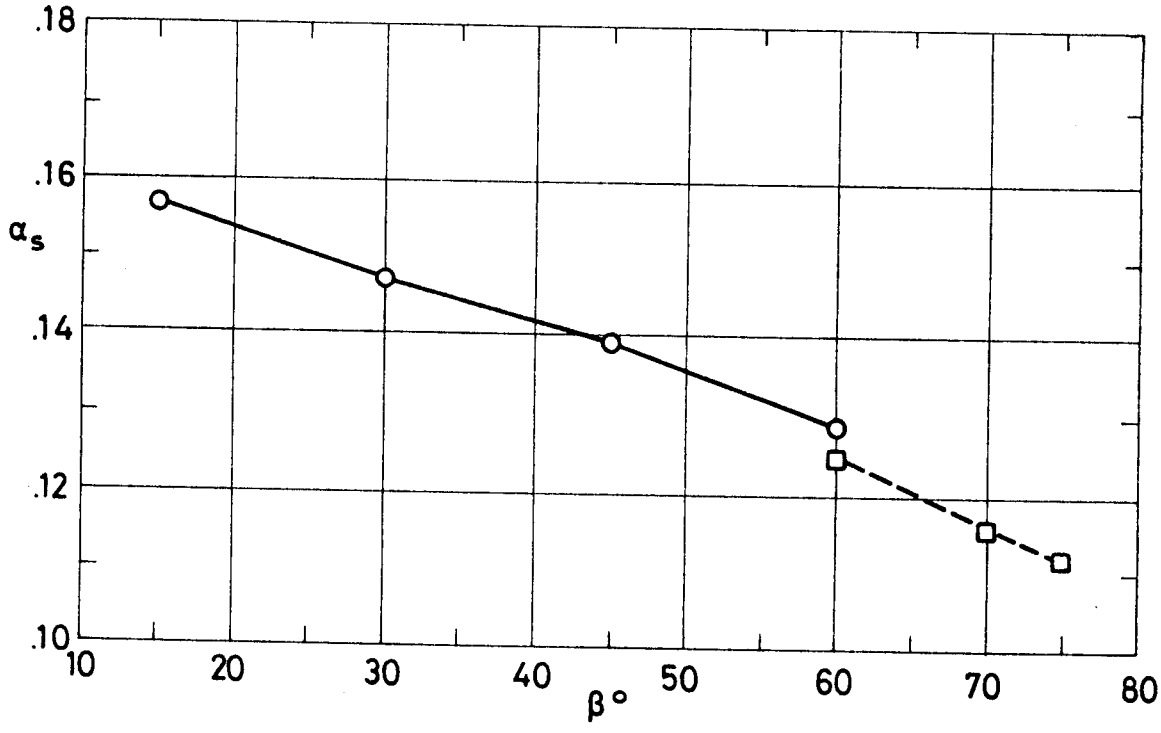

Fig 1-12. Solar absorptance, α_s, of Zinc Orthotitanate-Potassium Silicate coatings vs. incidence angle, β. SSR pigment, phosphated. From Keyte (1975).

7.3.2.5. Effects of the Space Environment on absorptance.

7.3.2.5.1. Ultra-Violet Radiation. Table 1-7.

Low-orbit (UV-only environment) data appear in pp. 1-39 and 1-40. UV, protons and electrons are present in geosynchronous orbit (pp. 1-76 or 1-135). See pp. 1-40.1 and 1-40.2 for several experiments.

COATINGS

Solar Reflectors

Table 1-7

Ultra-Violet Radiation Effects on Solar Absorptance of Zinc Orthotitanate-Potassium Silicate Coatings [a]

Sample [b] No.	Exposure Time [ESH]	Test Conditions	$\Delta\alpha_s$	References
1	690	Irradiated in vacuum	.019	Zerlaut, Gilligan & Harada (1964), quoted by Touloukian, DeWitt & Hernicz (1972).
2			.032	
4	170	Irradiated in vacuum (below 1.3×10^{-3} Pa). Intensity 3.5 Suns.	.031	
5	2 400	Irradiated in vacuum (1.3×10^{-4} Pa - 1.3×10^{-5} Pa) with 1 kw General Electric AH-6 Mercury-Argon lamp. Spectral reflectance measured in situ.	.020	Zerlaut, Gilligan & Ashford (1972). Test Conditions, Zerlaut & Courtney (1967).
6	2 000		.010	
7			.011	
8	1 200		.002	
9	700	Irradiated in vacuum (below 1.3×10^{-5} Pa) with 1 kw Thorn Mercury discharge lamp (type LRD 94-0151). Intensity 3.5 Suns. Measured in situ.	.026 to .040	Keyte (1975).
	700+10 min in Air	Same as above except measured after 10 min exposure in Air	.038 to .061	
10	1 000		.006	Harada & Wilkes (1979).
11				
12			.004	
13				
14			.003	
15			.005	
16			.006	
17			.003	
18				
19			.008	
20			.004	
21			.006	

[a] Values deduced from spectral reflectance data.
[b] Sample numbers in this Table correspond to those in Table 1-6.

COATINGS

Solar Reflectors

OSO-H

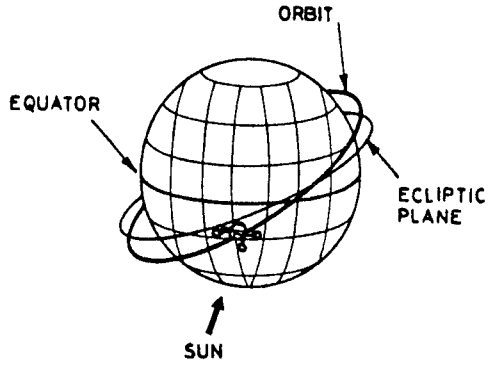

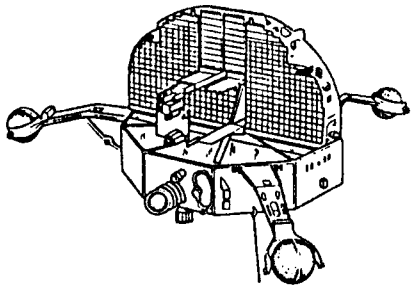

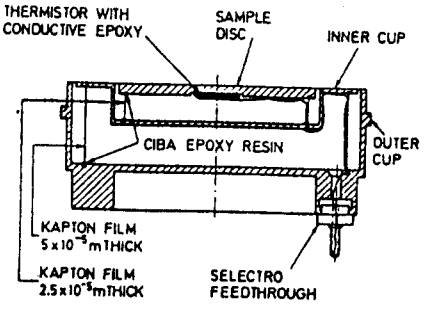

TEST CONDITIONS

Spacecraft & Programme

Orbiting Solar Observatory (OSO-H).
Thermal Control Coating Experiments (TCCE).

Orbit

Launched on September 29, 1971 into a 327 km by 560 km near to Earth elliptical orbit with a 33°inclination angle.

Configuration

OSO satellites have two main parts: a lower section, consisting of a nine-sided wheel, which rotates to provide gyroscopic stabilization, and a stabilized semicircular upper section, or sail, aimed at the Sun.

Thermal Test

Twelve samples (Triolo (1973)) were placed in the Sun-oriented, non-spinning sail. Data up to 8 225 orbits for eight of these samples are given by Triolo, Heaney & Hass (1978).

SAMPLE

Sample Description

SSR- processed Zn_2TiO_4 pigment, plasma calcined. PS7 binder.

Sample Mounting

The sample is mounted on a disc 2×10^{-2} m diameter. The disc is supported by a Kapton film cylinder fastened to both the disc and an inner cup. The thermistor and its leads were attached to the underside of the sample disc with conductive silver epoxy. Another Kapton film cylinder was used for attaching the inner cup to the outer cup. The two Kapton cylinders and the film covering the thermistor network were vapor-aluminized during assembly. Dimpled Mylar sheets were placed inside each cylinder for the reduction of radiative losses.
Holes were cut in the cylinders and the bases of both cups for venting when the assembly is exposed to a vacuum environment.
In order to prevent contamination during cup fabrication, the coating was applied to the cup once assembled.
The aim of the inner cup is to act as a thermal guard for the back of the sample disc and thermistor leads. The inner cup flange has the same area and thermal coating as the sample disc. In addition, the thermal capacity of the disc and the inner cup are made as close as possible, thus the sample disc and the inner cup temperatures are maintained close to each other under both steady and transient conditions.

CALCULATION METHOD

α_S/ε is measured calorimetrically from the disc temperature, T. The terms which appear in the heat balance equation are:
$c(T)dT/dt$, Sensible heat of the sample and substrate. This term disappears since the sample is in thermal equilibrium when readings are taken.
$\varepsilon A\sigma(T_S^4-T^4)$, Radiation to outer space. The hemispherical total emittance of the sample is measured before launch. The equivalent surrounding temperature, T_S, is assumed to be zero.
$\alpha_S AS$, Radiation from the Sun. Recall that the sail, where the coating is located, remains Sun-oriented.
Q, Heat transfer between the back of the sample and the outer cup. Measured before launch.
Albedo and Earth infrared radiations do not appear since reads were only taken at the Earth subsolar points.
α_S/ε is deduced from the resulting simplified equation, assuming that Q/ε is equal to its prelaunch value.

RESULTS

α_S/ε=.17 Measured in the laboratory.
α_S/ε=.21 Deduced from flight data after 20, 780 and 8 225 orbits.

COMMENTS

The first usable data point corresponded to the 20th orbit because of malfunction of the tape recorder.
Data on a "model coating" (Alzak), previously tested both in the laboratory and in orbit, were used to convert from orbital time to ESH. (1.5 orbital hours ≈ 1 ESH. 1 orbit takes 1.5 orbital hours).
The difference between the laboratory and the first in-flight data, (which is common to all the tested coatings) must have been caused by a systematic error in the measurements.

References: Triolo (1973), Triolo, Heaney & Hass (1978).

COATINGS

Solar Reflectors

PROSPERO

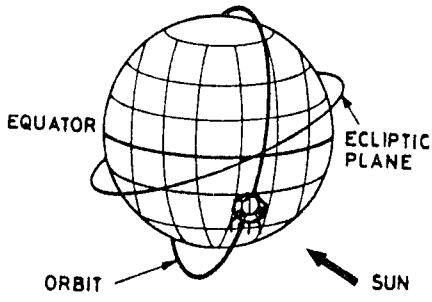

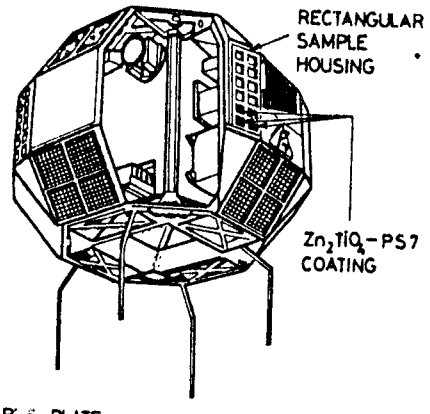

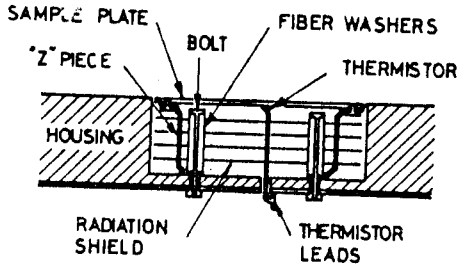

TEST CONDITIONS

Spacecraft & Programme

Prospero.
Thermal Control Surface Experiment (TCSE).

Orbit

Launched by the Black Arrow R3 launch vehicle on October 28, 1971. The initial orbit parameters were: Apogee, 1 580 km; Perigee, 547 km; Inclination, 82.06°; Period, 106.5 min (13.53 orbits per day).

Configuration

Prospero is a 26-faced polyhedron, .71 m height and 1.09 m in equatorial diameter. Mass, 65.8 kg. The satellite is spin stabilized and fitted with nutation dampers. The spin axis-Sun angle at launch was approximately 94°, providing roughly normal incidence of solar radiation on most of the coatings. Initial spin rate was 17.8 $rad.s^{-1}$.

Thermal Test

64 thermal control surfaces were flown, including 7 gold reference surfaces, 6 black gloss reference surfaces and 3 of each of 17 different coatings, among them 9 white paints. Two types of sample housing were used; 4 of rectangular shape each containing 12 samples and mounted in corner fillets parallel to the satellite spin axis, and 4 of triangular geometry, each containing 4 samples and also mounted in corner fillets, but at an angle of about 30° to the spin axis.
The 3 samples of this coating were placed in a rectangular housing.

SAMPLE

Sample Description

SSR-processed Zn_2TiO_4 pigment, phosphated. PS7 binder.

Sample Mounting

The coating was applied on an aluminium clad alloy (L72) substrate, goldized on the edges and on the rear side. The sample plate was mounted in a cup, machined in a magnesium alloy housing, by means of four fiber-glass Z pieces. The cup was goldized on both sides.
4 goldized radiation shields were placed between the substrate and the cup. The shields were mutually separated by small fiber-glass washers, and held in position by four bolts. Slots were cut in the radiation shields for passage of the above mentioned Z pieces.
The temperature was measured by a YSI precision thermistor attached with Araldite in the center of the rear face of the plate.

CALCULATION METHOD

α_s is measured calorimetrically from the temperature, T, of the plate. The terms which appear in the heat balance equation are:
$c(T)dT/dt$, Sensible heat of the sample plate. Since readings were only taken with the surface in thermal equilibrium, this term vanishes.
$\varepsilon A\sigma(T_s^4-T^4)$, Radiation to outer space. ε measured before launch (ε=.91). The equivalent surrounding temperature, T_s, is assumed to be zero. Attempts were made to deduce ε from in-flight measurements during the eclipse part of the orbit. This effort was unsuccessful because of the many parameters involved.
$\alpha_s AS(t)$, Radiation from the Sun. S is the solar flux, a known function of time, t.
$\alpha_s F_a A a S$, Albedo radiation. F_a view factor, a is the mean albedo of the Earth.
$\alpha_s F_{sp} AP$, Earth infrared radiation. F_{sp} is the view factor, and $F_{sp}P$ the flux of energy on the sample.
The last two terms were deduced from assumed values of α_s and ε for a reference surface (gold), using the balance equations for both the eclipse and the sunlit parts of the orbit.
$Q(T,T_c)$, Thermal coupling between the plate, at temperature T, and housing, at temperature T_c. Three methods for calculating Q were explored, none of them was completely successful. These methods were:
1) Calibration in a solar simulation vacuum chamber. Attempts to remove the many sources of error failed.
2) Thermal modelling of the sensor-housing assembly by a six-node network. Heat input was that on an orbiting-spinning plate. Temperatures for given α_s and ε were compared with in-flight data. Correlation was poor.
3) Calculation from in-flight data. ε was fixed for 4 samples. Only eclipse temperatures were used. Data of Q vs. $T-T_c$ were arranged as $Q=k+w_1(T-T_c)+w_2(T-T_c)^2$ and values of k, w_1 and w_2 for an average housing, as well as values of c(T) for each sample were deduced. The results for the 4 samples were fair, although discrepancies appeared.
Finally, a "best estimate" of Q vs. $T-T_c$ was made by a critical analysis of the above methods.

RESULTS

α_s=.109, measured in the laboratory. α_s=.110, after 15 days in orbit. α_s=.141, after 330 days in orbit.

COMMENTS

Owing to the design of the sample mounting, Q was 10 times too large for reaching sufficient sensitivity.

References: Adams (1973), Keyte (1975).

Rev. 3. 1986

COATINGS

Solar Reflectors

SPACECRAFT IN GEOSYNCHRONOUS ORBIT

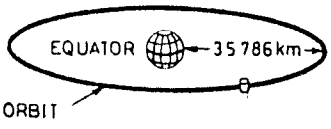

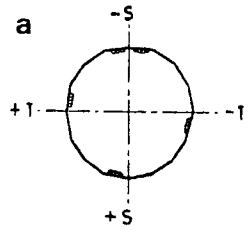

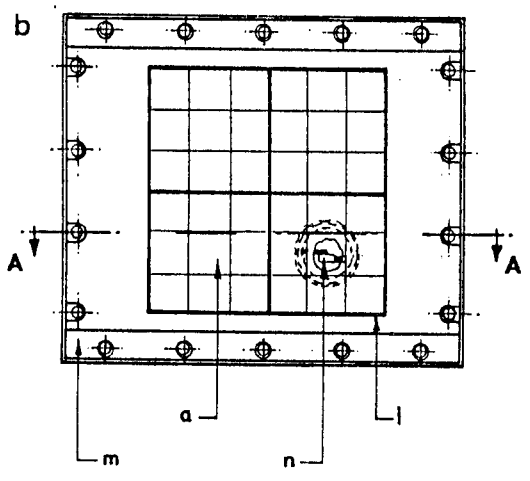

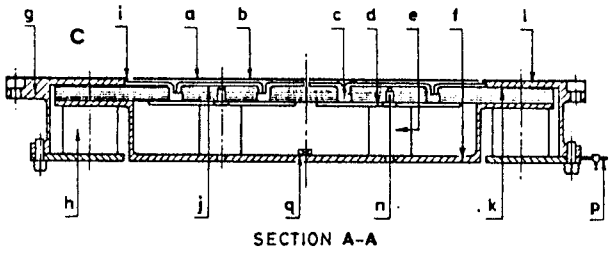

SECTION A-A

TEST CONDITIONS

Spacecraft & Programme
Different spacecraft in similar orbits.

Orbit
Geosynchronous.

Configuration
No data are given except that the calorimeters holding the samples were all installed in the same clean location (-T axis in the enclosed figure a) on several spacecraft. The calorimeter locations were so chosen as to minimize radiant heat exchange with spacecraft external surfaces. They were mounted in one of the main radiators of the satellite.

Thermal Test
Two set of data from calorimetric tests have been issued, Curran & Millard (1978), Ahern § Karperos (1983). The last set includes, among others, five ZOT coating samples of various thicknesses on different substrates. Calorimeter sample areas were 76×10^{-3} m by 76×10^{-3} m. See figure b.

SAMPLE

Sample Description
YB-71. Coating characteristics are given in the following Table.

Sample Designation	Thickness $t_c \times 10^4$ [m]	Substrate
9	2.03 - 2.54	Al alloy 6061-T6
10		
14	2.54 - 3.05	
18		
20		Mg alloy AZ31B

Sample Mounting (figures b and c)
Each sample (a) is bonded to a magnesium mounting platform (b) bonded to a series of thin-walled (10^{-4} m to 1.5×10^{-4} m) fiber-glass support cylinders for improved thermal isolation. Shown in the figure are, upper cylinders (c), discs (d) and lower cylinders (e). The lower cylinders are mounted to a magnesium housing (f). The housing is attached to the radiator mounting frame (g) (and thermally isolated from it) by fiber-glass support cylinders (h). All of the fiber-glass support cylinders and discs along with the housing are coated on both sides with vacuum-deposited aluminium ($\varepsilon < .1$) to minimize radiation heat transfer between surfaces. Silvered teflon gap seals (i) close the space between samples so that solar energy cannot reach the housing enclosure. An MLI (j) is held in place between the support discs and the corresponding mounting platform to minimize heat transfer between samples and the housing enclosure. This MLI (see J, § 3.10) is composed of several aluminized mylar sheets and has an aluminized side facing the housing enclosure. The MLI also extends outwards (k) and insulates the housing from the mounting frame, where it overlaps the housing adjacent to the samples. The top of the mounting frame in this overlapping region is covered with SSMs (see H, § 1.2.6 and 1.2.7) to minimize heat absorption adjacent to the samples ((l) in the figure). A strip of silvered teflon (m) serves the same purpose where the mounting frame bolts to the radiator.
Attached beneath each sample mounting platform is a thermal sensor (n), the leads of which travel through the fiber-glass cylinders to the terminal board (p). An additional thermal sensor (q) is mounted on the inside housing baseplate to provide data for the heat leak calculations of each individual sample.

CALCULATION METHOD

One of the main aims of the configuration design was simplicity of the computer thermal model.
Basically the sample temperature provides α/ε, where ε, although temperature dependent (Fig 1-10), does not change with time. A typical thermal network for one specimen is shown in the enclosed figure (next page).
For the nodes corresponding to external spacecraft surfaces viewing the sample, an AESC-developed Monte Carlo view factor programme was used. The temperatures of these external surfaces were supplied to the programme.

COATINGS

Solar Reflectors

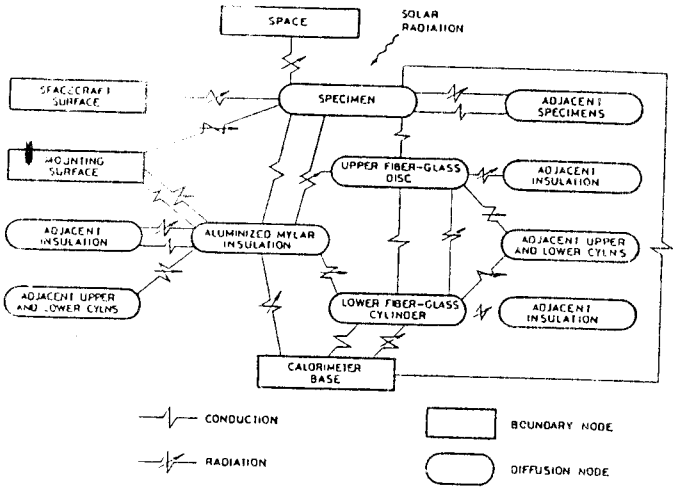

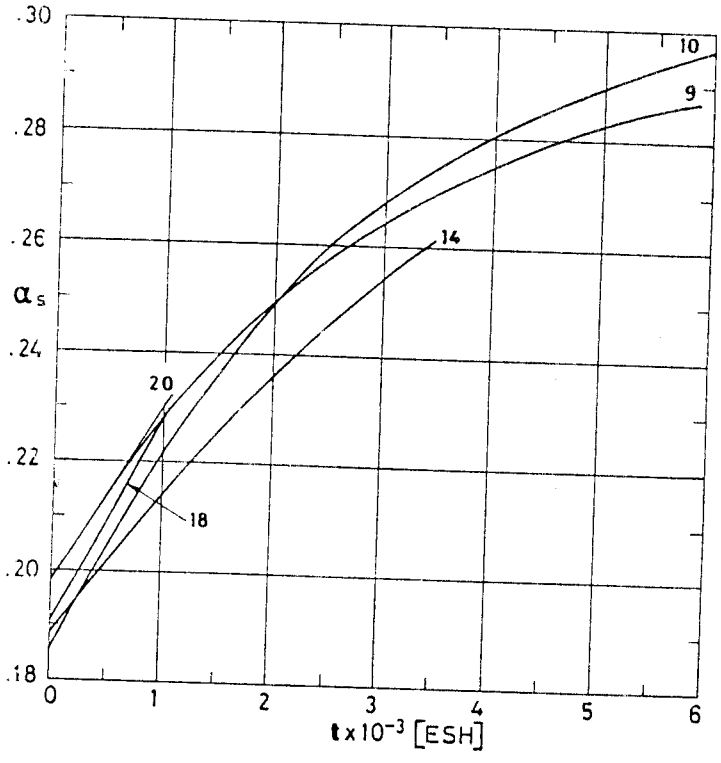

Fig 1-12.1. Solar absorptance, α_s, of several YB-71 coatings vs. exposure time, t, as deduced from data of various spacecraft in geosynchronous orbits. Numbers correspond to sample designations.

Solar heating of the sample was introduced in the computer model through a diurnal table automatically adjusted for solar angle and heat flux. The diurnal temperatures for the radiating spacecraft nodes (available at 15 min intervals) and the calorimeter base temperature, were introduced into the programme. Temperatures are then calculated on the basis of an assumed α_s value (normally the previous one). The computer then adjusts α_s and iterates until the calculated temperatures match the flight data within 1° F (.56 K) thus giving the α_s for the day. The analysis was repeated at varying intervals which generally were determined by the temperature rise rate. Usually large rises followed a roll-off trend and, thence, early data were obtained at time intervals of the order of one month, whereas at three years in orbit data were taken at approximately 3 months interval.
The measurements of the absolute solar absorptance involves the full calorimeter design errors, the thermal sensor calibration error and the telemetry quantization error. The estimated error in α_s is + .009, - .006.

RESULTS

Laboratory α_s data have been compared to initial flight measurements in the following Table. Laboratory measured hemispherical total emittance at 295 K was ε = .91 in any case (see also Fig 1-10).

Sample	Laboratory α_s	Flight α_s
9	.194	.197
10	.181	.185
14	.167	.177
18	.167	.190
20	.167	.199

Among the results for twenty samples reported by Ahern & Karperos (1983), ZOT samples are those giving the worst agreement between laboratory and flight data. The reason for this apparent ground-handling or launching degradation has not been determined.
The flight evolution of α_s with time **t** is shown in Fig 1-12.1. An exponential expression in t has been fitted to these data as follows:

$$\alpha_s = \alpha_o + (\alpha_m - \alpha_o)(1 - e^{-t/\tau})$$

Values of α_o, α_m and τ, together with the time range of validity of the expression are given in the enclosed Table.

Sample	α_o	α_m	τ ESH	t_{max} ESH
9	.198	.301	2863	5 800
10	.185	.314	2933	5 800
14	.188	.358	5920	3 400
18	α_s=.190+3.65 × 10^{-5}t, preliminary			1 100
20	α_s=.199+3.09 × 10^{-5}t, preliminary			1 100

COMMENTS

Solar absorptance, α_s, depends on coating thickness as shown in Fig 1-11. Samples 18 and 20 depart from this rule but the reasons for the discrepancy are not clear since the results given are only preliminary. On the other hand the rate of degradation seems to be independent of the coating thickness. Samples 14, 18 and 20 were tested in the same flight and that on magnesium substrate exhibits a slightly larger degradation rate.

References: Curran & Millard (1978), Ahern & Karperos (1983).

COATINGS

Solar Reflectors

7.3.2.5.3. Protons only exposure. The data below refer to a SSR pigment, phosphated.

α_s deduced from spectral reflectance measured in situ.

Radiation Exposure			α_{so}	$\Delta\alpha_s$	Comments
Intensity [keV]	Integrated Flux [protons.m^{-2}]	Flux [protons.$m^{-2}.s^{-1}$]	Initial		
1.2	8.4×10^{19}	5.4×10^{13}	.149	.038	Irradiations performed at 1.3×10^{-5} Pa. Sample temperature, 265 K. Reflectance measured in situ (initially at 8×10^{-6} Pa).

From Zerlaut, Gilligan & Ashford (1972). For a description of the experimental set up see Gilligan & Zerlaut (1971).

7.3.2.5.6. Combined exposure. α_s deduced from spectral reflectance measured in situ.

Chamber pressures and sample temperature as above.

Exposures in the order given from left to right, except those under Combined which are simultaneous.

UV Exposure Time [ESH]	Combined					$\Delta\alpha_s$	$\Delta\alpha_s$ after O_2 Bleach
	Protons				UV Exposure Time [ESH]		
	Intensity [keV]	Integrated Flux [protons.m^{-2}]	Flux [protons.$m^{-2}.s^{-1}$]	Exposure [a] Time [EWH]			
600						.033	
600	1.2	8.3×10^{18}	1.21×10^{13}	927	700	.074	.053
600					700	.019	.010

[a] EWH: Equivalent Wind Hours.

From Gilligan & Zerlaut (1971).

7.3.2.6. Effects of the Space Environment on solar absorptance to emittance ratio. See pp. 1-39 and 1-40.

7.3.3. Reflectance.

7.3.3.1. Normal-hemispherical spectral reflectance. See Fig 1-13.

COATINGS

Solar Reflectors

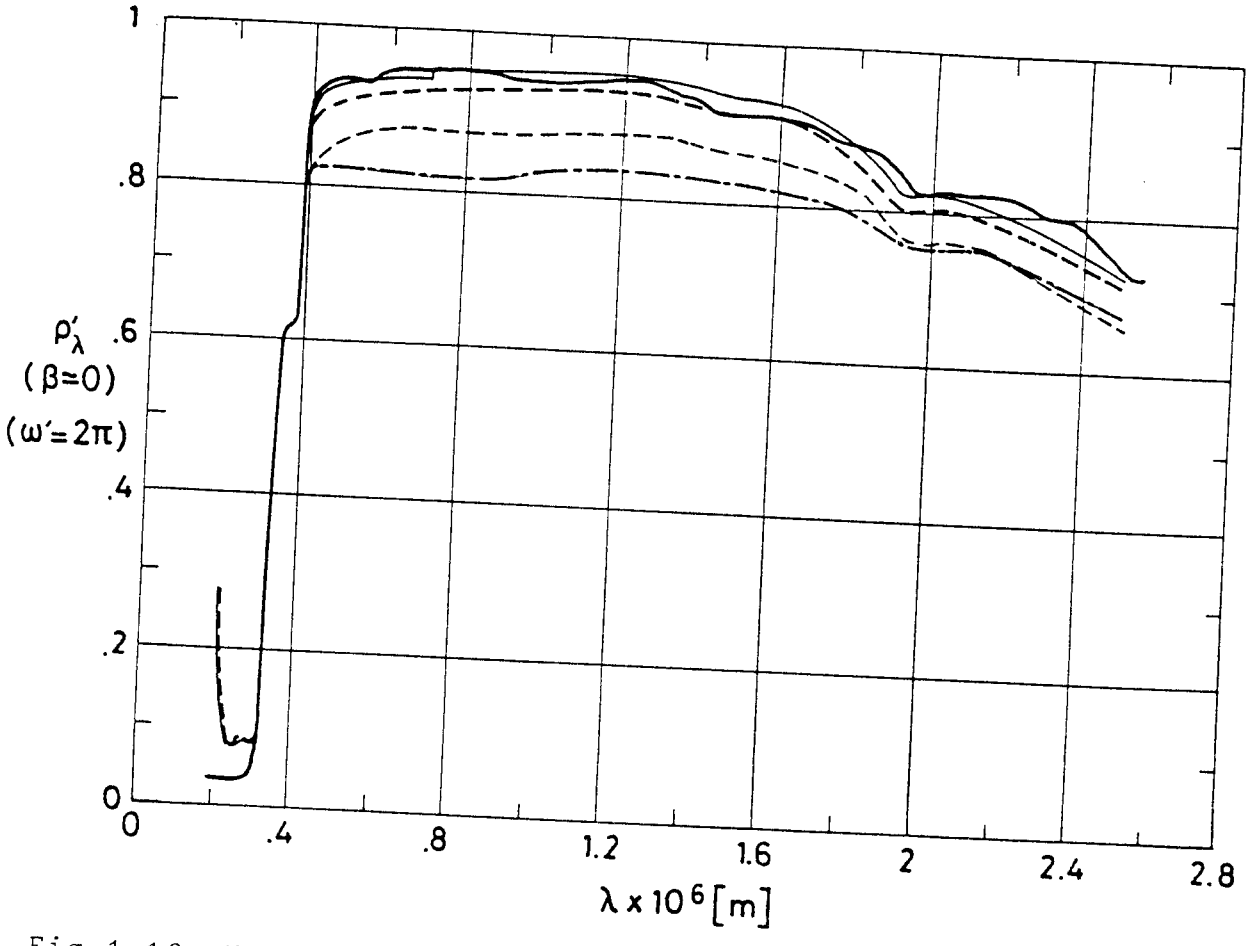

Fig 1-13. Normal-hemispherical spectral reflectance, ρ'_λ, of Zinc Orthotitanate-Potassium Silicate coatings vs. wavelength, λ.

Explanation

Key	Description			Comments	References
	Pigment Process and Encapsulation	Coating Thickness, $t_c \times 10^4$ [m]	α_s		
———	SSR Phosphated		.109	Measured in air with an integrating sphere attached to a Beckman DK2A reflectometer. β=0°.	Keyte (1975).
———	MOX	1.73	.108	Measured in vacuum (1.3×10^{-5} Pa) with an integrating sphere attached to a Beckman DK2A reflectometer. β=7°.	Harada & Wilkes (1979). Test Conditions Zerlaut & Courtney (1967).
- - - -		1.45	.125		
-----		.79	.178		
--·--		.56	.214		

COATINGS

Solar Reflectors

7.3.3.2. Effects of the Space Environment on reflectance.

7.3.3.2.1. Ultra-Violet Radiation. The data below refer to coatings based on SSR processed pigments.

Sample No.[a]	Exposure Time [ESH]	Spectral Reflectance Decrease, $10^2 \times \Delta\rho'_\lambda/\rho'_\lambda$, at Wavelengths, λ, below				
		$\lambda \times 10^7$ [m]				
		3.62	4.25	7.00	9.25	24.00
5	2 400	4.0	7.0	1.0	1.0	-1.0
6	2 000	7.0	5.5	.2	-.4	-2.2
7	2 000	4.2	5.0	1.8	1.0	-2.2
8	1 200	2.2	2.8	0	0	.5

[a] Sample numbers in this Table correspond to those in Tables 1-6 and 1-7.
Degrading Source: 1 kw General Electric AH-6 Mercury-Argon lamp, 6 Suns level.
Irradiated in vacuum (1.3×10^{-4} Pa - 1.3×10^{-5} Pa).
Measured in situ with an integrating sphere attached to a Beckman DK2A reflectometer.

From Zerlaut, Gilligan & Ashford (1972). For a description of the experimental set up see Gilligan & Zerlaut (1971).

Additional information, in graphical form, is given in Fig 1-14.

7.3.3.2.3. Protons only exposure. See Fig 1-15, p. 1-45.

COATINGS

Solar Reflectors

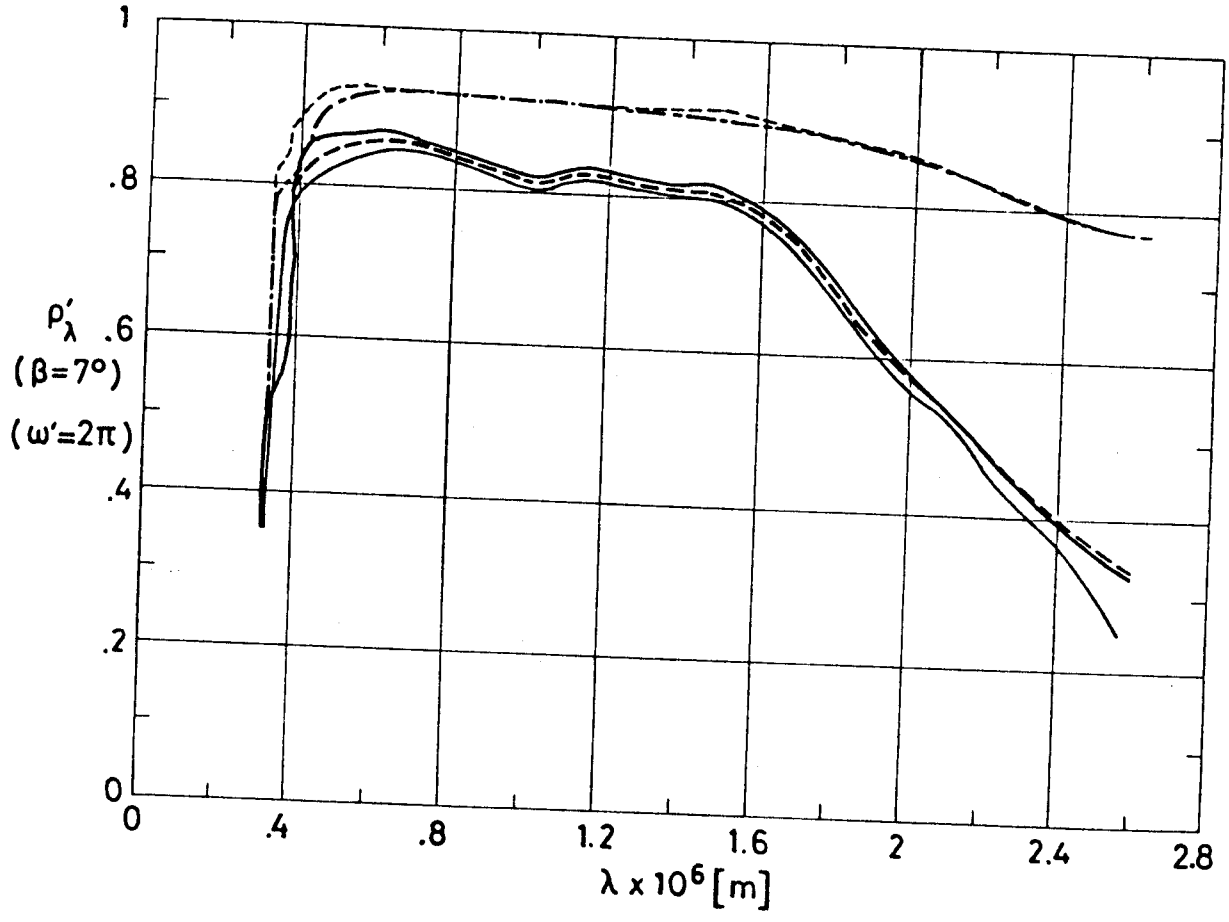

Fig 1-14. Effect of Ultra-Violet Radiation on normal-hemispherical spectral reflectance, ρ'_λ, of Zinc Orthotitanate-Potassium Silicate coatings vs. wavelength, λ.

Explanation

Key	Pigment Process and Encapsulation	Comments	References
———	SSR Phosphated.	Measured in vacuum (initially at 8×10^{-6} Pa). Sample temperature, 285 K.	Gilligan & Zerlaut (1971).
———		Same as above but irradiated in vacuum (1.3×10^{-5} Pa). 1 300 ESH.	
- - - -		Same as above. O_2 bleached. This is the same sample as in the lower Table p. 1-41.	
------	SSR Potassium hexafluorosilicate treated.	Coating cured at 773 K for 7 h. Sample No. 8 in Tables 1-6 and 1-7. Measured in vacuum (initially at 8×10^{-6} Pa).	Zerlaut, Gilligan & Ashford (1972).
-.-.-.-		Same as above but irradiated in vacuum (1.3×10^{-5} Pa). 1 200 ESH.	

COATINGS

Solar Reflectors

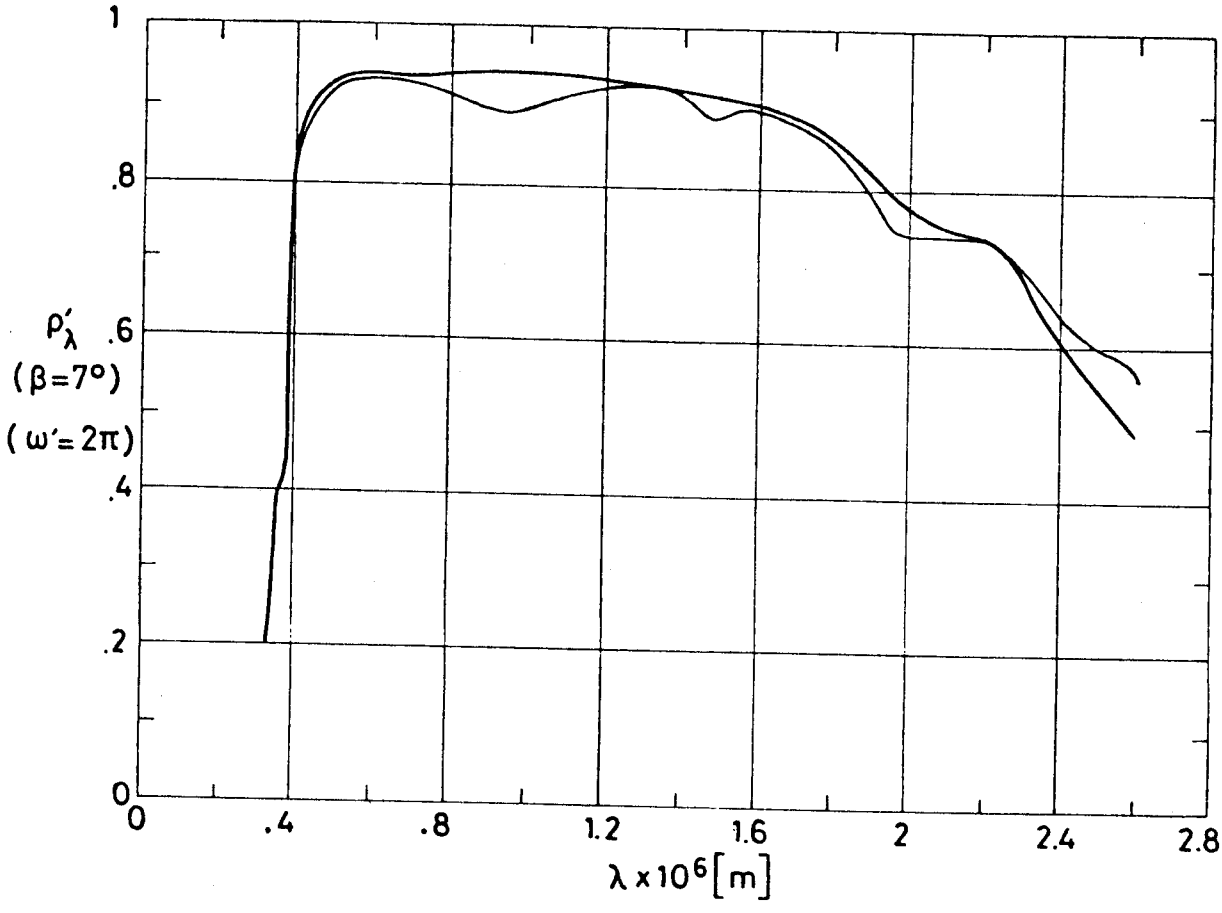

Fig 1-15. Effect of Protons Radiation on normal-hemispherical spectral reflectance, ρ'_λ, of Zinc Orthotitanate-Potassium Silicate coatings vs. wavelength, λ. From Gilligan & Zerlaut (1971).

Explanation

Key	Pigment Process and Encapsulation	Protons Exposure			Comments
		Intensity [keV]	Integrated Flux [protons.m^{-2}]	Flux [protons.$m^{-2}.s^{-1}$]	
———	SSR Phosphated.				Measured in vacuum (8×10^{-6} Pa). Sample temperature, 285 K.
———		1.2	2.7×10^{19}	5.4×10^{13}	Irradiated in vacuum (1.3×10^{-5} Pa). Measured in situ (initially at 8×10^{-6} Pa).

COATINGS

Solar Reflectors

8. ENVIRONMENTAL BEHAVIOR

8.1. Prelaunch. The adhesion to 6061-T6 aluminium alloy and cohesion of YB-71 coating appears to be similar to that for Z-93 (see § 1.2.2) which is a space-qualified paint. Scratching of the coating with a steel microspatula showed that the material is quite tough and could be removed only by applying strong pressure. Good adhesion was indicated in that after penetration to the substrate, complete removal of the coating at the coating-metal interface could not be effected. Initial conical mandrel bend tests have also revealed good adhesion (Harada & Wilkes (1979)).

According to Keyte (1975), who refers to a SSR pigment, phosphated, the coating is not as strong as Z-93 mechanically.

8.2. Postlaunch. Although this coating has been proposed for use in a number of satellites, actual in orbit performance data is very limited.

8.2.1. Ascent. The coating based on SSR processed pigment, phosphated, exhibits little tendency to change under vacuum (Keyte (1975)).

8.2.2. Orbital. The coating based on SSR processed pigment, phosphated, degrades itself very slightly, by about $\Delta\alpha_s = .03$, under ultra-violet radiation and near-to-Earth flight. (Keyte (1975)).

The initial degradation shown by all coatings tested on OSO-H has not been explained satisfactorily.

COATINGS

Solar Reflectors

9. THERMAL CYCLING

The maximum and minimum temperatures at which YB-71 has been tested, in a vacuum of 1.3×10^{-5} Pa, without any evidence of deterioration in adhesion were:

$$T_{min} = 116 \text{ K}$$

$$T_{max} = 380 \text{ K} .$$

Samples have been cooled to the range 33 K to 88 K for 45 min with no apparent loss in bond integrity.
(Harada & Wilkes (1979)).

10. SOURCE

IIT Research Institute, 10 West 35 Street, Chicago, Illinois 60616. Contact person: Mr. Yoshiro Harada.

11. COST

12. PAST SPATIAL USE

No information other than that given in pp. 1-39 and 1-40 has been found by the compiler.
Data on the performance of YB-71 coating samples in a geo-synchronous orbit is now being collected (Harada (1981)).
A sample of this coating, on aluminium substrate, will be tested, among others, onboard Long Duration Exposure Facility (LDEF) 1st Mission (scheduled for early 1984), Experiment S0010. In this experiment the coating will be examined before flight and after retrieval (Clark (1981)).

INTENTIONALLY BLANK PAGE

Rev. 3. 1986

COATINGS

Solar Reflectors

1.2.3.1. ZINC-OXIDE METHYLSILICONE

Three slightly different coatings will be introduced in this data item. For the time being they will be designated a, b and c respectively.

1. COMPOSITION

a) Pigment: New Jersey Zinc Co., SP500 zinc oxide
Binder: General Electric Co., RTV-602, methylsilicone
Solvent: Toluene

b) Pigment: New Jersey Zinc Co., SP500 zinc oxide, PS7-treated
Binder: General Electric Co., RTV-602, methylsilicone
Solvent: Toluene, USP (US Pharm.)

The pigment is reactively encapsulated to enhance its stability against UV radiation. The zinc oxide (the unstable component) is reacted in slurry with PS7 potassium silicate (Sylvania Electric Products Co.) The details vary from reference to reference. "Sweating" involves sealing in aluminium foil the slurry resulting from hot treatment of a slurry containing 1.7 parts PS7 and 1 part SP500 letting it to stand during 6 h at least. Satisfactory softness, whiteness and protection against UV is achieved with sweating times above 6 h. Paints prepared from 24 h-sweated pigment have extended shelf lives without the use of retarders. Sweating times of 48 h result

COATINGS

Solar Reflectors

in paints which cannot be easily applied or cured (Zerlaut, Rogers, Noble (1969)).

c) Pigment and solvent as in b

Binder: stripped methylsilicone

Outgassing characteristics are enhanced by devolatilization of the binder at 423 K ± 3 K and a vacuum of the order of 7×10^{-4} Pa for 24 h (Seidenberg, Park & Clatterbuck (1972)).

The properties (other than outgassing), application procedures and handling procedures are the same for both b and c coatings.

The silicones of General Electric were originally sold under the name of LTV (Low Temperature Vulcanizing). Sometime in the sixties the name LTV was changed into RTV (Room Temperature Vulcanizing) (Zwaal (1986)). Here either LTV or RTV will be used according to the corresponding source.

In 1982 General Electric Co. discontinued the manufacture of RTV-602. Since then IITRI, manufacturer of the coatings, is engaged in a program to find at least two new suitable replacement binders for RTV-602. See Cull et al (1984) for preliminary results with 21 commercial silicone resins.

2. FORMULATION

a) 2.4:1:1.7 by weight of pigment, binder and solvent

b) 2.4:1:1.75 by weight of pigment, binder and solvent

From Cunnington, Grammer & Smith (1969).

COATINGS

Solar Reflectors

c)

3. USUAL DESIGNATION

a) S-13

b) S-13 G

c) S-13 G/LO

IIT Research Institute.

4. SUBSTRATE

Any substrate to which the primer (General Electric propietary S-4044 silane) will adhere. This primer can be applied to either anodized or zinc-chromate-primed surfaces.

From Cunnington, Grammer & Smith (1969).

5. METHOD OF APPLICATION

5.1. Preparation of paint for application

a) S-13. The paint is furnished in 5 gal epoxy-lined metal pails. The paint should be thoroughly stirred before transfer to other containers or before additions of catalyst. The catalyst is SRC-05. The recommended concentration is 1 part SRC-05 in 20 parts of toluene to 670 parts of S-13 (by weight). This is equivalent to .76 % catalyst based on polymer solids. Lower catalyst concentrations are recommended to ensure optimum stability to UV irradiation in vacuum. For example a concentration of 1 part SRC-05 in 20 parts of toluene to 1 275 parts of S-13 (which represents .4 % catalyst based on polymer solids) provides optimum stability to UV irradiation in vacuum without great-

COATINGS

Solar Reflectors

ly sacrificing terminal-cure properties.

The catalyst solution is added only as the paint is used and only to the amount that can be applied in about 30 min. Allow the catalyst paint to set for 10 min before application to the primed surface.

b) S-13 G and S-13 G/LO. As above but now the recommended concentration of catalyst is 1 part SRC-05 in 10 parts of toluene to 1 030 parts of S-13 G (by weight), which corresponds to .75 % SRC-05. A concentration of .4 % based upon RTV-602 provides optimum stability without sacrificing terminal-cure properties.

The undiluted catalyst has a shelf life of six months and the diluted a shelf life of thirty days (Cull, Stevenson, Harada & Mell (1984)).

From Cunnington, Grammer & Smith (1969) unless otherwise stated.

5.2. Preparation of surfaces for painting. Greasy surfaces should be cleaned with standard detergent and water, and thoroughly dry prior to priming. Primer is SS-4044.

From Cunnington, Grammer & Smith (1969).

5.3. Application of paint. The primer can be spray-applied (Binks model 18 or comparable gun) at about 2×10^5 Pa. Only about 12.7×10^{-6} m thick primer is required. Allow primer to air dry for 1 h before application of the paint. Paint can be spray-applied (Binks model 18 or comparable

COATINGS

Solar Reflectors

gun) at about 4 x 10^5 Pa. Unless clean dry air is available prepurified nitrogen or prepurified air must be used. Paint viscosity is rated at 25 s to 31 s with a No. 4 Ford cup. It can be used until the viscosity exceeds 100 s No. 4 Ford. Paint should be thinned to 17 s - 23 s No. 4 Ford with X-99 thinner (Cull, Stevenson, Harada & Mell (1984)). From Cunnington, Grammer & Smith (1969) unless otherwise stated.

5.3.1. Pot life. Pot life of S-13 G/LO is one hour for the catalyzed paint.

From Cull, Stevenson, Harada & Mell (1984).

5.3.2. Shelf life. Shelf life of S-13 G/LO is guaranteed for 30 d after purchase, providing that paint is stored at 280 K.

From Cull, Stevenson, Harada & Mell (1984).

5.4. Coating thickness

a) S-13. 89 x 10^{-6} m to 140 x 10^{-6} m.

From Cunnington, Gramer & Smith (1969).

b) S-13 G. 127 x 10^{-6} m to 203 x 10^{-6} m.

From Breuch (1967).

c) S-13 G/LO. 17 x 10^{-6} m to 50 x 10^{-6} m per coat. Nominal total, 203 x 10^{-6} m (+ 50 x 10^{-6} m or -25 x 10^{-6} m) thick.

From Cull, Stevenson, Harada & Mell (1984).

5.5. Curing process. Airdrying cure for 16 h at room temperature, optionally 16 h at 394 K. Dust and debris must be

COATINGS

Solar Reflectors

kept off the surface during the curing process.

From Gilligan, Harada & Gates (1974).

There is a minimum time of 10 minutes required between coats and 50 h required before handling.

For the qualification testing, S-13 G/LO is allowed to cure for 7 days prior to testing.

5.6. Reapplication. Soiled or damaged areas can be recoated. Soiled areas must be cleaned thoroughly with detergent and water, and dried before application of additional paint. Damaged or gouged areas can be recoated by making a paste of paint in which the bulk of solvent is omitted. Such a material can be troweled or brushed over the damaged areas and cures can be tack free within a few hours.

From Cunnington, Grammer & Smith (1969).

6. SOLVENTS RESISTANCE

See a typical list of solvents in p. 1-4.

Optimum solvent composition based on Toluene (p. 1-48.41).

7. PHYSICAL PROPERTIES

7.1. Density

a)

b) S-13 G. Coating surface density is .03 $kg.m^{-2}$ as measured from test specimens (Breuch (1967)).

Paint density is between 1 425 $kg.m^{-3}$ and 1 475 $kg.m^{-3}$ (Cull, Stevenson, Harada & Gates (1984)).

c) Paint density as in b).

COATINGS

Solar Reflectors

7.2. Outgassing. See table below.

Coating	% TML [a]	% VCM [b]	Cure Time [h]	Cure Temp. [K] [c]	Vacuum Conditions [Pa]	References
S-13 G	.42	.09	48 16	298 394	10^5 $13x10^{-5}$	Campbell, Marriott & Park (1978)
	.26	.03				
	.82	.16	24	298	10^5	
S-13 G/LO	.56	.13	48 24	298 366	10^5 10^5	
A/B as 100/1 [d]	.54	.10	168	298	10^5	
	.40	.01	1	394	10^5	
No primer	.50	.12				
A/B as 100/1 [d]	.59	.11	168	298	10^5	
S-13 G/LO	.40 [e]	.05				INTA (1976)

a TML: Total Mass Loss.
b VCM: (Collected) Volatile Condensable Material.
c Each one of these cures was used in the order given.
d A refers to S-13 G/LO and B to SRC-05 catalyst in toluene. See b) in p. 1-48.4.
e Data for this sample have been obtained per Specification ESA PSS-09/QRM-02T (see p. 1-53). % RML = .25 %.

7.3. Thermal radiation properties

7.3.1. Emittance

7.3.1.1. Hemispherical total emittance. The data in the Table 1-7.1 overleaf have been taken from several sources. They correspond to samples under different conditions and have been determined by different procedures.

Rev. 3. 1986

COATINGS

Solar Reflectors

Table 1-7.1

Hemispherical Total Emittance of S-13 and S-13 G Coatings

Coating	T [K]	$t_c \times 10^3$ [m]	ε^a	ε^b	References
S-13	294			.87 b1	Cunnington, Grammer & Smith (1969)
	395	.090-.140	.87±.02 al	.84 b1	
	300	∿.127		.81 b2	Millard & Pearson (1973)
S-13 G	294			.84 b1	Cunnington, Grammer & Smith (1969)
	395	.090-.140	.89±.02 al	.85 b1	
	300	∿.127		.81 b2	Millard & Pearson (1973)

a Determined calorimetrically.
al 6061-T6 Al_3 alloy disc substrate. 25.4 x 10^{-3} m diameter, 1.27 x 10^{-3} m thick. Chamber pressure 1.33 x 10^{-5} Pa.
b From spectral reflectance data and the blackbody function for the quoted temperature.
b1 λ range 2 x 10^{-6} m to 2.5 x 10^{-5} m.
b2 OSO III preparation. Substrate primed with G.E. SS-4044.

Hemispherical total emittance vs. temperature is given in Fig 1-48.1 in the following page. The coating is S-13 G, 2 x 10^{-4} m thick, on molybdenum substrate. Hemispherical total emittance, absorptance and specific heat of the coating have been measured by a calorimetric cyclic radiation method (Spisz & Jack (1971)).

COATINGS

Solar Reflectors

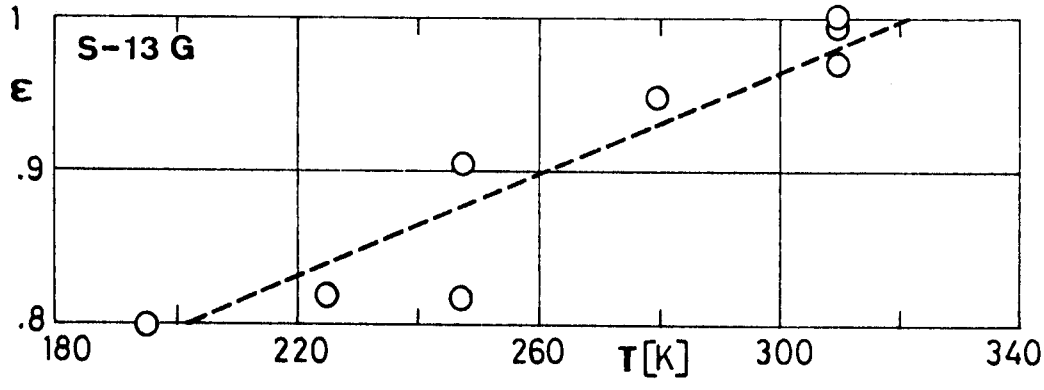

Fig 1-48.1. Hemispherical total emittance, ε, of S-13 G coating vs. temperature, T. 2 x 10^{-4} m thick coating on molybdenum substrate. From Spisz & Jack (1971).

The method consists basically in the following: First the substrate is irradiated in vacuum. After thermal equilibrium is reached, the radiant intensity is varied sinusoidally and the substrate temperature is measured as a function of time. From the temperature variation the properties of the substrate are deduced. The coating is then applied to the bottom side of the substrate and the process is repeated by irradiating the top side. Now the average hemispherical total emittance of both sides, the absorptance of the substrate, and the specific heat of coating plus substrate are deduced. The process is repeated again, irradiating the bottom side. The measurements indicate that the solar absorptance of this coating is practically temperature independent.

COATINGS

Solar Reflectors

7.3.1.3. Effects of the Space Environment on hemispherical total emittance

7.3.1.3.1. Ultra-Violet Radiation. Table 1-7.2 below has been prepared using data from Cunnington, Grammer & Smith (1969).

Table 1-7.2

Ultra-Violet Radiation Effects on Hemispherical Total Emittance of S-13 and S-13 G Coatings

Coating	Sample	T [K]	t [h]	n	ε_o	ε_f	$\bar{\varepsilon}$	σ
S-13	27	395	500	12	.86	.86	.862	.006
	28	395	636 [a]	14	.85	.87	.867	.005
S-13 G	43	395	500	10	.90	.91	.914	.008
	44	395	520	11	.91	.91	.911	.005

Degrading Source: 2×10^{-7} m to 4×10^{-7} m Xenon Lamp, 1 Sun level.
Method of obtaining data: Calorimetric. Chamber pressure: 1.33×10^{-5} Pa. 6061-T6 Al disc, 25.4×10^{-3} m diameter, 1.27×10^{-3} m thick.

t , total exposure time. [h]
n, number of data points given in the source at the quoted temperature.
ε_o, ε_f, initial and after-exposure values of the hemispherical total emittance.

$\bar{\varepsilon}$, mean value, $\bar{\varepsilon} = \dfrac{\sum_{i}^{n} \varepsilon_i \Delta t_i}{t}$.

σ, standard deviation, $\sigma = \sqrt{\dfrac{\sum_{i}^{n} (\varepsilon_i - \bar{\varepsilon})^2 \Delta t_i}{t-1}}$.

[a] Failure during test (electronic pump off, pressure increase to > 6.65 Pa (50×10^{-3} mm Hg) for 2 h).

COATINGS

Solar Reflectors

Test data have been represented in Fig 1-48.2 below.

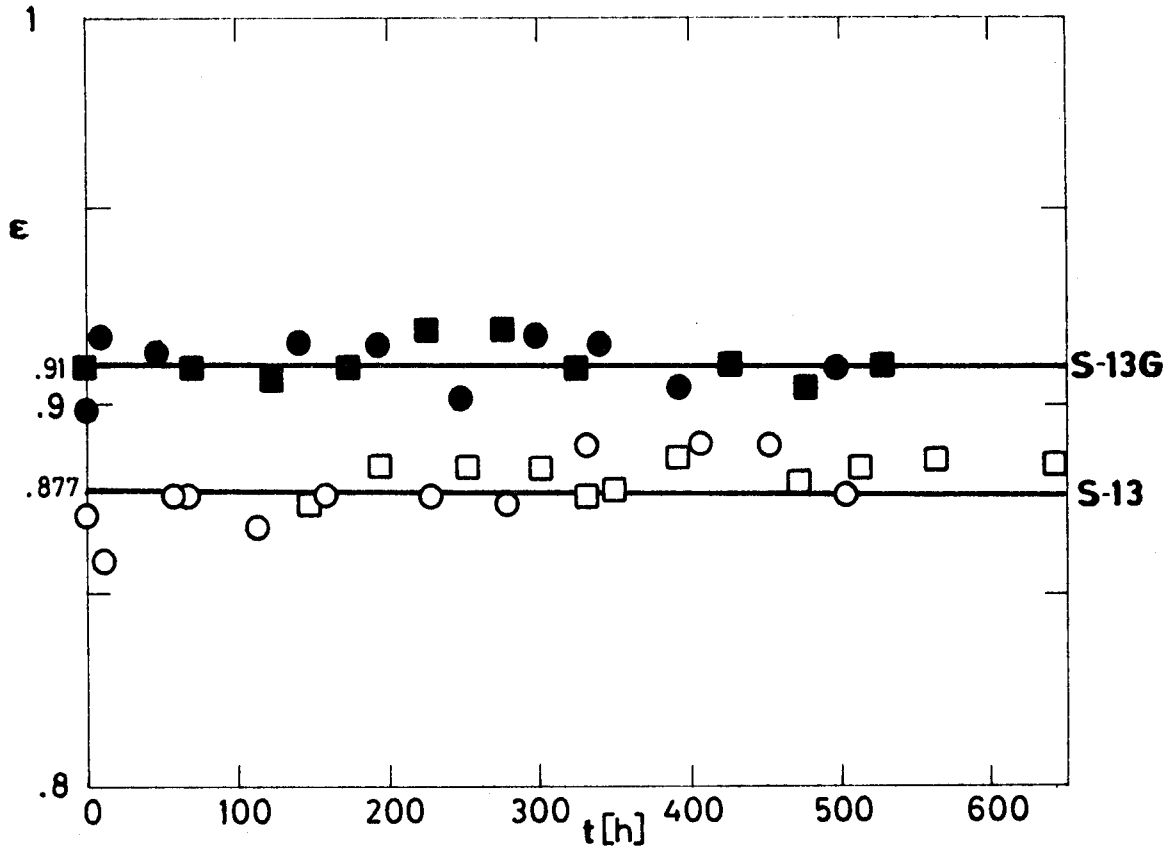

Fig 1-48.2. Hemispherical total emittance, ε, of S-13 and S-13 G coatings vs. exposure time, t, at 1-Sun level and 395 K. From Cunnington, Grammer & Smith (1969). Equal symbols correspond to the same sample.

○ Sample 27 ● Sample 43
□ Sample 28 ■ Sample 44

7.3.1.4. Normal total emittance.

See Table 1-7.3 overleaf.

Room-temperature emittance measurements were performed in the past using an infrared spectrophotometer with

COATINGS

Solar Reflectors

an attached heated cavity. The spectral reflectance data were then used to calculate the emittance. More recent data are being obtained with a Gier-Dunkle portable emissometer, model DB-100 (Henninger (1984)).

Table 1-7.3

Normal Total Emittance of S-13 G and S-13 G-LO Coatings

T [K]	Coating Description	ε'	References
311	S-13 G over B-1056 ZnO in methyl silicone binder ($.0508 \times 10^{-3}$ m thick), over ZnO in RTV-602 silicone resin binder substrate ($.254 \times 10^{-3}$ m thick). Property calculated from reflectance. Laboratory data taken on sample to be tested on LO IV.	.860	Touloukian DeWitt & Hernicz (1972)
	Similar to above specimen and conditions except sample to be tested on LO V.	.860	
	S-13 G, ZnO in methyl silicone binder ($.254 \times 10^{-3}$ m thick). Calculated from reflectance. Laboratory data taken on sample to be tested on LO IV.	.879	
	B-1060; SP-500 ZnO in silicone binder ($.264 \times 10^{-3}$ m thick). ZnO silicated. Property calculated from reflectance. Laboratory data taken on sample to be tested on LO IV.	.880	
300	S-13 G. Measured with a Gier-Dunkle portable emissometer. NASA specifications.	$.90 \pm .05$	Henninger (1984)
	S-13 G/LO. As above.	$.90 \pm .05$	Cull et al (1984)

COATINGS

Solar Reflectors

7.3.2. Absorptance

7.3.2.1. Solar absorptance

a) S-13. Near normal solar absorptance. Coating thickness $t_c = .127 \times 10^{-3}$ m, substrate primed with G.E. S-4044.

$\alpha_s = .19$, T = 300 K.

From spectral reflectance data.

From Millard (1969).

b) S-13 G. Near normal solar absorptance.

$t_c = .127 \times 10^{-3}$ m substrate primed with G.E. S-4044.

$\alpha_s = .23$, T = 300 K.

From spectral reflectance data.

From Millard (1969).

A recent value for S-13 G is

$\alpha_s = .20$, T = 300 K

From spectral reflectance.

Data on absolute reflectance, absorptance and transmittance are presently taken at NASA Goddard with a Beckman DK-2A spectrophotometer with a Gier-Dunkle absolute integrating sphere. The instrument covers the wavelength region from $.3 \times 10^{-6}$ m to 2.4×10^{-6} m. It is coupled to a microcomputer for data reduction. The manufacturer of the instrument lists an accuracy of $\alpha_s \pm .015$ units over the total measurement range.

From Henninger (1984).

COATINGS

Solar Reflectors

7.3.2.2. Variation of solar absorptance with coating thickness.

Data in Fig 1-48.3 are for S-13 coating.

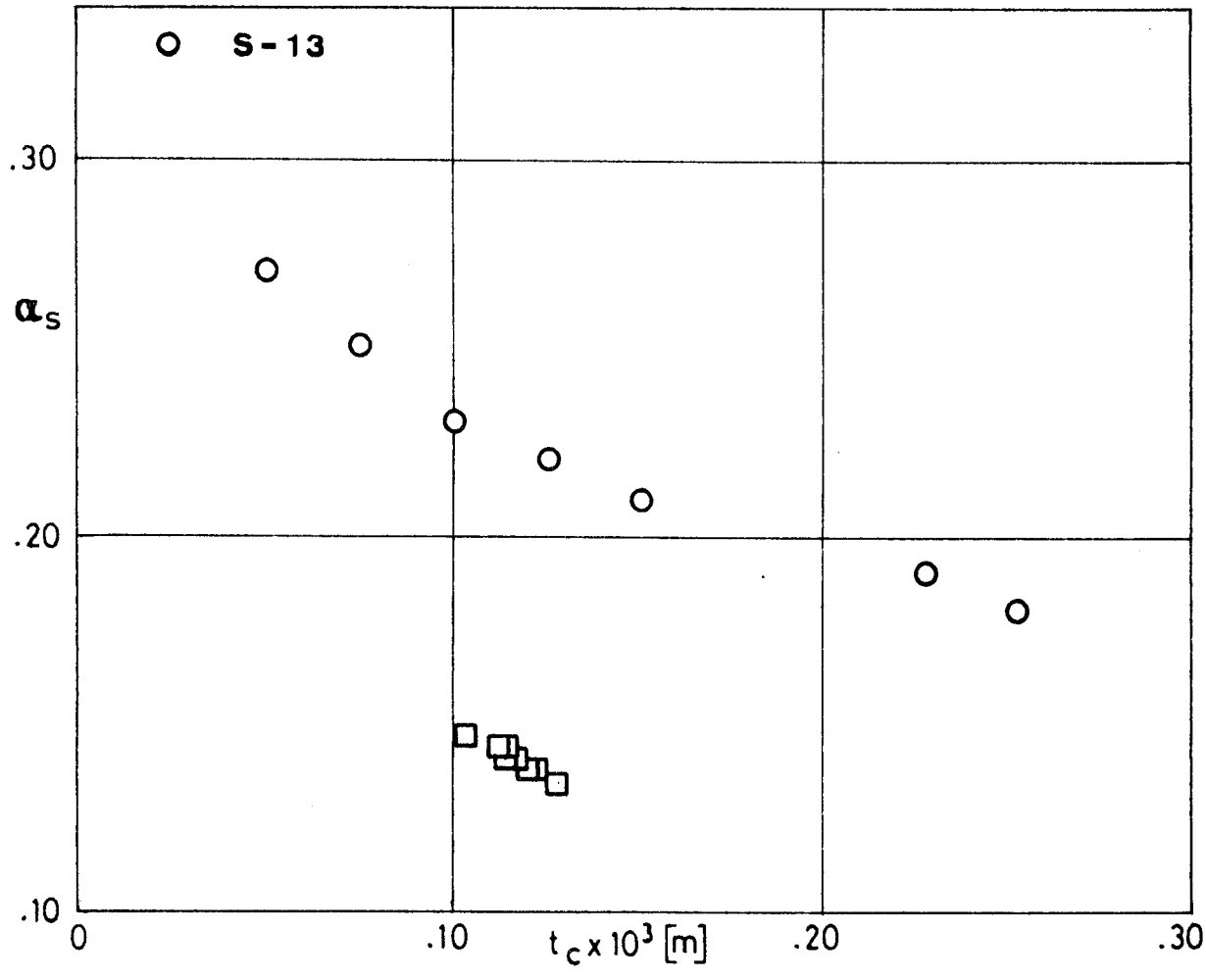

Fig 1-48.3. Variation of solar absorptance, α_s, of S-13 coating with coating thickness, t_c.

○ Nominal composition. Sprayed on primed surface. Air dryed. T = 298 K. (Designation in the ref.: 119 to 127).

□ ZnO in silicone binder. T = 298 K. (Designation in the ref.: 29, 30).

From Touloukian, DeWitt & Hernicz (1972).

COATINGS

Solar Reflectors

7.3.2.3. Variation of solar absorptance with incidence angle. Fig 1-48.4. Solar absorptance deduce from spectral reflectance measured in air. Two different sample sizes were used to assure full sample illumination at all incidence angles.

S-13 G coating, silicated pigment in silicone binder applied to aluminium substrate. Sample to be tested on Prospero.

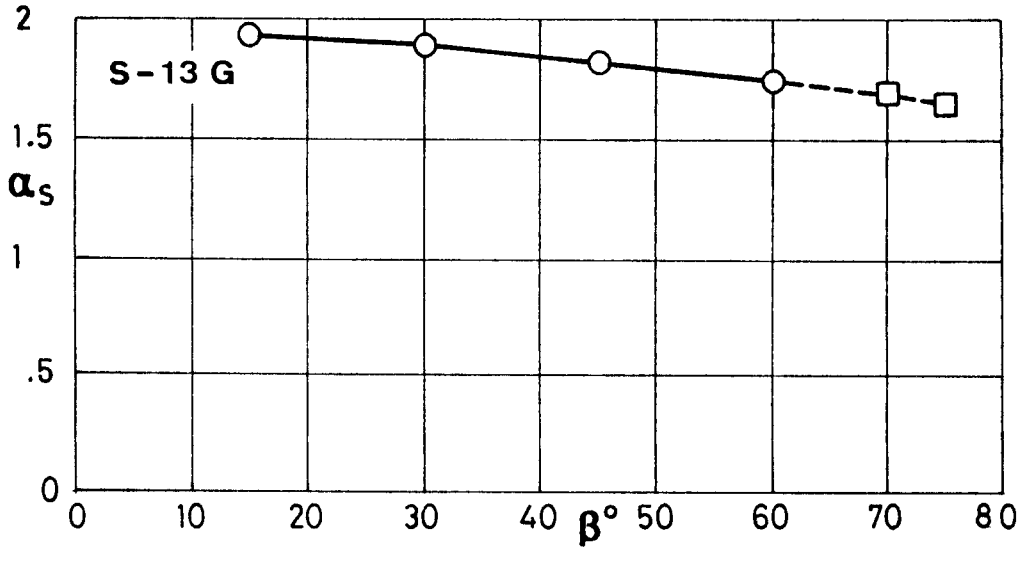

Fig 1-48.4. Solar absorptance, α_s, of S-13 G coating vs. incidence angle, β. From Keyte (1975).

7.3.2.5. Effects of Space Environment on absorptance

7.3.2.5.1. Ultra-Violet Radiation. Detailed laboratory data on the effects of UV radiation on spectral absorptance are given in Table 1-7.4.

COATINGS

Solar Reflectors

Table 1-7.4

Ultra-Violet Radiation Effects on Spectral Absorptance of S-13 Coating (Samples 27 & 28)

T [K]	t [h]	α for Xenon Lamp, Range of λ x 10^7 [m]					α_s
		2-4.1	4.1-6	6-8.5	8.5-	Total	
294	0	---	---	---	---	.21	---
339	0	---	---	---	---	.21	---
395	0	---	---	---	---	.21	---
395	4	.65	.08	.06	.24	.21	.21
395	53	.65	.10	.06	.27	.23	.23
395	61	.65	.15	.06	.28	.24	.24
395	113	.70	.15	.08	.30	.27	.26
395	158	.70	.19	.08	.28	.26	.26
395	230	.75	.21	.09	.28	.27	.27
395	280	.75	.25	.08	.29	.27	.28
395	330	.70	.26	.10	.28	.26	.28
395	402	.65	.26	.08	.28	.27	.28
395	450	.65	.27	.08	.30	.27	.28
395	500	.70	.27	.10	.28	.27	.28
Before Exposure [a]		.65	.08	.10	.14	.18	.18
After Exposure [a]		.76	.31	.15	.17	.26	.28
290	0	---	---	---	---	.21	---
342	0	---	---	---	---	.20	---
395	0	.70	.10	.10	.19	.21	.20
395	4	.70	.10	.10	.23	.22	.21
395	50	.65	.12	.10	.26	.23	.23
395	146	.65	.18	.10	.28	.26	.26
395	196	.65	.23	.08	.32	.27	.28
395	246	.70	.28	.08	.32	.30	.30
395	296	.70	.26	.09	.31	.29	.30
395	328 [b]	.70	.21	.10	.26	.25	.26
395	346	.70	.22	.10	.29	.27	.27
395	396	.70	.22	.10	.31	.28	.28
395	468	.70	.24	.11	.30	.27	.28
395	516	.70	.23	.14	.30	.27	.28
395	564	.70	.24	.14	.30	.27	.28
395	636	.70	.24	.14	.30	.27	.28
Before Exposure [a]		.65	.08	.10	.14	.19	.19
After Exposure [a]		.78	.32	.17	.21	.28	.31

(Continued onto next page)

COATINGS

Solar Reflectors

Table 1-7.4 (Continued)

Ultra-Violet Radiation Effects on Spectral Absorptance of S-13 G Coating (Samples 43 & 44)

T [K]	t [h]	α for Xenon Lamp, Range of λ x 10^7 [m]					α_s
		2-4.1	4.1-6	6-8.5	8.5-	Total	
294	0	---	---	---	---	.23	---
339	0	---	---	---	---	.21	---
395	0	---	---	---	---	.21	---
395	0	.85	.12	.05	.15	.20	.20
395	4	.90	.12	.05	.16	.21	.21
395	51	.90	.17	.08	.17	.23	.24
395	149	.90	.21	.09	.17	.24	.25
395	195	.92	.27	.10	.17	.26	.27
395	248	.90	.28	.10	.17	.26	.27
395	296	.90	.32	.09	.17	.26	.28
395	344	.85	.35	.11	.17	.26	.28
395	392	.85	.35	.11	.17	.26	.28
395	500	.85	.35	.10	.18	.26	.28
Before Exposure [a]		.70	.10	.10	.13	.19	.19
After Exposure [a]		.82	.37	.20	.15	.28	.31
294	0	---	---	---	---	.24	---
339	0	---	---	---	---	.22	---
395	0	.80	.10	.08	.14	.19	.19
395	5	.80	.10	.08	.14	.20	.20
395	75	.80	.16	.09	.15	.20	.21
395	123	.80	.16	.08	.16	.21	.22
395	172	.80	.21	.08	.16	.21	.22
395	227	.75	.27	.08	.16	.22	.23
395	274	.75	.27	.08	.16	.22	.23
395	327	.75	.27	.10	.16	.22	.24
395	423	.75	.27	.10	.17	.22	.24
395	471	.75	.27	.10	.17	.22	.24
395	520	.75	.28	.10	.18	.22	.25
Before Exposure [a]		.65	.10	.10	.13	.18	.20
After Exposure [a]		.75	.29	.12	.15	.23	.27

a Values from Cary room temperature reflectance measurements.
b Electronic pump off, pressure increase to >6.65 Pa (50 μm Hg).
Ultraviolet source is a 900 W Hanovia Xenon lamp, Model 538-CL.
Method of obtaining data: Calorimetric in situ absorptance.
Chamber pressure: 1.33×10^{-5} Pa.
From Cunnington, Grammer & Smith (1969).

COATINGS

Solar Reflectors

The UV radiation induced absorption of zinc oxide pigments is based on a photochemical evolution of oxygen. UV degraded zinc oxide rapidly recovers its initial optical properties upon reexposure to air. Table 1-7.5 (p. 1-48.19) lists results obtained under varied experimental conditions, and deduced from spectral reflectance given in pp. 1-48.41 to 1-48.50.

Data from flight experiments have been grouped in § 7.3.2.5.6 under Combined exposure. Reported measurements correspond to widely different orbits. Effects on solar absorptance of UV exposure and thermal cycling at cryogenic and room temperatures have been reported by Breuch (1967) and are given below. Coating is S-13.

Data Obtained by Cary Reflectometer

Chamber pressure:

For T = 136 K, p = 8×10^{-6} Pa to 13.3×10^{-6} Pa
For T = 133-297 K, p = 4×10^{-6} Pa to 8×10^{-6} Pa.

T [K]	t [ESH]	UV [Suns]	α_s	$\Delta\alpha_s$
136	2 790	14	.18	.01
133-297 (275 cycles)	2 560	12	.20	.03

From Breuch (1967).

COATINGS

Solar Reflectors

Table 1-7.5

Ultra-Violet Radiation Effects on Solar Absorptance of S-13 and S-13 G Coatings

Coating	Spectral Reflectance Data		t [ESH]	α_s	$\Delta\alpha_s$
S-13	p. 1-48.40	———	800	.21	.08
S-13 G	pp. 1-48.42 & 43	———	600	.21	.01
	p. 1-48.42	- - - -	600	.22	.03
	p. 1-48.43	- - - -	800	.20	.03
	p. 1-48.46	———	600	.22	.06
		- - - -	600	.22	.02
	pp. 1-48.47 & 48	———	1 400	.24	.01
	p. 1-48.48	- - - -	1 400	.22	.02
		—·—·—	1 400	.22	.03
		·····	1 400	.26	.05
		—··—··—	1 400	.23	.06
	p. 1-48.49	——— - - -	600+700		.039
		———	600+700+ O_2 bleaching		.013

7.3.2.5.3. Protons only exposure. Data for coatings S-13 and S-13 G are given in Fig 1-48.5. Data for S-13 have been measured in air after exposure and those for S-13 G in situ (see comments in p. 1-48.36).

COATINGS

Solar Reflectors

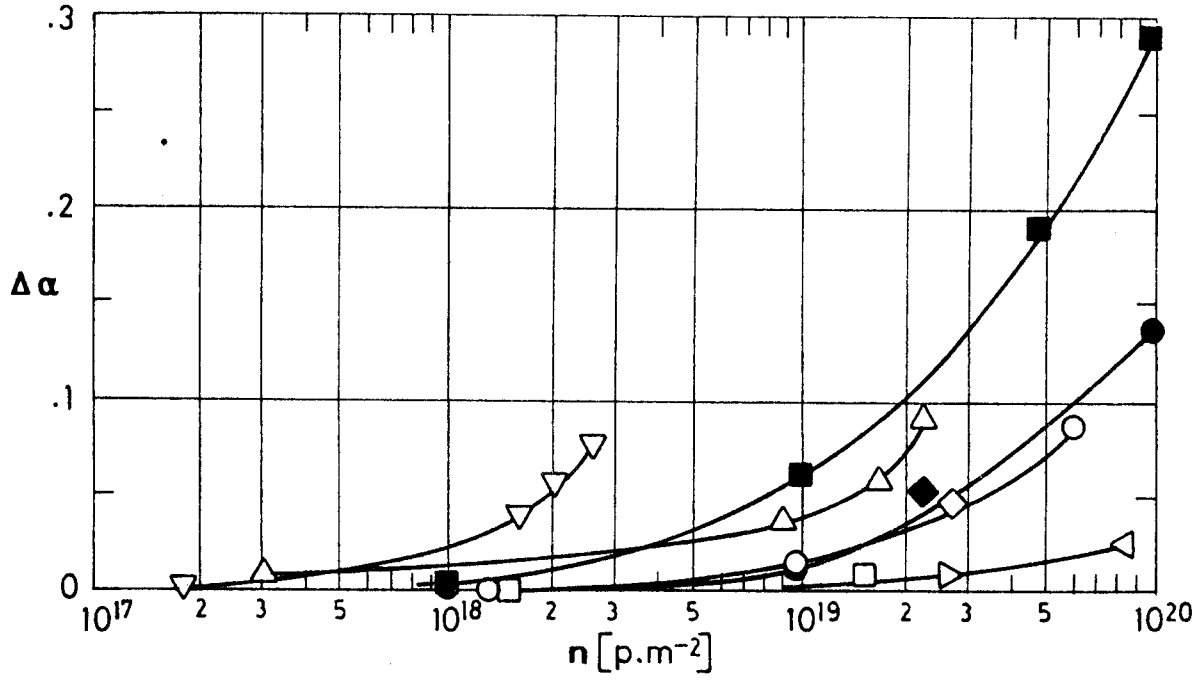

Fig 1-48.5. Change in solar absorptance, $\Delta\alpha_s$, of S-13 and S-13 G coatings due to Protons and Alpha Particles Radiation vs. integrated flux, n.

Explanation

Key	Coating	Intensity [keV]	Comments	References
○	S-13	8 p	$p \sim 10^{-4}$ Pa, T=303 K ± 5 K. Irradiated in vacuum by a low energy particle accelerator and a Dynamitron. From spectral reflectance measured in air (20 h-40 h delay. Cracking observed.	Gillette, Brown, Seiler & Sheldon (1966)
□		8 p		
△		2.5×10^3 p		
▽		5×10^3 α		
▷	S-13 G	1.2 p	4.9×10^{13} p.m^{-2}.s^{-1}. T=285 K	Compiled by Bourrieau, Paillous & Romero
◁		1.2 p	5×10^{13} p.m^{-2}.s^{-1}	
◇		2 & 10 p		
◆		10 & 20 p	7.3×10^{13} p.m^{-2}.s^{-1}. T=288 K	
●		40 p	T=293 K	
■		40 p	10^{14}-5×10^{14} p.m^{-2}.s^{-1}. T=291 K	

COATINGS

Solar Reflectors

Data for Protons Radiation up to 400 keV intensity are also given by Miller & Campbell (1966). The coating binder is Dow Corning Q 90016 methyl silicone. Reflectance data are presumably taken ex situ.

7.3.2.5.4. Electrons only exposure. Coating in the table below is GSFC, 101-7 (similar to S-13 G) on Al substrate. Absorptance deduced from spectral reflectance. See pp. 1-48.56, 1-48.57.

Intensity [keV]	Cumulative Integrated Flux [$e.m^{-2}$]	Measured in	α_s
20		Air T = 298 K	.22
	10^{17}	Vacuum T = 298 K	.22
	5×10^{17}	1.33×10^{-6} Pa	.23
	10^{18}		.23
	3×10^{18}		.24
	10^{19}		.26
	10^{20}		.29
80		Air T = 298 K	.22
	10^{17}	Vacuum T = 298 K	.23
	5×10^{17}	1.33×10^{-6} Pa	.24
	10^{18}		.26
	3×10^{18}		.32
	10^{19}		.37
	10^{20}		.41

From Fogdall, Cannaday & Brown (1970).

COATINGS

Solar Reflectors

Data from several sources are shown in Fig 1-48.6.

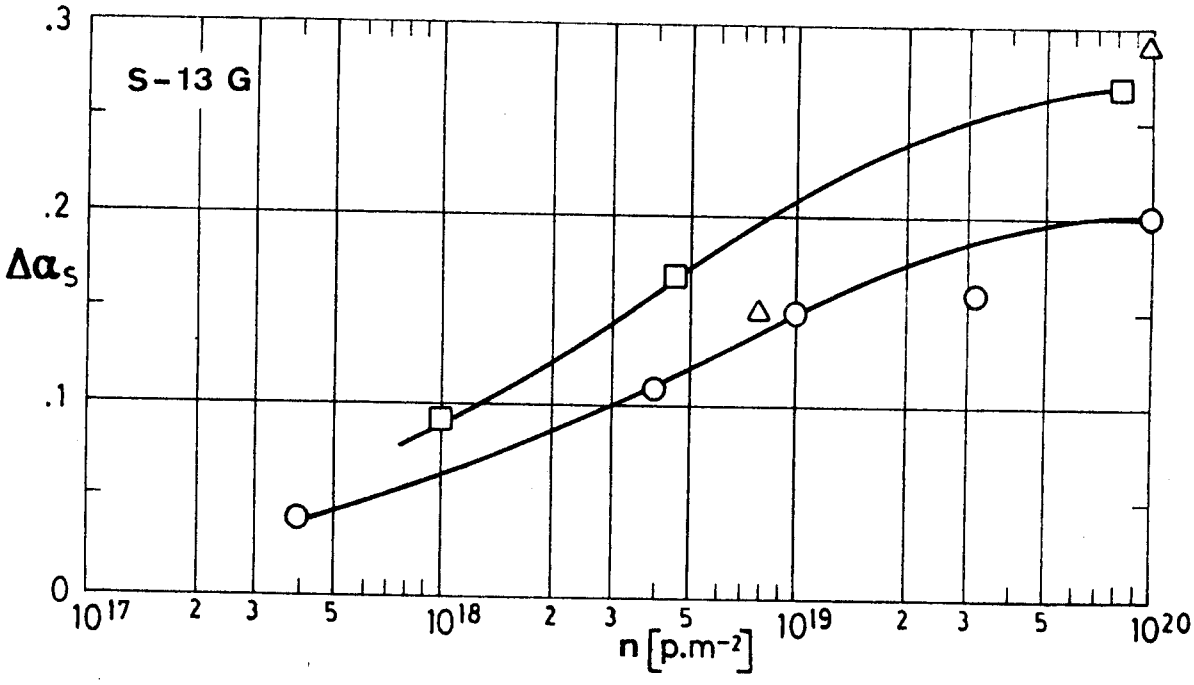

Fig 1-48.6. Change in solar absorptance, $\Delta\alpha_s$, of S-13 G coating due to Electrons Radiation vs. integrated flux, n. Data taken in situ. Compiled by Bourrieau, Paillous & Romero (1976).

Explanation

Key	Intensity [keV]	Flux [e.m^{-2}.s^{-1}]	T [K]
○	35	10^{14} - 7 x 10^{14}	291
□	50	2 x 10^{14} - 5 x 10^{15}	295
△	80		281

COATINGS

Solar Reflectors

7.3.2.5.5. Contamination. Changes in α_s and ε of S-13 G coating due to rocket exhaust impingement have been given by McCargo et al. (1971). The results are hardly useful due to their very limited scope (they depend on the motor generating the exhaust products) and to the inability to reproduce the space environment on a laboratory scale. The main phenomena inducing contamination and (or) degradation are heating, chemical reactions, deposition of solid particles and liquids, and erosion.

No change in emittance was observed, but the change in solar absorptance was appreciable.

Exhausts from non-chemical thrusters also affect the optical properties of the coating.

Results are summarized in the table below.

t [h]	ε	α_s	α_s/ε
0	.880	.163	.185
.167	.872	.309	.354
.667	.877	.344	.392
3.25	.876	.338	.386

From McCargo, Spradley, Greenberg & McDonald (1971).

7.3.2.5.6. Combined exposure

The available information regarding in flight meas-

COATINGS

Solar Reflectors

urements of solar absorptance is summarized in the following.

The experiments performed both before and during OSO III flight are described in Millard (1969) and Millard & Pearson (1973). An uncertitude analysis is given in Millard (1968).

a) Laboratory tests. The coatings were bombarded with Ultra-Violet radiation, 2 and 10 keV protons. and both UV and protons.

UV irradiations were made with a Xenon lamp and a mercury arc lamp at one Sun level up to 265 h, and with mercury arc lamps at 10 Suns intensity for the remaining ESH. Mercury arc irradiation at one Sun level seems to match the flight data to about 1 000 ESH.

Data were taken in situ.

Coating	UV [ESH]	p $[p.m^{-2}]$	UV + p [ESH + $p.m^{-2}$]	$\Delta\alpha_s$ UV	$\Delta\alpha_s$ p	$\Delta\alpha_s$ UV + p
S-13	90	$.43x10^{19}$	$90(.28x10^{20})$	.08	.01	.06
	432	$1.3x10^{19}$	$432(1.1x10^{20})$	.10	.02	.09
	1 098	$3x10^{20}$	$1\ 098(2.8x10^{20})$	.11	.10	.19
S-13 G	750	$2x10^{19}$	$750(2x10^{19})$	.01	.05	.08

From Millard (1969).

b) Flight Experiments. OSO III was launched on March 8, 1967 in a near circular orbit (of about 550 km)

COATINGS

Solar Reflectors

with a 33° angle of inclination relative to the Equator. The zone of the spacecraft on which the experiment was mounted continually spun at a rate of about 37 rpm. The plane of spin contained the satellite-Sun line. Thus the sensors alternatively viewed Sun and Earth without being affected by this spin because of their relatively large thermal mass. Upper and lower temperatures for each orbit were 255 K and 210 K respectively.

Data from OSO III coatings experiment up to four years are given by Millard & Pearson (1973).

Unfortunately, in the case of S-13, data are only available up to 2 400 ESH, afterward the temperature of the calorimeter exceeded the instrumentation range. On the other hand figures for S-13 and S-13 G in the mentioned reference are the same as those in 1969 Millard's paper.

The results, see Fig 1-48.7 overleaf, do not compare well with previous tests. It seems that the degradation of S-13 G coating depends on the exact method of preparation (see, however, comments in p. 1-48.36).

Figures 1-48.8 and 1-48.9 show data from several coatings experiments as compiled from Touloukian, DeWitt & Hernicz (1972). Agreement for the Pegasus I

COATINGS

Solar Reflectors

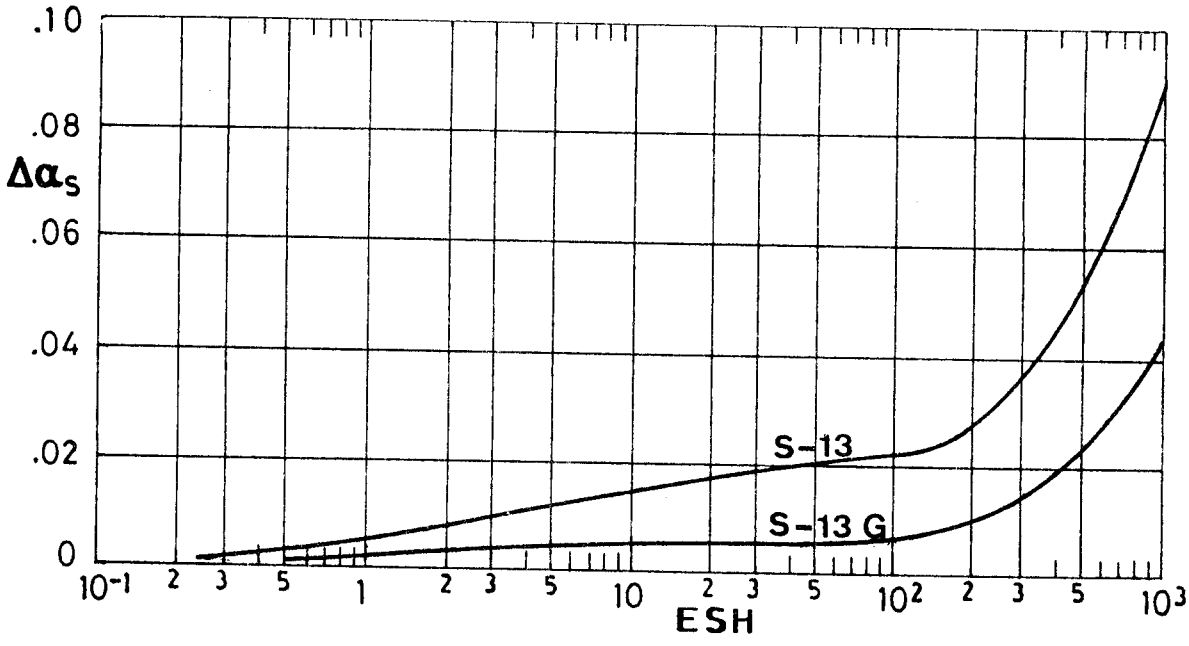

Fig 1-48.7. Changes in solar absorptance of S-13 and S-13 G coatings. OSO III experiment. From Millard (1969).

and II, OSO II and III is excellent. In flight contamination looks negligible for all four flights. Data for Mariner V and ATS-1 exhibit increased damage due to the particulate environment in deep space.

Comparison of the S-13 and S-13 G data confirms the increased protection in the later due to the silicate treated binder. This is now generally accepted, nevertheless, information on the contrary from the early seventies can be found (see f.e. Keyte (1972), p. 38). Although the reasons for the discrepancies remain unclear, they could be due to an unappropriate manipulation of the coating.

COATINGS

Solar Reflectors

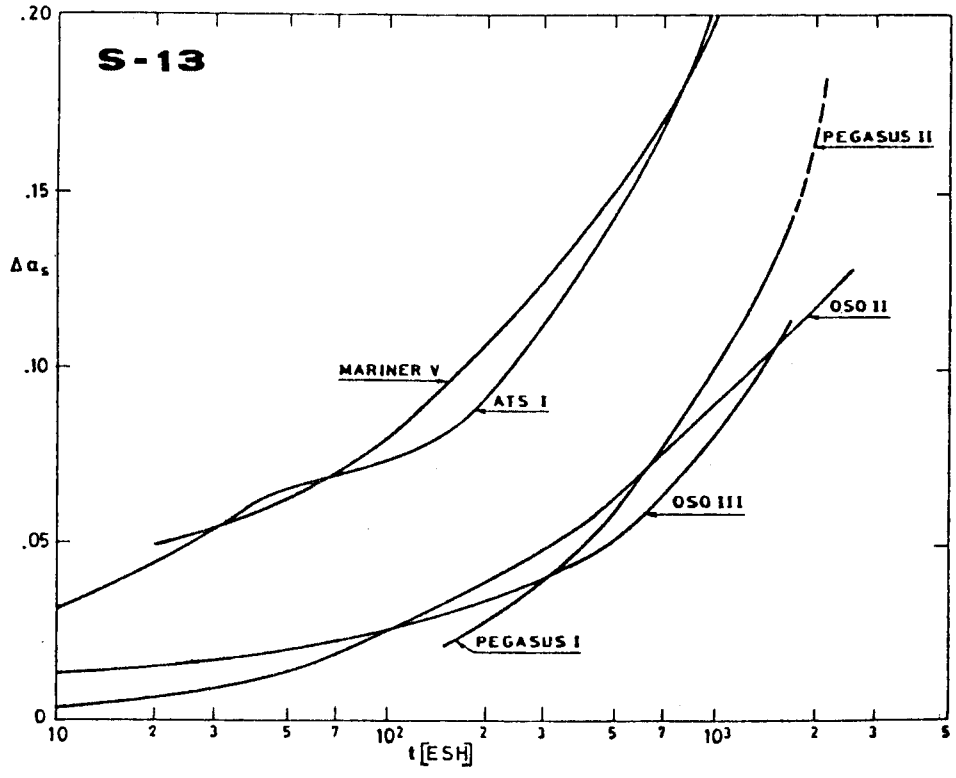

Fig 1-48.8. Change in solar absorptance, $\Delta\alpha_s$, of S-13 coatings vs. flight time in ESH as measured in orbital flight. Prepared by the compiler after Touloukian, DeWitt & Hernicz (1972).

Explanation

Satellite	Orbit Altitude [km]	Inclination [deg]	Duration of Data Acquisition [mo]
OSO II	550-630	33	16
OSO III	540-560	33	< 1
Pegasus I	500-740	32	< 26
Pegasus II	510-750	32	< 23
ATS I	35 790	0	< 4
Mariner V	Deep Space Venus probe	-	-

COATINGS

Solar Reflectors

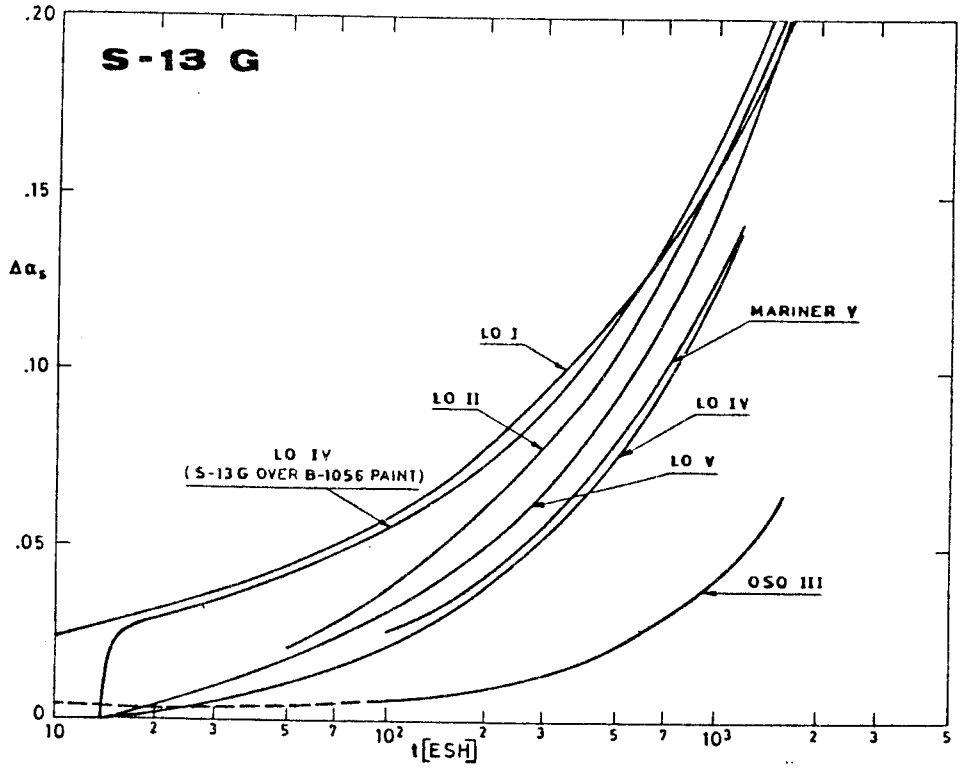

Fig 1-48.9. Change in solar absorptance, $\Delta\alpha_s$, of S-13 G coating vs. flight time in ESH as measured in orbital flight. Prepared by the compiler after Touloukian, DeWitt & Hernicz (1972).

Explanation

Satellite	Orbit Altitude [km]	Inclination [deg]	Duration of Data Acquisition [mo]
OSO III	540-560	33	< 1
Mariner V	Deep Space Venus probe	-	-
Lunar Orbiter I			
Lunar Orbiter II	-	-	-
Lunar Orbiter IV			
Lunar Orbiter V			

COATINGS

Solar Reflectors

More recent experimental data on S-13 G, plasma annealed and potassium silicate treated binder, are given in the adjacent table. Measurements have been performed in situ. Spectral reflectance curves and additional information are given in p. 1-48.61. Experimental data for S-13 G/LO on Al substrate are summarized in Table 1-7.6 overleaf, after DERTS.

Exposure	$\Delta\alpha_s$
600 ESH + 668 EWH	.044
Above plus 700 ESH	.065
Above plus O_2 bleaching	.032

From Gilligan and Zerlaut (1971).

CAUTION

See pp. 1-59 and 1-60. Now the initial value of the solar absorptance is:

$$\alpha_{so} = .18$$

The tests simulate geoshynchronous orbit exposure of the OTS equatorial faces. See **S** , Chap. 2.

Solar absorptance deduced from spectral reflectance (see pp. 1-48.63 to 1-48.65).

Two samples (here labelled Sample 1 and Sample 2) were tested among several others. Fig 1-48.10 shows the location of the different samples during the irradiation.

Test conditions are the same as in Table 1-13, p. 1-76. Irradiation and measurement procedures are explained in pp. 1-74 and 1-75.

COATINGS

Solar Reflectors

Table 1-7.6

Combined Exposure Effects on Solar Absorptance of S-13 G/LO Coating

Test Conditions	Sample 1						Sample 2					
	Measured in situ			Corrected [a]			Measured in situ			Corrected [a]		
	α_s	$\Delta\alpha_s$	$\Delta\alpha_s/\alpha_s$	α_s	$\Delta\alpha_s$	$\Delta\alpha_s/\alpha_s$	α_s	$\Delta\alpha_s$	$\Delta\alpha_s/\alpha_s$	α_s	$\Delta\alpha_s$	$\Delta\alpha_s/\alpha_s$
BEFORE IRRADIATION	.336			.180			.343			.180		
AFTER A UNDER VACUUM [b]	.456	.120	.358	.329	.149	.828	.471	.128	.373	.339	.159	.883
BEFORE B	.395	.059	.176	.253	.073	.406	.400	.057	.167	.251	.071	.394
AFTER B [b]	.517	.181	.539	.405	.225	1.250	.531	.188	.547	.414	.234	1.300
AFTER PUMP DAMAGE [c]	.384	.049	.146	.241	.061	.339	.391	.048	.139	.240	.060	.333
BEFORE C	.419	.083	.248	.283	.103	.572	.423	.080	.233	.279	.099	.550
AFTER C [b]	.537	.201	.600	.430	.250	1.388	.545	.202	.589	.413	.251	1.394
BEFORE D	.513	.177	.528	.400	.220	1.222	.519	.176	.514	.399	.219	1.217
AFTER D UNDER VACUUM [b]	.594	.258	.770	.501	.321	1.783	.599	.256	.746	.498	.318	1.767
AFTER D AND AIR EXPOSURE	.530	.194	.577	.421	.241	1.339	.541	.198	.577	.426	.246	1.367

[a] The correction has been made by the compiler as follows:

1) Value before irradiation, $\alpha_{so} = .18$

2) $$\frac{\Delta\alpha_{s\,corrected}}{\Delta\alpha_{s\,in\ situ}} = \frac{1 - \alpha_{so}}{1 - \alpha_{so\,in\ situ}} = \frac{.82}{.66}$$

where α_{so} has been measured (in air) with an integrating sphere attached to a Beckman DK2A reflectometer. $\alpha_{so\,in\ situ}$ is the value measured, before irradiation, as indicated in p. 1-65.

[b] Steps A to D correspond, respectively, to the following times in geosynchronous orbit.

A: .18 yr = 508 ESH
B: .94 yr = 2 443 ESH
C: 2.11 yr = 5 604 ESH
D: 3 yr = 7 949 ESH

[c] See p. 1-75 for further details.

From Paillous (1976).

COATINGS

Solar Reflectors

The "Corrected" values in Table 1-7.6 were used to estimate the degradation of the coating up to 3 years in orbit. Results are represented in Fig 1-48.11. Incidents during testing, see p. 1-75, could cast some doubts on the validity of the data beyond 1 year in orbit. Nevertheless, the comparison with OTS measurements, up to three years, is excellent, as can be seen in the figure.

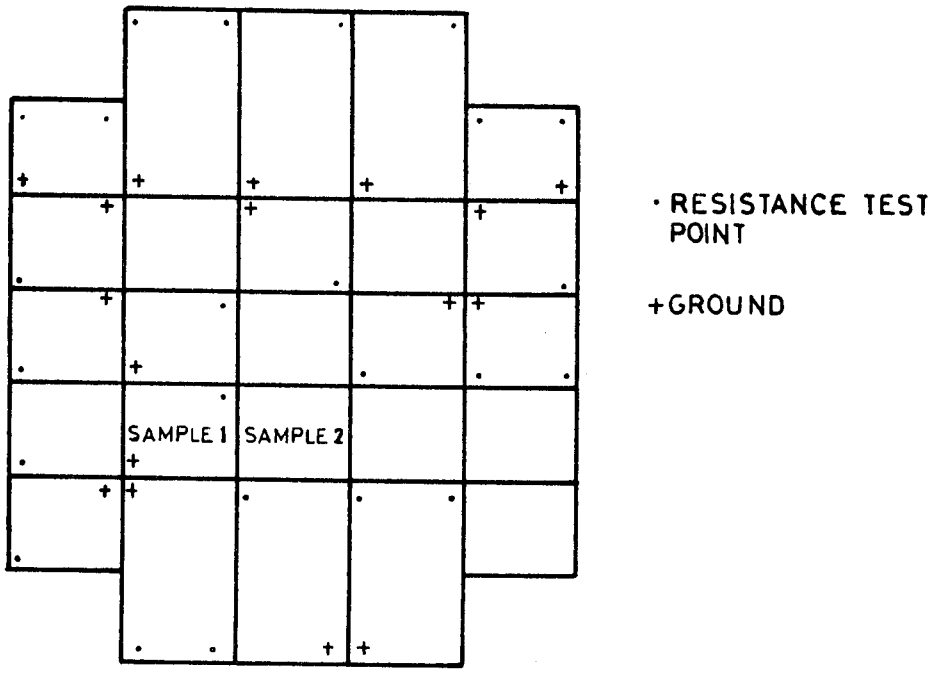

Fig 1-48.10. Position on the sample holder of the samples 1 and 2, for irradiation and measurement. From Paillous (1976).

Data in Fig 1-48.11 are recent in orbit measurements. They correspond to OTS and Navstar 6, respectively. The coating is S-13 G/LO.

COATINGS

Solar Reflectors

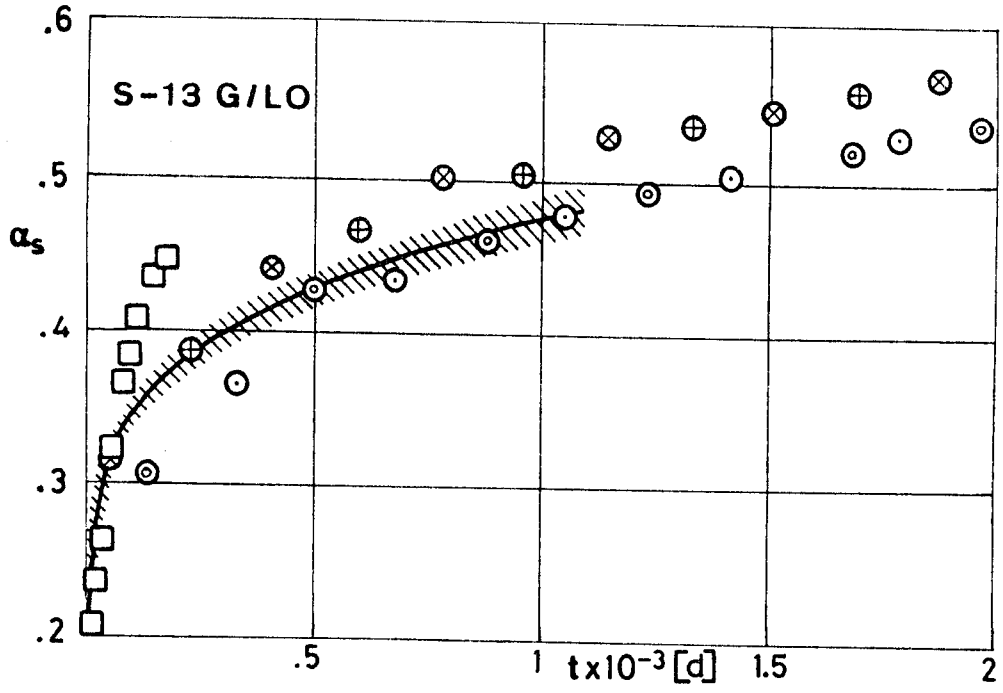

Fig 1-48.11. Solar absorptance, α_s, of S-13 G/LO coating vs. flight time, t.

○ OTS, see p. S 2-10.

⊗ SS
⊕ WS
⊙ VE
◎ AE

From Chalmers, Konzok, Bouchez & Howle (1983).

⫽ Prediction, up to three years in orbit by Paillous (1976). See Table 1-7.6, p. 1-48.30.

□ Navstar 6

From Pence & Grant (1981).

OTS was launched in May 11, 1978 in a geostationary orbit 35 779 km - 35 072 km.
Navstar 6 was launched in April 26, 1980. Orbit altitude 170 km - 20 288 km. Inclination 63.02°.
The reasons for the severe degradation of the coatings tested onboard Navstar series are unclear.
See pp. 1-123 and 1-40.2.

COATINGS

Solar Reflectors

7.3.2.6. Effects of the Space Environment on solar absorptance to emittance ratio. Results from several flight experiments are given in Figs 1-48.12 and 1-48.13.

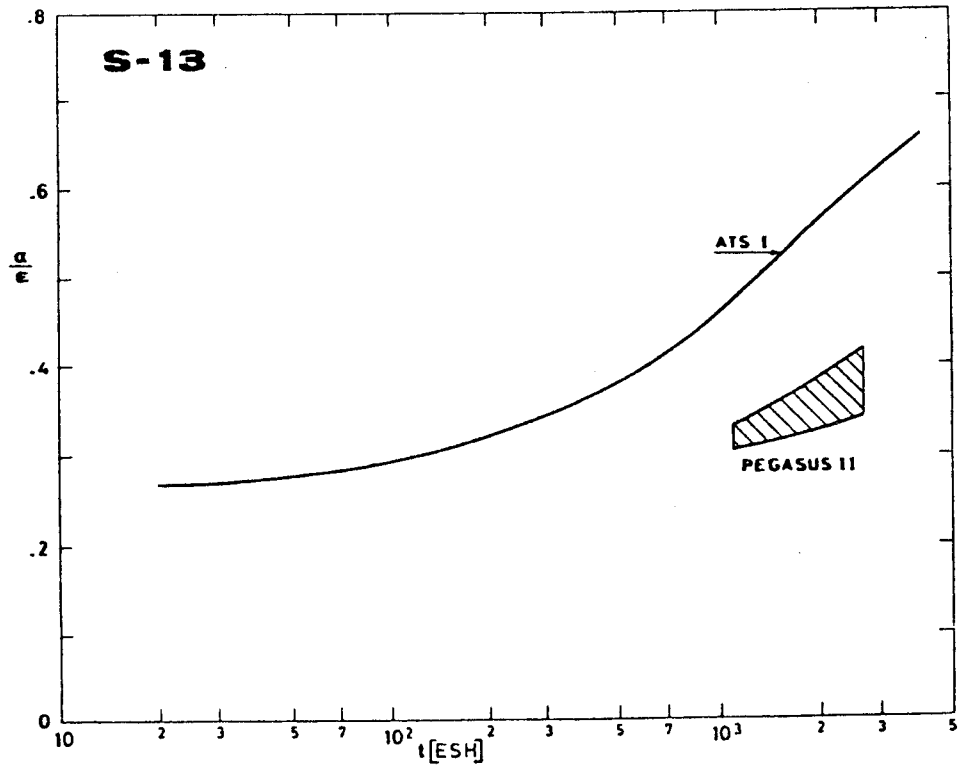

Fig 1-48.12. Variation of absorptance to emittance ratio, α/ε, of S-13 coating vs. flight time. Prepared by the compiler after Touloukian, DeWitt & Hernicz (1972) and Triolo (1973).

Explanation

Satellite	Orbit Altitude [km]	Inclination [deg]	Duration of Data Acquisition [mo]
Pegasus II	510-570	32	< 23
ATS I	35 790	0	< 36

COATINGS

Solar Reflectors

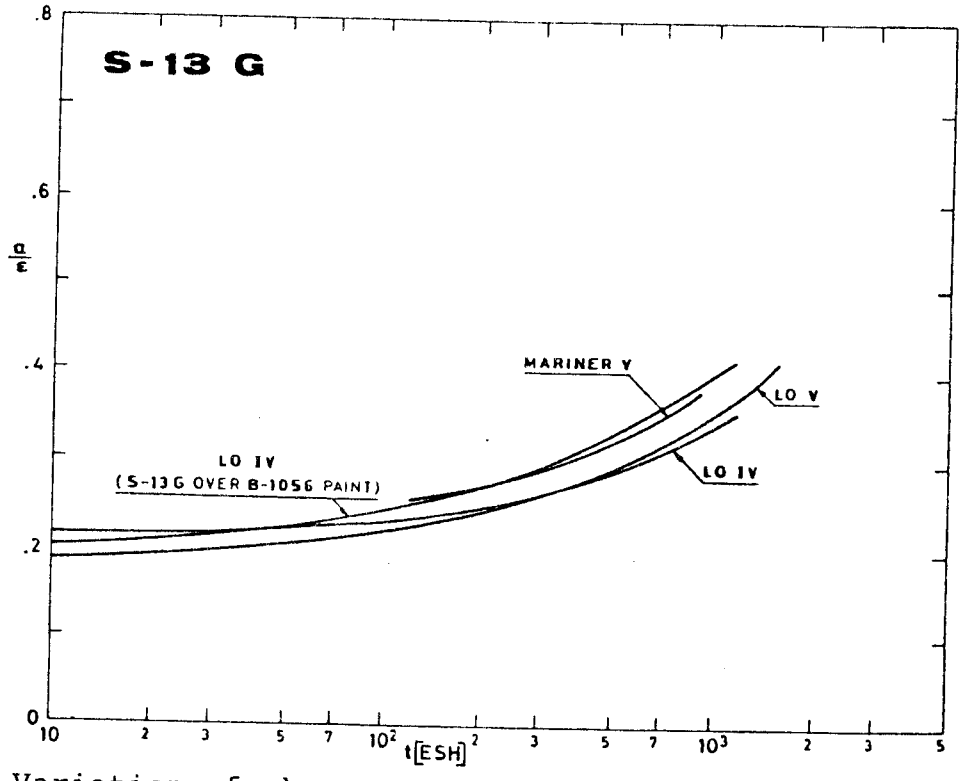

Fig 1-48.13. Variation of absorptance to emittance ratio, α/ε, of S-13 G coating vs. flight time. Prepared by the compiler after Touloukian, DeWitt & Hernicz (1972).

Explanation

Satellite	Orbit Altitude [km]	Inclination [deg]	Duration of Data Acquisition [mo]
Mariner V	Deep Space Venus probe		
Lunar Orbiter IV			
Lunar Orbiter V			

7.3.3. Reflectance.

7.3.3.1. Normal-hemispherical spectral reflectance. The available information regarding slightly different coating preparations is abundant. As an example Fig 1-48.14 shows the influence of pigment volume concentration (P-VC) on spectral reflectance.

COATINGS

Solar Reflectors

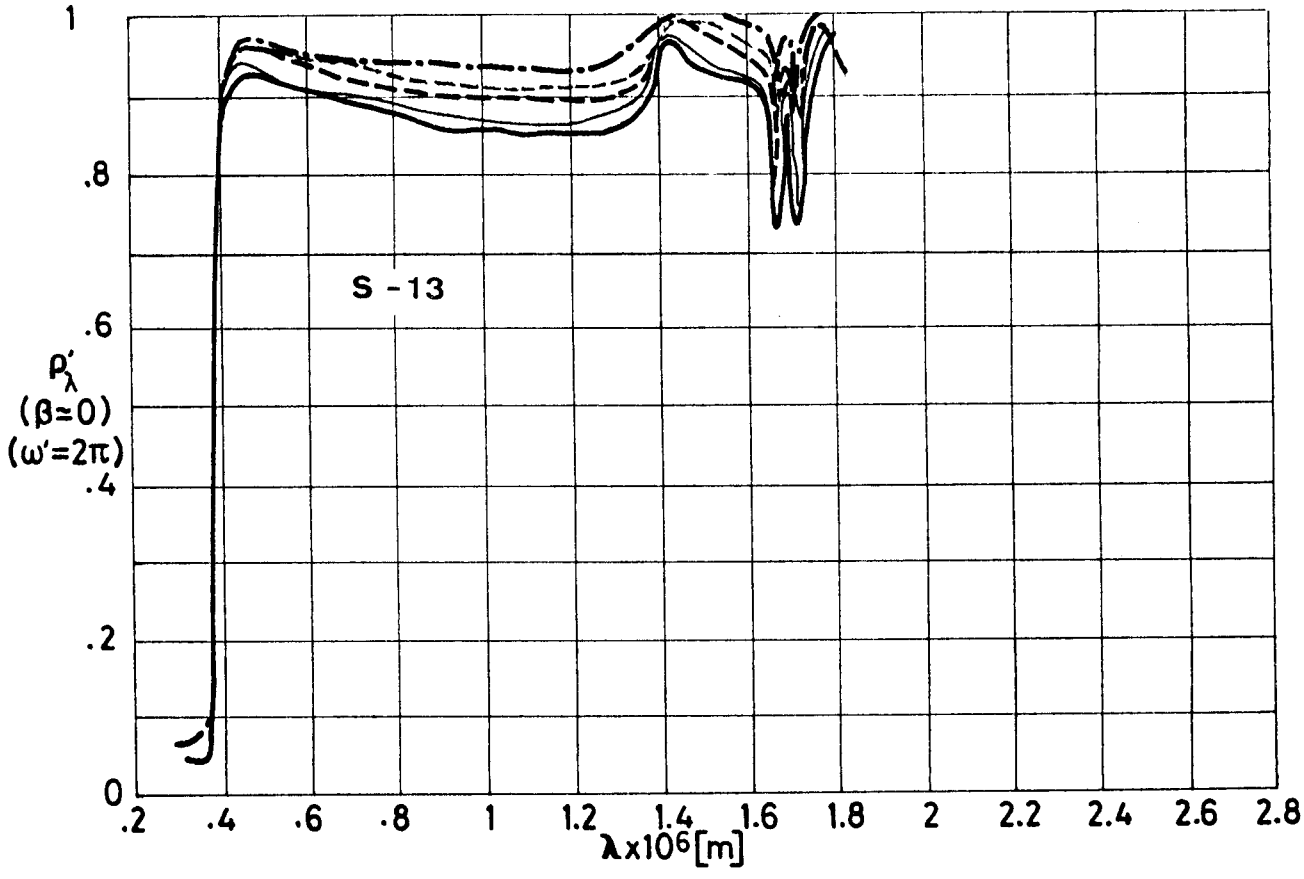

Fig 1-48.14. Normal-hemispherical spectral reflectance, ρ'_λ, of S-13 coating vs. wavelength, λ, for five different values of P-VC. G.E. LTV-602 binder. From Touloukian, DeWitt & Hernicz (1972).

Explanation

Key	P-VC	Comments
———	15	.17 x 10^{-3} m thick 6061 Al substrate. T ∿ 298 K Measured relative to magnesium carbonate. P-VC is the pigment volume concentration, percent
———	20	
– – – –	25	
– – – –	35	
—·—	40	

COATINGS

Solar Reflectors

7.3.3.2. Effects of the Space Environment on reflectance

7.3.3.2.1. Ultra-Violet Radiation. We will mention two points:

1st. Stability of these coatings to UV radiation strongly depends on their composition. The optimum composition has been obtained after a lengthy process and data exist to evaluate the sensibility of the coatings to small changes in composition.

2nd. Ex situ vs. in situ measurements. Up to 1965, the standard practice for space simulation was to irradiate the coatings with UV under vacuum, performing the measurements ex situ. Since a recovery exists after breaking vacuum, early flight tests showed an extreme degradation not foreseen at the light of the space simulation tests.

Figures 1-48.15 and 1-48.16 show the influence of pigment-binder ratio (PBR) on the stability against UV radiation. Data after irradiation have been obtained from ex situ measurements.

Figures 1-48.17 and 1-48.18, on the other hand, compare in situ with ex situ measurements.

Figure 1-48.18 indicates that S-13 exhibits a reflectance decrease of about 35% at $\lambda = 2 \times 10^{-6}$ m after approximately 800 ESH of UV radiation in vacuum and an almost instantaneous increase when the irradiated specimen is admitted to the atmosphere.

COATINGS

Solar Reflectors

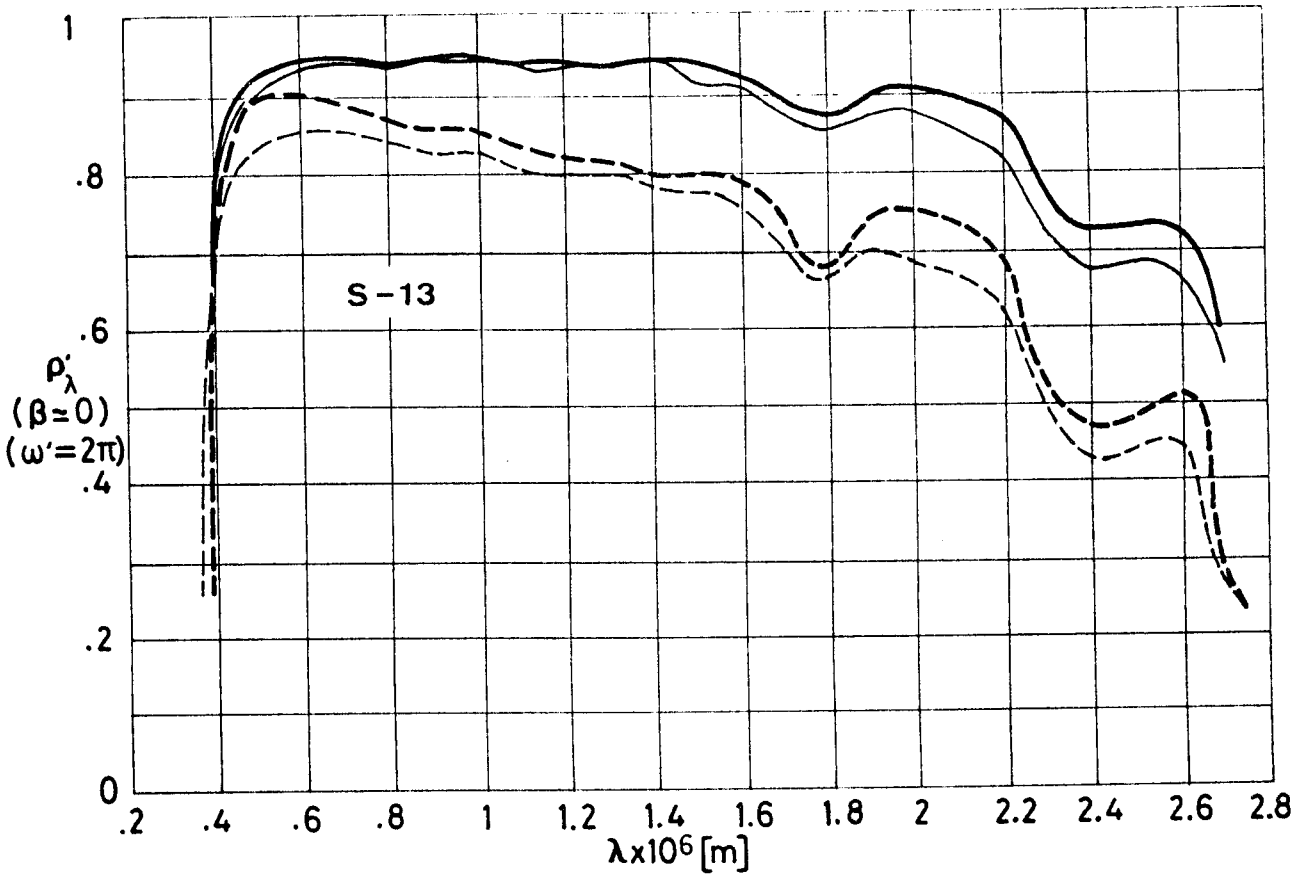

Fig 1-48.15. Effect of Ultra-Violet Radiation on normal-hemispherical spectral reflectance, ρ'_λ, of S-13 coating vs. wavelength, λ. LTV-602 silicone binder. Two different pigment-binder ratios (PBR). From Touloukian, DeWitt & Hernicz (1972).

Explanation

Key	PBR	P-VC	Exposure	Comments
———	3.73	40	In vacuum before irradiation.	Sample on Al substrate. Airbrush application T ∿ 298 K Exposed in vacuum. p ∿ $1.33x10^{-3}$ Pa. Measured ex-situ
———			UV. 1 200 ESH.	
- - -	1.40	20	In vacuum before irradiation.	Above specimen and conditions except Catalyst G.E. SRC-04 and toluene as solvent
- - -			UV. 1 460 ESH.	

COATINGS

Solar Reflectors

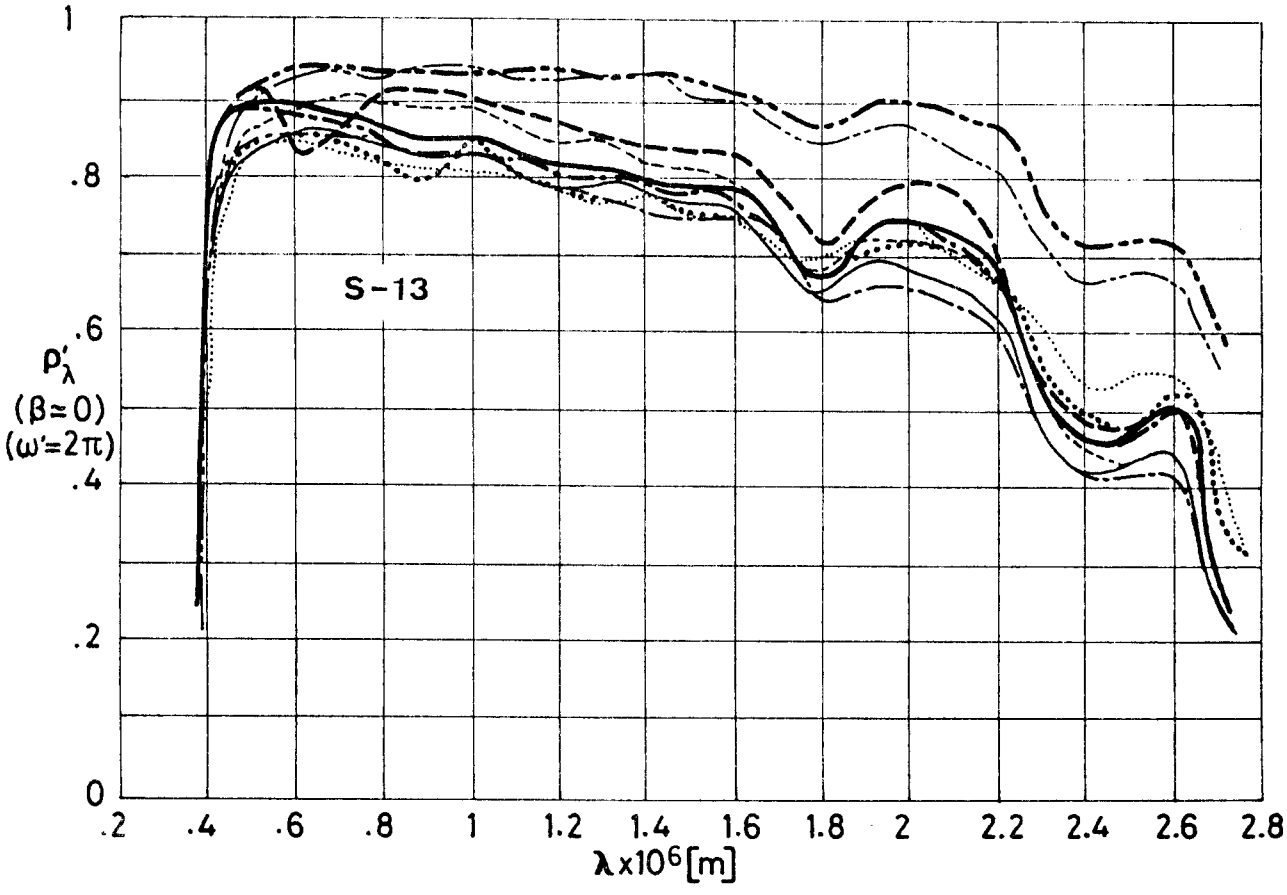

Fig 1-48.16. Effect of Ultra-Violet Radiation on normal-hemispherical spectral reflectance, ρ'_λ, of S-13 coating vs. wavelength, λ. Several binders and PBRs. From Touloukian, DeWitt & Hernicz (1972).

Explanation

Key	Binder	Me-Si Ratio	PBR	P-VC	Exposure	Comments
———	LTV-602		1.40	20	In vacuum before irradiation.	Catalyst, G.E. SRC-04; solvent, toluene. Sample on Al substrate. Airbrush application. T ∿ 298 K. Exposed in vacuum. p ∿ 1.33 x 10^{-5} Pa. Measured ex situ.
———					UV. 1 460 ESH.	
- - -	R-2	1.46	1.70	25	In vacuum before irradiation.	
- - -					UV. 1 460 ESH.	
—·—	R-5	1.38	1.63	25	In vacuum before irradiation.	
—·—					UV. 1 460 ESH.	
·····	R-7	1.33	1.64	25	In vacuum before irradiation.	
·····					UV. 1 600 ESH.	
—— —	LTV-602		3.73	40	In vacuum before irradiation.	
—— —					UV. 1 200 ESH.	

COATINGS

Solar Reflectors

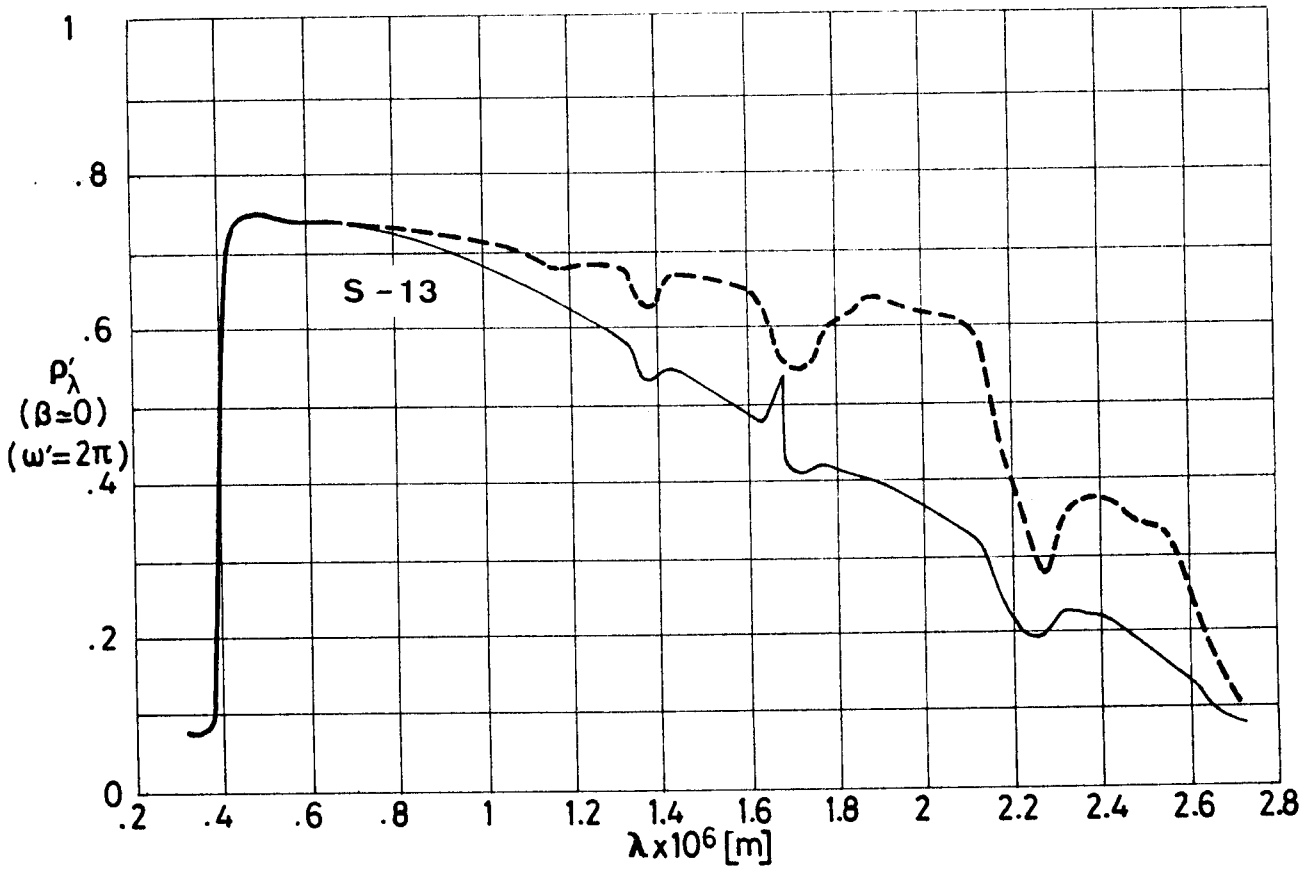

Fig 1-48.17. Effect of Ultra-Violet Radiation on normal-hemispherical spectral reflectance, ρ'_λ, of S-13 coating vs. wavelength, λ. From Touloukian, DeWitt & Hernicz (1972).

Explanation

Key	Exposure	Comments
———	In vacuum before irradiation.	T ∿ 298 K Measured and exposed in situ.
———	UV. 1 200 ESH.	
– – –	Above after breaking vacuum.	Recovery is complete.

COATINGS

Solar Reflectors

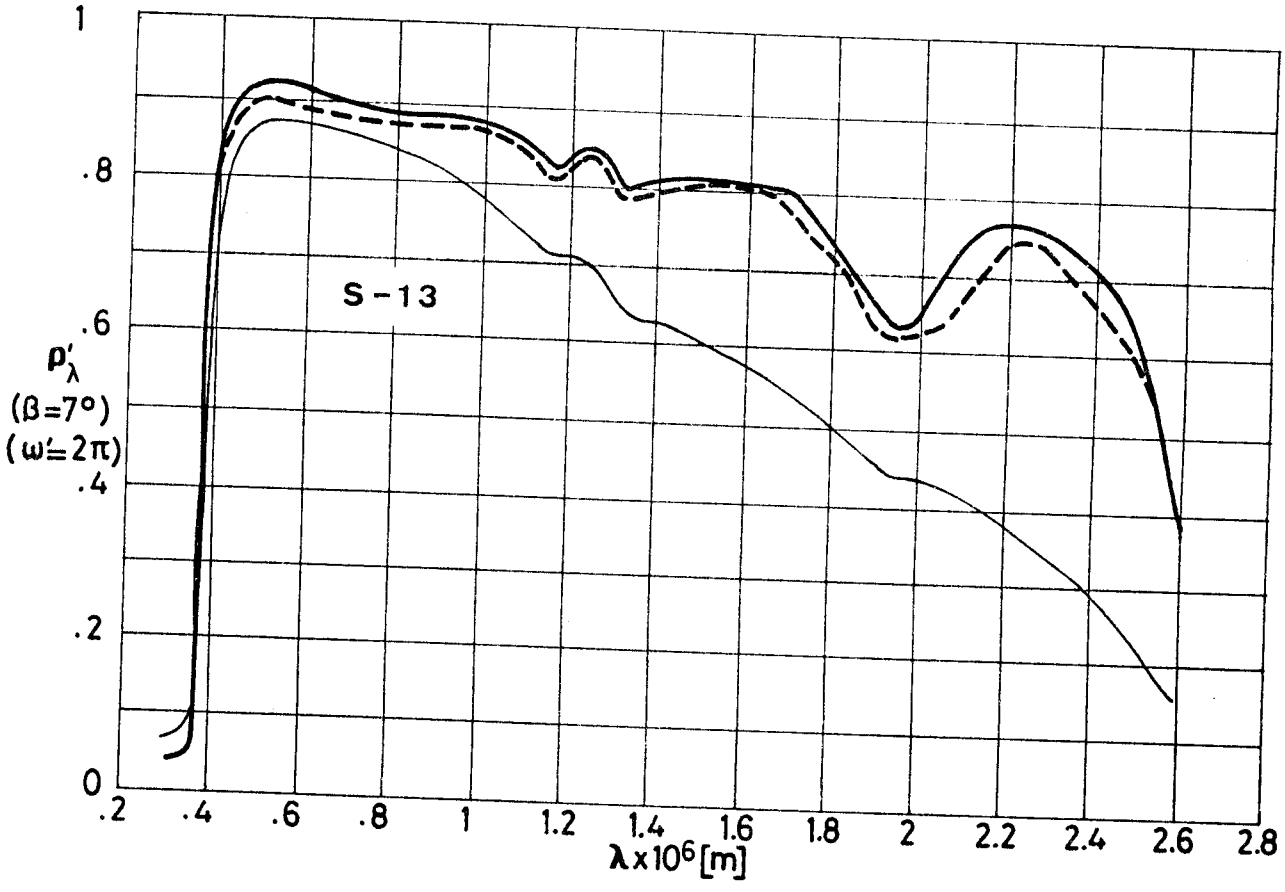

Fig 1-48.18. Effect of Ultra-Violet Radiation on normal-hemispherical spectral reflectance, ρ'_λ, of S-13 coating vs. wavelength, λ. From Zerlaut, Rogers & Noble (1969). Drawn from Touloukian, DeWitt & Hernicz (1972).

Explanation

Key	Exposure	Comments
———	In vacuum before irradiation.	T ∿ 298 K. p ∿ 1.33 x 10^{-5} Pa. Measured and exposed in-situ. UV source G.E. AH-6 lamp. IITRI test facility (In situ Reflectometer Irradiation Facility, see Zerlaut & Courtney (1967)). α_s and $\Delta\alpha_s$ in p. 1-48.19.
———	UV. 800 ESH.	
- - - -	Above after breaking vacuum.	

COATINGS

Solar Reflectors

Figures 1-48.19 to 1-48.24 present data taken when optimizing the composition of S-13 G.

Figure 1-48.19 compares sweating (see p. 1-48.1) versus sweating and calcining. Calcination of the sweated pigment decreases the stability in the infrared. This could be due to the greater grinding required to reduce the calcined pigment which yields ZnO surfaces devoided of barriers to photodesorption reactions which produce the bleachable degradation.

Figure 1-48.20 shows partial results in the process of solvent optimization. Originally toluene was used as the sole solvent. This resulted in excessive spray dust, in very poor shelf life, and in the production of "orange peel" in RTV-602 films (a pock marked appearance due to film failure to flow out to a level surface).

Films from solutions containing petroleum ether showed inferior stability. Paints prepared from sweated pigment are less sensitive to solvent composition. The optimum composition resulted to be

Toluene	40% by weight
Xilene	20% by weight
n-Butanol	15% by weigth
Isopropanol	20% by weight
Butyl acetate	5% by weight

This composition provides: 2 weeks shelf life, good spray flow-out, and good cure characteristics.

COATINGS

Solar Reflectors

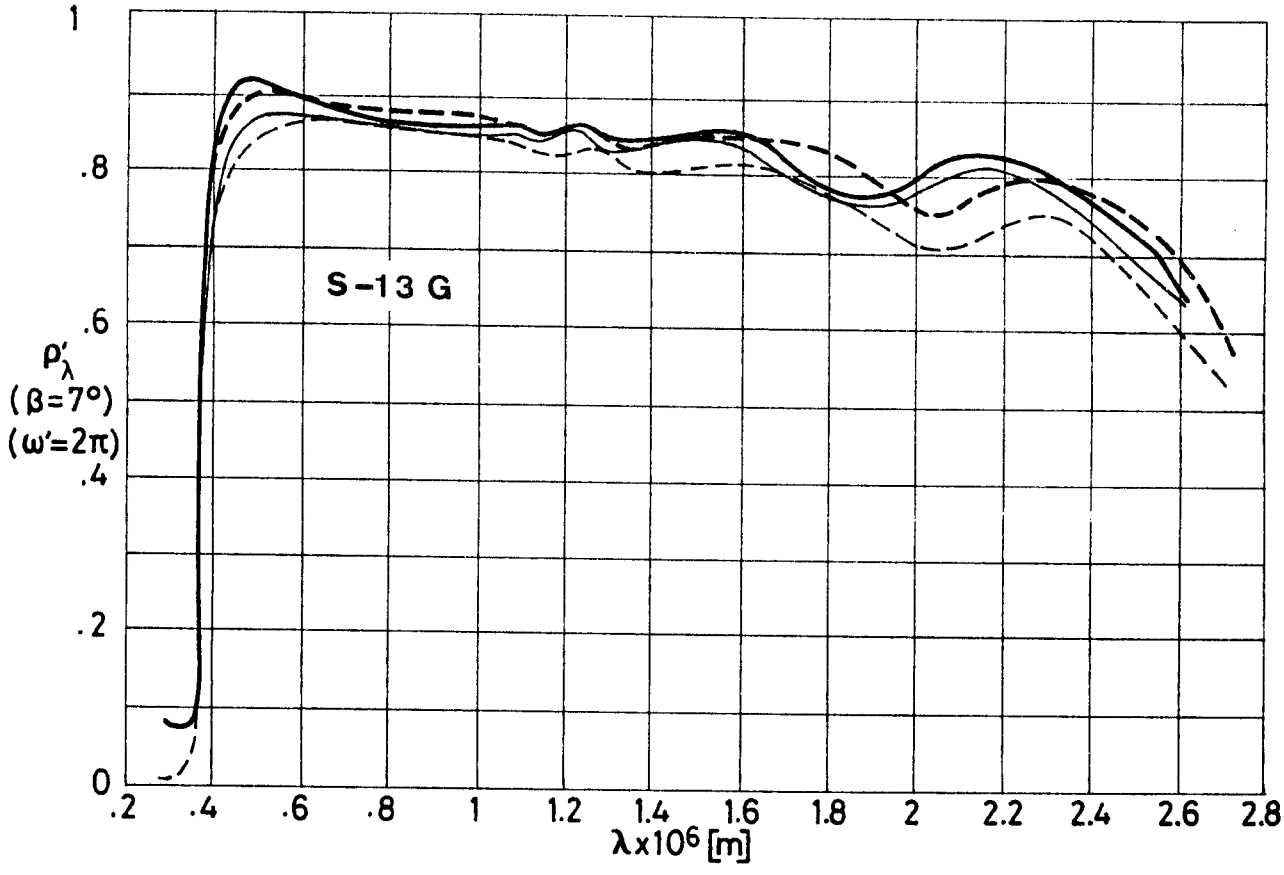

Fig 1-48.19. Effect of Ultra-Violet Radiation on normal-hemispherical spectral reflectance, ρ'_λ, of S-13 G coating vs. wavelength, λ. Two different pigment treatment processes. From Zerlaut, Rogers & Noble (1969). Drawn from Touloukian, DeWitt & Hernicz (1972).

Explanation

Key	Pigment Treatment	Exposure	Comments
———	16 h. sweating. Solvent toluene	In vacum before irradiation.	T ∿ 298 K. p ∿ 1.33 x 10^{-5} Pa. Measured and exposed in situ. UV source G.E. AH-6 lamp. IITRI test facility (In situ Reflectometer Irradiation Facility, see Zerlaut & Courtney (1967)). α_s and $\Delta\alpha_s$ in p. 1-48.19.
———		UV. 600 ESH.	
– – –	Sweating, calcining for 16 h at 293 K.	In vacuum before irradiation	
– – –		UV. 600 ESH.	

COATINGS

Solar Reflectors

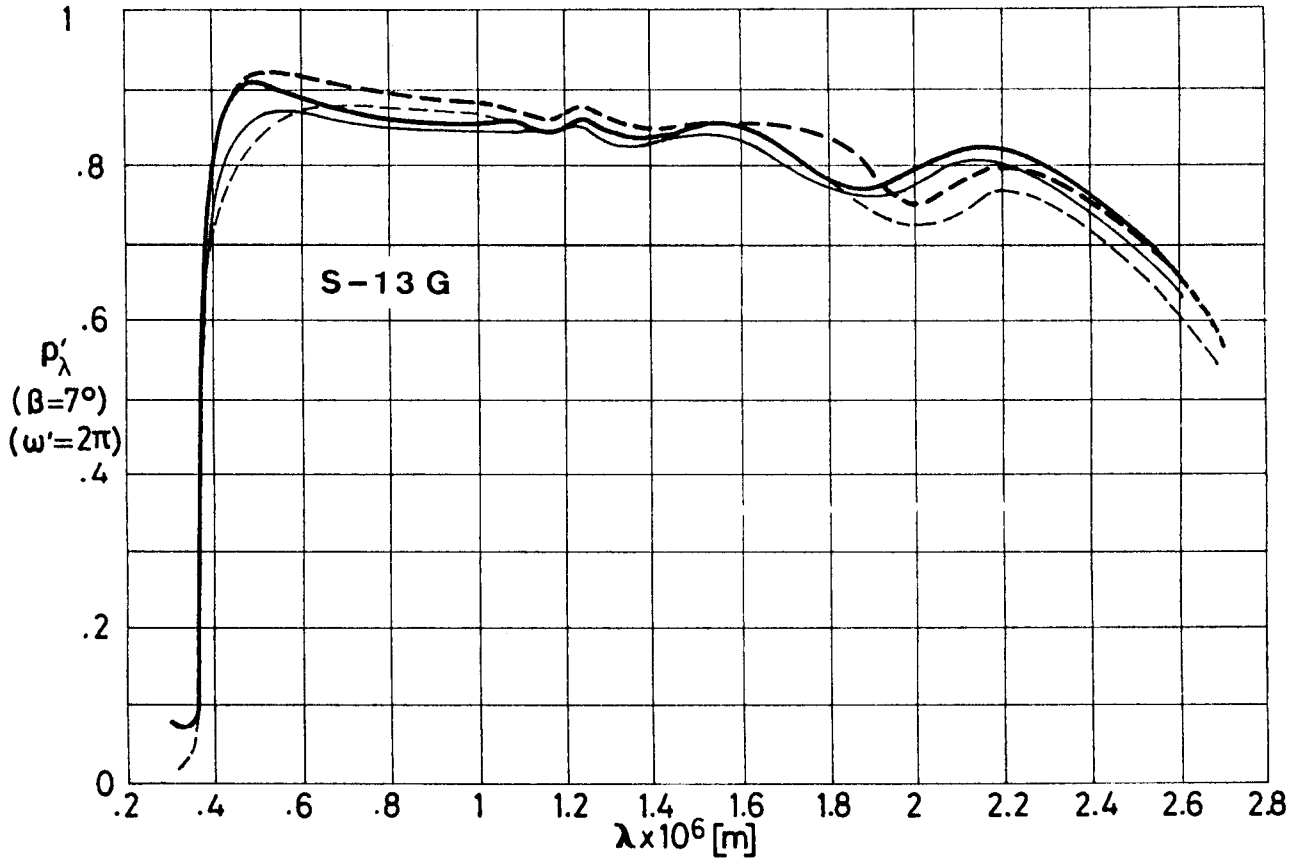

Fig 1-48.20. Effect of Ultra-Violet Radiation on normal-hemispherical spectral reflectance, ρ'_λ, of S-13 G coating vs. wavelength, λ. Sweated pigment. Two different solvent systems. From Zerlaut, Rogers & Noble (1969). Drawn from Touloukian, DeWitt & Hernicz (1972).

Explanation

Key	Solvent	Exposure	Comments
———	Toluene	In vacum before irradiation.	T ∿ 298 K. p ∿ 1.33 x 10^{-5} Pa. Measured and exposed in situ. UV source G.E. AH-6 lamp. IITRI test facility (In situ Reflectometer Irradiation Facility, see Zerlaut & Courtney (1967)). α_s and $\Delta\alpha_s$ in p. 1-48.19.
———		UV. 600 ESH.	
- - -	Toluene and petroleum ether	In vacuum before irradiation	
- - -		UV. 800 ESH.	

COATINGS

Solar Reflectors

Figure 1-48.21 shows results of two attempts made to neutralize the sweated pigment prior to manufacture. The specimen prepared from the sodium acid phosphate neutralized pigment exhibited the greatest UV stability that has been observed for S-13 G prepared from calcined pigment. On the other hand, stability at most wavelengths was destroyed by neutralization with formic acid.

Neutralization was required because in this case Owens-Illinois 650 resin was used. This resin is highly stable against UV irradiation and can be thermally cured at low temperatures without using catalysts. Unfortunately this causes nearly instantaneous gellation when mixed with silicate-treated zinc oxide. Gelled coatings exhibit a jelly-like condition.

Figures 1-48.22 and 1-48.23 show additional effects of different pigment treatment processes.

In Fig 1-48.22 pigment was sifted before wet grinding, a technique which is no longer used.

Reaction of ZnO with potassium silicate provides an effective barrier to photodesorption reactions on the surface of ZnO which the binder does not.

The idea behind this treatment was put forward in the Z-93 coating (see pp. 1-13 to 1-28) where the

COATINGS

Solar Reflectors

reactivity of ZnO with potassium silicate precluded the bleachable infrared degradation exhibited by ZnO powder and ZnO-silicone coatings.

Figure 1-48.23 deals with silicate treated pigments under different mechanical processes. The only difference between the different coatings was the manner in which the dried, treated ZnO powder was conditioned for grinding into the paint.

The data show that the stability to UV radiation in vacuum is an inverse function of the shear stress applied to the dry pigment prior to wet-grinding. A fivefold increase in damage, as measured by $\Delta\alpha_s$, was observed between the paint prepared from only sifted pigment and the hand-mulled prior to wet-grinding specimen (recall comment in p. 1-48.41 regarding Fig 1-48.19). Hand-mulling is no longer used after these studies.

Sifting out the millable pigment is a highly inefficient and costly technique, even though it permits shorter wet-grinding times and greater stability. At present only wet-grinding is used.

Figure 1-48.24 corresponds to the state of the art S-13 G coating.

From Zerlaut, Rogers & Noble (1969), Gilligan & Zerlaut (1971).

COATINGS

Solar Reflectors

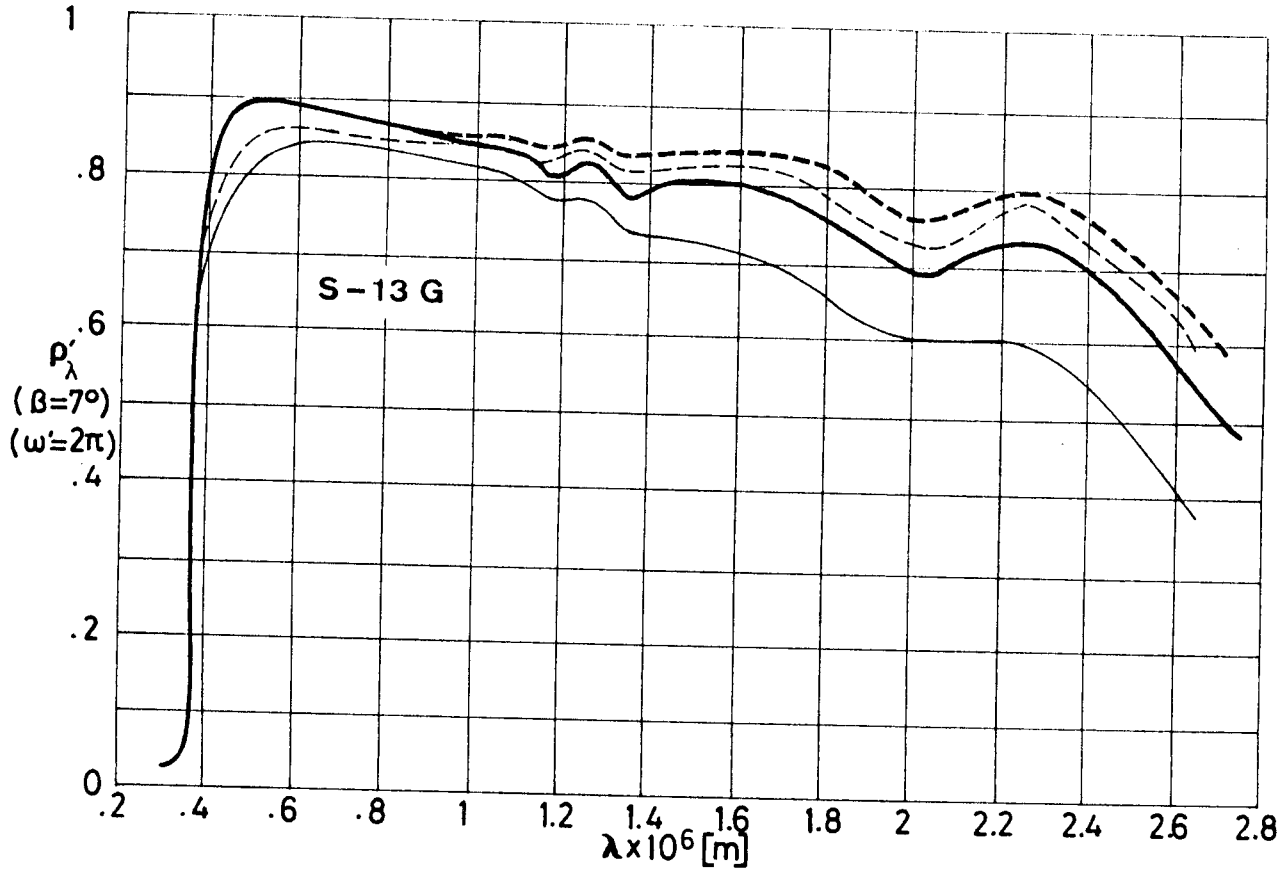

Fig 1-48.21. Effect of Ultra-Violet Radiation on normal-hemispherical spectral reflectance, ρ'_λ, of S-13 G coating vs. wavelength, λ. Two different pigment treatment processes. Owens-Illinois 650 binder. From Zerlaut, Rogers & Noble (1969). Drawn from Touloukian, DeWitt & Hernicz (1972).

Explanation

Key	Pigment Treatment	Exposure	Comments
———	Sweated, neutralized with formic acid and calcined for 16 h at 923 K.	In vacum before irradiation.	T ∿ 298 K. p ∿ 1.33 x 10^{-5} Pa. Measured and exposed in situ. UV source G.E. AH-6 lamp. IITRI test facility (In situ Reflectometer Irradiation Facility, see Zerlaut & Courtney (1967)). α_s and $\Delta\alpha_s$ in p. 1-48.19.
———		UV. 600 ESH.	
- - - -	Sweated, neutralized with sodium acid phosphate and calcined for 16 h at 923 K.	In vacuum before irradiation	
———		UV. 600 ESH.	

COATINGS

Solar Reflectors

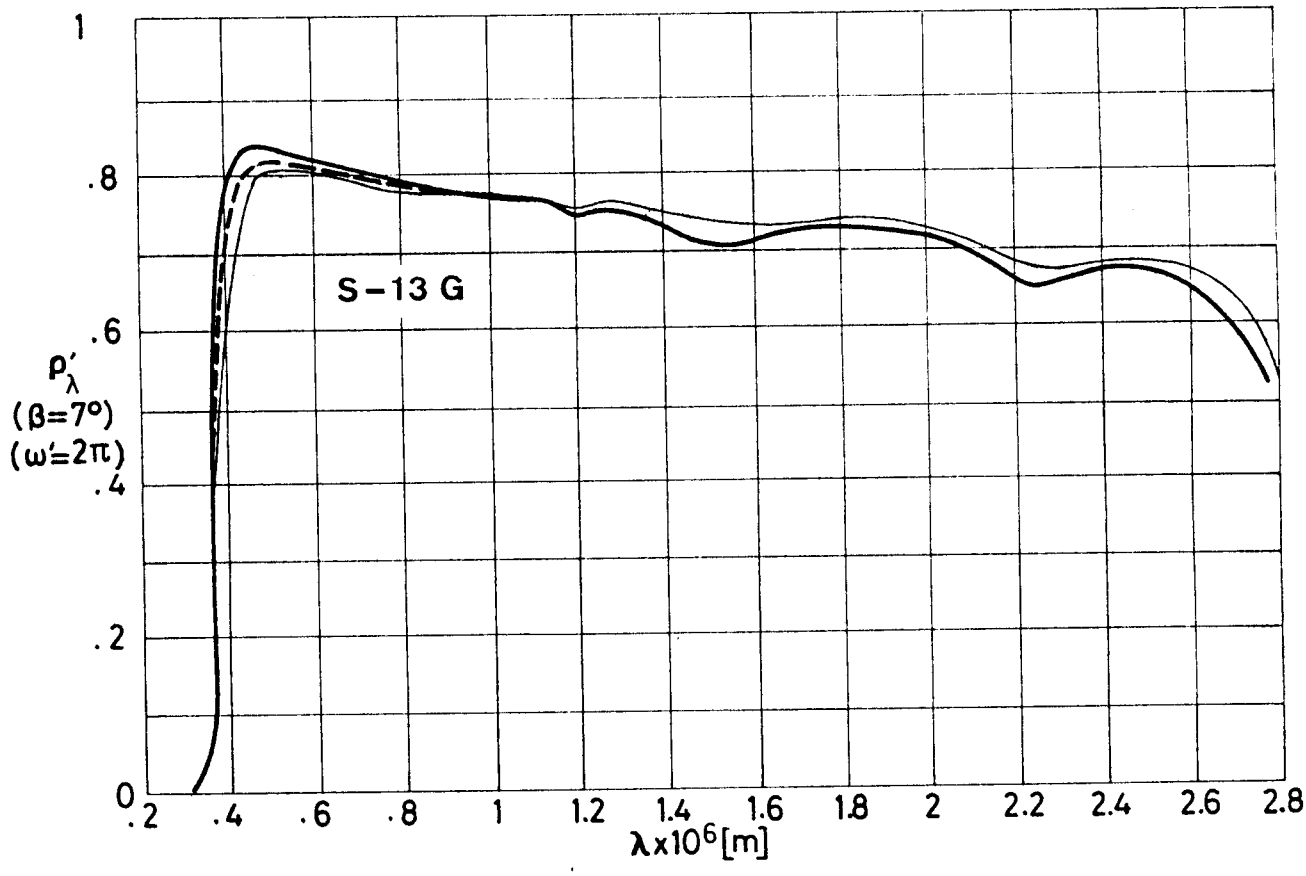

Fig 1-48.22. Effect of Ultra-Violet Radiation on normal-hemispherical spectral reflectance, ρ'_λ, of S-13 G coating vs. wavelength, λ. Pigment was sifted prior to wet grinding. Paint grind time 3 h. From Zerlaut, Rogers & Noble (1969). Drawn from Touloukian, DeWitt & Hernicz (1972).

Explanation

Key	Exposure	Comments
———	In vacuum before irradiation.	T ∿ 298 K. p ∿ 1.33 x 10^{-5} Pa. Measured and exposed in-situ. UV source G.E. AH-6 lamp. IITRI test facility (In situ Reflectometer Irradiation Facility, see Zerlaut & Courtney (1967)). α_s and $\Delta\alpha_s$ in p. 1-48.19.
_____	UV. 1 400 ESH.	
– – – –	Above after breaking vacuum.	

COATINGS

Solar Reflectors

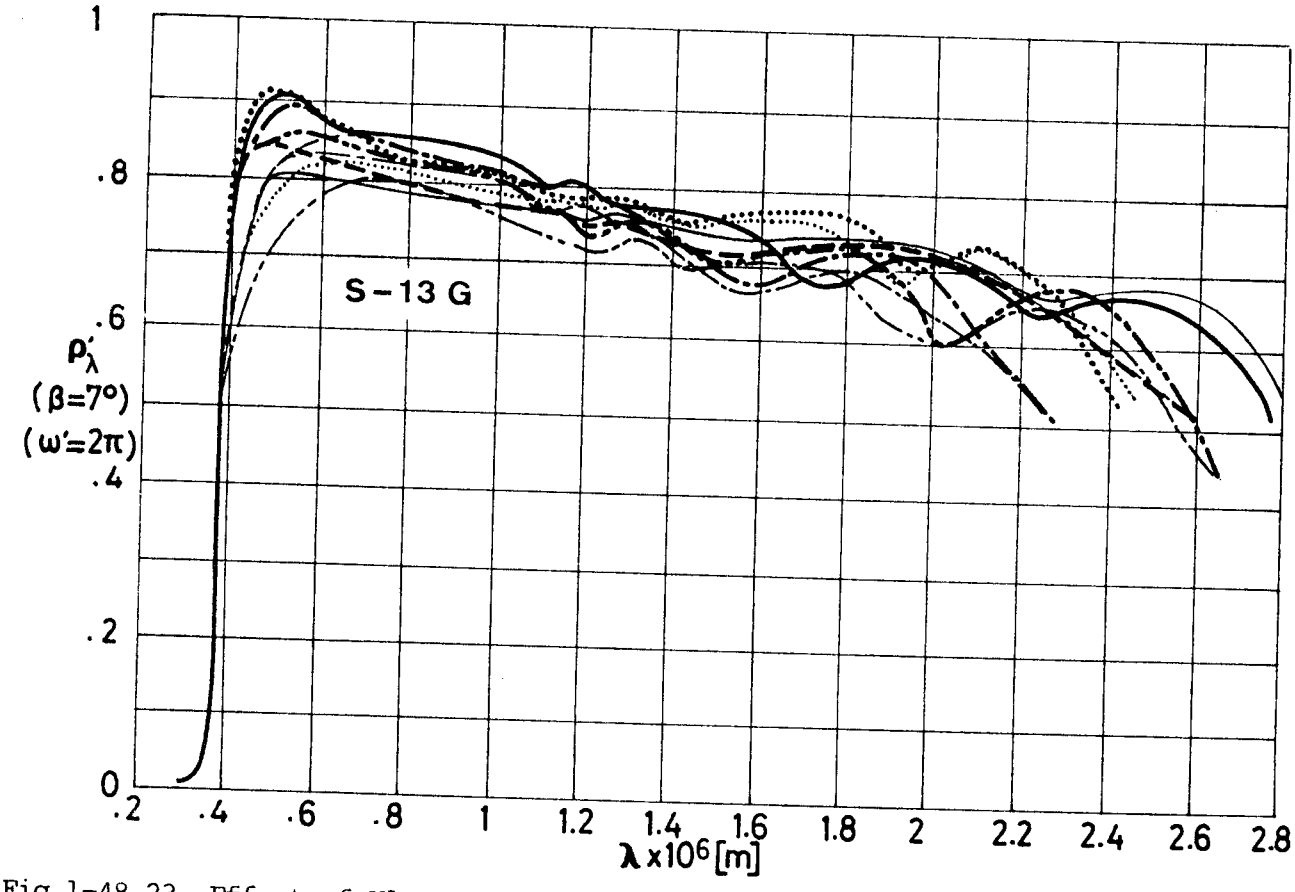

Fig 1-48.23. Effect of Ultra-Violet Radiation on normal-hemispherical spectral reflectance, ρ'_λ, of S-13 G coating vs. wavelength, λ. Silicated pigment with five mechanical perturbations. From Zerlaut, Rogers & Noble (1969). Drawn from Touloukian, DeWitt & Hernicz (1972).

Explanation

Key	Pigment Mechanical Perturbation	Exposure	Comments
———	Sifting prior to wet-grinding. Grind time 3 h.	In vacuum before irradiation. UV. 1 400 ESH.	T ∿ 298 K. p ∿ 1.33 x 10^{-5} Pa. Measured and exposed in situ. UV source G.E. AH-6 lamp. IITRI test facility (In Situ Reflectometer Irradiation Facility, see Zerlaut & Courtney (1967)). α_s and $\Delta\alpha_s$ in p. 1-48.19.
– – –	Unsifted and unground prior to wet-grinding. Grind time 4 h.	In vacuum before irradiation. UV. 1 400 ESH.	
—·—·	Dry-ground 30 min. Grind time 3 h.	In vacuum before irradiation. UV. 1 400 ESH.	
·····	Hand-mulling prior to wet grinding. Grind time 3 h.	In vacuum before irradiation. UV. 1 400 ESH.	
—··—	Remulled from first-hand mulling. Grind time 5 h.	In vacuum before irradiaton. UV. 1 400 ESH.	

COATINGS

Solar Reflectors

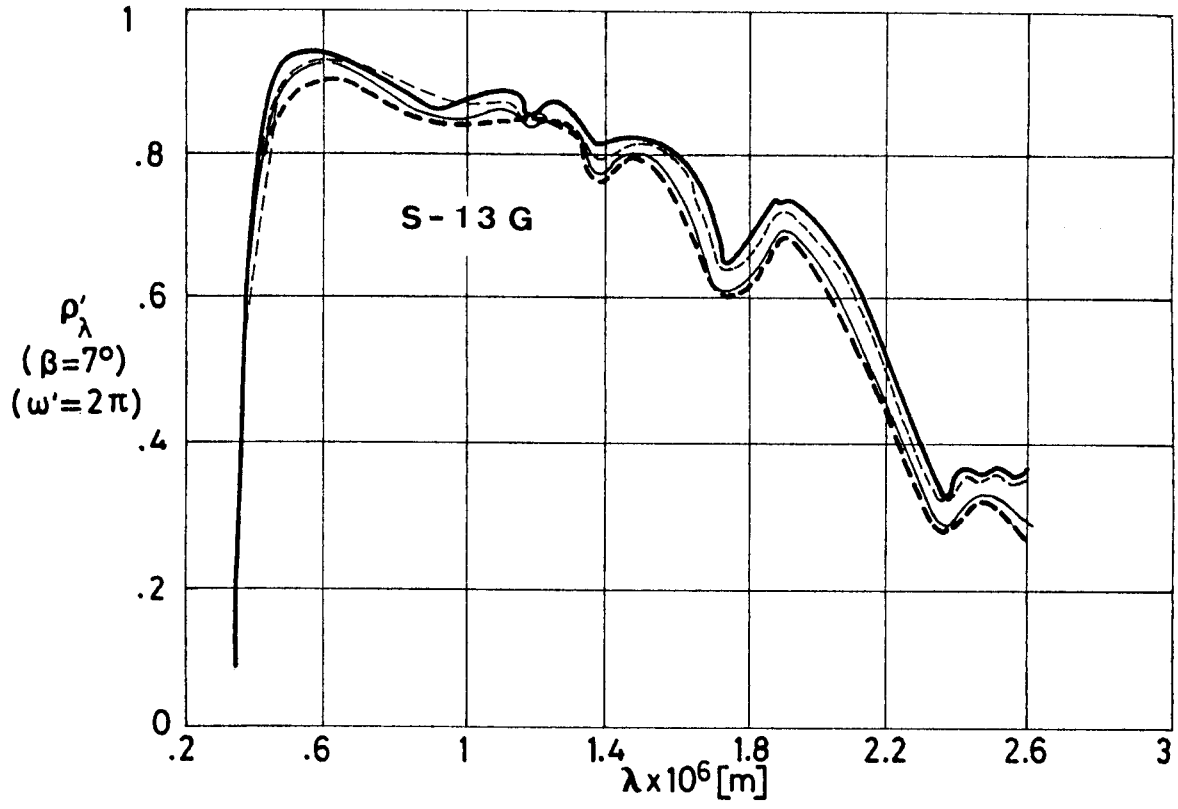

Fig 1-48.24. Effect of Ultra-Violet Radiation on normal-hemispherical spectral reflectance, ρ'_λ, of S-13 G coating vs. wavelength, λ. Plasma annealed and potassium silicate treated pigment. From Gilligan & Zerlaut (1971).

Explanation

Key	Exposure	Comments
———	In vacuum before irradiation.	T = 285 K. Measured in-situ. Initially at 8×10^{-6} Pa pressure. Irradiation performed at 1.33×10^{-5} Pa. IITRI test facility. (Combined Environment Radiation Facility) $\Delta\alpha_s$ in p. 1-48.19.
_____	UV. 600 ESH. First part of exposure.	
_ _ _ _	Above plus UV. 700 ESH. Second part of exposure.	
_ _ _ _ _	Above plus O_2 bleaching.	

COATINGS

Solar Reflectors

7.3.3.2.3. Protons only exposure. Fig 1-48.25 refers to S-13 and Fig 1-48.26 to S-13 G coating.

Unfortunately both the exposure conditions and the measuring method widely differ in either case.

In Fig 1-48.25 an Earth to Mars Mission has been simulated whereas Fig 1-48.26 seems to represent the conditions of a high altitude (200 000 km to 250 000 km) nearly circular orbit.

After exposure data in Fig 1-48.25, which were taken in the early sixties, were measured in air and those in Fig 1-48.26, from the seventies, in situ.

Figure 1-48.25 shows that changes in reflectance include a slight increase in the UV region ($\lambda < .35 \times 10^{-6}$ m) a shift in the Ultra-Violet absorption cut off, and a general increase in the infrared wavelength region.

The reflectance of a typical exposed sample was measured at time intervals of 14 h to 2 070 h after irradiation. No annealing of damage was observed between reflectance measurements at 14 h and 2 070 h after exposure.

Changes in solar absorptance of similar samples are given in p. 1-48.20.

From Gillette, Brown, Seiler & Sheldon (1966).

COATINGS

Solar Reflectors

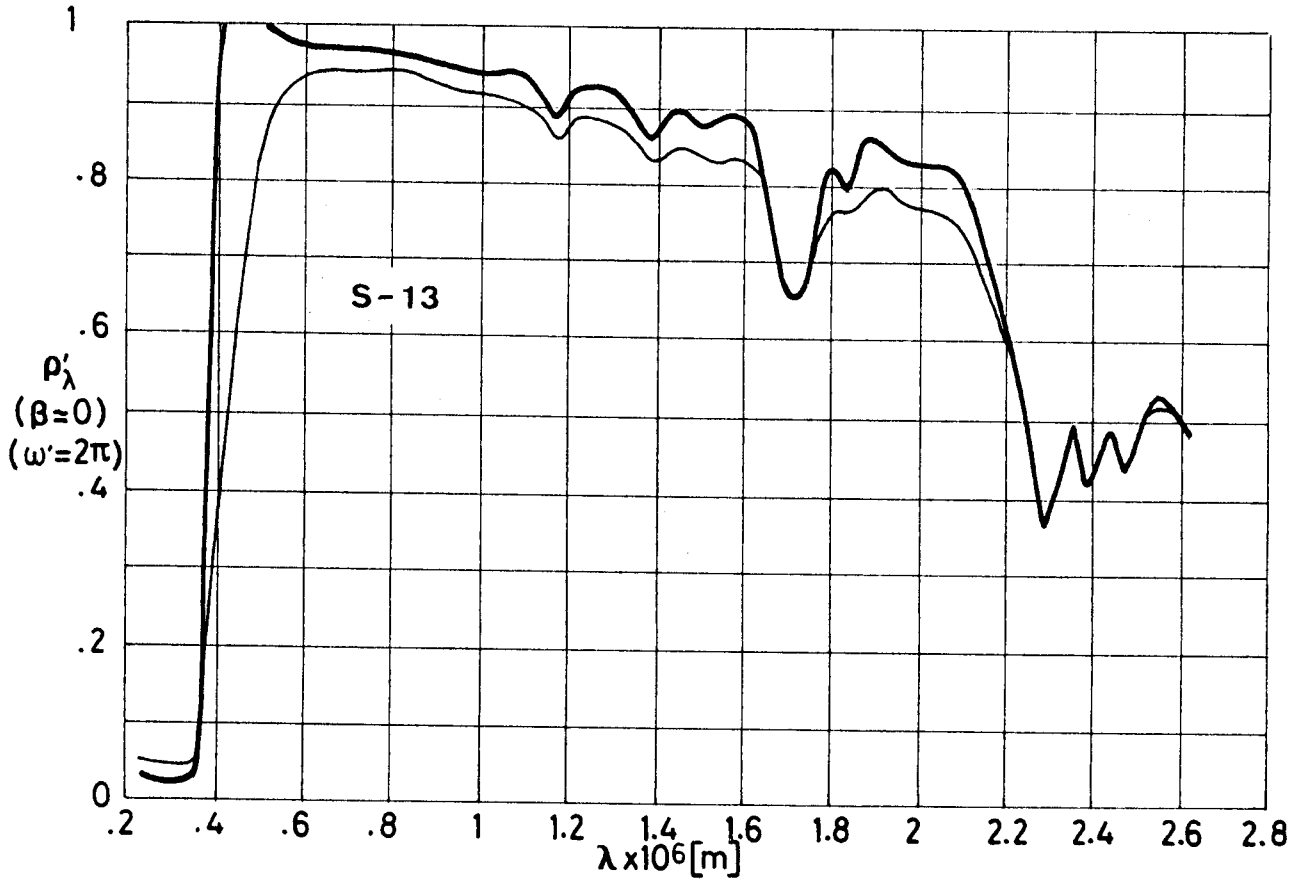

Fig 1-48.25. Protons exposure effects on normal-hemispherical spectral reflectance, ρ'_λ, of S-13 coating vs. wavelength, λ. LTV-602 silicone binder. From Gillette, Brown, Seiler & Sheldon (1966). Drawn from Touloukian, DeWitt & Hernicz (1972).

Explanation

Key	Exposure	Comments
———	In air before irradiation.	Sprayed on aluminium substrate. T = 300 K. Measured in air, exposed in vacuum (1.33×10^{-4} Pa). Measurement relative to MgO. Boeing low-energy particle accelerator.
– – –	Protons. 8.2 keV. 6.1×10^{19} p.m^{-2} Integrated Flux. In air 20 h - 40 h after irradiation.	

COATINGS

Solar Reflectors

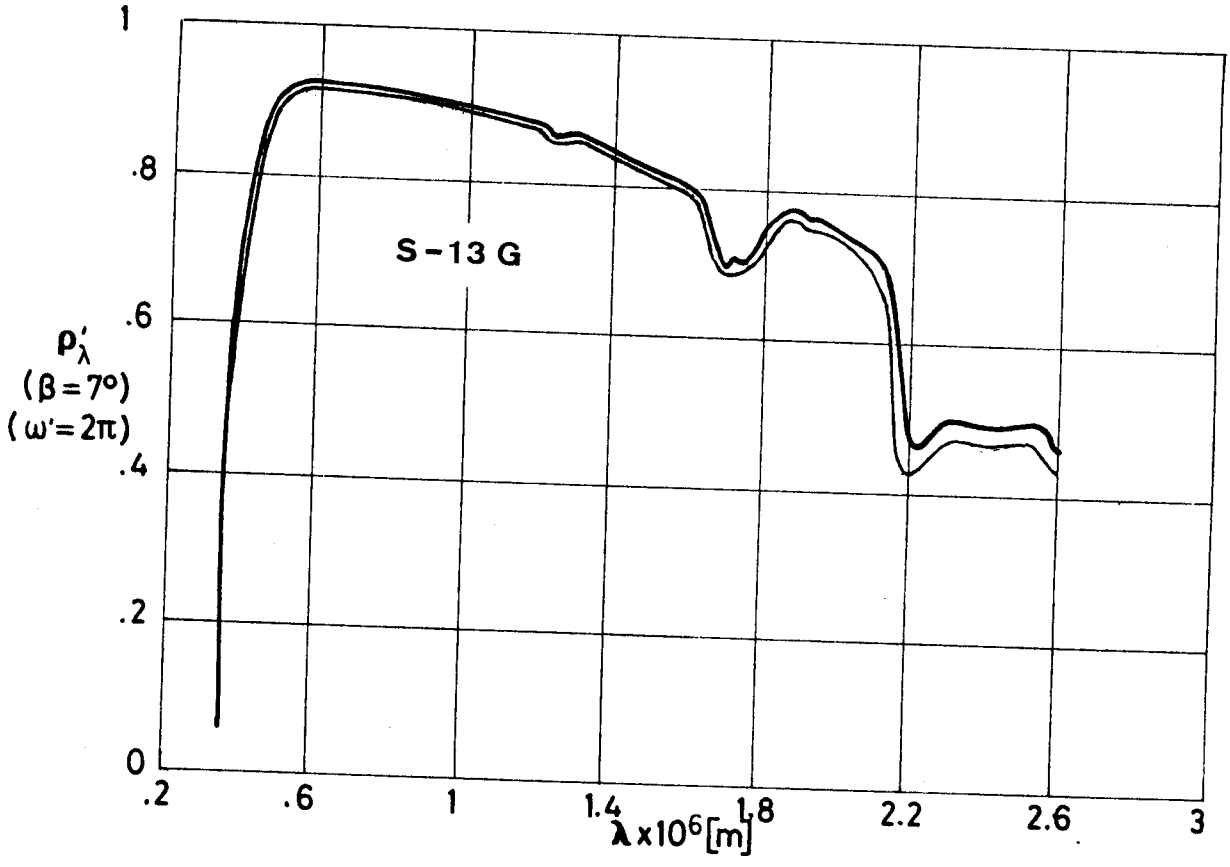

Fig 1-48.26. Protons exposure effects on normal-hemispherical spectral reflectance, ρ'_λ, of S-13 G coating vs. wavelength, λ. Plasma annealed and potassium silicate treated pigment. From Gilligan & Zerlaut (1971).

Explanation

Key	Exposure	Comments
———	In vacuum before irradiation.	T = 285 K. Measured in situ. Initially at 8×10^{-6} Pa pressure. Irradiation performed at 1.33×10^{-5} Pa. IITRI facility (In situ Reflectance Irradiation Facility - IRIF).
- - -	Protons. 1.2 keV 4.9×10^{13} p.m^{-2}.s^{-1} Flux. 2.5×10^{19} p.m^{-2} Integrated Flux	

COATINGS

Solar Reflectors

7.3.3.2.4. Electrons only exposure. Figs 1-48.27 and 1-48.28 concern S-13 G coating, whereas Figs 1-48.29 to 1.48-32 are related to GSFC, 101-7, a similar coating developed by NASA Goddard.

Both coatings exhibit a slow improvement in reflectance with time after exposure, even when the samples remain in the dark in a 1.33×10^{-6} Pa vacuum. The mechanisms of recovery are not quite understood. They probably depend on time, temperature, chamber residual atmosphere species, sample composition, radiation particle type, flux and integrated flux. Recovery occurs after exposure whether the impinging particle is stopped in the sample or passes through to its substrate.

Recovery proceeds to a greater extent and at a faster rate after 20 keV exposure than after 80 keV exposure and is probably reduced at improved vacuum conditions.

Compared to S-13 G, series 101-7 recovers more slowly and to a smaller fraction of original degradation.

From Fogdall, Cannaday & Brown (1970).

COATINGS

Solar Reflectors

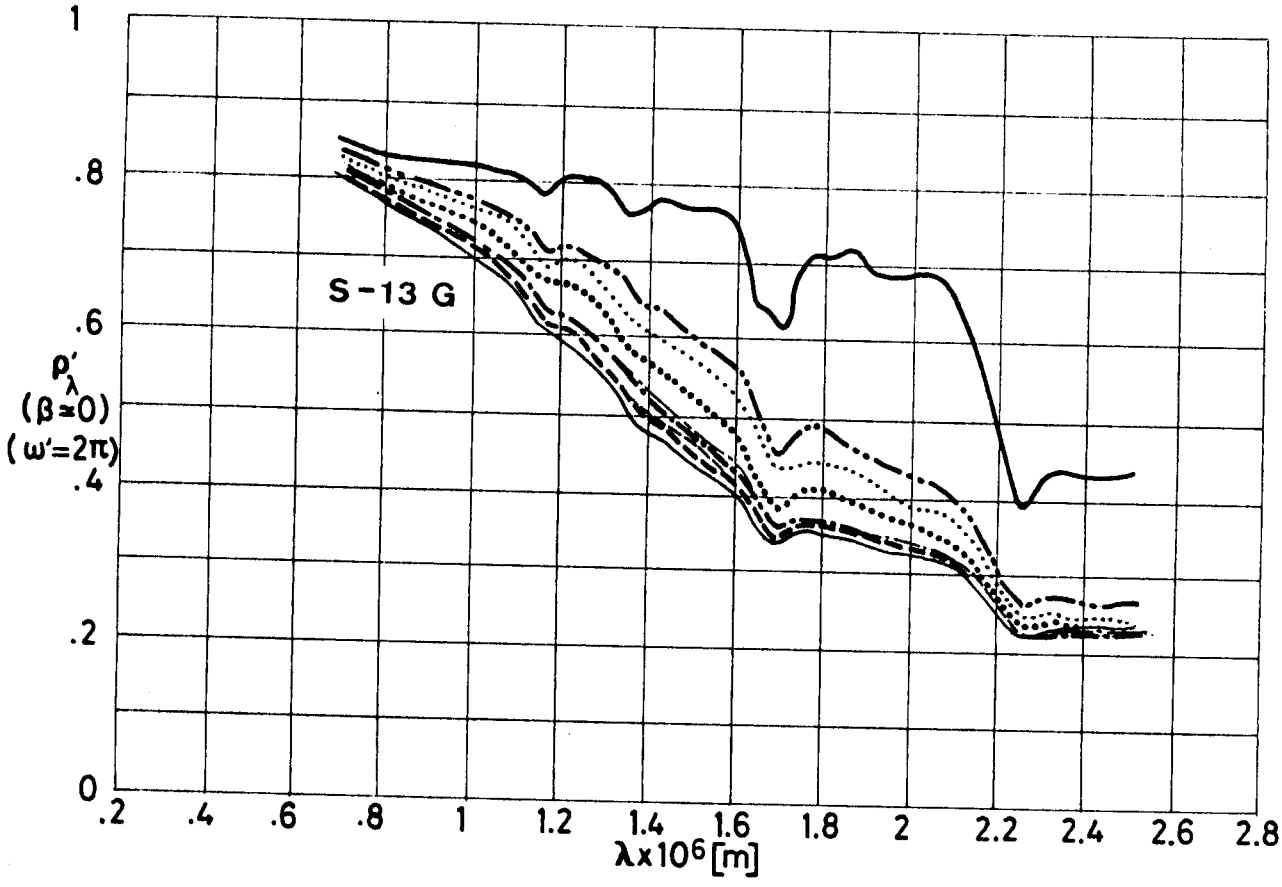

Fig 1-48.27. Electrons exposure effects on normal-hemispherical spectral reflectance, ρ'_λ, of S-13 G coating vs. wavelength, λ. Radiation intensity 20 keV. Recovery after exposure. From Fogdall, Cannaday & Brown (1970). Drawn from Touloukian, DeWitt & Hernicz (1972).

Explanation

Key	Intensity [keV]	Cumulative Integrated Flux [e.m^{-2}]	Time after Exposure [h]	Comments
———	In air before irradiation			Sample on Al substrate. T = 298 K.
———	20	10^{19} (10^{14} to 5x10^{15} e.m^{-2}.s^{-1})	.066	Sample on Al substrate. T = 281 K. 1.33 x 10^{-6} Pa vacuum maintained by ion pump. Measured in situ after exposure. Boeing test facility (Radiation Effects Laboratory) see Brown, Fogdall & Cannaday (1969).
– – – –			.82	
– – – –			1.65	
– · – · –			4.12	
– · – · –			6.92	
·····			23.07	
·····			53.68	
– – – –			122.87	

COATINGS

Solar Reflectors

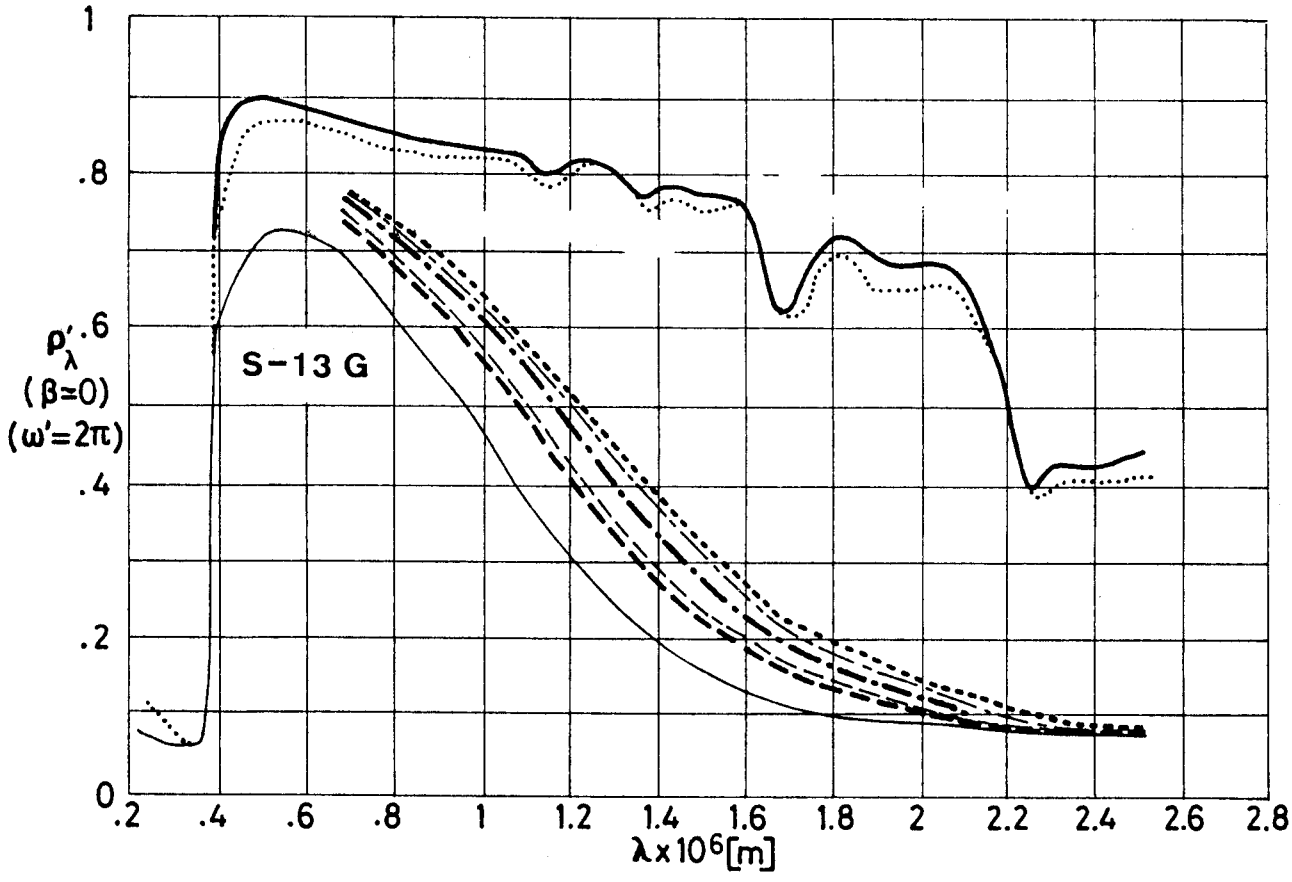

Fig 1-48.28. Electrons exposure effects on normal-hemispherical spectral reflectance, ρ'_λ, of S-13 G coating vs. wavelength, λ. Radiation intensity 80 keV. Recovery after exposure. From Fogdall, Cannaday & Brown (1970). Drawn from Touloukian, DeWitt & Hernicz (1972).

Explanation

Key	Intensity [keV]	Cumulative Integrated Flux [e.m^{-2}]	Time after Exposure [h]	Comments
———	In air before irradiation			Sample on Al substrate. T = 298 K.
———	80	10^{20} (10^{14} to 5×10^{15} e.m^{-2}.s^{-1})	0	Sample on Al substrate. T = 281 K. 1.33×10^{-6} Pa vacuum maintained by ion pump. Measured in situ after exposure. Boeing test facility (Radiation Effects Laboratory) see Brown, Fogdall & Cannaday (1969).
- - - -			48	
— — —			72	
—·—·—			96	
—·— —			168	
.....			432	
.....			Measured in air after the above tests had been made. T = 298 K.	

COATINGS

Solar Reflectors

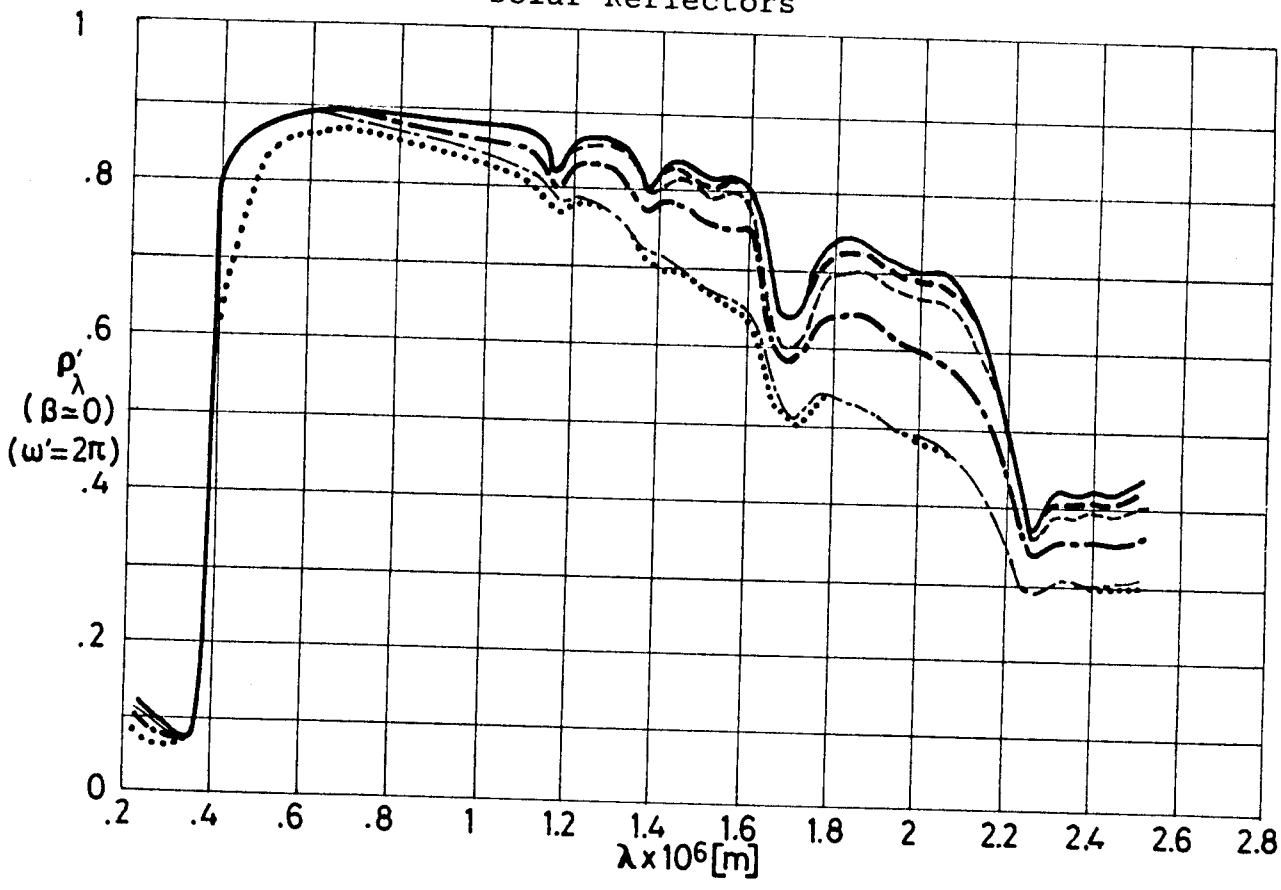

Fig 1-48.29. Electrons exposure effects on normal-hemispherical spectral reflectance, ρ'_λ, of GSFC, 101-7 coating vs. wavelength, λ. Radiation intensity 20 keV. Different integrated fluxes. 101-7 is a coating, similar to S-13 G, developed by NASA Goddard. From Fogdall, Cannaday Brown (1970). Drawn from Touloukian, DeWitt & Hernicz (1972).

Explanation

Key	Intensity [keV]	Flux [e.m^{-2}.s^{-2}]	Cumulative Integrated Flux [e.m^{-2}]	Comments
———	In air before irradiation			Sample on Al substrate. T = 298 K.
———	20	10^{14} to 5x10^{15}	10^{17}	Sample on Al substrate. T = 281 K. 1.33 x 10^{-6} Pa vacuum maintained by ion pump. Measured in situ after exposure. Boeing test facility (Radiation Effects Laboratory) see Brown, Fogdall & Cannaday (1969). α_s in p. 1-48.21.
- - - -			5 x 10^{17}	
– – – –			10^{18}	
—·—			3 x 10^{18}	
—·—·			10^{19}	
·····			10^{20}	

COATINGS

Solar Reflectors

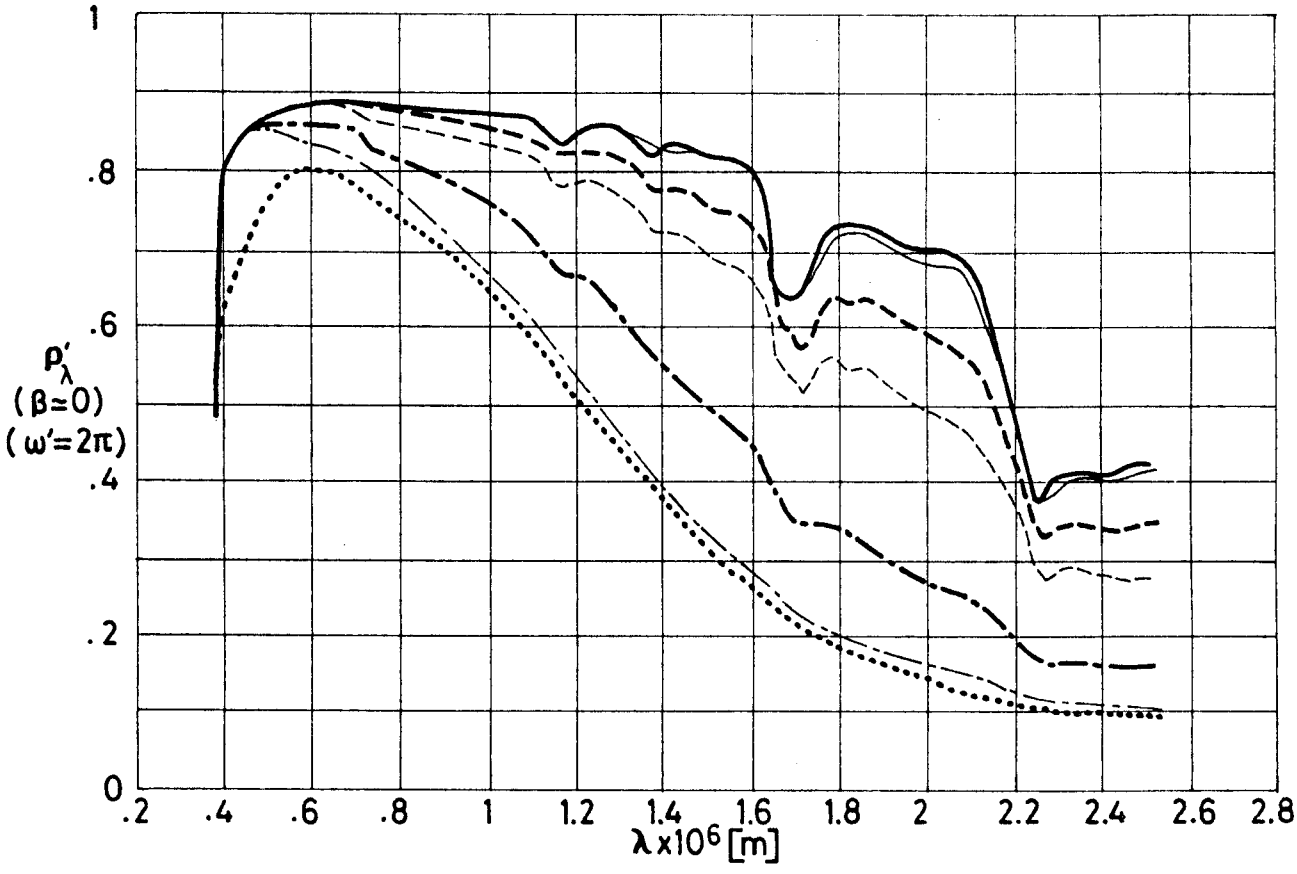

Fig 1-48.30. Electrons exposure effects on normal-hemispherical spectral reflectance, ρ'_λ, of GSFC, 101-7 coating vs. wavelength, λ. Radiation intensity 80 keV. Different integrated fluxes. 101-7 is a coating, similar to S-13 G, developed by NASA Goddard. From Fogdall, Cannaday & Brown (1970). Drawn from Touloukian, DeWitt & Hernicz (1972).

Explanation

Key	Intensity [keV]	Flux [$e.m^{-2}.s^{-2}$]	Cumulative Integrated Flux [$e.m^{-2}$]	Comments
———	In air before irradiation			Sample on Al substrate. T = 298 K.
———	80	10^{14} to $5x10^{15}$	10^{17}	Sample on Al substrate. T = 281 K. 1.33×10^{-6} Pa vacuum maintained by ion pump. Measured in situ after exposure. Boeing test facility (Radiation Effects Laboratory) see Brown, Fogdall & Cannaday (1969). α_s in p. 1-48.21.
- - - -			5×10^{17}	
----			10^{18}	
—·—			3×10^{18}	
—·—·			10^{19}	
.....			10^{20}	

COATINGS

Solar Reflectors

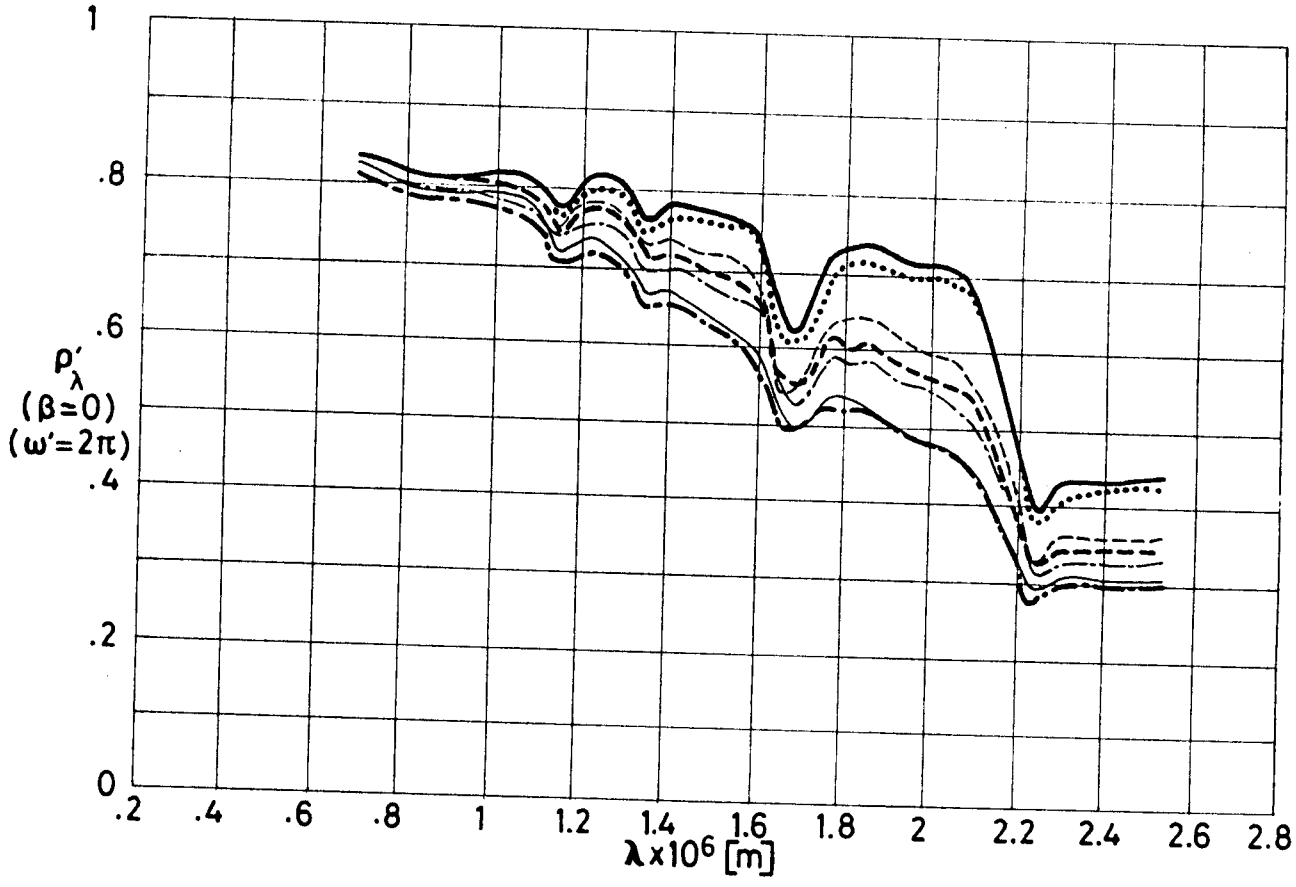

Fig 1-48.31. Electrons exposure effects on normal-hemispherical spectral reflectance, ρ'_λ, of GSFC, 101-7 coating vs. wavelength, λ. Radiation intensity 20 keV. Recovery after exposure. 101-7 is a coating, similar to S-13 G, developed by NASA Goddard. From Fogdall, Cannaday & Brown (1970). Drawn from Touloukian, DeWitt & Hernicz (1972).

Explanation

Key	Intensity [keV]	Cumulative Integrated Flux [e.m^{-2}]	Time after Exposure [h]	Comments
———	In air before irradiation			Sample on Al substrate. T = 298 K.
———	20	10^{19}	3.87	Sample on Al substrate. T = 281 K. 1.33×10^{-6} Pa vacuum maintained by ion pump. Measured in situ after exposure. Boeing test facility (Radiation Effects Laboratory) see Brown, Fogdall & Cannaday (1969).
– – –			54.	
– – – –			123.	
—·—		10^{20}	1.08	
—·—·			50.	
.....			168.	120 h after dry air back fill. T = 298 K.

COATINGS

Solar Reflectors

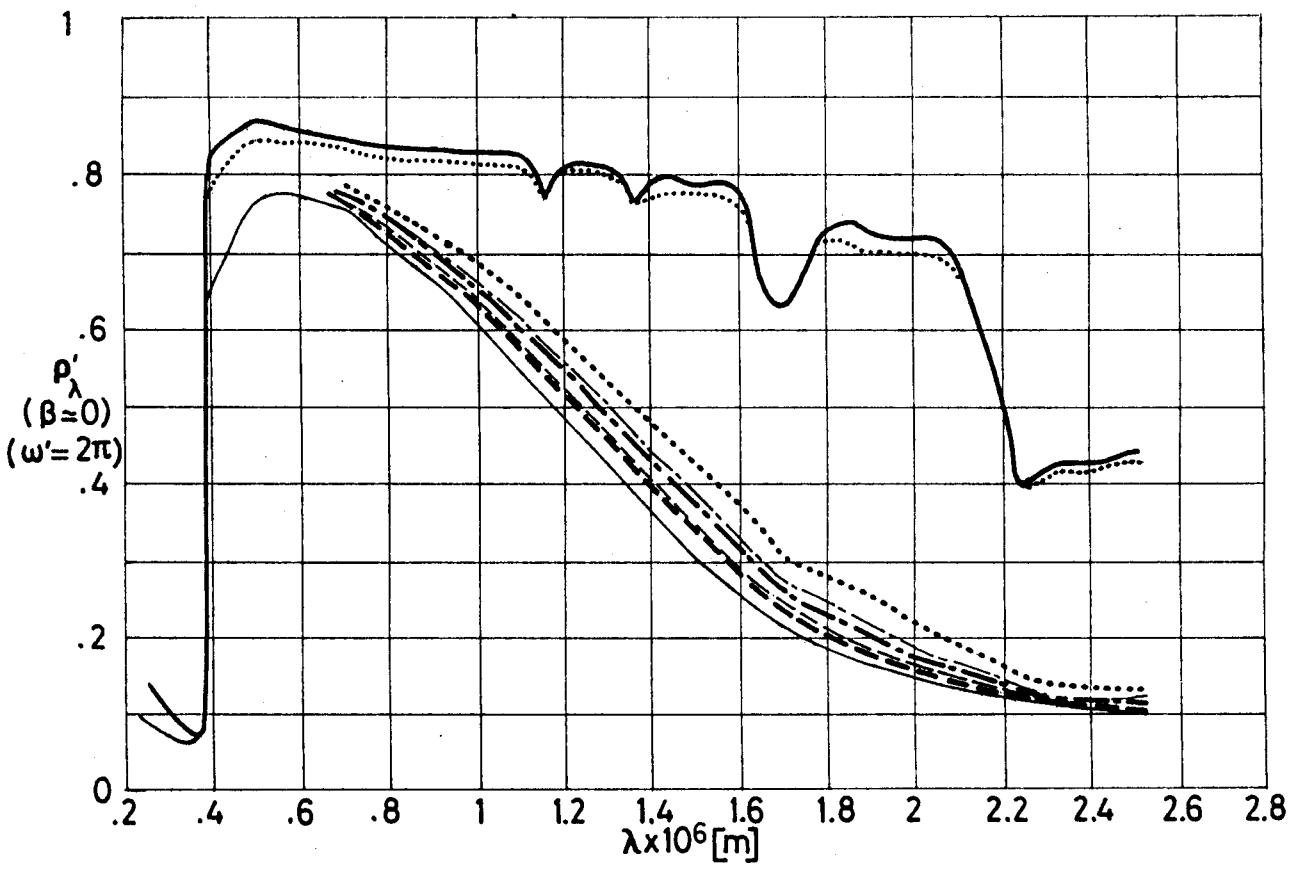

Fig 1-48.32. Electrons exposure effects on normal-hemispherical spectral reflectance, ρ'_λ, of GSFC, 101-7 coating vs. wavelength, λ. Radiation intensity 80 keV. Recovery after exposure. 101-7 is a coating, similar to S-13 G, developed by NASA Goddard. From Fogdall, Cannaday Brown (1970). Drawn from Touloukian, DeWitt & Hernicz (1972).

Explanation

Key	Intensity [keV]	Cumulative Integrated Flux [$e.m^{-2}$]	Time after Exposure [h]	Comments
———	In air before irradiation			Sample on Al substrate. T = 298 K.
———	80	10^{20} (10^{14} to 5×10^{15} $e.m^{-2}.s^{-1}$)	0	Sample on Al substrate. T = 281 K. 1.33×10^{-6} Pa vacuum maintained by ion pump. Measured in situ after exposure. Boeing test facility (Radiation Effects Laboratory) see Brown, Fogdall & Cannaday (1969).
– – – –			48	
– – – –			72	
—·—			96	
—·—			168	
·····			432	
·····			Measured in air after the above tests had been made. T = 298 K.	

COATINGS

Solar Reflectors

7.3.3.2.6. Combined exposure. Two different set of data are presented here.

Fig 1-48.33 shows the effect of Ultra-Violet and Protons exposure on S-13 G coating.

The damage in the visible spectrum ($\lambda = .4 \times 10^{-6}$ m to $.7 \times 10^{-6}$ m) is fairly slight and bleacheable. The exposure produces displacement of atoms, ionization and excitations. After exposure most of the atoms return to the previous or similar equilibrium positions and a recovery process follows, in which X ray and Ultra-Violet radiations are emitted. When long wavelength radiation is not present the damage is not bleached.

Charged particle damage produces effects which Ultra-Violet produces, as well as others which result from massive interactions. In combined exposures radiative bleaching will produce "synergism" and invalidate any reciprocity which might have existed in single environment testing.

$\Delta\alpha_s$ is given in p. 1-48.29.

From Gilligan & Zerlaut (1971).

The other set of data, Figs 1-48.34 to 1-48.36, are for S-13 G/LO on Al substrate and are intended to represent up to three years exposure in geosynchro-

COATINGS

Solar Reflectors

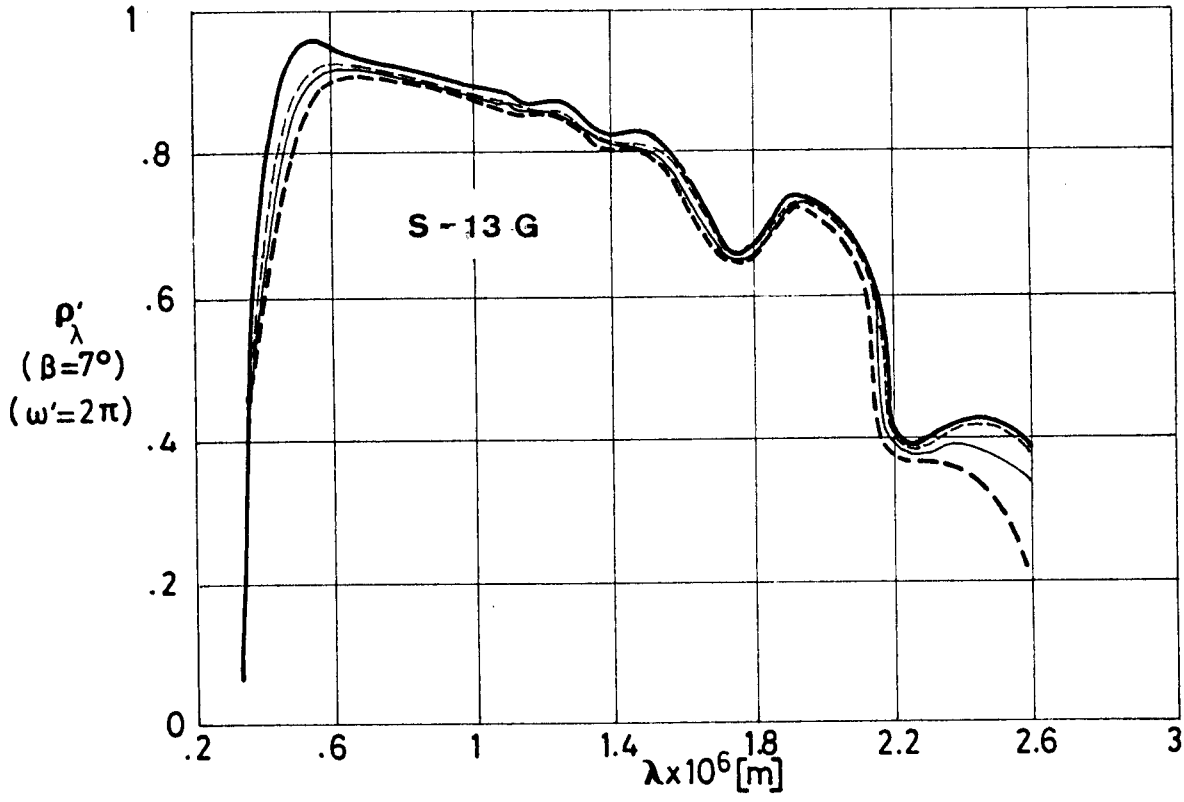

Fig 1-48.33. Effect of Combined Exposure on normal-hemispherical spectral reflectance, ρ'_λ, of S-13 G coating vs. wavelength, λ. Plasma annealed and potassium silicate treated pigment. From Gilligan & Zerlaut (1971).

Explanation

Key	Exposure	Comments
———	In vacuum before irradiation.	T = 285 K. Measured in situ. Initially at 8×10^{-6} Pa pressure. Irradiation performed at 1.33×10^{-5} Pa. IITRI facility (In situ Reflectance Irradiation Facility - IRIF). $\Delta\alpha_s$ in p. 1-48.29.
– – –	UV. 600 ESH. Protons. 668 EWH. 1.05×10^{13} p.m^{-2}.s^{-1} Flux. $\sim 6 \times 10^{18}$ p.m^{-2} Integrated Flux. First part of exposure.	
– – – –	Above plus UV. 700 ESH. Second part of exposure.	
– – – – –	Above plus O_2 bleaching.	

COATINGS

Solar Reflectors

nous orbit of the Orbital Test Satellite (OTS) equatorial faces. Solar absorptance data have been presented and evaluated in pp. 1-48.29 to 1.48-32. Figure 1-48.34 indicates that in the visible range ($\lambda = .4 \times 10^{-6}$ m to $.7 \times 10^{-6}$ m) the reflectance decreases regularly with the exposure time; whereas the decrease in the infrared ($\lambda > .8 \times 10^{-6}$ m) rapidly reaches a saturation.

Figure 1-48.35 shows the influence of air exposure after irradiation. To this aim the upper and lower reflectance curves in Fig 1-48.34 have been compared with that resulting from air exposure.

Figure 1-48.36 indicates that bleaching appears after pump damage but an increased reflectance also results when an irradiation with Ultra-Violet and particles is followed by an irradiation with particles only. Again the infrared part of the spectrum ($\lambda > .8 \times 10^{-6}$ m) is the most affected, as can be seen by comparing the curves corresponding to data taken after step C and before step D.

COATINGS

Solar Reflectors

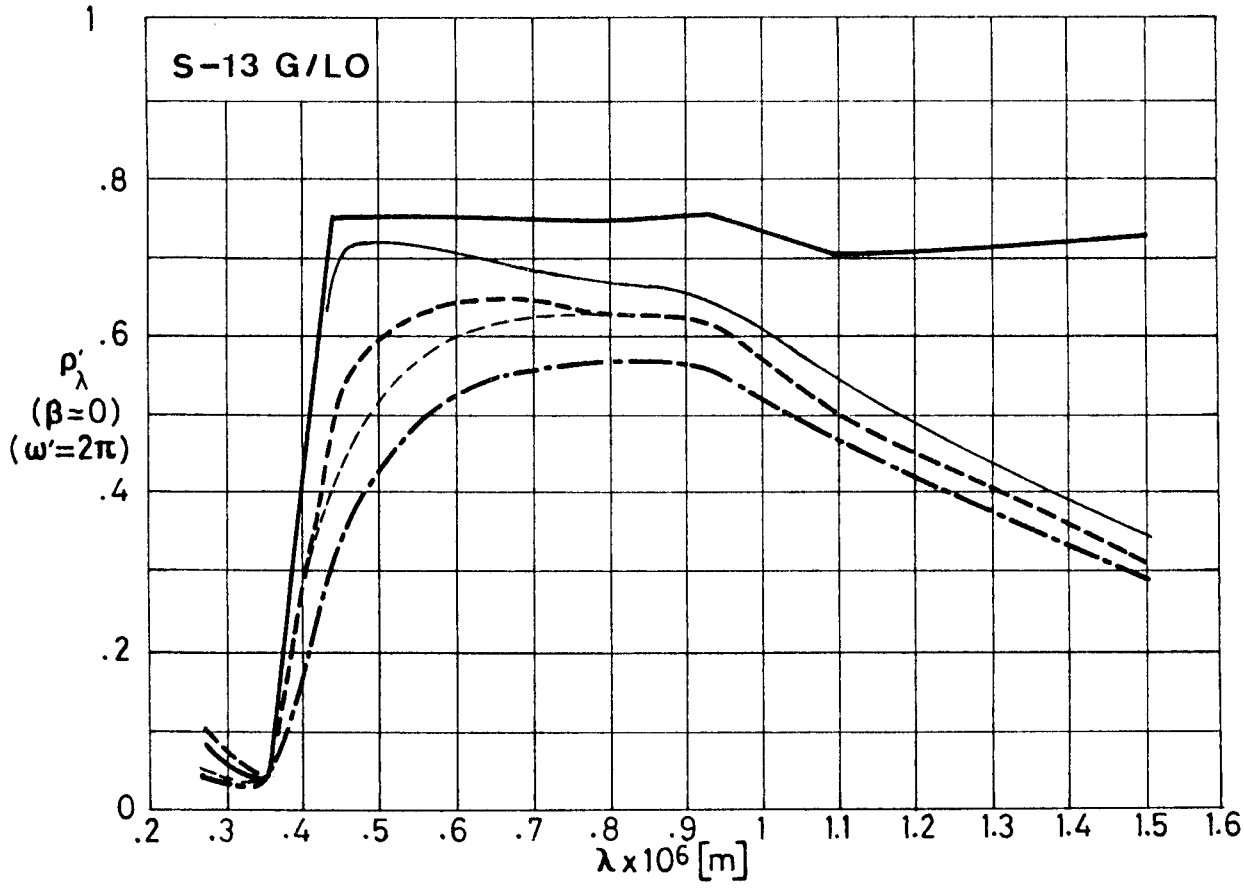

Fig 1-48.34. Effect of Combined Exposure, simulating up to three years in geosynchronous orbit, on normal-hemispherical spectral reflectance, ρ'_λ, of S-13 G/LO coating vs. wavelength, λ. From Paillous (1976).

Explanation

Key	Description	Comments
———	After 125 h below 1.3 x 10^{-4} Pa pressure. T = 363 K.	Test conditions: See Table 1-13, p. 1-76.
_____	After step A (.18 years in orbit). T = 363 K.	
- - - -	After Step B (.94 years in orbit). T = 363 K.	
_ _ _ _	After Step C (2.11 years in orbit) T = 363 K.	After unintentional O_2 bleaching.
—·—	After Step D (3 years in orbit) T = 363 K.	

COATINGS

Solar Reflectors

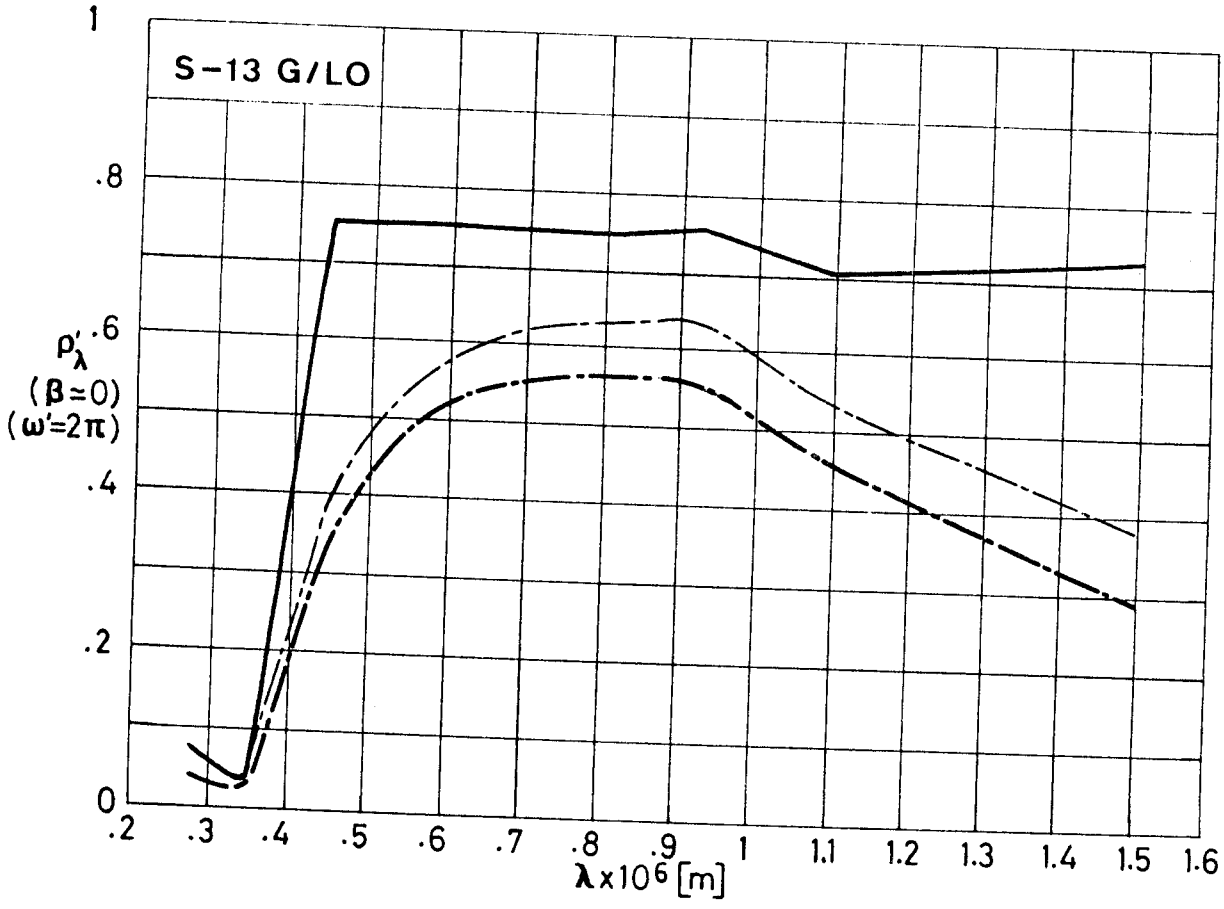

Fig 1-48.35. Effect of O_2 bleaching, after Combined Exposure, on normal-hemispherical spectral reflectance, ρ'_λ, of S-13 G/LO coating vs. wavelength, λ. Curves ——— and —·— are those shown in Fig 1-48.34. From Paillous (1976).

Explanation

Key	Description	Comments
———	After 125 h below 1.3 x 10^{-4} Pa pressure. T = 363 K.	Test conditions: See Table 1-13, p. 1-76.
—·—	After Step D (3 years in orbit) T = 363 K.	After unintentional O_2 bleaching.
— - —	After Step D and Air exposure. T = 293 K.	

COATINGS

Solar Reflectors

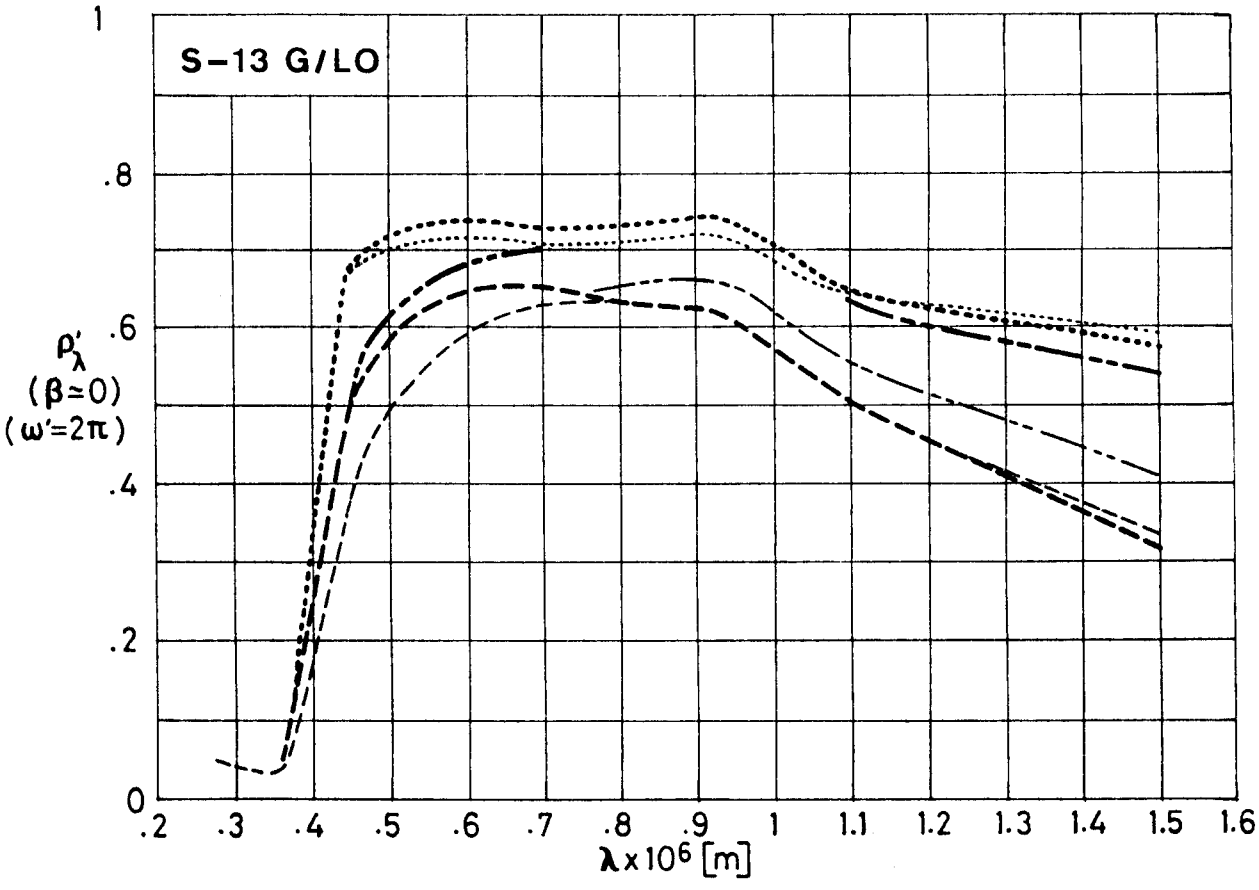

Fig 1-48.36. Effect of Combined Exposure, simulating up to three years in geosynchronous orbit, on normal-hemispherical spectral reflectance, ρ'_λ, of S-13 G/LO coating vs. wavelength, λ. Curves ---- and ----- are those shown in Fig 1-48.34. From Paillous (1976).

Explanation

Key	Description	Comments
.....	Before step B. T = 363 K.	Test conditions: See Table 1-13, p. 1-76.
----	After step B (.94 years in orbit). T = 363 K.	
.....	After pump damage. T = 363 K.	After unintentional O_2 bleaching.
—·—·—	Before step C. T = 363 K.	
-----	After Step C (2.11 years in orbit). T = 363 K.	
—··—	Before step D. T = 363 K.	

COATINGS

Solar Reflectors

7.4. Electrical resistance.

These coatings are non conductive.

A slight conductivity has been observed in S-13 G/LO by Paillous (1976) under two experimental conditions:

1) For the sample in air. Conductivity vanished to zero after exposure in vacuum. This was attributed to sample moisture.

2) When the sample was UV irradiated. Now the effect was attributed to photo-emission on the electrodes attached to the sample.

8. ENVIRONMENTAL BEHAVIOR

8.1. Prelaunch. These paragraphs concern S-13 G and S-13 G/LO coatings. Early information on S-13 can be found in Breuch (1967).

Two NASA Specifications cover the properties, qualification test and preparation of S-13 G and S-13 G/LO coatings. These are NASA Specification 10M01835, entitled "Paint, S-13 G, Temperature Control, Specification For" and 10M01836, entitled "Paint, S-13 G, Temperature Control, Application of, Specification For". Although these specifications are for S-13 G, they apply to S-13 G/LO since the only difference between them is that S-13 G/LO uses a stripped binder (see p. 1-48.2).

These coatings are easy to apply, flexible, cleanable and reparable. The surface is soft, rubbery and should be

COATINGS

Solar Reflectors

protected from sand, dust, salt, smog and human sebum with appropriate plastic coverings. No ill effects were evident when exposed to UV and vacuum after 14 months in storage under Mylar, H-polymer, Lexan, Teflon A or Tedlar films.

8.2. Postlaunch. These coatings have an accepted low α_s ($\alpha_s \leq .22$) high emittance ($\varepsilon \sim .90$) and a low outgassing (the LO version).

8.2.1. Ascent. These coatings are thermal shock resistant when cured as indicated in § 5.5, p. 1-48.5, provided that the primer is not too thick.

8.2.2. Orbital. UV and vacuum degradation are fair (UV degradation is due to damage in the binder).

These coatings have been often used on short flights at low altitudes.

From Cull, Stevenson, Mell & Harada (1984).

9. THERMAL CYCLING

The maximum and minimum temperatures at which these coatings have been tested with no cracking or spalling evident to the unaided eye or at 100x magnification were

T min = 83 K

T max = 395 K Chamber pressure below $.7 \times 10^{-3}$ Pa.

(Cunnington, Grammer & Smith (1969)).

COATINGS

Solar Reflectors

10. SOURCE

IIT Research Institute. 10 West 35 Street, Chicago, Illinois 60616.

11. COST

Quotations in the early eighties were of the order of 350 US $/pint (FOB, Chicago) for 1-7 pints and 300 US $/pint for 8 or more pints of S-13 G. (1 US pint = 473.2×10^{-6} m^3). Quotations for S-13 G/LO were 30 % higher.

12. PAST SPATIAL USE

Spacecraft or Programme	Launching Date	Used or Tested	References
OSO-II	Feb. 3, 1965	Tested	McCargo, Spradley, Greenberg & McDonald (1971)
Pegasus I	Feb. 16, 1965	Tested	Touloukian, DeWitt & Hernicz (1972)
Pegasus II	May 25, 1965	Tested	McCargo, Spradley, Greenberg & McDonald (1971)
Pegasus III	July 30, 1965	Tested	
Lunar Orbiter I	Aug. 10, 1966	Tested	Touloukian, DeWitt & Hernicz (1972)
Lunar Orbiter II	Nov. 6, 1966	Tested	
ATS-I	Dec. 7, 1966	Tested	Reichard & Triolo (1967) Triolo (1973) Triolo, Heaney & Hass (1978)
OSO-III	March 8, 1967	Tested	Millard (1969)

COATINGS

Solar Reflectors

Spacecraft or Programme	Launching Date	Used or Tested	References
ATS-II	Apr. 5, 1967	Tested	McCargo, Spradley, Greenberg & McDonald (1971)
Lunar Orbiter IV	May 4, 1967		Touloukian, DeWitt & Hernicz (1972)
Mariner V	June 14, 1967	Tested	
Lunar Orbiter V	Aug. 1, 1967	Tested	McCargo, Spradley, Greenberg & McDonald (1971)
Prospero	Oct. 28, 1971	Tested	Keyte (1975)
OTS	May 11, 1978	Used on the antenna dishes. See p. S 2-10.	Chalmers, Konzok, Bouchez & Howle (1983)
NAVSTAR 6	Apr. 26, 1980	Tested	Pence & Grant (1981)
LANDSAT D	July 16, 1982	Used on antennae. See p. S 3-3.	Bachofer (1979)
LDEF	Apr. 6, 1984	Tested	Clark (1981)

INTENTIONALLY BLANK PAGE

COATINGS

Solar Reflectors

1.2.4. ZINC OXIDE-METHYLSILICONE

1. COMPOSITION

Pigment: New Jersey Zinc Co., SP500 zinc oxide.

Binder: RTV 121 silicone elastomer.

From Guillaumon & Guillin (1979, 1981).

RHODORSIL RTV 121 is a bicomponent liquid silicone elastomer. This liquid, once mixed with catalyst 10028 and vulcanized at room temperature, yields a transparent material which is used as a potting and encapsulating compound.

From RHONE-POULENC (1978).

2. FORMULATION

Not given by the producer.

3. USUAL DESIGNATION

PSG 120. ASTRAL.

PSG 120 FD CNES has the same composition as above, but with the RTV 121 binder purified by CNES (Toulouse).

From Guillaumon & Guillin (1979, 1981).

4. SUBSTRATE

Practically any metallic substrate. Fiber-glass also quoted.

See Preparation of surfaces for painting.

5. METHOD OF APPLICATION

5.1. Preparation of paint for application. PSG 120 is delivered as a system consisting of:

Base PSG 120: 1 kg ,

Hardener CT 122: .2 kg ,

COATINGS

Solar Reflectors

Thinner S 105: 10^{-3} m^3 ,

to mix when using it.

Shelf life, in the temperature range 288 K - 298 K, between 10 h and 12 h.

Storage time of the unmixed components, held in closed containers, in the above temperature range, is 6 months.

From ASTRAL (1976)a.

5.2. Preparation of surfaces for painting. Excellent adhesion is obtained on metallic substrates such as: ferrous metals, steels and light alloys, as well as on fiber-glass composites, by use of P 128 primer which can be applied either by hand-rubbing or by spray painting.

Adhesion to electrolytic gold is excellent provided that the substrate is primed either with P 123 or with P 131, using P 128 as post-primer.

5.2.1. Use of P 123 primer. The surface should be cleaned from any trace of oxide or die lubricant and degreased with a rag soaked with toluene, trichloroethylene, acetone or ether.

The primer consists of three components which should be mixed as follows:

Base	P 123:	4 parts by volume,
Hardener	CX 124:	1 part by volume,
Thinner	S 125:	2 parts by volume.

The mixing should be filtered through a nylon net, mesh

COATINGS

Solar Reflectors

size 5×10^{-5} m.

Shelf life in the temperature range 288 K - 298 K is 8 h.

The primer can be spray-applied. Use Kremlin model Junior or comparable gun, at about 2×10^{5} Pa air pressure. Also recommended, Blinks model Wren B or comparable at 2.4×10^{5} Pa air pressure. In the last case, an additional thinning of 1 part by volume of S 125 should be used.

A single crosswise layer should be applied in an environment at 288 K to 298 K temperature.

Polymerization times at 293 K are:

Dust off : 30 min,

Dry to be handled : 4 h,

Final polymerization: 8 d.

The primer should be allowed to air-dry for 8 h at 293 K before application of the finishing coat.

Use paint remover D 165 for cleaning.

From ASTRAL (1976)b.

5.2.2. Use of P 128 primer. Ferrous metals, steels, light alloys and fiber-glass composites should be cleaned as above.

In the case of electrolytic gold, the surface should be degreased before application of a thin layer of primer P 123 or P 131, using P 128 as post-primer after at least 8 h drying at 293 K.

Primer P 128 is delivered ready for use. It can be applied as a thin and uniform single crosswise layer, either by hand rubbing or by spray painting. Application temperature

COATINGS

Solar Reflectors

in the range 288 K - 298 K.

Polymerization times at 293 K are:

Dust off : 15 min,

Dry to be handled : 30 min,

Final polymerization: 3 h.

The primer should be allowed to air-dry for 30 min at 293 K before application of the finishing coat.

From ASTRAL (1976)c.

5.3. Application of paint. By spray gun.

Yield (five layers): 1 $kg.m^{-2}$.

From ASTRAL (1976)a.

5.4. Coating thickness. Measured on A-U4G T4 aluminium alloy substrate, primed with P 128. $t_c = .9 \times 10^{-4}$ m to 1.1×10^{-4} m.

From ASTRAL (1976)a.

5.5. Curing process. On the above substrate and primer, the polymerization times at 293 K are:

Dust off : 3 h,

Dry to be handled : 24 h,

Final polymerization: 5 d.

Once cured, the coating appears as a glossless white surface.

From ASTRAL (1976)a.

CAUTIONS

Flammability. Primers P 123, P 128 and P 131, and coating PSG 120 must be handled far from any flame and in properly

COATINGS

Solar Reflectors

ventilated rooms.

Flash points of coating components, per NF M 07-019, are:

PSG 120: 278 K,

CT 122: 278 K,

S 105: 290 K.

Toxicity. Avoid breathing vapors during application.

Avoid frequent and lasting contacts on the skin, particularly while handling hardeners CT 122 and CX 124.

From ASTRAL (1976)a.

6. SOLVENTS RESISTANCE

A list of solvents of silicone elastomers is given in p. 1-4.

RHODORSIL HUILE 47 V 50 can be used for decreasing the viscosity of RTV 121.

From RHONE-POULENC (1978).

7. PHYSICAL PROPERTIES

7.1. Density. On A-U4G T4 aluminium alloy, primed with P 128, the surface density is: .26 $kg.m^{-2}$ to .30 $kg.m^{-2}$.

These values, together with the above quoted coating thicknesses yield a density close to 2 800 $kg.m^{-3}$.

The densities of the wet components are:

Base PSG 120: 1 380 $kg.m^{-3}$,

Hardener CT 122: 860 $kg.m^{-3}$,

Thinner S 105: 910 $kg.m^{-3}$.

From ASTRAL (1976)a.

7.2. Outgassing. See Table 1-8 overleaf. Outgassing characteristics given in that Table have been measured per Specifica-

COATINGS

Solar Reflectors

tion ESA PSS-09/QRM-02T. According to this specification, the sample is heated at 398 K, below 1.3×10^{-4} Pa pressure, during 24 h. The condensing plate is held at 298 K.

Table 1-8

Outgassing Characteristics of PSG 120 Coating

Coating	% TML [a]	% CVCM [b]	Cure Time [h]	Cure Temp. [K]	References
PSG 120 FD (binder purified by CNES). On aluminium substrate. Primer P 128.	.70	.03	120	298	Guillaumon & Guillin (1979, 1981).
	.79	.05	120	298	
	.80	.03	120	298	
	.43	.03	120 [c] 24	298 333	
	.49	.03	120 [c] 24	298 333	
	.24	.02	120 [c] 24	298 373	
	.24	.03	120 [c] 24	298 373	
PSG 120 FD (binder purified by CNES). Primer P 128.	.63 % RML: .61 [d]	.04			ESTEC (1980).
PSG 120 FD (binder purified by CNES). Primer P 128.	.65 % RML: .62 [d]	.03		298	ESTEC (1981).

[a] TML: Total Mass Loss.
[b] CVCM: Collected Volatile Condensable Materials.
[c] Each one of these cures was used in the order given.
[d] RML: Remainder Mass Loss.

7.3. Thermal radiation properties.

7.3.1. Emittance.

7.3.1.1. Hemispherical total emittance.

$$\varepsilon = .87 \pm .02 \quad .$$

COATINGS

Solar Reflectors

From ASTRAL (1976)a.

The following value refers to PSG 120 FD.

$$\varepsilon = .88 \quad .$$

From Guillaumon & Guillin (1979, 1981).

7.3.1.3. Effects of the Space Environment on hemispherical total emittance.

7.3.1.3.1. Ultra-Violet Radiation.

$$\Delta\varepsilon < .01$$

Chamber pressure below 1.3×10^{-3} Pa.

Sample temperature: 353 K.

Exposure time: 120 ESH.

From ASTRAL (1976)a.

7.3.2. Absorptance.

7.3.2.1. Solar absorptance.

$$\alpha_s = .17 \pm .02$$

From ASTRAL (1976)a, Guillaumon & Guillin (1979, 1981).

7.3.2.5. Effects of the Space Environment on absorptance.

7.3.2.5.1. Ultra-Violet Radiation. Figs 1-16 to 1-18, from CNES.

Data measured in vacuum (below 1.3×10^{-5} Pa), several sample temperatures, with an integrating sphere attached to a Beckman DK2A reflectometer, $\beta=0°$.

Aluminium used as standard.

Irradiated in vacuum.

Degrading source: OSRAM type XBO 900 W, Arc Xenon lamp, quartz Suprasil envelope. Around 1 Sun level.

From Simon (1973).

COATINGS

Solar Reflectors

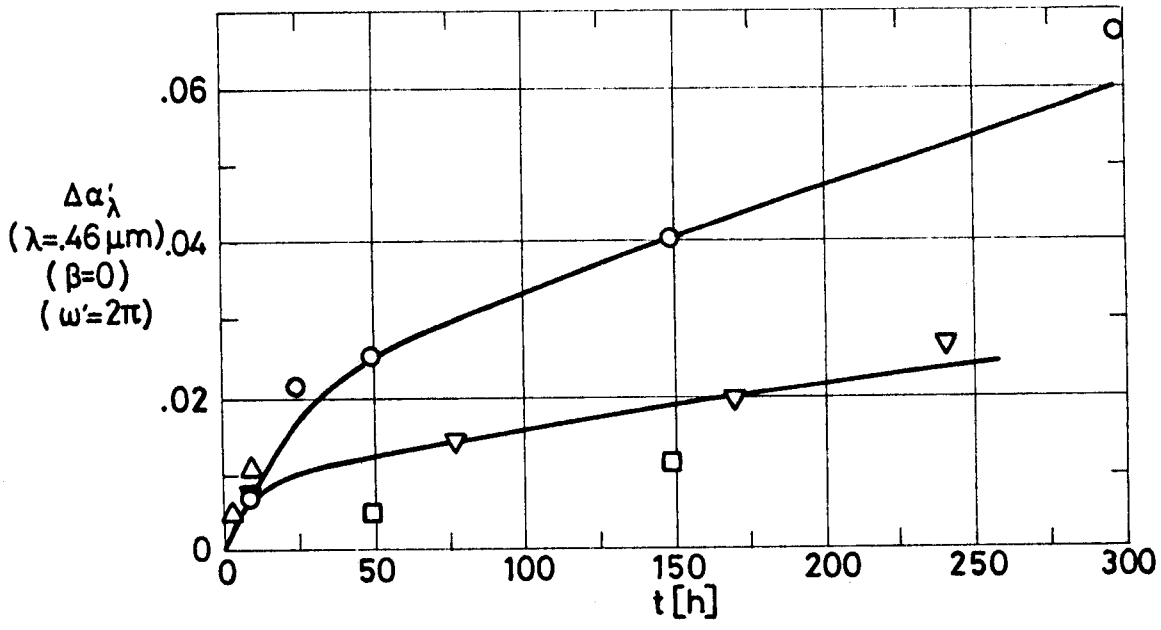

Fig 1-16. Change in normal-hemispherical spectral absorptance, $\Delta\alpha'_\lambda$, of PSG 120 coating, due to Ultra-Violet Radiation, vs. exposure time, t. Wavelength, $\lambda = .46 \times 10^{-6}$ m. From Simon (1974).

Explanation

Key	T [K]	$\lambda \times 10^6$ [m]	Comments
○	393	.46 (Fig 1-16).	
□	353	2.5 (Fig 1-17).	
△	283		
▽	283		After 9 h of UV radiation plus 25 h in nitrogen (bleaching).

COATINGS

Solar Reflectors

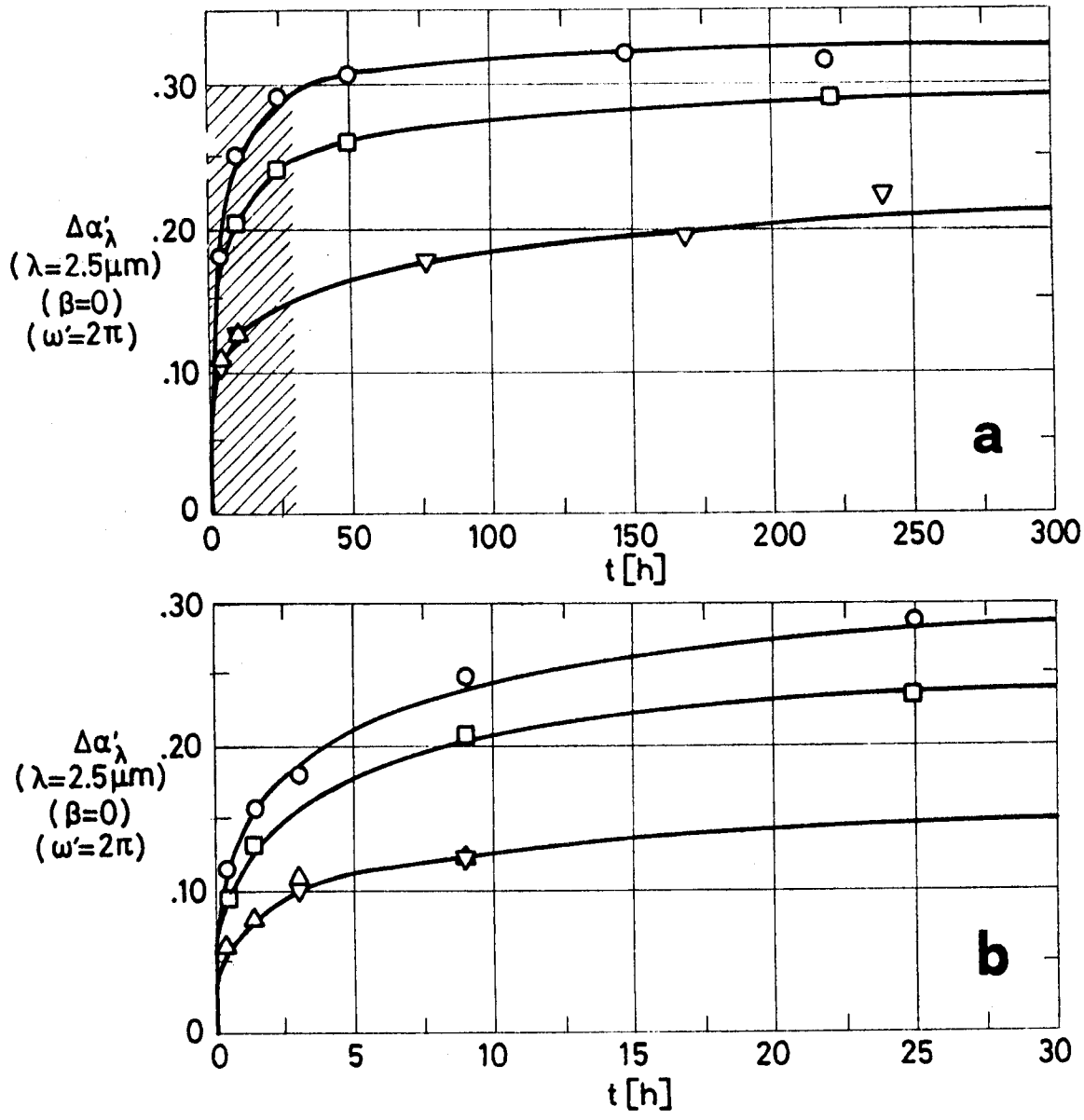

Fig 1-17. Change in normal-hemispherical spectral absorptance, $\Delta\alpha'_\lambda$, of PSG 120 coating, due to Ultra-Violet Radiation, vs. exposure time, t. Wavelength, $\lambda=2.5\times10^{-6}$ m. Shaded zone in a is enlarged in b.
See Explanation in the caption of Fig 1-16.
From Simon (1974).

Data concerning the effect of ultra-violet radiation on solar absorptance are given in Fig 1-18. α_s deduced from spectral reflectance measured as above.

COATINGS

Solar Reflectors

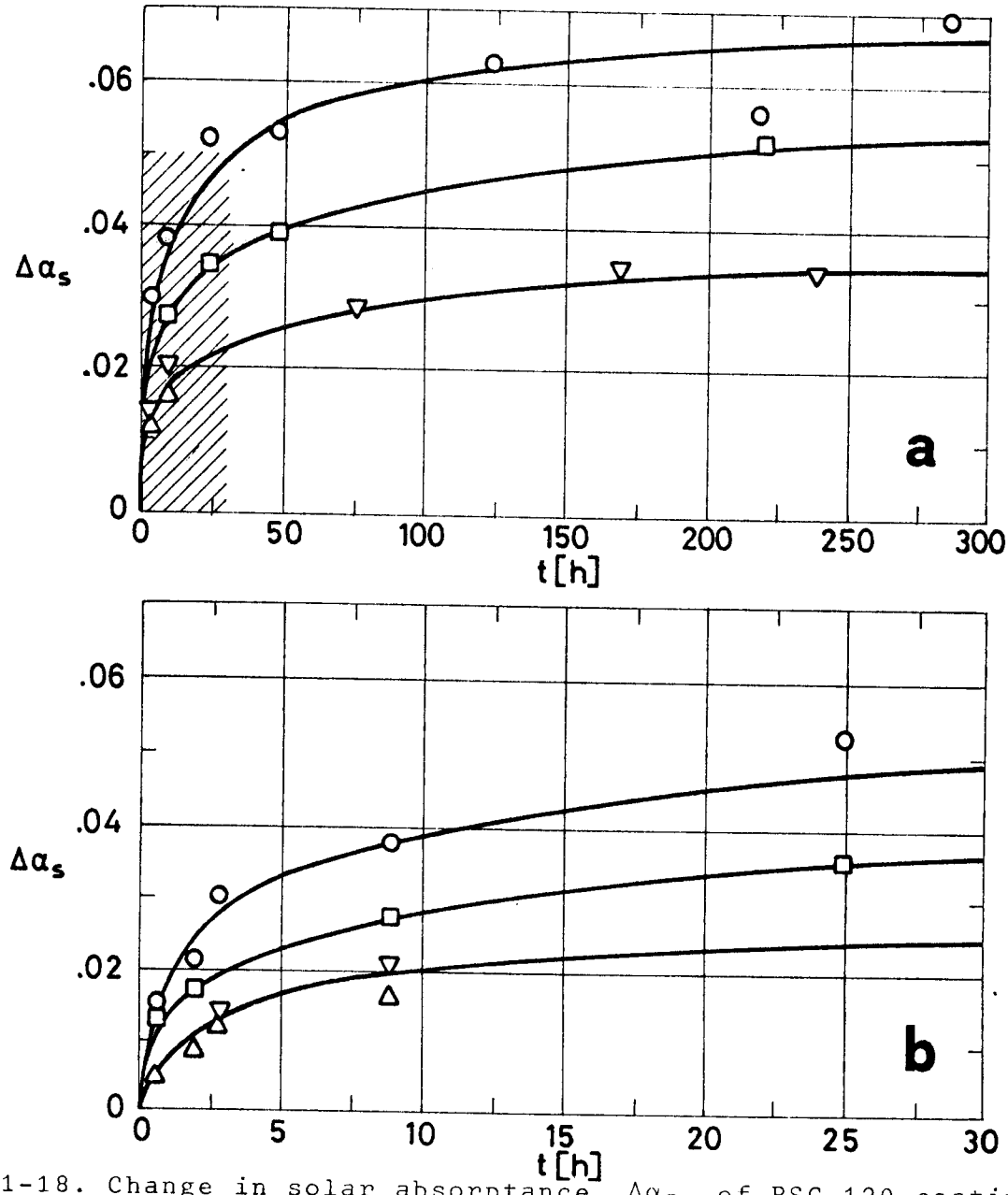

Fig 1-18. Change in solar absorptance, $\Delta\alpha_s$, of PSG 120 coating, due to UV Radiation, vs. exposure time, t. Shaded zone in a is enlarged in b. From Simon (1974).

Explanation

Key	T [K]	Comments
○	393	
□	353	
△	283	
▽	283	After 9 h of UV radiation plus 25 h in nitrogen (bleaching).

COATINGS

Solar Reflectors

7.3.2.5.3. Protons only exposure. Table 1-9 has been prepared after results reported by DERTS (Toulouse).

Solar absorptance is deduced from the spectral reflectance data given in p. 1-65 and ff.

CAUTION

Solar absorptance values of white paints deduced from spectral reflectance data by DERTS group, are larger, by a factor close to 2, than other widely accepted values.

The following table has been prepared by the compiler. Values of α_s before irradiation.

Solar Absorptance, α_s, of Four White Paints

Coating	S 13 IITRI	PSG 120 ASTRAL	Z 93 IITRI	PSZ 184 ASTRAL
DERTS	.37±.03	.38±.02	.33±.02	.36±.03
Other	.19±.04	.17±.02	.15±.02	.14±.02

Sources of data

S 13 DERTS, 6 values from Paillous (1976).
Other, 42 values from Touloukian, DeWitt & Hernicz (1972).

PSG 120 DERTS, 9 values from Paillous (1976) and Paillous, Amat, Marco & Panabiere (1977).
Other, p. 1-55.

Z 93 DERTS, 6 values as for S 13.
Other, p. 1-16 (soiled specimen has been excluded).

PSZ 184 DERTS, 9 values as for PSG 120.
Other, p. 1-86.

Spectral reflectance is measured in situ by DERTS group using a movable integrating sphere one of whose apertures faces successively each one of the samples in the sample holder, and the standard coating. See for further details p. 1-65.

A distance of the order of 3×10^{-3} m (not the same for all samples) exists

COATINGS

Solar Reflectors

between the sample and the sphere during reflectance measurements. This results in a loss of reflected light for diffusely reflecting coatings which affects ALL THE DATA regarding protons, electrons and combined exposure effect on reflectance (and absorptance) of PSG 120 coating.

Integrated values of solar absorptance from DERTS in Table 1-11 have been corrected, according to Paillous (1976), as follows:

1) The initial value for PSG 120 has been assumed to be,

$$\alpha_{so}=.20 \ ,$$

measured (in air) by ESTEC and by CNES using an integrating sphere attached to a Beckman DK2A reflectometer.

2) $\Delta\alpha_{s_{corrected}}$ has been related to $\Delta\alpha_{s_{in\ situ}}$ as follows,

$$\frac{\Delta\alpha_{s_{corrected}}}{\Delta\alpha_{s_{in\ situ}}}=\frac{\Delta\rho_{s_{corrected}}}{\Delta\rho_{s_{in\ situ}}}=\frac{.80}{1-\alpha_{so_{in\ situ}}} \ .$$

α_s variations in the different subranges of the spectrum (ultra-violet, visible, infrared) are given by Paillous, Amat, Marco & Panabiere (1977) regarding protons and electrons, and by Paillous (1976) regarding combined exposure. These data have not been compiled here.

Table 1-9

Protons Radiation Effects on Solar Absorptance of PSG 120 Coating

Intensity [keV] →	45			75			150		
↓ Integrated Flux [$p.m^{-2}$]	α_s	$\Delta\alpha_s$	$\Delta\alpha_s/\alpha_s$	α_s	$\Delta\alpha_s$	$\Delta\alpha_s/\alpha_s$	α_s	$\Delta\alpha_s$	$\Delta\alpha_s/\alpha_s$
Before (in air)	.293			.353			.348		
Before (in vacuum)	.326			.384			.383		
10^{17}	.325	-.001	-.004	.397	.013	.033	.385	.002	.005
10^{18}	.333	.007	.020	.401	.017	.043	.397	.014	.036
10^{19}	.383	.057	.148	.459	.075	.164	.495	.112	.226
2.1×10^{19} for 45 keV 2.8×10^{19} otherwise	.456	.130	.285	.528	.144	.273	.582	.199	.342
After (in air)	.390			.438			.458		

From Paillous, Amat, Marco & Panabiere (1977).

COATINGS

Solar Reflectors

7.3.2.5.4. Electrons only exposure. Table 1-10 after results from DERTS.

Solar absorptance is deduced from the spectral reflectance data given in p. 1-68 and ff.

Table 1-10

Electrons Radiation Effects on Solar Absorptance of PSG 120 Coating

Intensity [keV] →	40			80			210		
↓ Integrated Flux [e.m^{-2}]	α_s	$\Delta\alpha_s$	$\Delta\alpha_s/\alpha_s$	α_s	$\Delta\alpha_s$	$\Delta\alpha_s/\alpha_s$	α_s	$\Delta\alpha_s$	$\Delta\alpha_s/\alpha_s$
Before (in air)	.333			.335					
Before (in vacuum)	.341			.366			.346		
2×10^{14}	.354	.013	.035	.392	.026	.066	.412	.066	.160
5×10^{14}	.356	.015	.043	.403	.037	.091	.411	.065	.158
10^{15}	.365	.024	.067	.416	.049	.119	.426	.080	.189
2×10^{15}	.375	.034	.091						
After (in air)	.334			.363			.355		

From Paillous, Amat, Marco & Panabiere (1977).

7.3.2.5.6. Combined exposure. Table 1-11 after DERTS.

Solar absorptance from spectral reflectance data.

The tests simulate geosynchronous orbit exposure of the Orbital Test Satellite (OTS) equatorial faces.

"Corrected" values in Table 1-11 were used to estimate coating degradation up to 3 years in orbit, Fig 1-19.

Also shown data from Guillaumon & Guillin (1981), CNES.

Incidents during testing, see p. 1-75, cast doubts on the validity of the data beyond 1 year in orbit.

COATINGS

Solar Reflectors

Table 1-11

Combined Exposure Effects on Solar Absorptance of PSG 120 Coating

Test Conditions	Sample 1						Sample 2					
	Measured in situ			Corrected [a]			Measured in situ			Corrected [a]		
	α_s	$\Delta\alpha_s$	$\Delta\alpha_s/\alpha_s$	α_s	$\Delta\alpha_s$	$\Delta\alpha_s/\alpha_s$	α_s	$\Delta\alpha_s$	$\Delta\alpha_s/\alpha_s$	α_s	$\Delta\alpha_s$	$\Delta\alpha_s/\alpha_s$
BEFORE IRRADIATION	.358			.200			.367			.200		
AFTER A UNDER VACUUM [b]	.422	.063	.177	.279	.079	.395	.440	.073	.199	.291	.091	.455
BEFORE B	.388	.029	.082	.236	.036	.180	.402	.035	.096	.244	.044	.220
AFTER B [b]	.410	.051	.144	.264	.064	.320	.451	.084	.230	.305	.105	.525
AFTER PUMP DAMAGE [c]	.378	.020	.055	.225	.025	.125	.390	.023	.062	.229	.029	.145
BEFORE C	.425	.067	.188	.284	.084	.420	.440	.073	.200	.291	.091	.455
AFTER C [b]	.485	.127	.354	.359	.159	.795	.502	.135	.369	.369	.169	.845
BEFORE D	.474	.116	.323	.345	.145	.725	.487	.120	.327	.350	.150	.750
AFTER D UNDER VACUUM [b]	.505	.147	.410	.384	.184	.920	.516	.149	.405	.386	.186	.930
AFTER D AND AIR EXPOSURE	.430	.072	.201	.290	.090	.450	.557	.190	.518	.438	.238	1.19

[a] The correction has been made by the compiler as follows:

1) Value before irradiation, α_{so}=.20 .

2) $$\frac{\Delta\alpha_{s\,corrected}}{\Delta\alpha_{s\,in\ situ}} = \frac{1-\alpha_{so}}{1-\alpha_{so\,in\ situ}} = \frac{.80}{.64}\ ,$$

where α_{so} has been measured (in air) with an integrating sphere attached to a Beckman DK2A reflectometer. $\alpha_{so\,in\ situ}$ is the value measured before irradiation as indicated in p. 1-65.

[b] Steps A to D correspond, respectively, to the following times in geosynchronous orbit.
A : .18 yr = 508 ESH.
B : .94 yr = 2 443 ESH.
C : 2.11 yr = 5 604 ESH.
D : 3 yr = 7 949 ESH.

[c] See p. 1-75 for further details.

From Paillous (1976).

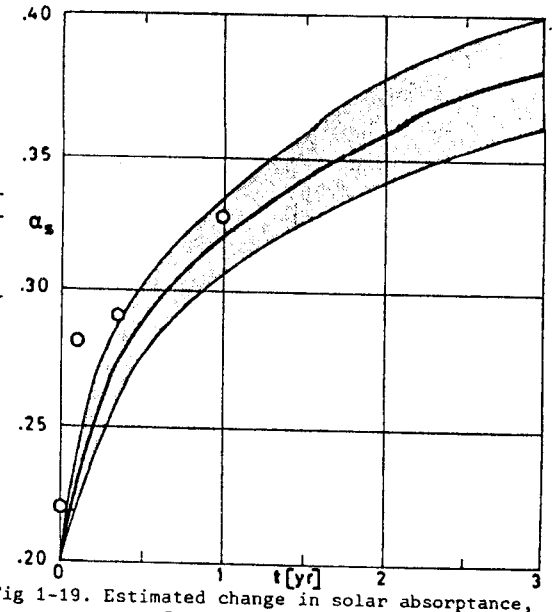

Fig 1-19. Estimated change in solar absorptance, α_s, of PSG 120 vs. time, t. From Paillous (1976).
O From Guillaumon & Guillin (1981).

COATINGS

Solar Reflectors

7.3.3. Reflectance. Data related with bidirectional total reflectance are given in Fig 1-20.

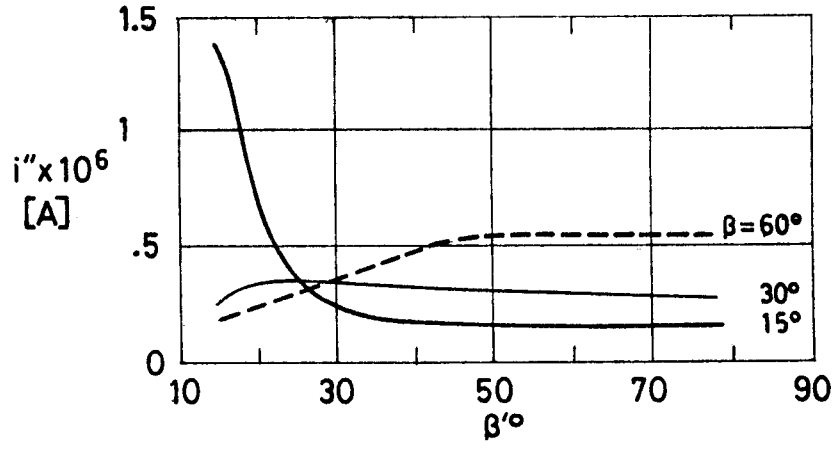

Fig 1-20. Bidirectional total radiation intensity of reflected flux, i", vs. cone angle, β', for several values of the cone angle of the incident flux, β. PSG 120 coating. Incident and reflected fluxes are coplanar. i" is measured by the response of a photocell attached to a photogoniometer. From ASTRAL (1976)a.

7.3.3.1. Normal-hemispherical spectral reflectance. Fig 1-21 from CNES.

Chamber pressure below 1.3×10^{-5} Pa.

Sample temperature: 348 K.

Spectral reflectance measured in situ with an integrating sphere, operating in the direct mode, attached to a Beckman DK2A reflectometer.

Aluminium used as standard. Sample and standard are alternatively illuminated.

See Simon (1973) for further details on the measurement procedure.

7.3.3.2. Effects of the Space Environment on reflectance.

7.3.3.2.1. Ultra-Violet Radiation. Fig 1-21.

COATINGS

Solar Reflectors

Sample conditions and spectral reflectance measurements as above.

Sample irradiated in vacuum.

Degrading source: OSRAM type XBO 900 W, Arc Xenon lamp, quartz Suprasil envelope.

Radiation flux density at the sample level: ∿1 Sun.

Exposure time: 212 ESH.

See Fig 1-16 and ff. where similar data from CNES are presented.

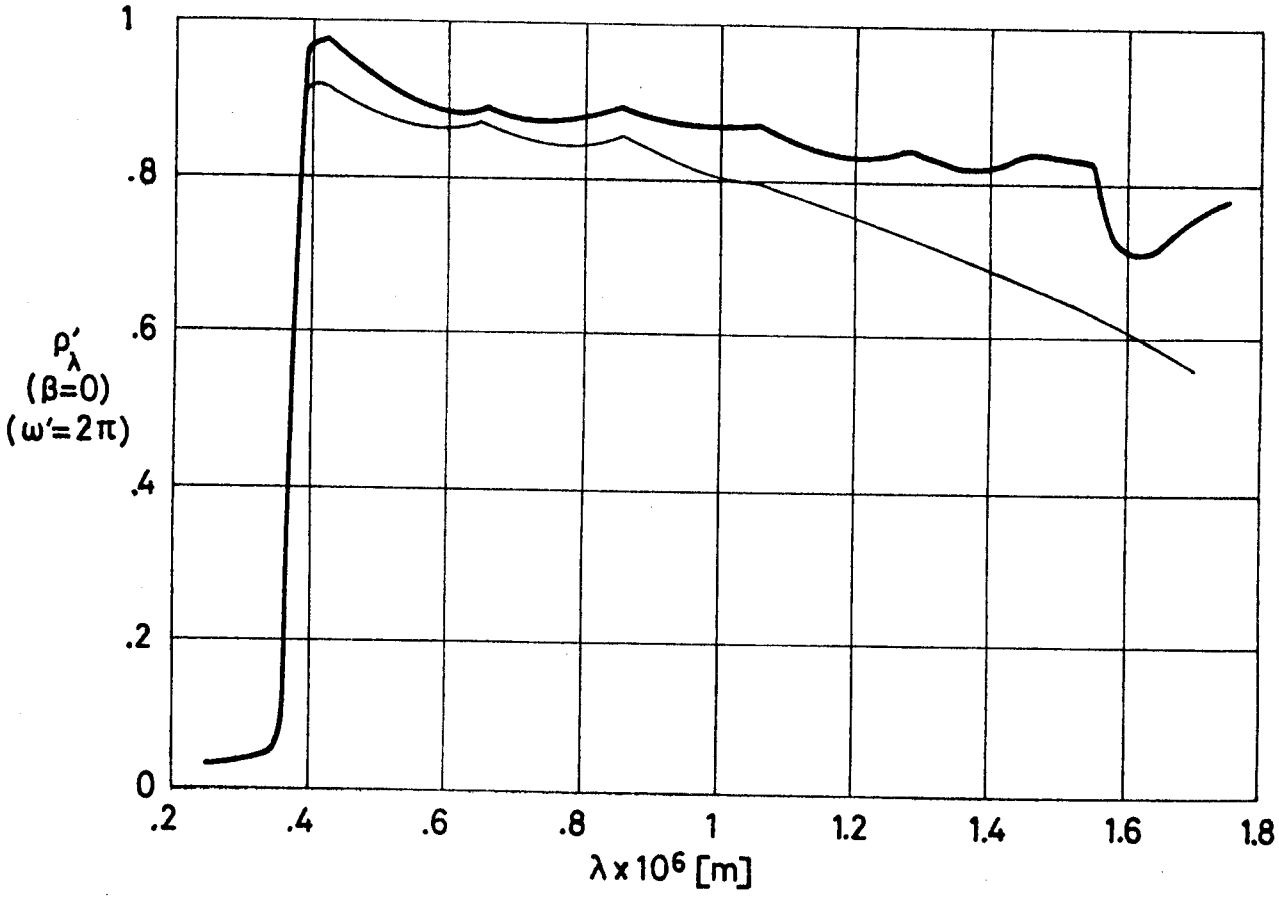

Fig 1-21. Effect of Ultra-Violet Radiation on normal-hemispherical spectral reflectance, ρ'_λ, of PSG 120 coating vs. wavelength, λ.
——— Before irradiation. $p<1.3\times10^{-5}$ Pa. T=348 K.
——— After irradiation. $p<1.3\times10^{-5}$ Pa. T=348 K.
1 Sun level. t = 212 ESH. From Simon (1973).

COATINGS

Solar Reflectors

7.3.3.2.3. Protons only exposure. Fig 1-22 and ff., from DERTS.

Sample on aluminium substrate.

A SAMES proton accelerator has been used. The proton beam impinges normally on the sample.

Tests were performed in four successive steps. Data, which were taken before 3 h from the end of each step, are for cumulative damage.

Chamber pressure in the range 6.7×10^{-5} Pa to 10^{-4} Pa.

Sample temperature: 303 K ± .5 K.

Spectral reflectance measured in situ with an integrating sphere, operating in the direct mode, and appropriate detectors (depending on the λ range) viewing an area of the sphere inner wall.

A Zeiss monochromator can be displaced, together with the sphere, to successively illuminate the sample (2×10^{-2} m square) and a vacuum deposited aluminium standard (not exposed to the damaging irradiation).

Readings for the sample and for the standard provide the directional-hemispherical reflectance factor, given in the following figures as directional-hemispherical spectral reflectance.

The experimental set-up is basically that described by Paillous (1975), except for minor improvements in the optical detector system.

Neither the incidence angle, β, nor a schematic of the sphere are given in the source.

COATINGS

Solar Reflectors

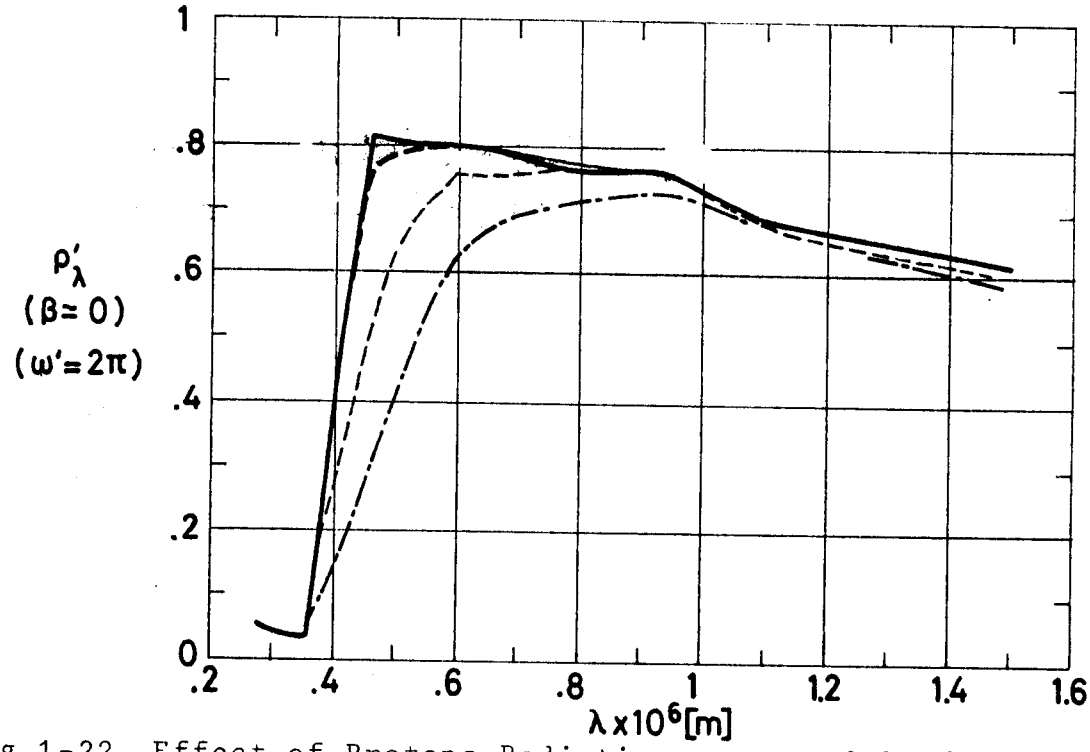

Fig 1-22. Effect of Protons Radiation on normal-hemispherical spectral reflectance, ρ'_λ, of PSG 120 coating vs. wavelength, λ. Radiation intensity ≃45 keV. See Explanation in the caption of Fig 1-24. From Paillous, Amat, Marco & Panabiere (1977).

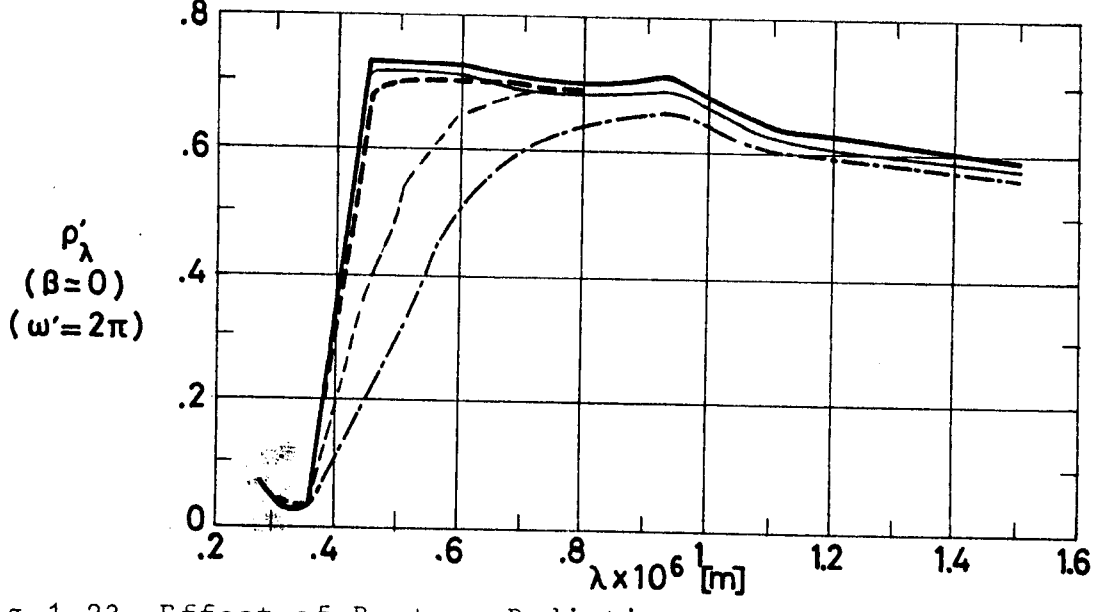

Fig 1-23. Effect of Protons Radiation on normal-hemispherical spectral reflectance, ρ'_λ, of PSG 120 coating vs. wavelength, λ. Radiation intensity ≃75 keV. See Explanation in the caption of Fig 1-24. From Paillous, Amat, Marco & Panabiere (1977).

COATINGS

Solar Reflectors

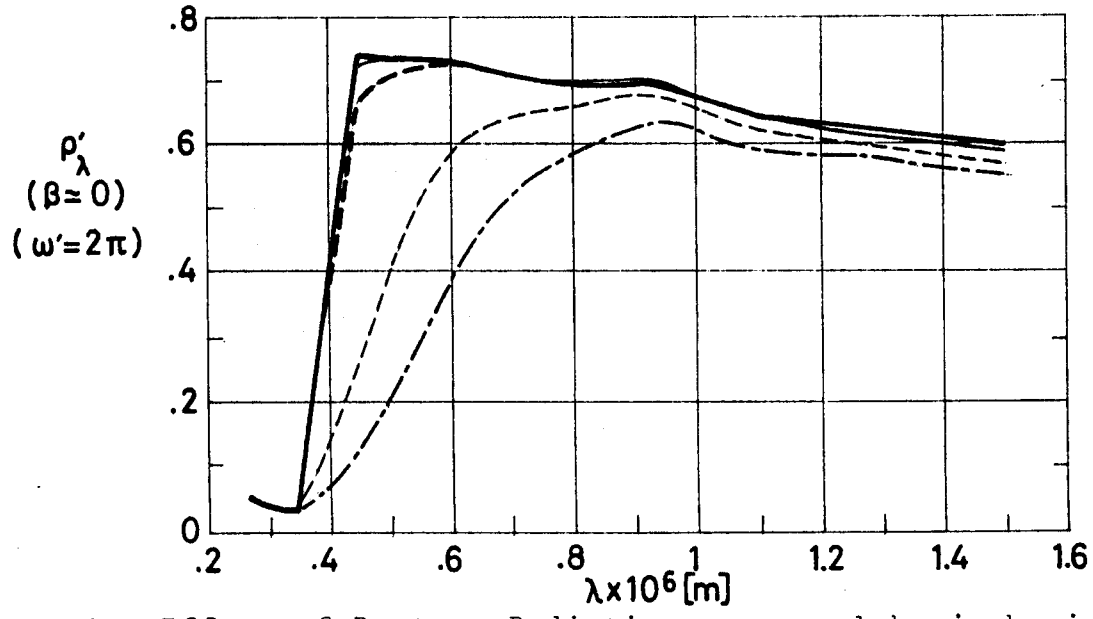

Fig 1-24. Effect of Protons Radiation on normal-hemispherical spectral reflectance, ρ'_λ, of PSG 120 coating vs. wavelength, λ. Radiation intensity ≃150 keV. From Paillous, Amat, Marco & Panabiere (1977).

Explanation

Key	Intensity [keV]	Flux [$p.m^{-2}.s^{-1}$]	Integrated Flux [$p.m^{-2}$]	Cumulative Integrated Flux [$p.m^{-2}$]	Comments
———	45 keV in Fig 1-22. 75 keV in Fig 1-23. 150 keV in Fig 1-24.				Sample on aluminium substrate. $p = 1.3\times10^{-4}$ Pa. T = 303 K ± .5 K. Incidence of the protons beam: 0°.
———		1.3×10^{14}	10^{17}	10^{17}	
– – –		2.5×10^{14}	9×10^{17}	10^{18}	
— — —		2.5×10^{14} (Fig 1-22). 6.2×10^{14} (Figs 1-23 & 1-24).	9×10^{18}	10^{19}	
—·—·—		6.2×10^{14}	1.1×10^{19} (Fig 1-22). 1.8×10^{19} (Figs 1-23 & 1-24).	2.1×10^{19} (Fig 1-22). 2.8×10^{19} (Figs 1-23 & 1-24).	

COATINGS

Solar Reflectors

7.3.3.2.4. Electrons only exposure. Fig 1-25 and ff., from DERTS.

Sample on aluminium substrate.

A SAMES electron accelerator has been used. The electron beam impinges on the sample at 45°, but this has been taken into account for estimating the mean flux and the deviation from the mean. This is kept within ±35% for the 25 samples being irradiated all at once. The achievable electrons energy at the samples is of the order of 200 keV.

See Paillous (1975) for further details.

The tests were performed in four successive steps, and readings were taken at the end of each step. Sample conditions and reflectance measurements as in p. 1-65.

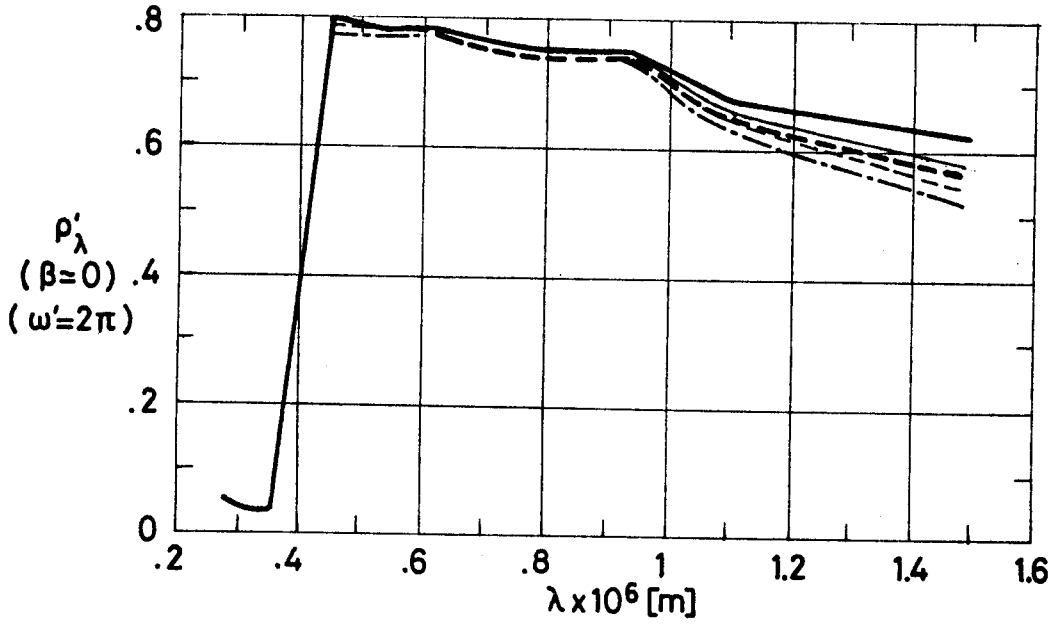

Fig 1-25. Effect of Electrons Radiation on normal-hemispherical spectral reflectance, ρ'_λ, of PSG 120 coating vs. wavelength, λ. Radiation intensity ≃40 keV.
See Explanation in the caption of Fig 1-26.
From Paillous, Amat, Marco & Panabiere (1977).

COATINGS

Solar Reflectors

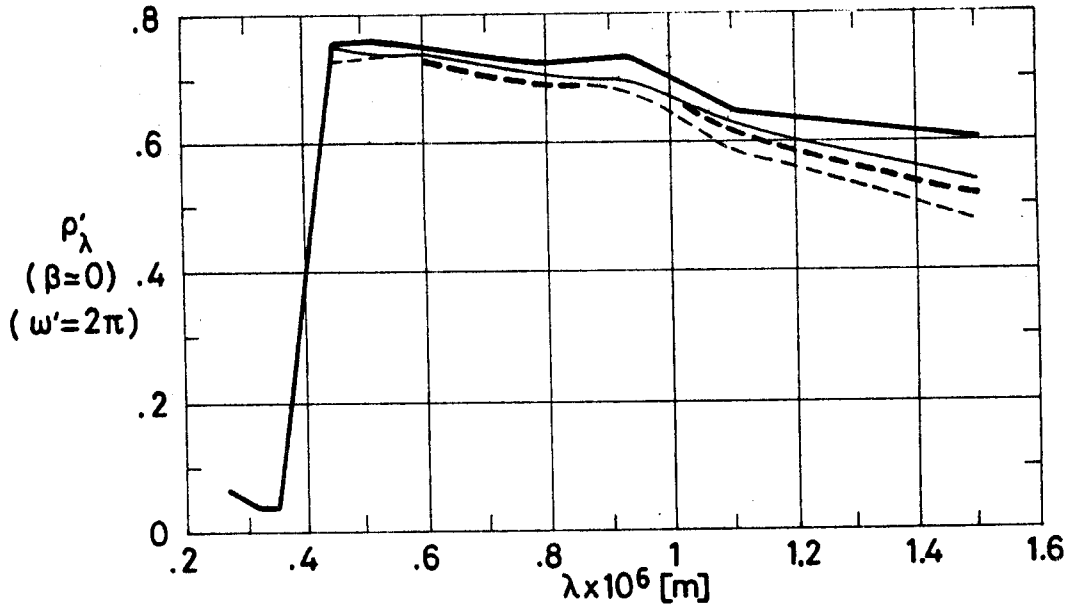

Fig 1-26. Effect of Electrons Radiation on normal-hemispherical spectral reflectance, ρ'_λ, of PSG 120 coating vs. wavelength, λ. Radiation intensity ≈80 keV. From Paillous, Amat, Marco & Panabiere (1977).

Explanation

Key	Intensity [keV]	Flux [$e.m^{-2}.s^{-1}$]	Integrated Flux [$e.m^{-2}$]	Cumulative Integrated Flux [$e.m^{-2}$]	Comments
———	40 keV in Fig 1-25. 80 keV in Fig 1-26.				Sample on aluminium substrate. $p = 1.3\times10^{-4}$ Pa. T = 303 K ± .5 K. Incidence of the electron beam: 45°.
———		2.7×10^{14} (Fig 1-25). 2.9×10^{14} (Fig 1-26).	2×10^{18}	2×10^{18}	
– – –		4×10^{14} (Fig 1-25). 2.8×10^{14} (Fig 1-26).	3×10^{18}	5×10^{18}	
– – –		4×10^{14} (Fig 1-25). 5.3×10^{14} (Fig 1-26).	5×10^{18}	10^{19}	
—·—		5.4×10^{14} (Fig 1-25).	10^{19} (Fig 1-25).	2×10^{19} (Fig 1-25).	

COATINGS

Solar Reflectors

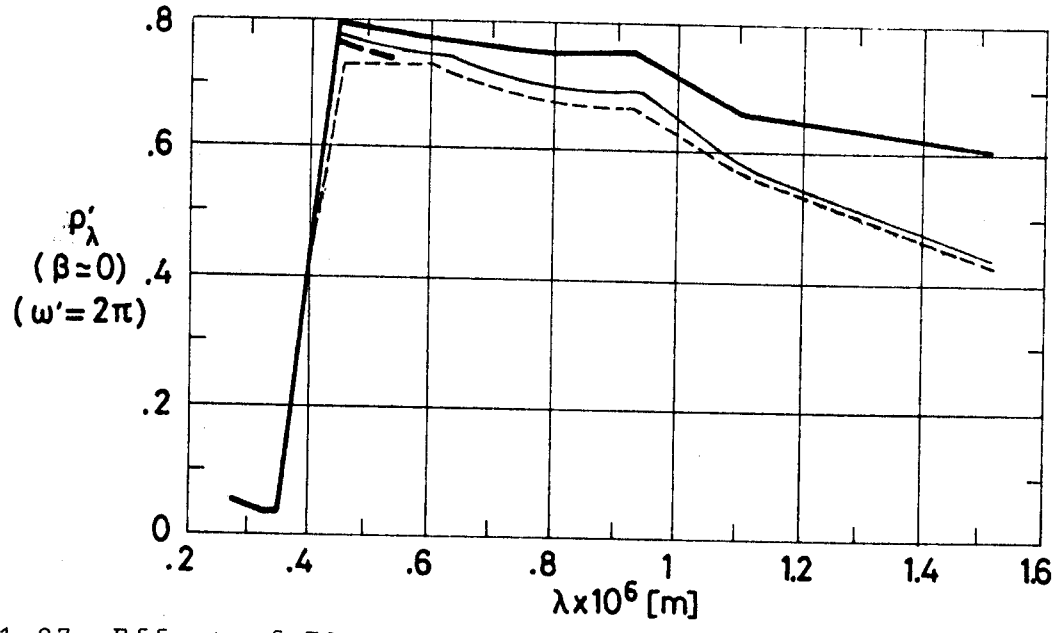

Fig 1-27. Effect of Electrons Radiation on normal-hemispherical spectral reflectance, ρ'_λ, of PSG 120 coating vs. wavelength, λ. Radiation intensity ≃210 keV. From Paillous, Amat, Marco & Panabiere (1977).

Explanation

Key	Intensity [keV]	Flux [$e.m^{-2}.s^{-1}$]	Integrated Flux [$e.m^{-2}$]	Cumulative Integrated Flux [$e.m^{-2}$]	Comments
———	210				Sample on aluminium substrate. $p = 1.3 \times 10^{-4}$ Pa. T = 303 K ± .5 K. Incidence of the electrons beam: 45°.
———		3.0×10^{14}	2×10^{18}	2×10^{18}	
- - -		3.1×10^{14}	3×10^{18}	5×10^{18}	
- - -		6.3×10^{14}	5×10^{18}	10^{19}	

An analytical model of the solar absorptance degradation because of the irradiation of protons and electrons, with application to white paints, has been set forth by Bourrieau (1978), Bourrieau & Paillous (1979).

COATINGS

Solar Reflectors

The model ascribes the changes in solar absorptance to the creation within the coating of defect centers, the concentration of which depends only on the local absorbed dose.

The defect density produces an absorption band which results in the optical degradation of the coating. The intensity of that absorption band is assumed to depend only on the defect density.

The absorption bands become apparent when the spectral reflectance curves before and after irradiation are compared to each other.

The distribution of absorbed dose in the coating can be calculated by use of available computational techniques (Bourrieau (1978)). In practice a mean dose, $\overline{D}$, is assumed to be uniformly distributed throughout a disturbed layer, the thickness of which, X_d, is called the penetration range.

The analytical model shows that:

1) When the disturbed layer is much thicker than the layer of photon absorption and scattering (optical range, X_u), the change in spectral reflectance does not depend on X_d. This occurs for high energy particles or very large irradiation doses.

2) On the other hand, when $X_d << X_u$ the changes in spectral reflectance are proportional to the penetration range, X_d.

COATINGS

Solar Reflectors

In the case of PSG 120 coating two absorption bands are present, probably at $\lambda=.41\times10^{-6}$ m and $\lambda=2.1\times10^{-6}$ m. None of them was clearly detected, since measurements of spectral reflectance were made at discrete values of λ, and the nearest values were, respectively, $\lambda=.45\times10^{-6}$ m and $\lambda=2.5\times10^{-6}$ m.

The experimental results for $\lambda=2.05\times10^{-6}$ m have been used to test the applicability of the analytical model to PSG 120 coating degradation.

The relevant irradiation parameters are summarized in Table 1-12.

Table 1-12

Application of the Degradation Model to PSG 120 Coating

Type of Particle	Protons			Electrons		
Intensity [keV]	45	75	150	40	80	210
Flux [particles.$m^{-2}.s^{-1}$]	1.3×10^{14} to 6.2×10^{14}			2.7×10^{14} to 5.4×10^{14}	2.9×10^{14} to 5.3×10^{14}	3.0×10^{14} to 6.3×10^{14}
Cumulative Integrated Flux [particles.m^{-2}]	10^{17} to 2.8×10^{19}			2×10^{18} to 2×10^{19}	2×10^{18} to 10^{19}	
Penetration Range, X_d [$kg.m^{-2}$]	2.4×10^{-3}	3.4×10^{-3}	5.6×10^{-3}	2.5×10^{-2}	9.0×10^{-2}	5.0×10^{-1}
Mean Dose, $\bar{D}$ GY/particle [a]	3.0×10^{-8}	3.6×10^{-8}	4.3×10^{-8}	1.7×10^{-9}	10^{-9}	5.8×10^{-10}
Related Figure	1-22	1-23	1-24	1-25	1-26	1-27

[a] 1 GY (Gray) = 1 $J.kg^{-1}$.

From Bourrieau (1978).

COATINGS

Solar Reflectors

Experimental have been compared to theoretical results as can be seen in Fig 1-28. Data from protons irradiation at 75 keV, not deemed to be reliable, are not shown. Agreement is fair, even though the assumption of an uniformly-distributed mean dose (throughout the disturbed layer) cannot be justified for high energy electron irradiations.

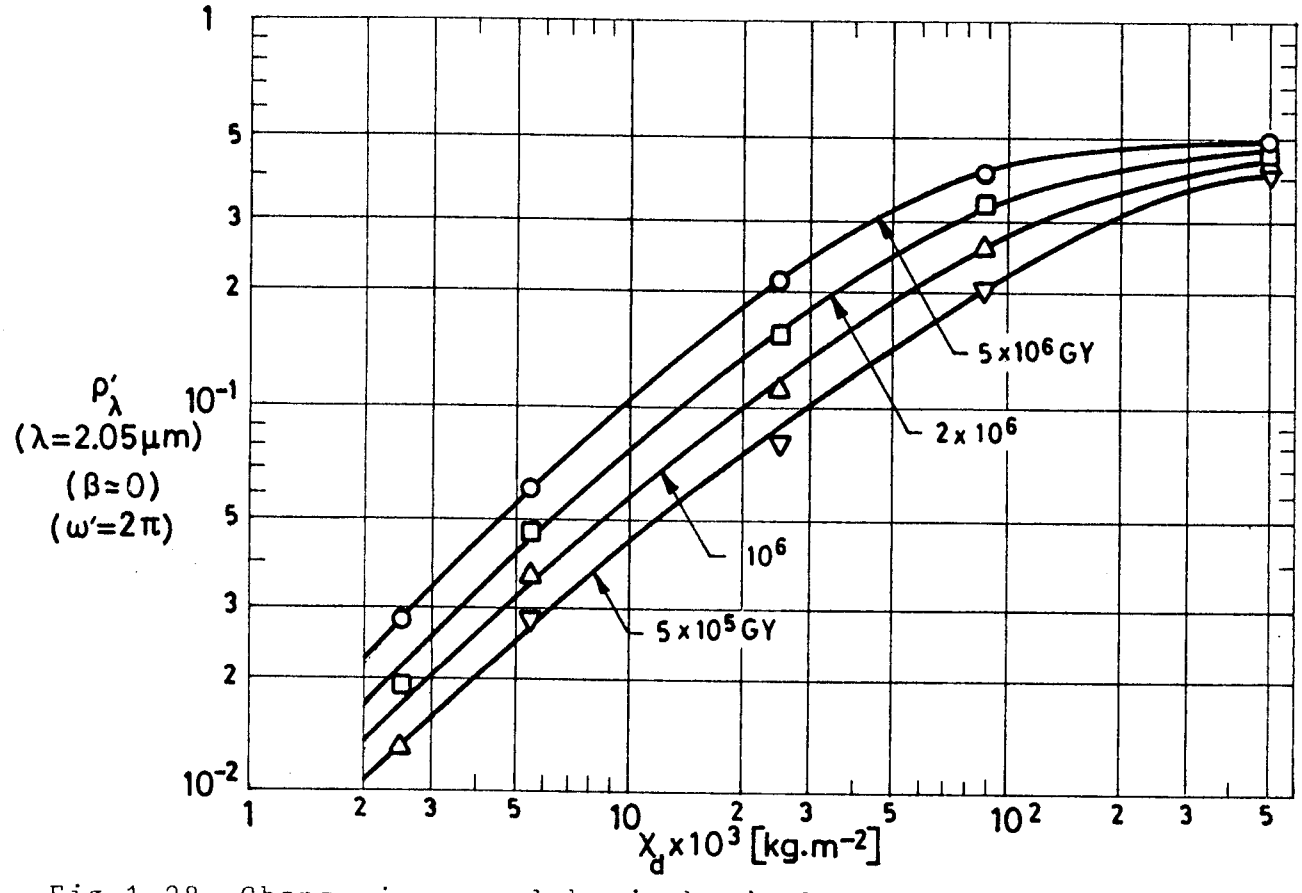

Fig 1-28. Change in normal-hemispherical spectral reflectance, ρ'_λ, of PSG 120 coating, due to particulate irradiation, vs. penetration range, X_d. Wavelength, $\lambda=2.05\times10^{-6}$ m. From Bourrieau (1978).

COATINGS

Solar Reflectors

7.3.3.2.6. Combined exposure. Figs 1-29 and 1-30 from DERTS.

Sample on aluminium substrate.

Irradiations were performed under the following conditions:

Chamber pressure below 1.3×10^{-4} Pa.

Sample temperature: 363 K.

Reflectance measured in situ without breaking vacuum, unless otherwise stated.

The exposure is intended to simulate 3 years in geo-synchronous orbit of the three-axis stabilized Orbital Test Satellite (OTS) equatorial faces. The tests reproduced the simultaneous action of vacuum and temperature, and of ultra-violet, protons and electrons irradiations.

Ultra-violet irradiation was only possible at or below 3 Suns. Because of this limited capability, particle irradiations were performed intermittently, within the constraint of a correct simulation of the integrated fluxes at the end of the four main steps of the test (Table 1-13). Ultra-violet irradiation, on the contrary, was performed continuously.

For the ultra-violet exposure, the samples were irradiated at 45° incidence, through a Suprasil ultra-pure silica window. Two different high pressure Xenon lamps were needed to reproduce the full ultra-violet spectrum. Uniformity of illumination was within ±17% for

COATINGS

Solar Reflectors

the whole ensemble of 25 samples in the sample holder. Particulate irradiations and in situ reflectance measurements were achieved as in pp. 1-65 and 1-68.

The following measurements were performed:

1) Solar reflectance (in air) before and after irradiation was measured, by ESTEC and by CNES, with an integrating sphere attached to a Beckman DK2A reflectometer. Standards of polished aluminium. The resulting α_s before irradiation has been given in p. 1-60.

2) In situ measurements of global reflectance. A solar-simulating high pressure Xenon lamp, 75 W, was used. The lamp was attached to the integrating sphere via a glass and quartz fiber optical tube. The resulting data have not been compiled here.

3) In situ spectral reflectance, as in p. 1-65. A limited amount of data are given in Figs 1-29 and 1-30. An incident occurred during ultra-violet only irradiation between steps B and C. The chamber pressure rose up to 1.3 Pa because of some damage in the secondary vacuum pump. This incident resulted in an increase in the reflectance, which was measured and reported. Since test were resumed after repairing the pump and some bleaching occurred, the data for steps C and D should be looked at cautiously.

COATINGS

Solar Reflectors

Table 1-13

Test Conditions Simulating up to Three Years in Geosynchronous Orbit

		Step A	Step B	Step C	Step D
Years in Orbit		.18	.94	2.11	3
Simulation Test Time [h]		160	883	1 868	2 650
ESH		508	2 443	5 604	7 949
Protons Exposure 40 keV	Starting Time, First Run [h]	90	790	1 850	2 630
	Stopping Time, Last Run [h]	169	831	1 868	2 650
	Net Running Time [h]	16	32	16	12
	Flux [Protons.$m^{-2}.s^{-1}$]	1.33×10^{13}	3.04×10^{13}	8.33×10^{13}	8.80×10^{13}
	Integrated Flux [Protons.m^{-2}]	$.77\times10^{18}$	$.35\times10^{19}$	$.48\times10^{19}$	$.39\times10^{19}$
	Cumulative Integrated Flux [Protons.m^{-2}]	$.77\times10^{18}$	$.43\times10^{19}$	$.91\times10^{19}$	1.30×10^{19}
Protons Exposure 150 keV	Starting Time, First Run [h]	0	548	1 700	2 615
	Stopping Time, Last Run [h]	90	790	1 850	2 630
	Net Running Time [h]	16	32	16	12
	Flux [Protons.$m^{-2}.s^{-1}$]	4.51×10^{11}	9.98×10^{11}	2.73×10^{12}	2.92×10^{12}
	Integrated Flux [Protons.m^{-2}]	$.27\times10^{17}$	1.17×10^{17}	1.58×10^{17}	1.27×10^{17}
	Cumulative Integrated Flux [Protons.m^{-2}]	$.27\times10^{17}$	1.44×10^{17}	3.02×10^{17}	4.29×10^{17}
Electrons Exposure 200 keV	Starting Time, First Run [h]	0	548	1 700	2 615
	Stopping Time, Last Run [h]	169	831	1 868	2 650
	Net Running Time [h]	32	64	32	24
	Flux [Electrons.$m^{-2}.s^{-1}$]	1.34×10^{13}	3.08×10^{13}	8.23×10^{13}	8.80×10^{13}
	Integrated Flux [Electrons.m^{-2}]	$.15\times10^{19}$	$.71\times10^{19}$	$.95\times10^{19}$	$.76\times10^{19}$
	Cumulative Integrated Flux [Electrons.m^{-2}]	$.15\times10^{19}$	$.86\times10^{19}$	1.81×10^{19}	2.57×10^{19}

Prom Paillous (1976).

COATINGS

Solar Reflectors

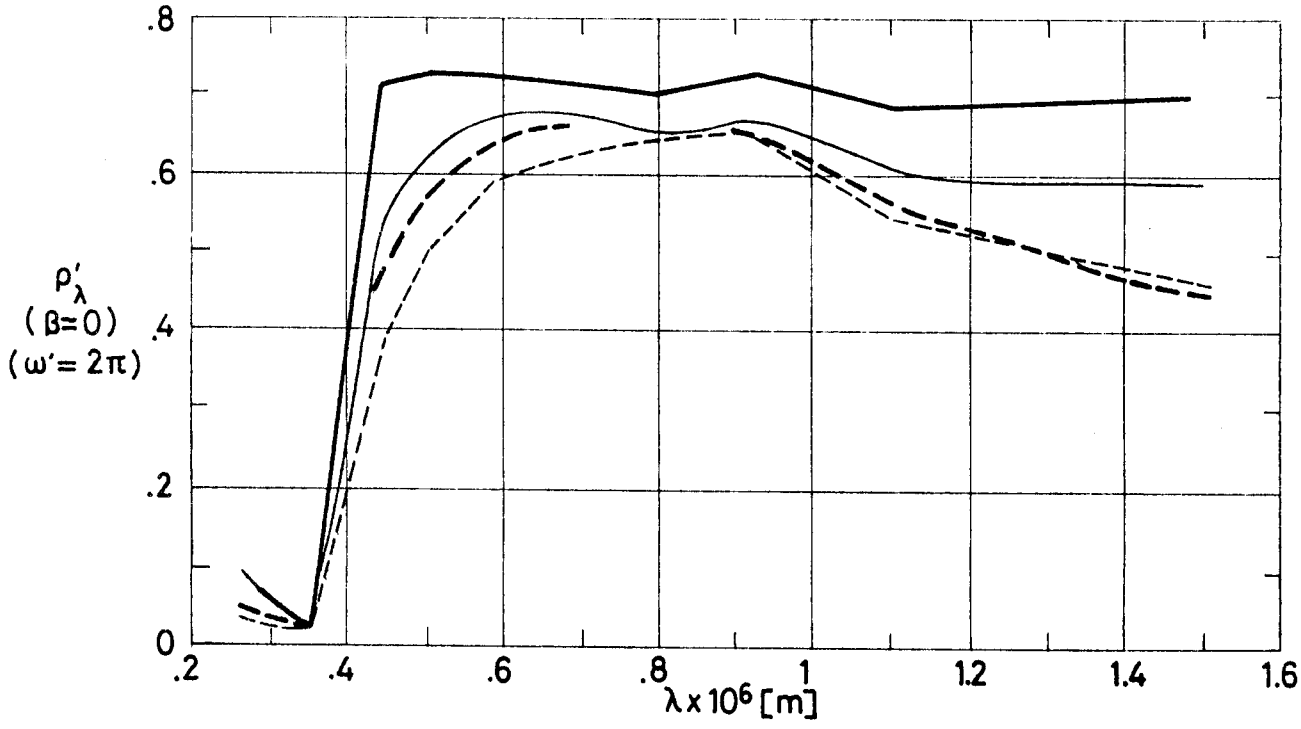

Fig 1-29. Effect of Combined Exposure, simulating up to three years in geosynchronous orbit, on normal-hemispherical spectral reflectance, ρ'_λ, of PSG 120 coating vs. wavelength, λ. From Paillous (1976).

Explanation

Key	Description	Comments
———	After 125 h below 1.3×10^{-4} Pa pressure. T = 363 K.	
——	After step B (.94 years in orbit). T = 363 K.	
– – –	After step C (2.11 years in orbit). T = 363 K.	After unintentional O_2 bleaching.
– – – –	After step D (3 years in orbit). T = 363 K.	

COATINGS

Solar Reflectors

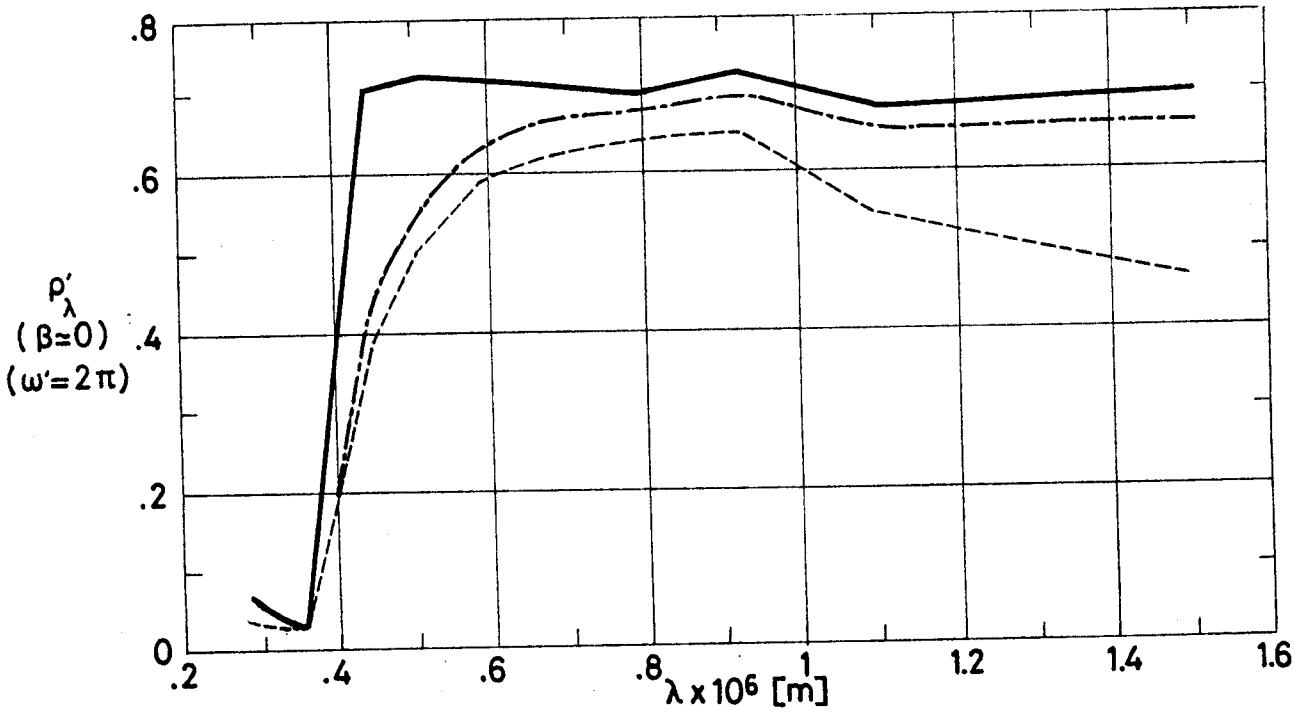

Fig 1-30. Effect of O_2 bleaching, after Combined Exposure, on normal-hemispherical spectral reflectance, ρ'_λ, of PSG 120 coating vs. wavelength, λ. Curves ——— and ---- are those shown in Fig 1-29. From Paillous (1976).

Explanation

Key	Description	Comments
———	After 125 h below 1.3×10^{-4} Pa pressure. T = 363 K.	
----	After step D (3 years in orbit). T = 363 K.	After unintentional O_2 bleaching.
—·—·	After step D and Air exposure. T = 293 K.	

COATINGS

Solar Reflectors

7.4. Electrical resistance. According to Paillous (1976) this coating exhibited a small electrical conductivity during particulate irradiation. After air exposure the electrical conductivity vanished to zero. The reason for this effect remains unclear.

8. ENVIRONMENTAL BEHAVIOR

PSG 120 has been space-qualified by CNES. The qualification tests include:

8.1. Prelaunch. Moisture resistance test.

Relative humidity: above 90%.
Temperature : 363 K.
Duration : 5 d.

The coating showed no failures, not even tiny unstuck spots. From Guillaumon & Guillin (1979). ASTRAL (1976)a quotes a duration of 7 d.

8.2. Postlaunch. Cure time for minimizing outgassing, in p. 1-54. The coating withstood vibrations per D2 Spacecraft Specification with no apparent change in adhesion.

8.2.1. Ascent. Thermal soak at normal pressure.

Temperature: 523 K.
Duration : 100 h.

Thermal soak under vacuum.

Pressure : below 1.3×10^{-5} Pa.
Temperature: 523 K.
Duration : 100 h.

From ASTRAL (1976)a.

COATINGS

Solar Reflectors

8.2.2. Orbital. Data on Ultra-violet and particulate irradiation damage of this coating show a moderate increase in the solar absorptance which ceases before long. Compare, for example, the values of α_s after 2 and 3 years in orbit, as given in Fig 1-19, p. 1-62.

9. THERMAL CYCLING

No cracking of the surface was observed after the following tests:

Pressure: below 1.3×10^{-4} Pa.

Temperature:

Tmin = 173 K

Tmax = 373 K.

Number of cycles: 200.

Cycle time : 1.5 h.

From ASTRAL (1976)a, Guillaumon & Guillin (1979).

10. SOURCE

ASTRAL, Peintures et Vernis, 164 rue Ambroise Croizat, boîte postale 140.

93024 Saint-Denis. Cédex 1, France.

Contact Person: Mr. B. Dumont. Département Aéronautique.

11. COST

P 123 primer.

1 kit consists of:

. 1 l Base P 123

. 2.5 l Hardener CX 124

. 1 l Thinner S 125 Cost: 1 550 FF.

COATINGS

Solar Reflectors

P 128 primer.

1 kit consists of:

. .25 l P 128 Cost: 230 FF.

PSG 120 FD

1 kit consists of:

. 1 kg Base PSG 120 FD

. .2 kg Hardener CT 122

. 1 l Thinner S 105 Cost: 3 300 FF.

These costs are FOB, factory of Montataire, Oise-France.

From a quotation dated Aug. 1984.

12. PAST SPACIAL USE

This coating has been used in several satellites, and considered for use in some other cases. Several examples of spacial use are given in the following Table.

Spacecraft or Programme	Launching Date	Used or Tested	References
D2A(Tournesol) D2B (Aura)	April 15, 1971 Sept. 27, 1975	Used	ASTRAL (1976)a
SRET 2 (MAS 2)	June 5, 1975	Tested in two different experiments.	ASTRAL (1976)a Rolfo (1976).
Meteosat 1 Meteosat 2	Nov. 23, 1977 June 19, 1981	Used in SRET 2-tested radiant cooler. (See L, § 2.6.3).	Rolfo (1976).
LDEF	April 6, 1984. Launched from Challenger.	Experiment A0138-6 by A. Paillous & J.C. Guillaumon.	Clark (1981).
Olympus	Scheduled for early 1988.	Used in the Propagation Antenna Package.	Domingo (1987)

INTENTIONALLY BLANK PAGE

COATINGS

Solar Reflectors

1.2.5. ZINC OXIDE-POTASSIUM SILICATE

1. COMPOSITION

Pigment: New Jersey Zinc Co., SP500 zinc oxide.

Binder: Potassium silicate.

Filler: Chopped glass fibers (Triton).

From Simon (1974) and ASTRAL (1981).

2. FORMULATION

Not given by the producer.

3. USUAL DESIGNATION

PSZ 184. ASTRAL.

4. SUBSTRATE

Any clean substrate, particularly aluminium alloys, stainless steel, copper alloys. See Preparation of surfaces for painting.

5. METHOD OF APPLICATION

5.1. Preparation of paint for application. PSZ 184 is delivered as a system consisting of:

Pigment.

Binder.

Chopped glass fibers (Triton).

Glass balls.

Distilled water (as much as required for grinding).

In order to prepare the paint:

1) Mix Triton, glass balls and distilled water.

2) Grind the resulting mixing for 30 min by use of a "Red Devil" stirrer.

COATINGS

Solar Reflectors

3) Add to above mixing the pigment and the binder.

4) Grind the solution for 30 min by use of a "Red Devil" stirrer.

5) Add 8×10^{-2} kg of distilled water.

6) Filter through a nylon 30 mesh (6.3×10^{-4} m mesh size) in order to separate the glass balls.

7) Add 20% by weight of distilled water.

8) Filter through a nylon 300 mesh (5×10^{-5} m mesh size).

Shelf life of the paint: 24 h.

From ASTRAL (1981).

5.2. Preparation of surfaces for painting.

1) For aluminium alloys, stainless steel, copper alloys.

The substrate should be thoroughly degreased with trichloroethylene, then scraped with an alkaline paint remover (steel wool and commercial detergent type VIM), or sandblasted, and copiously rinsed with water.

When the above preparation becomes unfeasible, a satisfactory result is achieved by use of the procedure given below, which can be applied to other substrates.

2) For other substrates.

Careful degreasing with trichloroethylene followed by a final cleaning with Freon TF or ethyl ether and a spray coat of P 131 primer.

From ASTRAL (1981).

5.3. Application of paint. By spray techniques using a Kremlin model Junior or comparable gun at about 2.8×10^{5} Pa air or

Rev. 1. 1981

COATINGS

Solar Reflectors

nitrogen pressure.

Compulsory conditions for application are:

Ambient temperature in the range 291 K - 298 K.

Relative humidity above 65%.

3 very thin layers should be applied to start with. Then 8 or 9 crosswise layers are sprayed on. The last layers must show a glossy appearance during application. The successive layers should be allowed to dry slowly and uniformly until the gloss has disappeared (30 min - 35 min) before spraying on the next layer.

After curing the surface can be rinsed with soapy water. Areas to be retouched should be slightly polished with steel wool and water. Then, a thin layer is applied. After around 5 min drying, one or two crosswise layers can be sprayed on.

From ASTRAL (1981).

5.4. Coating thickness. Between 10^{-4} m and 1.2×10^{-4} m.

From ASTRAL (1981).

5.5. Curing process. At 293 K.

Dust off: 3 h,

Deep dry: 24 h.

From ASTRAL (1981).

6. SOLVENTS RESISTANCE

Not attacked by solvents.

The paint can be removed mechanically.

7. PHYSICAL PROPERTIES

7.1. Density. Not given by the producer.

Rev. 1. 1981

COATINGS

Solar Reflectors

7.2. Outgassing. Sample at 398 K to 423 K, below 1.3×10^{-3} Pa pressure, during 24 h. Condensing plate held at 298 K.

Total mass loss, % TML: 2.26.

Collected volatile condensable materials, % CVCM: .01.

Water is the only volatile component of this inorganic coating.

From ASTRAL (1981).

7.3. Thermal radiation properties.

7.3.1. Emittance.

7.3.1.1. Hemispherical total emittance. See Table 1-14, which also gives information on solar absorptance, α_s.

Table 1-14

Hemispherical Total Emittance, ε, and Solar Absorptance, α_s, of PSZ 184

Description	Comments	ε	α_s
As received. Initial value.		.94±.02	.14±.02
After moisture resistance test. Relative humidity: 90%. Temperature: 363 K. During 7 d.	Emittance measured by use of a portable emissometer.	.93±.04	.14±.02
After thermal cycling under vacuum. 200 cycles. Temperature range: 173 K - 373 K. Pressure: 1.3×10^{-3} Pa.		.94±.04	.14±.02
After cumulative tests, moisture resistance plus thermal cycling, both as above.		.90±.04	.14±.02

From ASTRAL (1981).

7.3.2. Absorptance.

7.3.2.1. Solar absorptance. See Table 1-14 above.

7.3.2.5. Effects of the Space Environment on absorptance.

COATINGS

Solar Reflectors

7.3.2.5.1. Ultra-Violet Radiation. Figs 1-31 to 1-33, from CNES.

Data measured as in p. 1-55.

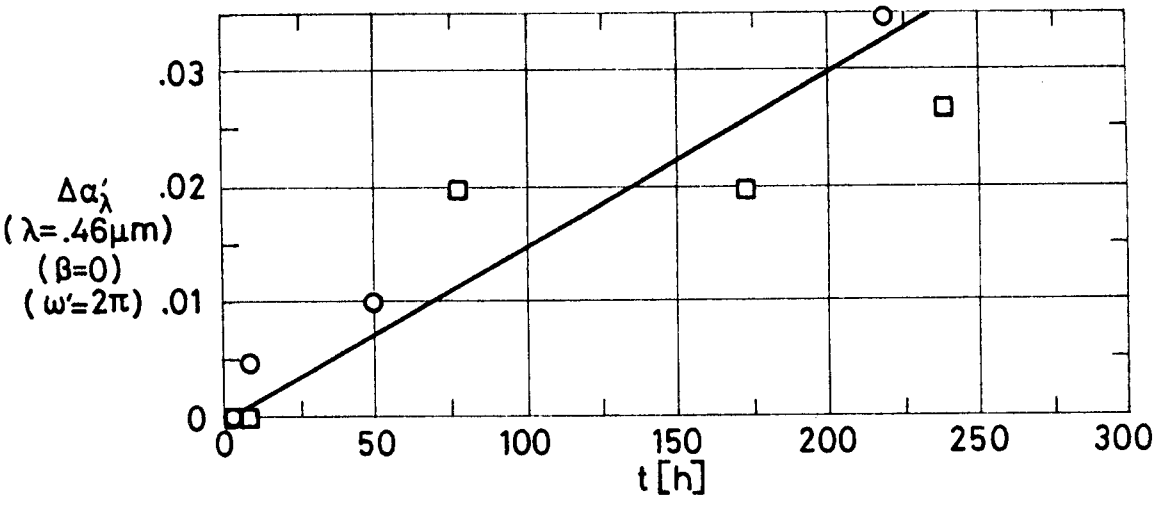

Fig 1-31. Change in normal-hemispherical spectral absorptance, $\Delta\alpha'_\lambda$, of PSZ 184 coating, due to UV Radiation, vs. exposure time, t. Wavelength, $\lambda=.46\times10^{-6}$ m. See Explanation in the caption of Fig 1-32. From Simon (1974).

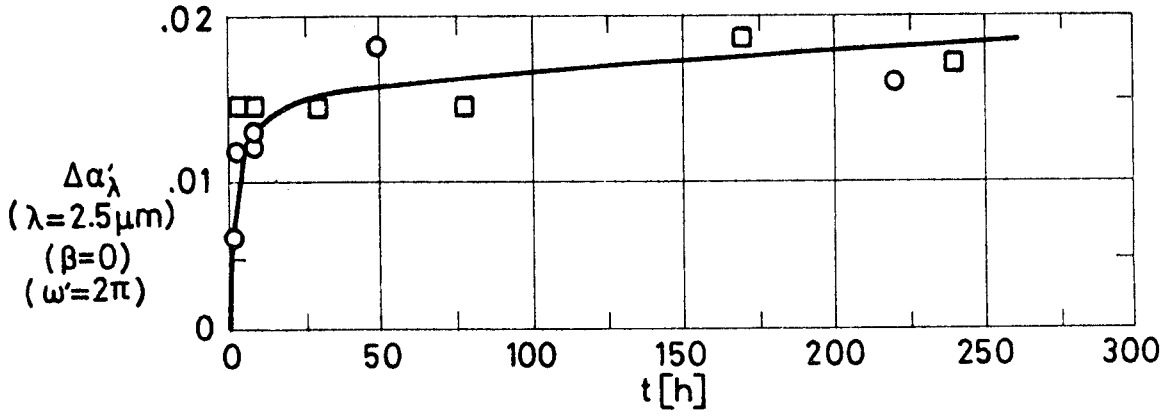

Fig 1-32. Change in normal-hemispherical spectral absorptance, $\Delta\alpha'_\lambda$, of PSZ 184 coating, due to UV Radiation, vs. exposure time, t. Wavelength, $\lambda=2.5\times10^{-6}$ m. From Simon (1974).

Explanation

Key	Sample Temperature [K]	Comments
○	353	
□	283	After 9 h of UV radiation plus 25 h in nitrogen (bleaching).

Rev. 1. 1981

COATINGS

Solar Reflectors

Data concerning the effects of ultra-violet radiation on solar absorptance are given in Fig 1-33. α_s deduced from spectral reflectance measured as above.

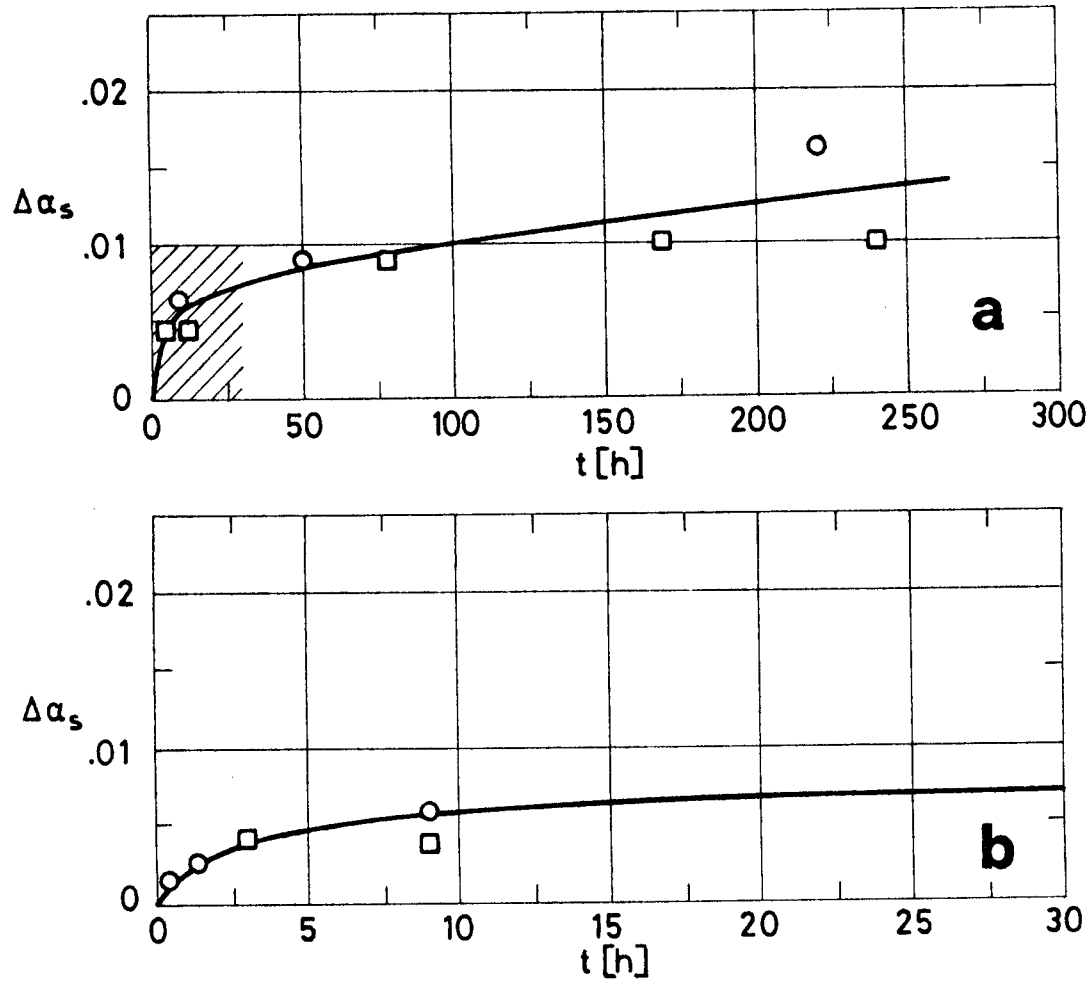

Fig 1-33. Change in solar absorptance, $\Delta\alpha_s$, of PSZ 184 coating, due to UV Radiation, vs. exposure time, t. Shaded zone in a is enlarged in b. From Simon (1974).

Explanation

Key	Sample Temperature [K]	Comments
o	353	
□	283	After 9 h of UV radiation plus 25 h in nitrogen (bleaching).

COATINGS

Solar Reflectors

7.3.2.5.3. Protons only exposure. Table 1-15 after DERTS.

Solar absorptance from spectral reflectance data given in p. 1-93 and ff.

CAUTION

Comments in pp. 1-59 and 1-60 are relevant here. Now the initial value is, α_{so}=.16 .

Table 1-15

Protons Radiation Effects on Solar Absorptance of PSZ 184 Coating

Intensity [keV] →	45			75			150		
↓ Integrated Flux [p.m^{-2}]	α_s	$\Delta\alpha_s$	$\Delta\alpha_s/\alpha_s$	α_s	$\Delta\alpha_s$	$\Delta\alpha_s/\alpha_s$	α_s	$\Delta\alpha_s$	$\Delta\alpha_s/\alpha_s$
Before (in air)	.307								
Before (in vacuum)	.349								
10^{17}	.348	-.001	-.002						
10^{18}	.348	-.001	-.002						
10^{19}	.376	.027	.071						
2.1×10^{19}	.407	.058	.142						
After (in air)	.386								
Before (in air)	.279			.328			.332		
Before (in vacuum)	.318			.375			.383		
10^{17}	.323	.005	.015	.384	.009	.024	.396	.013	.033
10^{18}	.334	.016	.047	.394	.019	.049	.411	.028	.068
10^{19}	.362	.044	.122	.420	.045	.107	.442	.059	.134
2.1×10^{19}	.396	.078	.196	.443	.068	.154	.471	.088	.187
After (in air)	.358			.392			.405		
Comments (for silicated primer only).	Small cracks appeared after tests.			Severe cracking, particularly in the lower part of the sample (held upright). Substrate badly primed.					

ON P 131 PRIMER

ON SILICATED PRIMER

From Paillous, Amat, Marco & Panabiere (1977).

COATINGS

Solar Reflectors

7.3.2.5.4. Electrons only exposure. Table 1-16 after DERTS.

Solar absorptance from the spectral reflectance data given in p. 1-97 and ff. Sample on silicated primer.

Table 1-16

Electrons Radiation Effects on Solar Absorptance of PSZ 184 Coating

Intensity [keV] →	40			80			210		
↓ Integrated Flux [e.m^{-2}]	α_s	$\Delta\alpha_s$	$\Delta\alpha_s/\alpha_s$	α_s	$\Delta\alpha_s$	$\Delta\alpha_s/\alpha_s$	α_s	$\Delta\alpha_s$	$\Delta\alpha_s/\alpha_s$
Before (in air)	.344			.330					
Before (in vacuum)	.351			.360			.341		
2×10^{14}	.422	.071	.168	.450	.090	.199	.471	.130	.277
5×10^{14}	.457	.106	.232	.486	.126	.259	.523	.182	.348
10^{15}	.480	.129	.269	.517	.157	.304	.533	.192	.361
2×10^{15}	.493	.142	.288						
After (in air)	.326			.360			.359		
Comments	Very severe cracking. The paint becames almost scaled off.			Small cracks away from the center of the sample.			Small cracks. Substrate badly primed.		

From Paillous, Amat, Marco & Panabiere (1977).

7.3.2.5.6. Combined exposure. Table 1-17 after DERTS.

Solar absorptance from spectral reflectance data.

The test simulate geosynchronous orbit exposure of the Orbital Test Satellite (OTS) equatorial faces.

The "Corrected" values in Table 1-17 were used to estimate coating degradation up to 3 years in orbit, Fig 1-34.

Incidents during testing, see p. 1-75, cast doubts on the validity of the data beyond 1 year in orbit.

COATINGS

Solar Reflectors

Table 1-17

Combined Exposure Effects on Solar Absorptance of PSZ 184 Coating

Test Conditions	Sample 1						Sample 2					
	Measured in situ			Corrected [a]			Measured in situ			Corrected [a]		
	α_s	$\Delta\alpha_s$	$\Delta\alpha_s/\alpha_s$	α_s	$\Delta\alpha_s$	$\Delta\alpha_s/\alpha_s$	α_s	$\Delta\alpha_s$	$\Delta\alpha_s/\alpha_s$	α_s	$\Delta\alpha_s$	$\Delta\alpha_s/\alpha_s$
BEFORE IRRADIATION	.319			.160			.349			.160		
AFTER A UNDER VACUUM [b]	.332	.013	.041	.176	.016	.100	.372	.023	.066	.189	.029	.181
BEFORE B	.347	.028	.089	.195	.035	.219	.356	.008	.022	.170	.010	.062
AFTER B [b]	.390	.071	.225	.249	.089	.556	.405	.056	.161	.230	.070	.437
AFTER PUMP DAMAGE [c]	.373	.055	.080	.229	.069	.431	.386	.037	.107	.206	.046	.287
BEFORE C	.396	.078	.243	.258	.098	.612	.417	.069	.197	.247	.087	.544
AFTER C [b]	.421	.103	.322	.289	.129	.806	.438	.089	.256	.272	.112	.700
BEFORE D	.415	.097	.304	.282	.122	.762	.435	.086	.247	.268	.108	.675
AFTER D UNDER VACUUM [b]	.425	.107	.335	.294	.134	.838	.438	.089	.257	.272	.112	.700
AFTER D AND AIR EXPOSURE	.395	.076	.238	.255	.095	.594	.415	.066	.189	.243	.083	.519

[a] The correction has been made by the compiler as follows:

1) Value before irradiation, α_{so}=.16 .

2) $$\frac{\Delta\alpha_{s\,corrected}}{\Delta\alpha_{s\,in\ situ}} = \frac{1-\alpha_{so}}{1-\alpha_{so\,in\ situ}} = \frac{.84}{.67}\ ,$$

where α_{so} has been measured (in air) with an integrating sphere attached to a Beckman DK2A reflectometer. $\alpha_{so\,in\ situ}$ is the value measured before irradiation as indicated in p. 1-65.

[b] Steps A to D correspond, respectively, to the following times in geosynchronous orbit.
A : .18 yr = 508 ESH.
B : .94 yr = 2 443 ESH.
C : 2.11 yr = 5 604 ESH.
D : 3 yr = 7 949 ESH.

[c] See p. 1-75 for further details.

From Paillous (1976).

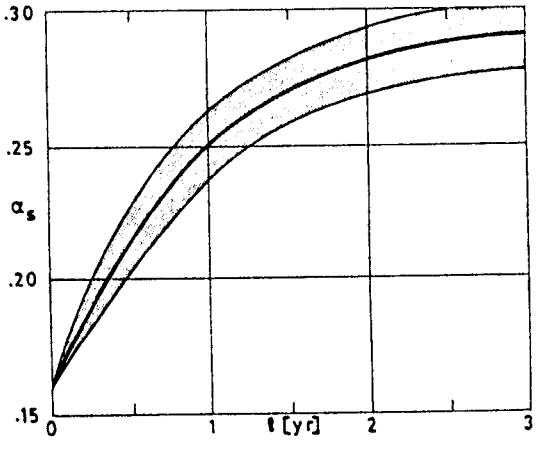

Fig 1-34. Estimated change in solar absorptance, α_s, of PSZ 184 vs. time, t. From Paillous (1976).

Rev. 3. 1986

COATINGS

Solar Reflectors

7.3.3. Reflectance.

7.3.3.1. Normal-hemispherical spectral reflectance. Fig 1-35 from CNES.

Chamber pressure below 1.3×10^{-5} Pa.

Sample temperature not given.

Spectral reflectance measured in situ as indicated in p. 1-63.

7.3.3.2. Effects of the Space Environment on reflectance.

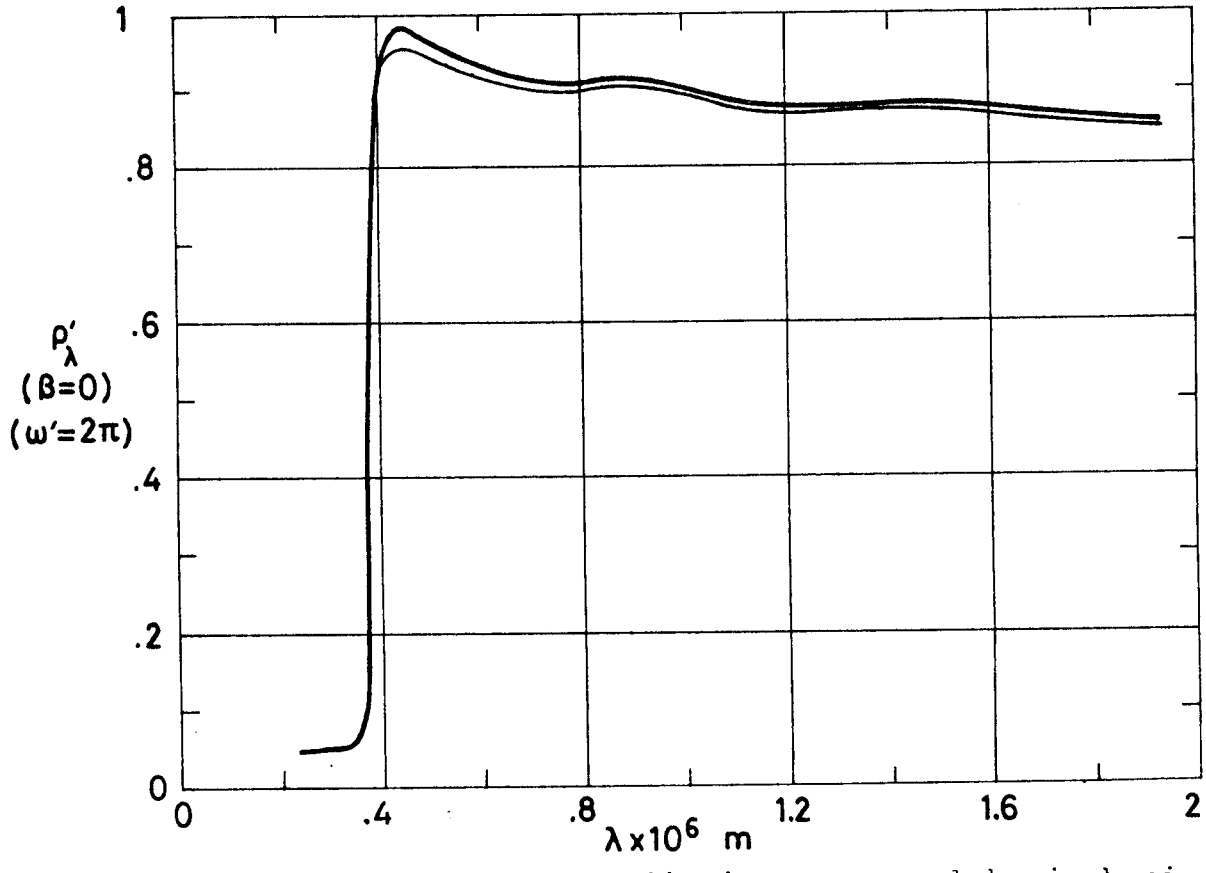

Fig 1-35. Effect of Ultra-Violet Radiation on normal-hemispherical spectral reflectance, ρ'_λ, of PSZ 184 coating vs. wavelength, λ.
——— Before irradiation. $p<1.3\times10^{-5}$ Pa.
——— After irradiation. $p<1.3\times10^{-5}$ Pa. 1 Sun level.
Neither sample temperature nor exposure time are given.
From Simon (1974).

COATINGS

Solar Reflectors

7.3.3.2.1. Ultra-Violet Radiation. Fig 1-35.

Sample conditions and spectral reflectance measurements as above.

Sample irradiated in vacuum as in p. 1-64.

Radiation flux density at the sample level: ∿1 Sun.

Exposure time not given.

See Fig 1-31 and ff. where similar data from CNES have been also presented.

Fig 1-35 is interesting from a qualitative point of view when compared with Fig 1-21. In particular, the decreased reflectance in the infrared ($\lambda > .7 \times 10^{-6}$ m) resulting from ultra-violet radiation, which is characteristic of silicone-binded white paints such as PSG 120, does not appear in this case where the binder is potassium silicate.

7.3.3.2.3. Protons only exposure. Fig 1-36 and ff., from DERTS.

Sample on aluminium substrate.

Irradiation and measurements as for PSG 120, p. 1-65.

One of the samples (that on silicated primer) exhibited severe cracks after exposure. These cracks have been attributed to bad priming of the substrate as it was made clear by the fact that a specimen using PSZ 184 on P 131 primer did not crack after a 45 keV proton irradiation. See Fig 1-36, and also Table 1-15, p. 1-89.

Rev. 1. 1981

COATINGS

Solar Reflectors

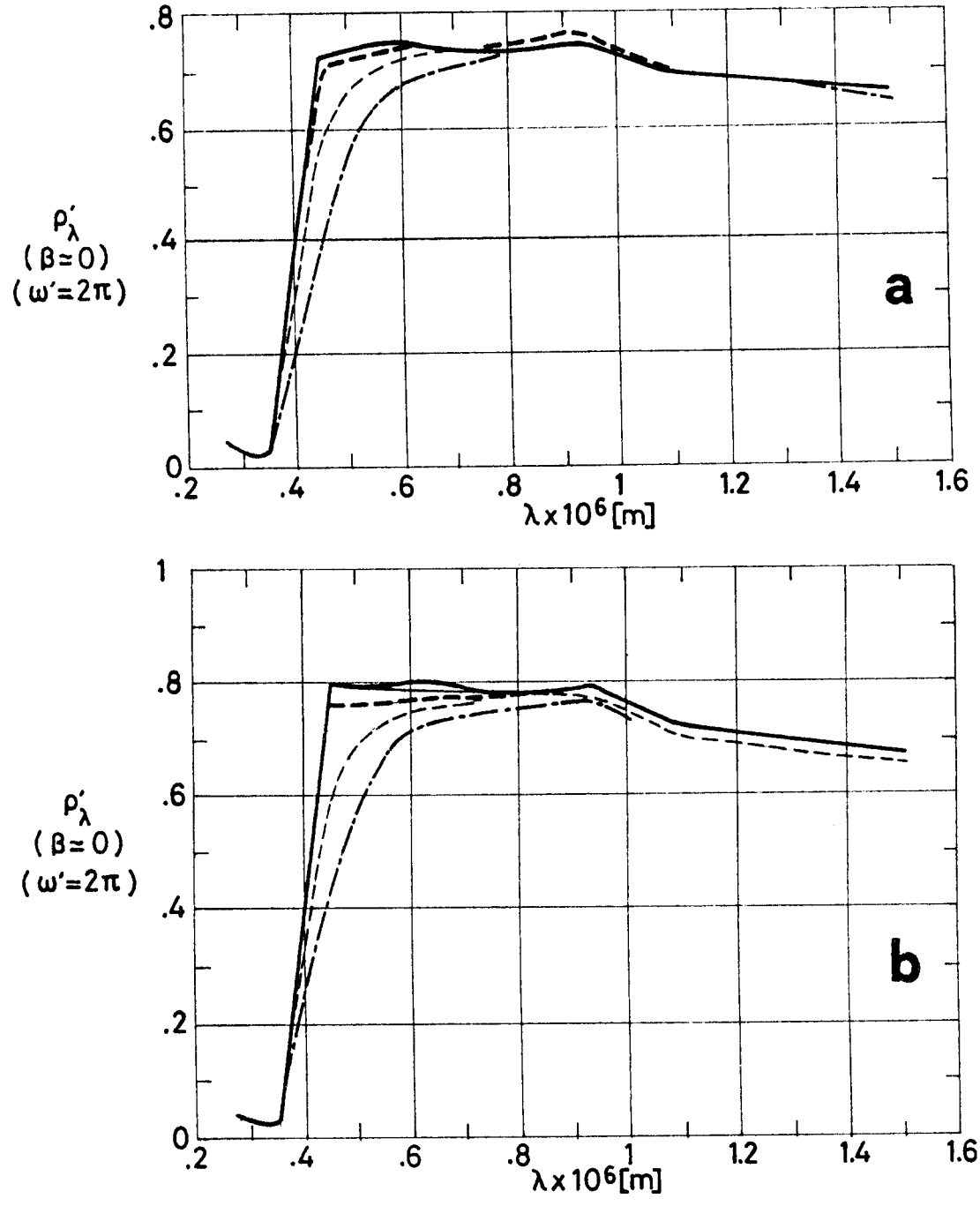

Fig 1-36. Effect of Protons Radiation on normal-hemispherical spectral reflectance, ρ'_λ, of PSZ 184 coating vs. wavelength, λ. a Coating on P 131 primer. b Coating on silicated primer. Radiation intensity ≈45 keV. See Explanation in the caption of Fig 1-37. From Paillous, Amat, Marco & Panabiere (1977).

COATINGS

Solar Reflectors

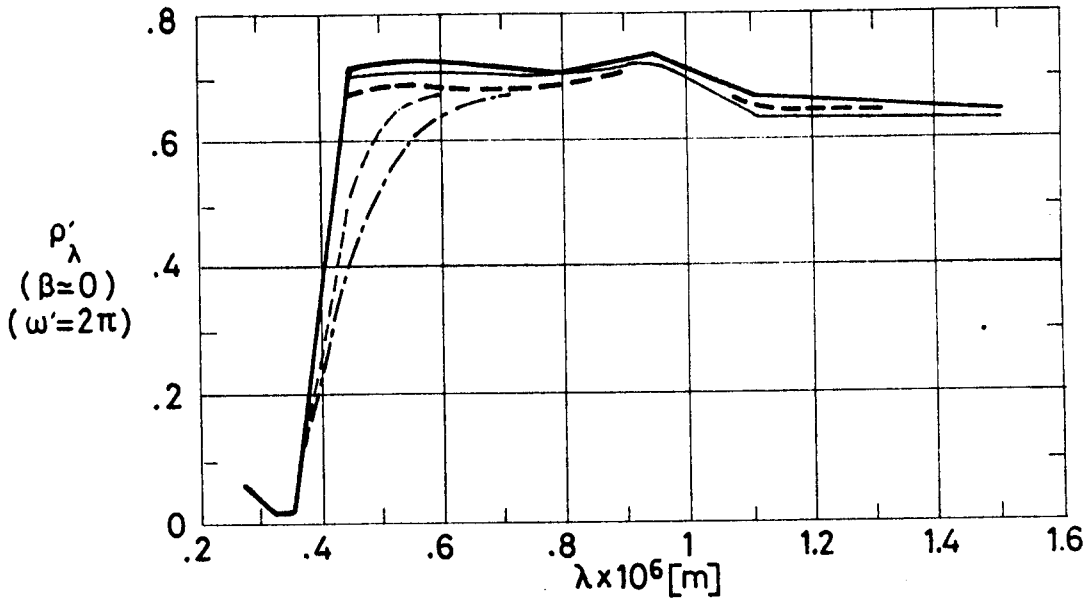

Fig 1-37. Effect of Protons Radiation on normal-hemispherical spectral reflectance, ρ'_λ, of PSZ 184 coating, on silicated primer, vs. wavelength, λ. Radiation intensity ≃75 keV. From Paillous, Amat, Marco & Panabiere (1977).

Explanation

Key	Intensity [keV]	Flux [$p.m^{-2}.s^{-1}$]	Integrated Flux [$p.m^{-2}$]	Cumulative Integrated Flux [$p.m^{-2}$]	Comments
———	45 keV in Fig 1-36. 75 keV in Fig 1-37.				Sample on aluminium substrate. $p = 1.3\times10^{-4}$ Pa. T = 303 K ± .5 K. Incidence of the protons beam: 0°. Small cracks appeared after tests in the case of Fig 1-36b. Cracking was severest in the case of Fig 1-37. Cracks attributed to bad priming of the substrate.
———		1.3×10^{14}	10^{17}	10^{17}	
– – – –		2.5×10^{14}	9×10^{17}	10^{18}	
– – – –		2.5×10^{14} (Fig 1-36). 6.2×10^{14} (Fig 1-37).	9×10^{18}	10^{19}	
—·—·—		6.2×10^{14}	1.1×10^{19} (Fig 1-36). 1.8×10^{19} (Fig 1-37).	2.1×10^{19} (Fig 1-36). 2.8×10^{19} (Fig 1-37).	

COATINGS

Solar Reflectors

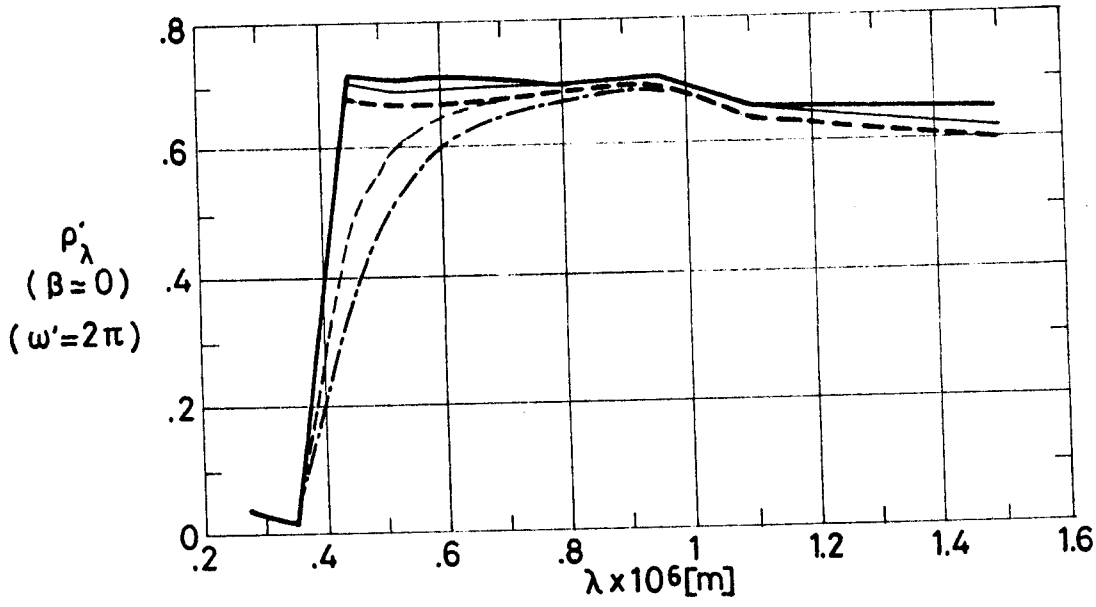

Fig 1-38. Effect of Protons Radiation on normal-hemispherical spectral reflectance, ρ'_λ, of PSZ 184 coating, on silicated primer, vs. wavelength, λ. Radiation intensity ≈150 keV. From Paillous, Amat, Marco & Panabiere (1977).

Explanation

Key	Intensity [keV]	Flux [$p.m^{-2}.s^{-1}$]	Integrated Flux [$p.m^{-2}$]	Cumulative Integrated Flux [$p.m^{-2}$]	Comments
———	150				Sample on aluminium substrate. Silicated primer. $p = 1.3\times10^{-4}$ Pa. T = 303 K ± .5 K. Incidence of the protons beam: 0°. Severe cracking appeared after tests, particularly in the lower part of the sample (held upright). Substrate badly primed.
——		1.3×10^{14}	10^{17}	10^{17}	
— — —		2.5×10^{14}	9×10^{17}	10^{18}	
— — —		6.2×10^{14}	9×10^{18}	10^{19}	
—·—·—		6.2×10^{14}	1.8×10^{19}	2.8×10^{19}	

COATINGS

Solar Reflectors

7.3.3.2.4. Electrons only exposure. Fig 1-39 and ff., from DERTS

Sample on aluminium substrate. Silicated primer.

Irradiation as for PSG 120, p. 1-68.

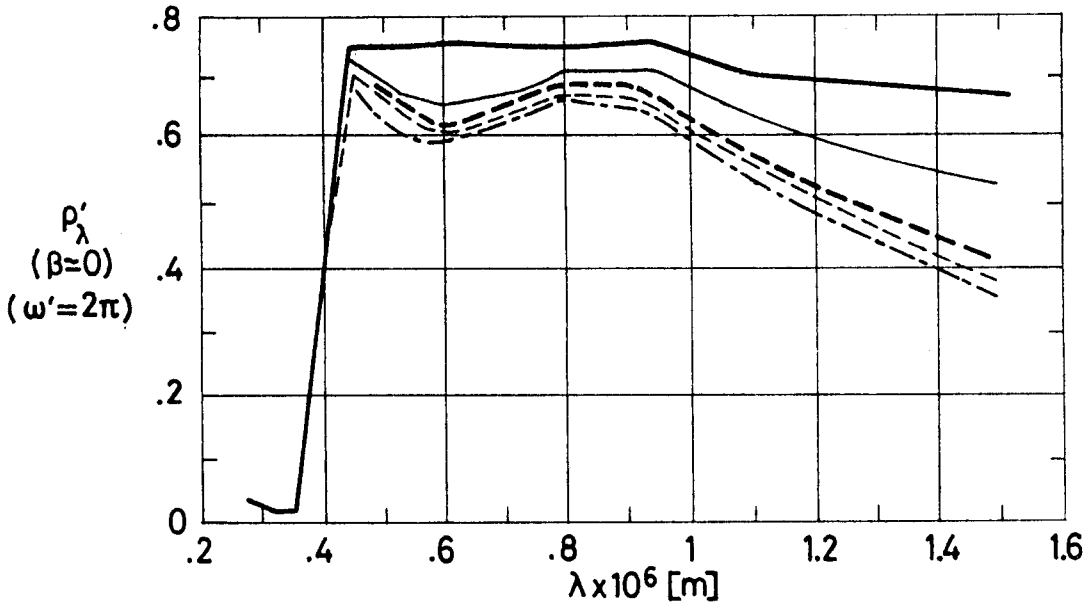

Fig 1-39. Effect of Electrons Radiation on normal-hemispherical spectral reflectance, ρ'_λ, of PSZ 184 coating, on silicated primer, vs. wavelength, λ. Radiation intensity ≃40 keV. From Paillous, Amat, Marco & Panabiere (1977).

Explanation

Key	Intensity [keV]	Flux [$e.m^{-2}.s^{-1}$]	Integrated Flux [$e.m^{-2}$]	Cumulative Integrated Flux [$e.m^{-2}$]	Comments
———	40				Sample on aluminium substrate. Silicated primer. $p = 1.3\times10^{-4}$ Pa. T = 303 K ± .5 K. Incidence of the electrons beam: 0°. Very severe cracking. The paint becames almost scaled off. Substrate badly primed.
———		2.7×10^{14}	2×10^{18}	2×10^{18}	
– – –		4×10^{14}	3×10^{18}	5×10^{18}	
- - - -		4×10^{14}	5×10^{18}	10^{19}	
·—·—·		5.4×10^{14}	10^{19}	2×10^{19}	

COATINGS

Solar Reflectors

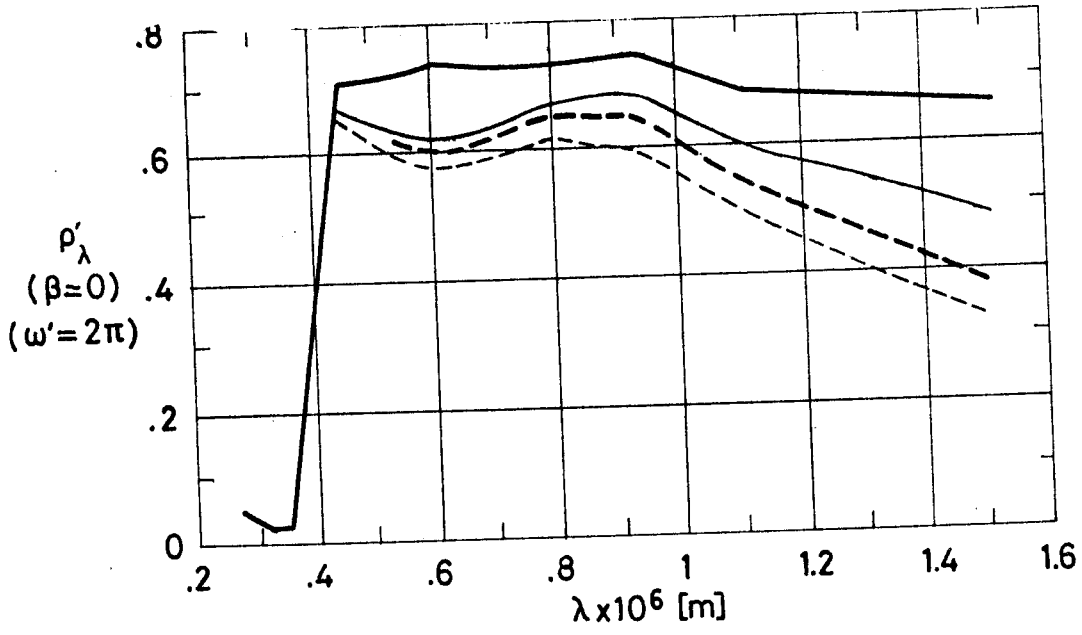

Fig 1-40. Effect of Electrons Radiation on normal-hemispherical spectral reflectance, ρ'_λ, of PSZ 184 coating, on silicated primer, vs. wavelength, λ. Radiation intensity ≃80 keV. From Paillous, Amat, Marco & Panabiere (1977).

Explanation

Key	Intensity [keV]	Flux [$e.m^{-2}.s^{-1}$]	Integrated Flux [$e.m^{-2}$]	Cumulative Integrated Flux [$e.m^{-2}$]	Comments
———	80				Sample on aluminium substrate. Silicated primer. $p = 1.3\times10^{-4}$ Pa. T = 303 K ± .5 K. Incidence of the electrons beam: 45°. Small cracks away from the center of the sample Substrate badly primed.
——		2.9×10^{14}	2×10^{18}	2×10^{18}	
– – –		2.8×10^{14}	3×10^{18}	5×10^{18}	
—– —–		5.3×10^{14}	5×10^{18}	10^{19}	

COATINGS

Solar Reflectors

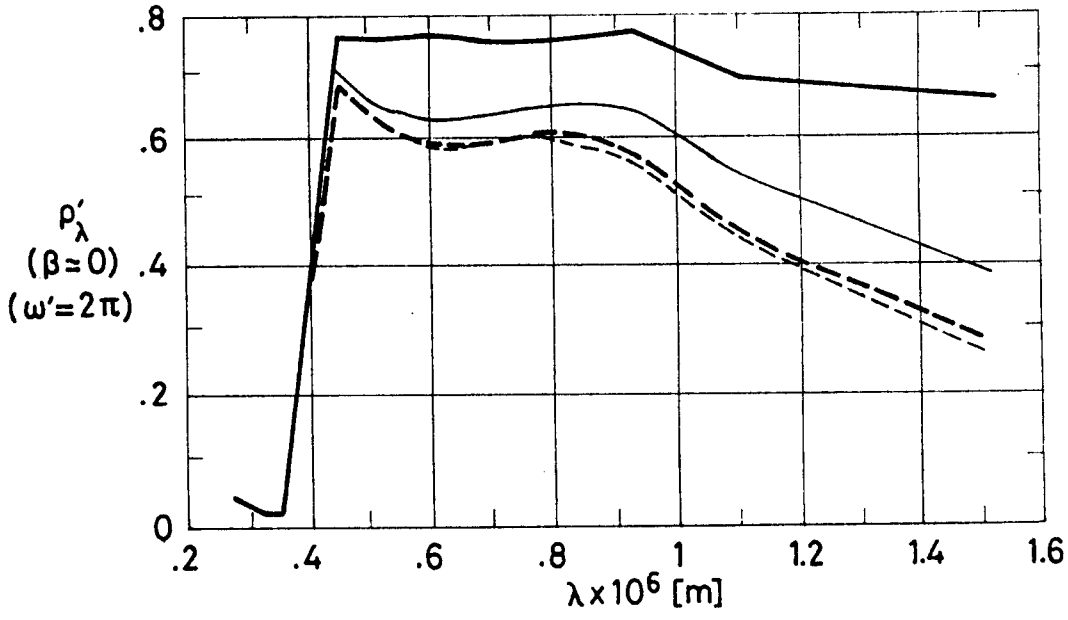

Fig 1-41. Effect of Electrons Radiation on normal-hemispherical spectral reflectance, ρ'_λ, of PSZ 184 coating, on silicated primer, vs. wavelength, λ. Radiation intensity ≈210 keV. From Paillous, Amat, Marco & Panabiere (1977).

Explanation

Key	Intensity [keV]	Flux [$e.m^{-2}.s^{-1}$]	Integrated Flux [$e.m^{-2}$]	Cumulative Integrated Flux [$e.m^{-2}$]	Comments
———	210				Sample on aluminium substrate. Silicated primer. $p = 1.3\times10^{-4}$ Pa. T = 303 K ± .5 K. Incidence of the electrons beam: 45°. Small cracks. Substrate badly primed.
———		3.0×10^{14}	2×10^{18}	2×10^{18}	
– – –		3.1×10^{14}	3×10^{18}	5×10^{18}	
– – –		6.3×10^{14}	5×10^{18}	10^{19}	

COATINGS

Solar Reflectors

An attempt has been made to check the validity of the analytical model of solar absorptance degradation, set forth by Bourrieau (1978), against the experimental results which have been presented in pp. 1-94 to 1-99. For a description of the mentioned analytical model see pp. 1-70 to 1-73.

The comparison was deceptive in the case of PSZ 184 because of the already mentioned cracks. Two absorption bands were detected, $\lambda=.61\times10^{-6}$ m and $\lambda=2.1\times10^{-6}$ m, but only the last one was workable, the first being masked by a drift of the absorption threshold of the paint. No definite results were obtained.

7.3.3.2.6. Combined exposure. Figs 1-42 and 1-43 from DERTS.

Sample on aluminium substrate.

Irradiation and measurements as for PSG 120, pp. 1-74 and 1-75.

Data presented are:

1) Solar reflectance (in air) before irradiation, $\alpha_{so}=.16$, given in p. 1-89.

2) In situ spectral reflectance, Figs 1-42 and 1-43. See also Table 1-17, p. 1-91.

The chamber pressure rose up to 1.3 Pa because of some damage in the secondary vacuum pump. This incident resulted in an unintentional bleaching of the coating. Test were resumed after repairing the pump. Data beyond 1 year in orbit should be used cautiously.

Rev. 1. 1981

COATINGS

Solar Reflectors

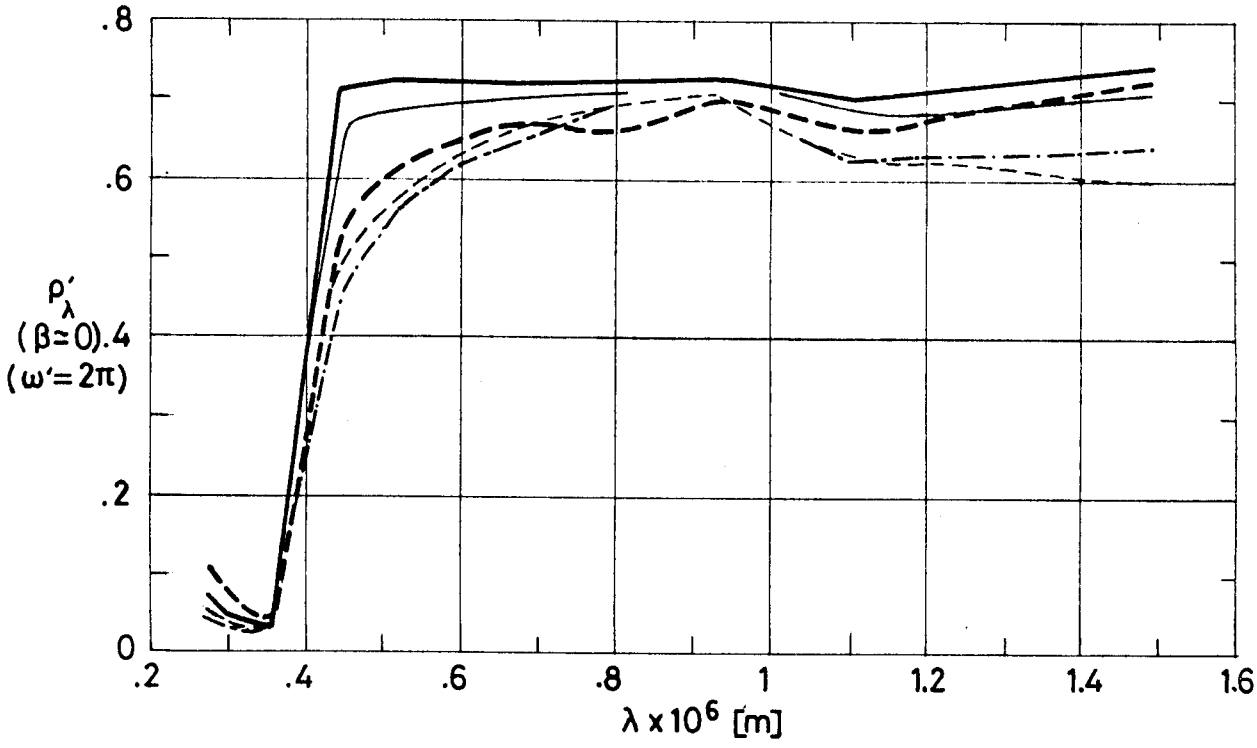

Fig 1-42. Effect of Combined Exposure, simulating up to three years in geosynchronous orbit, on normal-hemispherical spectral reflectance, ρ'_λ, of PSZ 184 coating vs. wavelength, λ. From Paillous (1976).

Explanation

Key	Description	Comments
———	After 125 h below 1.3×10^{-4} Pa pressure. T = 363 K.	
——	After step A (.19 years in orbit). T = 363 K.	
– – –	After step B (.94 years in orbit). T = 363 K.	
– – –	After step C (2.11 years in orbit). T = 363 K.	After unintentional O_2 bleaching.
—·—·	After step D (3 years in orbit). T = 363 K.	

COATINGS

Solar Reflectors

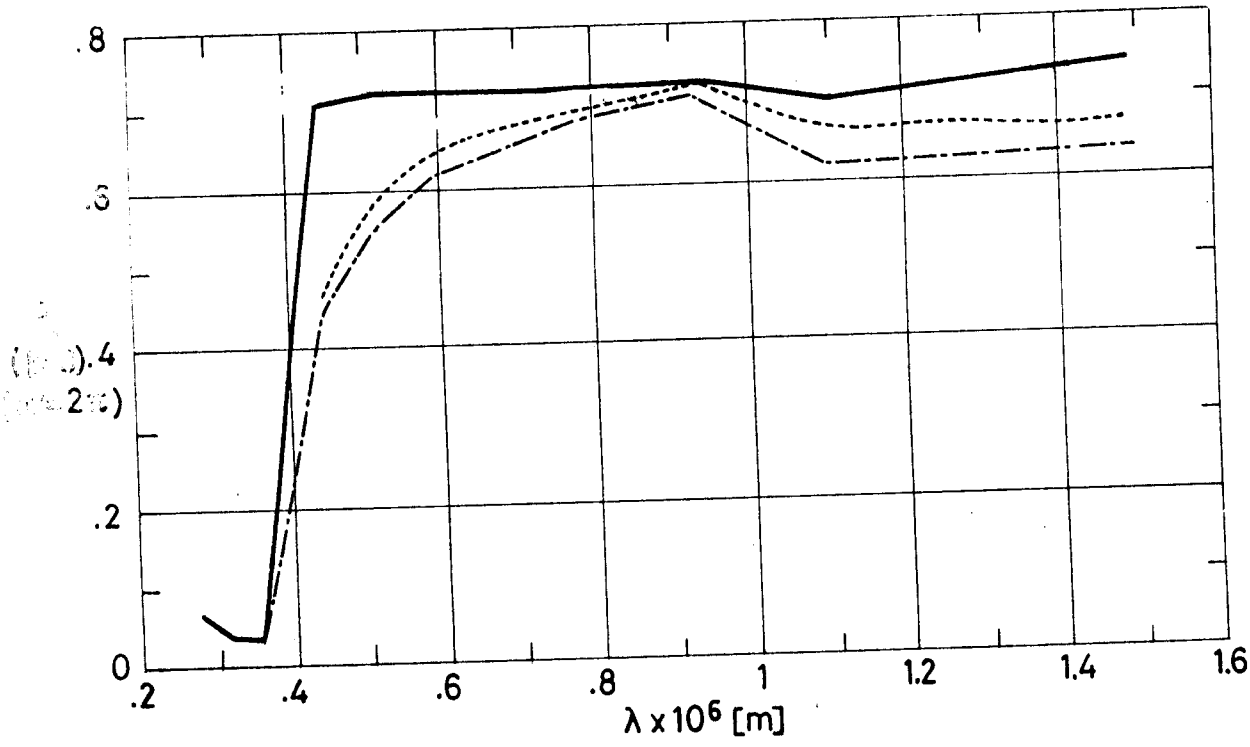

Fig 1-43. Effect of O_2 bleaching, after Combined Exposure, on normal-hemispherical spectral reflectance, ρ'_λ, of PSZ 184 coating vs. wavelength, λ. Curves ——— and —·—·— are those shown in Fig 1-42. From Paillous (1976).

Explanation

Key	Description	Comments
———	After 125 h below 1.3×10^{-4} Pa pressure. T = 363 K.	
—·—·—	After step D (3 years in orbit). T = 363 K.	After unintentional O_2 bleaching.
·····	After step D and Air exposure. T = 293 K.	

COATINGS

Solar Reflectors

7.4. Electrical resistance. PSZ 184 coating is nonconductive (Paillous (1976)).

8. ENVIRONMENTAL BEHAVIOR

8.1. Prelaunch. The use of this coating in spacecraft demands great care. In addition to compulsory application conditions (preparation of the surface, humidity level, ambient temperature,...), it requires a particularly well trained applier. The coating withstood moisture resistance tests (Table 1-14, p. 1-86). Neither degradation of its optical properties nor of its adhesion were observed.

8.2. Postlaunch. Outgassing characteristics are given in p. 1-86.

8.2.1. Ascent. See Table 1-14 for influence of thermal cycling under vacuum and moisture resistance plus thermal cycling. Changes look minimal. Nevertheless, some craks and slight scaling off near the borders resulted from cumulative tests (moisture plus thermal cycling).

From ASTRAL (1981).

8.2.2. Orbital. Data on ultra-violet and particulate irradiation damage of this coating compare favourably with those of other white paints which have been tested by Paillous (1976).

9. THERMAL CYCLING

No cracking of the surface was observed after the following tests:

Pressure below 1.3×10^{-4} Pa.

Rev. 1. 1981

COATINGS

Solar Reflectors

Temperature:

Tmin = 173 K

Tmax = 373 K.

Number of cycles: 200.

Cycle time not given.

From ASTRAL (1981).

10. SOURCE

ASTRAL, Peintures et Vernis, 164 rue Ambroise Croizat, boîte postale 140.

93204 Saint-Denis. Cédex 1, France.

Contact Person: Mr. B. Dumont. Département Aéronautique.

11. COST

12. PAST SPACIAL USE

No spacial use has been reported.

A sample of this coating, among others, will be tested on board Long Duration Exposure Facility (LDEF) 1st Mission (scheduled for early 1984), Experiment A0138-6, by Paillous & Guillaumon. The sample will be examined before flight and after retrieval. (Clark (1981)).

COATINGS

Solar Reflectors

1.2.5.1. ZINC ORTHOSTANNATE-METHYLSILICONE

1. COMPOSITION

Pigment: Zinc Orthostannate (Zn_2SnO_4).

Binder: RHODORSIL 10 336 purified by CNES method. This purification consists in a number of cures (usually three) which reduce outgassing without modifying the properties of the polymerized binder (see Guillaumon & Guillin (1979)).

From Guillaumon & Blet (1982).

RHODORSIL 10 336 is a methyl phenyl silicone used for the production of industrial coatings which must withstand temperatures up to 650 K - 700 K, and for producing fast-pressing and recooking insulation bricks.

Contains xilene.

Also commercialized as Silicex 717.

From Siliconas Hispania (1985).

Preparation of the pigment: 162.8 g (2 moles) of SP500 ZnO, New Jersey Zinc Co., and 150.7 g (1 mol) of Sn_4O_2, Merck (quality PUR) are dispersed in deionized water (.6 l and 1.2 l respectively) during 5 min. Both dispersions are mixed and thoroughly stirred for 15 min. The mixture is then allowed to stand during 3 h. Then it is transferred to a Buchner funnel and filtered at reduced pressure. The filter cake is removed from the funnel and dried for 16 h at 380 K. The resulting powder is calcined for 16 h at 1 220 K. In order to enhance the stability under UV radiation, mixtures with

COATINGS

Solar Reflectors

.5 % excess ZnO have been calcined at different temperatures (1 200 K, 1 270 K, 1 320 K, 1 370 K) and then treated with acetic acid.

From Guillaumon (1982).

2. FORMULATION

Not given by the producer.

3. USUAL DESIGNATION

PCBZ Conductive White Paint.

4. SUBSTRATE

Any light alloy, also fiber-glass, Kevlar or carbon fiber laminates.

5. METHOD OF APPLICATION

5.1. Preparation of paint for application. (See also § 5.2.2).

Add sufficient thinner to 100 kg of paint in order to reach a viscosity of 33 s - 34 s at 293 K per AFNOR No. 2.5 cup ($\sim$ 30 g of thinner).

This viscosity should be closely kept.

From Guillaumon & Blet (1982).

Cup type viscometers are widely employed in the paint industry (Demmler, Ford, Zahn, Gardner, ...). They consist of an orifice cup with a metal orifice and a receiver cup. The measured efflux time, **t**, in seconds, is related to the kinematic viscosity ($\nu = \mu/\rho$) through

$$\nu = kt - \frac{K}{t}$$

where k and K are empirical values for each instrument.
For a table with the most widely used viscometers see Van Wazer et al. (1963).
An account of AFNOR cups and pertinent procedures can be found in NF T 30-014 (1983).
The range of standard AFNOR cups is given in the following Table.

t vs. ν Range of Standard AFNOR Cups

Cup	t [sec]	$\nu \times 10^3$ [Pa.s]
2.5	30 to 250	5 to 140
4	20 to 300	50 to 1 100
6	30 to 300	510 to 5 100

From NF T 30-014 (1983).

Storage time in full, closed containers at 278 $\pm$ 2 K, is 4 months.

5.2. Preparation of surfaces for painting.

1) Metallic surfaces should be cleaned from any trace of oxide, grease or die lubricant by immersion or with a rag soaked with acetone and then with flugene 113 (or equivalent).

From Guillaumon & Blet (1982).

Flugene 113: Trichloro 1,1,2-Trifluoro 1,2,2 Ethane, is a product from Rhone-Poulenc.

2) Fiber-glass, Kevlar or carbon-fiber epoxy laminates should be grinded with abrasive cloth no. 320 and cleaned with acetone and then flugene 113 (or equivalent).

From MASTER (1985).

COATINGS

Solar Reflectors

5.2.1. Application of primers. Two alternative types of primers are quoted:

1) Primer P 128 could be applied either by hand rubbing or sprayed with a type Kremlin "Junior" or J3 spray gun. A single crosswise layer should be applied. Layer thickness, 5×10^{-6} m. Drying time, 30 min.

From Guillaumon & Blet (1982).

Very similar properties as those of the nominal coating on this primer have been obtained on light alloys without using P 128 primer (Guillaumon (1983)).

In the case of epoxy substrates it is advisable to apply a crosswise layer of P 123 primer (see p. 1-50).

2) PCBZ Primer.

Ambient temperature in the range 291 K to 298 K.

Relative humidity above 40 %.

Throughput: $.150 \pm .020$ kg.m^{-2} (dry) which corresponds to around .230 kg.m^{-2} as delivered.

Thickness (dry) around 45×10^{-6} m.

2a) For small surfaces (less than .5 m^2).

Thining: 20 to 25 % of PCBZ thinner.

Viscosity at application: 16 s to 20 s at 293 K per AFNOR No. 4 cup.

Filtering: through nylon filter 300 µ.

Application with Kremlin "Junior" or equivalent spray gun. Nozzle 203.

COATINGS

Solar Reflectors

Vector gas: air at 2.5×10^5 Pa. Suction feeding.

Needle valve aperture: 4.5 turns. Oval jet.

A slight wet plus 2 crosswise layers wet on wet in order to obtain a wet and uniform appearance.

2b) For large surfaces (beyond .5 m^2).

Thinning: 20 to 25 % of PCBZ thinner.

Viscosity at application: 18 s to 22 s at 293 K per AFNOR No. 4 cup.

Filtering: through nylon filter 300 µ.

Application with Kremlin type SKM17. Head H 10. Nozzle No. 16.

Pressure: 3×10^5 Pa. Aspiration can.

Needle valve aperture: 4.5 turns. Semi-oval jet.

Vent opening: 3/4 turn.

A slight wet plus 2 crosswise layers wet on wet in order to obtain a wet and uniform appearance.

After the last layer of PCBZ primer, wait 3 min before applying the layers of white finishing.

From MASTER (1985).

5.2.2. Application of white finishing layers.

Thinning: 40 to 50 % of PCBZ thinner.

Viscosity at application: 33 s to 35 s at 293 K per AFNOR No. 2.5 cup.

Filtering: through nylon filter 50 µ.

Throughput: .170 ± .010 $kg.m^{-2}$ (dry) which corresponds

COATINGS

Solar Reflectors

to around .230 kg.m^{-2} as delivered.

Thickness (dry) around 40 x 10^{-6} m.

1) For small surfaces (less than .5 m^2).

Application with Kremlin "Junior" or equivalent spray gun. Nozzle 203.

Vector gas: air at 1.8 x 10^5 Pa. Suction feeding.

Needle valve aperture: 4 turns. Oval jet.

2 to 5 crosswise layers depending on applicator.

Delay between layers so as to reach a semi-matte appearance.

2) For large surfaces (beyond .5 m^2).

Application with Kremlin type SKM17. Head H 10. Nozzle No. 14.

Pressure: 2 x 10^5 Pa. Aspiration can.

Needle valve aperture: 4.5 turns. Oval jet.

2 to 5 crosswise layers depending on applicator.

Delay between layers so as to reach a semi-matte appearance.

From MASTER (1985).

5.5. Curing process. The coating should be air-dry during 5 d, at 293 K and normal humidity.

Dust off : 1 to 2 h.

Dry to be handled: 24 h.

Final curing : 5 d.

From MASTER (1985).

COATINGS

Solar Reflectors

5.6. Appearance. White Matte.

6. CLEANING

Cleaning. Use ethyl alcohol. Chlorinated, fluorochlorinated or benzene solvents must be avoided.

Pickling. Use D165 Astral or chlorinated solvents like trichlorethylene, chloroform, etc.

CAUTIONS

This coating is flammable, noxius through breathing, swallowing and skin contact.

It must be handled far from any flame and applied only in properly ventilated rooms. If this is not the case a suitable mask must be used.

7. PHYSICAL PROPERTIES

7.1. Density. Data below correspond to specific density of wet components in the coating system.

PCBZ primer	1.73 ± .05
PCBZ finishing	2.02 ± .05
PCBZ thinner	.93 ± .02

From MASTER (1985).

Surface density, depending on the number of layers: .26 $kg.m^{-2}$ to .37 $kg.m^{-2}$ (see § 7.4).

7.2. Outgassing. Sample heated at 398 K, below 1.3×10^{-4} Pa pressure, during 24 h. Condensing plate held at 298 K. (Specification ESA PSS-09/QRM-02T) (see Table overleaf).

COATINGS

Solar Reflectors

Table 1-17.1

Outgassing Characteristics of PCB Z Coating

Coating	TWL [a] %	RWL [b] %	VCM [c] %	Cure Time [h]	Cure Temp. [K]	References
PCBZ on A-U4G [d] substrate primed with P 128	.65	.64	.12	120	293	Guillaumon & Blet (1982)
PCBZ system (primer and finishing layers) on A-U4G [d] substrate.	.65	.64	.12	360	298	MASTER (1985)
	.53	.40	.08	144 [e] 24	298 323	
	.26	.13	.07	120 [e] 24	298 373	
	.11	.01	.02	96 [e] 26	298 423	
PCBZ	.85	.81	.09			INTA (1984)

[a] TWL: Total Weight Loss.
[b] RWL: Relative Weight Loss.
[c] VCM: Volatile Condensable Materials.
[d] Al-4CuMgSi Alloy.
[e] Each one of these cures was used in the order given.

7.3. Thermal radiation properties.

7.3.1. Emittance

7.3.1.1. Hemispherical total emittance.

$$\varepsilon_p = .80 \pm .04$$

$$\varepsilon_c = .83$$

On A-U4G substrate. ε_p has been measured with a portable emissometer and ε_c by calorimetry.

COATINGS

Solar Reflectors

From Guillaumon & Blet (1982), Guillaumon (1983).

See Millard & Streed (1969)for a comparison of portable emissometer vs. calorimetric values.

7.3.2. Absorptance

7.3.2.1. Solar Absorptance

$\alpha_s = .26 \pm .02$

On A-U4G substrate.

From Guillaumon & Blet (1982), Guillaumon (1983).

7.3.2.2. Variation of solar absorptance with coating thickness

See p. 1-104.16.

7.3.2.5. Effects of the Space Environment on absorptance

7.3.2.5.1. Ultra-Violet Radiation. After 1 045 ESH at 298 K

$\Delta\alpha_s = .03$

On A-U4G substrate with P 128 primer.

From Guillaumon & Blet (1982).

See also Fig 1-43.1.

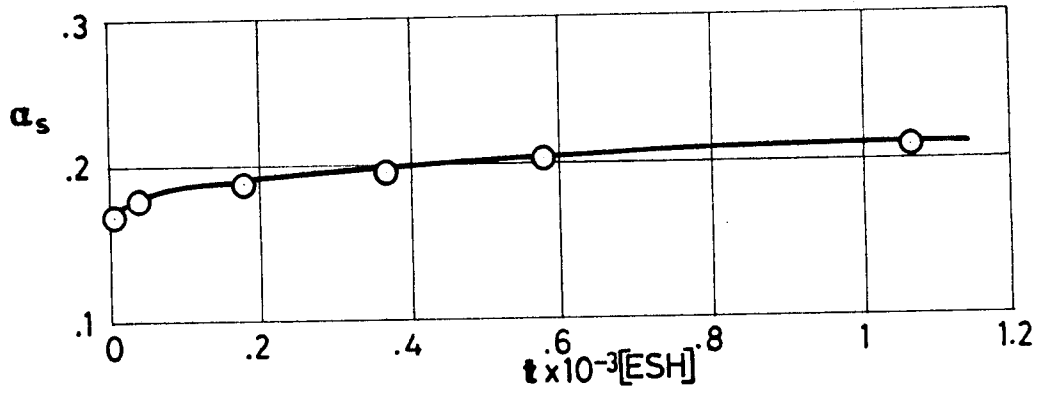

Fig 1-43.1. Solar absorptance, α_s, of PCBZ coating vs. UV Radiation exposure time, t. From Guillaumon (1982).

COATINGS

Solar Reflectors

From spectral reflectance data measured as in pp. 1-104.11 - 1-104.13.

Table 1-17.2

Ultra-Violet Radiation Effects on Solar Absorptance of PCBZ Coating.

Test conditions	α_s TOTAL	α_s UV	α_s Visible	α_s Infrared
Sample A: PCBZ b4f5 four primer layers, five white finishing layers. Substrate not given.				
In air, Beckman	.244	.863	.187	.203
UV in vacuum 0 ESH	.224	.863	.169	.178
120 ESH	.239	.866	.192	.186
293 ESH	.246	.876	.203	.189
586 ESH	.247	.854	.200	.197
1 086 ESH	.251	.877	.209	.195
1 597 ESH	.258	.890	.222	.194
2 090 ESH	.255	.878	.214	.197
2 625 ESH	.256	.878	.222	.192
After breaking vacuum	.240	.874	.199	.180
In air, Beckman	.262			
Sample C: PCBZ b4f8 four primer layers, eight white finishing layers. Substrate not given.				
In air, Beckman	.230	.864	.178	.181
UV in vacuum 0 ESH	.210	.860	.156	.161
110 ESH	.217	.864	.175	.157
268 ESH	.230	.868	.187	.172
536 ESH	.233	.861	.193	.174
994 ESH	.241	.881	.204	.176
1 459 ESH	.237	.881	.204	.167
1 910 ESH	.241	.883	.206	.174
2 400 ESH	.243	.884	.217	.166
After breaking vacuum	.225	.874	.190	.156
In air, Beckman	.246			

COATINGS

Solar Reflectors

UV degradation increases up to 1 000 ESH, becoming invariable beyond this time. Recovery after breaking the vacuum is noteworthy particularly in the infrared band. The number of white finishing layers (5 or 8) is immaterial except in the infrared. From Paillous & Millan (1983).

7.3.3.2. Effect of the Space Environment on reflectance.

7.3.3.2.1. Ultra-Violet Radiation.

Test performed at ONERA-CERT.

Two samples of PCBZ coating.

Author's designation: A PCBZ b4f5

C PCBZ b4f8

As in p 1-104.10.

Substrate not quoted.

Irradiation performed under a vacuum better than 1.3×10^{-4} Pa.

Sample temperature, T = 353 K $\pm$ 1 K controlled by a thermostatic bath.

Degrading source: Xenon lamp 2 500 W. Two independent filters are used, for the $.2 \times 10^{-6}$ m to $.3 \times 10^{-6}$ m band and for the $.3 \times 10^{-6}$ m to $.38 \times 10^{-6}$ m band respectively. Infrared and visible bands of lamp are thus suppressed.

COATINGS

Solar Reflectors

The illumination from the lamp was independently measured on a standard target and on the sample position (four samples were irradiated simultaneously). Thus corrective factors, f_c, are asigned to each sample. f_c = 1.045 for sample A and f_c = .955 for sample C.

The solar radiant energy in ESH, received by each sample, is given by

$$t_s = f_c \frac{t_{s.2} x 16.2 + t_{s.3} x 78.4}{16.2 + 78.4} ,$$

where $t_s = Q_s/\Phi_s$ (radiant energy over radiant flux) and $t_{s.2}$ and $t_{s.3}$ are radiant energies, in ESH, within each band. 16.2 $W.m^{-2}$ is the mean intensity of the spectral irradiation (one Sun) in the .2 x 10^{-6} m to .3 x 10^{-6} m, and 78.4 $W.m^{-2}$ that in the .3 x 10^{-} m to .38 x 10^{-6} m band.

Spectral reflectance was measured as follows:

1) Before irradiation, measurements where performed in air using an integrating sphere attached to a Beckman DK 2A reflectometer.

   Once finished the run, the reflectance was measured as in 2) but breaking the vacuum.

2) During irradiation spectral reflectance was measured in situ by an integrating sphere operating in the direct mode. The sample is irradi-

COATINGS

Solar Reflectors

ated directly and the detector views an area on the sphere wall. A standard coating of known reflectance is then measured under the same conditions. The directional-hemispherical reflectance factor $R(\beta,2\pi)$ is the ratio of the sample reading to the standard reading times the known reflectance of the standard. According to the sketch in the reference report (Paillous & Millan (1983)) $\beta \sim 0^{o}$. In the following R, will be given as normal-hemispherical spectral reflectance.

Solar reflectance is calculated as

$$\rho_s = \frac{\int_{.27x10^{-6}}^{2.5x10^{-6}} R(\lambda)E_s(\lambda)d\lambda}{\int_{.27x10^{-6}}^{2.5x10^{-6}} E_s(\lambda)d\lambda} \quad ,$$

where $E_s(\lambda)$ is the solar irradiance.

For the numerical computation the integrals have been discretized taking 30 selected wavelengths. Solar reflectance was calculated in the whole band (total), in the UV, in the visible and in the infrared.

Since for each wavelength $\alpha(\lambda) = 1 - R(\lambda)$ it follows that $\alpha_s = 1 - \rho_s$.

COATINGS

Solar Reflectors

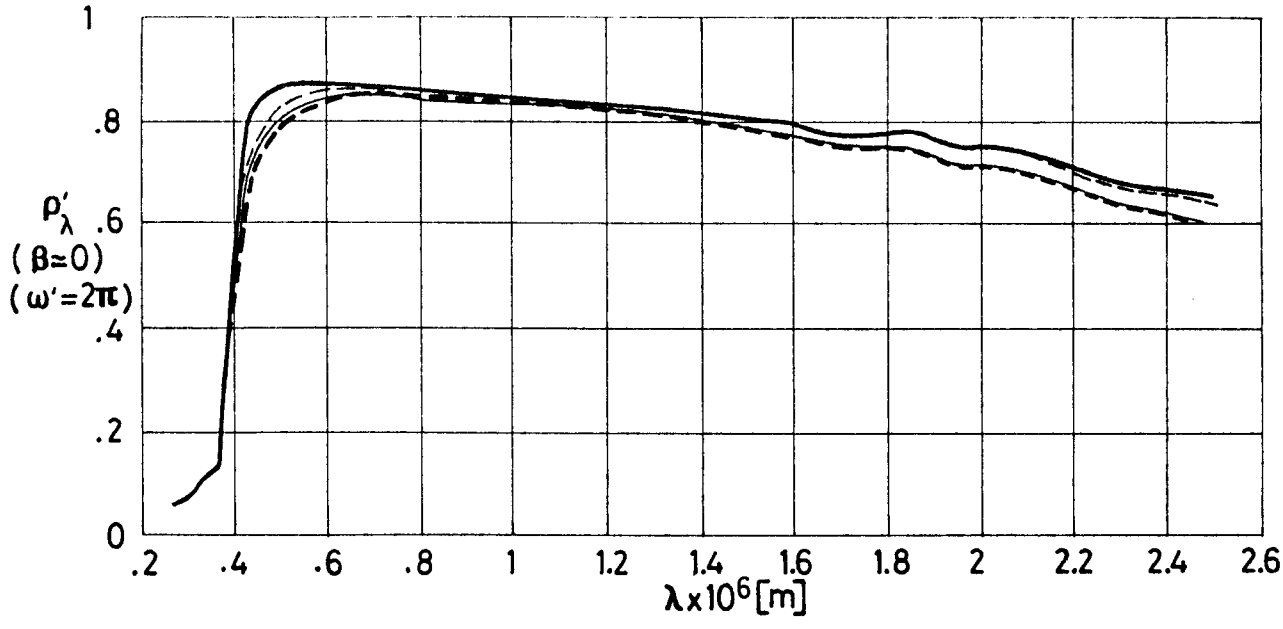

Fig 1-43.2. Normal-hemispherical spectral reflectance, ρ'_λ, of PCBZ coating, sample A, vs. wavelength, λ. Effect of Ultra-Violet radiation.

Explanation

$T \sim 353$ K $\beta \sim 0^\circ$ $\omega' = 2\pi$ Vacuum less than 1.3×10^{-4} Pa

Zinc Orthostannate in Rhodorsil 10 336. Four primer layers, five white finishing layers.

Key	Test Conditions
———	UV in vacuum, 0 ESH
———	1 086 ESH
- - - - - - -	2 625 ESH
———	2 625 ESH after breaking vacuum

From Paillous & Millan (1983).

COATINGS

Solar Reflectors

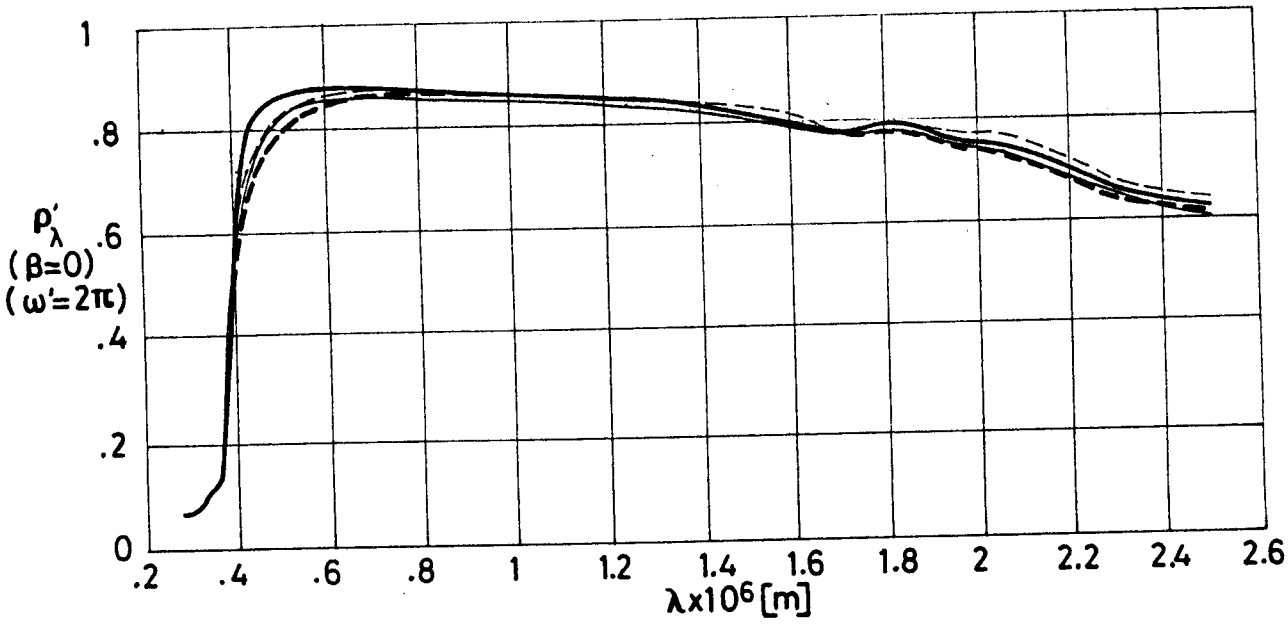

Fig 1-43.3. Normal-hemispherical spectral reflectance, ρ'_λ, of PCBZ coating, sample C, vs. wavelength, λ. Effect of Ultra-Violet radiation.

Explanation

$T \sim 353$ K $\beta \sim 0^\circ$ $\omega' = 2\pi$ Vacuum less than 1.3×10^{-4} Pa

Zinc Orthostannate in Rhodorsil 10 336. Four primer layers, eight white finishing layers.

Key	Test Conditions
———	UV in vacuum, 0 ESH
— — — —	994 ESH
- - - - - -	2 400 ESH
— — — — — —	2 400 ESH after breaking vacuum

From Paillous & Millan (1983).

COATINGS

Solar Reflectors

7.4. Electrical resistance.

Coating on glass substrate with P 128 primer.

.260 $kg.m^{-2}$ dry ($\sim$ 4 layers, α_s = .35) , R = 2 $\Omega/\square$ [a]

.310 $kg.m^{-2}$ dry ($\sim$ 5 layers, α_s = .29) , R = 150 $\Omega/\square$

.370 $kg.m^{-2}$ dry ($\sim$ 6 layers, α_s = .26) , R = 10^4 $\Omega/\square$

From Guillaumon & Blet (1982).

[a] From MASTER (1985). In this case primer is PCBZ primer. Measured per ASTM D 257-66.

The reason for the drastic increase in surface electrical resistance with thickness is twofold; 1) volume resistance of the semiconducting white layer increases with the number of layers, and 2) the diffusion of conducting particles through this white layer weakens when thickness increases (Guillaumon (1986)).

7.4.3. Charging

The surface potential of PCBZ coating irradiated with electrons has been measured at DERTS. Coating on glass substrate with P 128 primer.

Although surface resistance was very high (of the order of 10^{10} $\Omega/\square$), surface potential was low in any case. Results are given in Table 1-17.3 for different impinging electron beam energies, in keV.

Beam current density, 10^{-6} $A.m^{-2}$.

COATINGS

Solar Reflectors

Table 1-17.3

Charging Tests with PCBZ Coating

Exposure Time [h]	Surface Potential [V]			
	5 keV	10 keV	15 keV	20 keV
0	0	-	1	-
.008	4	3	3	1
.025	4	4	4	3
.058	4	4	5	4
.142	4	5	5	5
.308	5	6	6.5	6

From Guillaumon & Blet (1982).

8. ENVIRONMENTAL BEHAVIOR

PCBZ has been space-qualified by CNES. Results of the qualification tests are given in the following.

8.1. Prelaunch.

Moisture resistance test

Test conditions. Relative humidity: 90 %
Temperature : 323 K
Duration : 7 d

Coating Behavior.

	Appearance	Adhesion to scotch adhesive	ε	α_s
Before test	Matte	4/5 good	$.80 \pm .04$[a] $.83$	$.26 \pm .02$
After Test	No change	5/5 very good	$.80 \pm .04$	$.29 \pm .04$

[a] $\varepsilon_p = .80 \pm .04$ (portable emissometer), $\varepsilon_c = .83$ (calorimetric)

From Guillaumon & Blet (1982), Guillaumon (1983).

Adhesion of a coating to the substrate is the subject of several standards (ISO 2409 - 1972; UNE 48032; ASTM-D-3359, method B; DIN 53151; INTA 160299, ...) All of them deal with the so called cross-cut test. A lattice pattern is cut into the coating, penetrating through it to the substrate, by use of a standard cutting tool. The resulting pattern is then visually examined and the coating classified by comparison

COATINGS

Solar Reflectors

with an illustrative figure (0 to 5 or 5 to 0 from good to bad depending on the particular standards). Removal of flaked portions of coating film is made by a brush. Under certain circumstances, and through agreement between interested parties, an adhesive tape is used for removal. In other standards this procedure is mandatory. The above data have been presumably obtained per ASTM-D-3359.

---

9. THERMAL CYCLING

Test conditions. Pressure: 1.3×10^{-4} Pa
Temperature, Tmin: 123 K
Tmax: 373 K
Number of cycles: 200

Coating behavior.

	Appearance	Adhesion to scotch adhesive	ε	α_s
Before test	Matte	4/5 good	.80±.04	.26±.02
After Test	No change	4/5 good	.80±.04	.29±.04

Cummulative tests. Environmental + Thermal cycling.

After Test	No change	4/5 good	.80±.04	.29±.04

From Guillaumon & Blet (1982), Guillaumon (1983).

10. SOURCE

This coating, which has been developed by CNES, is commercialized by Société MASTER Peintures (ZI 09100 PAMIERS, France, Phone (61) 67.07.40).

11. COST

Not stated by supplier.

COATINGS

Solar Reflectors

1.2.6. SILVER VACUUM DEPOSITED ON FUSED SILICA

1. COMPOSITION

Metallic Silver, vacuum deposited on one surface of fused silica. The silver is overcoated with dielectric or conductive materials to protect it from degradation.

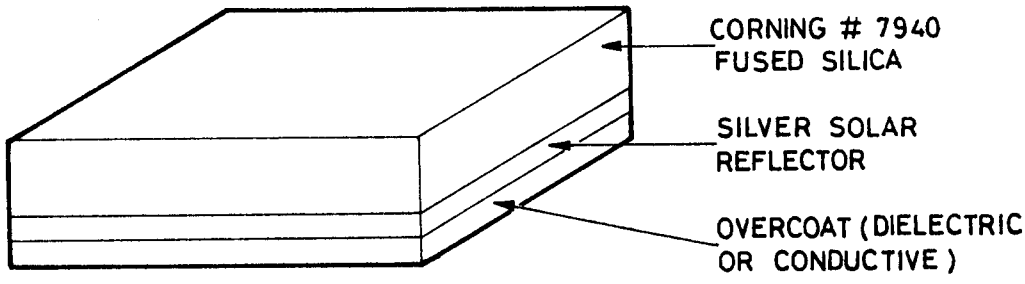

From OCLI (1980).

The following description is given by Cunnington, Grammer & Smith (1969).

Coating: Silver 10^{-7} m thick.

Overcoating: Inconel 5×10^{-8} m thick.

Both depositions made in the same chamber without breaking vacuum.

Fused Silica: Corning Glass Works No. 7940, .008" (2×10^{-4} m) thick.

3. USUAL DESIGNATION

Second Surface Thermal Control Mirror OCLI Type SI-100. Optical Coating Laboratory, Inc.

This coating system is also called Rigid Optical Solar Reflector (Rigid OSR), or Second Surface thermal control Mirror (SSM).

COATINGS

Solar Reflectors

In the following the first designation will be applied when the coating system is clearly identified in the reference, otherwise the more general designation, OSR fused silica, will be used.

4. SUBSTRATE

Any clean substrate.

5. METHOD OF APPLICATION

The OSR fused silica mirrors can be bonded to the substrate with an adhesive or a double-backed tape. Silicone cements provide the most desirable characteristics.

5.1. Background. The OSR fused silica mirrors can be fabricated in a variety of shapes and sizes. The most common configuration presently in use is that of 2.54×10^{-2} m squares. Squares of 3.81×10^{-2} m have been also manufactured. Larger sizes can be produced while maintaining the fused silica thickness mentioned above, however, the breakage factor during fabrication and handling leads to increased costs. These larger sizes are available on request.

Special sizes and/or shapes are required for application on highly curved surfaces. Application to a 2.5×10^{-2} m diameter tube has been reported by Marshall & Breuch (1968).

5.1.1. Geometrical tolerances. Unless superseded by customer specifications, the fused silica substrates of the SI-100 mirrors are fabricated to the following tolerances:

Rev. 1. 1981

COATINGS

Solar Reflectors

	Dimensional Tolerance
Length	±.002" (5.08×10^{-5} m)
Width	±.002"
Thickness	±.002"
Perpendicularity of sides	90°±0°15'
Edge Chips	.010" (2.54×10^{-4} m) max. projection into face.
Parallelism of sides	±.002"

From OCLI (1980).

5.1.2. Surface quality. F-F (80-50) or better per MIL-C-48497.

From OCLI (1980).

5.1.3. Appearance. The coated surface gives the appearance of uniform coverage when observed through the fused silica substrate (face) by the unaided eye. The surface shall be free of all metal deposition and other contamination. The overcoated surface (back) inherently has a distinct color when viewed under white light. This characteristic may be used to facilitate identification of the back face.

From OCLI (1980).

5.2. Preparation of surfaces for bonding. Depends on the substrate used. A detailed description of the several methods for preparing substrates for adhesive bonding can be found in Cagle (1968). Substrates considered are, among others, aluminium alloys, steels, titanium alloys, magnesium, copper and copper alloys, nickel and nickel base alloys, beryllium, chromium,... Manual methods for repair, as well as methods for

COATINGS

Solar Reflectors

evaluating surface preparation are also given by Cagle.

5.3. Application. Detailed application procedures must be worked out for each case. Sometimes each mirror must be applied individually. For other applications the mirrors are assembled in strings with tapes before transfer into the substrate. A small spacing between individual mirrors will allow for differences in thermal expansion between the mirrors and the substrate.

5.4. Curing process. Depends on the adhesive used. Table 1-18 gives a list of candidate adhesives, with pertinent outgassing data, as well as references on past experience in the attachment of OSR fused silica mirrors.

See also THERMAL CYCLING, p. 1-146.

5.5. Quality of adhesive bonding. Mechanical stability could not be a reliable test of the bond. In some instances the thermal conductance between the mirror and the substrate and, thence, the effective thermal emittance of the system, decreased as a result of thermal cycling.

6. SOLVENTS RESISTANCE

Fused silica is not attacked by solvents. Carbon tetrachloride, isooctane and xilene are silicone solvents. See p. 1-4. Solvent cleaning for repairing purposes would only be used when there is no other alternative. Very little cleaning is achieved, and porous bond lines will appear unless solvent completely evaporates before bonding.

COATINGS

Solar Reflectors

Table 1-18

Candidate Adhesives for OSR Fused Silica Application

Adhesive	% TML [a]	% CVCM [b]	Cure Time [h]	Cure Temp. [K]	Vacuum Conditions	References	Comments
DC 58C [e]							Used in Helios (Winkler & Stampfl (1975)).
DC 6-1104 [e]	.22 %RML:.14 [c]	.01	72	298	1.3×10^{-4} Pa-1.3×10^{-5} Pa	ESTEC (1980)	Prequalified by ESTEC for bonding CC-OSR fused silica on Aluminium substrate. (Bosma & Levadou (1979)).
DC 92-024 [e]							According to Marshall & Breuch (1968), has proven to have excellent properties.
DC 93-500 A/B as 11/1 by weight Silicone [e]	.09	.01	168	298	Air	Campbell, Marriott & Park (1978).	Used in radiators, Beacon Experiment, COMSTAR satellites. (Hyman (1981)).
DC 93-500 A/B as 20/1 by weight Silicone [e]	.04	.00	48	298	Air		
Eccobond 57C A/B as 1/1 by weight [f]	.52	.04	168	298	Air		Conductive Epoxy-Silver Adhesive. Used in SCATHA, ML12 experiment. (Hall & Fote (1979, 1980)).
Eccobond 57C A/B as 1/1 by weight [f]	.36	.03	.5	423	Air		
RTV-S 691 A/B as 9/1 by weight G790 Primer/Al foil [g]	.25 %RML:.22 [c]	.02	168	298	Below 1.3×10^{-4} Pa	ESTEC (1981)	Qualified by AEG-TELEFUNKEN as solar cell adhesive. (Koch (1978)).
RTV 560/T-12 as .1% T-12 [h]	2.22	.49	3600	298	Air	Campbell, Marriott & Park (1978).	Used in Boeing tests simulating HELIOS orbit. (Fogdall & Cannaday (1974)). Used in HELIOS. (Winkler & Stampfl (1975)).
RTV 560/T-12 as .1% T-12 [h]	.08	.04	3600 [d] 24	298 398	Air 1.3×10^{-6} Pa		
RTV 560/577/T-12 as 1/1/.5% by weight Silicone [h]	.63	.11	720 [d] 48	298 348	Air 1.3×10^{-6} Pa		
RTV 560/577/T-12 as 1/9/.5% by weight Silicone [h]	3.30	.57	720	298	Air		
RTV 560/577/T-12 as 1/9/.5% by weight Silicone [h]	.45	.08	336 [d] 144	298 348	Air 1.3×10^{-6} Pa		

(Continued onto next page)

Rev. 1. 1981

COATINGS

Solar Reflectors

Table 1-18 (Continued)

Candidate Adhesives for OSR Fused Silica Application

Adhesive	% TML [a]	% CVCM [b]	Cure Time [h]	Cure Temp. [K]	Vacuum Conditions	References	Comments
RTV 566 [h] .07% by weight Catalyst Silicone	.12	.00	168	298	Air	Campbell, Marriott & Park (1978).	Used in Boeing tests simulating HELIOS orbit. (Fogdall & Cannaday (1974)). It was not used in HELIOS because of technical problems. (Winkler & Stampfl (1975)). Used in several USAF geosynchronous satellites. (Curran & Millard (1978)).
RTV 566 [h] .075% by weight Catalyst Silicone	.11	.01	168	298	Air		
RTV 566 [h] .08% by weight Catalyst Silicone	.11	.01	168	298	Air		
RTV 566 [h] .09% by weight Catalyst Silicone	.10	.01	168	298	Air		
RTV 566 [h] .1% by weight Catalyst Silicone	.10	.02	168	298	Air		
RTV 566 [h] .1% by weight Catalyst Silicone/DC 1200 Primer/ /Sandwich	.12	.01	4	353	Air		
RTV 566 [h] .1% by weight Catalyst Silicone/GE 554155 Primer/ /Sandwich	.13	.01	4	353	Air		
RTV 615 [h] GE SS4120 Primer							Good thermal cycling results. (Marshall & Breuch (1968)). Used in USAF satellites. (Curran & Millard (1978)).

[a] TML: Total Mass Loss.
[b] CVCM: Collected Volatile Condensable Materials.
[c] RML: Remainder Mass Loss. Per Specification ESA PSS-09/QRM-02T.
[d] Each one of these cures was used in the order given.
[e] Manufactured by Dow Corning Corporation, Midland, Michigan, USA.
[f] Manufactured by Emerson & Cuming, Incorporated, Canton, Massachusetts, USA.
[g] Manufactured by Wacker-Chemie GmbH, Munich, Germany.
[h] Manufactured by General Electric Company, Silicone Products Department, Waterford, New York, USA.

COATINGS

Solar Reflectors

7. PHYSICAL PROPERTIES

7.1. Density. 2 200 $kg.m^{-3}$ (Cunnington, Grammer & Smith (1969)).

The surface density, including adhesive, is (Marshall & Breuch (1968)).

.49 $kg.m^{-2}$ for .008" (2×10^{-4} m) thick fused silica.

.27 $kg.m^{-3}$ for .004" thick fused silica.

7.2. Outgassing. Outgassing of adhesives, or of organic materials may degrade the optical properties of these mirrors. Outgassing characteristics of adhesives given in Table 1-18 have been measured per ASTM E595-77.

7.3. Thermal radiation properties

7.3.1. Emittance.

7.3.1.1. Hemispherical total emittance: Fig 1-44.

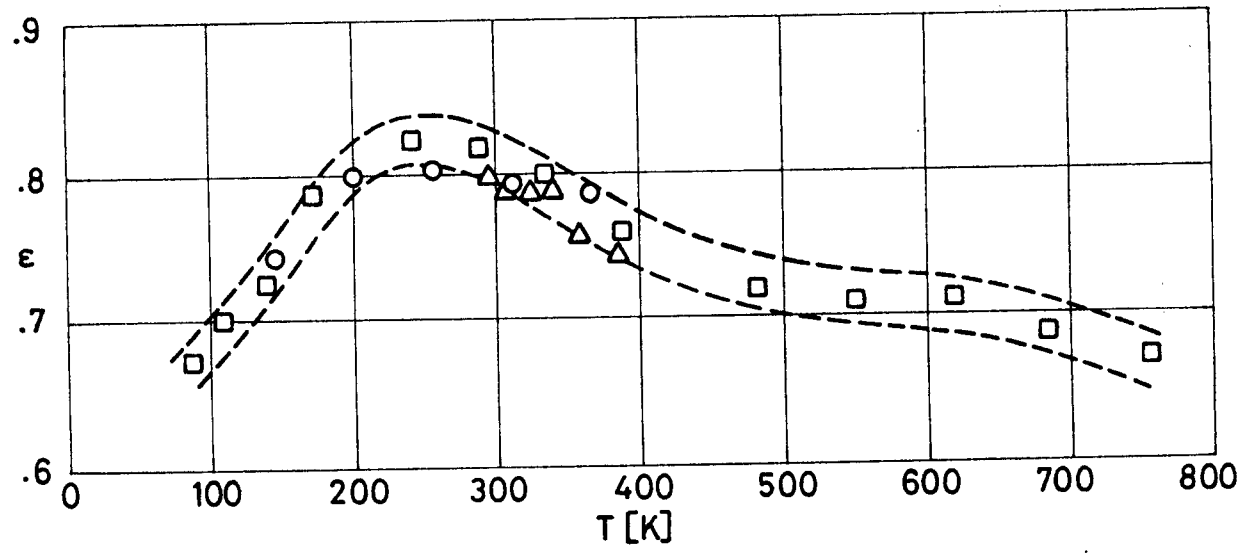

Fig 1-44. Hemispherical total emittance, ε, of OCLI Type SI-100 Thermal Control Mirrors as a function of temperature, T. ○ From Breuch (1967). □ From Marshall & Breuch (1968). △ From Cunnington, Grammer & Smith (1969). Uncertainty limits are from Marshall & Breuch (1968).

COATINGS

Solar Reflectors

7.3.1.2. Effects of the Space Environment on hemispherical total emittance.

7.3.1.2.1. Ultra-Violet Radiation. No significant change is anticipated. The following short table has been prepared using data from Cunnington, Grammer & Smith (1969).

T [K]	t [h]	n	ε_o	ε_f	$\bar{\varepsilon}$	σ
339	2040	31	.80	.78	.790	.010

Degrading Source: 2×10^{-7} m to 4×10^{-7} m Xenon Lamp, 1 Sun Level.
Method of obtaining data: Calorimetric.
Chamber pressure: 1.33×10^{-5} Pa.

t, total exposure time. [h].

n, number of data points given in the source.

ε_o,ε_f, initial and after-exposure values of the hemispherical total emittance.

$\bar{\varepsilon}$, mean value. $\bar{\varepsilon} = \frac{\sum_1^n \varepsilon_i \Delta t_i}{t}$.

σ, standard deviation. $\sigma = \sqrt{\frac{\sum_1^n (\varepsilon_i - \bar{\varepsilon})^2 \Delta t_i}{t-1}}$.

7.3.2. Absorptance.

7.3.2.1. Solar absorptance. According to Marshall & Breuch (1968), values obtained from spectral reflectance data and the appropriate solar radiation intensity fall within the range,

$\alpha_s = .050 \pm .005$, T from 180 K to 294 K.

COATINGS

Solar Reflectors

OCLI (1980) gives,

$$\alpha_s \leq .060 \quad ,$$

as deduced from spectral reflectance data (Cary 14 spectrophotometer) in the wavelength range 2.8×10^{-7} m to 2.5×10^{-6} m.

Slightly higher values can be found in the literature. For example, Fogdall & Cannaday (1974) quote

$$\alpha_s = .065 , \quad T = 153 \text{ K} ,$$

from spectral reflectance data measured, at 100 selected wavelengths, in the range 2.5×10^{-7} m to 2.5×10^{-6} m, with in situ reflectometer and spectrophotometer outside the vacuum chamber.

7.3.2.3. Variation of solar absorptance with incidence angle. Fig 1-45a shows data (Stultz (1976)) which correspond to:

1) Theoretical results, based on the electromagnetic wave theory and geometrical ray tracing, for the mirror geometries sketched in Fig 1-45b. The adhesive used to attach the mirrors is assumed to be totally absorbing, although the calculated α_s is based only on that energy directly impinging on the fused silica. Because of the internal reflection at the nonsunlit edge (Fig 1-45b) both configurations labelled A are equivalent, the same is true for B. In the analysis of configurations A both face and sunlit edge are taken into account, but only the face in the analysis B. Further details of the analysis are given in Stultz (1974).

COATINGS

Solar Reflectors

It was seen during the analysis that for $\beta \geq 86°$ total capture of the refracted ray occurs if the first and second faces are out of parallel by as less as .13° (.002" in 1"). Although these mirrors are out of standards (see p. 1-107), the probability of capture of the refracted ray increases when β becomes larger than 86°.

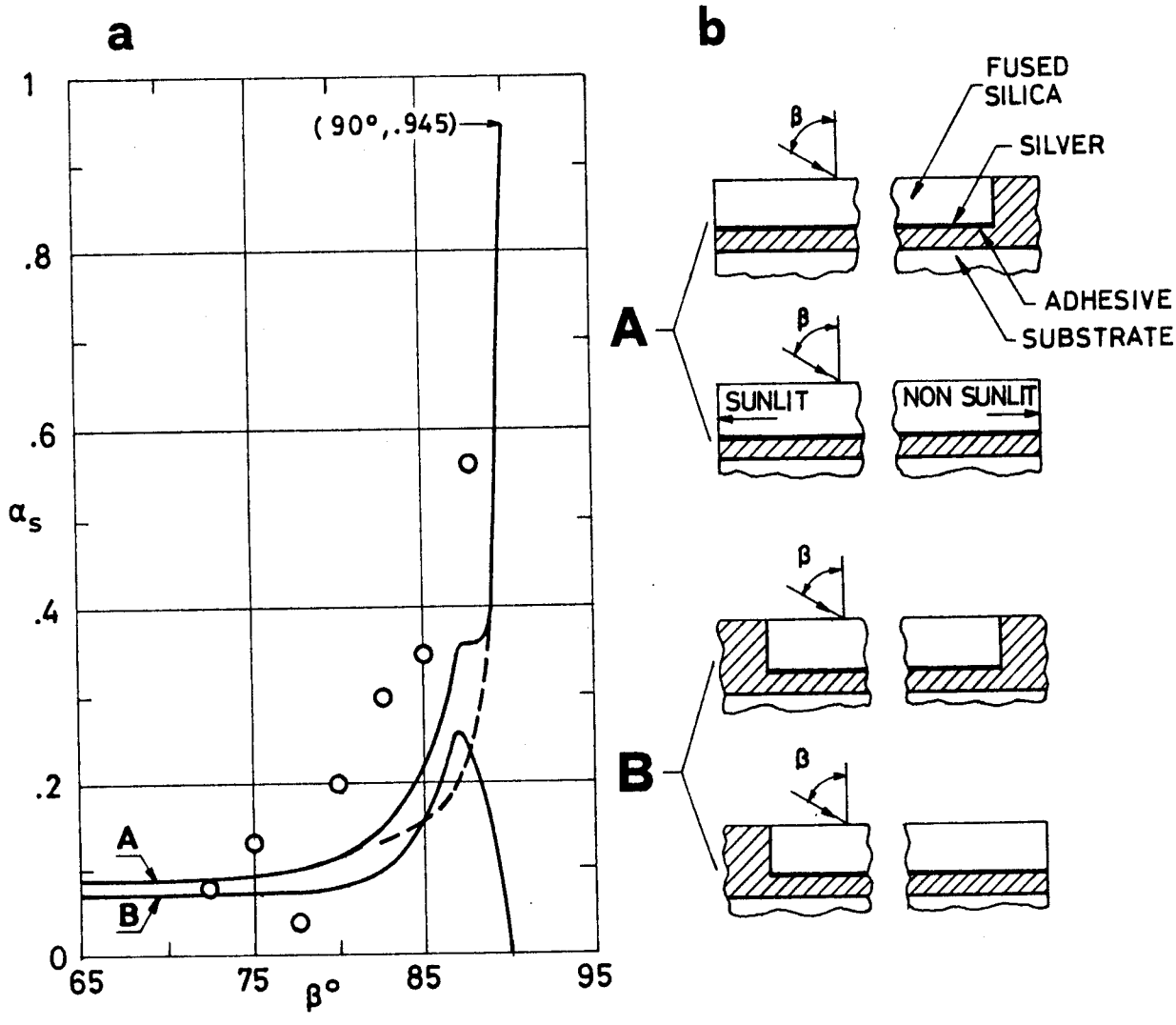

Fig 1-45. Solar absorptance, α_s, of OCLI Type SI-100 Thermal Control Mirrors vs. incidence angle, β. The full lines in a correspond to the analytical geometries sketched in b. O are from solar reflectance measurements, and the dotted line is based on flight temperatures of the NEMS radiator. From Stultz (1976).

COATINGS

Solar Reflectors

Mirrors of these geometrical characteristics would exhibit an α_s higher than that shown in Fig 1-45a.

2) Measurements made on a radiator, like those on board Nimbus E, Microwave Spectrometer (NEMS), which is covered by OSR fused silica mirrors. The JPL Celestarium was used for these measurements (Stultz (1974)).
These results are relative in the sense that they give the solar energy specularly reflected from a row of six mirrors. In order to locate the data points **O** in Fig 1-45a it is assumed that the maximum reflected energy at $\beta=72.5°$ represents an average solar reflectance of ρ_s = =.925 ($\alpha_s=1-\rho_s$), and that the maximum values for other β angles are proportional to this reflectance.

3) The calculated solar absorptance for the NEMS radiator based upon the flight temperature data corresponding to a period of constant solar intensity (November 20, 1973 to February 7, 1974). Although outgassing contamination could increase α_s by at least 10% (see Fig 1-47), the trend of the dotted line in Fig 1-45a is similar to those of the other curves.
Evidence of this β effect for smaller values of β has been reported by Hyman (1981). The analysis of radiator temperature data from COMSTAR satellites showed a seasonal increase and decay of α_s.
Since a seasonal variation of β also occurred, the curves giving the solar absorptance, α_s, vs. time, t, were

smoothed and the difference between original and smoothed curves was plotted as a function of the incidence angle, β. The results for COMSTAR D-1, D-2 and D-3 satellites are given in Fig 1-46. See also Fig 1-49, p. 1-125. No explanation for the larger slope of D-1 is given by the author.

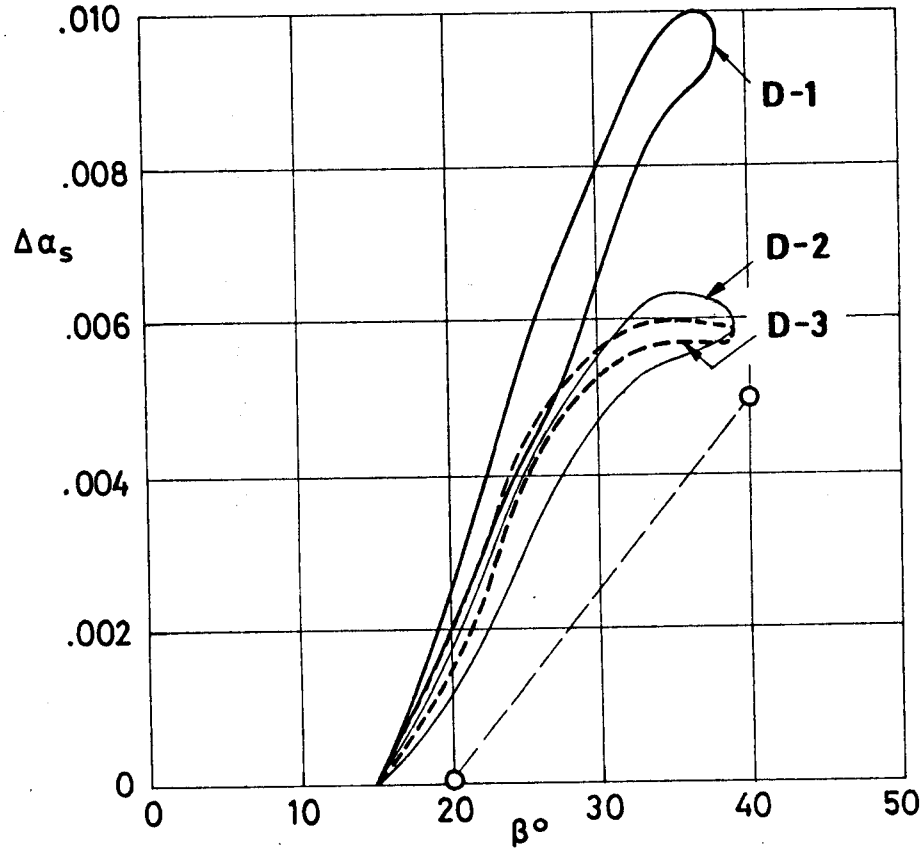

Fig 1-46. Change in solar absorptance, $\Delta\alpha_s$, of OCLI Type SI-100 Thermal Control Mirror vs. incidence angle, β, as deduced from data of COMSTAR D-1, D-2 and D-3 satellites. The envelopes contain all the data points. O Integrated sphere spectroreflectometer measurements made on a single mirror. From Hyman (1981).

7.3.2.5. Effects of the Space Environment on absorptance.

OSR fused silica mirrors are very stable when exposed to

COATINGS

Solar Reflectors

space environment, although contamination may significantly compromise their stability and performance. It is due to this reason that considerable discrepancy arose in the past several years between earlier and recent data obtained from spaceborne experiments.

A list of test conditions under which no change in the solar absorptance of OSR fused silica mirrors was detected is given in Table 3 of Marshall & Breuch (1968).

7.3.2.5.1. Ultra-Violet Radiation. Table 1-19 has been borrowed from Cunnington, Grammer & Smith (1969).

Table 1-19

Ultra-Violet Radiation Effects on Spectral Absorptance of OCLI Type SI-100 Thermal Control Mirrors

T [K]	t [h]	α for Xenon Lamp					α_s
		Range of $\lambda \times 10^7$ [m]					
		2-4.1	4.1-6	6-8.5	8.5-	Total	
339	0	.26	.05	.03	.03	.056	.061
339	122	.23	.05	.02	.04	.054	.058
339	170	.25	.05	.03	.03	.057	.060
339	242	.26	.05	.04	.03	.057	.062
339	338	.23	.07	.03	.03	.055	.062
339	410	.25	.06	.04	.03	.056	.062
339	458	.25	.06	.02	.03	.055	.059
339	528	.26	.05	.02	.04	.057	.059
339	648	.26	.06	.04	.03	.057	.063
339	696	.23	.07	.03	.03	.055	.061
339	768	.27	.05	.03	.03	.057	.061
339	816	.25	.05	.03	.03	.056	.059
339	864	.25	.05	.04	.03	.057	.061
339	936	.24	.05	.04	.03	.058	.058
339	984	.25	.05	.05	.03	.057	.063
339	1032	.25	.05	.04	.03	.056	.061
339	1104	.26	.04	.04	.03	.057	.059

(Continued onto next page)

Rev. 1. 1981

COATINGS

Solar Reflectors

Table 1-19 (Continued)

Ultra-Violet Radiation Effects on Spectral Absorptance of OCLI Type SI-100 Thermal Control Mirrors

T [K]	t [h]	α for Xenon Lamp, Range of λ×10^7 [m]					α_s
		2-4.1	4.1-6	6-8.5	8.5-	Total	
339	1152	.23	.07	.03	.03	.055	.062
339	1200	.26	.05	.03	.03	.056	.059
339	1272	.24	.06	.03	.03	.056	.060
339	1320	.23	.08	.03	.03	.056	.064
339	1468	.22	.08	.02	.03	.054	.061
339	1536	.20	.07	.02	.03	.052	.060
339	1608	.22	.08	.03	.03	.054	.063
339	1656	.25	.05	.03	.03	.056	.059
339	1704	.25	.06	.03	.03	.057	.061
339	1776	.24	.07	.03	.03	.056	.063
339	1824	.23	.07	.05	.03	.057	.057
339	1944	.24	.06	.05	.03	.058	.063
339	1994	.25	.04	.04	.03	.056	.058
339	2040	.24	.06	.05	.03	.059	.063
Before Exposure [a]		.25	.05	.03	.01	.052	.055
After Exposure [a]		.27	.06	.03	.01	.055	.061

[a] Values deduced from spectral reflectance data. See p. 1-132.
Degrading Source: 2×10^{-7} m to 4×10^{-7} m Xenon Lamp, 1 Sun level.
Method of obtaining data: Calorimetric in situ absorptance.
Chamber pressure: 1.33×10^{-5} Pa.
From Cunnington, Grammer & Smith (1969).

The data presented seems to indicate that change in α_s due to ultra-violet radiation is negligible.

7.3.2.5.5. Contamination. Fig 1-47 gives data (curves ○ and ◑) which, being obtained under similar radiation exposures, substantially differ in the amount of contamination.

COATINGS

Solar Reflectors

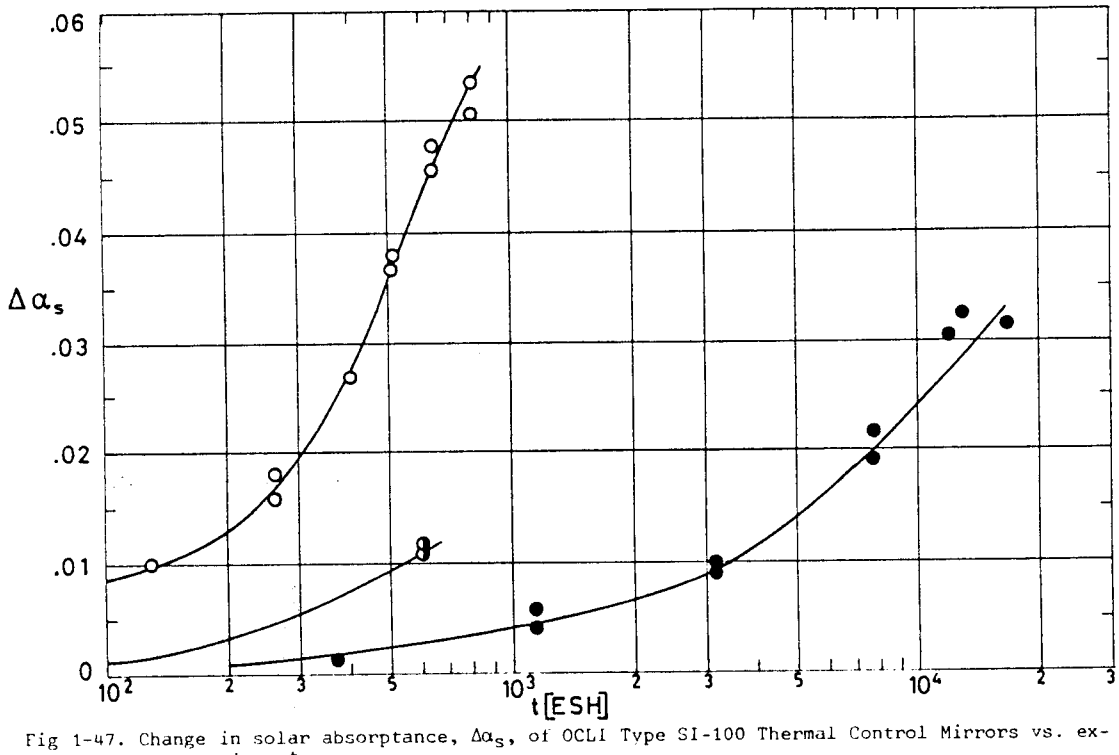

Fig 1-47. Change in solar absorptance, $\Delta\alpha_s$, of OCLI Type SI-100 Thermal Control Mirrors vs. exposure time, t.

Explanation

Key	Test Conditions					Comments
	Temp. [K]	Time [ESH]	Radiation Exposure: UV [Suns]	Charged Particles: Intensity [keV]	Charged Particles: Integrated Flux [Particles.m^{-2}]	
O	153	up to 800	1	80	7×10^{17} p.m^{-2}	Adhesive migrates toward the mirrors contaminating them. The degradation can be increased by repolymerization of the silicone because of the subsequent impinging radiation. The original values of ρ'_λ and α_s are restored when the adhesive is removed from the faces.
				20-230	5×10^{18} e.m^{-2}	
◑	288	up to 600	1	80	5×10^{17} p.m^{-2}	Degradation rates are much lower since outgassed RTV is more effectively trapped on the cold samples than on those at room temperature.
				20-230	4×10^{18} e.m^{-2}	
●	448	up to 17×10^3	16	10	4×10^{20} p.m^{-2}	Intended to reproduce HELIOS orbit conditions at .25 AU. Samples bonded to the substrate were tested adjacent to like samples clipped bare. Space was left between all samples so that a fin-type cryogenic baffle could form walls between the samples in order to avoid cross-contamination. Nevertheless, a portion of the reported α_s changes may represent the influence of cross-contamination from other samples.
				25×10^{-3}	electron neutralization	

SAMPLE

Sample Description

OCLI Type SI-100 Mirror. Fused Silica, .009" (2.29×10^{-4} m) thick. Polished with Barnsite. Initial solar absorptance, α_{so}=.065 .

Sample Mounting

Sample was bonded to a copper substrate with RTV 560 or RTV 566 silicone adhesives.

CALCULATION METHOD

α_s deduced from spectral reflectance measured at 100 selected wavelengths, in the range 2.5×10^{-7} m to 2.5×10^{-6} m, with in situ reflectometer and a spectrophotometer outside the vacuum chamber. Chamber pressure not given.

Reference: Fogdall & Cannaday (1974).

COATINGS

Solar Reflectors

7.3.2.5.6. Combined exposure. Results from in-orbit experiments are presented in the following. Typical exposures are given below. Data from both in-orbit and simulation experiments are summarized in Fig 1-52, p. 1-130.
See also Tables 1-20 and 1-21, pp. 1-135 and ff.

Orbit	Satellite	Typical Radiation Exposures					Comments	Pages
		UV	Protons		Electrons			
		[Suns]	Intensity [keV]	Flux [$p.m^{-2}.s^{-1}$]	Intensity [keV]	Flux [$e.m^{-2}.s^{-1}$]		
Near to Earth ∿500 km altitude	OSO-III	1					The Earth's magnetosphere shields the satellite from charged particles.	1-120 and 1-121
Subsynchronous ∿20 200 km altitude.	NAVSTAR	1	$<4\times10^3$ $>4\times10^4$	10^{12} $<10^6$ (time dependent).	>40 $>1.5\times10^3$	10^{10} 10^7	Crosses Van Allen radiation belt. Typical exposures estimated by the compiler after Johnson (1965).	1-122 and 1-123
Geosynchronous 35 800 km altitude.	COMSTAR SCATHA	1	20	5×10^{12}	20	2×10^{13}	More than 75% of the charged particles are of low energy (<20 keV). See further details in pp. 1-76 and 1-135.	1-124 to 1-127
Solar	HELIOS	up to 16	10	2.5×10^{13}			Also high temperatures T∿450 K. Solar wind is the only source of particles. Solar flares could increase the quoted protons value. (Winkler & Brungs (1975)).	1-128 and 1-129

OSO-III

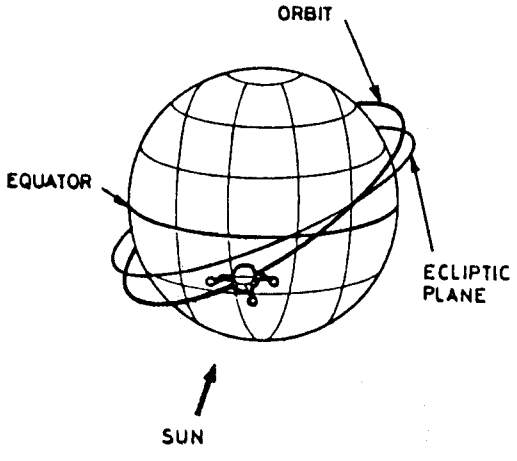

TEST CONDITIONS

Spacecraft & Programme
Third Orbiting Solar Observatory (OSO-III).
Thermal Control Coatings Experiment (TCCE).

Orbit
Launched on March 8, 1967 into a near circular orbit with an altitude of about 550 km and an inclination of about 33° relative to the Equator.

Configuration
OSO satellites have two main parts: a lower section, consisting of a nine-sided wheel, which rotates to provide gyroscopic stabilization, and a stabilized semicircular upper section, or sail, aimed at the Sun. The plane of spin contains the satellite-Sun line.

Thermal Test
Test of this OSR fused silica mirror was part of an experiment involving twelve coatings mounted on a single tray. This tray was located in the spinning wheel (about 3.9 $rad.s^{-1}$).
Data for the first year in orbit were reported by Millard (1969). Shortly after this year, the spacecraft tape recorders failed, but data to deduce $\Delta\alpha_s$ were still obtainable. Millard & Pearson (1973) gave $\Delta\alpha_s$ up to June 1971, a little over four years in orbit.

COATINGS

Solar Reflectors

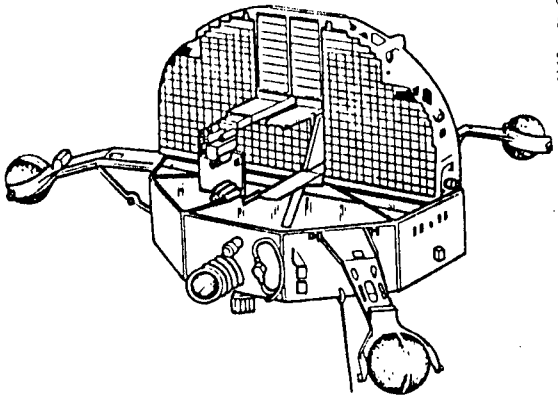

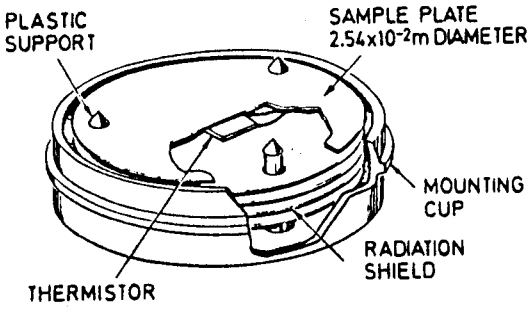

SAMPLE

Sample Description

OCLI Type SI-100 Mirror. It was furnished by Lockheed Missiles & Space Co.

Sample Mounting

The mirror is bonded to a thin aluminium disc, about 2.54×10^{-2} m in diameter, which is mounted in a cup to minimize heat leaks to the back side of the disc.
"Sample plate" will henceforth indicate the mirror plus the support disc.
The details of the sample mounting are described by Neel (1964). The sample plate is supported by three small Kel-F supports. The radiative coupling between the sample plate and the mounting cup is minimized by use of four radiation shields. All inner surfaces are polished and goldized to further reduce the radiant heat exchange. The temperature of the sample plate is measured by means of a thermistor soldered to the underside of the disc. The cups are in thermal contact with the tray base plate, whose temperature is measured with a thermistor. In order to evaluate the heat exchange between the sample plate and the mounting cups, it is assumed that the cups are at all times at the temperature of the tray base plate.
The tested thermal control surfaces alternatively view the Sun and the Earth, but their temperatures do not oscillate because of the relatively large thermal mass of the sample plates.

CALCULATION METHOD

α_S is measured calorimetrically from tray temperature, T_c, and sample plate temperature, T. The terms which appear in the heat balance equation are:
$c(T)dT/dt$, Sensible heat of the sample plate. It is, presumably, negligible. The temperature excursions in orbit of this sample plate remained in the range 210 K - 235 K, the narrowest among the twelve tested samples. In addition, the effect of this term can be minimized by taking the temperature data from a region of the orbit where time variations are small. This happens to be the case just before day-night transition when the sensor temperatures are near the maximum values.
$K(T_c^4-T^4)$, Radiation from the tray. K can be deduced as it will be indicated below.
$C(T_c-T)$, Conduction from the tray. It has been neglected.
$\varepsilon A\sigma(T_s^4-T^4)$, Radiation to outer space. The hemispherical total emittance, ε, of the sample plate is measured before launch. ε=.76 at 300 K. An evaluation of the different measurement techniques applied to nine of the coatings in this experiment has been made by Millard & Streed (1969). The equivalent surrounding temperature, T_s, is assumed to be zero.
$\alpha_S FAS/\pi$, Radiation from the Sun. F is the view factor. S is the solar constant. The factor $1/\pi$ accounts for the fact that the sample is placed in the spinning wheel.
$\alpha_S F_a A a S$, Albedo radiation. F_a is the view factor, and a the mean albedo of the Earth. This term can be neglected provided that only data very near the terminator (day-night transition), when the satellite does not see the sunlit side of the Earth, are taken.
$\alpha_p F_{sp} A P$, Earth infrared radiation. α_p is the hemispherical Earth radiation absorptance of the sample plate ($\alpha_p=\varepsilon$). F_{sp} is the view factor, and P_{sp} the flux on the sample plate. This term was deduced from the balance equation for the day side of the orbit for a reference surface, which was a V-groove.
Another energy balance, this for the night side of the orbit ($\alpha_S=0$), would yield either ε or (if ε is assumed to be known) the radiative transfer coefficient, K.
The effect of the uncertainty of the several unknown variables on α_S has been analyzed following Millard (1968). In this particular case the uncertainty is of the order of .05 α_S.

RESULTS

The laboratory value was α_S=.05 .
The mirror exhibited no changes in α_S after 7 500 ESH in orbit.

COMMENTS

No figure is given because, according to the reported results, $\Delta\alpha_S$ is practically zero.

References: Neel (1964), Millard (1968,1969), Millard & Streed (1969), Millard & Pearson (1973).

Rev. 1. 1981

COATINGS

Solar Reflectors

NAVSTAR

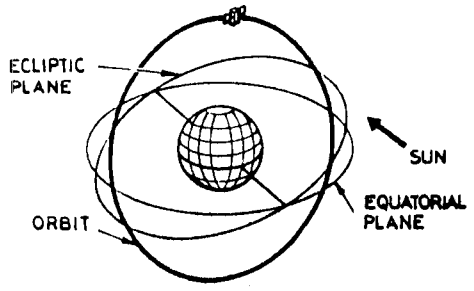

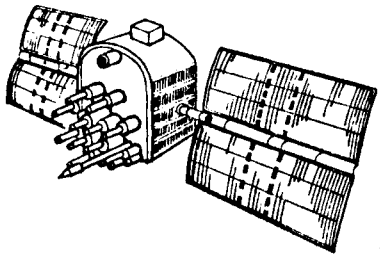

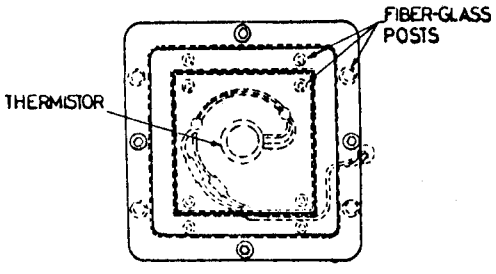

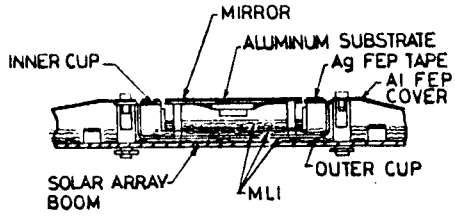

TEST CONDITIONS

Spacecraft & Programme

NavStar Global Positioning System (GPS).
Data in this item are from NavStar 5.

Orbit

NavStar satellites are being placed in subsynchronous, 12 h circular orbits of about 20 170 km, in three orbital planes at 63° inclination, with eight satellites per ring. The complete system of 24 satellites should be operational by 1985 (Taylor (1979)). NavStar provides three-dimensional position, velocity and time information to suitably equipped vehicles near or on the Earth's surface.
Six NavStar spacecraft were launched between February 1978 and April 1980.
NavStar 5 was launched on February 9, 1980 (Kruczynski (1980)).

Configuration

The spacecraft uses three nickel-cadmium batteries operating within a very narrow temperature range (273 K to 303 K), while the other spacecraft components have less restrictive temperature limits. Thence the batteries are thermally insulated from the spacecraft main structure. Heat from the batteries is rejected to the outer space. Thermostatically controlled heaters provide heating as required.

Thermal Test

Analysis of the NavStar 1 to 4 battery temperature data showed that the radiator coating utilized (silvered Teflon), degraded much faster than anticipated. Thermal experiments on subsequent satellites aimed at evaluating alternate solar reflectors. In particular, OSR fused silica mirrors and 1.27×10^{-4} m silvered Teflon were tested on board NavStar 5.
The experiments were flown in pairs, one attached to each of two solar array booms. The sample holder contained four 2.54×10^{-2} m square mirrors.
Once the spacecraft becomes 3-axis stabilized and the solar arrays are deployed, the booms are rotated so that the solar arrays (and thermal experiments) remain in full normal sunlight for the entire orbit.

SAMPLE

Sample Description

OSR fused silica mirror 2.54×10^{-2} m square. Not clearly identified in the reference.

Sample Mounting

The mirror is bonded to an aluminium substrate thermally insulated from the spacecraft. Substrate temperature is measured by a thermistor. Mirror and substrate form the sample plate.
The sample plate is partially surrounded by an inner aluminium cup. The gap between the sample plate and the edge of this cup, which was considered critical, was controlled to 1.27×10^{-4} m $\pm$ $\pm .51\times10^{-4}$ m. The inner cup is shaped such that the solar radiation through the gap will be absorbed inside. The sample plate is attached to the inner cup by .125" (3.175×10^{-3} m) diameter hollow fiberglass support posts. The rear surface of the substrate and the inner cup were covered with goldized Kapton to minimize radiative heat transfer.
A glass epoxy outer cup is used both to insulate the inner cup, to which it contacts through a flange coated with 1.27×10^{-4} m silvered Teflon, and as an attachment point for the entire assembly to the spacecraft through fiber-glass posts. The interstices between inner and outer cup and between outer cup and spacecraft solar array boom are filled with MLI blankets. An outer MLI cover (1.27×10^{-4} m aluminized Teflon) is attached to the outer cup by means of a double-faced tape (acrylic adhesive) and four screws.
The thermistor has leads gage No 22, as does the satellite wiring. To minimize heat leak through the leads, two pieces of constantan wire were spliced between the thermistor and the satellite wiring. The effect of the added electrical resistance on the accuracy level is negligible for α_s less than .5 .

CALCULATION METHOD

The in orbit sample plate temperature was calculated by using a 44 lumped-capacity steady-state Rockwell General Thermal Analyzer Programme. Nodes are interconnected with 242 conduction and radiation couplings. Boundary nodes are used to represent the solar array boom, the main body of the spacecraft and the outer space. The use of the steady state approach is justified since the solar heating is nearly constant for non-eclipse orbits.

COATINGS

Solar Reflectors

Parameters of the programme are: 1) Solar absorptance of the mirror and its hemispherical total emittance (which is assumed to be constant). 2) Solar absorptance of the inner cup, flange and MLI. 3) Radiation from the Sun, and 4) Temperature of the solar array boom. Albedo and infrared radiation from the Earth are neglected because only flight data when the mirror does not see the Earth are used.
Both pre-deployment of the solar array and in orbit configurations were modelled.
The output from the thermal model was compared to flight data. Small changes were made in the model values of the thermal conduction through the thermistor wires and through the fiber-glass posts, in the view factor from the mirrors to the remaining of the spacecraft, and in the effective emittance of the MLI in the cups. Using the same absorptance value for the beginning of orbital life as for the pre-deployment of the solar array, the calculated temperature values agreed with flight data to within 1 K.
Due to thermistor and telemetry errors the temperature readings have an uncertainty of 3.3 K, which means 0.01 uncertainty in α_s.

RESULTS

The solar absorptance, α_s, is plotted vs. orbital time, t. Since the mirrors remain in full normal sunlight for the entire orbit, orbital time is tantamount to ESH.

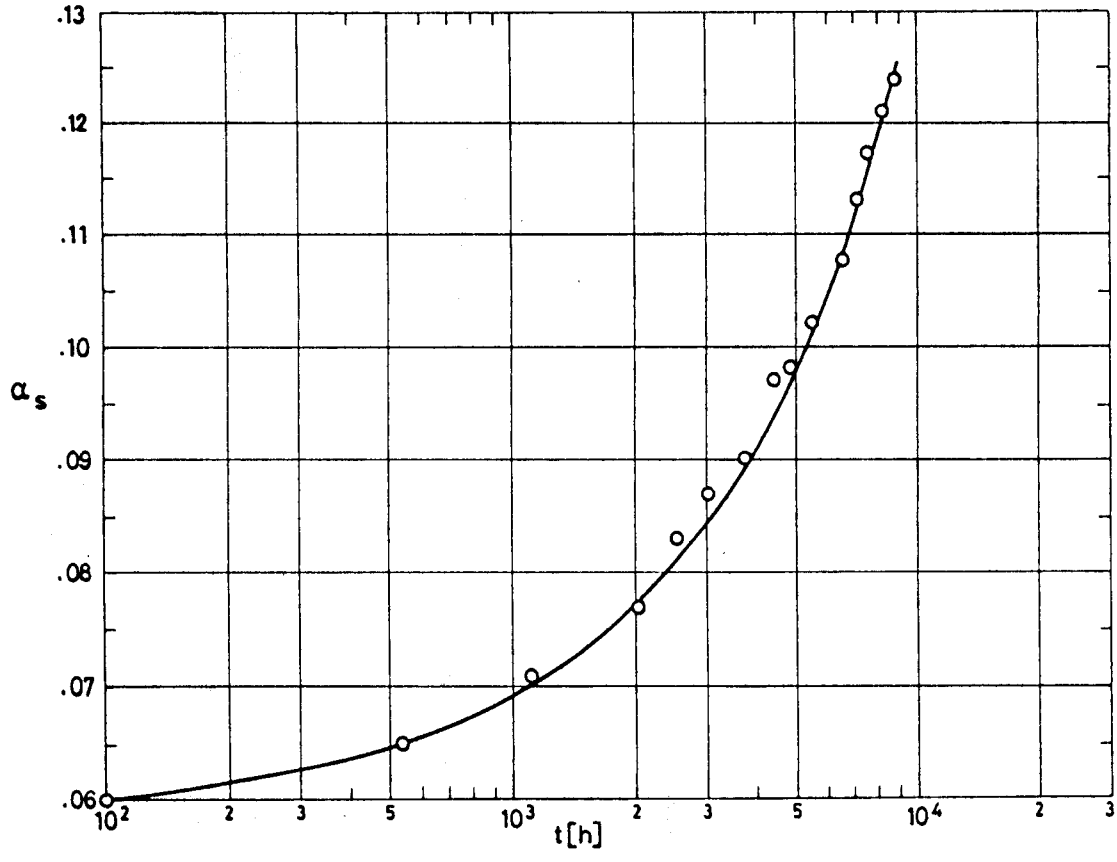

Fig 1-48. Solar absorptance, α_s, of OSR Fused Silica Mirrors vs. orbital time, t, as deduced from data of NavStar 5.

COMMENTS

Van Allen radiation is considered to be the most likely cause of the degradation experienced by these mirrors in orbital flight. The following reasons for ruling out contamination effects are quoted in the reference.

1) Any material used on NavStar should have a TML and CVCM below .1% .
2) NavStar satellites were assembled in a class 340 000 clean room.
   Air cleanlines class 340 000 implies at most 340 000 particles per cubic feet .5 micron ($5x10^{-7}$ m) and larger, and at most 2380 particles per cubic feet 5 microns and larger (Fed. Std. No. 209a (1966)).
3) Each spacecraft was subjected to a 30 day thermal vacuum test prior to launch and no degradation in optical properties was observed.
4) Test samples were installed after thermal vacuum tests.
5) The most likely potential contamination sources namely, the solar cell array (cover slides and RTV silicone adhesive), and the apogee kick motor are out of the direct line of sight of the samples.
6) Contamination effects would be expected to be less and less pronounced with time and no such trend is observed in Fig 1-48.

References: All the data in this item, unless otherwise stated, are from Pence & Grant (1981).

Rev. 1. 1981

COATINGS

Solar Reflectors

COMSTAR

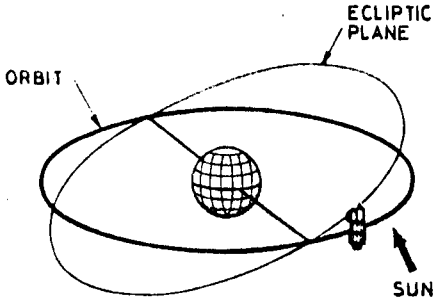

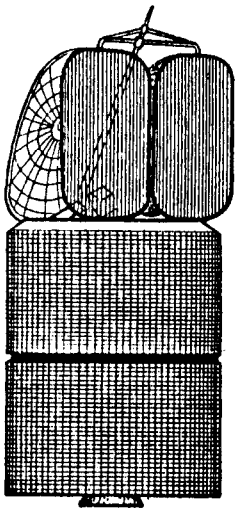

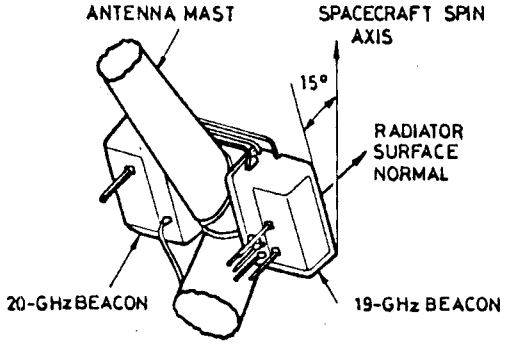

TEST CONDITIONS

Spacecraft & Programme
COMSTAR D-1, D-2 and D-3.
Beacon Experiment.

Orbit
Data for the first three COMSTAR satellites are given in the following table.

Satellite	Launching Date	Apogee [km]	Perigee [km]	Inclination [degrees]	Lifetime
D-1	May 13, 1976	35 810	35 790	1	Unlimited
D-2	July 22, 1976	35 795	35 780	1	
D-3	June 29, 1978	35 780	35 470	.08	

From Taylor (1977, 1979)

Configuration
The Beacon Experiment was devised to investigate microwave propagation. It was not intended to study the performance of the radiator thermal control surface.
The beacon package as a means for α_s measurement consists of an OSR radiator surface attached to a base plate upon which components are mounted that produce uniformly distributed and constant heat dissipation.
The radiator surface views only the diurnal Sun.

Thermal Test
The beacon serves as a coating experiment which is more realistic than dedicated flight experiments. It represents large OSR radiators not subjected to the extreme control, care and cleaning given to sample coatings.

SAMPLE

Sample Description
OCLI Type SI-100 Mirror. 2.54×10^{-2} m square.

Sample Mounting
The surface radiator is a .257 m × .437 m rectangle, 98% covered by the OSRs bonded to the aluminium honeycomb substrate with DC 93-500 adhesive. Heat flow other than that through the radiator is negligible due to an MLI blanket covering all other surfaces and to a low conductance mounting to the satellite mast. Heat dissipation, per package, is 29 W for D-1 and 32 W for D-2 and D-3, and is practically time-independent.
Temperature sensors within the beacon were provided for experiment performance evaluation.

CALCULATION METHOD

A thermal balance equation for the total package near temperature extremes (when $\partial/\partial t=0$) will contain the following terms.
$Q(t)$, Net heat input from external sources other than via radiator. This contribution is small but can not be easily estimated. A 14 node thermal model, accounting for all sources and incorporating a thermal resistance between the radiator and the temperature sensor, was devised. The model was developed and improved after flight temperature data become available, making it possible to accurately introduce properties such as thermal mass, radiator to sensor thermal resistance, solar reflection from the insulator hump covering the mast and so on.
$\varepsilon A\sigma(T_s^4-T_r^4)$, Radiation to outer space. The hemispherical total emittance of the sample, ε, is measured before launch. $\varepsilon=.78$. The equivalent surrounding temperature, T_s, is assumed to be zero. Telemetry data revealed that change in temperature is very slow near maximum, approximately .1 $K.h^{-1}$. Thence, it was assumed that maximum temperatures for the radiator, $T_{r_{max}}$, the package, $T_{p_{max}}$, and the sensor, T_{max}, appeared simultaneously. It was also assumed that $T_{r_{max}}=T_{max}+\Delta T$ where ΔT, the temperature jump along the radiator-sensor thermal resistance, is the same throughout the year and for all values of α_s.
$\alpha_s AS(t)$, Radiation from the Sun. S is the solar flux, a known function of time.
Q_i, Internally dissipated power. It is kept constant at the above indicated values. This assumption has been confirmed through data of minimum temperatures. The thermal balance equation for the total package, when $\partial/\partial t=S(t)=0$ and for couples of days exactly differing in one year (in order to eliminate the unknown $Q(t)$), indicates that over a one year interval $\Delta Q_i=.09$ W and that, even if Q_i is assumed to be constant, the maximum uncertainty in $\Delta\alpha_s$ per year will range from 3.8% to 6.4%.
By using the balance equation for conditions near T_{max}, and the above mentioned numerical model for $Q(t)$, curves of $\partial T_{max}/\partial\alpha_s$ along the year for different values of α_s were produced, as well as a curve giving the

COATINGS

Solar Reflectors

predicted maximum temperature, T_{pr}, for the typical value α_s=.13. Values of α_s for measured T_{max} differing from T_{pr} were calculated by the linear iterative formula

$$\alpha_s = .13 + \frac{T_{max}-T_{pr}}{\partial T/\partial \alpha_s} \quad ,$$

where $\partial T/\partial \alpha_s$ was obtained from the curves for the previously derived α_s.
The random error introduced by this graphical data reduction process is estimated to be ±.02 K for temperature and 2% for $\partial T/\partial \alpha_s$. This is equivalent to an uncertainty of approximately 1% in $\Delta \alpha_s$/year.
Errors due to temperature measurements and to telemetry were considered negligible.

RESULTS

The results deduced by the above method are shown as solid curves in Fig 1-49. All the curves exhibit an abrupt linear rise in α_s beginning at autumnal equinox, and an equally sharp decay at normal equinox. This is due to the incidence effect discussed in p. 1-113 and ff. The significance of this effect is estimated by first assuming a linear variation of α_s vs. time for normal incidence from autumnal to normal equinox, following the general trend of the curves after excluding abnormal increases and decreases. The dashed curves are supposed to represent α_s vs. time corrected to normal solar incidence, and the difference is the effect of incidence. These last data fairly correlated (particularly those from D-2 and D-3) with integrating sphere spectroreflectometer measurements made on an OSR sample at 20° and 40° from normal (Fig 1-46). No explanation of the larger deviation of D-1 data is given.

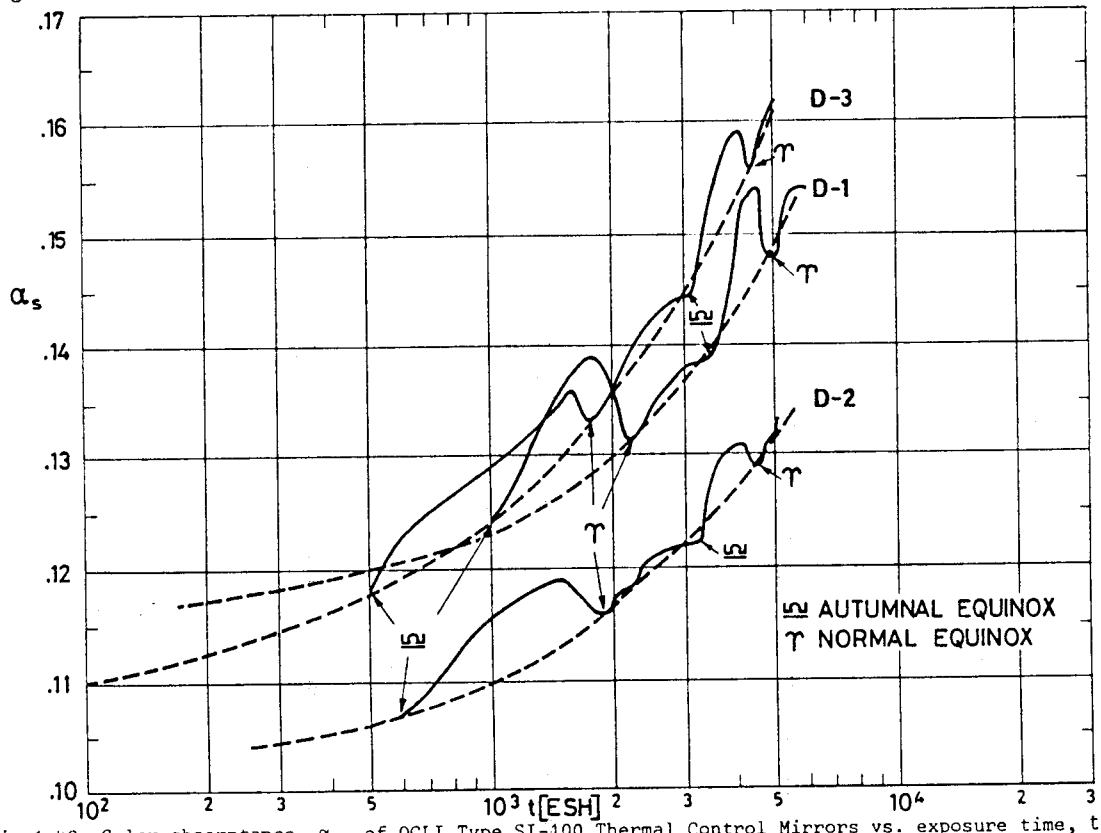

Fig 1-49. Solar absorptance, α_s, of OCLI Type SI-100 Thermal Control Mirrors vs. exposure time, t, as deduced from data of COMSTAR D-1, D-2 and D-3 satellites.
——— Derived from temperature telemetry.
------- Corrected to normal solar incidence.

COMMENTS

The curves corresponding to normal solar incidence given by Hyman (1981) exhibit a high initial slope until approximately the first summer solstice (2 000 to 3 000 ESH), afterwards the slope decreases and remains constant. This can not be appreciated in Fig 1-49 because of the logarithmic scale used in abscissae.
D-3 values are higher than the other two. The explanation could be based on the approximately 2 years longer storage time for D-3 mirrors. Although deposits on these mirrors were noticed, only standard cleaning procedures were used and cleaning effectiveness was not measured. According to Hyman (1981), telemetry data from D-4 satellite (launched February 1981), where only one of the beacon radiators has been cleaned, should clear up the present uncertainties.

References: All the data in this item, unless otherwise stated, are from Hyman (1981).

COATINGS

Solar Reflectors

SCATHA

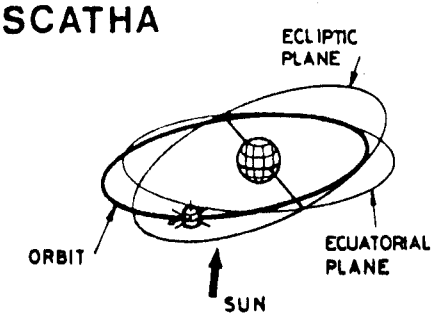

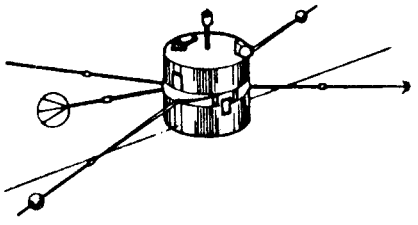

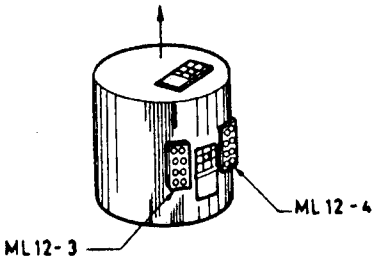

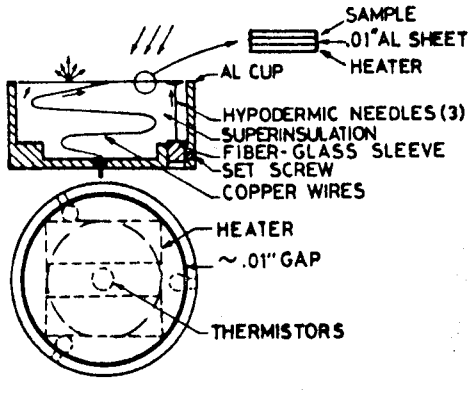

TEST CONDITIONS

Spacecraft & Programme

Spacecraft Charging at High Altitudes (SCATHA).
USAF Space Test Programme P78-2.

Orbit

Launched on January 30, 1979 into a 176 km by 43 278 km transfer orbit. On February 2 it was injected into a 27 600 km by 43 300 km, 7.9° inclination final orbit. P78-2 passes through geosynchronous altitude (35 786 km) twice per day and is always 23% of geosynchronism.

Configuration

The satellite is a circular cylinder approximately 1.75 m in both length and diameter. It spins with its axis approximately normal to the Sun line.

Thermal Test

Test of this OSR is a part of the ML12 experiment on board P78-2. The experiment consists of 16 calorimetrically mounted samples of thermal control coatings.
Another experiment concerning this OSR, among other coatings, has been performed on board P78-2 in the Satellite Surface Potential Monitor (SSPM) package which is devised to continually measure satellite frame to surface potential and bulk current of typical spacecraft thermal control materials (Koons, Mizera, Fennell & Hall (1980).

SAMPLE

Sample Description

OCLI Type SI-100 Mirror. 3.18×10^{-2} m diameter.

Sample Mounting

The mirror is mounted on an aluminium disc by means of diluted Eccobond EC 57C conductive epoxy. The disc is supported by three .014" (3.56×10^{-4} m) hypodermic needles, which are thermally insulated from the base of a cup by fiber-glass sleeving. The length and diameter of the instrumentation leads to the disc were chosen to minimize conduction. The tubing and wires together give approximately a thermal conductance of 9×10^{-4} $W.K^{-1}$. The volume enclosed by the sample plate and cup walls is filled with a combination of MLI and open-cell polyurethane insulation. The radiation coupling coefficient between sample plate and cup is approximately 7.9×10^{-12} $W.K^{-4}$. The underside of each sample plate carries two heaters in series and three thermistors. The heaters are used for preflight calibration and for allowing thermal desorption cleaning of the sample plate during flight. There are two trays, designated as ML12-3 and ML12-4 with eight samples each. This particular sample is placed on tray ML12-3. The trays were placed in the cylindrical surface of the satellite amid the end bases.

CALCULATION METHOD

α_S is measured calorimetrically from tray temperature, T_C, and sample plate temperature, T. The terms which appear in the heat balance equation are:

$c(T)dT/dt$, Sensible heat of the sample plate. The sample plate specific heat, c, is measured before launch.
$K(T_C^4-T^4)$, Radiation from the tray. K measured before launch.
$C(T_C-T)$, Conduction from the tray. C measured before launch.
$\varepsilon A\sigma(T_S^4-T^4)$, Radiation to outer space. ε measured before launch (ε=.80). The equivalent surrounding temperature, T_S, is assumed to be zero.
$\alpha_S FAS\sin\omega t$ for $0\leq\omega t\leq\pi$, and 0 for $\pi\leq\omega t\leq2\pi$, Radiation from the Sun. F, shading factor from spacecraft booms, is calculated as a function of spacecraft attitude (resolution 1°). S is the solar flux for the day of the evaluated data.
Q_j, Power from sample heater, if applied.
α_S is calculated assuming that sample plate temperature, T, weakly depends on time, t. A first approximation for α_S is obtained from the steady state equation ($\partial/\partial t=0$) taking for T the measured instantaneous value, T_O. Then $T(t)-T_O$ is deduced by integration of the linearized ($T^4-T_O^4\simeq4T_O^3(T-T_O)$) complete equation with the above α_S value. The process is repeated again with the new T.
An analysis of the expected degree of random errors has been performed. The results which are presented below are based on quick look data provided by the USAF Satellite Control Facility after one year in orbit.
The main sources of errors were. 1) Resolution of the telemetry system. The various input parameters which ap-

COATINGS

Solar Reflectors

pear in the balance equation were varied by amounts equal to the resolution inherent in the telemetry processing, and the change in α_s was calculated. Reduction of the uncertainty may be possible by averaging large data sheets contained on magnetic tape. 2) Shading from the booms. The errors arise from the resolution of the table of shading values vs. attitude angle, and from the uncertainty of the angle at a given time. Reduction of the uncertainty is anticipated when more accurate spacecraft attitude data become available, and by selecting data from times when the knowledge of the spacecraft attitude is not highly critical.

RESULTS

Since the spacecraft spins around an axis normal to the Sun line, it takes π hours to accumulate one ESH of exposure. Thus, the ESHs abscissae in Fig 1-50 below have been deduced multiplying by $24/\pi$ the times in julian days which appear in the references. This is not really justified for vacuum and energetic particle bombardment effects.

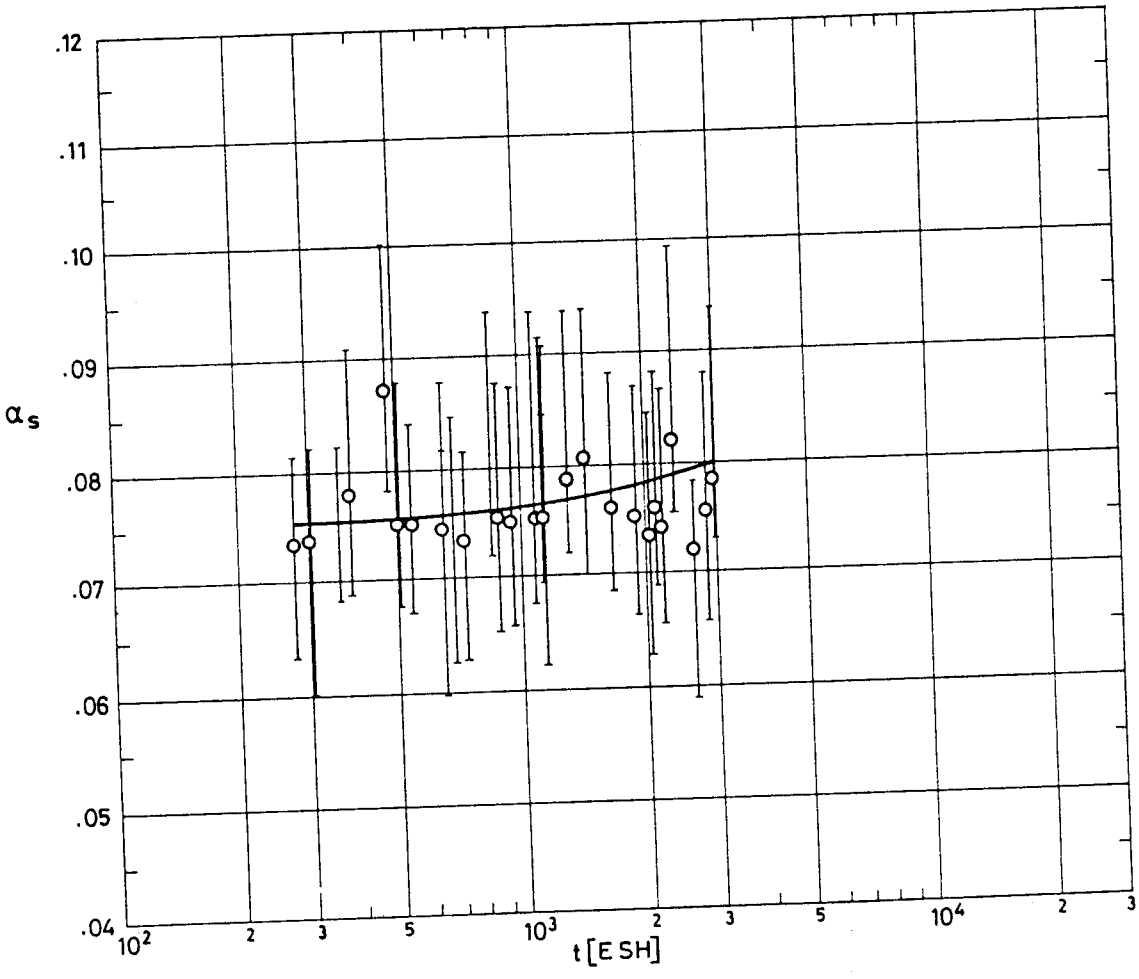

Fig 1-50. Solar absorptance, α_s, of OCLI Type SI-100 Thermal Control Mirrors vs. exposure time, t, as deduced from data of SCATHA spacecraft.

COMMENTS

α_s remained approximately constant over the year in orbit, which suggests that the coating is stable and that contamination effects were minor.

In order to calculate $\Delta\alpha_s$ plotted in the summary figure, Fig 1-52, p. 1-130, the value α_{so}=.075, resulting from the extrapolation to t=0 of the curve in Fig 1-50, has been taken. This fairly large value (compare with those given in pp. 1-112 and 1-113) seems to indicate that the initial degradation was relatively high.

References: All the data in this item, unless otherwise stated, are from Hall & Fote (1979, 1980).

Rev. 1. 1981

COATINGS

Solar Reflectors

HELIOS

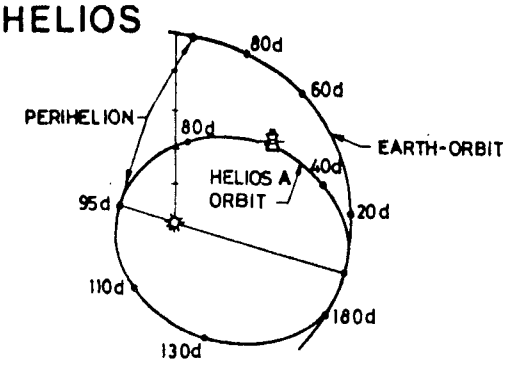

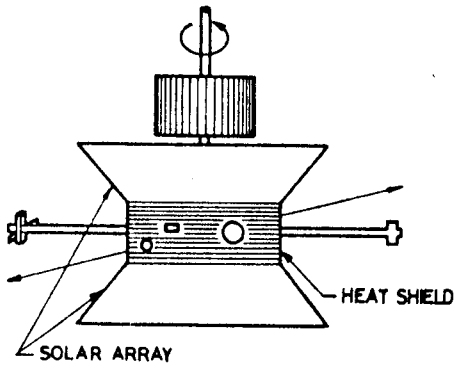

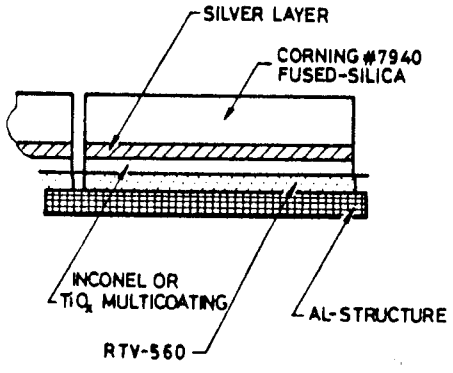

TEST CONDITIONS

Spacecraft & Programme

HELIOS-A and HELIOS-B solar probes.

Orbit

HELIOS-A was launched on December 12, 1974 on a highly eccentric elliptic solar orbit with a perihelion of .31 AU (1 AU = $=1.495\times10^{11}$ m). HELIOS-B was launched on January 15, 1976 on a slightly different orbit, perihelion of .29 AU.
Data presented here correspond to HELIOS-A first three orbits and HELIOS-B first orbit. Environmental conditions were similar to those assumed before launching (which correspond to ● in Fig 1-47, p. 1-119) although, according to measurements performed during HELIOS-A mission, the integrated flux of protons was 3.2×10^{20} p.m^{-2}. Solar flares where not detected, but an additional integrated flux of 2×10^{20} p.m^{-2} is estimated for an average Sun (1978-1980).

Configuration

HELIOS is an automatically-functioning solar probe. The basic structure is spool-shaped, with a cylindrical central compartment 1.75 m in diameter by .55 m long. A conical solar array is attached to each end, completing the spool-shape.
The telecomunications antenna system is placed on the central body, within and protruding above the upper solar array. Two deployable double-hinged booms are fitted to carry experiments. Two other deployable booms, diametrically opposed, are used as antennae for radio-wave experiments.

Thermal Test

HELIOS was devised to investigate the solar wind, but temperatures in specific points were recorded for house-keeping purposes. The records were used for coating behavior evaluation. HELIOS-A and B were practically similar, only the ion guards of the horizontal antennae of HELIOS-B were modified and enlarged.

SAMPLE

Sample Description

OCLI Type SI-100 Mirror.

Sample Mounting

Sample was bonded to an aluminium substrate, RTV 560 adhesive. Data were deduced from a single temperature sensor (S2) placed at the upper edge of the heat shield, under the mirror substrate, within easy reach of the conical solar array IR radiation. This location, not chosen for reasons connected with sample monitoring, presents the following drawbacks. 1) High thermal coupling, both conductive and radiative, with the solar array. This effect is stronger the lower the temperature, in relative terms. 2) A thick contamination layer resulting from the sensor location near the corner. Thus $\Delta\alpha_s$, both initial and after the first perihelion was very pronounced in the particular case of this sample.

CALCULATION METHOD

•A first estimate of α_s was made neglecting thermal couplings between spacecraft and sensor. Thence, $\alpha_s S=\varepsilon\sigma T$, where ε is assumed to be constant. Results from the first HELIOS-A orbit, as given by Winkler & Brungs (1975), are shown in Fig 1-51. The estimated initial value of α_s is $\alpha_s=.062$. Data near perihelion and near aphelion were lost since the measuring range of the sensor was limited to 233 K - 333 K.
The analysis of the results was mostly speculative at that stage both because of the above oversimplified calorimetric approach, and of the incomplete simulation of the following effects during ground tests. 1) Sample contamination, influenced by sources location, cold and hot surfaces,... 2) Sample degradation (physicochemical damage effects) which depends on the temperature. 3) Non-steady conditions (spin, varying Earth-Sun distance). 4) Combined effects.
Solar input data were considered reliable, and in fair agreement with those used for ground testing.
Errors due to the resolution of the telemetry system are, for instance, at aphelion: $\Delta\alpha_s=\pm.006$ for $\Delta T=\pm1$ K.
•Data from the first three orbits of HELIOS-A and the first orbit of HELIOS-B have been analyzed by Winkler (1977). The following effects have been considered. 1) Conductive thermal coupling between the spacecraft surface and the central compartment where the sensor is located. This introduces a correction which, for sensor S2, is $\Delta\alpha_s=.17(T_o-T_i)$, where T_o and T_i are outer and inner spacecraft temperatures, respectively. This correction accounts for most of the improvement in the analysis particularly near the perihelion. 2) Radiative thermal coupling and shading effects, which can be neglected for both HELIOS-A and B regarding this particular sample. 3) Influence of temperature on the hemispherical total emittance. 4) Degradation and contamination.

COATINGS

Solar Reflectors

RESULTS

Results from Winkler & Brungs (1975) and Winkler (1977) are shown in Fig 1-51. Time in ESH has been calculated by assuming that the flux, for both UV and protons, varies as the square of the distance to the Sun. Time for HELIOS-B has been compressed by a factor of 1.14, so that the perihelion and aphelion of both orbits correspond to the same ESH values.

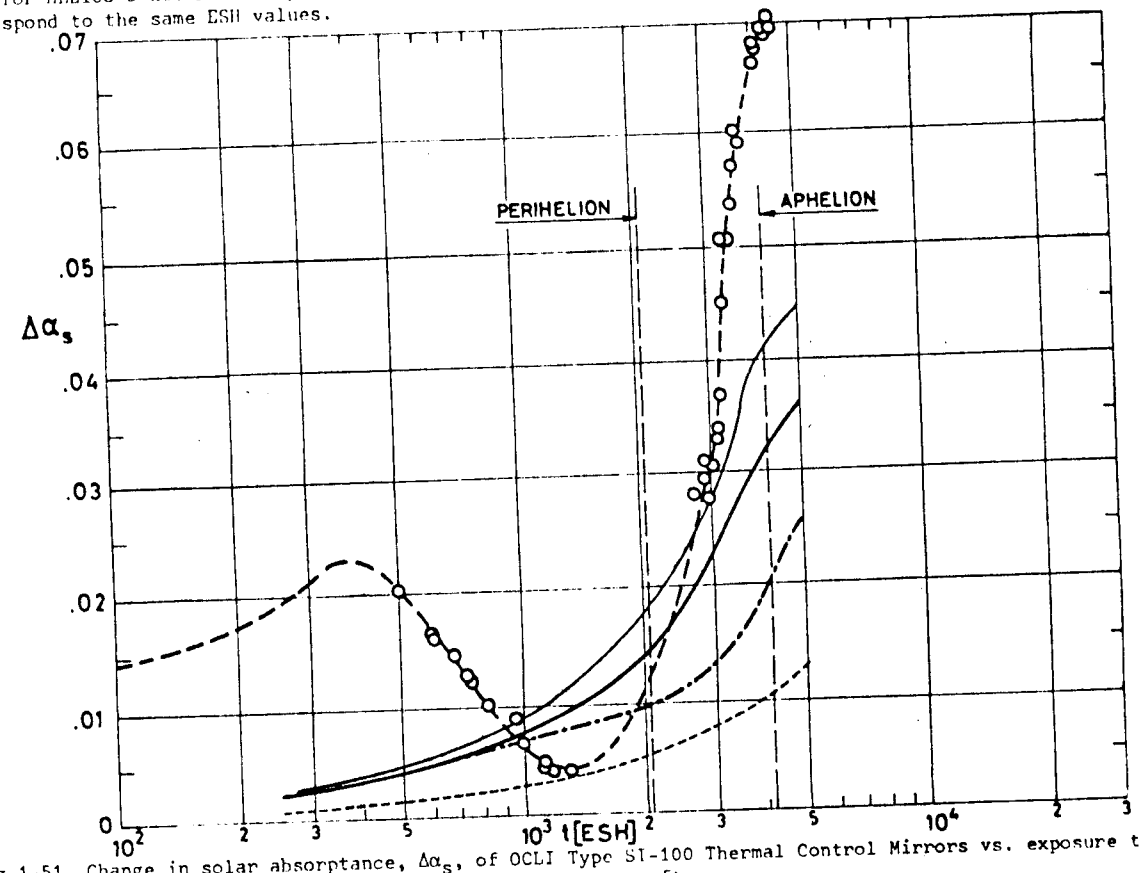

Fig 1-51. Change in solar absorptance, $\Delta\alpha_s$, of OCLI Type SI-100 Thermal Control Mirrors vs. exposure time, t, as deduced from data of HELIOS-A and B spacecraft.
-o- First HELIOS-A orbit. Simplified model of data analysis.
—— Average of the first three HELIOS-A orbits. Improved model of data analysis.
—— First HELIOS-B orbit. Improved model of data analysis.
----- Average of the first three HELIOS-A orbits. Effect of degradation alone. Fig 1-47, α_{so}=.062.
-·-·- Average of the first three HELIOS-A orbits. Effect of contamination alone. Calculated.

COMMENTS

In addition to the usual phenomena associated to outgassing under vacuum conditions, long time missions with extended periods at elevated temperatures, such as in HELIOS satellites, pose several peculiar problems.

1) Due to elevated temperatures a small fraction of the surrounding adhesive begins to creep into the surface sticking there. Incoming particles or high energy photons partially crack this creeping material. The resulting ions and neutral particles escape into open space (secondary outgassing). To estimate the influence of this effect on $\Delta\alpha_s$ it is assumed that, at least for the five or six first orbits, the rate of deposition on the spacecraft surface is constant. From the analysis of the results one can deduce that the thickness of the layer deposited in each orbit is 4.16×10^{-8} m.
2) Since the electric potential of the spacecraft surface is unevenly distributed and different from that of the undisturbed surrounding plasma, a boundary layer appears around the spacecraft whose thickness depends on the potential difference, and on plasma density and temperature. Outgassing material, which is ionized within the boundary layer, will rebound onto the surface creating a deposit of ionized molecules which increase α_s. One can estimate the thickness of the deposit on the basis of ad hoc values of the fraction of the ionized particles which will build up the contamination layer, and of outgassing kinetic data (not readily available). Such processes as cracking, creeping, polymerization and others, leading to long term effects upon adhesives, are accounted for by means of an additional constant term.

The $\Delta\alpha_s$ value is related to the contamination thickness, Δt, by means of $\Delta\alpha_s=1-e^{B\Delta t}$ where $B=1.2\times10^5$ m^{-1}.
Values calculated by Winkler (1977) for the first three HELIOS-A orbits are:
1st orbit $\Delta t=4.16\times10^{-8}$ m + 8.50×10^{-8} m, $\Delta\alpha_s$=.016. The real value was $\Delta\alpha_s$=.019, because of sample position.
2nd orbit $\Delta t=4.16\times10^{-8}$ m + 12.76×10^{-8} m, $\Delta\alpha_s$=.029 .
3rd orbit $\Delta t=4.16\times10^{-8}$ m + 16.92×10^{-8} m, $\Delta\alpha_s$=.043 .

References: Winkler & Stampfl (1975), Winkler & Brungs (1975), Winkler (1977).

COATINGS

Solar Reflectors

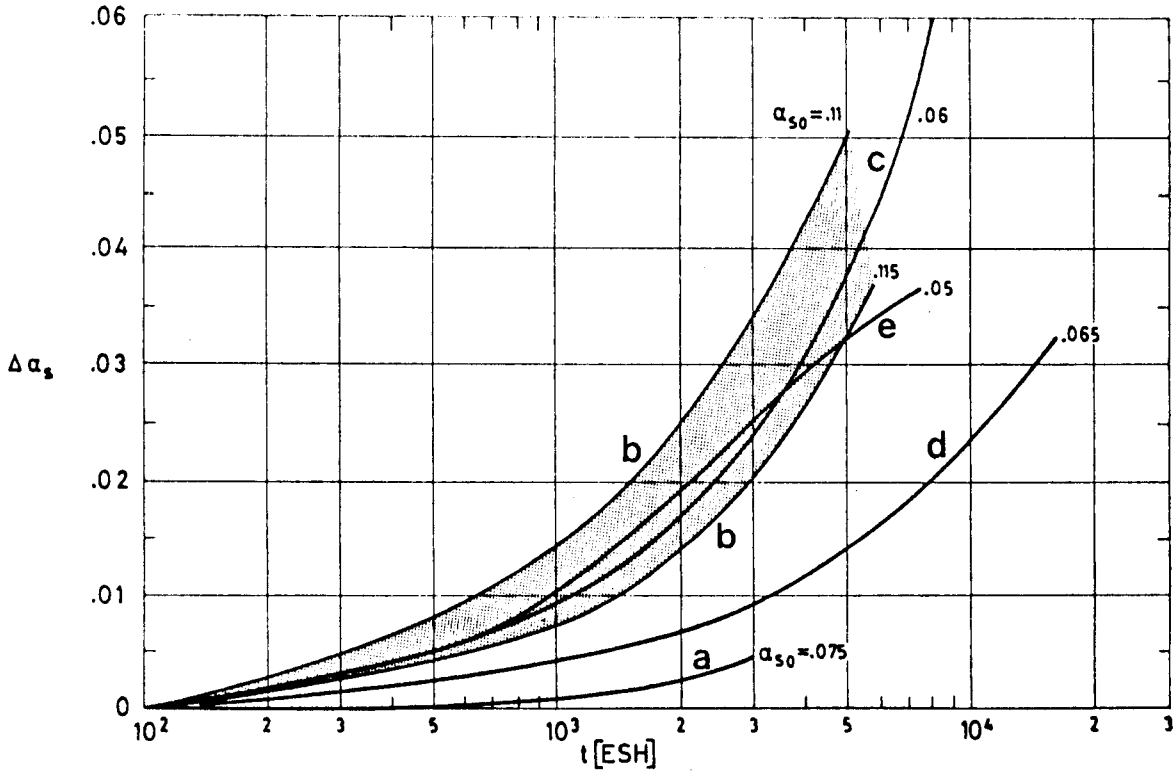

Fig 1-52. Summary data on the change in solar absorptance, $\Delta\alpha_s$, of OCLI Type SI-100 Thermal Control Mirrors vs. exposure time, t.
The estimated values of the initial solar absorptance, α_{so}, are shown near each curve.

- **a** From SCATHA. Partially geosynchronous orbit. α_{so}=.075 .
  See pp. 1-126 and 1-127.
- **b** From COMSTAR. Geosynchronous orbit. Contaminated before launching.
  α_{so}=.11 (COMSTAR D-3)
  α_{so}=.115 (COMSTAR D-1)
  See pp. 1-124 and 1-125.
- **c** From NAVSTAR. Influenced by Van Allen radiation. α_{so}=.06
  See pp. 1-122 and 1-123.
- **d** Ground test. "Clean" simulation of HELIOS orbit. α_{so}=.065
  See p. 1-119.
- **e** Ground test. Simulation of OTS orbit. α_{so}=.05
  See pp. 1-133 to 1-140.

The figure clearly shows the need for revised flight data acquisition procedures, improved satellite materials and careful ground-handling techniques, and the inadequacy of a data presentation in terms of the ultra-violet exposure time.

COATINGS

Solar Reflectors

7.3.3. Reflectance.

7.3.3.1. Normal-hemispherical spectral reflectance. Data in Fig 1-53 are from Cunnington, Grammer & Smith (1969).

Sample bonded to a 6061-T6 aluminium substrate. Adhesive not identified in the source.

Spectral reflectance in the wavelength range 2.7×10^{-7} m to 1.8×10^{-6} m was measured with a Cary Model 14 spectrophotometer with an integrating sphere operating in the indirect mode, i.e.: the sphere is illuminated from the external optics while the detector views the sample. The Cary sphere is small and has relatively large apertures. This results in significant errors which can be minimized by calibration against known surfaces. A limited number of absolute measurements were made using a much larger integrating sphere, Gier-Dunkle Model SP 210, attached to a Perkin-Elmer Model 98 monochromator. When the Gier-Dunkle instrument is used to calibrate Cary measurements on identical samples, the accuracy in reflectance readings with the latter instrument is .02 . Measurements in the wavelength range 2×10^{-6} m to 25×10^{-6} m were made with a Gier-Dunkle Model HC-300 heated cavity reflectometer in conjunction with a Perkin-Elmer Model 98 monochromator and a Brewer Model 129 chopper-amplifier system. The maximum relative error is, for most samples, no greater than ±.010. This instrument does not allow exactly normal ($\beta'=0$) measurements with perfectly

COATINGS

Solar Reflectors

specular samples, since then the reflected flux from the sample originates from the viewing port itself.

Measurements were performed in ambient air.

See also data "before exposure" in Fig 1-54.

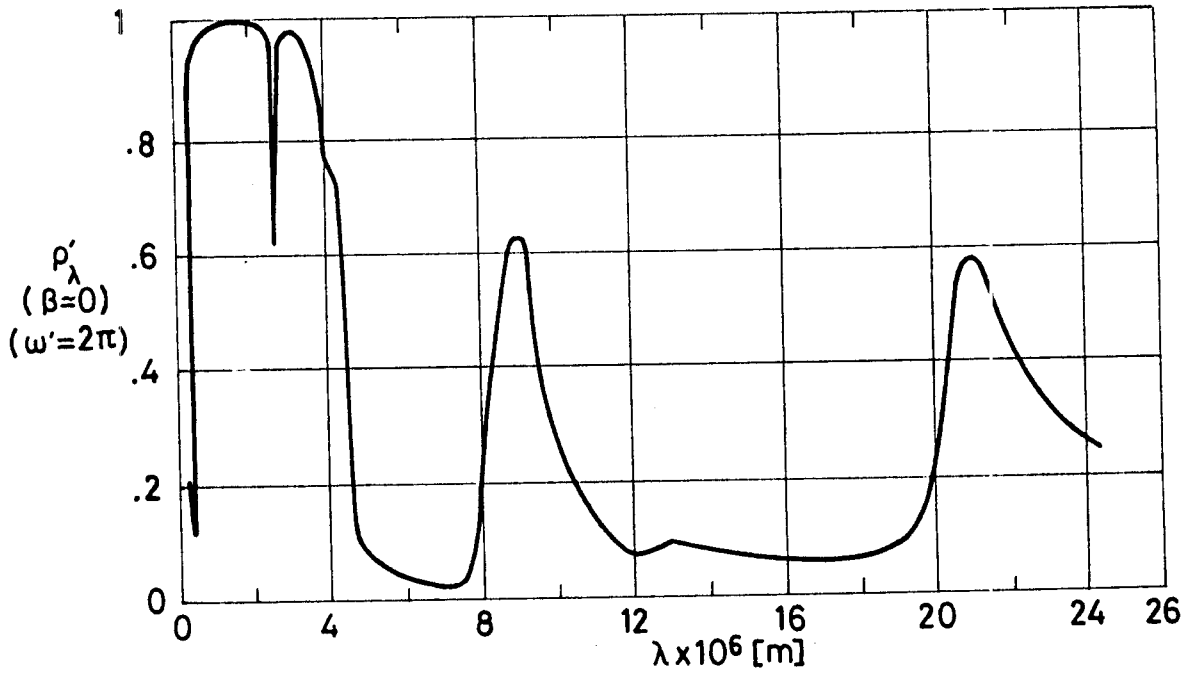

Fig 1-53. Normal-hemispherical spectral reflectance, ρ'_λ, of OCLI Type SI-100 Thermal Control Mirrors vs. wavelength, λ. From Cunnington, Grammer & Smith (1969).

7.3.3.2. Effects of the Space Environment on reflectance.

7.3.3.2.1. Ultra-Violet Radiation. Data in Fig 1-54 are from Cunnington, Grammer & Smith (1969). The ultra-violet source was a 900 W Hanovia Xenon lamp, Model 530-CL. Uniformity of the source total irradiance was better than 10% within 10^{-2} m of the sample center.

A 1 000 W, controllable and programmable tungsten iodide lamp, GE DXW, is used to heat the back of the substrate, so that the sample can be maintained at a

COATINGS

Solar Reflectors

given temperature or thermally cycled.

Radiation flux density at the sample level: 1 Sun.

Temperature: 339 K.

Chamber pressure: 1.33×10^{-5} Pa.

Exposure time: 2 040 h.

Spectral reflectance measured at ambient pressure and temperature, before and after irradiation.

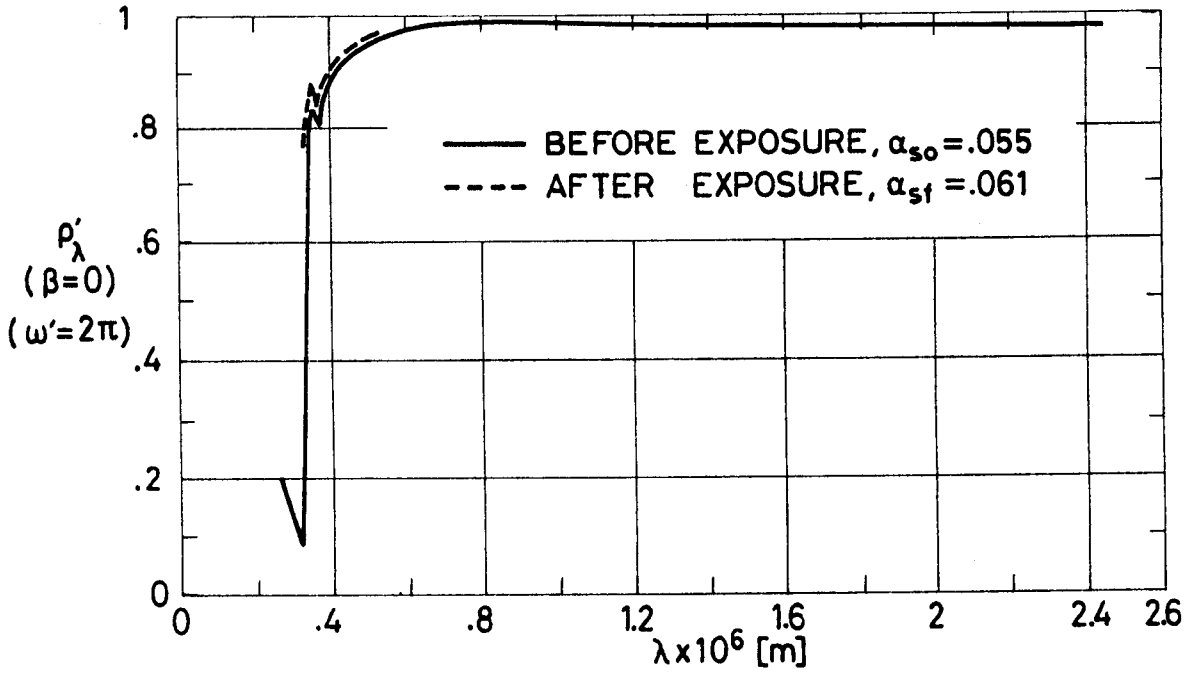

Fig 1-54. Effect of Ultra-Violet Radiation on normal-hemispherical spectral reflectance, ρ'_λ, of OCLI Type SI-100 Thermal Control Mirrors vs. wavelength, λ. From Cunnington, Grammer & Smith (1969).

7.3.3.2.6. Combined exposure. The following data are from Paillous (1975), DERTS.

Sample on aluminium substrate. Three of the samples (labelled 1 to 3) were bonded with RTV 560 adhesive, and two more samples (4 and 5) were fastened bare.

COATINGS

Solar Reflectors

Irradiations made under the following conditions:

Chamber pressure below 1.3×10^{-4} Pa.

Sample temperature: 363 K.

Reflectance measured in situ without breaking vacuum, unless otherwise stated.

Comments under **CAUTION** in p. 1-59 do not apply here because of the specular behavior of the mirrors.

The exposure is intended to simulate 7 years in geosynchronous orbit of the three-axis stabilized Orbital Test Satellite (OTS) north and south faces. The tests reproduced the simultaneous action of vacuum and temperature, and of ultra-violet, protons and electrons. The experimental facilities are those mentioned in pp. 1-65, 1-68 and 1-74. The procedures are also similar. See for further details Paillous (1975).

Simulation time was controlled by the maximum achievable solar radiation flux density at the sample level, which was smaller than 3 Suns. Thence, protons and electrons, which could require shorter simulation times, were irradiated intermittently, whereas ultraviolet irradiation was performed continuously within the constraint of a correct simulation of the integrated fluxes at the end of the seven main steps of the test (Table 1-20).

The following measurements were made:

1) Spectral reflectance at ambient conditions in air,

COATINGS

Solar Reflectors

Table 1-20

Test Conditions Simulating up to Seven Years in Geosynchronous Orbit

		Step A	Step B	Step C	Step D	Step E	Step F	Step G
Years in Orbit		.17	1.11	2.05	3.15	4.05	5.40	7.14
Simulation Test Time [h]		96	612	1 134	1 740	2 240	2 982	3 946
ESH		192	1 224	2 268	3 480	4 480	5 964	7 892
Protons Exposure 40 keV	Starting Time, First Run [h]	48	564	1 110	1 728	2 228	2 970	3 934
	Stopping Time, Last Run [h]	96	612	1 134	1 740	2 240	2 982	3 946
	Net Running Time [h]	48	48	24	12	12	12	12
	Flux [Protons.$m^{-2}.s^{-1}$]	4.05×10^{12}	2.26×10^{13}	4.86×10^{13}	1.07×10^{14}	9.03×10^{13}	1.32×10^{14}	1.67×10^{14}
	Integrated Flux [Protons.m^{-2}]	6.92×10^{17}	3.90×10^{18}	4.25×10^{18}	4.69×10^{18}	3.87×10^{18}	6.01×10^{18}	6.97×10^{18}
	Cumulative Integrated Flux [Protons.m^{-2}]	6.92×10^{17}	4.59×10^{18}	8.84×10^{18}	1.35×10^{19}	1.74×10^{19}	2.34×10^{19}	3.04×10^{19}
Protons Exposure 150 keV	Starting Time, First Run [h]	24	516	1 086	1 716	2 216	2 958	3 922
	Stopping Time, Last Run [h]	48	564	1 110	1 728	2 228	2 970	3 934
	Net Running Time [h]	24	48	24	12	12	12	12
	Flux [Protons.$m^{-2}.s^{-1}$]	2.90×10^{11}	7.52×10^{11}	1.49×10^{12}	3.68×10^{12}	3.01×10^{12}	4.47×10^{12}	5.65×10^{12}
	Integrated Flux [Protons.m^{-2}]	2.51×10^{16}	1.40×10^{17}	1.26×10^{17}	1.58×10^{17}	1.29×10^{17}	1.98×10^{17}	2.36×10^{17}
	Cumulative Integrated Flux [Protons.m^{-2}]	2.51×10^{16}	1.65×10^{17}	2.91×10^{17}	4.49×10^{17}	5.78×10^{17}	7.76×10^{17}	1.01×10^{18}
Electrons Exposure 200 keV	Starting Time, First Run [h]	0	516	1 086	1 716	2 216	2 958	3 922
	Stopping Time, Last Run [h]	96	612	1 134	1 740	2 240	2 982	3 946
	Net Running Time [h]	96	96	48	24	24	24	24
	Flux [Electrons.$m^{-2}.s^{-1}$]	4.05×10^{12}	2.28×10^{13}	4.83×10^{13}	1.06×10^{14}	9.03×10^{13}	1.38×10^{14}	1.66×10^{14}
	Integrated Flux [Electrons.m^{-2}]	1.43×10^{18}	7.92×10^{18}	8.44×10^{18}	9.13×10^{18}	7.70×10^{18}	1.19×10^{19}	1.44×10^{19}
	Cumulative Integrated Flux [Electrons.m^{-2}]	1.43×10^{18}	9.35×10^{18}	1.78×10^{19}	2.69×10^{19}	3.46×10^{19}	4.65×10^{19}	6.09×10^{19}

From Paillous (1975).

COATINGS

Solar Reflectors

before and after irradiation. An integrating sphere attached to a Beckman DK2A reflectometer was used. Standards of polished aluminium. Total solar reflectances from these data, ρ_s, are given in Table 1-21.

2) In situ measurements of global reflectance, as in p. 1-75. The illuminating source was a solar-simulating high-pressure Xenon lamp, 75 W. Results appear in Table 1-21 as ρ.

3) In situ spectral reflectance, as in p. 1-65. The incident flux came from a Zeiss monochromator. The spectral measurements were made with two detectors attached to the integrating sphere: a photodiode for λ in the range 5.46×10^{-7} m to 1.5×10^{-6} m, and a photomultiplier for the range 2.75×10^{-7} m to 6.50×10^{-7} m. A limited amount of data are given in Figs 1-55 and 1-56. The resulting spectral data were integrated against the solar spectral irradiance to obtain the reflectance for the different spectral bands (ultra-violet, visible, infrared and solar). Results appear in Table 1-21.

An incident occurred during ultra-violet only irradiation between steps E and F, around the 2 360 experiment hours (nearly 4.5 simulated years). One night the chamber pressure rose up to 1 Pa to 10 Pa. The damage was repaired the next morning. Duration of the malfunction was not determined. The results look fairly insensitive to this incident.

COATINGS

Solar Reflectors

Table 1-21

Combined Exposure Effects on Reflectance of OCLI Type SI-100 Thermal Control Mirrors

	From Global Measurements					From Spectral Measurements									
	ρ for Xenon Lamp					ρ_{SUV} $2.35 \leq \lambda \times 10^7 [m] \leq 3.80$					ρ_{SV} $2.95 \leq \lambda \times 10^7 [m] \leq 7.30$				
Sample	1	2	3	4	5	1	2	3	4	5	1	2	3	4	5
In Air before irradiation															
Under vacuum $<1.3\times10^{-4}$ Pa. 293 K.	.97	.97	.95	.96	.97	.48	.46	.46	.47	.47	.89	.88	.89	.92	.91
After 1 h under vacuum $<1.3\ 10^{-4}$ Pa. 363 K.	.989	.982	.970	.977	.977										
After 48 h under vacuum $<1.3\times10^{-4}$ Pa. 363 K.	.986	.965	.970	.981	.971	.46	.45	.46	.47	.46	.92	.92	.92	.91	.90
48 h after starting step A	.982	.974	.984	.987	.972										
After step A	.989	.969	.979	.975	.969	.45	.46	.45	.46	.44	.91	.91	.91	.91	.89
Before step B	.968	.970	.970	.975	.970										
After step B	.975	.972	.975	.978	.970										
Before step C	.980	.975	.975	.965	.967										
After step C	.969	.964	.971	.974	.971			.42	.43				.89	.89	
Before step D	.962	.962	.964	.977	.969										
After step D	.965	.965	.967	.970	.957	.42	.44	.43	.43	.42	.88	.88	.88	.88	.88
Before step E	.966	.968	.968	.971	.963										
During step E (no details are given)	.971	.966	.971	.971	.977										
After step E	.968	.965	.976	.971	.957										
After vacuum pump incident (4 800 ESH)	.969	.971	.971	.974	.969			.43	.43				.87	.87	
5 300 ESH	.963	.964	.971	.986	.967										
Before step F	.964	.967	.967	.976	.967			.42	.42				.87	.86	
After step F	.972	.959	.972	.985	.969			.41	.42				.88	.86	
Before step G	.970	.951	.969	.983	.970			.41	.41				.86	.86	
After step G (First readings)	.967	.965	.965	.967	.955	.41	.42	.42	.39	.40	.88	.86	.87	.84	.85
After step G (Second readings)	.961	.961	.963	.971	.961	.42	.43	.43	.42	.41	.88	.88	.87	.85	.84
After Exposure, 12 h in Air at 293 K.	.963	.964	.964	.971	.961			.43	.42				.86	.86	
In Air after irradiation															

(Continued onto next page)

Rev. 1. 1981

COATINGS

Solar Reflectors

Table 1-21 (Continued)

Combined Exposure Effects on Reflectance of OCLI Type SI-100 Thermal Control Mirrors

	From Spectral Measurements									
	$\rho_{S_{IR}}$ $7.30 \leq \lambda \times 10^{7}[m] \leq 40$					ρ_S				
Sample	1	2	3	4	5	1	2	3	4	5
In Air before irradiation						.95	.95	.95	.95	.95
Under vacuum $<1.3\times10^{-4}$ Pa. 293 K.	.97	.95	.96	.97	.96	.93	.92	.93	.95	.93
After 1 h under vacuum $<1.3\times10^{-4}$ Pa. 363 K										
After 48 h under vacuum $<1.3\times10^{-4}$ Pa. 363 K.	.99	.99	.98	.99	.99	.96	.95	.95	.96	.94
48 h after starting step A										
After step A	1.00	.99	.98	1.00	.99	.96	.95	.94	.96	.94
Before step B										
After step B										
Before step C										
After step C			.98	1.00				.94	.94	
Before step D										
After step D	.97	.98	.97	.99	.97	.93	.93	.92	.94	.92
Before step E										
During step E (no details are given)										
After step E										
After vacuum pump incident (4 800 ESH)			.97	.99				.92	.93	
5 300 ESH										
Before step F			.96	.96				.92	.91	
After step F			.97	.99				.93	.92	
Before step G			.97	.99				.92	.93	
After step G (First readings)	.97	.98	.97	.97	.96	.92	.92	.92	.91	.91
After step G (Second readings)	.98	.98	.98	1.00	.98	.93	.93	.93	.93	.91
After Exposure, 12 h in Air at 293 K.			1.02	1.00				.94	.93	
In Air after irradiation						.94	.94	.94	.94	.94

From Paillous (1975).

COATINGS

Solar Reflectors

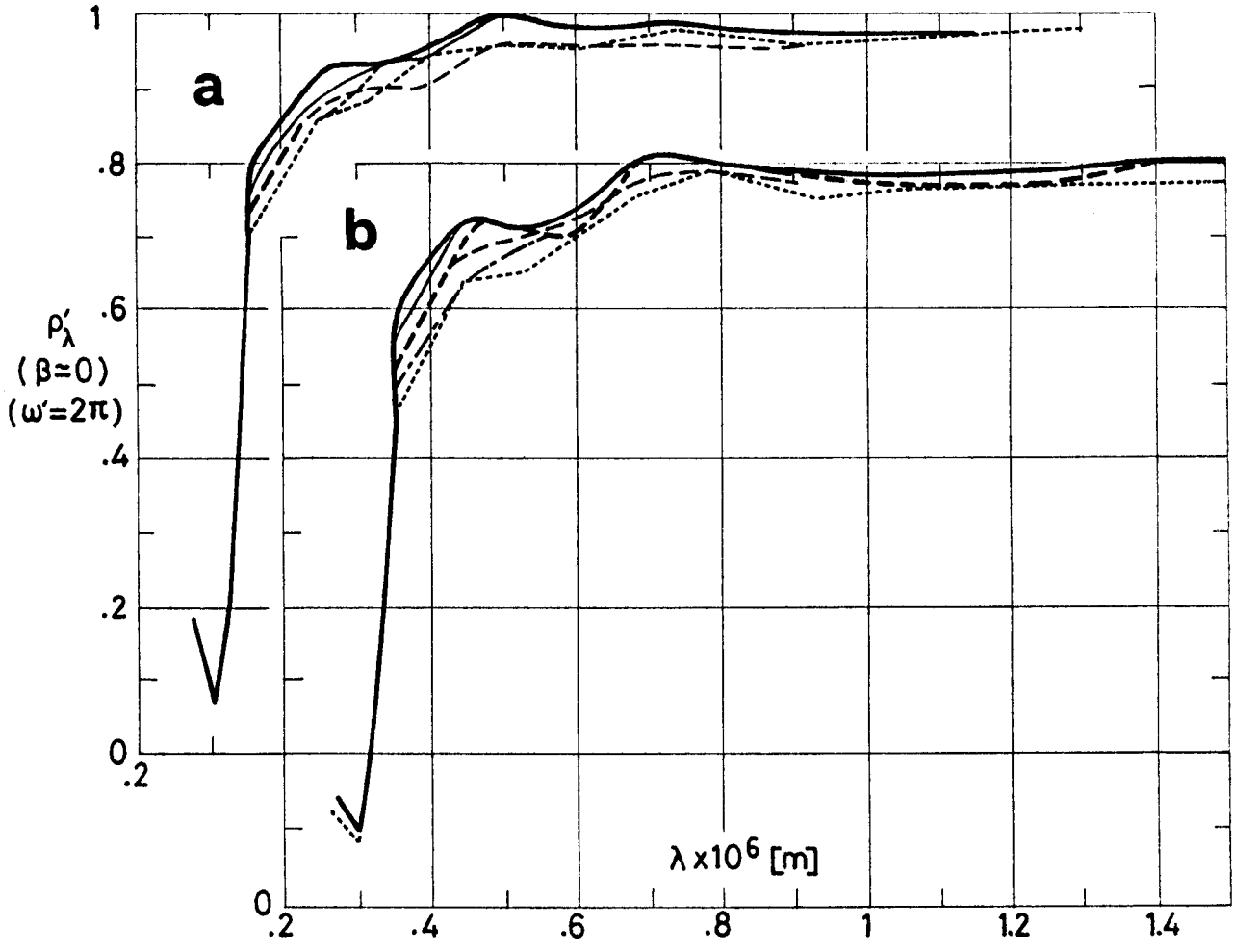

Fig 1-55. Effect of Combined Exposure, simulating up to seven years in geosynchronous orbit, on normal-hemispherical spectral reflectance, ρ'_λ, of OCLI Type SI-100 Thermal Control Mirrors vs. wavelength, λ. a Bonded sample. b Sample fastened bare. From Paillous (1975).

Explanation

Key	Description	Comments
———	After 48 h below 1.3×10^{-4} Pa pressure. T = 363 K.	
——	After step A (.17 years in orbit). T = 363 K.	
– – –	After step C (2.05 years in orbit). T = 363 K.	
– – –	After step D (3.15 years in orbit). T = 363 K.	
—·—·	After step F (5.4 years in orbit). T = 363 K.	After vacuum pump incident.
·····	After step G (7.14 years in orbit). T = 363 K.	

COATINGS

Solar Reflectors

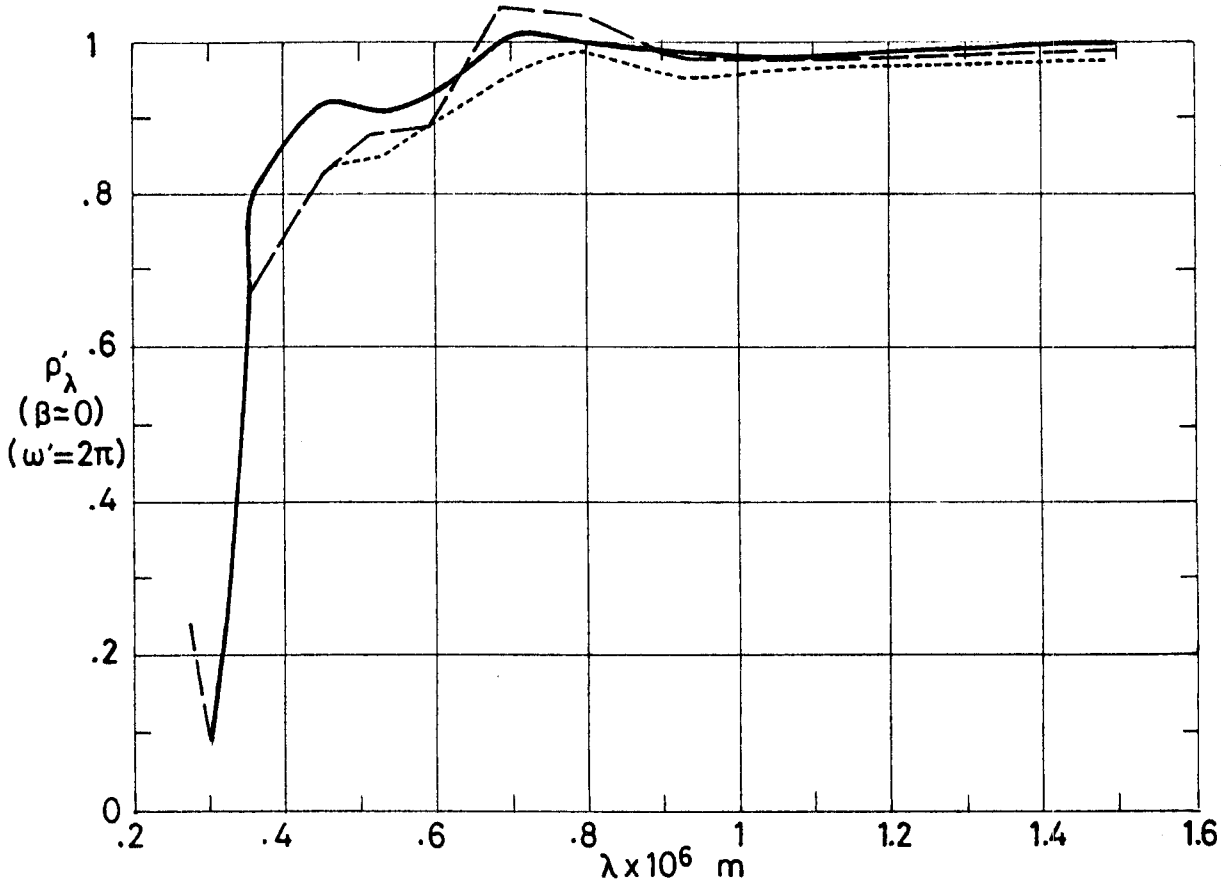

Fig 1-56. Effect of Combined Exposure, simulating up to seven years in geosynchronous orbit, on normal-hemispherical spectral reflectance, ρ'_λ, of OCLI Type SI-100 Thermal Control Mirrors vs. wavelength, λ. Sample fastened bare. From Paillous (1975).

Explanation

Key	Description	Comments
———	After 48 h below 1.3 10^{-4} Pa pressure. T = 363 K.	Same curves as in Fig 1-55.
-------	After step G (7.14 years in orbit). T = 363 K.	
— —	After Combined Exposure followed by 12 h in air at 293 K.	ρ'_λ>1. Could give an estimate of the uncertainty level associated to data acquisition and handling.

COATINGS

Solar Reflectors

7.4. Electrical resistance. OCLI Type SI-100 mirrors are nonconductive. Thence, the mirrors show a tendency to be charged electrostatically, particularly when the spacecraft becomes immersed in a substorm plasma.

7.4.3. Charging. The differential charging of the spacecraft components to a high voltage may generate a discharge (vacuum arc, arcing) if the voltage level exceeds the breakdown potential of the material.

The implications of these phenomena are:

1) On the thermal control mirrors.

Charging might accelerate the deposition of contaminants.

The discharges liberate contaminants.

The discharges damage the mirrors.

2) On the onboard instrumentation.

The components are irradiated by the electromagnetic waves associated with the vacuum arc.

Transient pulses of sufficient magnitude to activate (or even burn) the circuits could result.

3) On the surrounding electric field.

Electrical charges built up in the satellite would interfere with the space field.

For an account of the phenomena involved in spacecraft charging and arcing see Rosen (1975).

Relevant tests with OCLI Type SI-100 mirrors are presented in Table 1-22.

The outcome from these tests can be summarized as follows.

Rev. 1. 1981

COATINGS

Solar Reflectors

Table 1-22

Charging-Arcing Tests with OCLI Type SI-100 Thermal Control Mirrors

1

Sample. Nine mirrors on an aluminium substrate, 6.5×10^{-2} m square. Overcoat not quoted. Furnished by ESTEC. RTV 560 adhesive (nonconductive).

Tests. The experimental facility has been described by Lévy (1976). An electron accelerator is connected to a vacuum chamber, where the sample holder and irradiation monitoring devices are placed. Uniformity of irradiation is held within ±40% by diffusion of the beam through a 2×10^{-6} m thick aluminium foil. Pressure not given. The energy of the impinging electron beam is increased from 5 keV to 30 keV, with current densities in the range 10^{-6} A.m^{-2} to 2×10^{-5} A.m^{-2}, until breakdown results. Thereafter irradiation is pursued for 40 h under constant conditions.

Ultra-violet irradiation was superposed to electron exposure for some time. No effect was detected.

Measurements. The substrate is grounded through electrical resistors and a nanoammeter, the output of which is recorded. Potential at a point in the grounding line is measured with an oscilloscope.

For each value of the electrons beam energy, the surface potential is related to the ratio of measured intensity to beam current. The surface potential-intensity ratio relationship was established by a previous calibration with a metal sheet, placed in the sample holder, to which known voltages were applied while reading the ammeter output.

Surface currents were measured with an intensity probe placed in a grounding line from the exposed face of the mirror. Peak amplitudes of the current pulses up to 25 A, with durations in the range 2×10^{-7} s to 4×10^{-7} s, were detected. Discharge intensities as large as 7×10^{3} A.m^{-2} resulted.

Beam Energy [keV]	Beam Current Density [A.m^{-2}]	Exposure Time [h]	Temp. [K]	Surface Potential [V]	Electrostatic Discharges			Voltage Breakdown [V]	Comments
					Occurrence	Rate [min^{-1}]	Total Number in 6 h		
25	2×10^{-5}	40						Between 4 000 and 9 000	Minimum conditions for breakdown. Estimated error in voltage readings was ±1 000 V.
30					Many		65		

From Lévy (1976).

2

Sample. Nine mirrors on an aluminium substrate, 6.5×10^{-2} m square. Overcoat not quoted. Furnished by ESTEC. Conductive adhesive.

Tests. As above.

Measurements. As above. Surface currents at breakage were not measured.

Beam Energy [keV]	Beam Current Density [A.m^{-2}]	Exposure Time [h]	Temp. [K]	Surface Potential [V]	Electrostatic Discharges			Voltage Breakdown [V]	Comments
					Occurrence	Rate [min^{-1}]	Total Number in 6 h		
15	10^{-5}	.5		5 500					First run. One of the mirrors showed a transversal crack (not ascribable to the test). The breakdown occurs at lower energies than in table above, where a nonconductive adhesive was used.
20		1.33			Both small and large	$\frac{1}{5}$ to $\frac{1}{7}$	60	6 000	
25		.6				$\frac{1}{4}$	90	5 400	
20		1.43				$\frac{2}{7}$ to $\frac{2}{9}$	90	4 500	
25		.42				$\frac{2}{7}$	100	4 400	
25	2×10^{-5}	.35				$\frac{2}{3}$	240	4 000	
30	10^{-5}	.73				$\frac{1}{3}$	120	4 700	15 h since the end of the above run. Voltage breakdown decreases with beam energy.
30	2×10^{-5}	.67				$\frac{2}{3}$ to $\frac{1}{2}$	200	4 600	
15	10^{-5}	.75				$\frac{1}{15}$ to $\frac{1}{20}$	20	7 500	Same energy and flux as in the first run.

From Lévy & Sarrail (1976).

3

Sample. Several mirrors (36 to 49) on a metal substrate. Neither overcoat nor adhesive are quoted.

Tests. An electron gun is used to irradiate a sample panel mounted on the floor of an evacuated chamber.

Measurements. The metal substrate of the sample panel is grounded through an ammeter. An electric field meter placed near the panel is used for measuring the field produced at its location by the surface charge on the sample. The relationship between (averaged) mirror surface potential and field meter output was established

(Continued onto next page)

COATINGS

Solar Reflectors

Table 1-22 (Continued)

Charging-Arcing Tests with OCLI Type SI-100 Thermal Control Mirrors

through calibration as in 1 above.
Surface potential and leakage current through the sample were recorded vs. time.
The electromagnetic field near the sample was explored, by use of suitable antennae, to look at the influence of the discharge on the vehicle circuitry. The tests indicate that negative charges can be expelled to distances of over 7×10^{-2} m from the mirror surface and, thence, noise pulses of considerable duration result.

Beam Energy [keV]	Beam Current Density [A.m^{-2}]	Exposure Time [h]	Temp. [K]	Surface Potential [V]	Electrostatic Discharges			Voltage Breakdown [V]	Comments
					Occurrence	Rate [min^{-1}]	Total Number		
10	10^{-5}				One			3	
	3.3×10^{-5}				Several	1		3	
	6.7×10^{-5}				Small and large	3		2.5	Little changes resulted from small discharges.

From Adamo & Nanevicz (1976).

4

Sample. Four mirrors on an aluminium substrate. Inconel overcoating.
Conductive adhesive. RTV 566 with silver powder Cho-Bond 1029B (see pp. 1-155 and 1-156).
Tests. Performed at DERTS (Toulouse) by use of the CEDRE substorm simulation facility (Bosma & Levadou (1979)). Pressure below 6.5×10^{-3} Pa. Temperature between 260 K and 310 K. Uniformity of irradiation is achieved by diffusing the electron beam through a 7.5×10^{-7} m thick aluminium foil.
Measurements. Leakage current through the sample continuously monitored at constant electron energy and current density. Surface potential measured when cutting-off the electron beam at regular intervals.
A DC electrical breakdown tester was used to determine the breakdown voltages in air.

Beam Energy [keV]	Beam Current Density [A.m^{-2}]	Exposure Time [h]	Temp. [K]	Surface Potential [V]	Electrostatic Discharges			Voltage Breakdown [V]	Comments
					Occurrence	Rate [min^{-1}]	Total Number		
5	10^{-5}	.5	291	990					No hint to know when the electron beam is cutted-off for surface potential measurements. Notice that surface potential depends on time when discharges occur. No voltage breakdown in air was observed up to 12 kV, upper limit of the breakdown tester used.
10				3 420					
15				6 840	One				
20				9 300	Many				
10	5×10^{-5}			3 530					
15				7 200					
20				10 360	Many	1 to $\frac{1}{15}$			
10	5×10^{-5}	8							
20					Many				
5	10^{-5}	.5	259	2 630					No discharges were recorded. Apparently, the room temperature test affected the ability to discharge at low temperature. The large discharge could have been triggered by the potential probe.
10				5 800					
15				10 260					
20				13 700	One large				
10	5×10^{-5}			5 800					
15				10 400					
20				14 400					

From Bosma (1979).

COATINGS

Solar Reflectors

1) Electrical charges on the mirror surface tend to discharge at a point of minimum resistance. This could be a discontinuity in the (nonconductive) adhesive, too narrow a gap between mirrors, or cracks in the mirror surface.

2) A typical discharge follows the mirror edge into the adhesive, through which it reaches the substrate.

3) Damage to the thermal control surface could appear as.

3.1) Erosion of the adhesive from the joints between mirrors, and deposition on the quartz surface.

3.2) Defects in the silver layer such as cracks, local evaporation,...

3.3) Defects in the substrate.

3.4) Erosion of the quartz surface itself, near the edges, at high current levels.

4) Damages under 3.1 and 3.2 above become more severe when a conductive adhesive is used. This could be due to the fact that the discharge takes place at the mirror-adhesive interface instead of within the adhesive.

5) Damage under 3.3 results from nonconductive overcoatings. In that case the surge current through the silver discharges on the substrate, through the overcoating.

6) The rate of discharge occurrence is proportional to the beam current density, as in any relaxation oscillator. Nevertheless, the discharges tend to modify the later behavior of the sample in the most unpredictable way.

6.1) The discharge rate decreases with time.

COATINGS

Solar Reflectors

6.2) The minimum beam energy for arcing depends on the history of the process. Evidence that many discharges contribute to lower the threshold energy, and evidence on the contrary are both available.

7) Conductive coated mirrors have been devised to avoid all these shortcomings. See § 1.2.7.

8. ENVIRONMENTAL BEHAVIOR

8.1. Prelaunch. These mirrors are fragile and should be protected from mechanical damage during shipping and storage. Each mirror shall be individually wrapped in paper that will not scratch, leave a residue or corrode the metal surface. Surface contamination including finger-prints, oil, dust and atmospheric weathering does not cause permanent degradation after application. However, temporary contamination should be removed prior to launch.

From OCLI (1980).

According to Winkler & Stampfl (1975) Inconel overcoating is humidity-sensitive.

8.2. Postlaunch. Outgassing can be minimized by an appropriate curing process, see Table 1-18, pp. 1-109 and 1-110.

OSR panels have successfully passed sinusoidal and random vibration tests per "Lockheed Aircraft Corporation General Environmental Specification for Agena Satellite Programs".

8.2.1. Ascent. The effect of ascent heating on this rigid OSR is unknown. However no significant change in α_s is anticipated up to the upper operating temperature

COATINGS

Solar Reflectors

of the adhesive.

8.2.2. Orbital. Data on ultra-violet damage reveal no noticeable change in α_s due to near ultra-violet radiation. This rigid OSR is stable for extended missions up to two years in all space environments. It has been extensively investigated and has never been damaged. Nevertheless, many authors report space flight data, and laboratory results, indicating gradual degradation of α_s (see pp. 1-119 to 1-130). In general, contamination adversely affects the thermophysical properties of the mirrors when the satellite is exposed to either ultra-violet or charged particles irradiations.

From Breuch (1967), and Fogdall & Cannaday (1974).

9. THERMAL CYCLING

According to the manufacturer, certification of thermal cycling is supplied after the following test: The temperature is lowered from ambient to 143 K ± 5 K, a dwell of 30 minutes, raising the temperature to 358 K ± 5 K, a dwell of 30 minutes, and returning the temperature to ambient. The cycle will be repeated twice more. The rate of temperature change shall be not less than 2 $K.min^{-1}$. During the test, no condensation shall be allowed to form on the mirror. The mirror shall show no evidence of degradation after this test.

From OCLI (1980).

Factors limiting the useful temperature range of these mirrors

Rev. 1. 1981

COATINGS

Solar Reflectors

are controlled by the methods used for attachment to the substrate.

Several rigid OSR samples bonded to aluminium substrate by use of GE-RTV 615 silicone adhesive were tested in a vacuum chamber at 1.3×10^{-3} Pa approximately. The test consisted of 20 cycles of near-sinusoidal temperature cycling between 166 K and 366 K. Each cycle had a period of approximately 20 min. Performance of these rigid OSRs and adhesive was satisfactory, with no mechanical failures occurring during the test.

From Marshall & Breuch (1968).

10. SOURCE

Optical Coating Laboratory, Inc., 2789 Giffen Ave. P.O. Box 1599, Santa Rosa, California 95403, USA.

Manufacturing facilities serving Europe, OCLI Optical Coatings Limited.

621 London Road, High Wycombe, Buckinghamshire, HP11 1ET, England.

Telephone: High Wycombe (0494) 36286.

Telex: 83239.

Contact Person: Mr. J.A. Fawcett, Technical Products Manager.

11. COST

A large quantity price of 15 000 US $.m^{-2} has been estimated on the basis of 1980 quotations. Adhesive is not included.

From Bosma (1981).

12. SPATIAL EXPERIENCE

This rigid OSR was originally developed at Lockheed in 1964

COATINGS

Solar Reflectors

for use on an USAF satellite. It has been used in a number of satellites, some of them are listed in the following table. Additional sources of information, which has not been compiled in this item, are given in the mentioned table.

Spacecraft or Programme	Launching Date	Used or Tested	References
Lunar Orbiter 1st Lunar Orbiter 5th	Aug. 10, 1966 Aug. 1, 1968	Used.	Marshall & Breuch (1968).
OSO III	March 8, 1967	Tested, TCCE experiment. See pp. 1-120 and 1-121.	Millard (1969), Millard & Pearson (1973).
Nimbus E	Dec. 11, 1972	Used in the radiator of the Nimbus E Microwave Spectrometer (NEMS). See pp. 1-113 to 1-115.	Stultz (1974, 1976).
ATS-F	May 30, 1974	Used in the radiator of the Advanced Thermal Control Flight Experiment (ATFE), and in the baseplate of the Louvers (see p. P 3-9).	Kirkpatrick & Brennan (1973), Kemp, Beynon, Luedke & Hall (1973).
HELIOS A B	Dec. 12, 1974 Jan. 15, 1976	Used. Data available for analysis. See pp. 1-128 and 1-129.	Winkler & Brungs (1975, 1976), Winkler (1975, 1977).
Symphonie A B	Dec. 19, 1974 Aug. 26, 1975	Used in radiator.	Morelli (1974).
INTELSAT IV A	Jan. 29, 1976	Used.	Rolfo (1981).
COMSTAR D-1 D-2 D-3	May 13, 1976 July 22, 1976 June 29, 1978	Used. Data available for analysis. See pp. 1-124 and 1-125.	Hyman (1981).
OTS 2	May 11, 1978	Used, north & south faces. Data available for analysis.	Bouchez & Gülpen (1980), Bouchez & Howle (1981).
SCATHA	Jan. 30, 1979	Tested, ML12 and SSPM experiments. See pp. 1-126 and 1-127.	Hall & Fote (1979, 1980).

(Continued onto next page)

COATINGS

Solar Reflectors

Spacecraft or Programme	Launching Date	Used or Tested	References
ANIK B	Dec. 12, 1979	Used in radiators, north & south faces.	Rajagopalan & Willson (1980).
NAVSTAR 5	Feb. 9, 1980	Tested. See pp. 1-122 and 1-123.	Pence & Grant (1981).
USAF Geosynchronous	Several.	Tested.	Curran & Millard (1978).
LDEF	Scheduled for early 1984.	Experiment AO138-6 by A. Paillous & J.C. Guillaumon. Experiment S0010 by W.S. Slemp. Experiment S1002 by L. Preuss.	Preuss & Schäfer (1979), Clark (1981).

INTENTIONALLY BLANK PAGE

COATINGS

Solar Reflectors

1.2.7. SILVER VACUUM DEPOSITED ON FUSED SILICA WITH A CONDUCTIVE COATING

1. COMPOSITION

Metallic Silver, vacuum deposited on the second surface of fused silica with a transparent electrically conductive coating on the front surface. The silver is overcoated with dielectric or conductive materials.

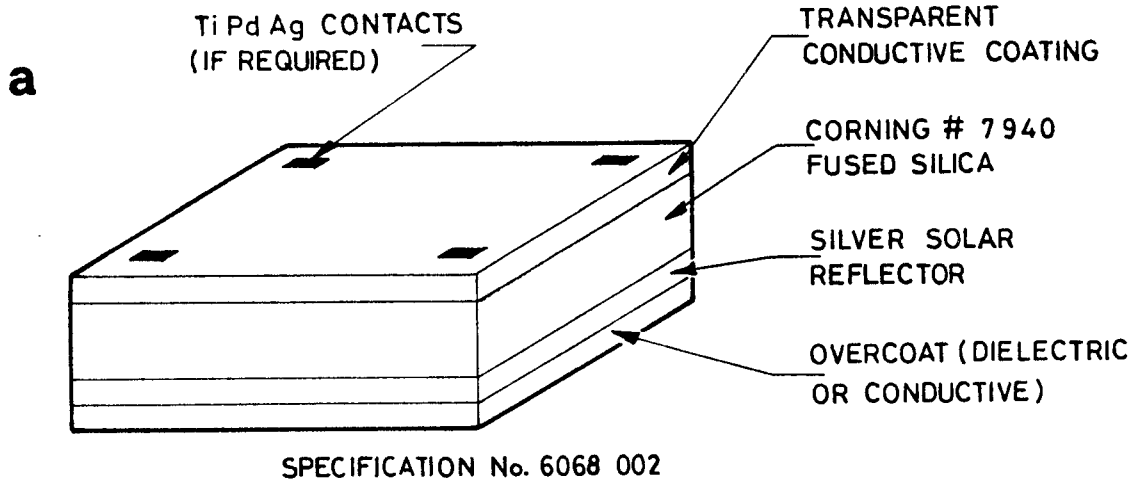

SPECIFICATION No. 6068 002

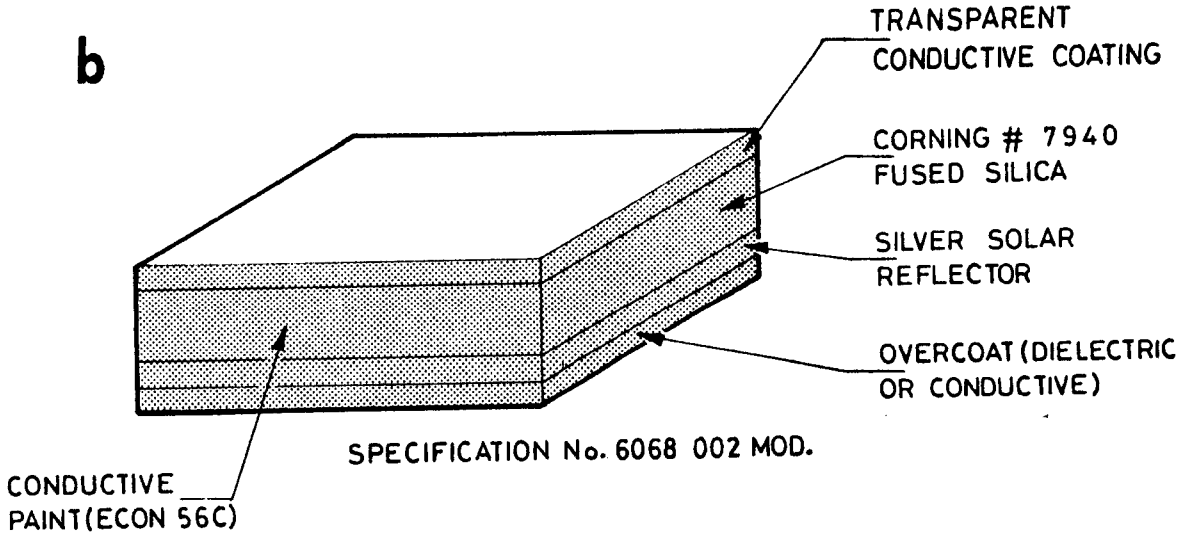

SPECIFICATION No. 6068 002 MOD.

From OCLI (1980).

COATINGS

Solar Reflectors

The protective overcoating could be either Inconel, Indium-Tin oxide, or a multicoating on TiO_x base. Inconel is humidity sensitive. The TiO_x based multicoating, on the other hand, exhibits an instability beyond 400 K leading to a substantial increase in solar absorptance, as discussed in connection with Fig 1-59, p. 1-161.

Conductive coating: Tin-doped In_2O_3 1.5×10^{-8} m to 2.0×10^{-8} m thick.

From Winkler & Stampfl (1975).

Electrical contacts as in a above are furnished on request (Specification No. 6068 002). b shows a recent development where the edges of the mirrors have been coated with a conductive paint (Specification No. 6068 002 Modified).

From Fawcett (1981).

3. USUAL DESIGNATION

Conductive Coated Second Surface Thermal Control Mirror (CC-SSM or SSM/CC). Optical Coating Laboratory, Inc.

Also known as In_2O_3/rigid OSR or ITO/rigid OSR, as CC/rigid OSR or CC-OSR fused silica, and as OCLI Conductive Coating.

SSM/WC indicates a second surface mirror with conductive coating and welding or soldering contacts as in a above.

4. SUBSTRATE

Any clean substrate.

5. METHOD OF APPLICATION

5.1. Background. Typically square mirror substrates of 2×10^{-2} m side, 2×10^{-4} m thick are fabricated. The panels flown on the

COATINGS

Solar Reflectors

GEOS and ISEE-B satellites consisted of small individual units 2×10^{-2} m × 4×10^{-2} m (Bosma & Levadou (1979)).

5.1.1. Geometrical tolerances. Typical fused silica substrates are fabricated to the following tolerances.

	Dimensional Tolerance
Length	$\pm5\times10^{-5}$ m
Width	$\pm5\times10^{-5}$ m
Thickness	$\pm5\times10^{-5}$ m
Perpendicularity of sides	90°±0°15'
Edge chips	2.5×10^{-4} m max. projection into face.
Corner chips	5×10^{-4} m max. length of leg, 4×10^{-4} m max. projection into face.
Parallelism of sides	5×10^{-5} m

From OCLI (1974).

5.1.1.1. Electrical contacts. The contacts shown in a above may vary in size depending upon application. Typical dimensions and tolerances are as follows:

Width	1.3×10^{-3} m ± $.2\times10^{-3}$ m
Length	2.1×10^{-3} m ± $.1\times10^{-3}$ m
Thickness	10^{-5} m ± $.3\times10^{-5}$ m

From OCLI (1974).

5.1.2. Surface quality. 80-50 or better per MIL-O-13830A.

From OCLI (1974).

5.1.3. Appearance. The coated surface gives the appearance of

uniform coverage when viewed through the conductive coated substrate (front surface). The overcoat back surface has a distinct color when viewed under white light.

From OCLI (1974).

5.2. Preparation of surfaces for bonding. As in § 1.2.6, p. 1-107.

5.3. Application. As in § 1.2.6, p. 1-108. See also Contacting.

5.4. Curing process. As in § 1.2.6, p. 1-108.

5.5. Quality of adhesive bonding. As in § 1.2.6, p. 1-108.

5.6. Contacting. A Titanium/Palladium/Silver contacting with the appropriate welding process and repair technique has been developed by AEG for the OCLI Conductive Coating used in HELIOS (Product Specification No. 6068 002. a in the figure of p. 1-151). The modules were interconnected through conductive contacts in the Indium oxide coating and electrically bonded by a silver string to the spacecraft structure.

The above mentioned technique, based in interconnecting individual units, is highly reliable from the electrostatic cleanliness point of view. It is, however, very expensive and involves considerable labour due to mounting and interconnection processes. A solution to avoid interconnection is the mounting of the mirror with a conductive adhesive, as in the next figure, which has been borrowed from Lehn (1979). See COST, p. 1-177, where a cost comparison between both contacting procedures is made.

In order to ease the contacting through the conductive adhesive, OCLI has recently developed a mirror with conductive

COATINGS

Solar Reflectors

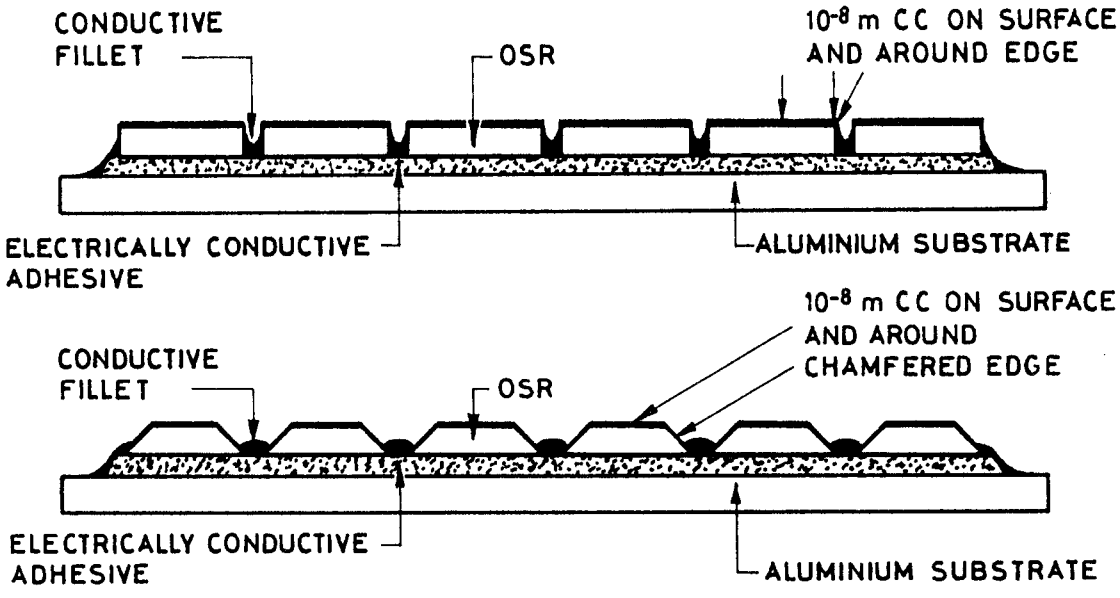

coated edges (Product Specification No. 6068 002 Modified. b in the figure of p. 1-151). The edges of the mirror are coated with ECON 56C conductive paint. Optionally other paints may be requested.

A silicone-silver conductive adhesive based on,

Silicone rubber RTV 566. General Electric, USA,

(General Electric Company. Silicone Products Department. Waterford, New York).

Silver powder Cho-Bond 1029B. Chomerics, USA,

(Chomerics, Incorporated, Arlington, Massachusetts), has been prequalified by ESTEC for conductive adhesion of OSRs, both rigid and flexible. This formulation is not applicable as underlying adhesive (Bosma & Levadou (1979)). The adhesive is prepared as follows (Benaïssa, Lévy, Paillous & Sarrail (1979), Bosma & Froggatt (1980)).

RTV 566A: 100 parts by weight,

Rev. 1. 1981

COATINGS

Solar Reflectors

Cho-Bond 1029B: 250 parts by weight.

Thorough mixing, then addition to the mixture,

RTV 566B catalyst: .15 parts by weight.

After further mixing, the adhesive is degassed under vacuum. Contact resistance of a 10^{-4} m thick layer between two aluminium plates is smaller than 10 Ω (Bosma & Levadou (1979)). By assuming a cross-sectional area of the electrical path through the conductive adhesive of the order of 70×10^{-6} m^2 (see Benaïssa, Lévy, Paillous & Sarrail (1979), p. 22, or Bosma & Froggatt (1980), p. 28), the resistivity of the conductive adhesive can be estimated as $\rho\simeq7$ Ω.m, i.e., 4×10^{4} times the resistivity of pure silver which, according to Weast (1976), is $\rho=1.6\times10^{-4}$ Ω.m.

Another conductive adhesive, quoted by Lehn (1979), consists of silicone rubber filled with 13% by weight of chopped graphite fibers, as follows:

Silicone rubber RTV 566 or 560. General Electric, USA.

2.5×10^{-4} m chopped graphite fibers HERCULES HMS. Hercules, USA.

(Hercules, Incorporated, Wilmington, Delaware 19899. HMS calls for high modulus fibers).

The resistivity of this formulation is about 750 Ω.m. That of pure graphite is: $\rho=.138$ Ω.m (Weast (1976)).

An epoxy-silver conductive adhesive has been used in SCATHA, ML12 experiment. See pp. 1-109, 1-126 and 1-162.

COATINGS

Solar Reflectors

6. SOLVENTS RESISTANCE

As in § 1.2.6, p. 1-108.

7. PHYSICAL PROPERTIES

7.1. Density

7.2. Outgassing. As in § 1.2.6, p. 1-111.

7.3. Thermal radiation properties

7.3.1. Emittance.

7.3.1.1. Hemispherical total emittance. According to Lehn (1979), the dependence of the hemispherical total emittance of OSR surfaces on the thickness of the Indium oxide conductive layer, in the range of layer thicknesses from 0 to 9×10^{-8} m, is small.

In the particular case of this rigid OSR, a slight decrease in emittance due to the Indium oxide layer has been consistently observed, as will be shown below.

Values measured calorimetrically by Hall & Pote (1980) are:

$$\varepsilon = .78 \text{ for the CC-SSM,}$$

contrasting with

$$\varepsilon = .80 \text{ for the SI-100 (uncoated).}$$

Values in Table 1-23 correspond to normal total emittance, $\varepsilon'(\beta'=0)$, and solar absorptance, α_s, of several types of OCLI Type thermal control mirrors. Both ε' and α_s have been measured per Specification ESA PSS-16/QRM--09T. The maximum absolute error was ±.02, and the reproducibility ±.005, in all the cases

COATINGS

Solar Reflectors

Table 1-23

Normal Total Emittance, ε', and Solar Absorptance, α_s, of Several OCLI Type Thermal Control Mirrors

Description	ε' ($\beta'=0$)	α_s
Specification No. 6068 002. Indium oxide top layer and Indium-Tin oxide rear side overcoating.	.758	.069
Specification No. 6068 002 Modified. Indium oxide top layer, Indium-Tin oxide rear side overcoating and ECON 56C conductive coated edges.	.744	.069
SI-100. Uncoated.	.788	.066
Uncoated. Indium-Tin oxide rear side over-coating.	.785	.063

From Bosma (1981).

The influence of temperature has not been assessed.

7.3.2. Absorptance.

7.3.2.1. Solar absorptance. Values in Table 1-23, above, indicate that there is a small increase in solar absorptance due to the Indium oxide layer.

Other values given in the literature are:

α_s=.06 Fogdall & Cannaday (1974). See p. 1-161.

Hall & Fote (1979). See p. 1-162.

α_s=.062 Winkler & Brungs (1975). See p. 1-163.

A strong temperature influence above 400 K has been reported by Winkler & Stampfl (1975), see also Fig 1-59, p. 1-161. This effect, which has been attributed to thermal instability of TiO_x based rear side overcoating, does

COATINGS

Solar Reflectors

not appear when using Inconel.

7.3.2.3. Variation of solar absorptance with incidence angle. Fig 1-57, from Winkler & Stampfl (1975), shows the same trends as Fig 1-45, p. 1-114, for the uncoated mirror.

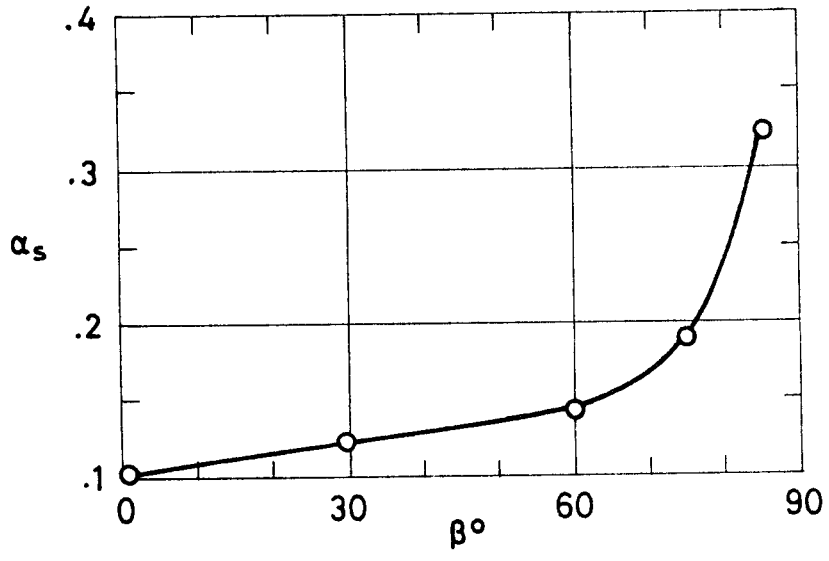

Fig 1-57. Solar absorptance, α_s, of OCLI Type CC-SSM vs. incidence angle, β. O are calculated values. From Winkler & Stampfl (1975).

7.3.2.5. Effects of the Space Environment on solar absorptance.

7.3.2.5.6. Combined exposure. Data presented are:

1) Results from ground experiments simulating either geosynchronous orbit exposure of the OTS equatorial faces (Fig 1-58, p. 1-160) or HELIOS orbit conditions at .25 AU (Fig 1-59, p. 1-161).

2) Results from in orbit experiments. Those from a nearly geosynchronous orbit (SCATHA) are given in Fig 1-60, p. 1-162, whereas those from HELIOS A and B appear in Fig 1-61, p. 1-163.

COATINGS

Solar Reflectors

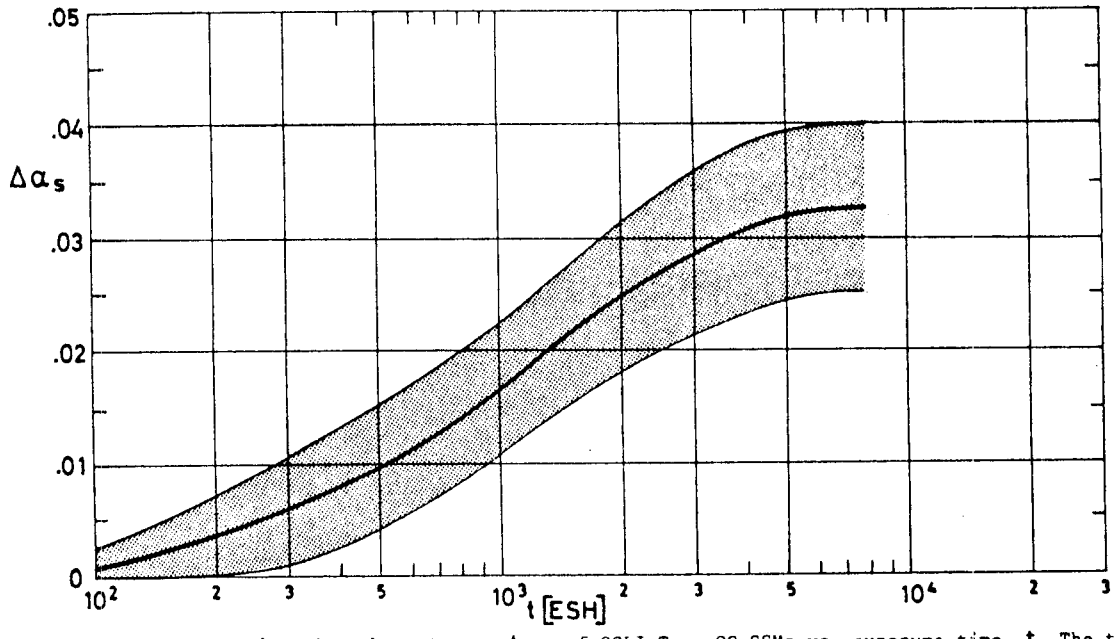

Fig 1-58. Estimated change in solar absorptance, $\Delta\alpha_s$, of OCLI Type CC-SSMs vs. exposure time, t. The tests simulate geosynchronous orbit exposure of the Orbital Test Satellite (OTS) equatorial faces.

Details concerning test procedures are given in pp. 1-74 to 1-76. Results from measurements with three samples appear in Table 1-24, below. See p. 1-76 for a precise definition of the test conditions.

Table 1-24

Effects of Simulated Geosynchronous Orbit Exposure on Solar Absorptance of OCLI Type CC-SSMs

Test Conditions	SAMPLE 1			SAMPLE 2			SAMPLE 3		
	Measured in situ		Corrected [a]	Measured in situ		Corrected [a]	Measured in situ		Corrected [a]
	α_s	$\Delta\alpha_s$	α_s	α_s	$\Delta\alpha_s$	α_s	α_s	$\Delta\alpha_s$	α_s
BEFORE IRRADIATION	.065		.090	.050		.090	.053		.090
AFTER A UNDER VACUUM	.075	.010	.101	.066	.016	.107	.066	.013	.103
BEFORE B	.069	.004	.094	.074	.024	.113	.054	.001	.091
AFTER B	.075	.010	.101	.079	.029	.119	.067	.014	.104
AFTER PUMP DAMAGE	.083	.017	.106	.081	.031	.120	.081	.028	.117
BEFORE C	.083	.018	.107	.085	.035	.124	.081	.028	.117
AFTER C	.081	.016	.105	.082	.032	.121	.076	.023	.112
BEFORE D	.085	.020	.109	.083	.033	.122	.083	.030	.119
AFTER D UNDER VACUUM	.080	.015	.104	.077	.027	.117	.088	.035	.124
AFTER D AND AIR EXPOSURE	.074	.009	.099	.077	.027	.117	.077	.024	.113

[a] The correction has been made, according to Paillous (1976), as follows:
1) The initial value for OCLI Type CC-SSMs has been assumed to be, α_{so}=.09. Measured in air.
2) $\Delta\alpha_{s_{corrected}}$ has been related to $\Delta\alpha_{s_{in\ situ}}$ as follows,

$$\frac{\Delta\alpha_{s_{corrected}}}{\Delta\alpha_{s_{in\ situ}}} = \frac{1-\alpha_{so}}{1-\alpha_{so_{in\ situ}}} = \frac{.91}{.94} .$$

Reference: Paillous (1976).

COATINGS

Solar Reflectors

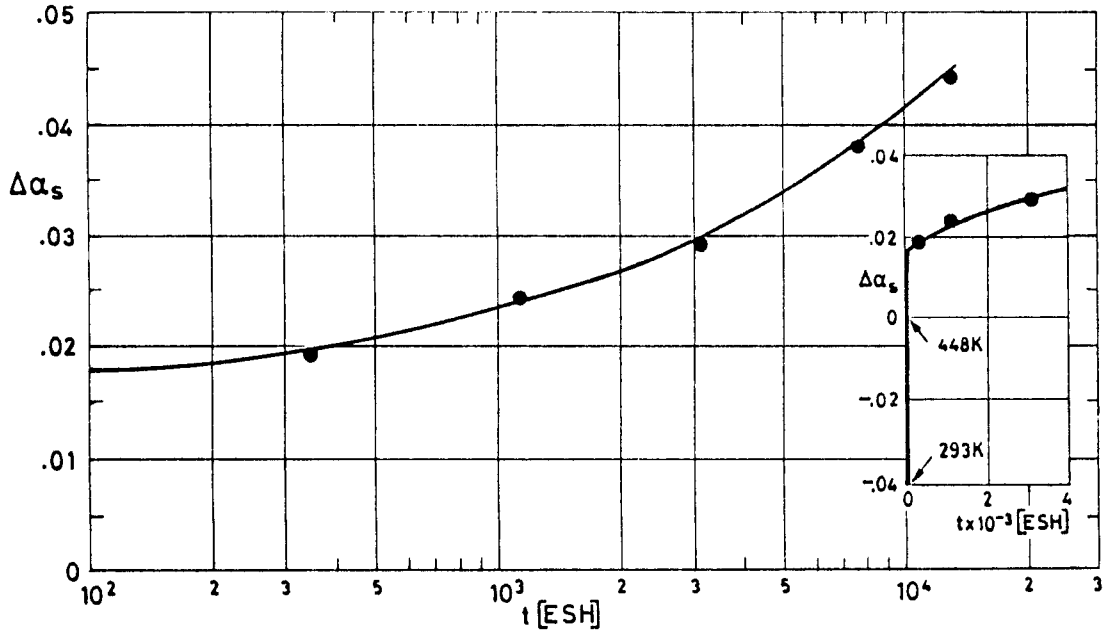

Fig 1-59. Change in solar absorptance, $\Delta\alpha_s$, of OCLI Type CC-SSMs vs. exposure time, t. The insert shows the changes in α_s which suddenly result when ultra-violet exposure, at 16 Suns, begins.

Explanation

Key	Test Conditions					Comments
	Temp. [K]	Time [ESH]	Radiation Exposure			
			UV [Suns]	Charged Particles		
				Intensity [keV]	Integrated Flux [Particles.m^{-2}]	
●	448	up to 17×10^3	16	10	4×10^{20} p.m^{-2}	Intended to reproduce HELIOS orbit conditions at .25 AU. The zero line for $\Delta\alpha_s$ in Fig 1-59 corresponds to unexposed samples at 448 K (α_s=.10 to .11). The figure indicates that illumination with 16 Suns solar radiation as exposure begins, raises the sample temperature sufficiently to produce a quasi-initial α_s value of perhaps .115. This effect has been attributed by Winkler & Stampfl (1975) to thermal instability of the rear side overcoating. The instability appears beyond 400 K and is due to the multicoating on TiO_x base. This multicoating seems to stabilize by diffusion and chemical reaction at high temperature, creating free activated oxygen atoms, which react with the silver forming black silver oxide.
				25×10^{-3}	electron neutralization	

SAMPLE

Sample Description

OCLI Type CC-SSM. Details not given.
Initial solar absorptance, α_{so}=.06 .

Sample Mounting

Sample was bonded to a copper substrate with RTV 560 or RTV 566 silicone adhesives.

CALCULATION METHOD

α_s deduced from spectral reflectance measured at 100 selected wavelengths, in the range 2.5×10^{-7} m to 2.5×10^{-6} m, with in situ reflectometer and a spectrophotometer outside the vacuum chamber.
Chamber pressure not given.

Reference: Fogdall & Cannaday (1974).

COATINGS

Solar Reflectors

SCATHA

Details concerning TEST CONDITIONS, Sample Mounting and CALCULATION METHOD for the OCLI Type SI-100 thermal control mirrors (uncoated) can be seen in pp. 1-126 and 1-127.
The main distinguishing features of the test bearing upon the CC-SSMs are summarized in the following.

SAMPLE

Sample Description

OCLI Type CC-SSM. 3.18×10^{-2} m diameter.

Sample Mounting

The sample is placed on tray ML12-4.

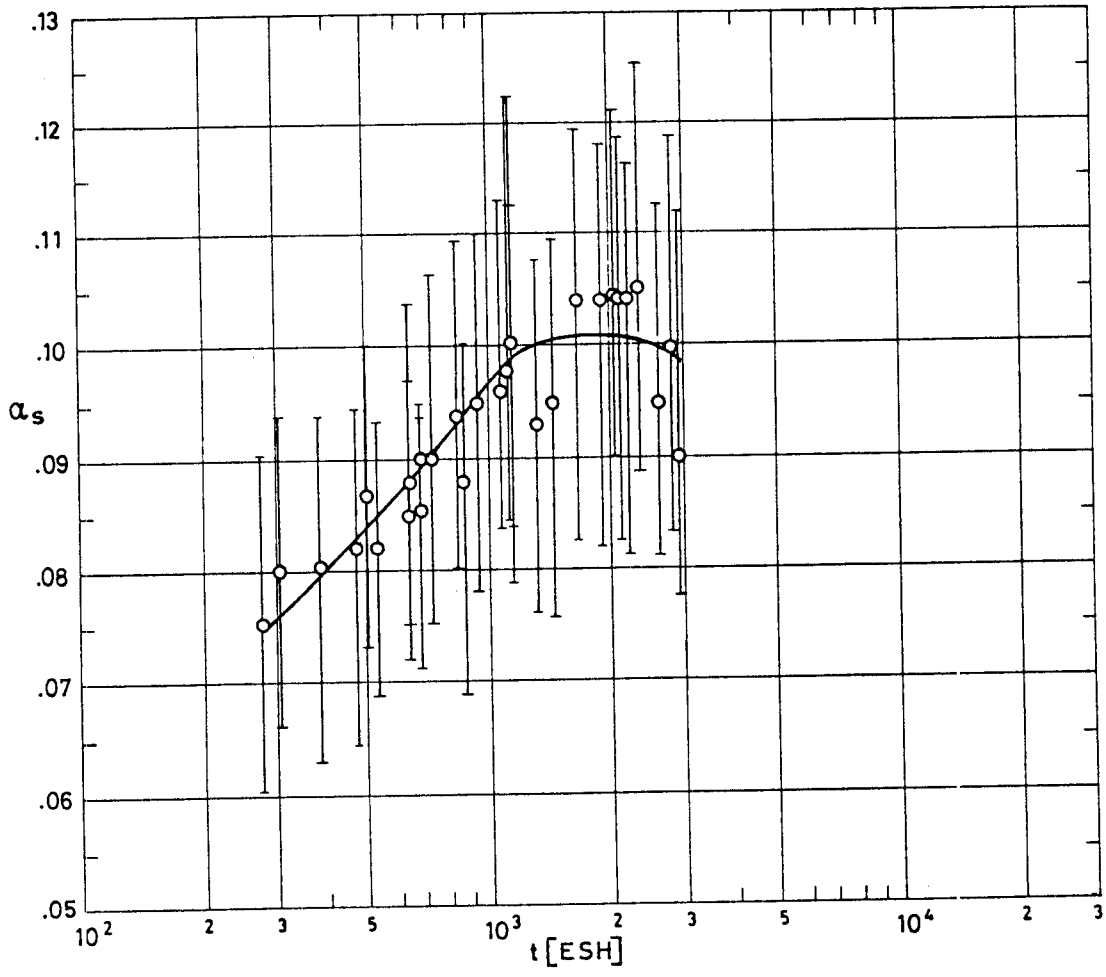

Fig 1-60. Solar absorptance, α_s, of OCLI Type CC-SSMs vs. exposure time, t, as deduced from data of SCATHA spacecraft.

COMMENTS

The data seems to indicate that the conductive coated mirrors degrade more rapidly than their uncoated counterparts. Compare Fig 1-60 above with Fig 1-50, p. 1-127.
An initial value α_{so}=.06 results from extrapolation to t=0 of the α_s vs. t curve given by the authors.

References: Hall & Fote (1979, 1980).

Rev. 1. 1981

COATINGS

Solar Reflectors

HELIOS

The information given in pp. 1-128 and 1-129 is relevant here, unless otherwise stated.

SAMPLE

Sample Description
OCLI Type CC-SSM. Inconel overcoating.

Sample Mounting
Data were deduced from a single temperature sensor (S1) placed on the center of the heat shield, underneath the mirror substrate. These data are deemed to be fairly reliable.

CALCULATION METHOD

- Simplified model of data analysis as in p. 1-128.
- The following effects were considered in the analysis of the first three orbits of HELIOS-A and the first orbit of HELIOS-B (Winkler (1977)). 1) Conductive thermal coupling between the spacecraft surface and the central compartment, where the sensor is placed. This effect is, in this case, small but not quite negligible; near perihelion, $\Delta\alpha_s$=.005, and near aphelion, $\Delta\alpha_s$=.0006. 2) Radiative input from the two solar array cones (already included in the simplified model). 3) Shading effects from the ion guard in HELIOS-B. This shading prevents 1/3 of the expected flux from reaching the surface, and distorts the temperature field, particularly near the perihelion, around the sensor location. 4) Influence of temperature on the hemispherical total emittance. 5) Degradation and contamination.

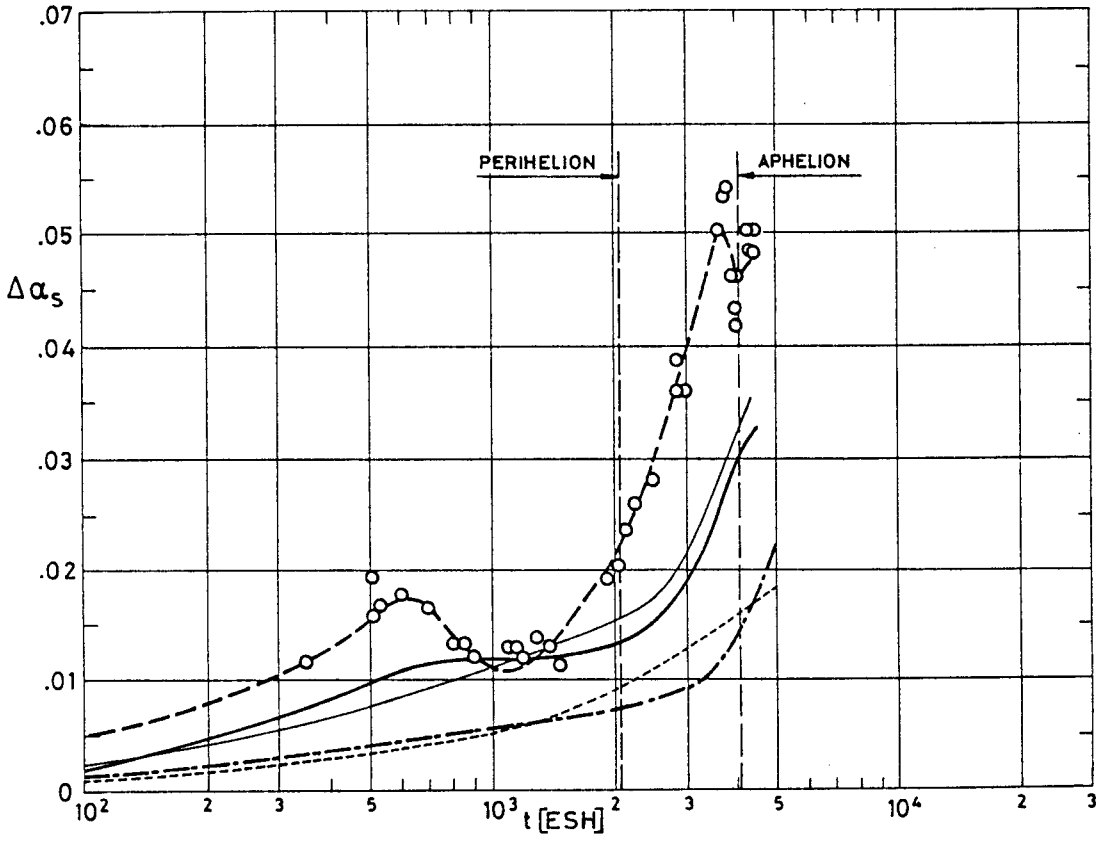

Fig 1-61. Change in solar absorptance, $\Delta\alpha_s$, of OCLI Type CC-SSMs vs. exposure time, t, as deduced from data of HELIOS-A and B spacecraft.
—o— First HELIOS-A orbit. Simplified model of data analysis.
——— Average of the first three HELIOS-A orbits. Improved model of data analysis.
——— First HELIOS-B orbit. Improved model of data analysis.
------ Average of the first three HELIOS-A orbits. Effect of degradation alone. Tests akin to Fig 1-59, α_{so}=.062 .
—·— Average of the first three HELIOS-A orbits. Effect of contamination alone. Calculated.

References: Winkler & Brungs (1975), Winkler (1977).

COATINGS

Solar Reflectors

The results shown in the above figures are summarized in Fig 1-62, below.

The data are presented in terms of the change in solar absorptance, $\Delta\alpha_s$, based on an initial value α_{so}. This value results to be very large (α_{so}=.115) in the case of HELIOS ground tests (curve d in Fig 1-62) because of the initial degradation at high temperature which has been mentioned in pp. 1-158 and 1-161.

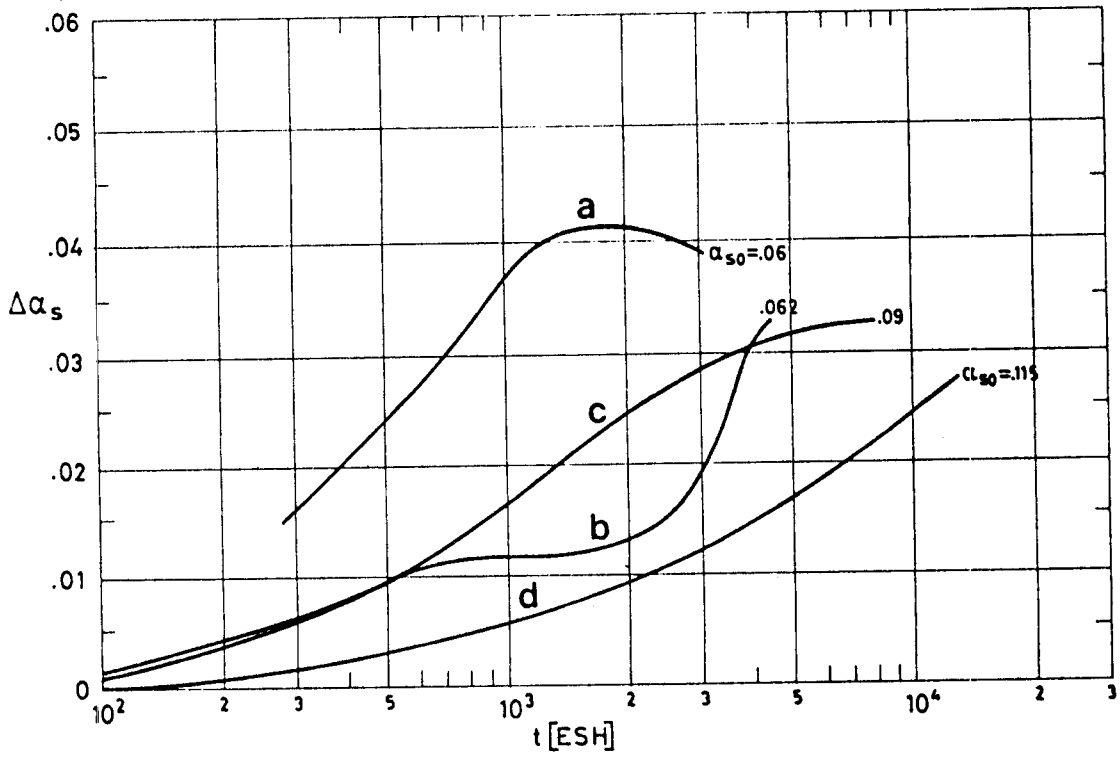

Fig 1-62. Summary data on the change in solar absorptance, $\Delta\alpha_s$, of OCLI Type CC-SSMs vs. exposure time, t. The estimated values of the initial solar absorptance, α_{so}, are shown near each curve.

a From SCATHA. Partially geosynchronous orbit. α_{so}=.06
See p. 1-162.

b From HELIOS-A. Solar orbit. α_{so}=.062
See p. 1-163.

c Ground test. Simulation of OTS orbit. α_{so}=.09
See p. 1-160.

d Ground test. "Clean" simulation of HELIOS orbit. α_{so}=.115
See p. 1-161.

COATINGS

Solar Reflectors

7.3.3. Reflectance.

7.3.3.2. Effects of the Space Environment on reflectance.

7.3.3.2.6. Combined exposure. Fig 1-63 from DERTS.

Sample: Three OCLI Type CC-SSMs, 2×10^{-2} m × 5×10^{-2} m, bonded with DC C6 1104 adhesive to aluminium substrate.

Irradiation and measurements as in pp. 1-74 and 1-75.

Data in Fig 1-63 are related to those in p. 1-160.

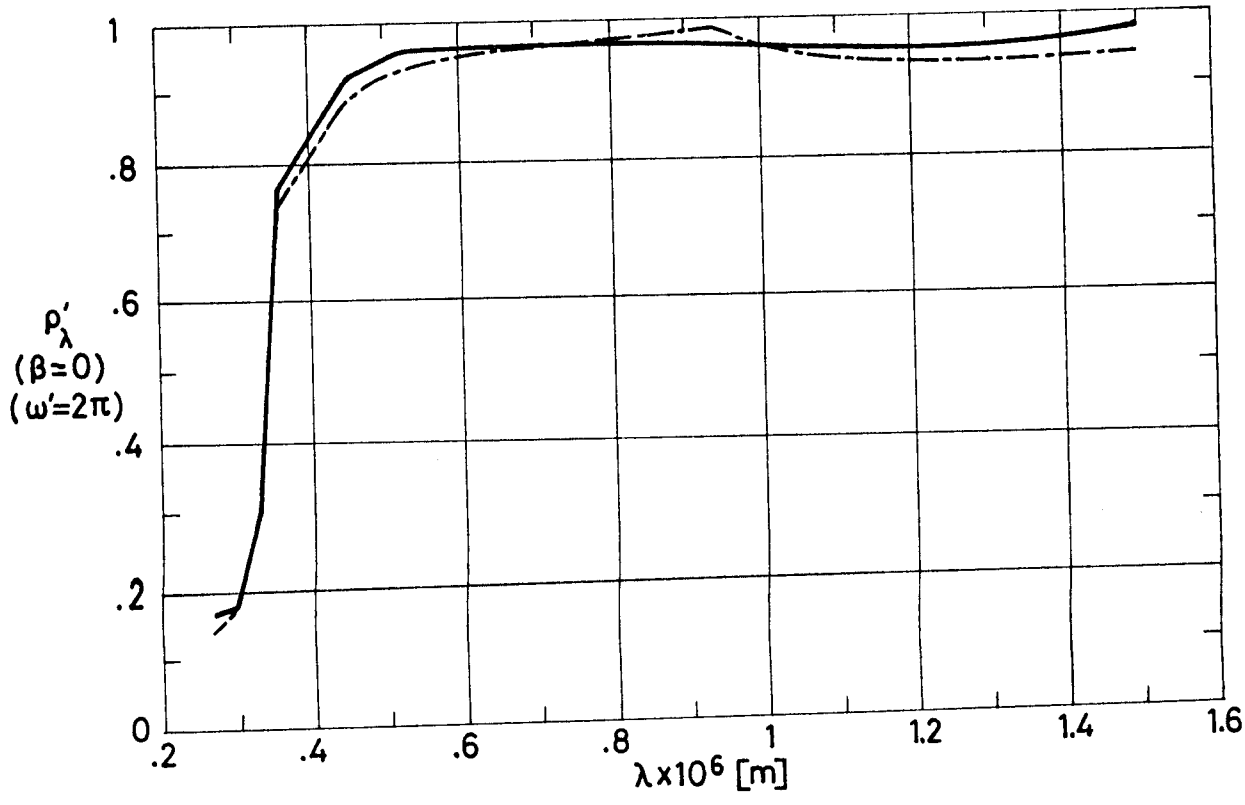

Fig 1-63. Effect of Combined Exposure, simulating up to three years in geosynchronous orbit, on normal-hemispherical spectral reflectance, ρ'_λ, of OCLI Type CC-SSMs vs. wavelength, λ. From Paillous (1976).

Explanation

Key	Description	Comments
———	After 125 h below 1.3×10^{-4} Pa pressure. T = 363 K.	
—·—·—	After step D (3 years in orbit). T = 363 K.	After pump damage. Influence is minimal.

COATINGS

Solar Reflectors

7.4. Electrical resistance. Fused silica is an insulator, thus it shows a tendency to be charged electrostatically in space. This may cause problems such as: coating degradation, transfer of contaminants, malfunction of electrical circuits,... (see pp. 1-141 and ff.). Particularly acute are the problems faced by the sun probe Helios (Winkler & Stampfl (1974,1975)) which was developed with the aim of measuring low energy particle (in the 10-100 eV) fluxes and their distribution function in space. Perturbations because of electrical charges built up in the sunlit and in the shadowed part of the satellite will disturb the field being measured, unless rapid charge exchange between the different parts of the spacecraft occurs through a conductive coating.

The electrical resistance of conductive coated second surface thermal control mirrors is considered in the following.

7.4.1. Effects of temperature on electrical resistance. Fig 1-64a shows the sheet resistance as a function of temperature for several samples of CC-SSM. Electrical contacts were placed either in mode A or in mode B as in Fig 1-64b. The results are interpreted as the electrical resistance of the surface, in Ω/□, although strictly speaking this property should be measured under conditions assuring that the electric field is uniform and one-dimensional.

Values given in Fig 1-64 conflict with the 40 kΩ quoted by Winkler & Stampfl (1975). Nevertheless, these authors also mention values of the order of 2-3 kΩ for temperatures

COATINGS

Solar Reflectors

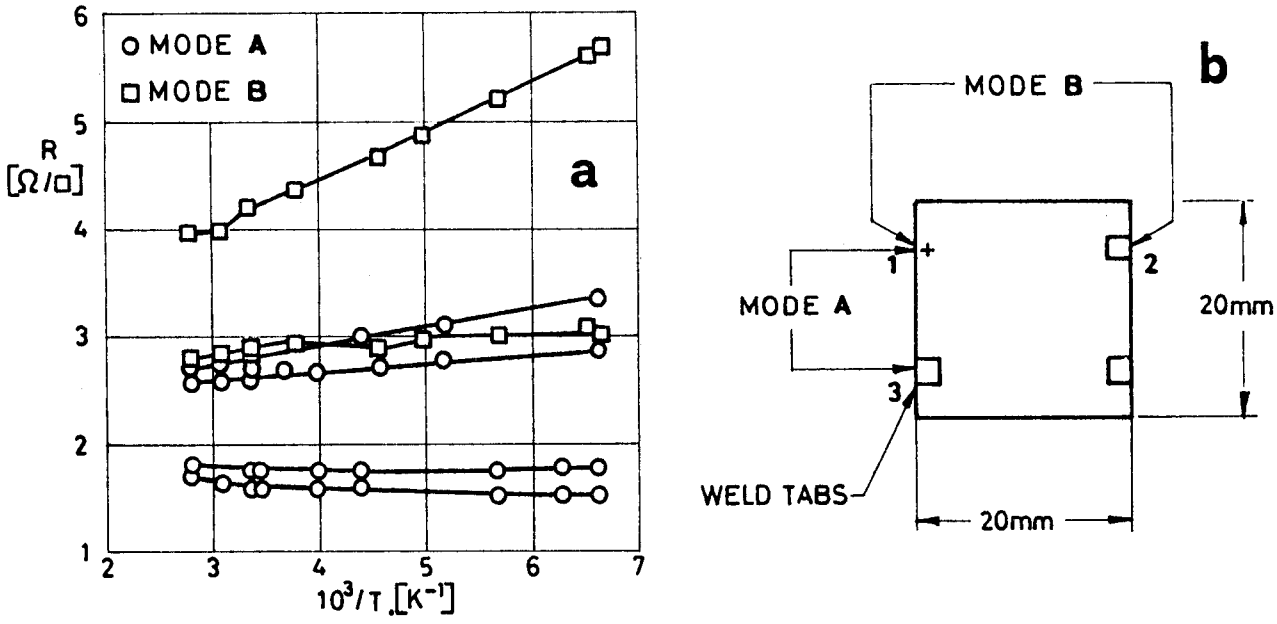

Fig 1-64. a. Electrical resistance, R, of six CC-SSM samples as a function of temperature, T. b shows the two alternative configurations of the electrical contacts set for performing the measurements. From Joslin & Kan (1975).

above 373 K. They attribute this change in electrical resistance to two effects. 1) Influence of the contact resistance between the Ti/Pd/Ag-contacts and the In_2O_3 coating, and 2) Change of the coating behavior from semi-conducting to metallic. (See also Table 2 in Bentlage, Spanier & Wilkens (1976), where changes in R with thermal load (573 K) in a high vacuum are reported).

7.4.2. Effects of the Space Environment on electrical resistance.

7.4.2.1. Ultra-Violet Radiation. The sample consisted of Corning 7940 fused silica, 2.54×10^{-2} m by 2.15×10^{-2} m and about 1.5×10^{-4} m thick, with Indium oxide conductive coating, 10^{-7} m thick, on the front surface, and a blue reflector

COATINGS

Solar Reflectors

coating, 8×10^{-7} m thick, on the rear surface. Although this sample is a solar cell-cover slide, the data are believed to be relevant for the purpose of evaluating space environment effects on the electrical resistance of the CC-SSM.

Irradiated in vacuum: Chamber pressure not given.

Sample temperature: 418 K ± 10 K.

Degrading source: General Electric AH-6 Mercury-Argon lamp.

Radiation flux density at the sample level: 16 Suns.

Exposure time: 800 ESH.

Sheet resistance measured, in air, with a Cambridge Four Point Probe, accuracy ±2%.

The comparison of the values measured before and after test indicated that the sheet resistance decreased from about .9 kΩ/□ to about .8 kΩ/□.

From Fry & Nicoletta (1972).

7.4.2.3. Protons only exposure. Data in Table 1-25, below, have been obtained with the same samples as above. All samples were exposed in vacuum at approximately 1.3×10^{-4} Pa. A 300 keV Texas Nuclear accelerator was used for the two lower fluxes, and an ORTEC RF source in the third case. Sheet resistance measured as above.

Electrons only exposure effects are also given in the table.

The values in the table indicate that a large jump in

Rev. 1. 1981

COATINGS

Solar Reflectors

Table 1-25

Protons (Electrons) Only Exposure Effects on Sheet Resistance of OCLI Solar Cell Cover Slides

Radiation Exposure		Sheet Resistance [kΩ/□]	
Intensity [keV]	Integrated Flux [Particles.m^{-2}]	Before Exposure	After Exposure
4 Protons	10^{16}	.9	1.1
	10^{18}	1.	1.2
	10^{20}	.8	1.3
4.5 Electrons	10^{16}	.8	1.
	10^{18}	1.	1.7
	10^{20}	1.	3.6

From Fry & Nicoletta (1972).

sheet resistance results from the 10^{20} e.m^{-2} exposure. The next table corresponds to two strings of six conductive coated Corning 7940 substrates connected in series, furnished by AEG Telefunken. One string was shielded and used as control, whereas the other string was exposed to radiation. Resistance was measured with a General Radio resistance bridge, Model GR 1650 A, accuracy ±1%. Although the contact resistance between elements is not given, it is presumably both negligible and insensitive to degradation effects. Thus, changes in electrical resistance can be traced back to the degradation of the coating. Notice that values given in Table 1-26, once divided by six, are comparable to those in Fig 1-64 and in Table 1-25.

Rev. 1. 1981

COATINGS

Solar Reflectors

Table 1-26

Protons (Electrons) Only Exposure Effects on Resistance of Conductive Coated Fused Silica

Radiation Exposure		Electrical Resistance [Ω]		Comments
Intensity [MeV]	Integrated Flux [Particles.m^{-2}]	Shielded Sample	Exposed Sample	
1 Protons	Initial	12.4	11.5	In vacuum. Sample removed from machine for each resistance measurement.
	10^{15}	11.1	10.2	
	10^{16}	10.8	10.0	
	10^{17}	10.7	10.2	
	10^{18}	10.4	10.2	
	10^{19}	12.5	11.0	
1 Protons	Initial	9.8	10.5	In vacuum. Resistance measured simultaneously with irradiation. 167 minutes to reach 10^{19} p.m^{-2}.
	10^{16}	9.8	10.5	
	10^{17}	9.8	10.4	
	10^{18}	9.8	10.4	
	2.5×10^{18}	9.8	10.4	
	5×10^{18}	9.8	10.3	
	7.5×10^{18}	9.8	10.3	
	10^{19}	9.8	10.4	
1 Electrons	Initial	12.8	11.8	In air. Sample removed from machine for each resistance measurement.
	10^{15}	12.8	12.2	
	10^{16}	12.8	12.5	
	10^{17}	12.8	12.1	
	10^{18}	12.5	12.0	
	2 h after exposure	12.5	11.8	
	16 h after exposure	12.5	11.9	
	10^{19}	12.6	11.2	
	2 h after exposure	12.6	10.9	
	16 h after exposure	12.7	10.8	
1 Electrons	Initial	12.5	11.0	In vacuum. Sample removed from machine for each resistance measurement.
	10^{16}	12.3	10.1	
	10^{17}	12.1	10.3	
	10^{18}	12.0	10.4	
	10^{19}	11.8	10.4	
1 Electrons	Initial	13.6	11.4	In vacuum. Resistance measured simultaneously with irradiation. 110 minutes to reach 10^{19} e.m^{-2}.
	1.4×10^{18}	13.6	11.6	
	2.7×10^{18}	13.6	11.6	
	4×10^{18}	13.6	11.6	
	5.4×10^{18}	13.6	11.7	
	6.7×10^{18}	13.5	11.7	
	8×10^{18}	13.4	11.5	
	9.5×10^{18}	13.4	11.6	
	10^{19}	13.4	11.6	
	10^{17}	13.6	11.4	

From Fry & Nicoletta (1972).

COATINGS

Solar Reflectors

7.4.2.4. Electrons only exposure. Effects of the electron exposure on electrical resistance of conductive coated fused silica substrates are given in Tables 1-25 and 1-26.

Data on charging of simulated heat shields consisting of OCLI Type CC-SSMs appear in Charging, pp. 1-174 and 1-175.

7.4.2.5. Contamination. When outgassing products from several sources collect on the conductive coating, the electrical path must go through the deposited layer toward the coating. Thence, the effect of contamination is measured in terms of the electrical resistance perpendicular to the surface coating of a given cross-section of contaminating layer (specific cross resistance, ρ_c).

Relevant results are given in Table 1-27 overleaf.

The contaminating source is silicone Silastic 35 rubber material with several admixtures. The target is the conductive coating, the surface area of which is 4×10^{-4} m^2.

Changes in the specific electrical cross resistance of the conductive coating are measured in situ with the simultaneous microgravimetric determination of the build up of contaminating layers due to outgassing material.

Measurements are performed by means of a diode measuring apparatus whose anode, the target, is hung on the load side of a special electronic microbalance.

Chamber pressure below 1.3×10^{-4} Pa.

Both source and target temperatures can be monitored independently from each other.

COATINGS

Solar Reflectors

Table 1-27

Change in the Specific Electrical Cross Resistance, ρ_c, of OCLI Type CC-SSMs by Outgassing Silastic Materials

Outgas Material	Source Temp. [K]	% TML	% CVCM	Target Temp. [K]	Contaminant Mass on Target $m_s \times 10^5$ [$kg.m^{-2}$]	$\rho_c \times 10^{-2}$ [$\Omega.m^2$]	Comments
Silastic 35 with ZnO_2	573	10.5	2.8	373	135	42	
	573	10.4	2.9	373	141	52	
Silastic 35 with TiO	573	6.5	1.6	373	68.5	19.8	
	573	6.8	1.65	373	77.2	28.5	
Silastic treated with TiO	573	2.9	.77	373	37.5	22	
	573	2.5	.65	373	30.0	24	
	523	1.2	.43	423	20.0	14	
	523	1.1	.46	423	21.0	16	
	523	1.2	<.05	443	<2.5	3.5	UV irradiation. 1.8 Suns
	523	1.1	.09	443	5	No change	
	523	1.2	<.05	443	<2.5	No change	

From Bentlage, Spanier & Wilkens (1976).

The total mass loss, TML, in Table 1-27 was deduced by thoroughly weighting the contaminating sample before and after test. The outgassing mass was about 1.8×10^{-4} kg differing somewhat from sample to sample, 1.7×10^{-4} kg up to about 2×10^{-4} kg, (Wilkens (1981)).

The CVCM data are deduced from the contaminant mass on target, m_s, and the test geometry. Due to this geometry only 10%±1% of the outgassing products reached the target. Thus the CVCM was calculated as follows:

$$\% \text{ CVCM} = 10^2 \times 4 \times 10^{-4} \frac{m_s}{\text{outgassing mass}/10} \quad .$$

COATINGS

Solar Reflectors

Three Hg high-pressure lamps are used as UV radiators. Neither these lamps nor the thermoionic cathode do affect the outgas specimen temperature. There is no interference between the electron current flowing from cathode to target and the contamination process, because of the relatively low electron energies (1.5 eV) used.

7.4.2.6. Combined exposure. Data in Fig 1-65 correspond to three simulated years in geosynchronous orbit.

Sample: The same samples as in pp. 1-160 and 1-165.

Irradiations were performed as was indicated in p. 1-74.

In order to perform the measurements, permanent electrical contacts were soldered to the front surface of the mirrors. The position of the electrical contacts as well as that of the mirrors on the sample-holding plate are shown in Fig 1-65b, overleaf.

The electrical resistance is measured by establishing a voltage of $1\ V \pm 10^{-4}\ V$ DC between the terminals for 1 min, reading the intensity with an ammeter.

Measurements were performed in air at 293 K before and after irradiation; in vacuum at 293 K before irradiation, and in vacuum at 363 K before and after the steps A to D which appear in Table 1-13, p. 1-76.

Fig 1-65 indicates that the measured electrical resistance was, within experimental error, quite insensitive to the irradiation.

COATINGS

Solar Reflectors

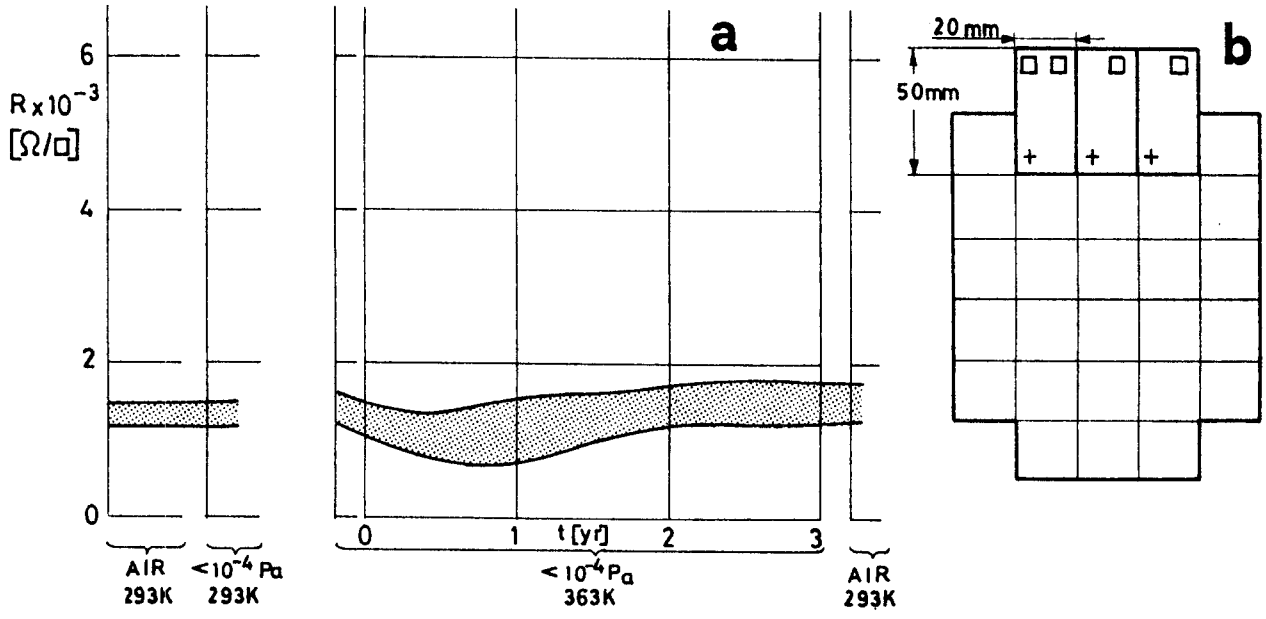

Fig 1-65. a. Sheet electrical resistance, R, of three OCLI Type CC-SSMs vs. time in simulated geosynchronous orbit, t. b. Configuration of the electrical contacts and position of the mirrors on the sample holder for irradiation and measurement. From Paillous (1976).

7.4.3. Charging. An isolated surface in a plasma will charge to a potential depending on the characteristics of the impinging electrons, illumination of the surface, geometry,...

Two surfaces connected through a high-resistance bridge will charge to differential potentials. For a large enough potential buildup, a current discharge will occur.

To what extent should the electrical resistance be decreased to avoid charging is an open question because of the many variables involved. Thence, the charging of materials should be tested through appropriate simulation of the magnetic substorm conditions and realistic electric contacting and grounding of the surfaces.

Tests with OCLI Type CC-SSMs are summarized in Table 1-28.

COATINGS

Solar Reflectors

Table 1-28

Charging Tests with OCLI Type CC-SSMs

1

Sample. Four mirrors on an aluminium substrate. Product Specification No. 6068 002. Indium-Tin oxide overcoating. Furnished by ESTEC.
Conductive adhesive. RTV 566 with silver powder Cho-Bond 1029B (see pp. 1-155 and 1-156).
Tests. Performed at DERTS (Toulouse) by use of the CEDRE substorm simulation facility (Bosma & Levadou (1979)). Pressure close to 10^{-3} Pa. Tests made successively at 323 K, 253 K and 223 K. Uniformity of irradiation better than ±5% (on a .1 m × .1 m target), achieved by diffusing the electron beam through an 8×10^{-7} m thick aluminium foil.
Exposure time was of the order of 20 min for each set of values of ambient temperature, beam energy and beam current density. The electron beam was cutted-off at regular intervals for measuring the surface potential. Once finished the above tests, which will be referred to as step A, the samples were exposed to air for three weeks. After that, tests at 323 K and 10^{-5} A.m^{-2} (step B) were performed. These were followed by a long duration (8 h) exposure under the worst conditions (323 K, 20 keV, 5×10^{-5} A.m^{-2}) in order to detect long term degradation of the mirrors, which did not. The long exposure was followed by step C, tests at 323 K and 10^{-5} A.m^{-2}.
Measurements. Surface potential was measured by a TREK potential probe. The probe moves along an axis parallel to the mirrors surface, travelling straight over two side-by side mirrors. The output of the probe directly feeds an XY plotter. Plotting resolution was better than 10 V. The probe can be calibrated with a metal sheet, placed on the sample holder, to which known voltages are applied.
In order to measure the leakage current through the sample, the metallic substrate is grounded through a microammeter, the output of which is continuously recorded by a two-channel recorder, second channel being used to record the beam current density.
Electrostatics discharges would be measured by an inductive probe, detecting the current pulses through a grounding connection from the substrate. The probe output would be recorded by a storage oscilloscope. No such discharges were detected.
Results of the tests performed at 323 K are given in the following. Similar tests at 253 K and 223 K were performed (step A only). In no case the surface potential exceeded 10 V. This surprising result, which is not new (see data from Bosma (1979) in p. 1-143), is attributed by the authors to the enhanced electrical contacting between silver particles as a result of the adhesive contraction due to low temperatures.

T = 323 K

Beam Energy [keV]	5			10				15				20			
Beam Current Density [A.m^{-2}]	10^{-5}			10^{-5}			4×10^{-5}	10^{-5}			5×10^{-5}	10^{-5}			5×10^{-5}
Step [a]	A	B	C	A	B	C	A	A	B	C	A	A	B	C	A
Exposure Time [min]	Maximum Surface Potential [V]														
0	<10	<10	<10	75	40	28	<10	55	50	50	15	55	55	75	40
.5	60	55	40	160[b]	188	220	107	100	173	212	90	120	178	185	100
1.5	112	143	120	150	188	195	100	90	158	190	85	125	163	178	100
3.5	235	230	185	140	178	185	95	85	163	178	75	115	155	163	85
8.5	180	213	200	120	155	175	90	85	158	172	75	105	140	163	80
18.5	170	190	180	120	162	172	80	90	148	160	75	105	135	160	75

[a] Step A: Irradiations on samples as received.
B: After Step A followed by three weeks of air exposure.
C: After Step B followed by a long duration exposure under the worst achievable conditions.

[b] Value in p. 12 of the source is probably a misprint. Value given here is from Fig 4.

2

Sample. Four mirrors on an aluminium substrate. Product Specification No. 6068 002 modified. Indium-Tin oxide overcoating. Furnished by ESTEC.
Conductive adhesive, Tests and Measurements as above.
In no case the surface potential exceeded 10 V. No discharges were detected.
The improved charging behavior is due to the conductive painting of the edges of these mirrors.

From Amartin & Paillous (1981).

COATINGS

Solar Reflectors

8. ENVIRONMENTAL BEHAVIOR

8.1. Prelaunch. As in § 1.2.6, p. 1-145.

8.2. Postlaunch. As in § 1.2.6, p. 1-145.

8.2.1. Ascent. As in § 1.2.6, p. 1-145.

8.2.2. Orbital. The in orbit behavior of these conductive coated mirrors seems to be quite similar to that of the non-conductive ones. Although data from SCATHA do indicate a faster degradation of the conductive mirrors (compare Fig 1-60, p. 1-162 with Fig 1-50, p. 1-127), "clean" tests performed at Boeing (Fig 1-47, p. 1-119 and Fig 1-59, p. 1-161) do not support this contention.

Really comparable degradation data for conductive coated and for uncoated mirrors are scanty.

9. THERMAL CYCLING

According to the manufacturer, certification of thermal cycling is supplied after the following test: The temperature is lowered from ambient to 143 K ± 5 K, a dwell of 30 minutes, raising the temperature to 358 K ± 5 K, a dwell of 30 minutes, and returning the temperature to ambient. The cycle will be repeated twice more. The rate of temperature change shall be not less than 2 K/min. During the test, no condensation shall be allowed to form on the mirror. The mirror shall show no evidence of degradation after this test.

From OCLI (1974).

Factors limiting the useful temperature range of this coating

COATINGS

Solar Reflectors

are controlled by the methods used for attachment to the spacecraft.

10. SOURCE

Optical Coating Laboratory, Inc., 2789 Giffen Ave., P.O. Box 1599, Santa Rosa, California 95403, USA.

Manufacturing facilities serving Europe, OCLI Optical Coatings Limited.

621 London Road, High Wycombe, Buckinghamshire, HP11 1ET, England.

Telephone: High Wycombe (0494) 36286.

Telex: 83239.

Contact Person: Mr. J.A. Fawcett, Technical Products Manager.

11. COST

In the case of type 6068 002, with TiPdAg contacts, a cost of 55 000 US $.m^{-2} has been estimated.

When type 6068 002 modified is used, the estimated cost of the mirrors is 15 000 US $.m^{-2}. The cost of the conductive adhesive required (approximately .15 kg.m^{-2}) is close to 500 US $.

These estimates are based on 1980 quotations.

The balance will be even more favourable for the solution based on the 6068 002 modified mirrors when the manwork required for interconnecting the TiPdAg contacts is taken into account.

From Bosma (1981).

Rev. 1. 1981

COATINGS

Solar Reflectors

12. PAST SPATIAL USE

This coating was originally developed for the German-USA HELIOS programme. It has been used in several satellites, as indicated in the following Table.

Spacecraft or Programme	Launching Date	Used or Tested	References
HELIOS A B	Dec. 12, 1974 Jan. 15, 1976	Used. Data available for analysis. See p. 1-163.	Winkler & Brungs (1975, 1976), Winkler (1975, 1977).
GEOS	April 20, 1977	Used.	Bosma & Levadou (1979), Morelli (1974).
ISEE-B	Oct. 22, 1977	Used.	Bosma & Levadou (1979).
SCATHA	Jan. 30, 1979	Tested, ML12 and SSPM experiments. See p. 1-162.	Hall & Fote (1979, 1980).
USAF Geosynchronous	Satellite E (author's designation).	Tested.	Curran & Millard (1978).

COATINGS

Total Reflectors

1.3. TOTAL REFLECTORS

1.3.1. LEAFING ALUMINIUM-SILICONE

1. COMPOSITION

Pigment: Leafing Aluminium.

Vehicle: Silicone.

3. USUAL DESIGNATION

Fuller Aluminium Silicone Paint (172-A-1).

4. SUBSTRATE

Any clean, rigid, substrate which can withstand the cure cycle. (Breuch (1967)).

5. METHOD OF APPLICATION

5.3. Application of paint. By any method.

5.4. Coating thickness. For internal applications, where emittance is the value of interest, a minimum thickness of 2.5×10^{-5} m should be achieved. For external surfaces, where both ε and α_s are important, the minimum thickness for opacity is 7.5×10^{-5} m (Breuch (1967)).

5.5. Curing process. Baking at 514 K (Breuch (1967)).

6. SOLVENTS RESISTANCE

The following data, concerning resistance of elastomeric silicones to chemical attack, have been reported.

Rev. 1. 1981

COATINGS

Total Reflectors

Solvents and Fuels (after 7 d at room temperature)	Volume Variation (per cent)
Acetone	15 to 25
Carbon tetrachloride	above 150
Ethyl alcohol	0 to 20
Isooctane	above 150
Xylene	above 150
B type fuel	above 150
JP-4 jet fuel	above 150
Oils (after 70 h at T=423 K)	
ASTM No. 1 Oil	5 to 10
ASTM No. 3 Oil	35 to 60
Hydraulic fluid Mil-0-5606 (Univis J-43)	above 150
Oronite 8200 (silicate ester)	above 150

From DOW-CORNING (1970).

7. PHYSICAL PROPERTIES

7.3. Thermal radiation properties

7.3.1. Emittance.

7.3.1.1. Hemispherical total emittance: Table 1-29.

7.3.1.3. Effects of the Space Environment on hemispherical total emittance.

7.3.1.3.1. Ultra-Violet Radiation.

The available information indicates that ε is unaffected after 600 ESH (Breuch (1967)).

7.3.2. Absorptance.

7.3.2.1. Solar absorptance: Table 1-29.

COATINGS

Total Reflectors

Table 1-29

Hemispherical Total Emittance and Solar Absorptance of Leafing Aluminium-Silicone

T [K]	ε	α_s	References
294	.28±.07	.25±.07	Breuch (1967)

7.3.2.5. Effects of the Space Environment on solar absorptance.

The available information indicates that α_s increases by $\Delta\alpha_s$=.09±.04 after 600 ESH (Breuch (1967)).

7.3.3. Reflectance.

7.3.3.1. Normal-hemispherical spectral reflectance: Fig 1-66.

7.3.3.2. Effects of the Space Environment on reflectance.

7.3.3.2.2. Gamma Radiation: Fig 1-67.

8. ENVIRONMENTAL BEHAVIOR

8.1. Prelaunch. The surface must be protected and carefully handled.

8.2. Postlaunch.

8.2.1. Ascent. No change has been detected in ε and α_s as a result of ascent heating with peak temperatures below 747 k.

8.2.2. Orbital. The primary source of degradation appears to be the near-ultraviolet portion of incident solar and albedo radiation.

From Breuch (1967).

9. THERMAL CYCLING

The extreme temperatures at which this paint was tested without significantly changing its properties were:

Tmin = 122 K
Tmax = 294 K

Rev. 1. 1981

COATINGS

Total Reflectors

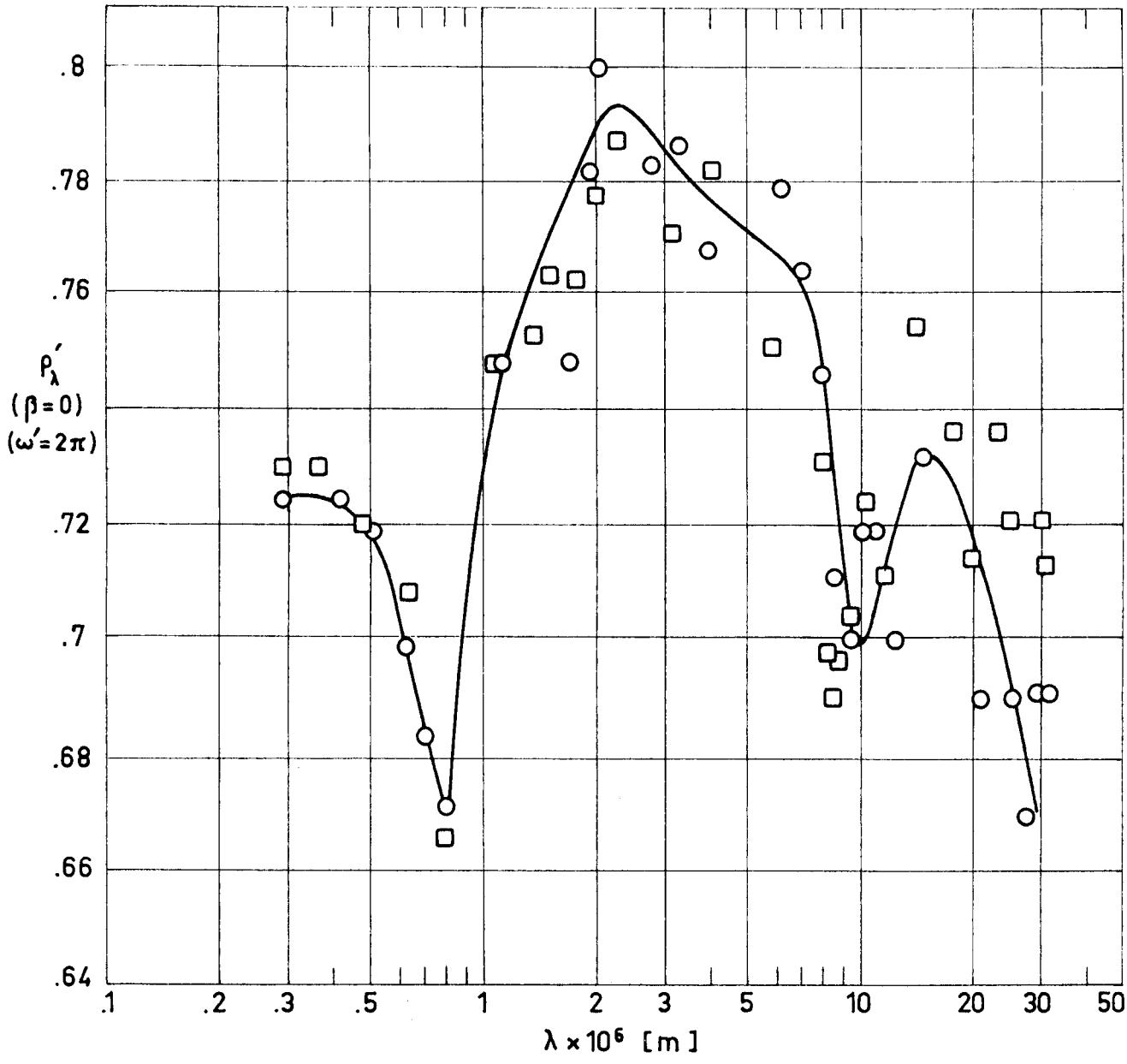

Fig 1-66. Normal-hemispherical spectral reflectance, ρ'_λ, of Fuller 172A1, vs. wavelength, λ. From Touloukian, DeWitt & Hernicz (1972).

Explanation

Key	Description	Comments
○	2024 aluminium substrate.	T = 310 K. Measured in air soon after preparation.
□	Same as ○ . Stored in dry chamber several days, then in N_2 several days.	T = 310 K.

COATINGS

Total Reflectors

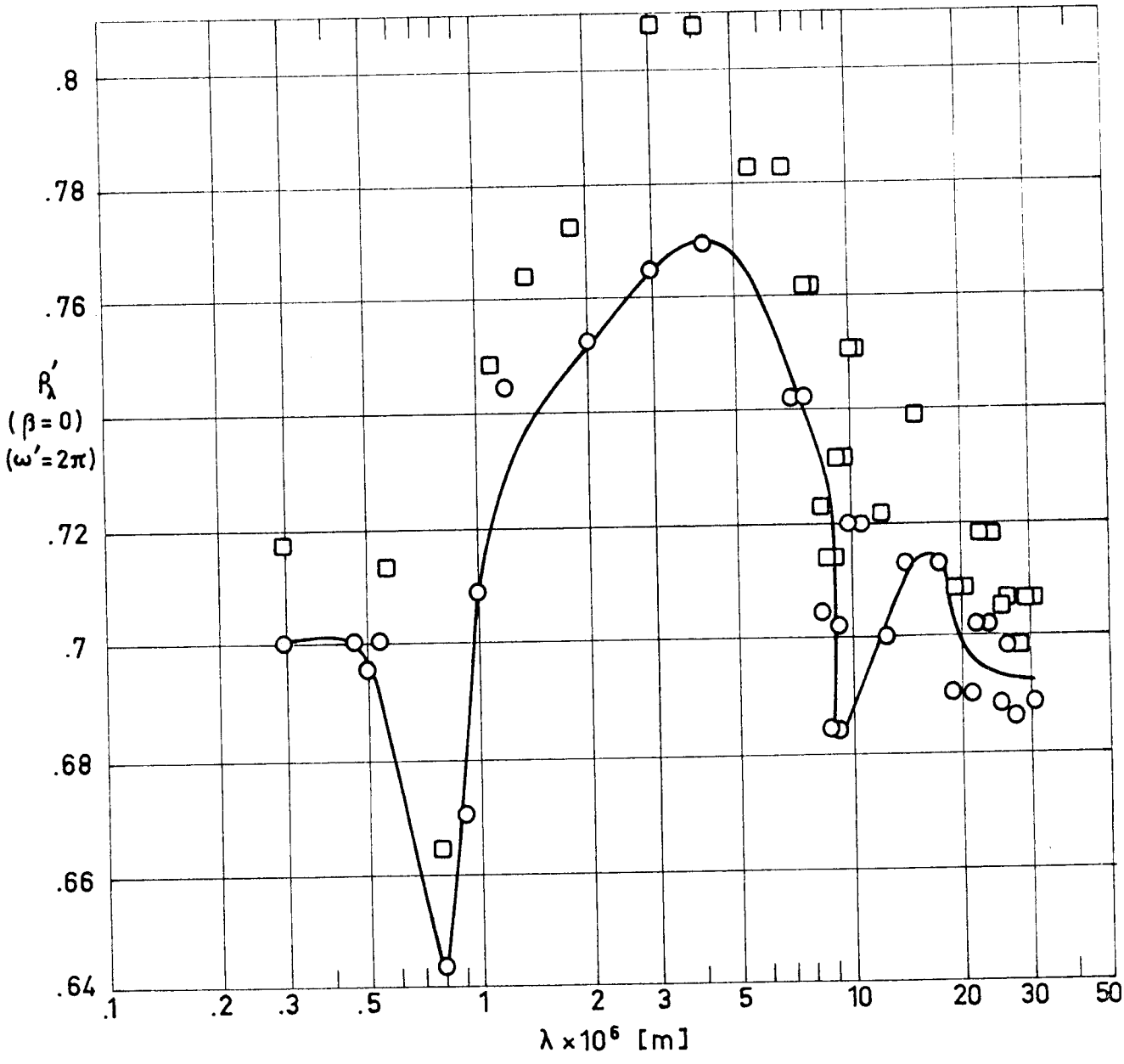

Fig 1-67. Normal-hemispherical spectral reflectance, ρ'_λ, of Fuller 172A1, exposed to gamma radiation, vs. wavelength, λ. From Touloukian, DeWitt & Hernicz (1972).

Explanation

Key	Description	Comments
○	2024 aluminium substrate, exposed to gamma radiation. Sample stored in nitrogen for several days before measuring property in air.	T = 310 K Gamma dose $\sim 1.7 \times 10^6$ J.kg^{-1}.K^{-1}. Exposure in vacuum ($\sim 1.33 \times 10^{-4}$ Pa) maintained by diffusion pump. Property measured in air.
□		

Rev. 1. 1981

COATINGS

Total Reflectors

Cycling: 06 Cycles. min^{-1}.

From Kittenhouse & Singletary (1969).

10. SOURCE

H.B. Fuller, Co. 1150 Eustis Street. St. Paul, Minn. 55108. USA.

COATINGS

Total Absorbers

1.4. TOTAL ABSORBERS

1.4.1. CARBON BLACK-ACRYLIC RESIN

1. COMPOSITION

Pigment: Carbon black.

Vehicle: Acrylic resin.

3. USUAL DESIGNATION

Flat Black Kemacryl Lacquer M49BC12. Sherwin Williams Co.

4. SUBSTRATE

Any clean substrate. Primer required (Breuch (1967)).

5. METHOD OF APPLICATION

5.2. Preparation of surfaces for painting. The substrate should be primed with Sherwin Williams P40GC1, or Dow 17 on Mg alloy substrates (Breuch (1967)).

5.3. Application of paint. By any method.

5.4. Coating thickness. Minimum thickness for opacity is 3.8×10^{-5} m (Breuch (1967)).

5.5. Curing process. Satisfactory physical properties for most applications are obtained by an air drying cure of 8 h (PROCOLOR (1974)). However, to avoid blistering during ascent heating, a minimum of 14 d at room temperature is recommended (Breuch (1967)).

6. SOLVENTS RESISTANCE

Acrylic resins are soluble in Benzene, Toluene, ketones and in most acetates (Sidney Gross (1970)).

Rev. 1. 1981

COATINGS

Total Absorbers

7. PHYSICAL PROPERTIES

7.1. Density. As received: 1 080 $kg.m^{-3}$. Solids content: 45% by weight, 30.2% by volume.

7.3. Thermal radiation properties

Table 1-30 contains data concerning the following topics.

7.3.1. Emittance.

7.3.1.1. Hemispherical total emittance.

7.3.1.3. Effects of the Space Environment on hemispherical total emittance.

7.3.1.3.1. Ultra-Violet Radiation.

7.3.2. Absorptance.

7.3.2.1. Solar absorptance.

7.3.2.5. Effects of the Space Environment on solar absorptance.

7.3.2.5.1. Ultra-Violet Radiation.

Table 1-30

Hemispherical Total Emittance and Solar Absorptance of Carbon Black-Acrylic Resin

T[K]	ε	α_s	Comments	References
294	.88±.03	.93±.03		Breuch (1967)
278	.83	.94	Substrate unknown. Value average of several determinations	Touloukian, DeWitt & Hernicz (1972)
278	.81	.94	Mg alloy substrate treated with Dow 17	
278	.79	.92	Above specimen exposed to UV radiation in vacuum (1.33×10^{-4} - 1.06×10^{-3} Pa) from an argon-filled A-H6 high pressure Hg arc lamp for 80 h.	

Rev. 1. 1981

COATINGS

Total Absorbers

7.3.3. Reflectance.

7.3.3.1. Normal-hemispherical spectral reflectance: Fig 1-68.

7.3.3.2. Effects of the Space Environment on reflectance.

7.3.3.2.2. Gamma Radiation: Fig 1-69.

8. ENVIRONMENTAL BEHAVIOR

8.1. Prelaunch. The surface is porous and requires protection from contamination.

8.2. Postlaunch. This paint requires a minimum of 14 days of room temperature curing to minimized blistering during ascent heating.

8.2.1. Ascent. This coating is not recommended for general use in locations reaching temperatures above 505 K. At peak temperatures above 517 K the paint blisters.

8.2.2. Orbital. No degradation has been detected.

From Breuch (1967).

9. THERMAL CYCLING

The extreme temperatures at which this paint was tested without significantly changing its properties were:

Tmin: 172 K.
Tmax: 294 K.
Cycling: 06 Cycles.min^{-1}

From Rittenhouse & Singletary (1969).

10. SOURCE

Sherwin Williams Co. 101 Prospect Avenue. Cleveland, Ohio, 44101. USA.

COATINGS

Total Absorbers

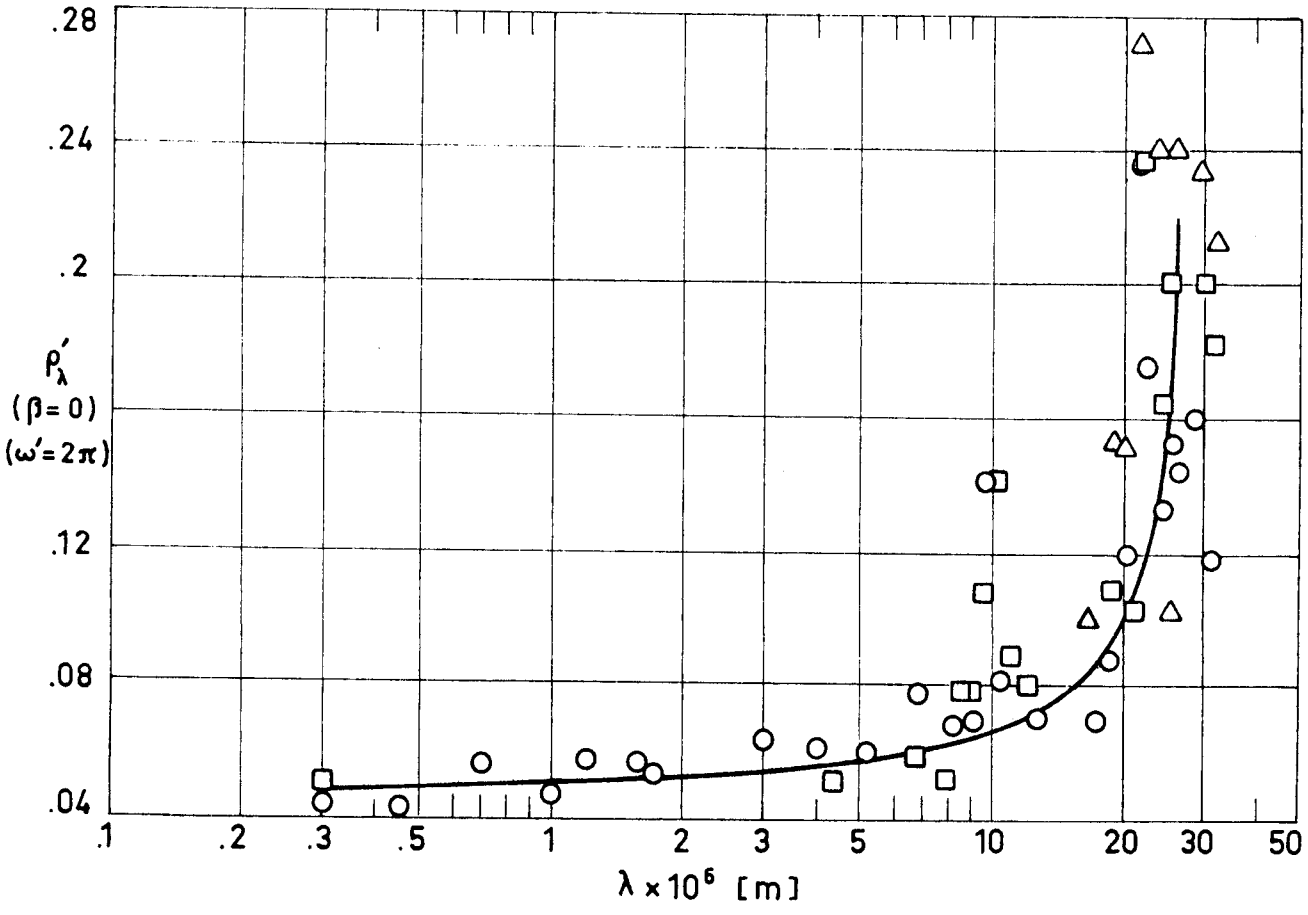

Fig 1-68. Normal-hemispherical spectral reflectance, ρ'_λ, of Kemacryl M49BC12 vs. wavelength, λ. From Touloukian, DeWitt & Hernicz (1972).

Explanation

Key	Description	Comments
○	2024 Aluminium substrate primed with Sherwin-Williams P40GC1.	T = 310 K Property measured in air soon after sample preparation. Representative values for 2 samples.
□	Same as ○ except stored in dry chamber for several days, then in nitrogen for several days, then property measured.	
△	Same as □	

COATINGS

Total Absorbers

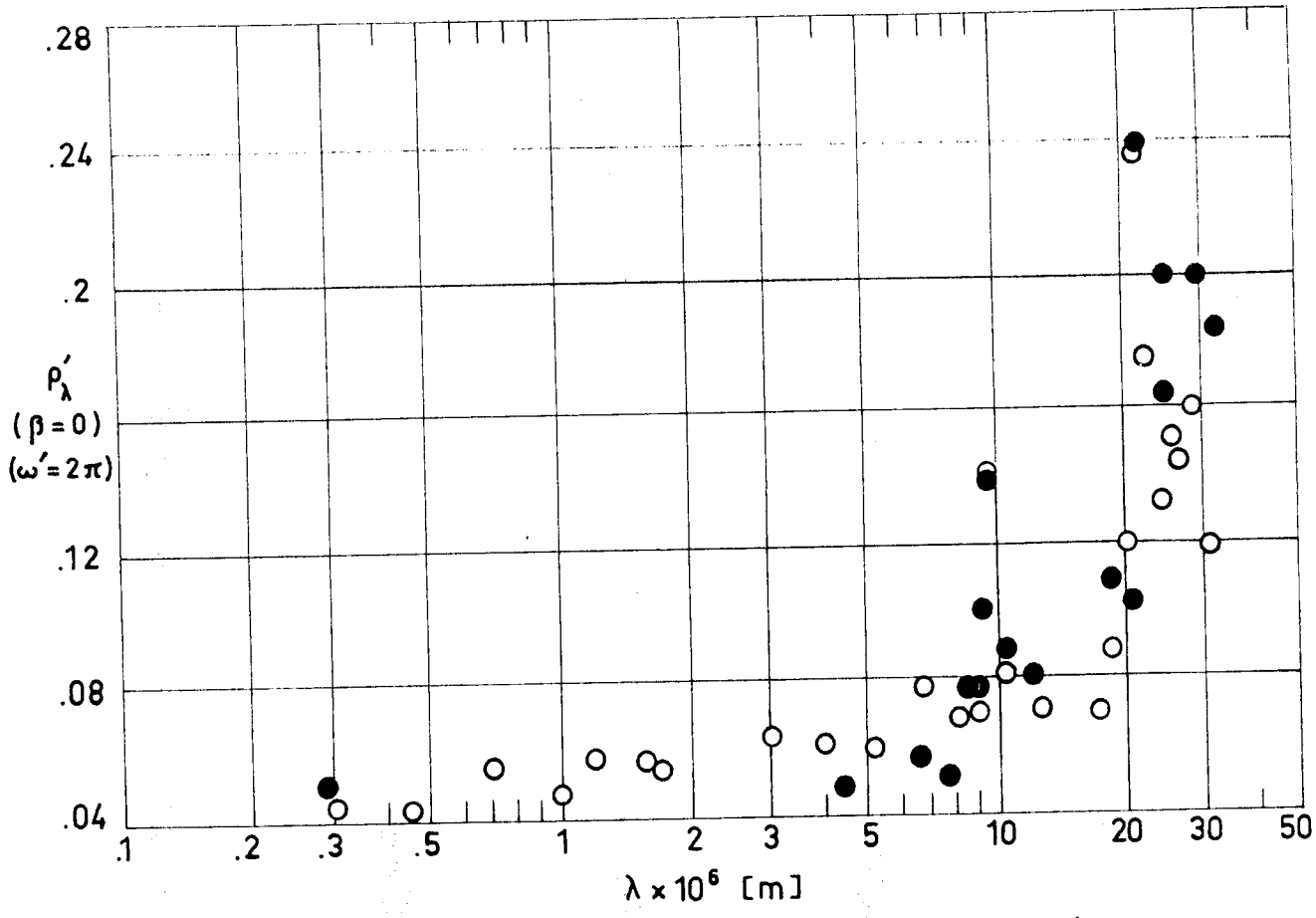

Fig 1-69. Normal-hemispherical spectral reflectance, ρ'_λ, of Kemacryl M49BC12, exposed to gamma radiation, vs. wavelength, λ. Points O are those represented in Fig 1-68. From Touloukian, DeWitt & Hernicz (1972).

Explanation

Key	Description	Comments
O	2024 aluminium substrate primed with Sherwin-Williams P40GC1. Unexposed sample.	T = 310 K. Property measured in air soon after sample preparation. Representative values for 2 samples.
●	Same as O except exposed to gamma radiation. Sample stored in nitrogen for several days, then property measured.	T = 310 K. Gamma dose $\sim 1.7 \times 10^6$ J.kg^{-1}.K^{-1}. Exposure in vacuum ($\sim 1.33 \times 10^{-4}$ Pa) maintained by diffusion pump. Property measured in air.

INTENTIONALLY BLANK PAGE

ADHESIVE TAPES

General

with modulus of backing film and thickness of adhesive, but the degree of these dependences is smaller than that of peel force value.

Tack is often measured by means of the Polyken probe tack tester (Toyama & Ito (1974)) which way of working consists in bringing the tip of probes of various composition and surface texture into contact with the adhesive at controlled rates, contact pressure, contact times and temperature, and afterwards in breaking the tack bond thus formed at controlled rates. The tack value is the maximum force during separation.

In the rolling ball tack test the tack value is related to the distance between the initial contact point of a rolling ball on the surface of the sample adhesive tape and the point at which the ball stops. The initial rolling motion of the ball is imparted by means of a special incline. When care is taken in avoiding sliding, the ball losses momentum at a constant rate, so that in some tests the tack force is measured by the rate of momentum loss. Rolling ball tests are supposed to measure the resistance to detachment after a very short period of contact with the adhesive surface.

The three test methods of estimating adhesive characteristics appraise different aspects of adhesion. The peel force test mainly measures the viscoelastic properties of the adhesive, while the probe tack estimates the initial condition of adhesion in addition to the viscoelastic properties of the adhesive. The rolling ball tack may be more sensitive to surface conditions as compared with the other test methods.

Several results obtained in a typical case are shown in Fig 2-1.

2.1.2. CURING OF ADHESIVE TAPES

Generally, adhesives used in pressure sensitive adhesive tapes are thermoplastic. However, a small amount of curing agents may be added to the adhesive in order to increase heat resistance, cohesive strength, and solvent resistance. In the first two cases the adhesive tape is normally supplied with the adhesive already cross-linked (pre-cured adhesive). In the last case, where solvent resistance is achieved by cross-linking, it is more usual to cure the adhesive after the tape has been applied to the relevant surface. The adhesive is normally cross-linked by the application of heat and, once cured, pre-curing characteristics are lost.

Pre-curing is performed by the manufacturer before applying the adhesive on a backing by solvent coating and calendering spreading.

The curing process, when performed by the user is fairly troublesome and the main advantage of the adhesive tapes, which is ease of application, is lost.

Normally there is an optimum cure temperature for achieving a given purpose. Fig 2-2 illustrates the effect of cross-linking of a rubber based adhesive on the peel adhesion measured at 393 K. It can be seen that by increasing the curing temperature, the peel force increases to a maximum. This will be due to the in-

2. ADHESIVE TAPES

2.1. GENERAL

Pressure-sensitive adhesives can spread over a surface by mere pressure to make an adhesive bond, and are expected to be removed from the surface without leaving an adhesive residue. Pressure-sensitive adhesives, other than thermosetting types, do not change their physical state from the initial stage of adhesion upon wetting the surface to the final breaking of the adhesive bond.

Structural adhesives, on the contrary, are applied in the liquid state and set to the highly cohesive form by release of a solvent, by cooling of a hot melt, or by chemical reaction.

Pressure sensitive adhesive tapes can be used in aerospace as thermal control surfaces, for attaching multilayer insulations, as electrical insulators, and as temporary fasteners of sensors and wires during qualification test.

Primary emphasis is placed in this Chapter on adhesive tapes as thermal control coatings, but data concerning adhesive films and general purpose low-outgassing tapes are also included.

Compared with other thermal control coatings such as paints, plating or vacuum depositions, the tapes have the following advantages.

1) They are available in various widths, and do not require setup or masking for application.

2) They are easy to remove. Damaged surfaces can easily be repaired in the field at any time, up to late prelaunch phases.

ADHESIVE TAPES

General

3) Mosaics can be prepared and easily changed by addition or removal of appropriate tapes.

2.1.1. ADHESIVE PROPERTIES

The adhesive force of pressure sensitive tapes is commonly related to their peel strength.

The most popular of the methods used for performing the peel test is the 180° peel adhesion. This test is usually carried on pendulum machines using stainless steel panels to be adhered to the test sample. The adhesive force is measured as the force necessary for stripping the adhesive tape at an angle of 180° at a constant jaw separation rate.

As the test sample is noticeably deformed, peel strength depends on rate of peeling, peel angle, thickness of adhesive, width of tape, Young moduli of adhesive and backing materials, temperature, and so forth. Peel force becomes larger in proportion to the width of the sample, and increases to a maximum value when the thickness of adhesive increases.

Peel test is considered not to measure adhesion but rather a combination of adhesion and the viscoelastic properties of the adhesive.

Tack is the force required to separate the adhesive from an adherent after only a brief time of contact under low pressure application. Factors affecting tack are contact time, contact pressure, rate of separation, and temperature. Tack values also vary

ADHESIVE TAPES

General

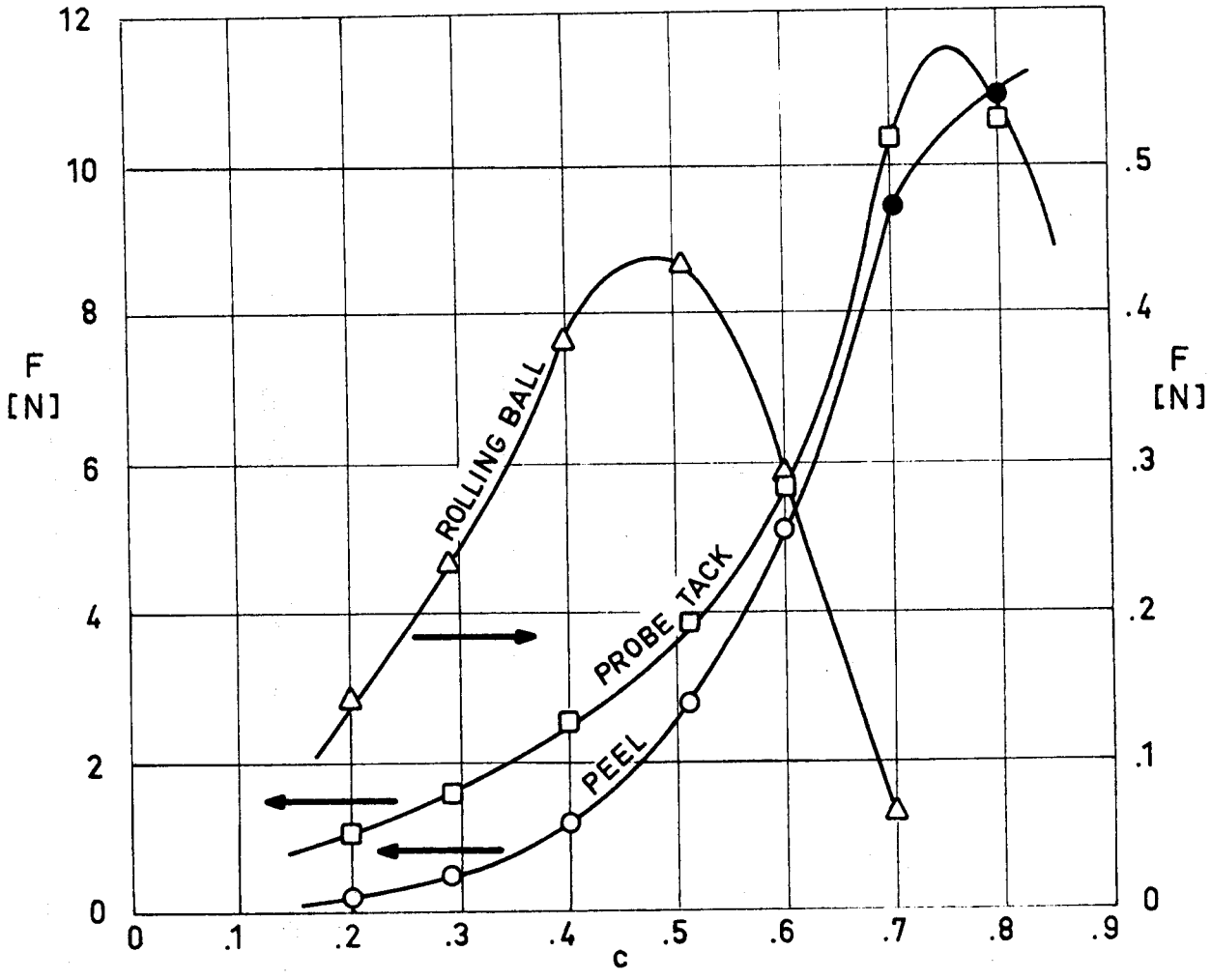

Fig 2-1. Peel force, probe tack and rolling ball tack, F, as functions of resin concentration, c, for a rubber adhesive on a polyethylene terephthalate (polyester) film. Peel force has been measured at a rate of separation of 5×10^{-3} m.s^{-1}. Tape width is 1.2×10^{-2} m. Labels correspond to experimental points. Closed circles indicate that the cohesive failure occurs during measurement. Probe tack is measured by using a probe of 5×10^{-3} m diameter at 9.8×10^{3} Pa of contact pressure, 1 s of contact time and 10^{-2} m.s^{-1} of rate of separation. Rolling ball tack is measured using No. 16 steel ball. The force given equals the rate of momentum loss of the rolling ball.
From Toyama & Ito (1974).

ADHESIVE TAPES

General

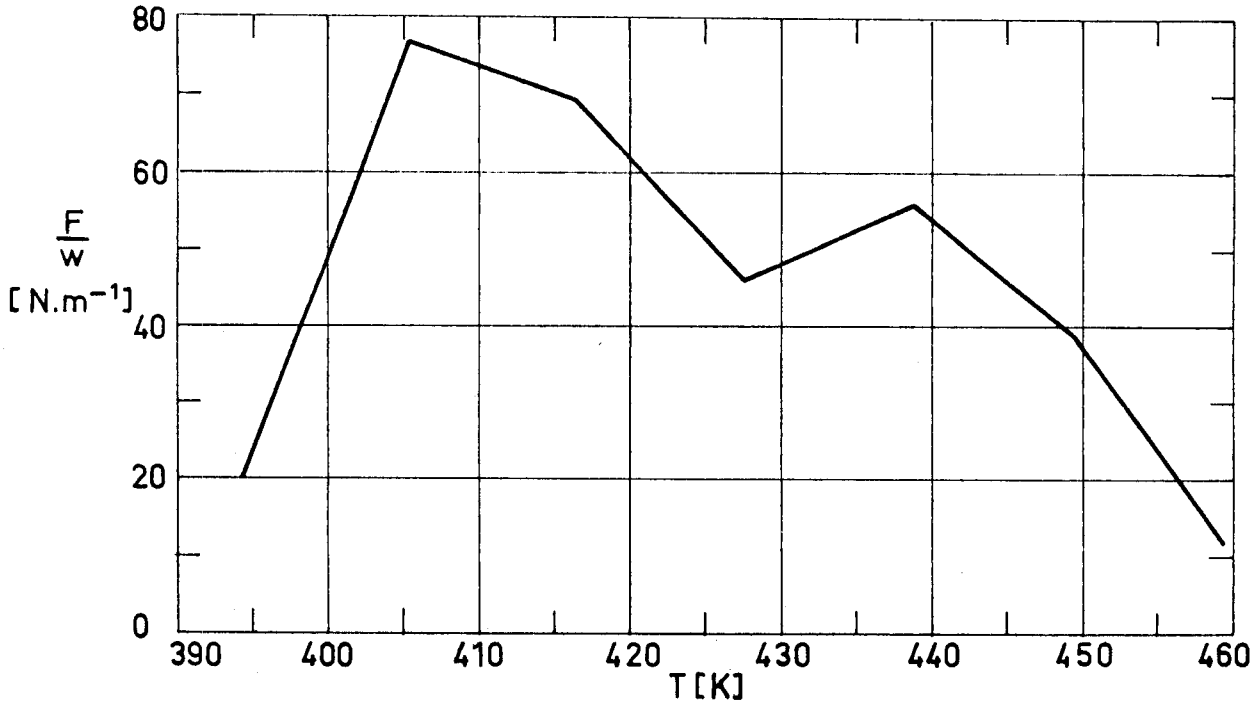

Fig 2-2. Peel adhesion, F/w, measured at 393 K as a function of curing temperature, T. Rubber based adhesive. From Toyama & Ito (1974).

Table 2-1

Thermosetting Cure Cycles and Useful Temperature Range of Several MYSTIK Adhesive Tapes.

Adhesive	Cure Time [h]	Cure Temp. [K]	Tape No.	Backing	Useful Temp. Range [K]
Rubber	3	394	7321, 7322, 7323, 7351, 7352, 7355.	Polyester	233 - 436
	2	408			
	1	422			
Acrylic	3	394	7367.	Kapton	211 - 450
	2	408			
	1	422			
Silicone	3	533	7300, 7331,	Polyester	211 - 469
			7361, 7362, 7366.	Kapton	193 - 561
			7502, 7503, 7505, 7510.	Teflon	193 - 505

From MYSTIK BRAND Insulation Tape Selector.

ADHESIVE TAPES

General

crease of cohesive strength of adhesive. After a maximum has been reached at 405 K, further increase in cure temperature or cross-linking results in a decrease in adhesion value.

Obviously both the backing film and the adherent must withstand the temperatures involved in the curing process. This condition introduces some coupling in the selection of the film and the adhesive, since it should be convenient that the optimum cross-linking temperature be as close as possible to the maximum operating temperature of the film. As an illustration Table 2-1 shows the suggested cure cycles for maximum cross-link density of several adhesives used in commercial tapes, together with the operating temperature range of the tape, as recommended by the manufacturer.

Unsupported adhesive tapes are normally thermoplastic. Although hand application of these tapes is easily accomplished, relatively high temperatures (of the order of 420 K) must be applied with a hand iron set. Thermoplastic adhesive tapes can be stored at room temperature for many months without deterioration.

Thermosetting adhesives are used sometimes to raise the service temperature of the system, the increase being of the order of 20 K. Thermosetting adhesive tapes are normally available upon request, they must be stored at 250-260 K, and have a shelf life of the order of 30 d.

Properties of several general purpose adhesive tapes are given in § 2.1.3. Table 2-2 concerns double faced adhesive tapes, and Table 2-3 unsupported adhesive tapes.

ADHESIVE TAPES

General

2.1.3. GENERAL PURPOSE ADHESIVE TAPES

Table 2-2

Properties of Double-Faced Adhesive Tapes [a]

Type	Description			Thickness, $t \times 10^4$ [m]				Temp. Range [K]
	Backing	Adhesive	Liner (Detachable)	Backing	Adhesive (each face)	Liner	Total	Intermit. / Continuous
3 M Co. 400	Paper						1.27	Up to 368 / Up to 338
3 M Co. 404	Paper						1.14	Up to 403 / Up to 378
3 M Co. 410	Paper	Natural Rubber	Paper				1.14	Up to 368 / Up to 338
3 M Co. 411	Polyvinyl Chloride						3.81	Up to 338 / Up to 318
3 M Co. 415	Polyester "Scotchpar"	Synthetic Rubber	Paper	.25			1.77	Up to 393 / Up to 353
3 M Co. 4004	Polyurethane Foam	Acrylic	Paper			1.25	60	Up to 463 / Up to 368
3 M Co. 4008	Polyurethane Foam	Acrylic	Paper			1.25	32	Up to 463 / Up to 368
3 M Co. 4016	Polyurethane Foam	Acrylic	Paper			1.25	16	Up to 463 / Up to 368
3 M Co. 4032	Polyurethane Foam	Acrylic	Paper			1.25	8	Up to 463 / Up to 368
Mystik 5855	Cotton Cloth			2.41			3.05	
Mystik 5856	Cotton Cloth			2.03			3.30	
Mystik 6360	Paper			1.40			1.78	
Mystik 6466	Polyester			.25			.97	

ADHESIVE TAPES

General

Mechanical Properties		Outgassing [d]			Comments
Peel Strength $(F/w) \times 10^{-2}$ $[N.m^{-1}]$	Tack $(F/w) \times 10^{-2}$ $[N.m^{-1}]$	% TWL % VCM	Cure t [h] Cure T [K]	ATMOS.	
					Excellent adhesion to rubber. Fair solvents resistance.
					Resists temperature and plasticizers. Good solvents resistance.
					Excellent adhesion. Fair solvents resistance. Easily strippable liner. Tape does not leave any residue upon removal. Standard lengths 10 m and 33 m.
					Good resistance to plasticizers and solvents. Used for holding metallic plates.
5.46		.605 .118			High tack values to many materials (except untreated polyurethane). Fair solvents resistance. Good resistance to UV irradiation and ageing. Resists low temperatures, vibrations and shocks. "Scotchpar" allows an easy detachment of liner. Length 33 m.
					Good solvents and moisture resistance. High tack values. Recommended temperature of application: 293 K to 313 K; once applied, low temperatures do not impair the adhesive characteristics. Good ageing. Can be applied to rough surfaces. Polyurethane foam insures good thermal insulating characteristics. Can be recommended as a vibration and noise damper.
4.38 [e] 9.85 [f]	1.31 [e] 4.38 [f]				High adhesion one side, low adhesion other side. Recommended for blend fastening, carpet seaming, splicing and holding. Color: White.
5.25 [e] 7.66 [f]	.015 m [e] .012 m [f] (Rolling ball)				Carpet tape. High internal strength, good adhesion. Color: Blue.
4.93 [e] 5.25 [f]	2.41 [e] 3.06 [f]				High maneuverability. Strong moisture resistant. Excellent tear and creep resistance. Used for holding nameplates, splicing paper, tabs or manifold forms. Color: White.
3.72 [e] 4.16 [f]	2.63 [e] 2.74 [f]				High strength, excellent adhesion. Thermosetting and electrically non-corrosive. Color: Transparent.

(Continued onto next page)

ADHESIVE TAPES

General

Table 2-2 (Continued)

Properties of Double Faced Adhesive Tapes [a]

Type	Description			Thickness, $t \times 10^4$ [m]				Temp. Range [K]
	Backing	Adhesive	Liner (Detachable)	Backing	Adhesive (each face)	Liner	Total	Intermit. / Continuous
Mystik 7100	Glass Cloth	Silicone		1.17			2.39±.13	193 to 561
Mystik 7366	Kapton	Silicone	Cloth	.25			1.24±.08	193 to 561
G.T. Schjeldahl Schjel-Bond GT 400	Polyester	Polyester		.51 [b]	.25 [b]			Up to 400 [c] / Up to 355 [c]

[a] All data in this table, unless otherwise stated, are from manufacturer's bulletins.

[b] Typical values. For more details see Table below. O indicates that the configuration is not available for inmmediate delivery.

[c] Specific for individual base material, not necessarily same as for composite tape.

SCHJEL-BOND GT-400. Thermoplastic adhesive on both sides of polyester film. 7.62 m rolls.					
Adhesive × Mylar × Adhesive	Width, $w \times 10^2$ [m]				
Thickness, $t \times 10^4$ [m]	1.3	2.5	5.1	10.2	53.3
.13 × .13 × .13					
.25 × .25 × .25					
.25 × .51 × .25					
.38 × .51 × .38	O			O	
.38×1.27 × .38	O				

ADHESIVE TAPES

General

Mechanical Properties		Outgassing [c]			Comments
Peel Strength $(F/w) \times 10^{-2}$ $[N.m^{-2}]$	Tack $(F/w) \times 10^{-2}$ $[N.m^{-2}]$	% TWL % VCM	Cure t [h] Cure T [K]	ATMOS.	
2.19 Min. [e] 3.28 Avg.		3.22 R 3.60 S			Thermosetting. High-low temperature resistant, non-corrosive. Electrically pure, does not shrink, rot or burn. High tensile strength, excellent thermal stability. Length 33 m on 7.62×10^{-2} m core. Color: White.
2.19 Min. [f] 3.17 Avg.		.670 R .790 S			
1.75 Min. [e] 2.19 Avg.		1.30 R 5.45 S	72	E-4	Thermosetting. High mechanical strength. Retains dielectric strength at elevated temperatures. Stable over a wide temperature range. Length 33 m on 7.62×10^{-2} m core. Color: Amber.
1.75 Min. [f] 2.08 Avg.		.940 R 1.680 S	328 0	E-4	
7 [g]		.631 .124	.083 .433	Air	Used to bond plastic films, fibers, paper, metals, glass, ferrites, plastics and finishes. Thicker resin coatings are recommended for sealing porous materials. Also available as GT-401 with thermosetting adhesive. Color: Milky-White; becomes clear when sealed.

[d] Outgassing characteristics have been borrowed from Campbell, Marriott & Park (1973).

TWL: Total Weight Loss VCM: Volatile Condensable Materials (by weight)

R: Several layers of the tape were rolled on a glass Rod to permit outgassing at the edges.

S: The tape was placed on a Screen exposing the adhesive of the first layer.

E-4: Chamber pressure 10^{-4} torr = .013 Pa.

A zero indicates that cure conditions are unknown.

[e] Roll Side.

[f] Liner Side.

[g] Bond adhesive to adhesive.

ADHESIVE TAPES

General

Table 2-3

Properties of Unsupported Adhesive Tapes [a]

Type	Description		Thickness, $t \times 10^4$ [m]			Temperature Range [K]	
	Adhesive	Liner (Detachable)	Adhesive	Liner	Total	Intermittent	Continuous
3 M Co. 465	Acrylic	Paper	.50	.75		Up to 393	Up to 353
3 M Co. 467	Acrylic	Paper				Up to 478	Up to 448
G.T. Schjeldanl Schjel-Bond GT-100	Polyester	Paper	.635 [b]			Up to 400 [c]	Up to 355 [c]

[a] All data in this table, unless otherwise stated , are from manufacturer's bulletins.

[b] Typical value. For more details see Table below. 0 indicates that the configuration is not available for immediate delivery.

[c] Specific for individual base material, not necessarily same as for composite tape.

SCHJEL-BOND GT-100. Unsupported thermoplastic adhesive. 8.38 m rolls.					
Adhesive Thickness, $t \times 10^4$ [m]	Width, $w \times 10^2$ [m]				
	1.3	2.5	5.1	10.2	53.3
.13				0	
.254				0	
.635				0	

ADHESIVE TAPES

General

Mechanical Properties		Outgassing [d]			Comments
Peel Strength $(F/w)\times10^{-2}$ $[N.m^{-1}]$	Tack $(F/w)\times10^{-2}$ $[N.m^{-1}]$	% TWL % VCM	Cure t h Cure T [K]	ATMOS.	
		.840 .209	0		Resistant to temperature, moisture and UV irradiation. Fair solvents resistance. High tack values. Excellent ageing. Can be applied to any smooth surface such as cloth, crystal, metal, paper, plastic, wood. Length 55 m.
		1.320 .080	4 311	AIR	Similar to above although it exhibits improved resistance to Sun irradiation and chemical attack. Excellent final adhesion. Can be applied to any surface, except polyurethane.
7 [e]		.250 [f] .082 [f]	.083 422	AIR	Used in bonding lap seams, constructing multi-layer circuits and joining parts and components. Also available as GT-101 with thermosetting adhesive on special order. Color: Milky-White; becomes clear when sealed.

[d] Outgassing characteristics have been borrowed from Campbell, Marriott & Park (1973).

TWL: Total Weight Loss VCM: Volatile Condensable Materials (by weight).

A zero indicates that cure conditions are unknown.

[e] Bond adhesive to adhesive.

[f] Composite Mylar - GT-100 - Mylar.

INTENTIONALLY BLANK PAGE

ADHESIVE TAPES
Application and Handling

2.2. APPLICATION AND HANDLING

2.2.1. APPLICATION

Thermal control tapes incorporate pressure sensitive adhesives such as acrylics, rubber or silicones which enable the tape to be positioned and set by applying pressure with a non-abrasive roller or ironing tool. Room-temperature-curing or elevated-temperature-curing adhesives are available.

Before applying the tapes it must be ensured that the adherent surface is clean enough, that the tape is regularly pressed, and that the adhesive surface is not damaged during the application.

Several commercially available metallic foils are protected with a nitrocellulose lacquer. This lacquer must be completely removed prior to application of the foil. The removal may be performed by wiping with a soft clean cloth, using the following solvents in this order (Breuch (1967)):

1) Lacquer thinner or methyl-ethyl-ketone.

2) Isopropyl or ethyl alcohol.

The lacquer is almost invisible to eye. Any doubt concerning whether it has been removed or not can be dissipated by using an ohmeter to measure the electrical resistance between points on the same foil face. If this resistance is large the lacquer has not been removed.

Films and foils can be applied to the substrate by using either a double faced or an unsupported adhesive tape. In these systems the film or foil is first attached to one adhesive side of the tape and subsequently applied by bringing the other side into

contact with the substrate. This method is time-consuming and increases the chances for tape missalignment and air entrapment.

2.2.2. CLEANING

Foils and metallized films can be cleaned by lightly rubbing the surface with a soft cloth or cotton swab wetted with solvent. Choice of solvent depends upon: type of contaminant to be removed, and compatibility of the solvent with the adhesive. Special care should be employed during cleaning to avoid the scratching of the metallized surface. In addition, cleaning solvents can be absorbed into the adhesive, the tape, or both, diffusing out under vacuum conditions.

Adhesive tapes which are applied temporally contaminate the substrate which should be carefully cleaned after tape removal. On the other hand, when the tape is applied permanently it may be displaced by creep, leaving a dirty trace of its past position.

Solvents of relevant adhesives are listed in Table 2-4.

Table 2-4

Several Solvents of the Adhesives

Adhesive	Solvents	References
Acrylic	Glacial acetic acid. Methylene chloride.	Katz (1964)
Rubber	Benzene.	Delmonte (1947)
Silicone	Carbon tetrachloride. Isooctane. Xylene.	DOW-CORNING (1970)

ADHESIVE TAPES

Application and Handling

2.2.3. HANDLING

Permanent damage to foils and metallized surfaces result from improper handling during installation or cleaning operation.

Data showing effects of abrading metallized surfaces are given in Table 2-5. Since the amount and degree of rubbing used in the tests was subjective, these data should be considered merely as qualitative.

Table 2-5

Rubbing Degradation of the Optical Properties of Aluminized Films

Material	Condition	α_s	ε [a]
First Surfaces			
Aluminized Mylar	As received	.081	.032
	Lightly rubbed	.116	.034
	Lightly rubbed	.145	.042
	Heavily rubbed	.429	.351
Aluminized Kapton	As received	.096	.032
	Lightly rubbed	.162	.067
	Lightly rubbed	.273	.100
	Heavily rubbed	.192	.075
Second Surfaces			
Aluminized FEP Teflon 1.27×10^{-4} m thick	As received	.134	.805
	Lightly rubbed	.137	.809
	Lightly rubbed	.147	.808
	Heavily rubbed	.138	.807

[a] Infrared Emittance. Measured by Gier-Dunkle Method. From Kordsmeier & Peters (1972).

Additional recommendations concerning handling may be found under Terrestrial Degradation § 2.3.2.

2.2.4. REPAIRING

Damaged surfaces can be removed and replaced.

INTENTIONALLY BLANK PAGE

2.3. DEGRADATION

2.3.1. INTRODUCTION

The degradation in the thermal performance of the tapes depends on the materials, the construction, the application technique, the substrate, and the environment. The main degradation effects are: change in the thermo-optical characteristics of the surface, and loss of contact between the tape and the substrate.

General ideas concerning the degradation of adhesive tapes, which have been mainly borrowed from Brown & Merschel (1970), are given in the following paragraphs.

2.3.2. TERRESTRIAL DEGRADATION

1) Humidity Exposure.

Emittance of almost all tapes having a metallic surface is seriously degraded.

Absorptance increases slightly.

Emittance and absorptance of the backing films are not affected.

Comments. The effects of moisture, which are especially noteworthy in the case of aluminized coatings, can be minimized through use of protective packaging and control of storage and assembly environments.

When environmental control cannot be exercised, substitution of goldized for aluminized films is recommended (Kordsmeier & Peters (1972)).

2) Long Term Exposure to Air.

ADHESIVE TAPES

Degradation

Emittance increases slightly.

Absorptance does not change significantly.

2.3.3. SPACE DEGRADATION

Thermo-optical properties of the first surface metallized films and metal foil tapes are essentially stable.

The second surface metallized and clear polyimide film tapes are relatively stable.

The second surface metallized and clear polyester film tapes exhibit large increases in solar absorptance.

FEP type A Teflon films are extremely resistant to damage from UV irradiation. Table 2-6 shows optical measurements and UV degradation data of commercially available sheets of FEP type A Teflon, 1.27×10^{-4} m thick, coated on one side with vaccum deposited Silver plus a protective layer of evaporated Inconel. All samples have been obtained from sheets or tapes produced by G.T. Schjeldahl Company except sample identified as "control" which was coated by NASA Goddard Space Flight Center's Engineering Applications Branch. Since the purpose of the study was to evaluate the acceptability of the commercially supplied coated film, several samples were cut from four different sheets as is indicated in the insert of Table 2-6. Roman numbers are used to distinguish between original sheets. In addition two tape rolls were tested which are identified as TI and TII.

Fig 2-3 gives the variation of solar absorptance in simi-

ADHESIVE TAPES

Degradation

Table 2-6

Thermal Radiation Properties of Second Surface Silver-Teflon (1.27×10^{-4} m thick)

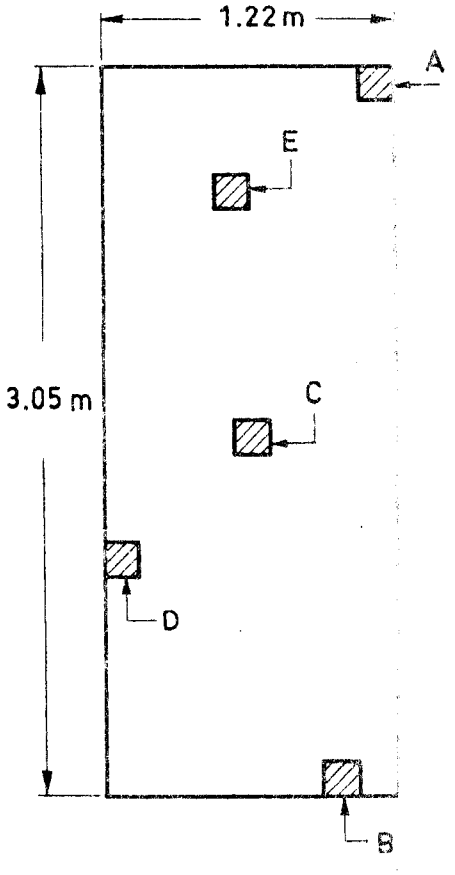

Sample	α_s [a]	$\Delta\alpha_s$ [b]	ε' [c] ($\beta'\sim0$)	ε [d]	α_s/ε
Control	.088	+ .003	.812	.767	.111
IA	.085		.804	.760	.112
IB	.082		.805	.761	.108
IC	.084	+ .001	.800	.756	.111
ID	.080		.799	.757	.106
IE	.082	+ .001	.802	.759	.108
IIA	.087	.000	.809	.765	.127
IIB	.087	- .002	.806	.762	.114
IIC	.084		.802	.759	.111
IID	.080		.803	.759	.105
IIIA	.085	- .002	.807	.763	.110
IIIB	.083		.806	.762	.110
IIIC	.083		.807	.763	.109
IIID	.091	- .001	.803	.759	.120
IVA	.082		.795	.755	.109
IVB	.078	- .003	.801	.757	.124
IVC	.078	- .002	.806	.762	.115
IVD	.078		.806	.762	.104
TI- (1/8 way in TI-End)	.087	+ .005	.814	.769	.113
TII-Beginning	.085	+ .002	.807	.763	.106
TII-Middle	.080		.801	.757	.119

[a] From spectral reflectance data. Integrating sphere reflectometer used to cover the region 2.9×10^{-5} to 2.4×10^{-6} m, and hohlraum reflectometer to extend the range up to 8×10^{-6} m.

Precision: ± .003; Accuracy: ± .010

[b] After 200 ESH UV irradiation from a filtered Xenon arc source (Spectrolab x-25).

[c] Measured at 300 K using a Gier-Dunkle DB-100 portable infrared reflectometer.

Precision: ± .005; Accuracy: ± .010

[d] Calculated assuming $\varepsilon = .945\ \varepsilon'$

From Heaney (1974).

ADHESIVE TAPES

Degradation

lar specimens, as measured on board OSO-H, IMP-I and IMP-H satellites.

The OSO-H was in near earth orbit and was not subjected to charged particle irradiation, thence the data indicate that Silver-Teflon is not degraded by UV irradiation only. The initial value quoted in Fig 2-3 corresponds to the 20th orbit (20th orbit ∿ 20 ESH ∿ 30 orbital h) due to a malfunction in the tape recorder.

The degradation experienced by the Silver-Teflon coating on board IMP-I is considered to be the result of solar wind and high energy proton irradiation rather than solar UV irradiation. During the first 9 months in orbit, the temperature of the detector plate gradually rose from 202.5 K to 219 K, corresponding to an increase in the coating solar absorptance of .077. This value remained constant for another 7 months, at which time data keeping was ceased. Nearly 4 months later the spacecraft passed through an apogee shadow of almost 6 h duration. Data acquired again after this event shown that there was a sudden increase in detector plate temperature to 223 K with a continual rise thereafter, indicating that Teflon is susceptible to damage by charged particles. The estimated fluxes are given in the Table 2-7.

Concerning IMP-H, the initial α/ε values measured in flight were 50% larger than the laboratory values. The discrepancy has been attributed to blistering of Teflon (Triolo (1973)). Data presented show again that Teflon may be damaged by charged particles.

ADHESIVE TAPES

Degradation

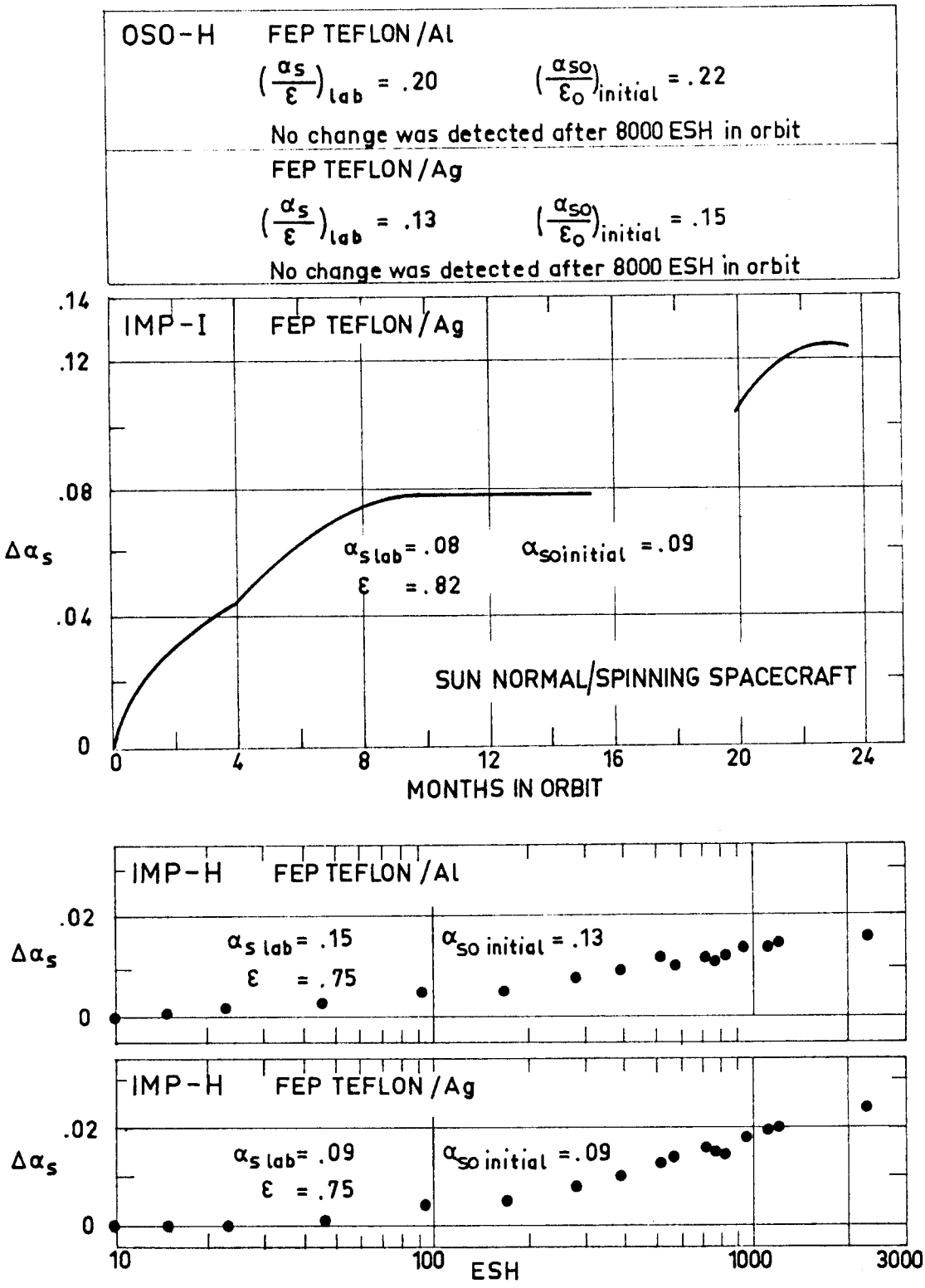

Fig 2-3. Space degradation of second surface mirrors based on 1.27×10^{-4} m thick FEP Teflon. All data are from Triolo (1973) except those corresponding to IMP-I which are from Hoffman (1973).

ADHESIVE TAPES

Degradation

Table 2-7

Exposure Conditions of Silver-Teflon on IMP-1 Spacecraft

Source	Intensity [MeV]	Integrated Flux [particles.m^{-2}]
Solar Wind		3×10^{19}
Electrons	All energies	10^{18}
Protons	.1 - 5	3×10^{18}
	4 - 50	3×10^{16}
	Above 50	3×10^{14}

From Hoffman (1973).

2.3.4. BLISTERING

Blistering, Fig 2-4, occurs whenever the adhesive bond strength is locally exceeded by a lifting force. These forces are mainly due to:

1) Thermal expansion of air entrapped in the bond area.

2) Outgassing of the adhesive or substrate.

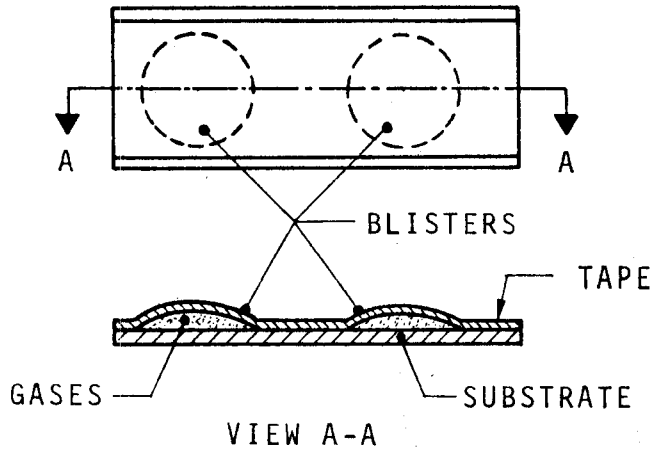

Fig 2-4. Sketch of a blistering tape. From Brown & Merschel (1970).

Blistering of thermal control tapes inhibit the heat transfer through the tape-surface interface. When the purpose of the tape is to increase the emittance of a hot-plate, blistering would tend to create

ADHESIVE TAPES
Degradation

a partial shield between the plate and its surrounding. The added thermal resistance increases the substrate temperature which may in turn increase the blister size. Similarly, blistering may seriously affect the thermal behavior of tapes used as a solar collector surfaces.

Table 2-8 gives the blistering temperature of tapes applied to an aluminium substrate and exposed to 13.3 to 133 Pa pressure while temperature was being increased in steps of 7 K up to 385 K.

2.3.4.1. PRECAUTIONS AGAINST BLISTERING

Several rules to avoid blistering are given by Stevens (1971). Although these rules concern a particular tape (aluminium foil Mystik 7402 L), it is hoped that they can be applied in more general cases.

1) The use of too wide tapes should be avoided. Tapes of $5\times\times10^{-2}$ m to 7.5×10^{-2} m width are recommended.
2) Whenever possible, the tapes should be baked in order to reduce outgassing.

As quoted by Stevens, samples baked at 394 K for 24 h had a significantly reduced blistering, as compared with unbaked samples, when applied on a piece of 2020 Aluminium plate washed with detergent and then cleaned with xylene.

The protective lacquer was removed before baking.

ADHESIVE TAPES

Degradation

Table 2-8

Blistering Temperatures of Tapes Applied to an Aluminium Substrate [a]

Type	Description			Temperature [K]			
	Coating	Backing	Adhesive	T_1	T_2	T_3	T_4
3M Co. 53	Aluminium	Mylar	Rubber	361	364	378	
3M Co. 56		Mylar	Rubber	311			
3M Co. 425	Al. Foil			336		344	366
3M Co. 428 A	Al. Foil		Acrylic	>383			341-389
3M Co. 850 S	Aluminium	Mylar	Acrylic	311	336	344	378
3M Co. 850 G	Gold	Mylar	Acrylic				383
3M Co. 853	Aluminium	Mylar		366	378		
3M Co. Y-9184 A	Gold	Kapton	Silicone	344	353	361	
Mystik 7390				<333			
Mystik 7402 L	Al. Foil		Silicone	311	319	328	
Mystik 7430	Lead Foil		Rubber	319	328	336	
Mystik 7453	Al. Foil		Acrylic	>386			366
Mystik 7455	Al. Foil	Glass Cloth		300	311	319	
G.T. Schjeldahl GT 102000-4	Al. on nylon tulle	Kapton	Acrylic	328		336	364
G.T. Schjeldahl GT 103300	Aluminium	Kapton	Silicone	297	311[b]	>380	
TF-12				308		333	

T_1, Temperature at which blistering first occurred in thermal vacuum. Sample applied to a cleanser scrubbed aluminium sheet stock.

T_2, Temperature at which an increase in blister size was noted.

T_3, Temperature at which blisters were so large and numerous that almost entire tape area was delaminated.

T_4, Temperature at which blisters occurred on tapes tested after 10 d of humidity per MIL-STD-202, Method 106 B; applied to aluminium sheet conversion coated per MIL-C 5541.

a Single sample per tape.

b There was some increase in size and number of blisters at that temperature, but not further increase at higher temperatures.

From Brown & Merschel (1970).

ADHESIVE TAPES

Degradation

Comments. There is some disagreement in connection with the usefulness of baking.

1) Brown & Merschel (1970) reported no increase in the blistering resistance of 3M Co. 850G tape after baking in vacuum at 366 K and $.34\times10^{4}$ to 1.4×10^{4} Pa for 24 h.

2) Baking does not appear to be a practical means to improve tape performance. If the baking process is performed by the manufacturer, large quantities of tape would have to be ordered to achieve a reasonable price. On the other side, the use of especial drying fixtures, vacuum ovens and high level clean room procedures would invalidate the main advantage of pressure sensitive adhesive tapes, which is the ease of application.

3) Tape application under vacuum conditions has been suggested by Brown & Merschel (1970). This process eliminates air entrapment reducing the cause of blister formation. However, taping under vacuum requires special tooling and equipment which makes the process expensive and cumbersome.

4) Perforating the tape to open ways out to entrapped air, solvents or volatile constituents, could improve the blistering characteristics of tapes. Perforations having $8\times\times10^{-4}$ m diameter on 1.5×10^{-2} m centers have been used by

ADHESIVE TAPES

Degradation

Stevens (1971). The thermo-optical characteristics of the coating are not seriously degraded by the presence of such a few small holes.

Spiked rollers to perforate the tapes are available.

In order to avoid introducing solvents within the adhesive, the protective lacquer (if present) must be removed prior to perforation of the foil.

5) Tests performed with different application pressures (13 N, 27 N and 45 N on approximately 4×10^{-3} m^2) shown that the tape should be just setted on the substrate. In the experiments reported by Stevens only the lightly applied tapes remained free of blisters after the test. It is believed that the light application pressure kept the adhesive from sealing the gas escape paths.

   Light application of pressure is also required when using perforated tapes to avoid the flowing of adhesive towards the perforations thereby sealing them.

6) When the tape is applied externally it is advisable to provide mechanical fastening on both ends to prevent lifting forces from peeling the tape away from its substrate. (Breuch (1967)).

7) As a general rule it should be said that rubber and silicone-based adhesives are unacceptable, because of poor outgassing behavior, unless baked at elevated temperatures (Kordsmeier & Peters (1972)).

ADHESIVE TAPES

Relevant Properties of Thermal Control Tapes

2.4. RELEVANT PROPERTIES OF THERMAL CONTROL TAPES

Thermal radiation, adhesion and outgassing properties of widely used adhesive tapes are given in Tables 2-9 to 2-11. Any tape whose solar absorptance, α_s, and total hemispherical emittance, ε, are known to the compiler has been included in the pertinent table.

As an aid in the selection of the most appropriate tape, the thermal radiation properties from these tables have been plotted in Fig 2-5. The number next to each data point identify the tape in the tables. The first digit in these numbers, 1, 2 or 0, indicates whether the tape is first surface metallized (Table 2-9), second surface metallized (Table 2-10) or clear (Table 2-11), respectively.

Values of the mass/area ratio for several films and tapes are given in Table 2-12.

Table 2-13 presents data on general-purpose tapes which meet two criteria concerning outgassing: they have a maximum of 1.0 percent weight loss, and a maximum of .1 percent (in weight) of volatile condensable materials.

Availability of the tapes is not always indicated in the brochures sent by the manufacturers. Tape dimensions are generally from 10^{-2} m to .5 m in width, and either 33 m or 66 m in length. Normal sheets are 1.22 m wide by 3.05 m long.

Concerning costs, the following approximate figures have been quoted by Scollon & Carpitella (1970)

Aluminized Teflon 45 US $.m^{-2}

Series Emittance 45-60 US $.m^{-2}.

INTENTIONALLY BLANK PAGE

ADHESIVE TAPES

Relevant Properties of Thermal Control Tapes

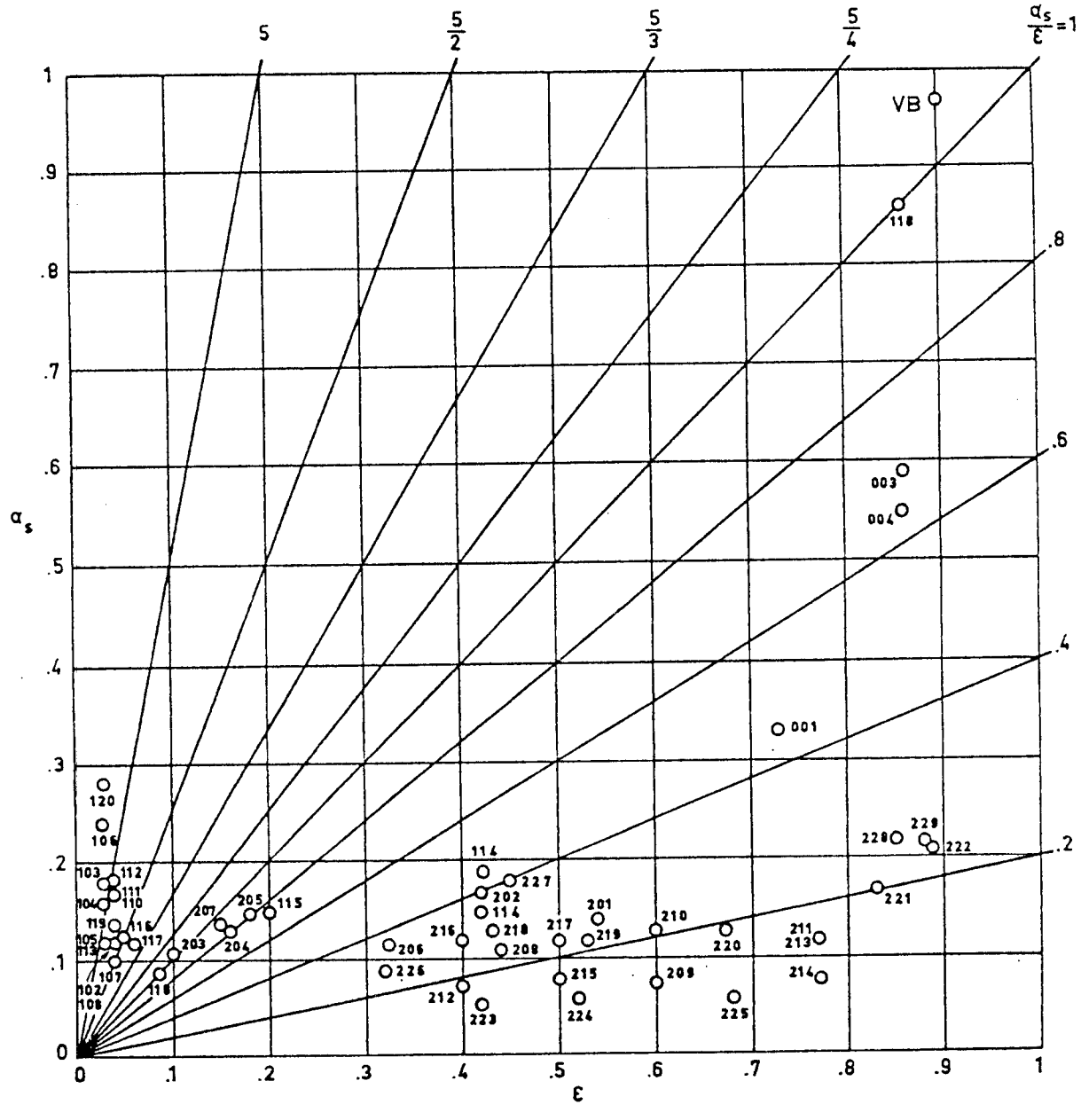

Fig 2-5. Solar absorptance, α_s, vs. total hemispherical emittance, ε, of several thermal control tapes.

ADHESIVE TAPES

Relevant Properties of Thermal Control Tapes

Table 2-9

Properties of First Surface Metallized Tapes [a]

Type	Description			Thickness, $t \times 10^4$ [m]		Temperature Range [K]	
	Coating	Backing	Adhesive	Backing	Total	Intermittent	Continuous
101. Fasson S-277 I	Al. Foil+ +Lacquer Coating		Acrylic S-277	.51 (metal foil)		464[b]	
102. Fasson S-277 II	Aluminium Foil		Acrylic S-277	.51 (metal foil)		464[b]	
103. 3M Co. 425	Aluminium Foil		Acrylic [c]	.76 [c]	1.27		Up to 588 [c]
104. 3M Co. Y-9040	Aluminium Foil		Silicone		.51		
105. 3M Co. Y-9050	Aluminium Foil	Glass Cloth	Silicone		1.52		
106. 3M Co. Y-9184	Gold vacuum deposited	Kapton	Silicone				
107. 3M Co. Y-9360	Al. vacuum depos. both sides	Mylar	Acrylic	.25			
108. Mystik 7402	Aluminium Foil		Silicone	.51 (metal foil)[c]	1.12[c]	700 (Internal)[b] 670 (External)[b]	
109. Mystik 7430	Lead Foil		Rubber	1.27 (metal foil)[c]	1.65[c]		
110. Mystik 7452	Aluminium Foil		Acrylic	.51 (metal foil)[c]	.94[c]		
111. Mystik 7453	Aluminium Foil		Acrylic	.76 (metal foil)[c]	1.30 [c]		
112. Mystik 7455	Aluminium Foil	Glass Cloth		1.14[c]	1.30 [c]	Up to 3600 short term[c]	194 to 560[c]
113. Permacel EE6600	Aluminium vacuum deposited	Mylar	Rubber				
114. G.T. Schjeldahl G 101500 [d]	SiO_x on Al. both vacuum deposited	Kapton	Silicone	.13		88 to 533	88 to 422
115. G.T. Schjeldahl G 10200-4	Al. vacuum depos. over nylon tulle	Kapton	Acrylic	.13			
116. G.T. Schjeldahl G 103300	Aluminium vacuum deposited	Kapton	Silicone	.25		88 to 533	88 to 42?
117. G.T. Schjeldahl G 103500	Aluminium vacuum deposited	Kapton	Silicone	.13			
118. G.T. Schjeldahl G 107000	Thick film black	Kapton	Silicone	.13		88 to 422	88 to 380

ADHESIVE TAPES

Relevant Properties of Thermal Control Tapes

Thermal Radiation Properties			Mechanical Properties		Outgassing [e]			Comments
α_s / ε	α_s/ε	Stability to Space Degradation	Peel Strength $(F/w)\times10^{-2}$ [N.m^{-1}]	Specification	% TWL / % VCM	CURE t [h] / CURE T [K]	ATMOS.	
					1.367 / .421	16 / 338	Air	
.04±.02 [b] / .12±.04 [b]	3.00							
.04±.02 [b] / .04±.01 [b]	3.00							
.18 / .03	6.00	Good	7.00 / 10.00 [f]	ASTM D1000	.240 / .030	0		
.16 / .03	5.33	Good			1.120 / .640	0		
.12 / .03	4.00	Good			.917 / .380	0		
.24 [e] / .03 [e]	8.00	Good	1.75	ASTM D1000	2.240 / .410	0		
.10 / .04	2.50	Good			.79R .79S / .06R .03S	0		
.12±.04 [b] / .04±.02 [b]	3.00	Good	4.71 [c] / 3.85	MIL-T-81287 / ASTM D1000	1.69R 2.09S / .35R .54S	0		α=.07. From blackbody [b] at 920 K
.09		Good	6.68 [c] / 10.70	HH-T-29 / ASTM D1000				
.17 / .04	4.25	Good	6.57 [c]		.37 .25R / .04 .03R	0		
.17 / .04	4.25	Good	7.99 [c] / 6.48 / 9.63 [f]	LT-80 / ASTM D1000	.092R / .003R	0		
.18 / .04	4.50	Good	4.60 [c] / 6.48	ASTM D1000	3.820 1.710 / 2.620 1.340	0 24 / 0 423	Air	
.12 [g] / .03 [g]	4.00				>8.50 / >3.80	0		
<.15 / .42	.35-.45		1.10	ASTM D1000 (to Al.)				
.15±.03 / .20±.07	.75	Good	3.15 / 5.43 [f]	ASTM D1000				
<.13 / .05	2.50	Good	1.75 [a] / 1.10 [d]	ASTM D1000 / ASTM D1000 (to Al.)	1.48P / .32R	0		
.10-.14 [h] / <.06	1.70-2.30 [h]							
.86 / >.76	1.00							

(Continued onto next page)

ADHESIVE TAPES

Relevant Properties of Thermal Control Tapes

Table 2-9 (Continued)

Properties of First Surface Metallized Tapes [a]

Type	Description			Thickness, $t \times 10^4$ [m]		Temperature Range [K]	
	Coating	Backing	Adhesive	Backing	Total	Intermittent	Continuous
119. G.T. Schjeldahl G 401000	Aluminium vacuum deposited	Kapton	Acrylic	.25		88 to 505	88 to 395
120. G.T. Schjeldahl G 402600	Gold vacuum deposited	Kapton	Silicone	.25		88 to 505	88 to 395

[a] All data in this table, unless otherwise stated, are from Brown & Merschel (1970).

[b] From Breuch (1967).

[c] Manufacturer's data.

[d] Data concerning G.T. Schjeldahl tapes are from bulletins issued by the producer, except those corresponding to GT 102000-4 which are given by Brown & Merschel (1970).

ADHESIVE TAPES

Relevant Properties of Thermal Control Tapes

Thermal Radiation Properties			Mechanical Properties		Outgassing [e]			Comments
α_s / ε	α_s/ε	Stability to Space Degradation	Peel Strength $(F/w)\times10^{-2}$ [N.m^{-1}]	Specification	% TWL / % VCM	CURE t [h] / CURE T [K]	ATMOS.	
.14 / .05	2.80		2.19	ASTM D1000 (to Al.)				
.25-.28 / .035	8.00		1.10	ASTM D1000 (to Al.)				

[e] Outgassing characteristics have been borrowed from Campbell, Marriott & Park (1973)
TWL: Total Weight Loss. VCM: Volatile Condensable Materials (by weight)
A zero indicates that cure conditions are unknown.
R: Several layers of the tape were rolled on a glass Rod to permit outgassing at the edges.
S: The tape was placed on a Screen exposing the adhesive of the first layer.

[f] 90° peel strength of tape bonded to aluminium sheet exposed to 340 K in air for 30 d. From Brown & Merschel (1970).

[g] From Kordsmeier & Peters (1972).

[h] From Scollon & Carpitella (1970).

ADHESIVE TAPES

Relevant Properties of Thermal Control Tapes

Table 2-10

Properties of Second Surface Metallized Tapes [a]

Type	Description			Thickness, t×10^4 [m]		Temperature Range [K]	
	Plastic	Metal	Adhesive	Plastic	Total	Intermittent	Continuous
201. 3M Co. 850 Silver	Mylar	Aluminium vacuum deposited	Acrylic		.63		223 to 423[b]
202. G.T. Schjeldahl [c] G 101500	Kapton	Al. vacuum deposited+ SiO_x	Silicone	.13		88 to 530	88 to 420
203. G.T. Schjeldahl G 101600	Kapton	Al. vacuum deposited+ SiO_x	Silicone	.13			
204. G.T. Schjeldahl G 101701	Kapton	Al. vacuum deposited+ SiO_x	Silicone	.13			
205. G.T. Schjeldahl G 101901	Kapton	Al. vacuum deposited+ SiO_x	Acrylic	.25			
206. G.T. Schjeldahl G 101902	Kapton	Al. vacuum deposited+ SiO_x	Acrylic	.25			
207. G.T. Schjeldahl G 102000	Kapton+Nylon tulle	Aluminium vacuum deposited	Acrylic	.13			
208. G.T. Schjeldahl G 107300	Kapton	Al. vacuum deposited+ SiO_x		.25			
209. G.T. Schjeldahl G 400100	FEP Teflon	Silver+Inconel both vacuum dep.	Acrylic	.51		88 to 505	88 to 395
210. G.T. Schjeldahl G 400200	FEP Teflon	Aluminium vacuum deposited	Acrylic	.51		88 to 505	88 to 395
211. G.T. Schjeldahl G 400400	Kapton	Aluminium vacuum deposited	Acrylic	1.27		88 to 505	88 to 395
212. G.T. Schjeldahl G 400600	FEP Teflon	Silver+Inconel both vacuum dep.	Acrylic	.13		88 to 505	88 to 395
213. G.T. Schjeldahl G 400800	FEP Teflon	Aluminium vacuum deposited	Acrylic	1.27		88 to 505	88 to 395
214. G.T. Schjeldahl G 401900	FEP Teflon	Silver+Inconel both vacuum dep.	Acrylic	1.27		88 to 505	88 to 395
215. G.T. Schjeldahl G 402500	FEP Teflon	Silver+Inconel both vacuum dep.	Acrylic	.25		88 to 505	88 to 395
216. G.T. Schjeldahl G 402800	FEP Teflon	Aluminium vacuum deposited	Acrylic	.13		88 to 505	88 to 395
217. G.T. Schjeldahl G 402900	FEP Teflon	Aluminium vacuum deposited	Acrylic	.25		88 to 505	88 to 395
218. G.T. Schjeldahl Series Emittance Tape	FEP Teflon	Aluminium vacuum deposited		.13			
219.				.25			

ADHESIVE TAPES

Relevant Properties of Thermal Control Tapes

Thermal Radiation Properties			Mechanical Properties		Outgassing [d]			Comments
α_s / ε	α_s/ε	Stability to Space Degradation	Peel Strength $(F/w)\times10^{-2}$ [N.m^{-1}]	Specification	% TWL / % VCM	CURE t [h] / CURE T [K]	ATMOS.	
.14 / .54	.26	Poor	4.38 / 13.84 [e]	ASTM D1000	.686 / .097	0		Kordsmeier & Peters (1972) give α_s=.15 ε=.61
<.15 / <.42 [f]	.35-.45 [f]							
/ .06-.14 [f]	1.00-1.20 [f]							
.10-.16 [f] / .11-.21 [f]	.70-1.00 [f]							
.12-.18 [f] / .14-.22 [f]	.70-1.00 [f]							
.09-.14 [f] / .28-.37 [f]	.32-.48 [f]							
.12-.16 [f] / .13-.17 [f]	.70-1.20 [f]							
.09-.13 [f] /	.19-.31 [f]							
.06-.09 / .6	.12		2.19	ASTM D1000 (to Al.)				
.13 / .6	.22		2.19	ASTM D1000 (to Al.)				
.10-.14 / .77	.14							
.06-.09 / .4	.18							
.10-.14 / .77	.18		2.19	ASTM D1000 (to Al.)				
.06-.10 / .77	.09		2.19	ASTM D1000 (to Al.)	.335R / .007R	0		
.06-.10 / .50	~.14		2.19	ASTM D1000 (to Al.)				
.10-.14 / .40	.27		2.19	ASTM D1000 (to Al.)				
.10-.14 / .50	.22		2.19	ASTM D1000 (to Al.)				
.13 [f] / .43 [f]	.30 [f]							
.12 [f] / .53 [f]	.23 [f]							

(Continued onto next page)

ADHESIVE TAPES

Relevant Properties of Thermal Control Tapes

Table 2-10 (Continued)

Properties of Second Surface Metallized Tapes [a]

Type	Description			Thickness, $t \times 10^4$ [m]		Temperature Range [K]	
	Plastic	Metal	Adhesive	Plastic	Total	Intermittent	Continuous
220. G.T. Schjeldahl Series Emittance Tape	FEP Teflon	Aluminium vacuum deposited		.51			
221.				1.27			
222.				2.54			
223. G.T. Schjeldahl Series Emittance Tape	FEP Teflon	Silver vacuum deposited		.13			
224.				.25			
225.				.51			
226.				1.27			
227. Series Emittance Tape	Polyvinyl butyral (Butvar)	Aluminium vacuum deposited		.19			
228.				.81			
229.				1.65			
230.				2.03			

[a] All data in this table, unless otherwise stated, are from Brown & Merschel (1970).

[b] Manufacturer's data. The tape remains flexible throughout the mentioned temperature range.

[c] Data concerning G.T. Schjeldahl tapes are from bulletins issued by the producer, unless otherwise stated.

ADHESIVE TAPES

Relevant Properties of Thermal Control Tapes

Thermal Radiation Properties			Mechanical Properties		Outgassing [d]			Comments
α_s / ε	α_s/ε	Stability to Space Degradation	Peel Strength $(F/w)\times10^{-2}$ [N.m^{-1}]	Specification	% TWL / % VCM	CURE t [h] / CURE T K	ATMOS.	
.13[e] / .67[e]	.19[f]	$\Delta\alpha_s$=0 [g]; $\Delta\alpha_s$=.07 [h]						
.17[e] / .83[e]	.20[f]							
.21[e] / .89[e]	.24[f]							Not included in G.T. Schjeldahl Bulletin
.055[e] / .42[e]	.13[f]							
.059[e] / .52[e]	.11[f]							
.059[e] / .68[e]	.087[f]	$\Delta\alpha_s$=0 [g]						
.090[e] / .82[e]	.11[f]							Data on degradation in Table 2-6 (Samples TI&TII)
.18[e] / .45[e]	.40[f]							
.22[e] / .85[e]	.26[f]							
.22[e] / .88[e]	.25[f]							
.17[e] /		$\Delta\alpha_s$=0 [i]; $\Delta\alpha_s$=.25 [j]						

[d] Outgassing characteristics have been borrowed from Campbell, Marriott & Park (1973)
TWL: Total Weight Loss. VCM: Volatile Condensable Materials (by weight)
A zero indicates that cure conditions are unknown
R: Several layers of the tape were rolled on a glass Rod to permit outgassing at the edges.
S: The tape was placed on a Screen exposing the adhesive of the first layer.

[e] 90° peel strength of tape bonded to aluminium sheet exposed to 340 K in air for 30 d. From Brown & Merschel (1970).

[f] From Scollon & Carpitella (1970).

[g] 180 EUVSH+4×10^6 rads X-ray. From Scollon & Carpitella (1970). EUVSH: Equivalent Ultraviolet Sun Hours.

[h] 51 EUVSH+1.5×10^{20} protons.m^{-2} at 3 KEV. From Scollon & Carpitella (1970).

[i] 250 EUVSH. From Scollon & Carpitella (1970).

[j] 70 EUVSH+2.1×10^{20} protons.m^{-2} at 4 KEV. From Scollon & Carpitella (1970).

ADHESIVE TAPES

Relevant Properties of Thermal Control Tapes

Table 2-11

Properties of Clear Tapes [a]

Type	Description			Thickness, $t \times 10^4$ [m]		Temperature Range [K]	
	Substrate	Plastic	Adhesive	Plastic	Total	Intermittent	Continuous
001. 3M Co. 850	Aluminium backside	Mylar	Acrylic	.51			223 to 423 [b]
002. 3M Co. 853	Aluminium	Mylar		.25			223 to 453 [b]
003. 3M Co. X-1173	low α_s Aluminium	Clear Kapton	Thermoset. Silicone	.51			
004. Mystik 7361	Aluminium	Kapton	Silicone	.25	.51±.05 [c]		195 to 560 [c]
005. G.T. Schjeldahl G 401100		Kapton	Acrylic	.25		88 to 505 [c]	88 to 395 [c]
Other Tapes							
3M Co. 53	Aluminium	Mylar	Thermoset. Rubber	.25			
VB 3M Co. Y-9244		Velvet Black/ Vinyl Film	Acrylic				

[a] All data in this table, unless otherwise stated, are from Brown & Merschel (1970).

[b] Manufacturer's data. The tape remains flexible throughout the mentioned temperature range.

[c] Manufacturer's data.

ADHESIVE TAPES

Relevant Properties of Thermal Control Tapes

Thermo-Optical Properties			Mechanical Properties		Outgassing [d]			Comments
α_s / ε	α_s/ε	Stability to Space Degradation	Peel Strength $(F/w)\times10^{-2}$ [N.m^{-1}]	Specification	% TWL / % VCM	CURE t [h] / CURE T [K]	ATMOS.	
.33 / .73	.45	Poor	2.74 [b]	ASTM D1000				Roll Length: 66m [c]
/ .76		Poor	4.38	ASTM D1000				Roll Length: 33m [c] 66m [c]
.59 / .86	.69	Good			2.150R 3.040S / 0.580R 1.390S	0 / 0		
.55 / .86	.64	Good	1.42 Min. [c] 1.64 Avg. [c]		1.150 1.380 / 0.200 0.550	0 / 0		Roll Length: 33 m [c] Roll Width: 7.62×10^{-2} m [c]
			2.19 [c]	ASTM D1000 (to Al.) [c]				
/ .79		Poor			1.026 / .131	3 / 394	Air	
.97 / .90	1.08	Good			6.760R 1.660S / .840R .160S	0 27 / 0 383	E-3	Additional outgassing data are given below [e]

[a] Outgassing characteristics have been borrowed from Campbell, Marriott & Park (1973).

TWL: Total Weight Loss. VCM: Volatile Condensable Materials (by weight)

A zero indicates that cure conditions are unknown.

R: Several layers of the tape were rolled on a glass Rod to permit outgassing at the edges.

S: The tape was placed on a Screen exposing the adhesive of the first layer.

E-3: Chamber pressure 10^{-3} torr = .133 Pa.

[e] These data have been obtained by Scannapieco (1967) by using the General Electric in-situ technique.

% TWL	% VCM	CURE t [h]	CURE T [K]	ATMOS.
4.8 ± .02	.40 ± .11	24	Room	$< 1.33\times10^{-3}$ Pa 341.5 ± 5 K
4.6 ± .02	.20 ± .11	24	Room	$< 1.33\times10^{-3}$ Pa 341.5 ± 5 K
		8	338 ± 5 Furnace pressure $<1.33\times10^{-3}$ Pa	

ADHESIVE TAPES

Relevant Properties of Thermal Control Tapes

Table 2-12

Mass-Area Ratio of Several Foils and Tapes

Type	Description			Plastic Thickness $\times 10^4$ [m]	(Mass/Area) $\times 10^2$ [kg.m^{-2}]
	Metal	Plastic	Adhesive		
Mystik 7361		Kapton	Silicone	.25	6.71
Mystik 7367		Kapton	Acrylic	.25	9.72
Mystik 7375		Tedlar	Acrylic	.51	11.92
G.T. Schjeldahl G 103300	Aluminium vacuum deposited	Kapton	Silicone	.25	7.75
G.T. Schjeldahl G 400300	Silver+Inconel both vacuum dep.	FEP Teflon		.51	10.85
G.T. Schjeldahl G 400900	Aluminium vacuum deposited	FEP Teflon		1.27	27.90
G.T. Schjeldahl G 401400	Silver+Inconel both vacuum dep.	FEP Teflon		.25	6.20
G.T. Schjeldahl G 402000	Aluminium vacuum deposited	FEP Teflon		.25	6.20
G.T. Schjeldahl G 402200	Inconel+Al. both vac. deposited	FEP Teflon		.25	6.20
G.T. Schjeldahl G 402300	Inconel+Al. both vac. deposited	FEP Teflon		.51	10.85

From manufacturers' bulletins.

ADHESIVE TAPES

Relevant Properties of Thermal Control Tapes

Table 2-13

Characteristics of Low-Outgassing Tapes [a]

Type	Description	Thick. $t \times 10^4$ [m]	Temp. Range [K]	Electrical	Mechanical	Outgassing [b]			Comments
	Backing	Backing	Intermit.	Dielectric Strength $\times 10^{-3}$ [V]	Peel Strength	% TWL	Cure t [h]	ATMOS.	
	Adhesive	Total	Continuous		Tack	% VCM	Cure T [K]		
3 M Co. 425	Aluminium	.76			7.11 9.98 [c]	.240	0		High temperature and reflectance qualities. Expands readily with thermal changes. Long ageing. Excellent moisture barrier.
	Acrylic	1.27	Up to 588			.030			
3 M Co. 850 Black	Mylar	.25			2.74	.770 R .650 R	0		Thermal, abrasion and solvent resistant. Long ageing. Bonds more firmly with time. Difficult to remove without adhesive transfer. Clear, red, white, and black tapes available
	Acrylic	.51	223 to 423			.020 R .090 R			
3 M Co. 850 Silver	Aluminized-Mylar				4.38 13.84 [c]	.686 R	0		Thermal and abrasion resistant. Good outdoor weathering. Excellent moisture barrier. Long ageing. Removal, after long bonding times, difficult without adhesive transfer. Length 66 m.
	Acrylic	.63	223 to 423			.097 R			
Mystik 7341	Mylar					.238 R	0		
	Acrylic					.041 R			
Mystik 7367	Kapton	.25		7.20 Min. 7.50 Avg.	3.28 Min. 4.70 Avg.	.639	0		High temperature, solvent, and moisture resistant. Electrically pure with excellent dielectric strength. High adhesion. Length 33 m on 7.62×10^{-2} m core. Color: Amber.
	Acrylic	.76±.08	211 to 450		1.42 Min. 1.75 Avg.	.049			
Mystik 7375	Tedlar	.51		4.90 Min 5.20 Avg.	5.58 Min. 6.79 Avg.	.341 R	0		Excellent outdoor weatherability, solvent and moisture resistant. High adhesion, conformability and elongation, and good dielectric strength. Abrasion resistant. Length 66 m on 7.62×10^{-2} m core. Color: White.
	Acrylic	.94±.10	211 to 450		2.41 Min. 3.06 Avg.	.007 R			
Mystik 7420	Copper	.41			6.02	.215 R	0		Temperature resistant, solderable.
	Acrylic	.89			1.14 m (Rolling ball)	.010 R			

[a] All data in this table, unless otherwise stated, are from manufacturer's bulletins.

[b] Outgassing characteristics have been borrowed from Campbell, Marriott & Park (1973).

TWL: Total Weight Loss. VCM: Volatile Condensable Materials (by weight)

A zero indicates that cure conditions are unknown.

R: Several layers of the tape were rolled on a glass Rod to permit outgassing at the edges.

S: The tape was placed on a Screen exposing the adhesive of the first layer.

[c] From Brown & Merschel (1970). 90° peel strength of tape bonded to aluminium sheet exposed to 338.5K in air for 30d.

INTENTIONALLY BLANK PAGE

2.5. PAST SPATIAL USE

Tapes are widely used in spacecraft as thermal control coatings. The following examples have been found. Launching date is given in parenthesis.

Explorers 12, 14, 15 and 26 - Energetic Particles Explorers (EPE). (Aug. 16, 1961. Oct. 2 and 27, 1962. Dec. 21, 1964). Aluminized tape or foil tape. (Rittenhouse & Singletary (1969)).

Mariner 2. (Aug. 27, 1962). Exposed wiring wrapped with Teflon-coated aluminium foil. (Rittenhouse & Singletary (1969)).

ERS. (Environmental Research Satellite). (Sept. 17, 1962, failed). External surface - Among other coatings, Gold vacuum deposited on Mylar tape 3M Co. Y-9181, and Aluminized foil tape 3M Co. 425, were used. (Rittenhouse & Singletary (1969)).

Vela. (Oct. 17, 1963). Aluminium foil tape (3M Co. 425) and aluminized Mylar tape (3M Co. 850) used as thermal control coatings. (Rittenhouse & Singletary (1969)).

Explorers 18, 21, and 28 - Interplanetary Monitoring Platform (IMP). (Nov. 27, 1963. Oct. 4, 1964. May 29, 1965). Small areas covered with aluminized or foil tape. (Rittenhouse & Singletary (1969)).

Ranger 6 through 9. (Jan. 30 and July 28, 1964. Feb. 17 and Mar. 21, 1965). Aluminized Mylar used for wrapping cable harnesses. (Rittenhouse & Singletary (1969)).

Nimbus 1. (Aug. 8, 1964). Aluminized Mylar and aluminized Teflon tapes used to cover the truss structure of the louvers. Electrical cable harnesses covered with the same tapes. (Rittenhouse & Singletary (1969)).

ADHESIVE TAPES

Past Spatial Use

Pegasus 1 and 2. (Feb. 16 and May 25, 1965). Tubing near electronics boxes-wrapped with aluminized Mylar tape. (Rittenhouse & Singletary (1969)).

Oscar 3. (Mar. 9, 1965). External surface - Non leafing aluminium paint on Mystik tape. (Rittenhouse & Singletary (1969)).

ERS 15 and 16. (July 20, 1965). Aluminized Mylar wrap, 3M Co. 850 applied over the bodies of valves prepared to perform several cold-welding experiments. (Rittenhouse & Singletary (1969)).

Apollo 1 through 15. (Feb. 26, 1966 - July 26, 1971). Gold tapes and aluminium tapes were used in the Command Module. (Rittenhouse & Singletary (1969)).

Aluminized tapes were used to attach multilayer insulations in the cryogenic propulsion systems of Saturn S-II stage. (Schroeder (1973)).

SERT II (Space Electric Rocket Test). (Feb. 3, 1970). About 27 m of 5×10^{-2} m wide Mystik 7402 L tape were used for thermal control. (Stevens (1971)).

OSO - H (Orbiting Solar Observatory). ( ). The following coatings, among others, were tested in the Thermal Control Coatings Experiment:

1) FEP Teflon 1.27×10^{-4} m thick coated with Silver ($\sim10^{-7}$ m thick), vacuum deposited, plus a layer of Inconel, attached to Al substrate by Mystik 7366 double backed adhesive tape.
2) Same as above except Aluminium is deposited instead of Silver-Inconel. (Triolo (1973)).

ADHESIVE TAPES

Past Spatial Use

IMP - I (Interplanetary Monitoring Platform). (March 13, 1971). A second surface mirror, vapor deposited Silver on 1.27×10^{-4} m thick FEP Teflon, was used to minimize the effect of the incident solar energy on a detector of the Energy Particle Experiment. The coating was applied by use of the pressure sensitive double sided adhesive tape Mystik 7366. Inconel is vapor deposited over the silver backing to protect this film from possible degradation by the adhesive. Data concerning the space degradation of this coating were already presented under the heading Space Degradation. (Hoffman (1973)).

IMP - H (Interplanetary Monitoring Platform). (Sept. 22, 1972). The following coatings, among others, were tested in the Thermal Control Coatings Experiment:

1) FEP Teflon 1.27×10^{-4} m thick coated with Silver ($\sim10^{-7}$ m thick), vacuum deposited, plus a layer of Inconel, attached to Al substrate by Mystik 7366 double backed adhesive tape. (metal side down).
2) Same as above except that Silver plus Inconel has been substituted for Aluminium. Preliminary results of the experiments undertaken during these two flights were compared with laboratory results in the paragraph dealing with Space Degradation. (Triolo (1973)).

Meteosat. (Geostationary European Meteorological Satellite). The following tapes are included in the Thermal Control Material List:

Fasson Bright Solid Aluminium Foil, $.51\times10^{-4}$ m thick, with S-277 adhesive. Used as thermal control coating.

G.T. Schjeldahl G 400200. FEP Teflon on Aluminium with Acrylic adhesive. Used as a Second Surface Mirror.

ADHESIVE TAPES

Past Spatial Use

Mystik 7300. Mylar film with Silicone Adhesive. Used for coating masks.

Mystik 7367. Kapton film with Acrylic Adhesive. Superinsulation assembly.

3M Co. 850. Mylar film with Acrylic Adhesive. Superinsulation assembly.

3M Co. 250. Adhesive tape, acrylic. Coating film adhesion.

THERMAL CONTROL SURFACES

References

Delmonte, J. 1947 "The Technology of Adhesives", Reinhold Publishing Corporation, New York, 1947, Chap. 8, pp. 178-228.

Van Wazer, J.R., Lyons, J.W., Kim, K.Y., Colwell, R.E. 1963 "Viscosity and Flow Measurement", Interscience Publishers, New York, 1963, Chap. 4, pp. 258-262.

Katz, I. 1964 "Adhesive Materials, Their Properties and Usage", Foster Publishing Company, Long Beach, California, 1964, Part I, Chap. 6, pp. 44-54.

Neel, C.B. 1964 "Measurement of Thermal-Radiation Characteristics of Temperature-Control Surfaces During Flight in Space", ISA Trans., Vol. 3, No. 2, pp. 108-122, April 1964.

Johnson, F.S. 1965 "Satellite Environment Handbook", 2nd ed. Stanford University Press, Stanford, California, 1965, Chap. 3, pp. 64-76.

Lewis, D.W., Thostesen, T.O. 1965 "Mariner-Mars Absorptance Experiment", in "Thermophysics and Temperature Control of Spacecraft and Entry Vehicles", Progress in Astronautics and Aeronautics, Vol. 18, G.B. Heller, Ed., Academic Press, New York, 1965, pp. 441-457.

Zerlaut, G.A., Harada, Y., Tompkins, E.H. 1965 "Ultraviolet Irradiation of White Spacecraft Coatings in Vacuum", in NASA SP-55, "Symposium on Thermal Radiation of Solids", Proceedings of a Symposium held at San Francisco, California, March 4-6, 1964, pp. 391-420.

Guillette, R.B., Brown, R.R., Seiler, R.F., Sheldon, W.R. 1966 "Effects of Protons and Alpha Particles on Thermal Properties of Spacecraft and Solar Concentrator Coatings", in "Thermophysics and Temperature Control of Spacecraft and Entry Vehicles", Progress in Astronautics and Aeronautics, Vol. 18, G.B. Heller, Ed., Academic Press, New York, 1966, pp. 413-440.

THERMAL CONTROL SURFACES

References

Miller, R.A., Campbell, F.J. 1966 "Effects of Low Energy Protons on Thermal Control Coatings", in "Thermophysics and Temperature Control of Spacecraft and Entry Vehicles", Progress in Astronautics and Aeronautics, Vol. 18, G.B. Heller, Ed., Academic Press, New York, 1966, pp. 399-412.

Breuch, R.A. 1967 "Handbook of Optical Properties for Thermal Control Surfaces", LMSC-A847882, Vol. III, Lockheed Missiles & Space Company, Sunnyvale, California, June 1967.

Neel, C.B. 1967 "Role of Flight Experiments in the Study of Thermal-Control Coatings for Spacecraft", in "Thermophysics of Spacecraft and Planetary Bodies", Progress in Astronautics and Aeronautics, Vol. 20, G.B. Heller, Ed., Academic Press, New York, 1967, pp. 411-438.

Reichard, P.J., Triolo, J.J. 1967 "Preflight Testing of the ATS-1 Thermal Coatings Experiment", in "Thermophysics of Spacecraft and Planetary Bodies", Progress in Astronautics and Aeronautics, Vol. 20, G.B. Heller, Ed., Academic Press, New York, 1967, pp. 491-513.

Scannapieco, J.F. 1967 "Final Report of Thermal Vacuum Weight Loss Study of Cat-a-Lac and 3M Velvet Black Paints", Radnor Project 73P057, General Electric, Missile and Space Division, Philadelphia, Pensylvania, Feb. 1967.

Schafer, C.F., Bannister, T.C. 1967 "Thermal Control Coating Degradation Data from the Pegasus Experiment Packages", in "Thermophysics of Spacecraft and Planetary Bodies", Progress in Astronautics and Aeronautics, Vol. 20, G.B. Heller, Ed., Academic Press, New York, 1967, pp. 457-473.

THERMAL CONTROL SURFACES

References

Zerlaut, G.A., Courtney, W.J. 1967 "Space-Simulation Facility for In Situ Reflectance Measurements", in "Thermophysics of Spacecraft and Planetary Bodies", Progress in Astronautics and Aeronautics, Vol. 20, G.B. Heller, Ed., Academic Press, New York, 1967, pp. 349-369.

Cagle, C.V. 1968 "Adhesive Bonding-Techniques and Applications", McGraw-Hill Book Company, New York, 1968, Chap. 5, pp. 86-123.

Caldwell, C.R., Nelson, P.A. 1968 "Thermal Control Experiments on the Lunar Orbiter Spacecraft", in "Thermal Design Principles of Spacecraft and Entry Bodies", Progress in Astronautics and Aeronautics, Vol. 21, J.T. Bevans, Ed., Academic Press, New York, 1969, pp. 819-852.

Marshall, K.N., Breuch, R.A. 1968 "Optical Solar Reflector: A Highly Stable Low α_s/ε Spacecraft Thermal Control Surface", Journal of Spacecraft and Rockets, Vol. 5, No. 9, Sept. 1968, pp. 1051-1056.

Millard, J.P. 1968 "An Uncertainty Analysis for Satellite Calorimetric Measurements", NASA TN D-4354, 1968.

Westcott, M. 1968 "The Measurement of Solar Abscrptance and Thermal Emittance", ESRO TN-23 (ESTEC), Jan. 1968.

Zerlaut, G.A., Noble, G., Rogers, F.O. 1968 "Development of Space Stable Thermal Control Coatings", Report No. IITRI-U6002-59, (NAS 8-5379), IIT Research Institute, Chicago, Illinois, 1968.

Brown, R.R., Fogdall, L.B., Cannaday, S.S. 1969 "Electron-Ultraviolet Radiation Effects on Thermal Control Coatings", in "Thermal Design Principles of Spacecraft and Entry Bodies", Progress in Astronautics and Aeronautics, Vol. 21, J.T. Bevans, Ed., Academic Press, New York, 1969, pp. 697-724

THERMAL CONTROL SURFACES

References

Cunnington, G.R., Grammer, J.R., Smith, F.J. 1969 "Emissivity Coatings for Low-Temperature Space Radiators", NASA CR-1420, (NAS 3-7630), Lockheed Missiles & Space Company, Sunnyvale, California, Sept. 1969.

Millard, J.P. 1969 "Results from the Thermal Control Coatings Experiment on OSO-III", in "Thermal Design Principles of Spacecraft and Entry Bodies", Progress in Astronautics and Aeronautics, Vol. 21, J.T. Bevans, Ed., Academic Press, New York, 1969, pp. 769-795.

Millard, J.P., Streed, E.R. 1969 "A Comparison of Infrared-Emittance Measurements and Measurement Techniques", Applied Optics, Vol. 8, No. 7, July 1969, pp. 1485-1492.

Rittenhouse, J.B., Singletary, J.B. 1969 "Space Materials Handbook", 3rd ed., NASA SP-3051, 1969, pp. 485-493.

Zerlaut, G.A., Rogers, F.O., Noble, G. 1969 "The Development of S-13 G-Type Thermal Control Coatings", in "Thermal Design Principles of Spacecraft and Entry Bodies", Progress in Astronautics and Aeronautics, Vol. 21, J.T. Bevans, Ed., Academic Press, New York, 1969, pp. 741-766.

Brown, G.L., Merschel, R.P. 1970 "Thermal Control Tapes for Spacecraft Applications", Proceedings of the Symposium on Thermodynamics and Thermophysics of Spacecraft Flight, Sponsored by USAF and Lockheed, Palo Alto, California, March 23-25, 1970, pp. 221-228.

DOW CORNING 1970 "Les Elastomères Silicones Silastic au Service des Bureaux d'Etudes", Dow Corning Int. Ltd., Chaussée de la Hulpe, 177, B-1170 Brussels, Belgium, 1970.

Fogdall, L.B., Cannaday, S.S., Brown, R.R. 1970 "Electron Energy Dependence for in Vacuum Degradation and Recovery in Thermal Control Surfaces",

THERMAL CONTROL SURFACES

References

in "Thermophysics: Applications to Thermal Design of Spacecraft", Progress in Astronautics and Aeronautics, Vol. 23, J.T. Bevans, Ed., Academic Press, New York, 1970, pp. 219-248.

Scollon, T.R., Carpitella, M.J. 1970 "Long Life High Reliability Thermal Control Systems Study Data Handbook", Contract NAS 8-26252, Space Systems Organization, General Electric Company, Valley Forge Space Technology Center, Philadelphia, Pennsylvania, 1970.

Sidney Gross 1970 "Modern Plastics Encyclopedia", McGraw-Hill Publications Company, New York, 1970, pp. 868-869.

Gilligan, J.E., Zerlaut, G.A. 1971 "The Space Environment Stability Problem in White Pigmented Coatings", 17th Annual Meeting Institute of Environmental Sciences, Los Angeles, California, April 1971, pp. 447-457.

McCargo, M., Spradley, L.W., Greenberg, S.A., McDonald, S.L. 1971 "Review of the Transient Degradation/Contamination of Thermal Coatings", LMSC-D1778, (NAS 8-26004), Lockheed Missiles & Space Company, Sunnyvale, California, 1971.

Spisz, E.W., Jack, J.R. 1971 "Thermal and Radiative Property Measurement of Thermal-Control Coatings by Cyclic Radiation" NASA TN D-6316, Apr. 1971.

Stevens, N.J. 1971 "Applicaton of Sert II Thermal Control Coatings", NASA TM X-2155, Feb. 1971.

Stevens, N.J., Smolak, G.R. 1971 "Report on the Flight Performance of the Z-93 White Paint Used in the Sert II Thermal Control System", in "Fundamentals of Spacecraft Thermal Design", Progress in Astronautics and Aeronautics, Vol. 29, J.W. Lucas, Ed., The MIT Press, Cambridge, Massachusetts, 1972, pp. 189-204.

THERMAL CONTROL SURFACES

References

Fry, J., Nicoletta, C.A. 1972 "Ultraviolet and Charged Particle Irradiation of Proposed Solar Cell Coverslide Materials and Conductive Coatings for the Helios Spacecraft", NASA TM X-65945, June 1972.

Kordsmeier, N.H., Peters, S.T. 1972 "Materials and Processes for Thermal Control Surfaces", in "Non-Metallic Materials Selection, Application and Environmental Effects", 4th National SAMPE Technical Conference and Exhibition, Palo Alto, California, 17-19 Oct. 1972, pp. 79-90.

Seidenberg, B., Park, J.J., Clatterbuck, C. 1972 "Achievement of a Low-Outgassing White Paint System for Spacecraft Thermal Control", NASA TN D-6892, August 1972.

Touloukian, Y.S., DeWitt, D.P., Hernicz, R.S. 1972 "Thermal Radiative Properties. Coatings", Thermophysical Properties of Matter, Vol. 9, IFI/Plenum, New York, 1972.

Zerlaut, G.A., Gilligan, J.E., Ashford, N.A. 1972 "Space Radiation Environmental Effects on Reactively Encapsulated Zinc Orthotitanates and Their Paints", in "Fundamentals of Spacecraft Thermal Design", Progress in Astronautics and Aeronautics, Vol. 29, J.W. Lucas, Ed., The MIT Press, Cambridge, Massachusetts, 1972, pp. 3-32.

Adams, V.W. 1973 "Prospero: The First Year in Orbit", RAE-TR-73 114, Royal Aircraft Establishment, Farnborough, England, Sept. 1973.

Campbell, Jr. W.A., Marriott, R.S., Park, J.J. 1973 "A Compilation of Outgassing Data for Spacecraft Materials", NASA TN D-7362, Sept. 1973, pp. 82-88.

Gilligan, J.E., Zerlaut, G.A. 1973 "Thermal Control Materials and Technology in the 1970s", Transactions of the ASME, Journal of Engineering for Industry, Vol. 95, Series B, No. 4, Nov. 1973, pp. 1065-1068.

Rev. 3. 1986

THERMAL CONTROL SURFACES

References

Hoffman, R.H. 1973 "Spaceflight Performance of Silver Coated FEP Teflon as a Thermal Control Surface on the IMP-I Spacecraft", NASA TM X-66242, April 1973.

Kemp, R.F., Beynon, J.C., Luedke, E.E., Hall, D.F. 1973 "Effects of Cesium Ions and Cesium Vapor on Selected ATS-F Samples", AIAA Paper No. 73-1099, AIAA 10th Electric Propulsion Conference, Lake Tahoe, Nevada, Oct. 31-Nov. 2, 1973.

Kirkpatrick, J.P., Brennan, P.J. 1973 "The Advanced Thermal Control Flight Experiment", AIAA Paper No. 73-757, AIAA 8th Thermophysics Conference, Palm Springs, California, July 16-18, 1973. Also Published in "Thermophysics and Spacecraft Thermal Control", Progress in Astronautics and Aeronautics, Vol. 35, R.G. Hering, Ed., The MIT Press, Cambridge, Massachusetts, 1974, pp. 409-430.

Millard, J.P., Pearson, Jr., B.D. 1973 "Optical Stability of Coatings Exposed to Four Years Space Environment on OSO-III", AIAA Paper No. 73-734, AIAA 8th Thermophysics Conference, Palm Springs, California, July 16-18, 1973. Also Published in "Thermophysics and Spacecraft Thermal Control", Progress in Astronautics and Aeronautics, Vol. 35, R.G. Hering, Ed., The MIT Press, Cambridge, Massachusetts, 1974, pp. 249-262.

Schroeder, C.J. 1973 "Insulation Commonality Assessment (Phase 1), Vol. 2", NASA CR-124473, Feb. 1973, Section 12.9, pp. 12-36.

Simon, J. 1973 "Actions des Ultra-Violets sur les Materiaux de Controle Thermique et Confrontation des Essais en Laboratoire avec les Performances Enregistrées en Vol", Séminaire International Simulation et Espace, Toulouse, France, Sept. 10-14, 1973.

THERMAL CONTROL SURFACES

References

Triolo, J.J. 1973 "General Aspects of Space Simulation Validity and Comparison between Laboratory and In-Flight Degradation", Séminaire International Simulation et Espace, Toulouse, France, Sept. 10-14, 1973.

Cunnington, G.R. 1974 Private communication, Lockheed, Palo Alto Research Laboratory, Palo Alto, California, Oct. 25, 1974.

ESTEC 1974 Private communication, Meteosat, Material List (Thermal Control), May 1974.

Fogdall, L.B., Cannaday, S.S. 1974 "Radiation Effects on Second Surface Mirrors", in "Evaluation de l'Action de l'Environnement Spatial sur les Materiaux", Centre National d'Etudes Spatiales, Toulouse, France, June 1974, pp. 549-560.

Gilligan, J.E., Harada, Y., Gates, D.W. 1974 "Current Technology for Development of Low α_s/ε Coatings", in "Evaluation de l'Action de l'Environnement Spatial sur les Materiaux", Centre National d'Etudes Spatiales, Toulouse, France, June 1974, pp. 567-587.

Heaney, J.B. 1974 "Evaluation of Commercially Supplied Silver Coated Teflon for Spacecraft Temperature Control Usage", NASA TM X-70588, Jan. 1974.

IITRI 1974 "Price Schedule for IITRI Services in Spacecraft Thermal Control Materials", IIT Research Institute, Chicago, Illinois 60616, July 1974.

Morelli, D. 1974 Private communicaton, OCLI, Santa Rosa, California, Oct. 23, 1974.

THERMAL CONTROL SURFACES

References

OCLI 1974 "Conductive Coated Second Surface Thermal Control Mirror - Product Specification 6068 002", OCLI Inc., P.O.B., 1599, Santa Rosa, California 95403, July 1974.

PROCOLOR 1974 Private communicaton, Procolor, Madrid, Oct. 28, 1974.

Simon, J. 1974 "Influence de la Temperature sur la Degradation des Revêtements de Contrôle Thermique Soumis a des Radiations Ultra-Violettes sous Vide", in "Evaluation de l'Action de l'Environnement Spatial sur les Materiaux", Centre National d'Etudes Spatiales, Toulouse, France, June 1974.

Stultz, J.W. 1974 "Solar Absorptance of Second Surface Mirrors for High Angles of Incidence", AIAA Paper No. 74-670, AIAA-ASME 1974 Thermophysics and Heat Transfer Conference, Boston, Massachusetts, July 15-17, 1974.

Toyama, M., Ito, T. 1974 "Pressure-Sensitive Adhesives", in "Polymer-Plastics Technology and Engineering", Vol. 2, L. Naturman, Ed., Marcel Dekker, Inc., New York, 1974, pp. 161-230.

Winkler, W., Stampfl, P. 1974 "Conductive Coatings (CC) a Concept to Achieve Electrostatic Cleanliness (ESC) on Satellites Completely Covered with Dielectric Materials. Scientific Requirements and Practical Approach on the Sunprobe Helios", in "Evaluation de l'Action de l'Environnement Spatial sur les Materiaux", Centre National d'Etudes Spatiales, Toulouse, France, June 1974, pp. 45-55.

Joslin, D.E., Kan, H.K.A. 1975 "Properties of Conductive Coatings for Thermal Control Mirrors and Solar Cell Covers", in NASA SP-379, "Eight Conference on Space Simulation", Proceedings of a Symposium held at Silver Spring, Maryland, Nov. 3-5, 1975, pp. 187-193.

THERMAL CONTROL SURFACES

References

Keyte, G.E. 1975 "The Prospero Thermal Control Surfaces Experiment-Investigation of Thermal Control Surface Materials in Space Environment", RAE-TR-75123, Royal Aircraft Establishment, Farnborough, England, Dec. 1975.

Paillous, A. 1975 "Qualification des Revêtements de Contrôle Thermique aux Rayonnements Ultra-Violets et Particulaires de l'Espace. Rapport Final", ONERA CERT DERTS EC 4025, Toulouse, France, 1975.

Rosen, A. 1975 "Large Discharges and Arcs on Spacecraft" Astronautics & Aeronautics, Vol. 13, No. 6, June 1975, pp. 36-44.

Winkler, W. 1975 "Helios Surface Materials, Test-Predictions and Test-Results of Orbit Conditions Compared with Mission Results", in NASA SP-379, "Eight Conference on Space Simulation", Proceedings of a Symposium held at Silver Spring, Maryland, Nov. 3-5, 1975, pp. 51-61.

Winkler, W., Brungs, W. 1975 "Helios Surface Materials Prediction for Orbit and Mission Results", IAF 75-021, XXVI Congress International Astronautical Federation, Lisbon, Sept. 21-27, 1975, Also published in Acta Astronautica, Vol. 3, No. 5-6, May-June 1976, pp. 395-406.

Winkler, W., Stampfl, W. 1975 "Conductive Coating: Problem of Electrostatic Cleanliness", Acta Astronautica, Vol. 2, No. 7-8, July-August 1975, pp. 745-754.

Adamo, R.C. Nanevicz, J.E. 1976 "Spacecraft-Charging Studies of Voltage Breakdown Processes on Spacecraft Thermal Control Mirrors", in "Spacecraft Charging by Magnetospheric Plasmas", Progress in Astronautics and Aeronautics, Vol. 47, A. Rosen, Ed., The MIT

THERMAL CONTROL SURFACES

References

Press, Cambridge, Massachusetts, 1976, pp. 225-235.

ASTRAL 1976a "Revêtement de Contrôle Thermique -PSG 120-", Astral Peintures et Vernis, 164 Rue Ambroise Croizat, 93204 Saint-Dénis, France, Janv. 1976.

ASTRAL 1976b "Primaire P 123", Astral Peintures et Vernis, 164 Rue Ambroise Croizat, 93204 Saint-Dénis, France, Janv. 1976.

ASTRAL 1976c "Primaire P 128", Astral Peintures et Vernis, 164 Rue Ambroise Croizat, 93204 Saint-Dénis, France, Janv. 1976.

Bentlage, H., Spanier, H.P., Wilkens, W. 1976 "Changes in Electrical Cross-Resistance of Conductive Coatings Due to Contamination by Outgassing of Silicon Rubber Material Silastic 35", NASA TT F-16727, April 1976.

Bourrieau, J., Paillous, A., Romero, M. 1976 "Degradations de Revêtements de Contrôle Thermique Sous L'Effect des Rayonements Ultraviolets et Particulaires. Rapport Final", ONERA CERT DERTS EC 4046, Toulouse, France, Oct. 1976.

INTA 1976 "S-13 G/LO Coating. Outgassing Test No. I-305", Private communication. Test performed on Aug. 2, 1976.

Lévy, L. 1976 "Irradiations par Electrons de Revêtements de Contrôle Thermique", ONERA CERT DERTS EC 4050, Toulouse, France, Oct. 1976.

Lévy, L., Sarrail, D. 1976 "Essai de Claquage sur un Echantillon de Paneau OSR de 65 mm x 65 mm Collés avec un Adhésif Conducteur", ONERA CERT DERTS EC 4052, Toulouse, France, Oct. 1976.

Paillous, A. 1976 "Degradation de Revêtements de Contrôle Thermique par Irradiations Ultraviolet-

THERMAL CONTROL SURFACES

References

tes et Particulaires",
ONERA CERT DERTS EC 4047, Toulouse, France, Oct. 1976.

Rolfo, A. 1976 "In Flight Results of a Cryogenic Cooler Designed for Meteosat", IAF 76-210, XXVII Congress International Astronautical Federation, Anaheim, California, Oct. 10-16, 1976.

Stultz, J.W. 1976 "Solar Absorptance of Second Surface Mirrors for High Angles of Incidence", Journal of Spacecraft and Rockets, Vol. 13, No. 1, Jan. 1976, pp. 57-59.

Weast, R.C. 1976 "Handbook of Chemistry and Physics", 57th ed., CRC Press, Inc., Cleveland, Ohio, 1976, p. F-170.

Winkler, W., Brungs, W. 1976 "Helios Surface Materials, Predictions for Orbit and Mission Results", Acta Astronautica, Vol. 3, No. 5-6, May-June 1976, pp. 395-406.

Paillous, A., Amat, M.T., Marco, J. Panabiere, G. 1977 "Irradiations par Protons et Irradiations par Electrons de Revêtements de Contrôle Thermique et de Films Polymériques. Tome 1 - Partie Expérimentale. Rapport Final", ONERA CERT DERTS EC 4059, Toulouse, France, 1977.

Taylor, J.W.R. 1977 "Jane's all the World's Aircraft, 1977-1978", Macdonald and Jane's Publishers Ltd., London, 1977, pp. 745-746.

Winkler, W. 1977 "Improved Model for Performance of Spacecraft Materials", Acta Astronautica, Vol. 4, No. 5-6, May-June 1977, pp. 709-726.

Bourrieau, J. 1978 "Irradiations par Protons et Irradiations par Electrons de Revêtements de Contrôle Thermique et de Films Polymériques. Tome 2 - Partie Théorique. Rapport Final", ONERA CERT DERTS EC 4059, Toulouse, France, 1978.

THERMAL CONTROL SURFACES

References

Campbell,Jr.,W.A., Marriott, R.S., Park, J.J. 1978 "An Outgassing Data Compilation of Spacecraft Materials", NASA RP 1014, Jan. 1978.

Curran, D.G.T., Millard, J.M. 1978 "Contamination/Degradation Measurements on Operational Satelite Thermal Control Surfaces", in "Heat Transfer and Thermal Control Systems", Progress in Astronautics and Aeronautics, Vol. 64, L.S. Fletcher, Ed., American Institute of Aeronautics and Astronautics, New York, 1978, pp. 236-289.

Koch, J. 1978 "Some Current Developments in Solar Array Technology at AEG-Telefunken", in ESA SP-140, "Photovoltaic Generators in Space", K. Bogus & T.D. Guyenne, Eds., Proceedings of a Symposium held at ESTEC, Noordwijk, The Netherlands, Sept. 11-13, 1978, pp. 33-40.

RHONE-POULENC 1978 "Rhodorsil RTV 121", Informations Silicones Rhodorsil E-09-6, Rhone-Poulenc, Département Silicones, 33, rue Jean Goujon, 75008 Paris, Cedex 08, Sept. 1978.

Triolo, J.J., Heaney, J.B., Hass, G. 1978 "Coatings in Space Environment", SPIE Vol. 121, Optics in Adverse Environment, Proceedings of the Seminar, San Diego, California, Aug. 25-26, 1977. Society of Photo-Optical Instrumentation Engineers, Bellingham, Washington, 1978, pp. 45-66.

Bachofer, B.T. 1979 "Landsat D - Case Study in Spacecraft Design", AIAA Professional Study Series, AIAA Educational Programs, New York, Aug. 1979.

Benaïsa, B., Lévy, L., Paillous, A., Sarrail, D. 1979 "Satellite Spacecraft Charging Control Materials", ONERA CERT DERTS Interim Scientific Report, Toulouse, France, July 1979.

Rev. 3. 1986

THERMAL CONTROL SURFACES

References

Bosma, S.J. 1979 "Microscopic Investigation of Electrostatic Discharge Phenomena on Nonconductive Optical Solar Reflectors with a Conductive Adhesive", ESA STM-211, March 1979.

Bosma, J., Levadou, F. 1979 "Electrostatic Charging and Space Materials", in ESA SP-145, "Spacecraft Materials in Space Environment", J. Dauphin & T.D. Guyenne, Eds., Proceedings of a Symposium held at ESTEC, Noordwijk, The Netherlands, Oct. 2-5, 1979, pp. 189-207.

Bourrieau, J., Paillous, A. 1979 "Effect of Radiations on Polymers and Thermal Control Coatings", in ESA SP-145, "Spacecraft Materials in Space Environment", J. Dauphin & T.D. Guyenne, Eds., Proceedings of a Symposium held at ESTEC, Noordwijk, The Netherlands, Oct. 2-5, 1979, pp. 227-245.

Guillaumon, J.C., Guillin, J. 1979 "Paints, Potting Compounds and Silicone Varnishes with Low Outgassing in Space Environment", in ESA SP-145, "Spacecraft Materials in Space Environment", J. Dauphin & T.D. Guyenne, Eds., Proceedings of a Symposium held at ESTEC, Noordwijk, The Netherlands, Oct. 2-5, 1979, pp. 63-66.

Hall, D.F., Fote, A.A. 1979 "Preliminary Flight Results from P78-2 (SCATHA) Spacecraft Contamination Experiment", in ESA SP-145, "Spacecraft Materials in Space Environment", J. Dauphin & T.D. Guyenne, Eds., Proceedings of a Symposium held at ESTEC, Noordwijk, The Netherlands, Oct. 2-5, 1979, pp. 81-90.

Harada, Y., Wilkes, D.R. 1979 "Inorganic Zn_2TiO_4 Thermal Control Coatings", in "The Enigma of the Eighties: Environment, Economics, Energy", SAMPE National Business Office, Azusa, California, 1979, Vol. 24, Book 2, pp. 936-944.

THERMAL CONTROL SURFACES

References

Lehn, W.L. 1979 "New Space Materials Developments in the United States", in ESA SP-145, "Spacecraft Materials in Space Environment", J. Dauphin & T.D. Guyenne, Eds., Proceedings of a Symposium held at ESTEC, Noordwijk, The Netherlands, Oct. 2-5, 1979, pp. 37-47.

Preuss, L., Schäfer, W. 1979 "Coating and Contamination Experiment on LDEF", in ESA SP-145, "Spacecraft Materials in Space Environment", J. Dauphin & T.D. Guyenne, Eds., Proceedings of a Symposium held at ESTEC, Noordwijk, The Netherlands, Oct. 2-5, 1979, pp. 71-80.

Taylor, J.W.R. 1979 "Jane's all the World's Aircraft, 1979-1980", Macdonald and Jane's Publishers, Ltd., London, 1979, pp. 677 and 680.

Bosma, J., Froggatt, M. 1980 "Evaluation of a Conductive Adhesive System for the Grounding of Aluminised Kapton Coated with Indium/Tin Oxide", ESA STM-213, Aug. 1980.

Bouchez, J.P., Gülpen, J. 1980 "The European Geostationary Communication Satellite OTS - Two Years of Thermal Control Experience in Orbit", AIAA Paper No. 80-1500, AIAA 15th Thermophysics Conference, Snowmass, Colorado, July 14-16, 1980.

ESTEC 1980 "Co-ordination of Materials Studies", Data Sheet No. 28, 4th Quarter 1980, ESTEC, Noordwijk, The Netherlands.

Hall, D.F., Fote, A.A. 1980 "α_s/ε Measurements of Thermal Control Coatings on the P78-2 (SCATHA) Spacecraft", AIAA Paper No. 80-1530. AIAA 15th Thermophysics Conference, Snowmass, Colorado, July 14-16, 1980. Also published in "Heat Transfer and Thermal Control", Progress in Astronautics and Aeronautics, Vol. 78, A.L. Crosbie, Ed., American Institute of Aeronautics and Astronautics, New York, 1981, pp. 467-486.

THERMAL CONTROL SURFACES

References

Kruczynski, L.R. 1980 "Astrodynamics", Astronautics and Aeronautics, Vol. 18, No. 12, Dec. 1980, pp. 32-33.

Koons, H.C., Mizera, P.F., Fennell, J.F. Hall, D.F. 1980 "Spacecraft Charging-Results from the SCATHA Satelite", Astronautics and Aeronautics, Vol. 18, No. 11, Dec. 1980, pp. 44-47.

OCLI 1980 "Second Surface Thermal Control Mirror (Standard Type) - Product Specification 6065 002", OCLI Inc., P.O.B. 1599, Santa Rosa, California 95403, June 1980.

Rajagopalan, R., Willson, W.J. 1980 "Thermal Performance of Anik-B Satellite in Orbit", AIAA Paper No. 80-1498, AIAA 15th Thermophysics Conference, Snowmass, Colorado, July 14-16, 1980.

Amartin, M., Paillous, A. 1981 "Comportement de Deux Types d'OSR en Silice Argentés a Couche d'ITO sous Irradiation par Electrons de 5 a 20 keV", ONERA CERT DERTS EC 4134, Toulouse, France, Juillet 1981.

ASTRAL 1981 "PSZ 184", Astral Peintures et Vernis, 164 rue Ambroise Croizat, 93204 Saint-Dénis, France, Avril 1981.

Bosma, J. 1981 Private communication, ESTEC, Noordwijk, The Netherlands, Dec. 14, 1981.

Bouchez, J.P., Howle, D. 1981 "The Orbital Test Satellite OTS-2-Two Years of Orbital Thermal Control Experience", ESA Bulletin, No. 26, May 1981, pp. 54-61.

Clark, L.G. 1981 "LDEF Mission 1 - Experiment Description", Preliminary Copy, Langley Research Center, NASA, Sept. 1981.

ESTEC 1981 "Co-ordination of Materials Studies", Data Sheet No. 30, 2nd Quarter 1981, ESTEC, Noordwijk, The Netherlands.

THERMAL CONTROL SURFACES

References

Fawcett, J.A. 1981 Private communication, OCLI Europe, High Wycombe, Buckinghamshire, England, June 10, 1981.

Guillaumon, J.C., Guillin, M.J. 1981 "Development of Low Outgassing Resins and Electrical Conductive Paints for Thermal Control and Space Applications", AIAA Paper No. 81-1182. AIAA 16th Thermophysics Conference, Palo Alto, California, June 23-25, 1981.

Harada, Y. 1981 Private communication. IITRI, Chicago, Illinois, Jan. 30, 1981.

Hyman, N.L. 1981 "Solar Absorptance Degradation of OSR Radiators on the COMSTAR Satelites", AIAA Paper No. 81-1185. AIAA 16th Thermophysics Conference, Palo Alto, California, June 23-25, 1981.

Pence, W.R., Grant, T.J. 1981 "α_s Measurements of Thermal Control Coatings on Navstar Global Positioning System Spacecraft", AIAA Paper No. 81-1186. AIAA 16th Thermophysics Conference, Palo Alto, California, June 23-25, 1981.

Rolfo, A. 1981 "In Flight Contamination and Changes in Thermo Optical Properties Measurements", AIAA Paper No. 81-1184. AIAA 16th Thermophysics Conference, Palo Alto, California, June 23-25, 1981.

Wilkens, W. 1981 Private communication, DFVLR, Braunschweig, Germany, March 19, 1981.

Guillaumon, J.C. 1982 "Development du Nouveaux Revêtements de Contrôle Thermique pour les Vehicles Spatiaux", in "Spacecraft Materials in Space Environment", A. Rolfo, J. Dauphin & T.D. Guyenne, Eds., ESA SP-178, Paris, 1982, pp. 21-26.

Guillaumon, J.C., Blett, L. 1982 "Peinture Blanche Conductrice (PCBZ CNES) - Compte Rendu de Qualification", CNES Report CT/PRT/SST/TH/331, Dec. 1982.

THERMAL CONTROL SURFACES

References

Ahern, J.E., Karperos, K.	1983	"Calorimetric Measurements of Thermal Control Surfaces on Operational Satellites", AIAA Paper No. 83-0075, AIAA 21st Aerospace Sciences Meeting, Reno, Nevada, Jan. 10-13, 1983.
Chalmers, D.R., Konzok, H.G., Bouchez, J.P., Howle, D.	1983	"OTS-2: Five Years of Thermal Testing on a Satellite in a Geostationary Orbit", in "Proceedings of the International Symposium on Environmental and Thermal Systems for Space Vehicles", T.D. Guyenne & J.J. Hunt, Eds., Toulouse, France, 4-7 Oct. 1983. ESA SP-200, Paris, 1983, pp. 425-436.
Guillaumon, J.C.	1983	"Peinture Blanche Conductrice (PCBZ CNES). Qualification de l'Application Directe (Sans Pl28) sur les Alliages Legers", CNES Report CT/DRT/SST/TH/2326, Oct. 1983.
NFT 30-0 14	1983	"Détermination du Temps d'Écoulement des Peintures, Vernis et Préparations Assimilées au Moyen des Coupes Françaises", Sept. 1983.
Paillous, A., Millan, Ph.	1983	"Irradiation Ultraviolette des Peintures Blanches Conductrices PCB-Z et PCB-T", ONERA CERT DERTS EC 4169, Toulouse, France, Mars 1983.
Cull, R.A., Stevenson, G., Harada, Y., Mell, R.	1984	"Requalification of S-13 G/LO", AIAA Paper No. 84-1775, AIAA 19th Thermophysics Conferences, Snowmass, Colorado, June 25-28, 1984.
Henninger, J.H.	1984	"Solar Absorptance and Thermal Emittance of Some Common Spacecraft Thermal-Control Coatings", NASA RP 1121, Apr. 1984.
INTA	1984	"PCB Z Coating. Outgassing Test", Private communication. Test performed on March 12, 1984.
MASTER	1985	"Departement Aerospatial", Master Peintures Pamiers, June 1985.

THERMAL CONTROL SURFACES

References

Siliconas Hispania	1985	Private communication, Barcelona, 1 Oct. 1985.
Guillaumon, J.C.	1986	Private communication, Toulouse, 25 Feb. 1986.
Zwaal, A.	1986	Private communication, Noordwijk, 13 March 1986.
Domingo, E.	1987	Private communication, Madrid, 30 Jan. 1987.
3M Co.		"Technical Data for Industry", Data Sheets D-14, D-20, D-21, D-22 and F-5. 3M Co., St. Paul, Minnesota 55101.
MYSTIK		"Mystik Brand Industrial Tape Selector", and "Mystik Brand Insulation Tape Selector", Mystik Tape Division, Winnetka, Illinois 60093.
SCHJELDAHL		Data Sheets G 4001, G 4002, G 4008, G 4015 and G 4019, "Capability Bulletin - Thermal Control Materials", Schjel-Bond, Product Bulletin No. EP-301, and Sample Bulletin No. EP-401, G.T. Schjeldahl Company, Northfield, Minnesota 55057.

INTENTIONALLY BLANK PAGE

INSULATIONS

Table of Contents

INSULATIONS

Table of Contents

INSULATIONS

List of Symbols

LIST OF SYMBOLS

A , Area. [m^2].

C , Coefficient for the Degradation Due to a Joint. [m].

D , Dissipation Factor.

D_K , Knudsen Diffusion Coefficient. [$m.s^{-1}$].

E , Modulus of Elasticity. [Pa].

E_c , Compressive Modulus of Elasticity. [Pa].

E_f , Flexural Modulus of Elasticity. [Pa].

F , Propagating Tear Strength in a Foil. [N].

F_{HC} , View Factor. Fraction of the Total Radiation which Arrives at C Coming from H.

K_0 , Constant Dependent on the Interaction between Gas and Porous Medium. [m].

L , Length. [m].

L^* , Equivalent Length for the Degradation because of a Joint. [m].

M , Gas Molecular Mass. [$kg.mol^{-1}$].

N , Chap. 1: Factor Relating the Radiative Contribution to the Effective Thermal Conductivity of a Foam to the Warm Boundary Temperature.

Chap. 3: Number of Shields in an MLI.

Number of Patch Layers in an MLI.

N_A , Avogadro Constant. $N_A = 6.02252 \times 10^{23}$ mol^{-1}.

P , Applied Compressive Load. [Pa].

INSULATIONS

List of Symbols

Q , Heat Flow through the Insulation. [W].

Outgassing Rate. [$Pa.m.s^{-1}$].

R , Electrical Resistance of a Foil. [Ω per Square].

Boltzmann Constant. $R = 1.38054 \times 10^{-23}$ $J.K^{-1}$.

$R(2\pi,\beta')$, Reflectance Factor. Irradiation over a Complete Hemisphere.

S , Steric Factor Accounting for the Distortion of the Heat Flow Path Due to Foam Expansion.

T , Temperature. [K].

Tm , Arithmetic Mean Temperature. [K].

V , Gas Volume Flow Rate per Unit Area of the Insulation. [$m.s^{-1}$].

a , Absorption Coefficient. [m^{-1}].

c , Specific Heat. [$J.kg^{-1}.K^{-1}$].

c_p , Gas Specific Heat at Constant Pressure. [$J.kg^{-1}.K^{-1}$].

$\bar{c}$, Average Molecular Speed. [$m.s^{-1}$]. $\bar{c}=\sqrt{8RT/\pi m}$.

d , Diameter. [m].

f , Frequency. [Hz].

h , Thermal Conductance. [$W.m^{-2}.K^{-1}$].

k , Thermal Conductivity. [$W.m^{-1}.K^{-1}$].

k_g , Gas Thermal Conductivity. [$W.m^{-1}.K^{-1}$].

k_{rad} , Radiative Contribution to the Effective Thermal Conductivity. [$W.m^{-1}.K^{-1}$].

m , Mass of One Molecule. [kg].

$\dot{m}$, Mass Flow Rate per Unit Cross-Sectional Area. [$kg.m^{-2}.s$].

INSULATIONS

List of Symbols

m_h , Mass Flow Rate per Unit Cross-Sectional Area of an Isolated Hole. [$kg.m^{-2}.s$].

n , Refractive Index.

n_s , Number of Spacer Layers per Shield.

p , Gas Pressure. [Pa].

Chap. 3: Fraction of the Electrons Suffering Specular Reflection at the Surface of a Metallic Film.

p_o , Ambient Pressure. [Pa].

s , Scattering Coefficient. [m^{-1}].

t , Insulation Thickness. [m].

t' , Spacer Thickness. [m].

t_c , Coating Thickness. [m].

$t_{c\Omega}$, Coating Thickness as Measured by the Electrical Resistance Method. [m].

t_u , Uncompressed Insulation Thickness. [m].

t , Time. [s] or [min].

w , Width. [m].

x , Geometrical Coordinate.

$\Delta L/L$, Linear Thermal Expansion.

α , Chap. 2: Sound Absorption Coefficient.

Chap. 3: Absorptance.

Thermal Diffusivity.

α_s , Normal Solar Absorptance.

α'_λ , Directional Spectral Absorptance.

INSULATIONS

List of Symbols

β , Chaps. 1 and 3: Linear Thermal Expansion Coefficient.

Chap. 3: Angle between Surface Normal and Direction of Incident Flux. [Angular Degrees].

β' , Angle between Surface Normal and Direction of Reflected, Emitted or Transmitted Flux. [Angular Degrees].

δ , Strain.

ε , Hemispherical Total Emittance.

ε_a , Apparent Emittance of a Groove.

ε_r , Dielectric Constant.

ε' , Directional Total Emittance.

θ , Groove Angle. [Angular Degrees].

κ , Permeability of a Porous Medium. [m^2].

λ , Wavelength of the Incident Radiation. [m].

Mean Free Path. [m].

μ , Dynamic Viscosity. [Pa.s].

π , Pressure Differential. [Pa].

ρ , Density. [$kg.m^{-3}$].

Chaps. 1 and 3: Reflectance.

Chap. 3: Bulk Electrical Resistivity. [$\Omega.m$].

σ , Chaps. 1 and 3: Stefan-Boltzmann Constant.

$\sigma = 5.6697 \times 10^{-8}$ $W.m^{-2}.K^{-4}$.

Chap. 1: Strength, Either Tensile, Compressive or Flexural. [Pa].

σ_0 , Yield Strength. [Pa].

INSULATIONS

List of Symbols

τ , Chap. 1: Shear Strength. [Pa].

Chap. 3: Fractional Area of Perforations or Transmittance of a Perforated Shield.

τ_0 , Shear Yield Strength. [Pa].

Subscripts

C , Cold Boundary.

H , Hot Boundary.

e , Concerns MLI Evacuation by Edge-Controlled Pumping.

eff , Effective.

eff$\perp$, Normal Effective ($\perp$ is omitted except when normal and lateral heat transfer appear simultaneously).

eff$\parallel$, Lateral Effective (same comment as for $\perp$).

h , Concerns MLI Evacuation by Hole-Controlled Pumping.

i , Concerns the ith Layer or the ith Joint of an MLI.

ult , Concerns Ultimate Strength.

Superscripts

j , Concerns Species j.

Acronyms

F , Flammable.

NF , Non-Flammable.

LS , Linear Shrinkage, Percent.

INSULATIONS

List of Symbols

MLI , Multilayer Insulations.

SE , Self-Extinguishing.

TWL , Total Weight Loss, Percent.

VCM , Volatile Condensable Materials, Percent by Weight.

gpd , Grams per Denier.

FOAMS

General

1. FOAMS

1.1. GENERAL

Foams are commonly used as insulating materials in building, storage vessels, sports equipment, spacecraft, and others. They can be also used for potting and encapsulation of shock-sensitive components and for packaging. Because they have many advantages for cryogenic and space applications, efforts have been made to develop suitable foams; establish their physical, chemical and structural properties, and integrate foams with thermal insulation systems.

Because of their cellular structure of discrete or interconnected voids, a large percentage of the foam volume is air, or whatever gas was used as the expanding agent, thence foams are lightweight and have very low thermal conductivity, that could be decreased further by evacuation. In most cryogenic applications the insulation efficiency is achieved by condensation of the gases contained in the cellular structure of the plastic material (cryopumping).

The main shortcomings of the foams are that they are not gas-tight, that their mechanical properties are relatively poor, and that thermal stresses induce cracks which require the use of constrictive wraps to maintain the insulation integrity.

According to their chemical composition foams may be classified in inorganic and organic.

Inorganic foams have been used at elevated temperatures. These foams are difficult to produce and have inferior physical properties than organic foams at low densities (16 to 80 $kg.m^{-3}$).

FOAMS

General

Organic foams, on the other hand, can be readily manufactured in low densities. These foams are used, in the range of cryogenic temperatures, either as a single insulation or combined with other materials to form an integrated system.

Three basic problems should be condidered regarding the application of organic foams as thermal insulators, namely: thermal conductivity, thermal expansion and contraction, and flammability and explosion hazards.

1. Thermal Conductivity. Thermal conduction through a foam combines solid conduction, gas conduction and radiation. Although an effective thermal conductivity, in the Fourier law sense, can be measured with relative ease, analytical models are available for predicting the thermal conductivity and the net heat flow through candidate foam materials to be used as thermal insulators.

The solid thermal conductivity of most foams varies with temperature in an almost linear manner as with many other materials. When the density decreases, the solid conductivity will be reduced, not only because the decreasing of the solid cross section, but also by the influence of a steric factor since, even assuming that the shape of the cells is independent of the density, expansion elongates the paths through which heat must flow. As an illustration Fig 1-1 shows the calculated variation of the thermal conductivity of a polyurethane resin as a function of foam density.

The second mode of heat transfer is gas conduction. In the case of closed-cell foams the gas thermal conductivity is a function

FOAMS

General

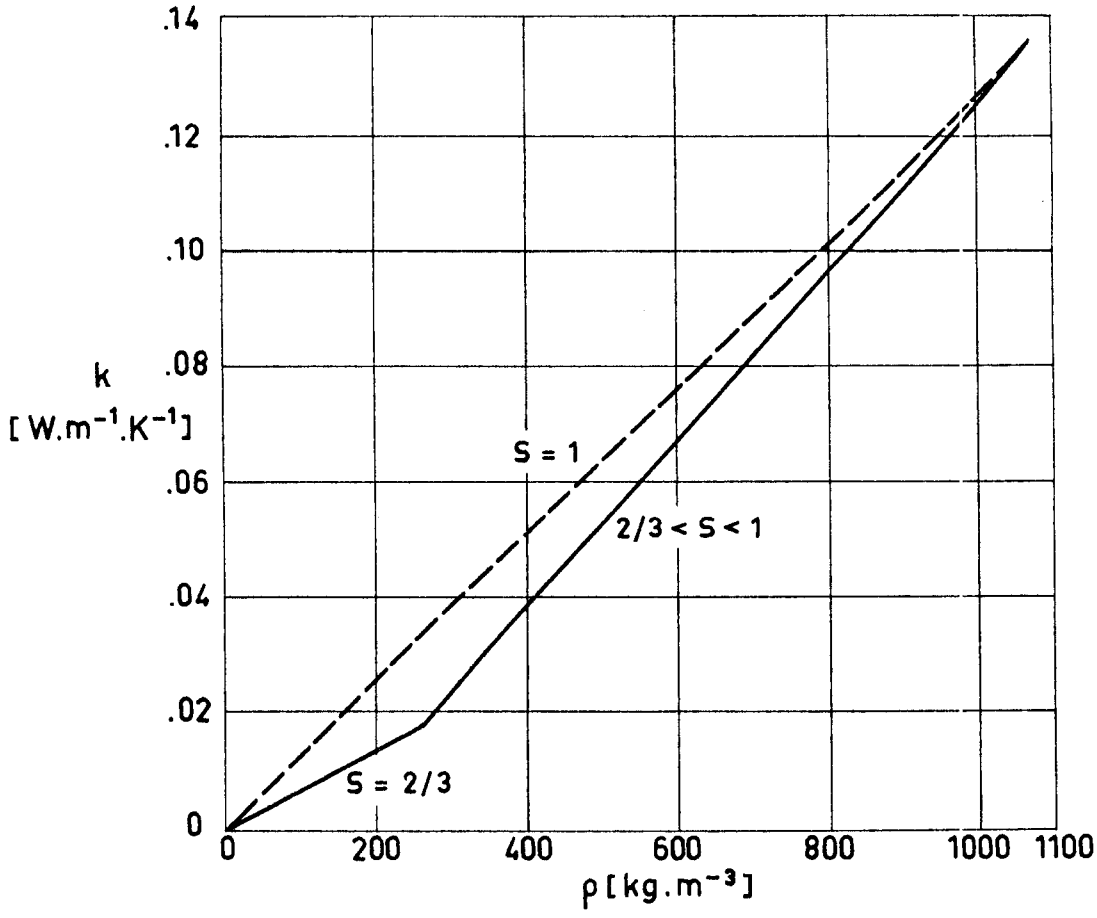

Fig 1-1. Resin thermal conductivity, k, as a function of foamed resin density, ρ. S is the steric factor which takes into account the distortion of the heat flow paths because expansion of the foam. Polyurethane resin. From Hammond (1969).

of the concentration of both the foaming agent and the air which may diffuse into the foam from outside. Since condensation can take place the thermal conductivities of both gases will depend not only on temperature but also on pressure. Fig 1-2 gives the gas thermal conductivity for mixtures of Freon 11, a typical foaming agent, and air, at atmospheric pressure, as a function of temperature.

In most spacecraft applications the foam is outgassed, so

FOAMS

General

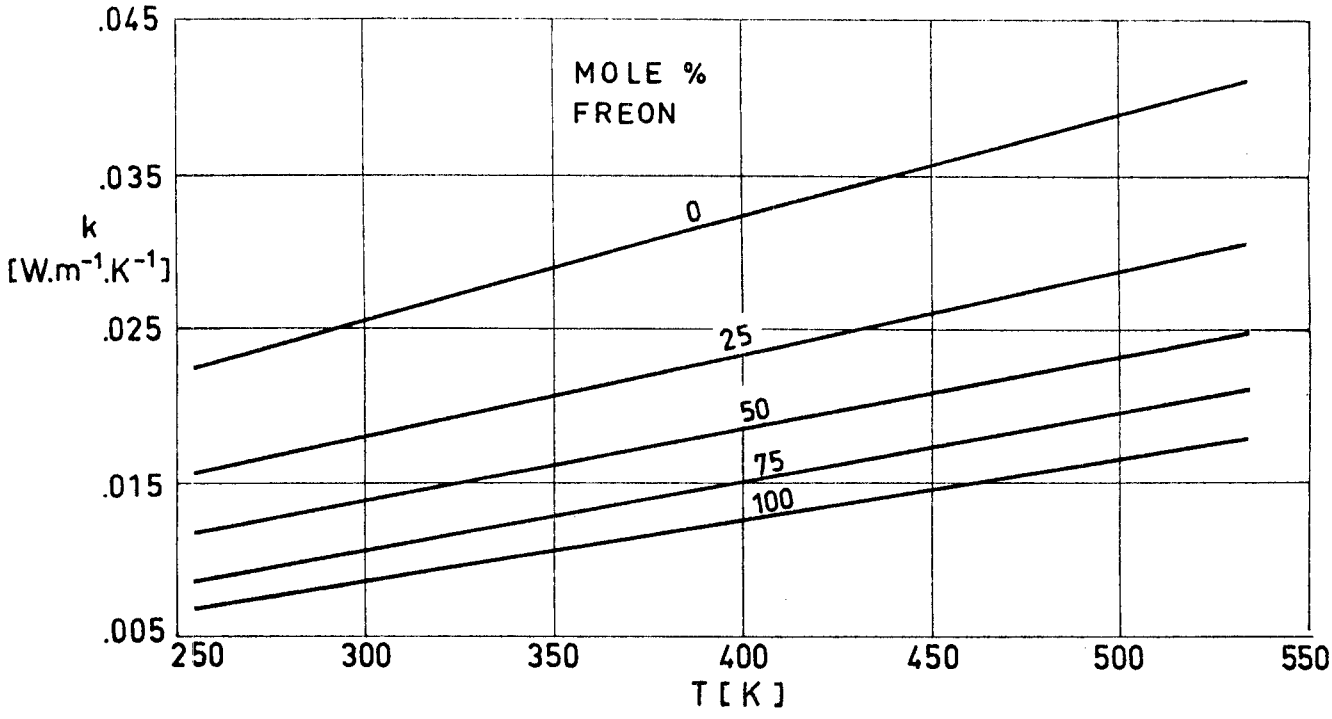

Fig 1-2. Gas thermal conductivity, k, for mixtures of Freon 11 and air as a function of temperature, T, for different concentrations of Freon 11. From Hammond (1969).

that gas conductivity is kept small enough to be neglected as compared with the other thermal conductivities. However, in the case of foams sprayed on cryogenic tanks for insulating purposes, the air has enough time to diffuse into the foam, possibly degrading the insulation characteristics in an amount which must be estimated. For example: in a typical case (Schroeder (1973)b) a total cure of 72 hours is required, after spraying the foam, before the cryogenic exposure of the tank wall.

The radiative transfer of heat within the foam involves simultaneous transmission, absorption and scattering. According to Hammond (1969) the radiative contribution to thermal conductivity of

FOAMS

General

the foam can be written as

$$k_{rad} = N\sigma \frac{T_H^4 - T_C^4}{a(T_H - T_C)} = 4N\sigma \frac{T_H^3}{a} \quad ,$$

where: N, constant factor which lies between .5 (for low temperatures) and 2 (for high temperatures).

T_C, T_H, cold and warm boundary temperatures, respectively. [K].

a, foam absorption coefficient. [m^{-1}].

σ, Stefan-Boltzmann Constant. [$W.m^{-2}.K^{-4}$].

Values of the radiation thermal conductivity are given in Fig 1-3 versus mean temperature, Tm. It can be deduced from this fig-

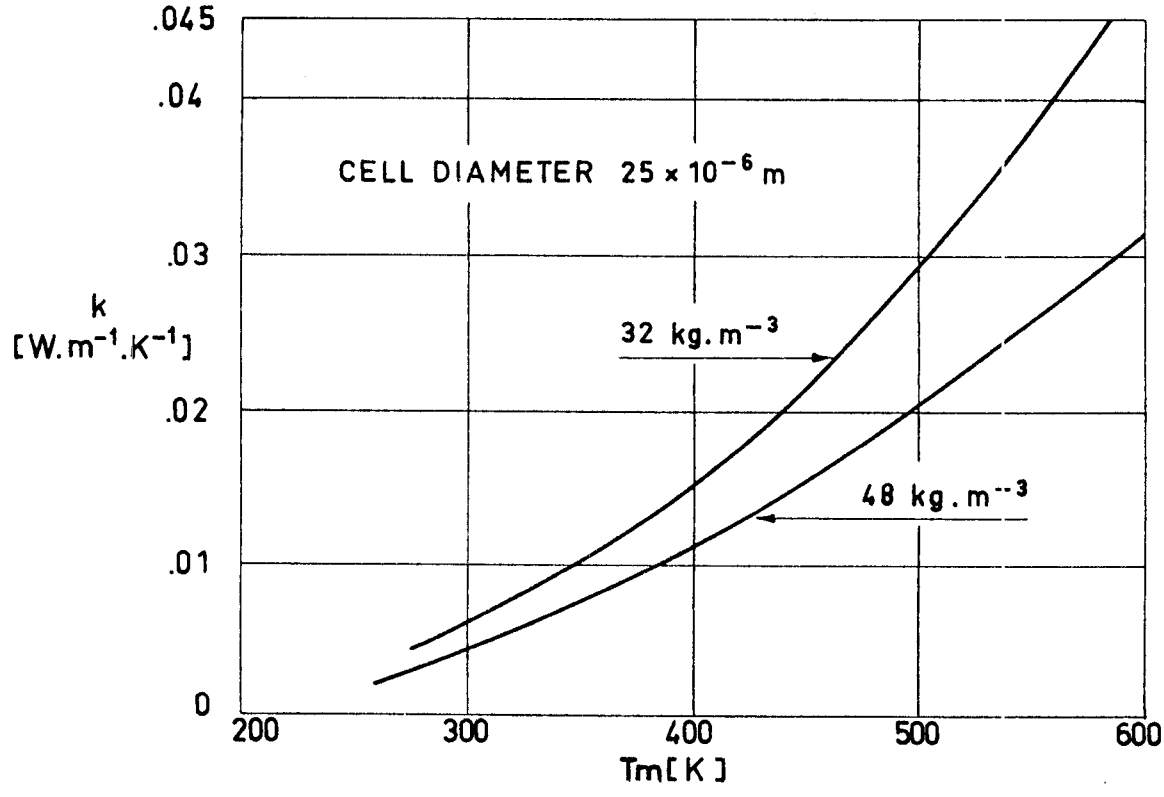

Fig 1-3. Radiation thermal conductivity, k_{rad}, as a function of mean temperature, Tm, for two polyurethane foams. From Hammond (1969).

ure that radiation becomes significant above 350 K.

2. Thermal Expansion and Contraction. Broadly speaking, the thermal expansion coefficient of polyurethane foams is 2 to 5 times that of aluminium and 4 to 10 times that of steel. Because of this large difference in thermal expansions, the foam cannot be foamed in place against the metal or bonded directly to it, since during chilldown from ambient temperature to cryogenic temperatures high stresses will be created in the foam, and it will fail either in shear along the tank surface or in tension in a direction normal to it.

Various techniques for overcoming the effects of thermal contraction have been developed. For example, Glaser et al. (1967), report that the addition of 10 percent (based on the weight of foam) of chopped glass fibers, 6.35×10^{-3} to 12.7×10^{-3} m long, to a low-viscosity one-shot foam eliminated cracking of the foam when exposed to liquid nitrogen. The same authors indicate that in work on the Saturn S-IV stage, where an internal insulation system was developed for the liquid-hydrogen propellant tank, urethane foam was reinforced with threads in order to prevent foam failure.

3. Fire and Explosion Hazards. The fire hazard of plastic materials has been demonstrated in the most dramatic fashion many times. Depending upon anticipated use, some polymeric materials are required to pass various flammability tests. The passing of these tests is assured by the addition of fire retardants.

When external foam insulation is used in spacecraft tank-

FOAMS

General

age, the possibility of ignition can be enhanced by the diffusion of air into the foam. Because of the low temperatures the air condenses, and this oxygen rich condensed air, in conjunction with an oxidizable organic foam, can create an explosion hazard.

Flame-retardant coatings can be applied to the exterior of the insulation, once it has been cured, to enhance its self-extinguishing characteristics. When this precaution has been taken, the possibility of ignition or explosion in a well-designed foam insulation system is remote.

A further hazard associated with burning of foams is the toxicity of their combustion products, which can be ascribed to the fire-retardant additives. Petajan et al. (1975) report that the physiological and toxicological effects of the combustion products of a laboratory-formulated fire-retarded rigid-polyurethane foam, proved fatal to rats in a matter of minutes, while the same rigid-polyurethane foam, without fire retardant, produced only minor signs of toxicity. The fire-retardant used in these experiments, a reactive phosphate, is not uncommon in commercial formulations.

INTENTIONALLY BLANK PAGE

FOAMS

Inorganic Foams

1.2. INORGANIC FOAMS

Porous ceramic foams have been developed to be used as high temperature insulators, for space applications. These foams provide the high strength required in many instances. Nevertheless, their use is somewhat limited because of their high density and relatively high thermal conductivity.

Table 1-1 gives the relevant properties of several ceramics foams.

The influence of temperature on thermal conductivity and linear thermal expansion of the same types of foam is shown in Figs 1-4 and 1-5 respectively.

Table 1-1

Relevant Properties of Ceramic Foams

	Alumina	Silica	Silicon Carbide	Zircon
Maximum Recommended Service Temperature [K]	2090	1920	2200	2470
Porosity [percent]	88	84	90	86
Density, $\rho \times 10^{-3}$ [$kg.m^{-3}$]	.51	.32	.32	.74
Thermal Conductivity, k [$W.m^{-1}.K^{-1}$]	.605	.158	.821	.137
Compressive Strength, $\sigma_{ult} \times 10^{-6}$ [Pa]	6.41	5.31	1.38	1.65

From Glaser et al. (1967).

Zircon foams that can be cast and later cured in place at temperatures below 390 K have been developed. These foams have excellent insulating and structural properties and are suitable for use in rigid heat shields. Fig 1-6 shows the temperature evolution

FOAMS

Inorganic Foams

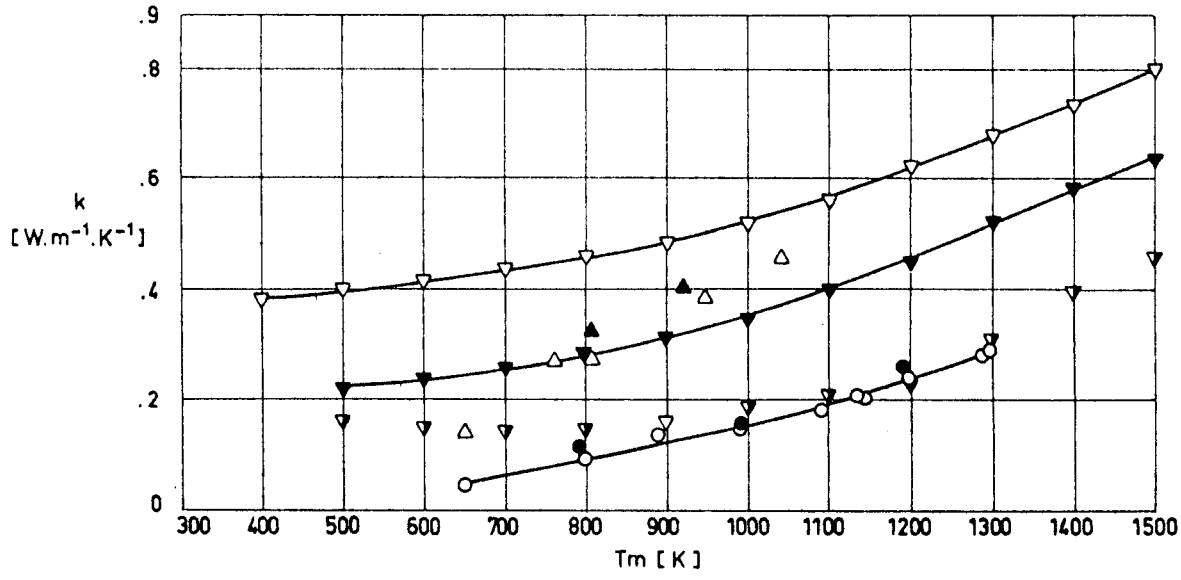

Fig 1-4. Thermal conductivity, k, of several ceramic foams as a function of arithmetic mean temperature, Tm.

Explanation

Key	Description	Comments	References
○	Alumina. Density, ρ=470 kg.m^{-3}.	Measured in 5.33×10^{-5} to 2.66×10^{-2} Pa pressure range.	Touloukian (1967)a.
●	Same as above.	Measured when cooled.	
△	Silicon Carbide. Density, ρ=460 kg.m^{-3}.	Measured in 5.33×10^{-5} to 4×10^{-2} Pa pressure range.	Touloukian (1967)b.
▲	Same as above.	Measured when cooled.	
▽	Zircon. Density, ρ=960 kg.m^{-3}.	Data extracted from smooth curve.	Glaser et al. (1967).
▼	Zircon Z-90. Density, ρ=940 kg.m^{-3}.		
▽	Zircon Z-67. Density, ρ=830 kg.m^{-3}.		

FOAMS

Inorganic Foams

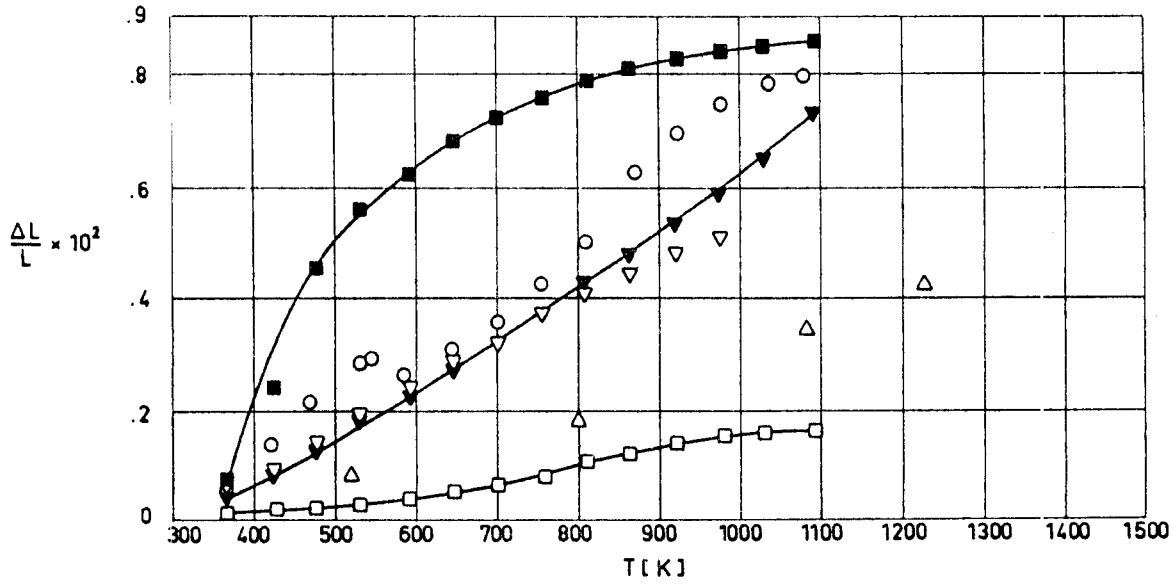

Fig 1-5. Linear thermal expansion, ΔL/L, of several ceramic foams as a function of temperature, T.

Explanation

Key	Description	Comments	References
○	Alumina. 35-40 alumina hidrate, 25-30 Al_2O_3, 22-27 H_3PO_4 (85%), 8-12 H_2O, 1-1.5 carbon powder, and .05-.1 Al powder Density, ρ=930 kg.m^{-3}. Dimensions, 5.08×10^{-2} m long by 6.35×10^{-3} m square.	Cured at 366.5 K; temperature raised continuously to 588.5 K during a 20 h period and then held at this temperature for 12 h. Reference temperature not given, assumed to be 293 K.	Touloukian (1967)a.
□	Silica. 50-55 Glasrock Slip, 30-35 Ludox (colloidal SiO_2), 5-7 SiO_2 400 mesh, 3-6 Al powder, 3-6 carbon powder, and 2-3 microballons. Density, ρ=640 kg.m^{-3}. Dimensions, 5.08×10^{-2} m long by 6.35×10^{-3} m square.	Cured at 366.5 K; temperature raised continuously to 588.5 K during a 24 h period and then held at this temperature for 8 h. Reference temperature not given, assumed to be 293 K.	
■	Same as above.	Second run.	
△	Silicon Carbide. Carborundum Company. Density, ρ=610 kg.m^{-3}. Dimensions, 7.62×10^{-2} m long by 1.27×10^{-2} m diameter.	Measured in vacuum of 1.7×10^{3} Pa up to 1200 K and with a slight purge of argon above 1200 K.	Touloukian (1967)b.
▽	Zircon. 30-35 ZrO_2 100 mesh, 20-25 ZrO_2 325 mesh, 20-25 of 90 rare-earth oxide, 10-12 H_3PO_4, 10-12 H_2O, 1-2 carbon powder, and .05-.1 Al powder. Density, ρ=1600 kg.m^{-3}. Dimensions, 5.08×10^{-2} m long by 6.35×10^{-3} m square.	Cured at 366.5 K; temperature raised continuously to 588.5 K during a 20 h period and then held at this temperature for 24 h. Reference temperature not given, assumed to be 293 K.	Touloukian (1967)c.
▼	Same as above.	Second run.	

FOAMS

Inorganic Foams

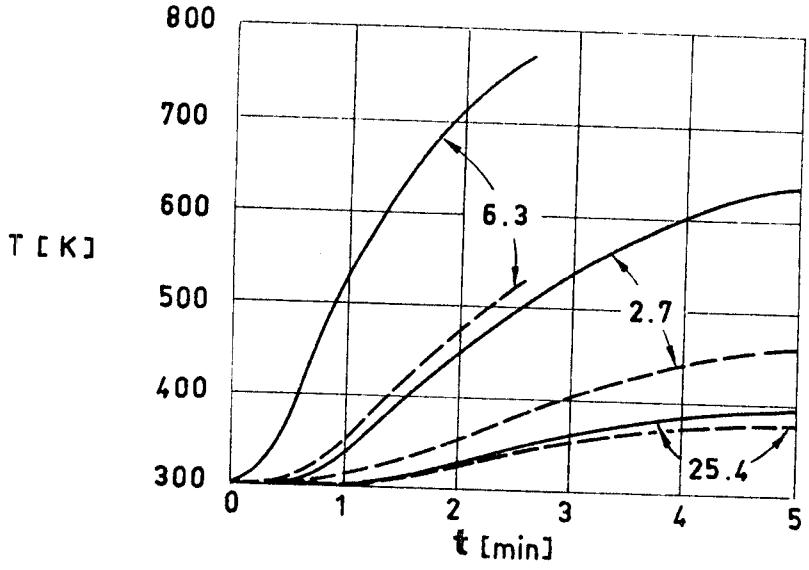

Fig 1-6. Temperature evolution of the hot and cold faces of several pieces of Zircon foam. ——— T_H, hot face. – – – – T_C, cold face. The numbers in the figure indicate the foam thicknesses in mm. From Glaser et al. (1967).

of the hot face, T_H, and backface, T_C, of several pieces of zircon foam which are heated by a heat flux of 4.5×10^5 $W.m^{-2}$. To perform the tests the foams were placed in contact with a stainless-steel honeycomb panel exposed to the heat flux.

Impregnated porous ceramics may also be used as insulating materials (Glaser et al. (1967)). These foams consist of a refractory porous base uniformly impregnated with a solid substance which sublimes or descomposes at elevated temperatures. Phenolics, and thermoplastics such as nylon, polyethylene, and polypropylene, have been used as the impregnating material. The composite is very similar to ablative substances used in reentry heat shields; although it

FOAMS

Inorganic Foams

presents the advantage that no changes in the shape of the surface occur.

Thermal switches formed by ceramic foams impregnated with metals such as silver or copper can be used to protect radioisotope capsules from reentry heating (Bustard, Princiotta & Barr (1970)). These composites are thermal conductors ($k \simeq 9$ $W.m^{-1}.K^{-1}$) below the melting point of the metal impregnant and switch to insulators ($k \simeq .2$ $W.m^{-1}.K^{-1}$) above its melting point. In this manner, the thermal conductance during normal power system operation is relatively high, facilitating the transfer of heat from the fuel capsule to the hot side of the energy conversion device, without excessive capsule and/ /or radioisotope temperatures. During reentry into the earth's atmosphere the capsule is protected against the aerothermodynamic heating by the unimpregnated ceramic foam.

Table 1-2, which has been borrowed from Bustard et al. (1970), gives additional properties of several ceramic foams.

FOAMS

Inorganic Foams

Table 1-2

Properties of Ceramic Foams

Description	Chemical Formula	Thermal Conductivity, k, at 1350 K, [W.m^{-1}.K^{-1}]	Specific Heat, cx10^{-3}, at 1350 K, [J.kg^{-1}.K^{-1}]	Melting Point [K]	Density, $\rho \times 10^{-3}$ [kg.m^{-3}]	Pore Structure	Thermal Shock Resistance	Compressive Strength, σ_{ult} x10^{-6} [Pa]	Shear Strength, τ_{ult} x10^{-6} [Pa]	Machinability
Alumina Ipsen 3300	Al_2O_3	.64	1.34	2320	0.92	Coarse pore-bubble structure	Good - hairline cracks developed	6.20	3.59	Fair
Alumina Ipsen 3400	Al_2O_3	.52	1.34	2320	0.56	Coarse pore-bubble structure	Fair to poor - spalling	4.83	3.03	Good
Alumina Astro Met 200	Al_2O_3	.69	1.34	2320	0.39	Open pore-lacey structure	Very poor - severe cracking	.34	.69	Very poor
Alumina Insalute	Al_2O_3	.40	1.34	2320	0.85	Irregular pore	Fair to poor - cracking and spalling	2.31	1.24	Fair
Fused Silica Glassrock 25	SiO_2	.28	1.46	2000	0.42	Fine pore-bubble structure	Excellent-no structural damage	3.10	1.72	Excellent
Fused Silica Thermo Matls. 50	SiO_2	.38	1.46	2000	0.80	Fine pore-bubble structure	Excellent-no structural damage	12.1	3.45	Excellent
Fused Silica Thermo Matls.HP50	SiO_2	.38	1.46	2000	0.80	Fine pore-bubble structure	Excellent-no structural damage	22.4	5.38	Excellent
Zircon Ipsen 4400	ZrO_2 [a]	.40	.75	2960	1.45	Coarse pore-bubble structure	Good - no structural damage	6.14	3.72	Fair
Zircon Ipsen 4300	ZrO_2 [b]	.40	.75	2960	1.10	Coarse pore-bubble structure	Poor - severe cracking	5.51	3.79	Good

[a] Partially stabilized to cubic structure.

[b] Fully stabilized to cubic structure.

From Bustard, Princiotta & Barr (1970).

FOAMS

Organic Foams

1.3. ORGANIC FOAMS

Low density organic foams are used for cryogenic insulation because they offer the following advantages: 1) Ease of fabrication, 2) Relatively low cost, and 3) Self-supporting structure.

Like plastics, organic polymer foams can be divided into two basic groups: thermoplastic foams and thermosetting foams.

Thermoplastic foams soften at temperatures of 340 to 390 K and, in most cases, tend to become brittle at cryogenic temperatures. These foams can be made from such polymers as cellulose acetate, polystyrene, styrene-acrylonitrile copolymer, polyvinylchloride, polyethylene, and polypropylene. Among these foams polystyrene and polyvinyl-chloride are the most commonly used. Polystyrene foams are rigid and polyvinyl chloride are flexible, although rigid PVC foams have been developed recently which are competitive with other rigid foams.

Thermosetting foams are commonly made with phenolic, urea-formaldehyde, epoxy, and polyurethane resins. Flexible polyurethane foams dominate the market; these foams exhibit very good properties at cryogenic temperatures with a minimum tendency to become brittle. Urea-formaldehyde foams are brittle and do not show good structural properties at low densities. Low density phenolic resin foams tend to be brittle and friable at room temperature and are difficult to manufacture. Epoxy foams have met only with limited use because of difficulties in controlling satisfactorily the foaming.

Tetrafluoroethylene foam (TFE) is an intermediate material

between a thermosetting and a thermoplastic foam. It melts at very high temperature, has very good physical properties at cryogenic temperatures and, because of its extreme chemical inertness, resists the effects of liquid oxygen, hydrazine, and other chemically reactive rocket fuels.

1.3.1. THERMAL PROPERTIES OF ORGANIC FOAMS

Fig 1-7 summarizes the available information on the thermal conductivity of polyurethane foams in a wide range of temperatures, and for different foam densities and preconditioning. Data for polystyrene foams are given in 1-8.

As has been already said, the thermal conductivity of foams can be reduced further by evacuation.

Evacuation by vacuum pumps is used when foams are employed as spacers of multilayer insulations. However, for insulating relatively large cryogenic tanks pump evacuation is normally impractical, nevertheless, in that case the gas contained in the cellular structure condenses because of the prevailing low temperature level, thus leaving the void space evacuated (cryopumping).

A close examination of the thermal conductivity-temperature curve in the proximity of the condensation temperature of the filling gas reveals the typical S-curve behavior shown in Fig. 1-9. This particular curve corresponds to a Freon 11-air filled foam. At atmospheric pressure Freon 11 condenses between 260 and 290 K. At temperatures below 260 K air controls the gas conduction contribu-

FOAMS

Organic Foams

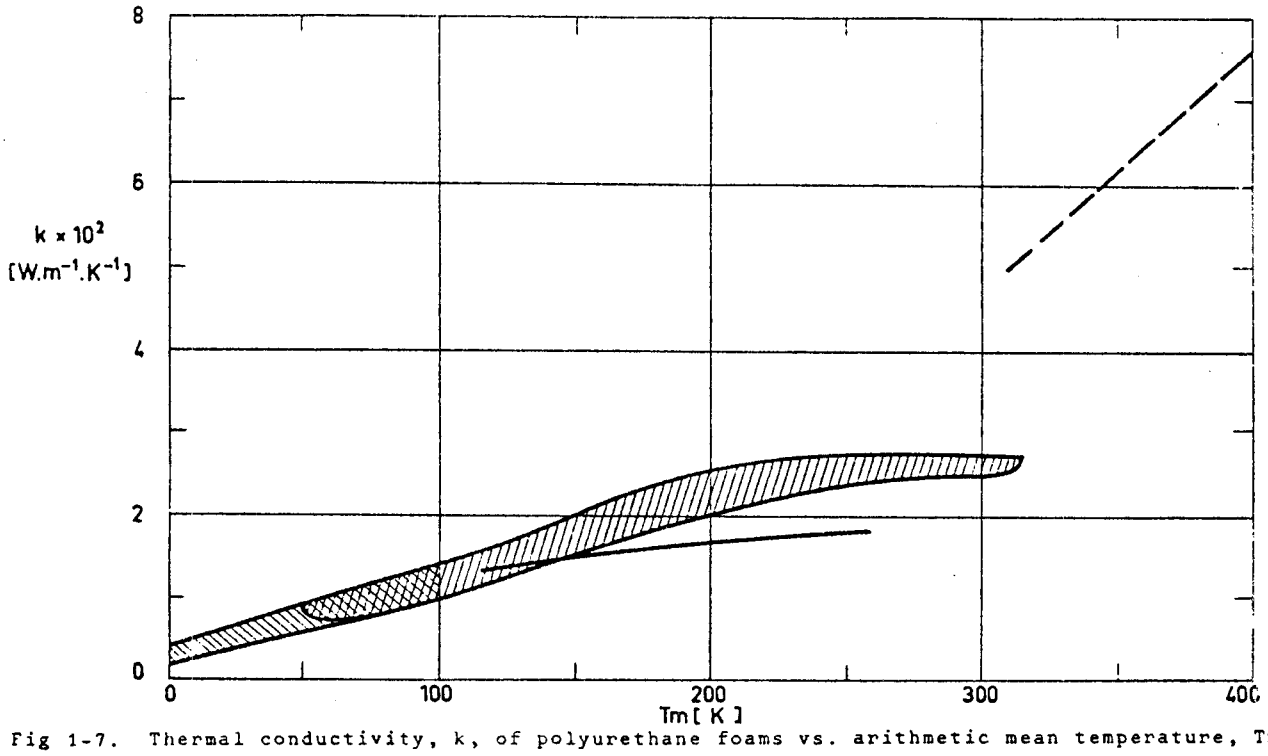

Fig 1-7. Thermal conductivity, k, of polyurethane foams vs. arithmetic mean temperature, Tm.
64 kg.m^{-3} > ρ > 32 kg.m^{-3}; cryopumped; from Coston (1967).
From Rosato (1968).
CO_2 blown, ρ = 32 kg.m^{-3}; evacuated; from Schroeder (1973)b.
The same foam at ambient pressure in air; from Schroeder (1973)b.

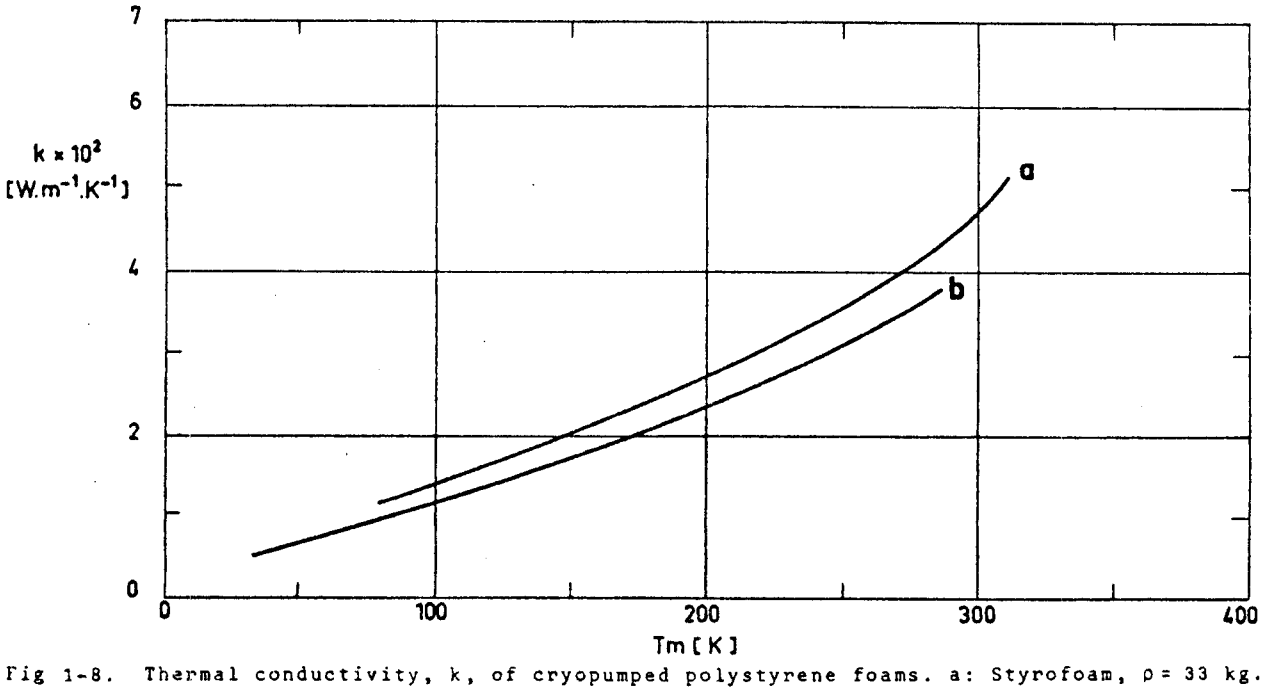

Fig 1-8. Thermal conductivity, k, of cryopumped polystyrene foams. a: Styrofoam, ρ = 33 kg.m^{-3}. b: Styrofoam, ρ = 22 kg.m^{-3}. Styrofoam is a registered trade name of Dow Chemical Co. From Rosato (1968).

FOAMS

Organic Foams

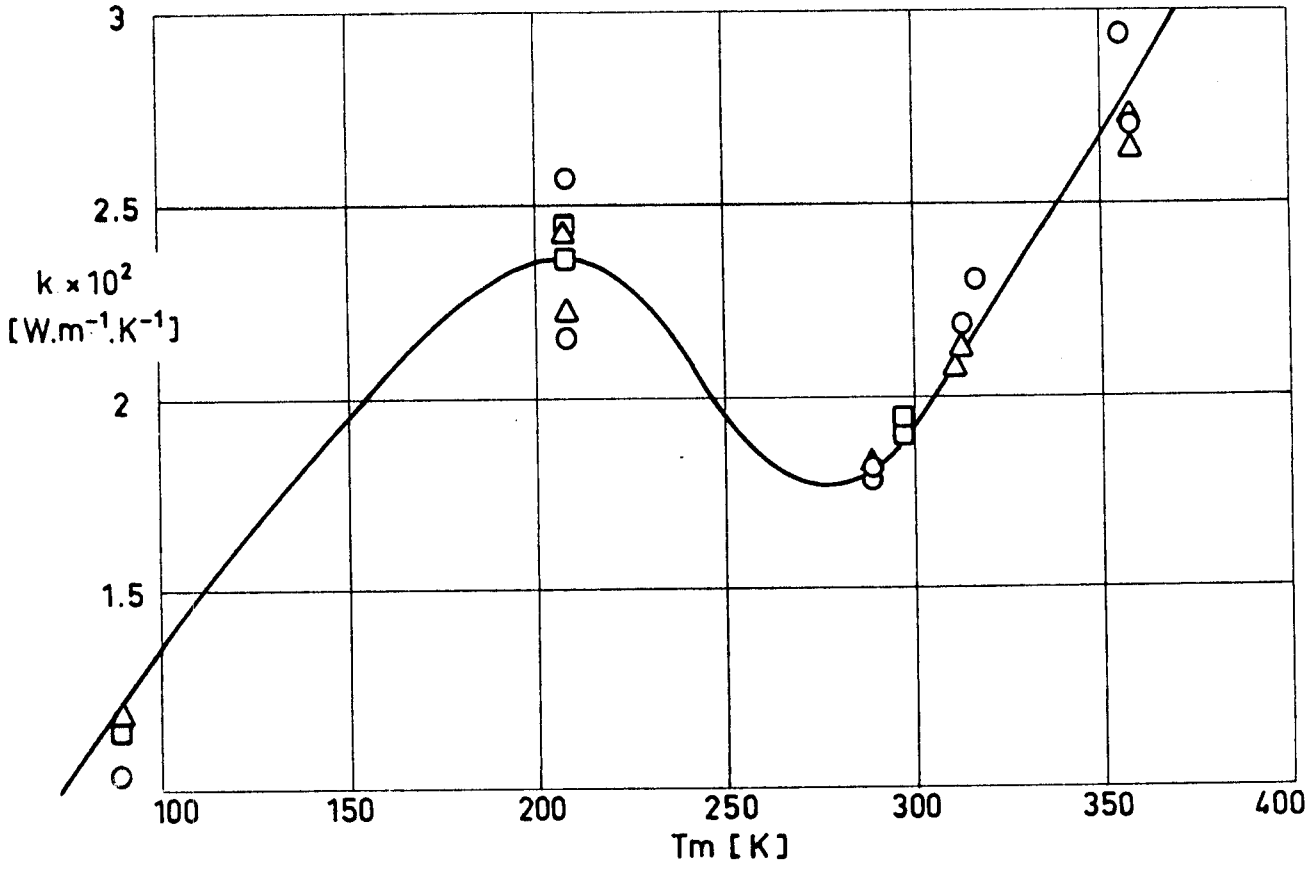

Fig 1-9. Thermal conductivity, k, vs. arithmetic mean temperature, Tm, of a polyurethane foam in the proximity of the condensation temperature of the filling gas. The temperature gradient is parallel to the foam rise direction. Foam: Nopcofoam BX-250, two-component, flame retardant, spray foam. Filling gas: Freon 11.

○ $\rho = 30.6$ kg.m^{-3}.

□ $\rho = 32.7$ kg.m^{-3}.

△ $\rho = 37.5$ kg.m^{-3}.

From Schroeder (1973)b.

tion to the foam thermal conductivity. This contribution decreases when the temperature decreases, reaching very low levels when the air condenses. In the temperature range above the Freon condensing temperature the gas conduction depends on the concentration of Freon in the binary Freon-air system, and on temperature, increasing when the temperature increases, as occurs with single-phase gaseous systems. In the intermediate temperature range, when Freon starts boiling, the conductivity of the gaseous system decreases since the thermal conductivity of Freon is about a fourth of that of air.

Linear thermal expansion of relevant foams is shown in Fig 1-10. It can be seen that Epoxy foams have the lowest thermal expansion. For a given foam, the thermal expansion increases when the temperature increases. Especially significant is the fact that in the cryogenic range all the foams have thermal expansion characteristics which can be reasonably considered as linear functions of temperature, the nonlinearities becoming apparent at room temperature.

1.3.2. MECHANICAL PROPERTIES OF ORGANIC FOAMS

In general, the main function of an insulation system is to provide thermal protection; it is not intended to be a primary load-carrying structure. However, since the insulation system is normally bonded or mechanically attached to the primary structure, it should match the strains and deflections of that structure, and therefore significant stresses could be introduced in it.

Low-temperature mechanical property data of foams are ex-

FOAMS

Organic Foams

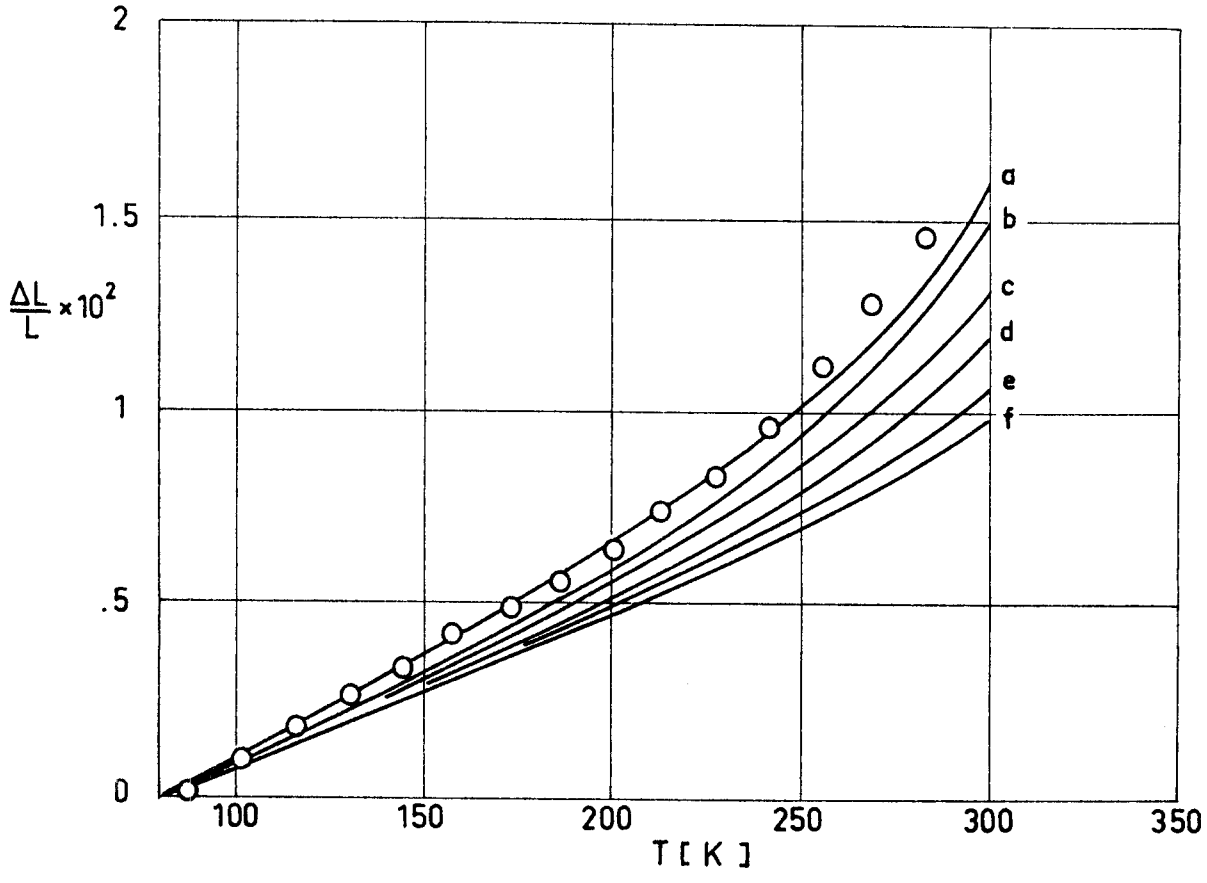

Fig 1-10. Linear thermal expansion, ΔL/L, of several organic foams as a function of temperature, T.

O Polyurethane foam. ρ=50 kg.m^{-3}. From Schroeder (1973)b.

a Urethane foam. ρ=80 kg.m^{-3}.

b Urethane joint filler.

c Syntactic foam. Urethane filler with hollow silica spheres.

d Semiflexible Urethane.

e Epoxy.

f Epoxy.

Curves a to f are from Glaser et al. (1967).

FOAMS

Organic Foams

tremely scarce, notwithstanding the fact that they are required for efficient design of foam-based insulations. Because of these reasons it seems advisable to collect these data in the present item.

The tensile strengths of a number of foams at temperatures ranging from 400 K down to 20 K are shown in Fig 1-11. At 20 K both the semirigid polyurethane and the epoxy foams have tensile strengths of the order of 4×10^5 Pa. At room temperature the rigid polyurethane foam has the highest tensile strength, closely followed by the semi-rigid polyurethane foam. At temperatures of the order of 400 K the tensile strength of all the organic foams practically vanishes.

The results of shear strength tests are summarized in Fig 1-12. All the foams tested exhibit minimum shear strengths at the two extreme temperatures. Again the rigid polyurethane foam has the highest shear strength among all of them.

The above or similar figures could give some order of magnitude idea useful for comparison purposes, however, the available information indicates that mechanical properties of foams are very sensitive to foam density, direction of cell-rise versus direction of loading, and test method.

All organic materials tested to date behave in a viscoelastic manner. Strictly speaking the thermal stresses caused on these materials by differential expansions or contractions cannot be expressed in terms of the standard modulus of elasticity and the free contraction constant.

Test methods have been devised to measure the thermal

FOAMS

Organic Foams

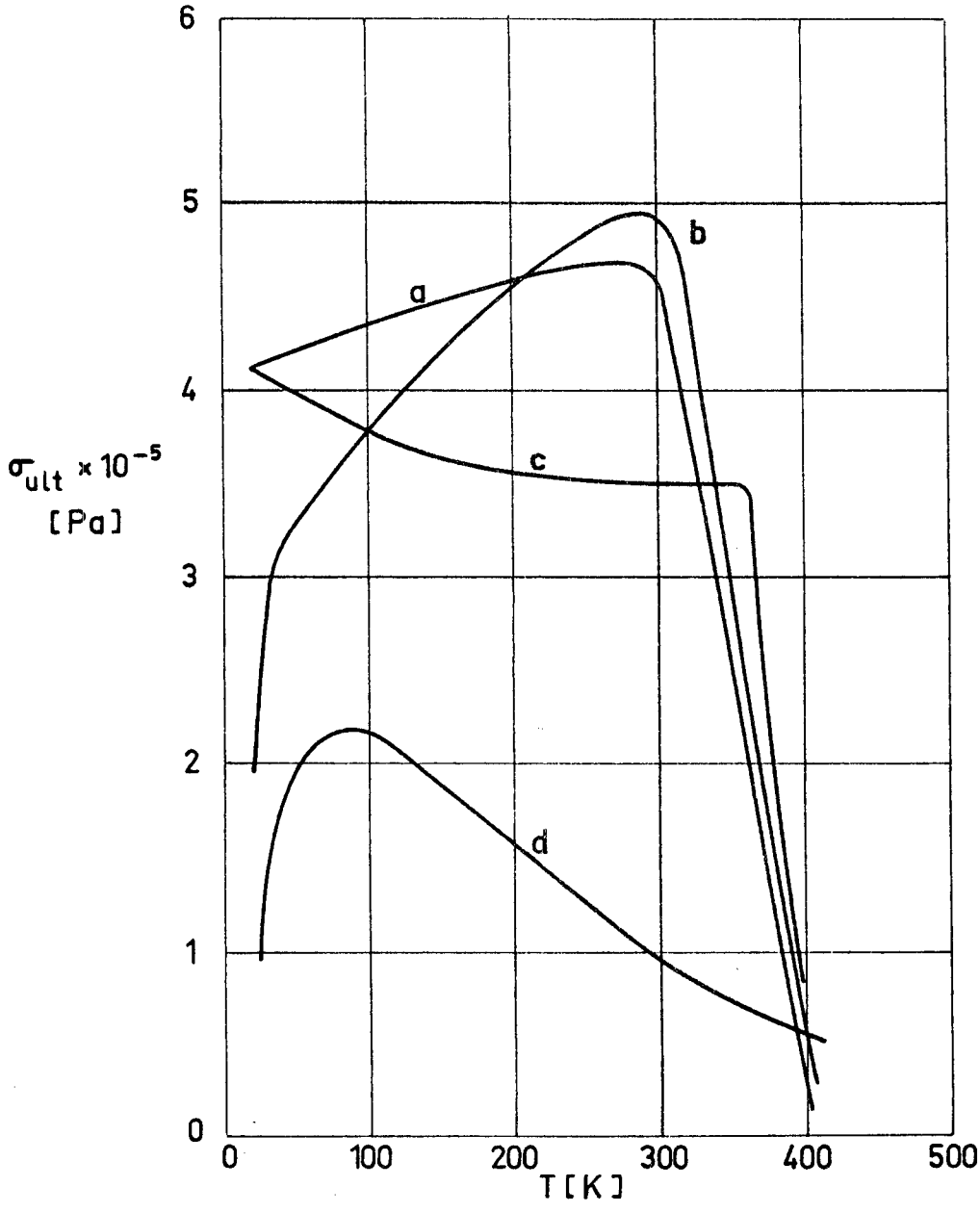

Fig 1-11. Ultimate tensile strength, of several foams as a function of temperature, T.
a: Barret semirigid polyurethane.
b: Hexcel 1414-2 polyester polyurethane rigid.
c: Magnolia 7015 epoxy.
d: Baron S-39 flexible polyether.
From Rosato (1968).

FOAMS

Organic Foams

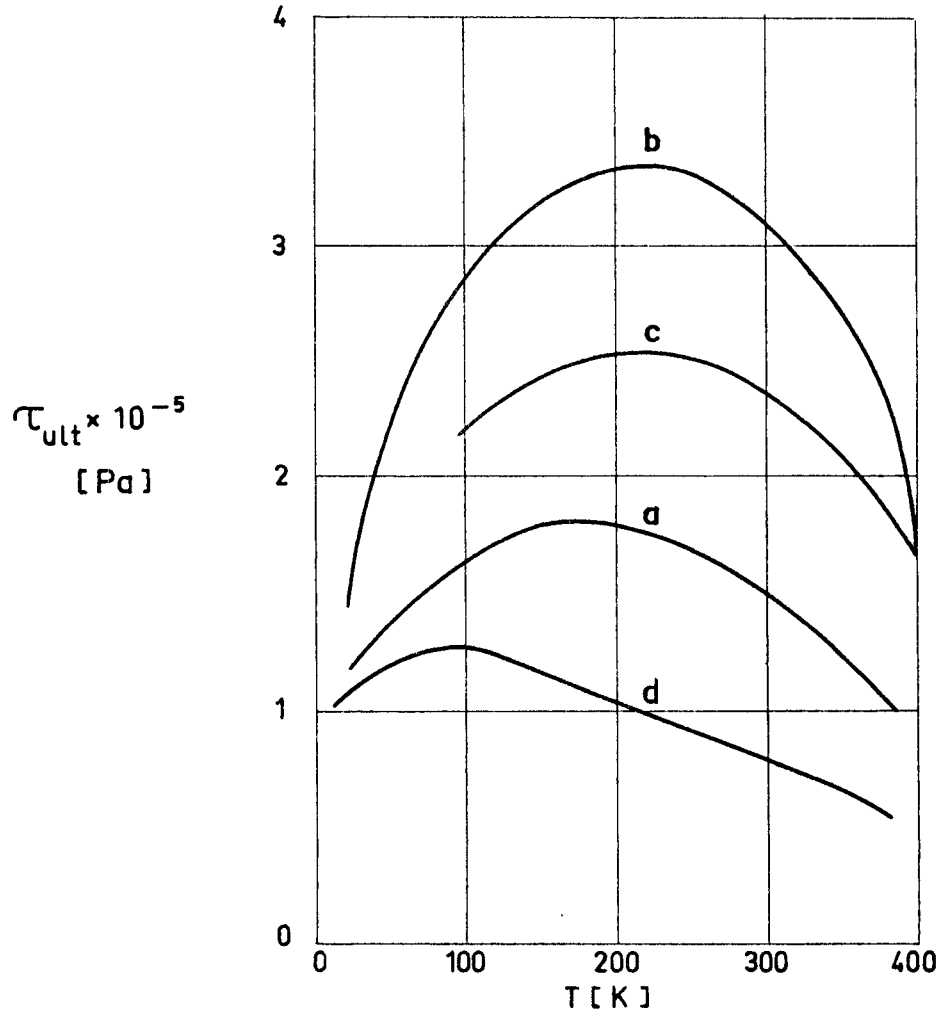

Fig 1-12. Ultimate shear strength, τ_{ult}, of several foams as a function of temperature, T.
a: Barret semirigid polyurethane.
b: Hexcel 1414-2 polyester polyurethane rigid.
c: Magnolia 7015 epoxy.
d: Baron S-39 flexible polyether.
From Rosato (1968).

FOAMS

Organic Foams

stress-thermal strain ratio (thermoelastic modulus) and the thermoelastic contraction as a function of temperature (Schroeder (1973)). The main objection to such type of data is that because of the non-linearity of the phenomenon it is not easy to superpose thermally induced and mechanically induced stresses. For example, tests reveal that the thermoelastic strain of a loaded specimen is not the same as that corresponding to the unloaded or free shrink specimen.

One way to circumvent these difficulties and still generate data which would be useful for engineering purposes, is to neglect non-linear effects, which at low temperatures seems to be justified, as was mentioned in connection with Fig 1-10 and will be confirmed later, and to obtain mechanical property data using normal widely used test techniques, with the obvious additions to reproduce the required low temperature environment and to minimize thermally induced stresses.

A collection of data generated by US National Bureau of Standards is presented in Tables 1-3 to 1-5 and Figs 1-13 to 1-18. These data concern both tensile and compressive strengths.

The main results of these tests can be summarized as follows:

1) The Modulus of Elasticity, yield strength, and ultimate strength increase with decreasing temperature, while the elongation decreases, Tables 1-4 and 1-5.

2) The Modulus of Elasticity is twice as great in tension compared to compression, but the difference diminishes at lower tem-

peratures. Compare Figs 1-14 and 1-17.

3) Most foams become brittle at low temperatures, whereas the ductility is considerable at 195 K and above (Figs 1-13 and 1-16). On the average, polystyrene foams are more ductile than polyurethane foams at 76 K (Fig 1-16).

4) The Modulus of Elasticity and the strength, both tensile and compressive, are approximately linearly dependent on density. At low temperatures the density dependence is greater (Figs 1-14, 1-15, and 1-17, 1-18). In the compressive case there is a minimum density below which the rigid foam cannot withstand any applied compressive force at low temperatures; by extrapolation of the straight lines corresponding to O and ∇ data points in Fig 1-17 one obtains a zero value of E at finite density.

5) Specimens loaded along the rise are stronger than those loaded transversally to rise (Figs 1-13 and 1-16). In the compressive case this is not necessarily true; notice, for instance, the foam YR-1 in Fig 1-16.

6) At most densities there is considerable data spread which can be attributed to foam components, manufacturing process, and blowing agent.

A second set of data - this one from North American Rockwell - is presented in Figs 1-19 to 1-22. Basically these data confirm the general trends mentioned above. Additional information concerning the influence of different loading directions on the compressive strength is shown in Fig 1-21.

FOAMS

Organic Foams

Shear strength data are given in Fig 1-22. Regarding these data, it should be said that mechanically and thermally induced stresses are strongly coupled, since in this particular test, which was performed using the ASTM C-273 standard method, the loading plates are bonded to the facings of the foam along their whole length. Thence, these results should be considered as merely qualitative.

1.3.3. DATA ON COMMERCIALLY AVAILABLE FOAMS

The physical characteristics, availability and information which concerns the processing of several organic foams are given in the last pages of this item.

The number of commercially available foams is very large and no attempt has been made to present an exhaustive list of all of them; rather it is hoped that the information presented is representative enough and could be used in a large number of cases.

FOAMS

Organic Foams

Table 1-3

Characterization of Foams Whose Properties Will Be Given Later

	Sample [a]	Type [b]	Density, ρ [kg.m^3]	Polyol Component	Isocyanate Component [c]	Blowing Agent	Flame Retardant
Flexible	AF-1	PU	34.8	Polyether	TDI	CO_2	No
	BF-4	PU	125	Polyether	PAPI/TDI	CO_2	No
	BF-5	PU	123	Polyether	PAPI/TDI	CO_2	No
	BF-6	PU	116	Polyether	PAPI/TDI	CO_2	No
	CF-7	PU	33.8	Polyester	TDI	CO_2	No
	CF-8	PU	32.7	Polyester	TDI	CO_2	No
	CF-9	PU	33.5	Polyester	TDI	CO_2	No
	DF-1	PU	110	Polyester	TDI	CO_2	No
	DF-2	PU	111	Polyester	TDI	CO_2	No
	DF-3	PU	105	Polyester	TDI	CO_2	No
Rigid	JR-1	PU	66.2	Polyether	PAPI Prepol	CO_2 and Freon 11	Yes
	KR-1	PU	30.6	Polyether	PAPI Prepol	CO_2 and Freon 11	Yes
	LR-3	PU	42.4	Polyether	TDI Prepol	CO_2	No
	MR-1	PU	68.4	Polyether	TDI Prepol	CO_2	No
	NR-1	PU	95.6	Polyether	TDI Prepol	CO_2	No
	OR-1	PU	47.6	Polyester	TDI Prepol	Freon 11	No
	OR-2	PU	47.7	Polyester	TDI Prepol	Freon 11	No
	PR-1	PU	48.1	Polyether	PAPI	Freon 11	No
	SR-2	PU	47.7	Polyether	PAPI	Freon 11	Yes
	TR-2	PU	32.4	Polyester	TDI Prepol	CO_2	No
	UR-2	PU	43.6	Polyester	TDI Prepol	CO_2	No
	VR-2	PU	61.0	Polyester	TDI Prepol	CO_2	No
	WR-2	PU	87.8	Polyester	TDI Prepol	CO_2	No
	XR-3	PU	48.2	Polyether	TDI Prepol	CO_2	No
	XR-4	PU	47.6	Polyether	TDI Prepol	CO_2	No
	YR-1	PS	52.2	Polystyrene	-	Pentane	No
	ZR-1	PS	100	Polystyrene	-	Pentane	No

[a] Material source: AF-1 to SR-2: CPR Division, Upjohn Company; TR-2 to ZR-1: Bendix Corporation.

[b] PU: Polyurethane foam; PS: Polystyrene foam.

[c] TDI: Tolylene diisocyanate; PAPI: Polymethylene polyphenylisocyanate, registered trade name of Upjohn Co.; Prepol: Prepolymerized.

From Reed, Arvidson & Durcholz (1972).

FOAMS

Organic Foams

Table 1-4

Average Tensile Data of Polyurethane and Polystyrene Foams

T [K]	Foam	Specimen Density, ρ [kg.m^{-3}]	Type [a]	Modulus of Elasticity, E × 10^{-6} [Pa]		Proportional limit, σ × 10^{-5} [Pa]		Yield [b] strength, σ_o × 10^{-5} [Pa]		Compressive strength, σ × 10^{-5} [Pa]		Elongation %			
												Plastic		Total	
				Trans.	Long.	Trans.	Long.	Trans.	Long.	Trans.	Long.	Trans.	Long.	Trans.	Long.
76	KR-1	30.6	PUR	12.5	-	3.2	-	-	-	3.7	-	0.06	-	3.05	-
	KR-1	29.5	PUR	-	18.2	-	1.4	-	-	-	4.6	-	0.03	-	1.81
	TR-2	32.4	PUR	20.4	-	3.0	-	-	-	3.6	-	0.03	-	1.80	-
	LR-3	42.4	PUR	38.5	-	6.8	-	-	-	8.3	-	0.04	-	1.86	-
	UR-2	43.6	PUR	33.4	-	4.7	-	-	-	6.0	-	0.01	-	1.88	-
	UR-2	44.5	PUR	-	27.1	-	4.1	-	-	-	6.1	-	0.07	-	2.40
	XR-4	47.6	PUR	31.7	-	-	-	-	-	5.6	-	0.00	-	1.77	-
	OR-1	47.7	PUR	37.0	-	-	-	-	-	10.1	-	0.00	-	2.72	-
	OR-1	46.3	PUR	-	45.0	-	-	-	-	-	6.3	-	0.00	-	2.03
	SR-2	47.7	PUR	38.7	-	-	-	-	-	6.6	-	0.00	-	1.67	-
	PR-1	47.7	PUR	32.8	-	5.0	-	-	-	5.4	-	0.02	-	1.70	-
	VR-2	61.0	PUR	51.0	-	6.3	-	-	-	9.2	-	0.02	-	1.62	-
	JR-1	64.6	PUR	40.4	-	-	-	-	-	7.9	-	0.00	-	1.93	-
	MR-1	68.2	PUR	44.5	-	6.5	-	-	-	9.4	-	0.05	-	2.17	-
	WR-2	87.8	PUR	63.0	-	11.0	-	-	-	14.4	-	0.05	-	2.22	-
	NR-1	95.6	PUR	95.8	-	14.4	-	-	-	18.5	-	0.04	-	1.98	-
	NR-1	94.8	PUR	-	85.4	-	13.2	-	-	-	15.7	-	0.06	-	2.21
	CF-7	33.8	PUF	16.5	-	1.9	-	2.7	-	4.4	-	1.79	-	4.63	-
	CF-7	32.5	PUF	-	17.6	-	2.6	-	3.7	-	4.9	-	0.83	-	3.54
	AF-1	34.8	PUF	15.4	-	2.0	-	2.8	-	4.2	-	2.40	-	5.35	-
	DF-1	108	PUF	102.7	-	6.6	-	12.3	-	26.3	-	3.27	-	5.90	-
	BF-4	124	PUF	120.1	-	7.8	-	-	-	10.4	-	0.08	-	0.73	-
	YR-1	52.2	PSR	57.4	-	7.2	-	9.9	-	11.2	-	0.72	-	2.02	-
	YR-1	51.3	PSR	-	50.4	-	6.5	-	9.4	-	10.9	-	0.83	-	2.95
	ZR-1	101	PSR	108.2	-	11.8	-	19.2	-	22.5	-	0.76	-	2.18	-
195	KR-1	30.6	PUR	10.1	-	2.2	-	2.6	-	3.2	-	0.88	-	4.01	-
	KR-1	30.6	PUR	-	11.2	-	1.04	-	2.1	-	4.0	-	1.98	-	5.69
	UR-2	39.2	PUR	11.9	-	2.6	-	4.1	-	6.1	-	0.96	-	6.10	-
	UR-2	42.0	PUR	-	15.9	-	4.6	-	6.1	-	6.8	-	0.12	-	4.40
	OR-1	47.1	PUR	14.5	-	3.8	-	7.5	-	8.1	-	0.16	-	5.70	-
	NR-1	95.8	PUR	38.7	-	6.2	-	10.5	-	17.1	-	1.15	-	5.57	-
	NR-1	94.3	PUR	-	45.2	-	6.3	-	11.4	-	17.4	-	1.14	-	4.03
	CF-7	32.2	PUF	3.7	-	.74	-	1.2	-	3.2	-	34.30	-	45.55	-
	CF-7	33.6	PUF	-	6.9	-	1.1	-	1.7	-	3.7	-	23.7	-	28.9
	YR-1	51.7	PSR	35.0	-	4.5	-	6.8	-	8.8	-	2.81	-	4.91	-
	YR-1	50.6	PSR	-	30.2	-	3.2	-	6.4	-	8.7	-	1.83	-	3.92
300	KR-1	30.8	PUR	5.6	-	1.03	-	1.3	-	2.9	-	4.84	-	9.96	-
	UR-2	40.0	PUR	16.1	-	1.0	-	2.4	-	5.0	-	2.86	-	5.89	-
	UR-2	41.2	PUR	-	13.7	-	1.5	-	2.6	-	4.9	-	2.42	-	6.02
	OR-1	47.3	PUR	17.2	-	2.4	-	3.7	-	5.4	-	1.57	-	4.35	-
	NR-1	94.7	PUR	26.4	-	3.7	-	6.1	-	10.8	-	3.09	-	7.05	-
	NR-1	94.7	PUR	-	31.0	-	3.4	-	6.3	-	10.4	-	2.00	-	5.68
	CF-7	33.0	PUF	0.12	-	.20	-	.28	-	.73	-	37.25	-	96.27	-
	CF-7	33.2	PUF	-	0.19	-	1.6	-	.28	-	.85	-	35.33	-	82.03
	YR-1	50.8	PSR	36.1	-	3.0	-	6.2	-	8.2	-	2.84	-	5.24	-
	YR-1	50.9	PSR	-	38.7	-	3.9	-	6.3	-	8.3	-	2.10	-	4.20

[a] PUR: polyurethane rigid; PUF: polyurethane flexible; PSR: polystyrene rigid.

[b] At .2% offset.

COMMENTS: 1) The rigid foam samples were cylindrical, 2.866×10^{-2} m in diameter and 7.62×10^{-2} m long. Specimens having a reduced middle section 2.21×10^{-2} m in diameter and 2.54×10^{-2} m long were also tested. Flexible foam samples were square cross-sectioned specimens 2.54×10^{-2} m × 2.54×10^{-2} m in side and 7.62×10^{-2} m long. The specimens were epoxied to polycarbonate grips. Polycarbonate was chosen because its thermal expansion matched that of the adhesive at low temperature.

2) The rate of head movement of the testing machine was 5×10^{-4} m.min^{-1}.

3) Each value represents the average of about four tests. Strength data variation from the reported average were ± 10%. Suggested inaccuracies of the reported average strength data are ± 5%. Averare elongation data are supposed to be inaccurate to ± 5%, and data variations from the reported averages are ± 10%. For a given test individual strength and elongation measurements are thought to be accurate to ± 1%.

From Reed, Arvidson & Durcholz (1972).

FOAMS

Organic Foams

Table 1-5

Average Compressive Data of Polyurethane and Polystyrene Foams

T [K]	Foam	Specimen Density, ρ [kg.m^{-3}]	Type [a]	Modulus of Elasticity, E × 10^{-6} [Pa]		Proportional limit, σ × 10^{-5} [Pa]		Yield [b] strength, σ_o × 10^{-5} [Pa]		Compressive [c] strength, σ × 10^{-5} [Pa]		Elongation %			
												Plastic		Total	
				Trans.	Long.	Trans.	Long.	Trans.	Long.	Trans.	Long.	Trans.	Long.	Trans.	Long.
76	UR-2	47.6	PUR	29.4	-	4.0	-	5.1	-	6.3	-	0.41	-	2.58	-
		46.8		-	36.1	-	5.4	-	-	-	6.5	-	0.11	-	1.92
	NR-1	48.4	PUR	13.6	-	2.3	-	3.8	-	6.2	-	2.69	-	7.32	-
		47.4		-	23.0	-	3.5	-	5.8	-	7.0	-	0.72	-	3.75
	NR-1	94.8	PUR	67.8	-	11.3	-	-	-	14.8	-	0.04	-	2.39	-
		95.6		-	81.7	-	10.8	-	-	-	14.2	-	0.13	-	1.87
	CF-7	34.1	PUF	12.0	-	2.1	-	2.8	-	3.0	-	0.35	-	2.88	-
		31.7		-	10.9	-	2.2	-	3.2	-	3.4	-	0.45	-	3.55
	YR-1	51.6	PSR	31.6	-	3.7	-	5.0	-	5.4	-	3.28	-	5.02	-
		51.3		-	32.4	-	3.7	-	4.6	-	5.1	-	4.65	-	6.28
	ZR-1	99.5	PSR	73.8	-	9.3	-	13.7	-	15.1	-	0.58	-	2.32	-
		99.2		-	74.8	-	9.4	-	13.2	-	14.5	-	0.95	-	2.93
195	UR-2	43.9	PUR	12.6	-	1.7	-	2.6	-	3.8	-	1.84	-	4.91	-
		41.3		-	11.2	-	1.7	-	2.3	-	3.4	-	2.35	-	5.59
	NR-1	94.2	PUR	40.4	-	4.1	-	7.0	-	(11.6)	-	7.10	-	10.00	-
		94.5		-	51.4	-	4.6	-	7.3	-	(11.7)	-	7.68	-	10.00
	CF-7	33.3	PUF	2.0	-	.33	-	.57	-	(.84)	-	5.96	-	10.00	-
		32.0		-	3.5	-	.72	-	.99	-	1.19	-	1.87	-	5.45
	YR-1	51.3	PSR	23.6	-	3.2	-	4.1	-	(5.2)	-	7.80	-	10.00	-
		51.4		-	21.5	-	3.0	-	3.8	-	(4.8)	-	7.70	-	10.00
300	UR-2	46.3	PUR	7.0	-	1.3	-	1.9	-	3.0	-	3.26	-	7.62	-
		40.8		-	7.2	-	1.4	-	2.2	-	3.0	-	2.04	-	6.34
	NR-1	95.1	PUR	17.2	-	3.5	-	5.2	-	8.0	-	3.27	-	7.93	-
		93.2		-	20.2	-	4.3	-	5.9	-	8.1	-	3.27	-	7.38
	CF-7	33.3	PUF	.06	-	.021	-	.024	-	(.035)	-	4.13	-	10.00	-
		33.3		-	.20	-	.014	-	.021	-	(.04)	-	7.31	-	10.00
	YR-1	51.9	PSR	19.8	-	3.4	-	3.7	-	(4.0)	-	7.94	-	10.00	-
		51.1		-	19.1	-	2.3	-	3.2	-	3.4	-	0.68	-	2.46

[a] PUR: polyurethane rigid; PUF: polyurethane flexible; PSR: polystyrene rigid.

[b] At .2% offset.

[c] Tests in which the stress continued to increase as the test progressed (i.e., the material did not exhibit an ultimate) were concluded at 10% total elongation. The corresponding values are in parentheses.

COMMENTS:

1) The rigid foam samples were cylindrical, 2.866×10^{-2} m in diameter and 2.54×10^{-2} m long. Flexible foam specimens were machined into a cube geometry with the length of each side equal to 2.54×10^{-2} m.

2) The rate of head movement of the testing machine was 5×10^{-4} m.min^{-1}.

3) Each value represents the average of at least three tests. The average strength deviations for a given type and loading direction were ± 9%, while the average elongation deviations were ± 8%. Individual strength and elongation measurements are accurate to ± 1%. Reported strength and elongation measurements are thought to be accurate to ± 7%, with the principal contributor to test inaccuracy being material inconsistency.

From Arvidson, Durcholz & Reed (1972).

FOAMS

Organic Foams

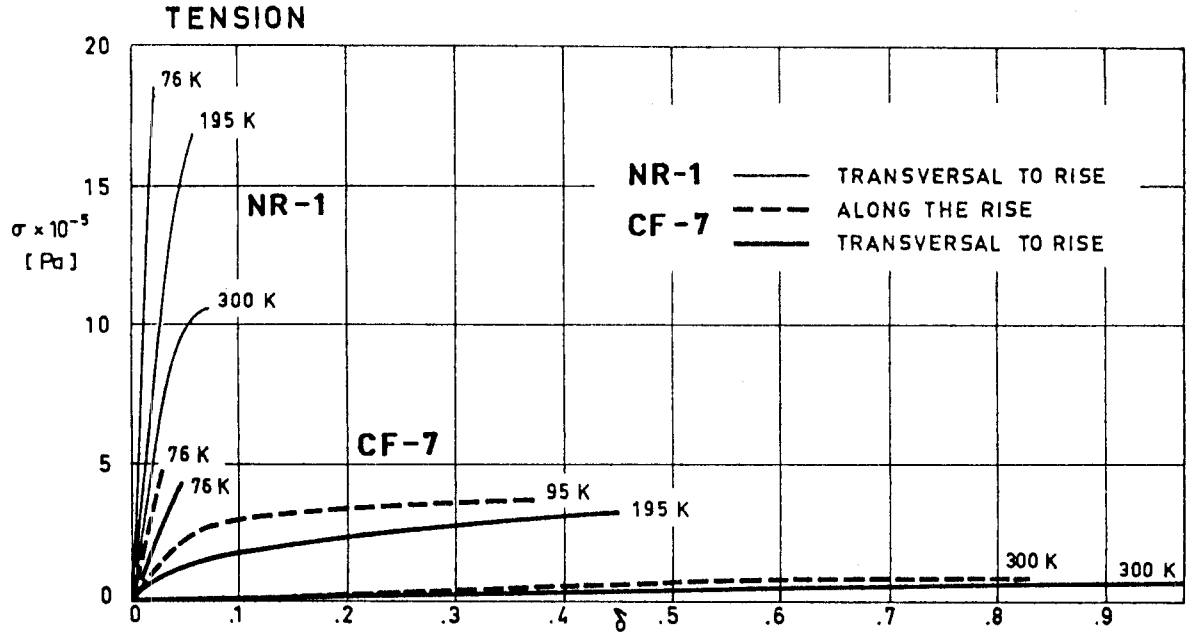

Fig 1-13. Tensile stress, σ, vs. strain, δ, for several polyurethane foams at 76, 195 and 300 K. From Reed, Arvidson & Durcholz (1972).

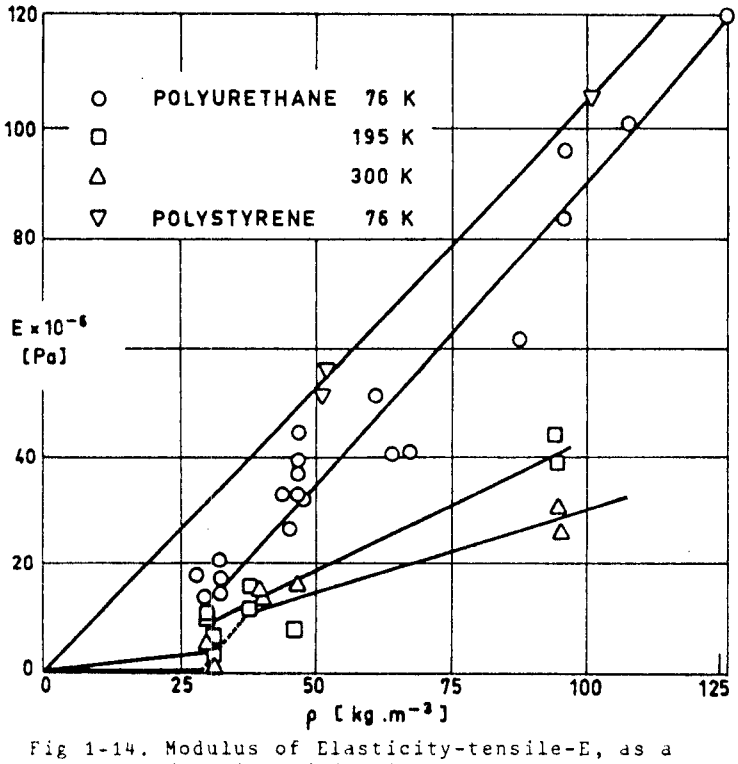

Fig 1-14. Modulus of Elasticity-tensile-E, as a function of density, ρ, for several organic foams. Solid lines show the estimated dependence of E on foam density; dashed lines indicate transition between rigid foams (large E) and flexible foams (small E). From Reed et al. (1972).

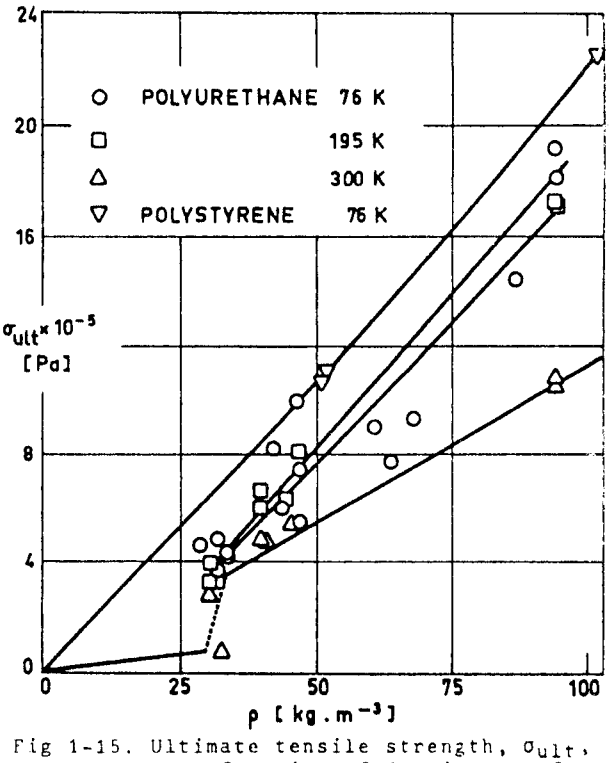

Fig 1-15. Ultimate tensile strength, σ_{ult}, as a function of density, ρ, for several organic foams. Solid and dashed lines have the same meaning as in Fig. 08. From Reed et al. (1972).

FOAMS

Organic Foams

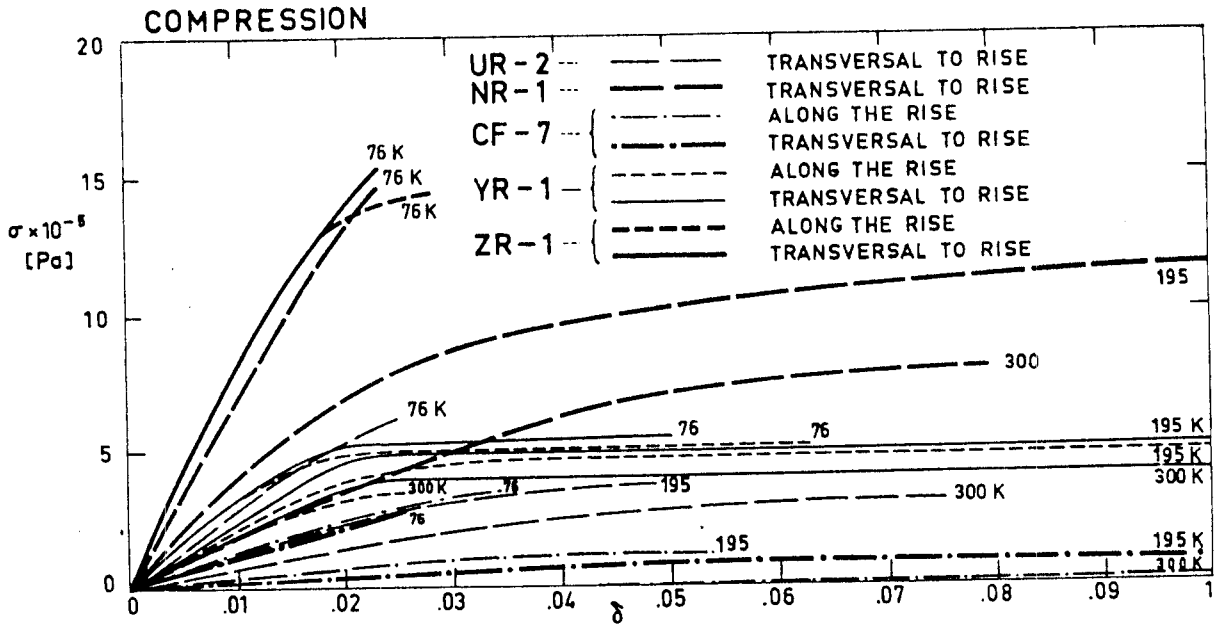

Fig 1-16. Compressive stress, σ, vs. strain, δ, for several organic foams at 76, 195 and 300 K. From Arvidson, Durcholz & Reed (1972).

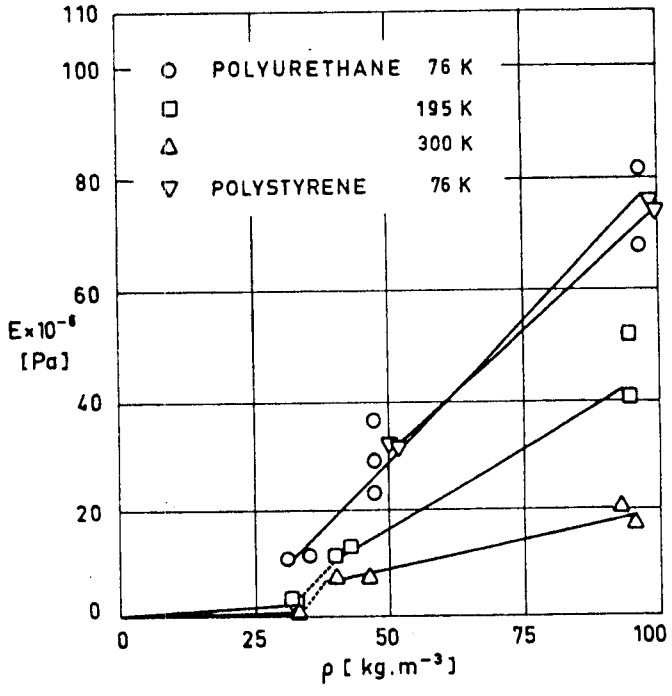

Fig 1-17. Modulus of Elasticity-compressive-E, as a function of density, ρ, for several organic foams. Solid lines show the estimated dependence of E on foam density; dashed lines indicate transition between rigid foams (large E) and flexible foams (small E). From Arvidson et al (1972).

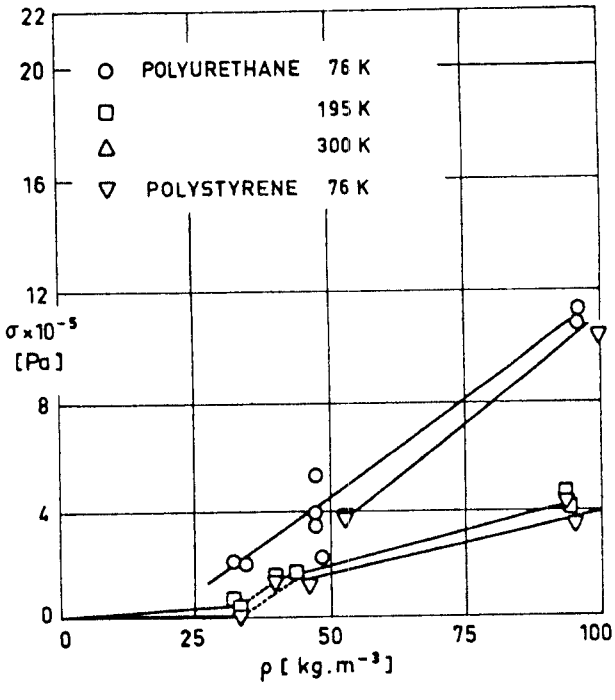

Fig 1-18. Proportional limit-compressive-σ, as a function of density, ρ, for several organic foams. Solid lines show the estimated dependence of E on foam density; dashed lines indicate transition between rigid foams (large E) and flexible foams (small E). From Arvidson et al (1972).

FOAMS

Organic Foams

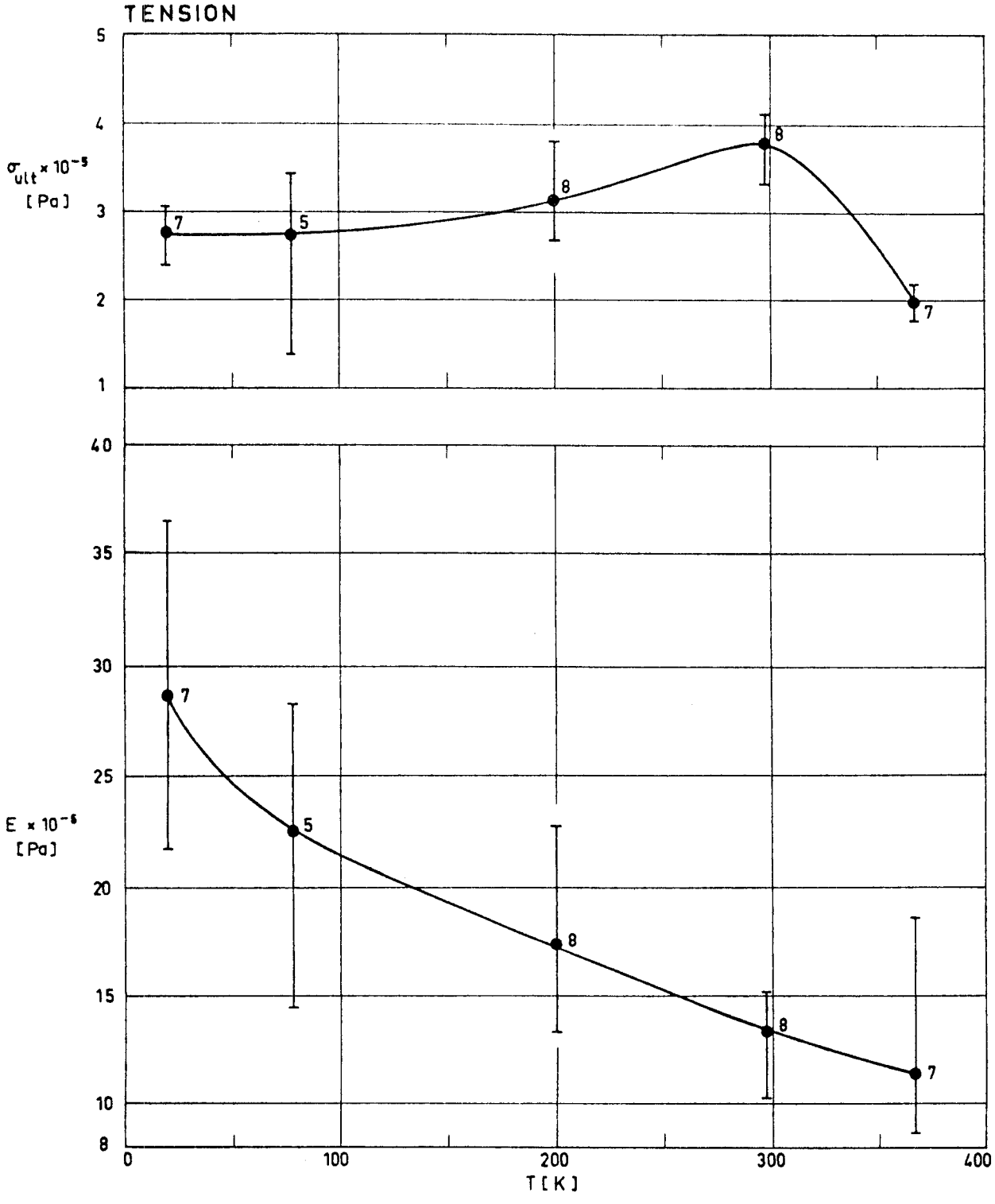

Fig 1-19. Ultimate tensile strength, σ_{ult}, and Modulus of Elasticity-tensile-E, as functions of temperature, T. Polyurethane spray foam, $\rho = 32$ kg.m^{-3}. Tested per ASTM D-1623; transversal to the rise. Numbers indicate how many tests were performed in each case. From Schroeder (1973)b.

FOAMS

Organic Foams

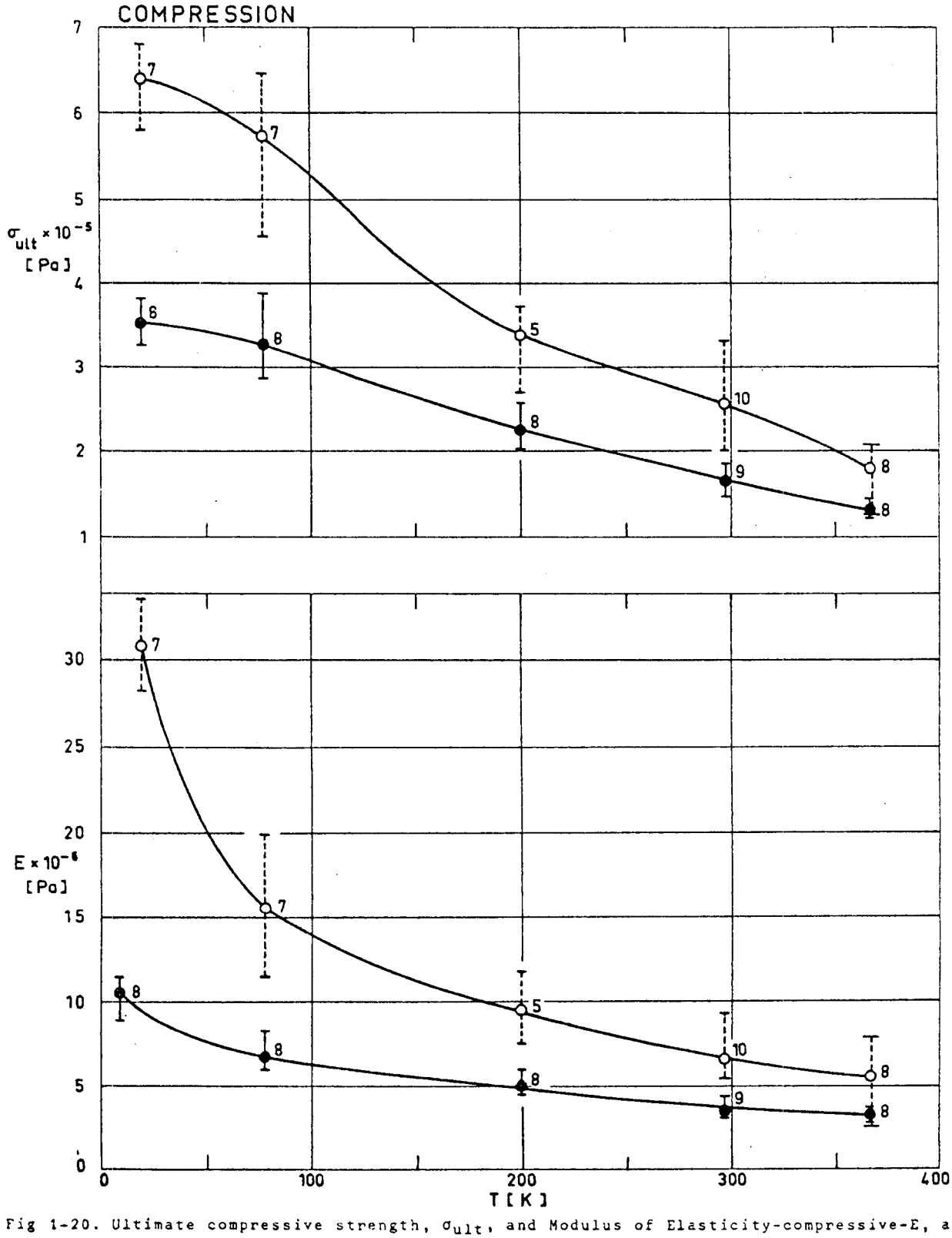

Fig 1-20. Ultimate compressive strength, σ_{ult}, and Modulus of Elasticity-compressive-E, as functions of temperature, T. Polyurethane spray foam, ρ=32 kg.m^{-3}. Tested per ASTM D-1621; O along the rise, ● transversal to the rise. Numbers indicate how many tests were performed in each case. From Schroeder (1973)b.

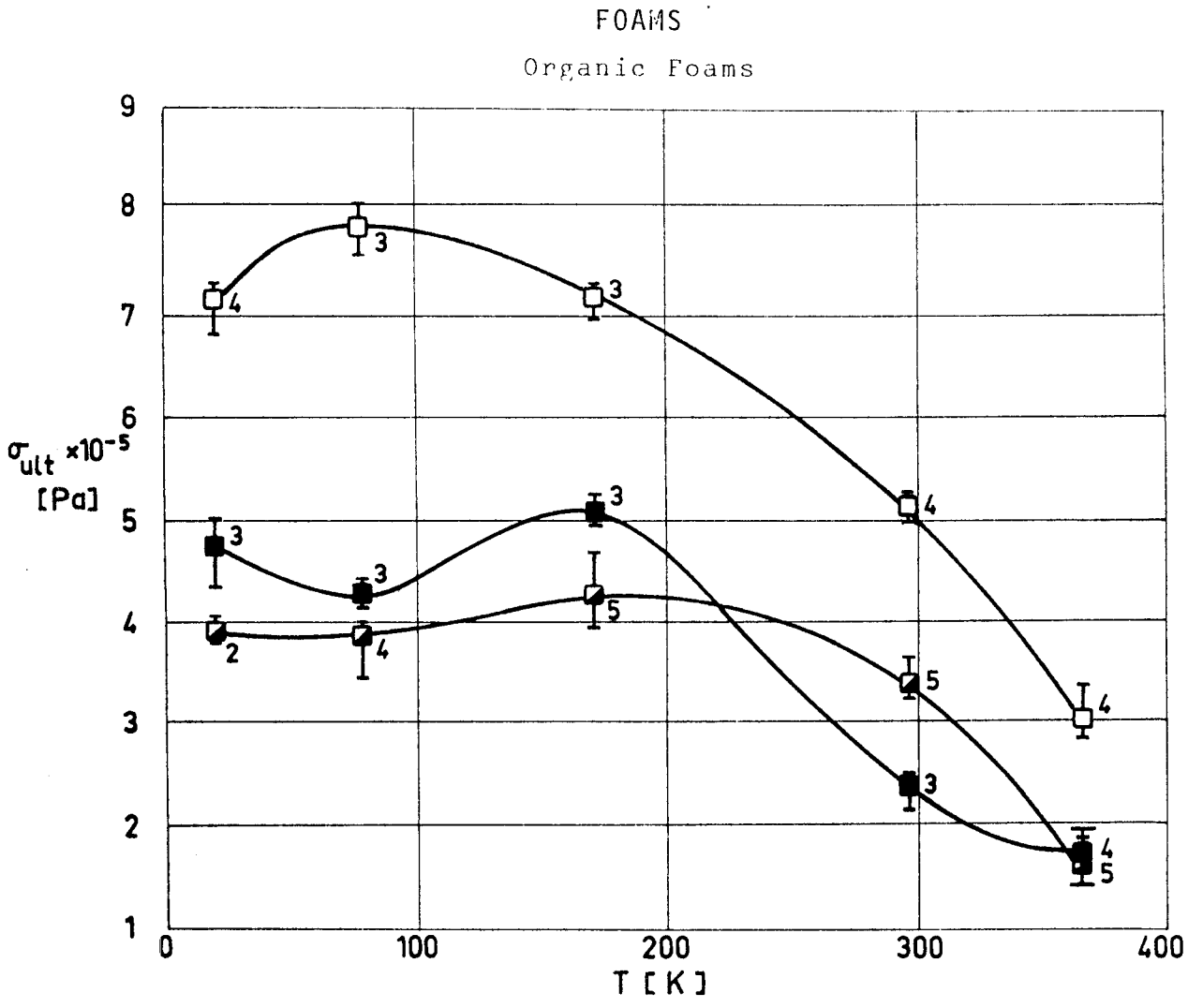

Fig 1-21. Ultimate compressive strength, σ_{ult}, as a function of temperature, T. Polyurethane spray foam, $\rho = 45$ kg.m^{-3}. Tested per ASTM D-1621; □ along the rise, ■ transversal to the rise, ◪ 45 degrees to the rise. Numbers indicate how many tests were performed in each case. From Schroeder (1973)b.

FOAMS

Organic Foams

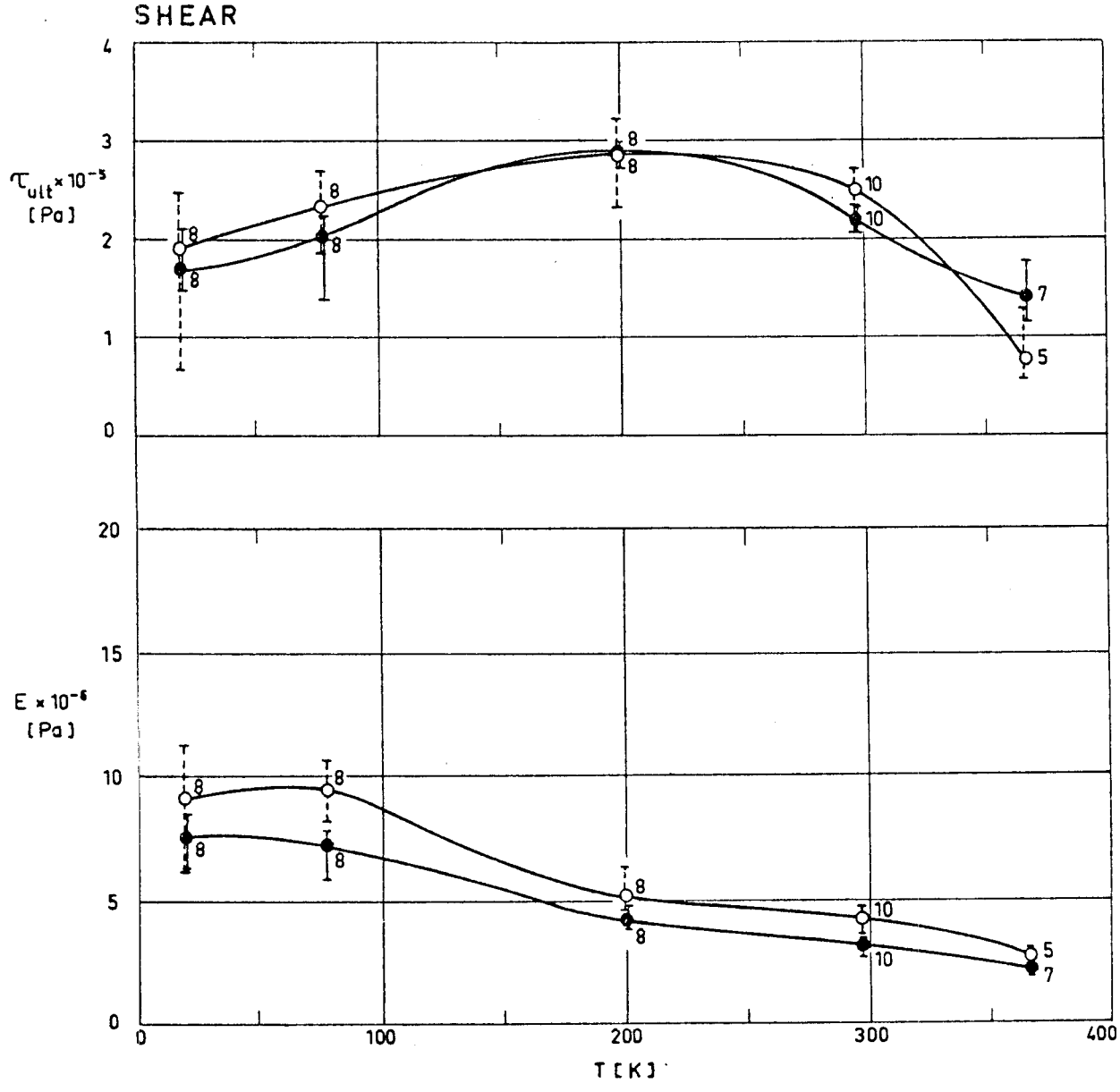

Fig 1-22. Ultimate block shear strength, τ_{ult}, and Modulus of Elasticity-shear block-E, as functions of temperature, T. Polyurethane spray foam, $\rho = 32$ kg.m^{-3}. Teste per ASTM C-273; O along the rise, ● transversal to the rise. Numbers indicate how many tests were performed in each case. From Schroeder (1973)b.

FOAMS

Organic Foams

MANUFACTURER	DOW CORNING	EMERSON & CUMING, INC						
TRADE NAME	SILASTIC S-5370	ECCOFOAM FPH			ECCOFOAM SH			ECCOBOND SF-40
NATURE	SILICONE	POLYURETHANE			POLYURETHANE			EPOXY
DESCRIPTION	Resilient rubbery foam, for molding and foaming in place	High temperature resistant foam in place			Sheets made from Eccofoam FPH.			Syntactic foam epoxy adhesive and rigid filler
PHYSICAL PROPERTIES								
Color	Tan	Pink			Pink			White
Cell Type	10% Closed	Closed			Closed			
Density, ρ [kg.m^{-3}]	154	32	128	224	32	128	224	641
OPERATING TEMPERATURE								
Max. Temperature [K]	470	408	408	408	408	408	408	422
THERMAL PROPERTIES								
Thermal Conductivity, k [W.m^{-1}.K^{-1}]	.045	.021	.043	.062	.017	.034	.034	.144
Linear Coefficient of Thermal Expansion, $\beta \times 10^{-5}$ [K^{-1}]		2.5	4	5				3.78
MECHANICAL PROPERTIES								
Tensile Strength, $\sigma \times 10^{-6}$ [Pa]		.28	1.38	3.10				
Compressive Modulus, $E \times 10^{-9}$ [Pa]								
Compressive Strength, $\sigma \times 10^{-6}$ [Pa]		.21	1.72	4.14	.21	1.72	4.14	68.94
Flexural Modulus, $E \times 10^{-6}$ [Pa]		4.45	48.26	137.8				
Flexural Strength, $\sigma \times 10^{-6}$ [Pa]		.17	1.55	5.51				
Shear Strength, $\tau \times 10^{-6}$ [Pa]		.24	.96	2.07				10.34 [a]
ELECTRIC PROPERTIES								
Dielectric Strength $\times 10^{-6}$ [V.m^{-1}]	3.15	1.57	1.57	1.57				13.8
Volume Resistivity [Ω.m]	10^{17}							10^{10}
Dielectric Constant, ε_r	1.42 (at 10^5 Hz)	1.04 (from 10^4 to 10^{10} Hz)	1.12	1.25	1.04 (from 60 to 10^{10} Hz)	1.12	1.25	2.5 (at 10^6 Hz)
Dissipation Factor $D \times 10^3$	1 (at 10^5 Hz)	1 (at 10^{10} Hz)	2	.5	.5 (from 60 to 10^{10} Hz)	1	3	20 (at 10^6 Hz)
WATER ABSORPTION								
% gain in 24 h		3	1.5	1	.8	.2	.1	.4
OUTGASSING [b]								
Cure Time [h]	72 / 16	16				0		48
Cure Temperature [K]	423 / 477	328				0		298
Atmosphere	E-4 / Air	Air				0		Air
% TWL	.592 / .315	1.182				1.030		.238
% VCM	.096 / .120	.040				.010		.043
AVAILABILITY	S-5370, foam base with catalyst, is supplied in .45 kg and 4.5 kg containers				Available in maximum sheet size of .3 m × .61 m Thickness: available from 25.4×10^{-3} m to 101.6×10^{-3} m			
PROCESSING	Table 1-6	Table 1-6						Table 1-6
APPLICATIONS	SILASTIC S-5370 RTV foam is a general purpose material used for vibration or thermal insulation, cushioning, foam rubber parts, etc. ECCOFOAM FPH is used for electronic embedments, radome cores, void filling, etc. This foam was used for encapsulation of electronic modules in Telstar, Sidewinder missile and Concorde SST aircraft ECCOFOAM SH sheets are used for high temperature structural members and thermal barriers. ECCOBOND SF-40: edge filler on honeycomb papel fabrication, fillet development, etc.							

[a] Sample placed between two aluminium plates.

[b] Outgassing characteristics have been borrowed from Campbell, Marriott & Park (1973).
TWL: Total Weight Loss. VCM: Volatile Condensable Materials (by weight).
A zero indicates that cure conditions are unknown.
E-4: Chamber pressure 10^{-4} torr = .013 Pa.

From manufacturer's bulletins.

FOAMS

Organic Foams

MANUFACTURER	EMERSON & CUMING	FIBERFIL DIVISION, DART INDUSTRIES INC.			MOSITES
TRADE NAME	STYCAST 1090	F-1200/20 ABSAFIL	F-60/20 PROFIL	F-30/20 STYRAFIL	FLUOREL 1093
NATURE	EPOXY	ABS [a]	POLYPROPYLENE	POLYSTYRENE	FLUOREL [b]
DESCRIPTION	Low weight epoxide casting	Fiberglass reinforced structural foams for molding			Sponge sheets
PHYSICAL PROPERTIES					
Color	Black				
Cell Type					Closed
Density, ρ [$kg.m^{-3}$]	880	840	730	840	240 - 480
OPERATING TEMPERATURE					
Max. Temperature [K]	477 (200 min.)				480 (240 min.)
THERMAL PROPERTIES					
Thermal Conductivity, k [$W.m^{-1}.K^{-1}$]	.187				
Linear Coefficient of Thermal Expansion, 8×10^{5} [K^{-1}]	4				
MECHANICAL PROPERTIES					
Tensile Strength, $\sigma \times 10^{-6}$ [Pa]		48.26	20.68	34.47	
Compressive Modulus, $E \times 10^{-9}$ [Pa]	2.41	See Fig 1-23: Deformation vs. Compressive load		See Fig 1-23: Deformation vs. Compressive load	
Compressive Strength, $\sigma \times 10^{-6}$ [Pa]					
Flexural Modulus, $E \times 10^{-6}$ [Pa]		5170	2760	5170	
Flexural Strength, $\sigma \times 10^{-6}$ [Pa]	28.96	82.74	41.37	58.60	
Shear Strength, $\tau \times 10^{-6}$ [Pa]					
ELECTRIC PROPERTIES					
Dielectric Strength $\times 10^{-6}$ [$V.m^{-1}$]	14.8				
Volume Resistivity [$\Omega.m$]	10^{10}				
Dielectric Constant, ε_r	Fig 1-24				
Dissipation Factor, $D \times 10^{3}$	Fig 1-24				
WATER ABSORPTION					
% gain in 24 h	.4				non-absorbent.
OUTGASSING [c]					
Cure Time [h]	16 [d] / 24 [e] / 24 [e]	0	0	0	0
Cure Temperature [K]	323 / 373 / 394	0	0	0	0
Atmosphere	Air / Air / Air	0	0	0	0
% TWL	.310 / .130 / .040	.339	.169	.269	.380
% VCM	.070 / .130 / .040	.010	.044	.022	.030
AVAILABILITY					Sheets up to .61 m × 1.22 m with thicknesses from 3.18×10^{-3} m to 12.7×10^{-3} m [f]
PROCESSING	Table 1-6	Table 1-7			
APPLICATIONS	STYCAST 1090: Airborne embedment applications. FIBERFIL PRODUCTS are used in fornitures, appliance cabinets, housings, automotive products, etc. FLUOREL 1090: Low pressure fluid and gas sealing, thermal insulation shock absorbing, padding, joint filling and flotation.				

[a] Acrylonitrile-Styrene-Butadiene.

[b] Fluorel is a trade name given to a series of compounds made from hexafluoropropene and vinylidene fluoride.

[c] Outgassing characteristics have been borrowed from Campbell, Marriott & Park (1973).
TWL: Total Weight Loss. VCM: Volatile Condensable Materials (by weight).
A zero indicates that cure conditions are unknown.

[d] These outgassing data concern STYCAST 1090 obtained using Catalyst 9.

[e] These outgassing data concern STYCAST 1090 obtained using Catalyst 11 (See also Table 1-6).

[f] Thickness tolerances are ± 1/4 of nominal thickness.

From manufacturer's bulletins.

FOAMS

Organic Foams

TABLE 1-6

INFORMATION CONCERNING PROCESSING

PRODUCT	SILASTIC S-5370	ECCOFOAM FPH	ECCOBOND SF-40	STYCAST 1090
COMPONENTS	SILASTIC S-5370 foam base SILASTIC S-5370 Catalyst	Resin component and Catalysts 12-2H, 12-4H, 12-6H and 12-10H	Part A and Part B	STYCAST 1090, and either Catalyst 9 or Catalyst 11
PROCESS	Catalize 100 parts by weight of foam base with 6 parts of catalyst mixing by stirring for about 30 seconds. The mixture should be poured in place within 60 seconds of the catalyst addition.	Mix thoroughly liquid resin component (preferably heated to about 305K) with an appropiate Catalyst (which may be at room temperature), and pour the mixture into a mold. The catalyst must be selected according to table below.[a]	Mix 100 parts by weight of Part A with 9 parts of Part B and apply the material with a suitable tool (trowel, spatula,..) Pot life of the blended material is 30 min.	Weight out the quantity required and add the percent by weight of the chosen catalyst as indicated below, blending thorougly. Catalyst 9: 9% Catalyst 11: 12%. Pour the blend into a mold. Pot life is 30 min, when Catalyst 9 is used and 4 h when using Catalyst 11.
CURE CONDITIONS	Cures at room temperature, reaching optimum strength after 24 h.	Cures at room temperature. For optimum dimensional stability a post cure for 3 h at 395 K is suggested.	Cure time is 48 h for optimum strength.	Cure time is 24 h at room temperature when Catalyst 9 is used. When using Catalyst 11, cure time is 2 h at 366 K - 377 K for casting up to .2 kg and at lower temperatures for larger castings.
STORAGE	Base products should be stored at temperatures below 305 K.		Base products should be stored at room temperature in unopened containers.	Stored uncatalyzed in well sealed, unopened containers at temperatures not above 298 K.
SHELF LIFE	Six months from date of shipment.		Six months at least when stored under the above mentioned conditions	Six months when stored under the above mentioned conditions.
WARNINGS	STYCAST S-5370 contains stannous octoate and may cause skin and eye irritation. During the expansion period a small quantity of hydrogen is outgassed.	ECCOFOAM FPH contains tolylene diisocyanate, an obnoxious and hazardous material which is an irritant to the skin and mucous membranes, especially eyes and upper respiratory tract.		Avoid breathing vapors and protect skin and eves.

a. ECCOFOAM FPH can be produced at any bulk density from 32 $kg.m^{-3}$ to 224 $kg.m^{-3}$ using a confined mold and the appropriate catalyst as indicated below. The resin component is the same in any case

Desired Bulk Density $[kg.m^{-3}]$	32 to 48	64 to 80	96 to 160	160 to 224
Catalyst Designation	12 - 2H	12 - 4H	12 - 6H	12 - 10H
Parts of Catalyst per 100 parts of Resin	65	75	75	85

FOAMS

Organic Foams

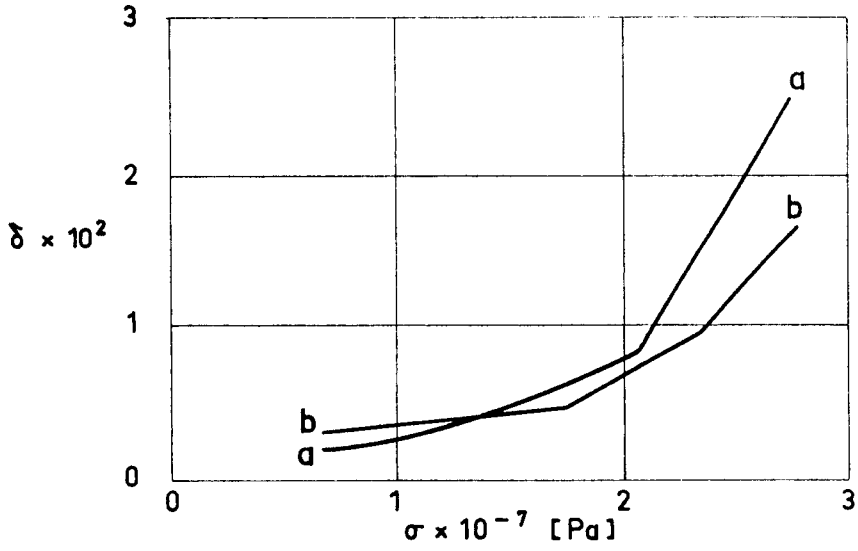

Fig 1-23. Strain, δ, vs. compressive stress, σ, of Fiberfil Structural Foams.
a: F-1200/20 Absafil.
b: F-30/20 Styrafil.
Specimen: 12.7×10^{-3} m × 12.7×10^{-3} m × × 12.7×10^{-3} m.
Test temperature: 323 K.

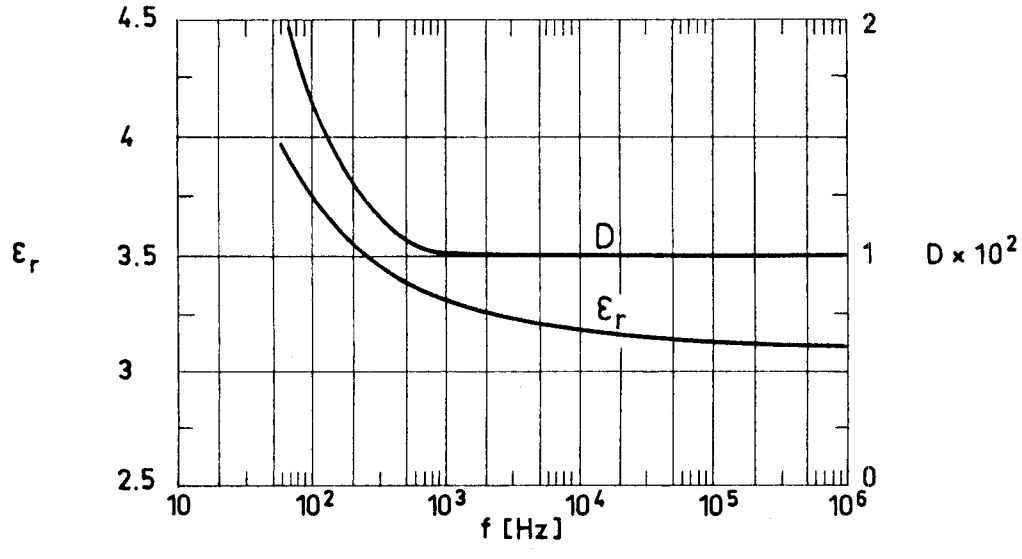

Fig 1-24. Dielectric constant, ε_r, and dissipation factor, D, vs. frequency, f. Stycast 1090.

FOAMS

Organic Foams

Table 1-7

INFORMATION CONCERNING PROCESSING OF FIBERFIL PRODUCTS

Recommendations for Molding

		STYRAFIL F-30	PROFIL F-60	ABSAFIL F-1200
Drying of material		Not necessary		
Preferred Melting Temperature [K]		477.5	450	477.5
Cylinder Temperatures [K]	Rear	444.5-455.5	416.5-427.5	444.5-455.5
	Center	461 -472	433 -444.5	461 -472
	Front	483 -505.5	455.5-477.5	483 -505.5
	Mold	483 -505.5	455.5-477.5	483 -505.5
When large voids appear in several parts		The stock temperature has been too high		

FIBROUS INSULATIONS

General

2. FIBROUS INSULATIONS

2.1. GENERAL

Fibrous materials are used both as internal and external insulations for many spacecraft applications.

The main advantages of these materials are:

Low thermal conductivity.

Low density.

Structural integrity.

Ease of integration into a thermal protection system.

Flexibility to conform to shapes and contours of the structural components.

Availability and relatively reduced cost.

Most of these materials have been developed for furnace insulations, ovens, and high-temperature processing. Their use in spacecraft, however, has been reported several times. In addition, the refractory fibers are used in composites as matrices for ablative materials, as localized insulators, and as spacers for multilayer insulations.

The use of fibrous materials for internal insulation is somewhat hampered by the extreme scarcity of data concerning outgassing. When binders are used to improve the dimensional stability of these materials, outgassing can be significant. In addition, there may be several other sources of gaseous products added in order to make easier the manufacturing process; these additives pose one of the major flammability threats to fibrous materials that,

FIBROUS INSULATIONS

General

being based on inorganic substances, are otherwise non-flammable.

A summary of thermal conductivity values for several fibrous insulations is shown in Fig 2-1. Detailed engineering and procurement data, as reported by the manufacturers, are given in the subsequent tables and figures.

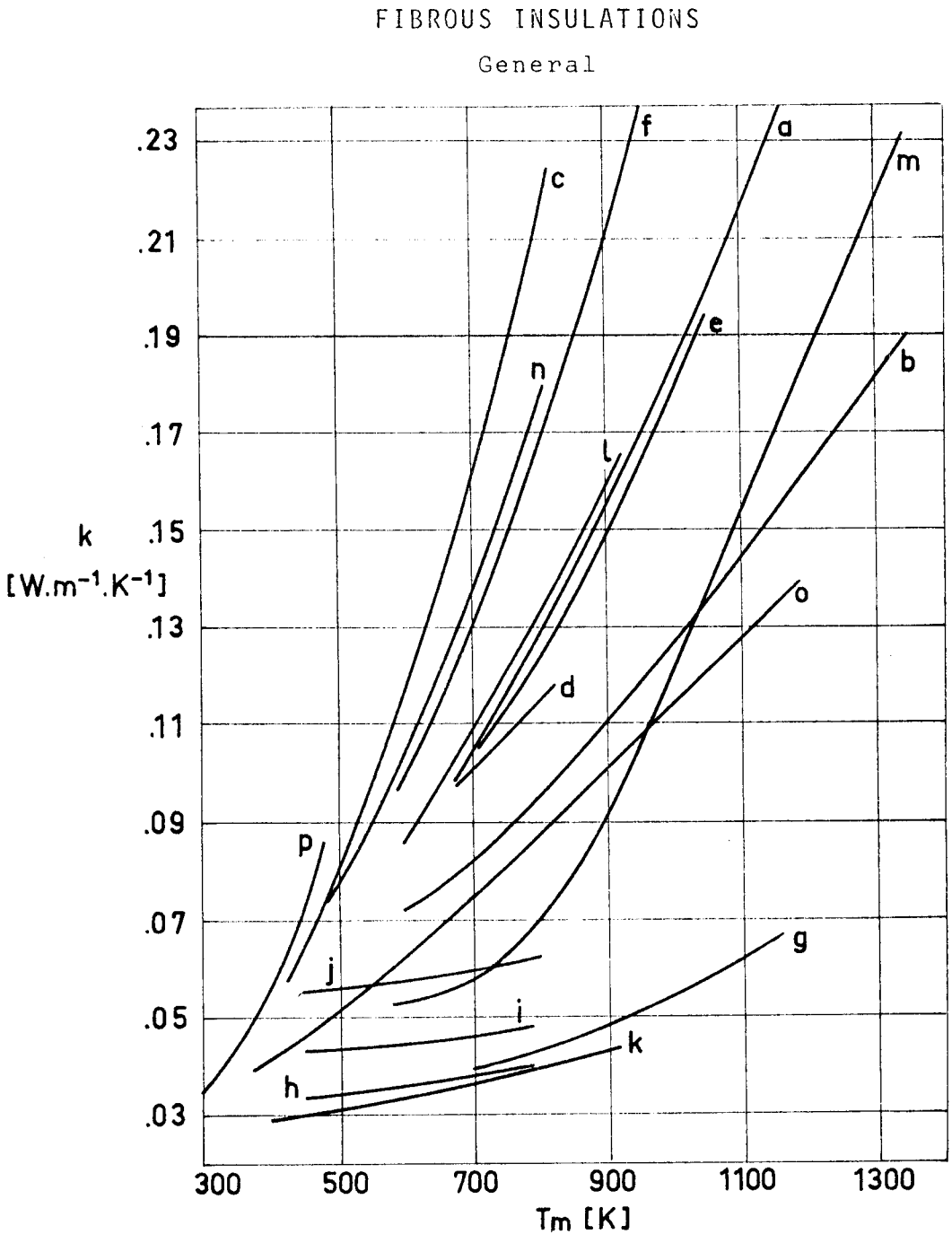

Fig 2-1. Thermal conductivity, k, vs. mean temperature, Tm, for several fibrous insulations. From Glaser et al. (1967).

Explanation

Key	Insulation	ρ [kg.m-3]	Key	Insulation	ρ [kg.m-3]	Key	Insulation	ρ [kg.m-3]
a	Fiberfrax Lo-Con	96	g	Min-K 2000	320	l	Micro-Quartz	48
b	Fiberfrax Paper	192	h	Min-K 2000	400	m	Dyna-Quartz	155
c	Kaowool bulk	48	i	Min-K 2000	480	n	Thermoflex	48
d	Kaowool bulk	160	j	Min-K 2000	561	0	Thermoflex	384
e	Refrasil Batt A-100	56	K	Min-K 1301	320	P	Microlite AA	24
f	Refrasil Batt B-100	48						

FIBROUS INSULATIONS

Bulks

2.2. BULKS

MANUFACTURER	BABCOCK & WILCOX. Trade name KAOWOOL				
NATURE	ALUMINA-SILICA				
FIBER FORM	High Purity Low percentages of iron oxide and titania	Bulk-A Lubricated	Bulk-B Unlubricated	Bulk-C Unlubricated Short fiber	Chopped Unlubricated Shorter fiber
PHYSICAL PROPERTIES					
Color	White			White	
Fiber Diameter, d [m]	2.8×10^{-6} Average			2.8×10^{-6} Average	
Fiber Length [m]	up to .254 (.102 Average)			shorts to .013	
Fiber Density, ρ [kg.m^{-3}]	2.56×10^{3}			2.56×10^{3}	
Shipping Density [kg.m^{-3}]					
Surface Area [m^{2}.kg^{-1}]					
OPERATING TEMPERATURE Continuous [K]	up to 1533				
MELTING POINT [K]	2033				
THERMAL PROPERTIES Specific Heat, c [J.kg^{-1}.K^{-1}]	1067 [a]				
Thermal Conductivity, k [W.m^{-1}.K^{-1}]	Fig 2-2				
Temperature Differential [K]					
MECHANICAL PROPERTIES Fiber Modulus of Elasticity [Pa]	1.15×10^{11}				
Bulk Modulus of Elasticity [Pa]					
Tensile Strength, Fiber [Pa]	1.3×10^{9}				
CHEMICAL COMPOSITION %					
Al_2O_3	47.0	45.1			
SiO_2	52.9	51.9			
ZrO_2					
Fe_2O_3	.05 (.1 max)	1.3			
P_2O_5					
TiO_2	.07 (.15 max)	1.7			
B_2O_3		.08			
Na_2O		.2			
CaO		.1			
MgO		trace			
Trace inorganics	trace				
		Leachable element on surface of fiber < 165 PPM.			
CHEMICAL DEGRADATION	Excellent resistance to chemical attack. Exceptions are hydrofluoric and phosphoric acids and strong alkalies. Unaffected by oil. Thermal and physical properties are restored after drying. The lubricant in Bulk-A should be burned out at 811 K prior to use in the proximity of liquid oxygen. Bulk-B, C, and Chopped do not require this treatment.				
MOISTURE ABSORPTION	Unaffected by water				
OUTGASSING					
AVAILABILITY					
APPROXIMATE COST	2.2 US $.kg^{-1} F.O.B.				
APPLICATIONS	INSULATION: Kiln car tops, walls and crowns of annealing, brazing, heat treating and holding furnaces. Fill for roofs and walls of furnaces and kilns. PACKING: Expansion joints, emergency repair and patching. SECONDARY PRODUCT PROCESSING: Paper, block, spray mix, vacuum formed shapes, monolithics, etc.. REINFORCEMENT FOR COMPOSITE STRUCTURES: Plastics, resins, etc..				
[a]	At 1255 K Mean Temperature				

From manufacturer's bulletins.

FIBROUS INSULATIONS

Bulks

MANUFACTURER	CARBORUNDUM. Trade name FIBERFRAX				
NATURE	ALUMINA-SILICA				
FIBER FORM	Bulk Fiber	Washed Low content of unfiberized particles	HI-FI Washed Lower content of unfiberized particles	Chopped Short fiber	Milled Shorter fiber
PHYSICAL PROPERTIES					
Color	White	White	White	White	White
Fiber Diameter, d [m]	$2\text{-}3 \times 10^{-6}$	$2\text{-}3 \times 10^{-6}$	1.6×10^{-6}	$2\text{-}3 \times 10^{-6}$	$2\text{-}3 \times 10^{-6}$
Fiber Length [m]	.1		up to .05	3×10^{-4}	14×10^{-6}
Fiber Density, ρ [kg.m^{-3}]	2.53×10^{3}	2.53×10^{3}	2.53×10^{3}	2.53×10^{3}	2.53×10^{3}
Shipping Density [kg.m^{-3}]	96	64 - 96		112 - 192	176
Surface Area [m^2.kg^{-1}]	500	500			
OPERATING TEMPERATURE Continuous [K]	1533				
MELTING POINT [K]	2066.5				
THERMAL PROPERTIES Specific Heat, c [J.kg^{-1}.K^{-1}]	1130 [b]	1130 [b]	1130 [b]	1130 [b]	1130 [b]
Thermal Conductivity, k [W.m^{-1}.K^{-1}]	Fig 2-3	Fig 2-3	Same as Washed	.144 [a]	.187 [a]
Temperature Differential [K]	Fig 2-4 to 2-6	Fig 2-7			
MECHANICAL PROPERTIES Fiber Modulus of Elasticity [Pa]	1.09×10^{11}				
Bulk Modulus of Elasticity [Pa]	2.74×10^{9}	2.74×10^{9}	2.74×10^{9}		
Tensile Strength, Fiber [Pa]					
CHEMICAL COMPOSITION %					
Al_2O_3	51.7				
SiO_2	47.6				
ZrO_2					
Fe_2O_3	.02				
P_2O_5					
TiO_2					
B_2O_3	.15				
Na_2O	.3				
CaO					
MgO					
Trace inorganics	.2				
	Leachable chlorides <50 PPM.				
CHEMICAL DEGRADATION	Excellent chemical stability, resisting attack from most corrosive agents. Exception are hydrofluoric and phosphoric acids and concentrated alkalies. Fiberfrax also resists oxidation and reduction. If wet by steam or oil, thermal and physical properties are restored upon drying.				
MOISTURE ABSORPTION	Unaffected by water.				
OUTGASSING					
AVAILABILITY	11.3 kg bags 18.2 kg bags for shipments over 906 kg.	Standard: 13.6 and 22.65 kg. Trial: .453 and 4.53 kg cartons		Standard 6.79 kg cartons Trial: .453 and 4.53 kg cartons	Standard: 90.6 kg drums Trial: .453 and 4.53 kg cartons
APPROXIMATE COST	For amounts below 11.3 kg: 7 US $.kg^{-1} For amounts above 45.3 kg: 5 US $.kg^{-1}				
APPLICATIONS	BULK: Expansion joints, burner openings, glass feeder bowls, fire boxes, furnace repairs, furnace base seals, kiln insulation. Bulk fiber is also used for the secondary processing of other Fiberfrax product forms: blanket, felt, paper, etc. WASHED: Manufacture of high temperature papers, as an additive for ablative compositions, insulation of aerospace vehicles and components, reinforcing additives to plastics and resins, resilient packing material. CHOPPED AND MILLED: Compact filler insulation.				
[a]	At 811 K Mean Temperature.				
[b]	At 1366.5 K Mean Temperature.				

From manufacturer's bulletins.

FIBROUS INSULATIONS

Bulks

MANUFACTURER	CARBORUNDUM. Trade name FIBERFRAX		
NATURE	ALUMINA-SILICA		
FIBER FORM	Long Staple Fine Extra Long Fiber	Long Staple Coarse Extra Long Fiber	H Bulk
PHYSICAL PROPERTIES			
Color	White	White	White
Fiber Diameter, d [m]	8×10^{-6}	18×10^{-6}	$2\text{-}4 \times 10^{-6}$
Fiber Length [m]	up to .25	up to .25	up to .025
Fiber Density, ρ [$kg.m^{-3}$]	2.62	2.62	2.6
Shipping Density [$kg.m^{-3}$]	48	48	
Surface Area [$m^2.kg^{-1}$]			
OPERATING TEMPERATURE Continuous [K]	1533		1700
MELTING POINT [K]	2066.5		2200
THERMAL PROPERTIES Specific Heat, c [$J.kg^{-1}.K^{-1}$]			
Thermal Conductivity, k [$W.m^{-1}.K^{-1}$]			Same as Bulk
Temperature Differential [K]			
MECHANICAL PROPERTIES Fiber Modulus of Elasticity [Pa]			
Bulk Modulus of Elasticity [Pa]			
Tensile Strength. Fiber [Pa]			
CHEMICAL COMPOSITION %			
Al_2O_3	43.9		62
SiO_2	50.1		38
ZrO_2	5.1		
Fe_2O_3			
P_2O_5			
TiO_2			
B_2O_3	.15		
Na_2O			
CaO			
MgO			
Trace inorganics	.75		
CHEMICAL DEGRADATION	Same characteristics as other Fiberfrax fibers		
MOISTURE ABSORPTION	Unaffected by water		
OUTGASSING			
AVAILABILITY	Standard Quantity: 11.32 kg cartons Trial Quantities: .453 and 4.53 kg cartons		
APPROXIMATE COST			
APPLICATIONS	LONG STAPLE FINE & COARSE: Catalyst recovery filter in nitric acid production, diffusion medium for fluidized beds, high temperature acoustical insulations, filtration and catalyst carrier medium for radioactive particles and hot exhaust gases, raw material for the manufacture of textiles, rope and square braid.		

From manufacturer's bulletins.

FIBROUS INSULATIONS

Bulks

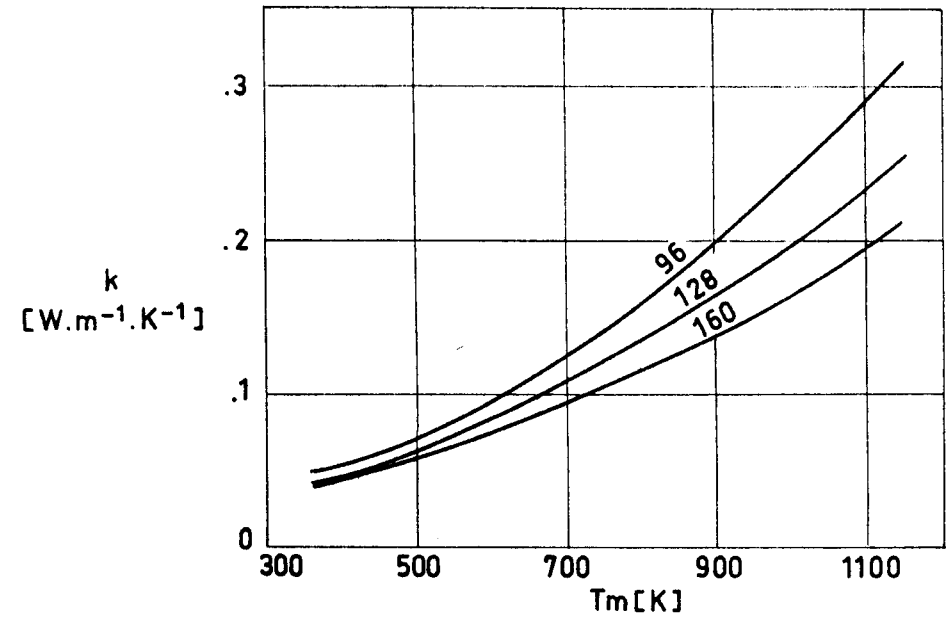

Fig 2-2. Thermal conductivity, k, of B & W Kaowool bulk vs. mean temperature, Tm. Numbers on curves indicate the density in $kg.m^{-3}$.

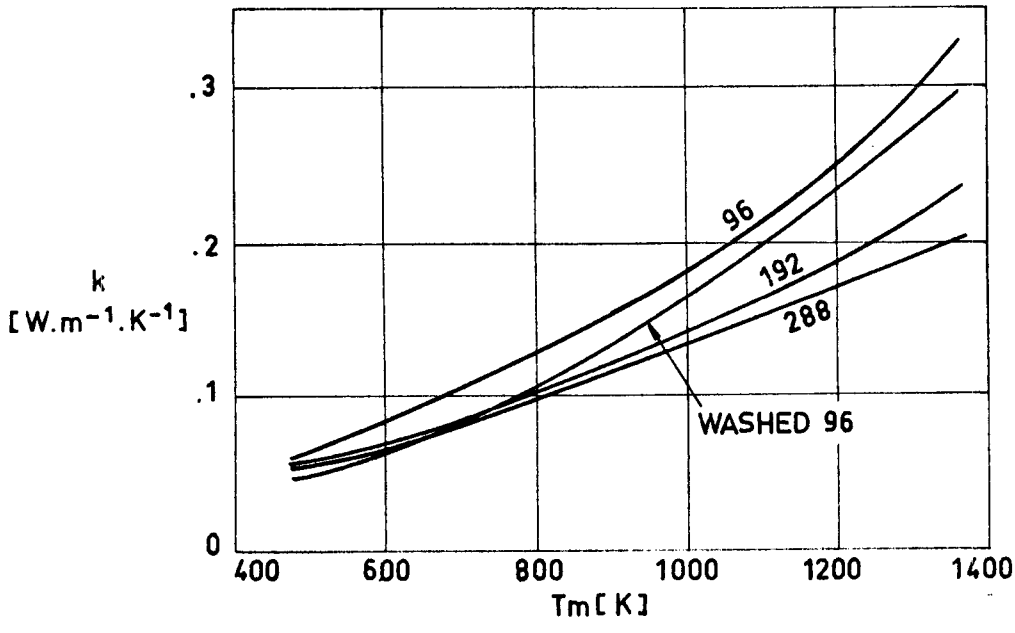

Fig 2-3. Thermal conductivity, k, of Carborundum Fiberfrax bulk and washed fibers vs. mean temperature, Tm. Numbers on curves indicate the density in $kg.m^{-3}$.

FIBROUS INSULATIONS

Bulks

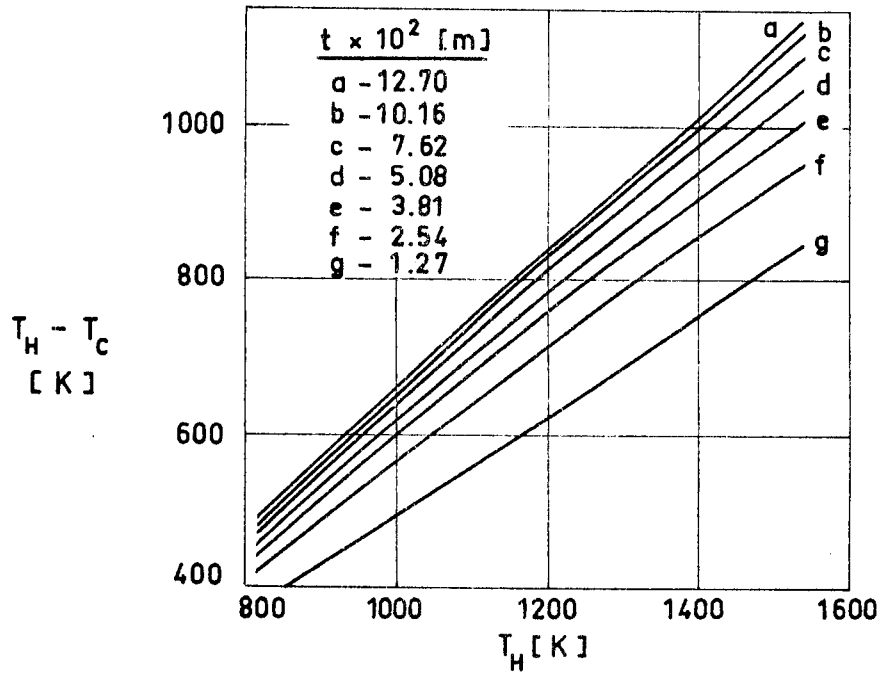

Fig 2-4. Temperature differential, T_H-T_C, vs. temperature of the hot face, T_H, for different values of the insulation thickness, t. Fiberfrax bulk, $\rho = 96$ kg.m^{-3}.

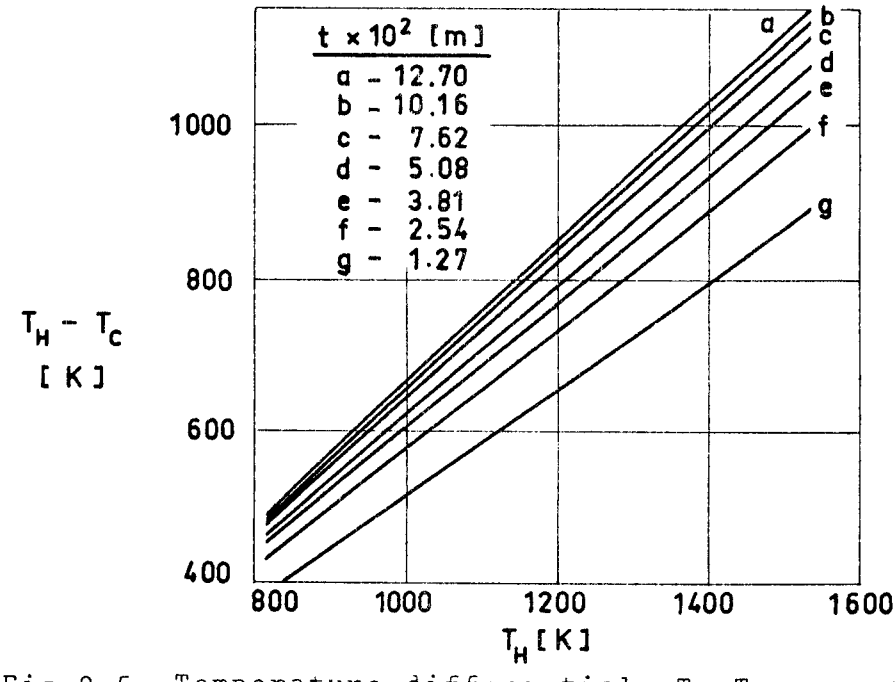

Fig 2-5. Temperature differential, T_H-T_C, vs. temperature of the hot face, T_H, for different values of the insulation thickness, t. Fiberfrax bulk, $\rho = 192$ kg.m^{-3}.

FIBROUS INSULATIONS

Bulks

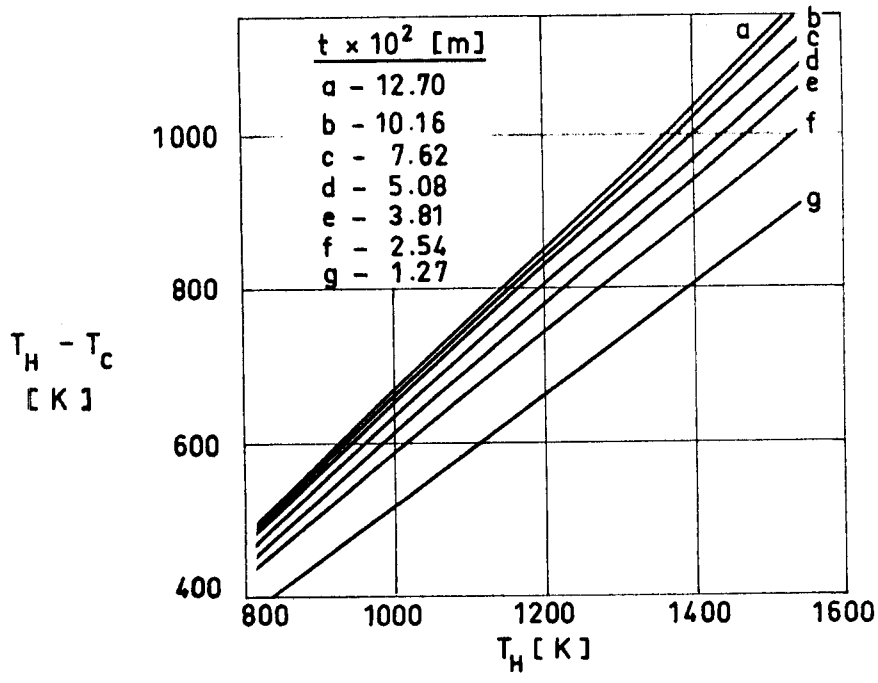

Fig 2-6. Temperature differential, T_H-T_C, vs. temperature of the hot face, T_H, for different values of the insulation thickness, t. Fiberfrax bulk, $\rho = 288$ kg.m^{-3}.

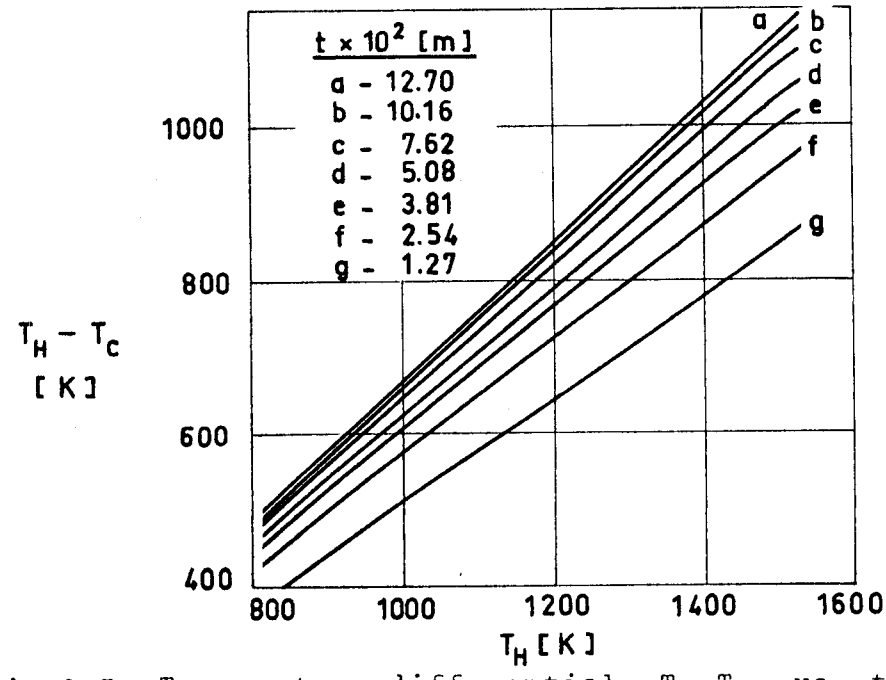

Fig 2-7. Temperature differential, T_H-T_C, vs. temperature of the hot face, T_H, for different values of the insulation thickness, t. Fiberfrax washed fiber, $\rho = 96$ kg.m^{-3}.

FIBROUS INSULATIONS

Blankets and Felts

2.3. BLANKETS AND FELTS

MANUFACTURER	BABCOCK & WILCOX		CARBORUNDUM		
TRADE NAME	KAOWOOL		FIBERFRAX		
NATURE	ALUMINA - SILICA		ALUMINA - SILICA		
FORM	Blanket, made from B&W Kaowool Ceramic Fibers	High Purity Blanket, made from B&W Kaowool High Purity Fibers	Lo-Con Blanket and Felt, made from Fiberfrax Bulk Ceramic Fibers	PH Blanket, made from Fiberfrax Long Staple Fine or Long Staple Coarse Fibers	H Blanket and Felt, made from Fiberfrax H Bulk
PHYSICAL PROPERTIES					
Color	White		White	Tan	White (Felt Tan)
Sound Absorption Coefficient	Fig 2-8		Fig 2-9	Fig 2-9	
Binder Content	No		Small in Felt	3 - 5%	Up to 3% in Felt
Air Permeability	Fig 2-10		Fig 2-11	Fig 2-11	
Dielectric Strength [V.m^{-1}]			3.3 x 10^6		
OPERATING TEMPERATURE Continuous [K]	1533		1533	1533	1700
MELTING POINT [K]	2033		2066.5	2066.5	2200
THERMAL PROPERTIES Specific Heat, c [J.kg^{-1}.K^{-1}]	1067 [a]		1130 [b]		
Thermal Conductivity, k [W.m^{-1}.K^{-1}]	Fig 2-12		Fig 2-13		Fig 2-13
Temperature Differential [K]			Fig 2-14, 2-15		
MECHANICAL PROPERTIES Compression Resistance					
Linear Shrinkage vs. Temp.					
CHEMICAL COMPOSITION	Same as B&W Kaowool Ceramic Fiber	Same as B&W Kaowool High Purity Fiber	Same as Fiberfrax Bulk Ceramic Fiber	Same as Fiberfrax Long Staple Fiber	Same as Fiberfrax H Bulk
CHEMICAL DEGRADATION	Excellent resistance to chemical attack. Exceptions are phosphoric and hydrofluoric acids and strong alkalies. Unaffected by oil. Thermal and physical properties are restored after drying.		These blankets and felts resist attack from most corrosive agents. Exceptions are hydrofluoric and phosphoric acids and concentrated alkalies. Also resist oxidation and reduction. If wet by steam or oil, thermal and physical properties are restored upon drying. No water of combination is present.		
MOISTURE ABSORPTION	Unaffected by water		Unaffected by water		
OUTGASSING					
AVAILABILITY	Available in nominal densities of 48, 64, 96 and 128 kg.m^{-3} Roll sizes: Width: .61 and 1.22 m Length: 7.31 m For thickness see Table 2-1		See Table 2-2	Roll sizes Thickness t x 10^2 m : 1.27 and .635 Width: 1.22 m Length: 15.24 and 7.62 m Density: 96 kg.m^{-3}	Roll sizes Thickness t x 10^2 m 2.54 1.27 and .635 Width: .3, .61 and 1.22 m Length: 7.62 m Density: 96 kg.m^{-3}
APPROXIMATE COST	6.5 US $.kg^{-1} F.O.B.				
APPLICATIONS	High temperature insulation: Furnace linings. Gas turbines. Fans. Boiler combustion chambers and heat exchangers, oil fired. Catalytic mufflers and automotive afterburners. Laboratory ovens. Steam valves of headers and steam separators. Thin walls kilns-back up. Water and steam tubes-back up Acoustical service for missiles and jet aircraft. Cryogenic vessel fire protection. High temperature filters. Superheater seals. Etc.		LO-CON Blanket: Furnace insulation, firewall protection, insulation for stress relieving welds, skid rail insulation, ingot cover insulation, titanium and beryllium hot forming insulation, heating element support bases, refractory back-up insulation, catalytic combustion surfaces, furnace base seals and high temperature filtration media. LO-CON Felt: Furnace, kiln and boiler linings, gas turbine silencer and muffler insulation, thermal reactor insulation, high temperature gaskets and expansion joint seals, etc. PH Blanket: Insulation for gas turbine and jet engines, high temperature acoustical insulation, diffusion medium for fluidized beds, etc.		

[a] At 1255.5 K Mean Temperature.
[b] At 1366.5 K Mean Temperature.

From manufacturer's bulletins

FIBROUS INSULATIONS

Blankets and Felts

MANUFACTURER	JOHNS-MANVILLE				
TRADE NAME	THERMOFLEX	MICRO-QUARTZ	DYNA-QUARTZ	MICROLITE AA & B	MICROLITE AA & B
NATURE	ALUMINA-SILICA	SILICA	SILICA	BOROSILICATE	
FORM	Felt	Felt, made from 98.5% pure silica fibers. Also in bulk form	Lightweight, semi-rigid tiles Specially heat treated Micro-Quartz	Standard Blanket and Felt bonded with a phenolic resin.	Silicone Binder Blanket and Felt bonded with a high temperature silicone binder.
PHYSICAL PROPERTIES					
Color					
Sound Absorption Coefficient				Fig 2-16	
Binder content	Small	No	No	Yes (Details not given)	
Air Permeability					
Dielectric Strengh [$V.m^{-1}$]					
OPERATING TEMPERATURE Continuous [K]	1366.5	1366.5	1783	477	677
MELTING POINT [K]					
THERMAL PROPERTIES Specific Heat, c [$J.kg^{-1}.K^{-1}$]	Fig 2-23	Fig 2-23	Fig 2-17		
Thermal Conductivity, k [$W.m^{-1}.K^{-1}$]	Table 2-3	Fig 2-18	Fig 2-19	Fig 2-20	
Temperature Differential [K]					
MECHANICAL PROPERTIES Compression Resistance			Fig 2-21		
Linear Shrinkage vs. Temp.			Less than 1% [a]		
CHEMICAL COMPOSITION		SiO_2 98.50 minimun B .01 maximun Fe .06 " Al_2O_3 .50 " CaO .35 " MgO .35 " Na_2O .15 "			
CHEMICAL DEGRADATION	Non-alkaline, contains no sulphur. Thermoflex will not cause nor accelerate corrosion.	Incombustible and resistant to most acids. Micro-Quartz will not cause nor accelerate corrosion.		Incombustible and non-corrosive (has no effect on aluminium or steel) Non cellular and non-hygroscopic	
MOISTURE ABSORPTION		Unaffected by moisture		Absorbs less than 3% by weight after exposure to 95% RH at 333 K for 96 hours.	
OUTGASSING		Fig 2-22			
AVAILABILITY	Width: 1.06 m Length (sheets) 1.22 and 2.44 m Length (rolls) 7.31 m Thickness and Density: Table 2-4	Sheet width: .914 m Sheet length: 1.52 and 3.04 m Thickness and Density: Table 2-5	Width: .304 m Length: .354 m Thickness: $t \times 10^2$ [m]: .63, 1.27, 2.54, 3.81, 5.08, 6.35 and 7.62 Density: 67, 99 and 128 $kg.m^{-3}$	Width: .61, .91 and 1.82 m Roll length: 30.48 m Thickness $t \times 10^2$ [m] / Density $kg.m^{-3}$ Type "AA" / Type "B" .95 — 24 1.27 — 9.6, 16 — 9.6, 16 2.54 — 9.6 — 8, 16	
APPROXIMATE COST					
APPLICATIONS	THERMOFLEX: Aircraft jet engine insulations. High flexibility and compressibility make Thermoflex an ideal insulation filler in complicated metallic enclosures fabricated from heat-resistant alloys. MICRO-QUARTZ: Thermal insulation for aircraft, missiles, spacecraft and special industrial applications. It is also designed to provide reinforcement for high-temperature plastics such as exhaust nozzles, nose cones and aerodynamically heated surfaces. MICROLITE: Thermal and acoustical insulation for aircraft. "AA" is used for applications requiring an insulation with superior thermal and acoustical properties. "B" is for less critical applications permitting the use of a more economical insulation.				
[a]	After a 24 h soak at 1783 K.				

From manufacturer's bulletins

FIBROUS INSULATIONS

Blankets and Felts

MANUFACTURER	JOHNS - MANVILLE				
TRADE NAME	MIN-K 1301	MIN-K 2000	UNBONDED B-FIBER	MICRO-FIBER "E"	
NATURE	SILICA		BOROSILICATE		
FORM	Standard Type Blanket of Min-K faced on both sides with No. 116 glass fabric.	High Temperature Blanket of Min-K faced on both sides with high silica fabric.	Batt or Blanket consists of flame-blown glass fibers loosely felted.	Felt, made by water disposition of fine glass fibers.	
PHYSICAL PROPERTIES					
Color					
Sound Absorption Coefficient					
Binder Content				No	
Air Permeability					
Dielectric Strengh [V.m^{-1}]					
OPERATING TEMPERATURE Continuous [K]	1255		728	922	
MELTING POINT [K]					
THERMAL PROPERTIES Specific Heat, c [J.kg^{-1}.K^{-1}]	Fig 2-23	Fig 2-23			
Thermal Conductivity, k [W.m^{-1}.K^{-1}]	Fig 2-24 to 2-26	Fig 2-27 to 2-29	Fig 2-30	Fig 2-31	
Temperature Differential [K]					
MECHANICAL PROPERTIES Compression Resistance	Fig 2-32	Fig 2-33			
Linear Shrinkage vs. Temp.					
CHEMICAL COMPOSITION					
CHEMICAL DEGRADATION			Under normal use Unbonded B-Fiber will not cause nor accelerate corrosion	Under normal use Micro-Fiber "E" will not cause nor accelerate corrosion	
MOISTURE ABSORPTION					
OUTGASSING					
AVAILABILITY	Table 2-6	Table 2-7	Roll sizes: Length: 30.48 m Width: .914 m Thickness: 6.35 x 10^{-3} m Density: 24 and 48 kg.m^{-3}	Sheet length: 1.52 and 3.05 m Width: .914 m Thickness: 4.7 x 10^{-3} and 12.7 x 10^{-3} m Density: 64 and 80 kg.m^{-3}	
APPROXIMATE COST					
APPLICATIONS	MIN-K: Insulation for operational missiles, aircraft and spacecraft. Flexible Min-K blankets lend themselves to bonding, lamination with plastics, service coatings, and as insulation system components. Gemini spacecraft walls were insulated with Min-K UNBONDED B-FIBER: Used by manufacturers as a source of basic glass fibers for other products and processes. It may be used as a back-up or cold face insulation as in thermal fabrications for jet aircraft engines. MICRO-FIBER: Thermal insulation, and air and gas filtration in the medium temperature range.				

From manufacturer's bulletins.

FIBROUS INSULATIONS

Blankets and Felts

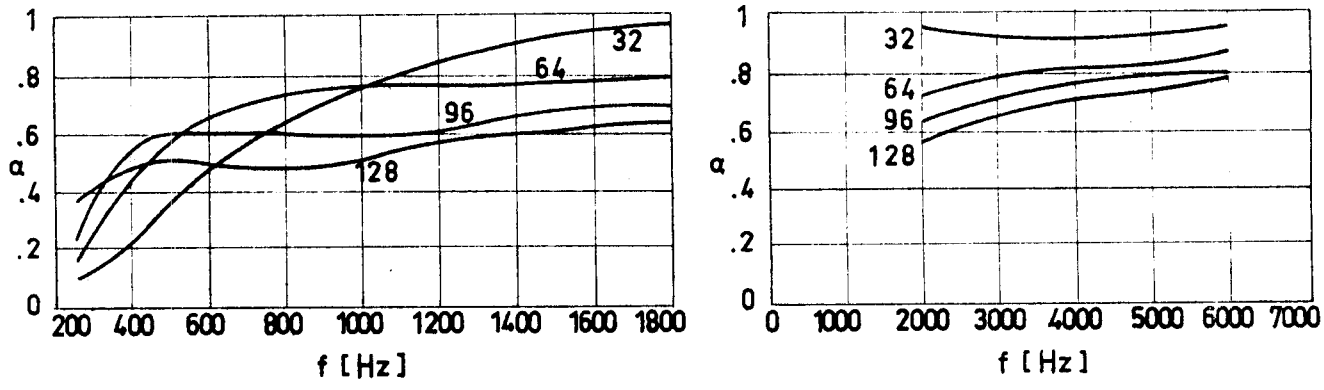

Fig 2-8. Sound absorption coefficient, α, as a function of frequency, f, for B & W Kaowool blanket 2.54×10^{-2} m thick. Numbers on curves indicate blanket densities in $kg.m^{-3}$.

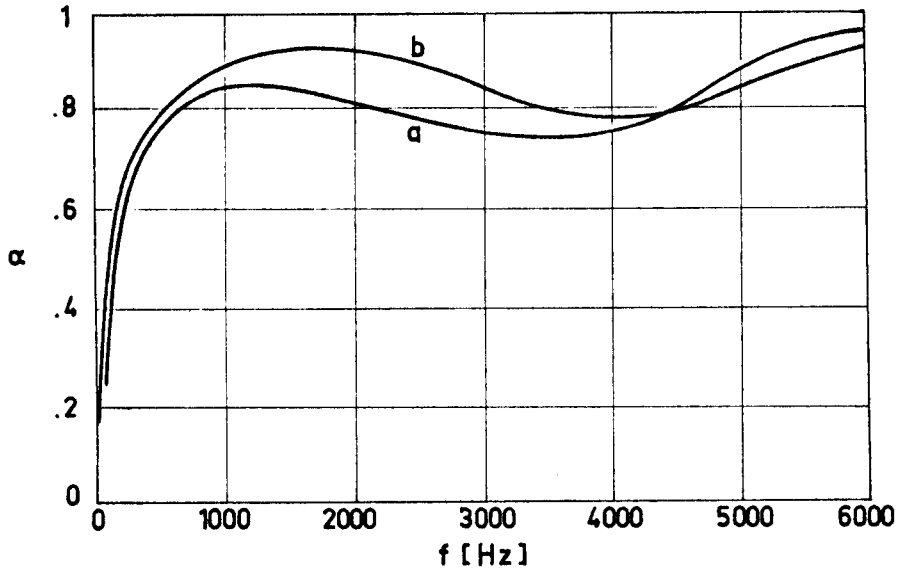

Fig 2-9. Sound absorption coefficient, α, as a function of frequency, f, for the following Fiberfrax products:

a Lo-Con blanket and felt. $t = 2.54\times10^{-2}$ m. $\rho = 96$ $kg.m^{-3}$.

b PH Fine blanket. $t = 2.54\times10^{-2}$ m. $\rho = 96$ $kg.m^{-3}$.

FIBROUS INSULATIONS

Blankets and Felts

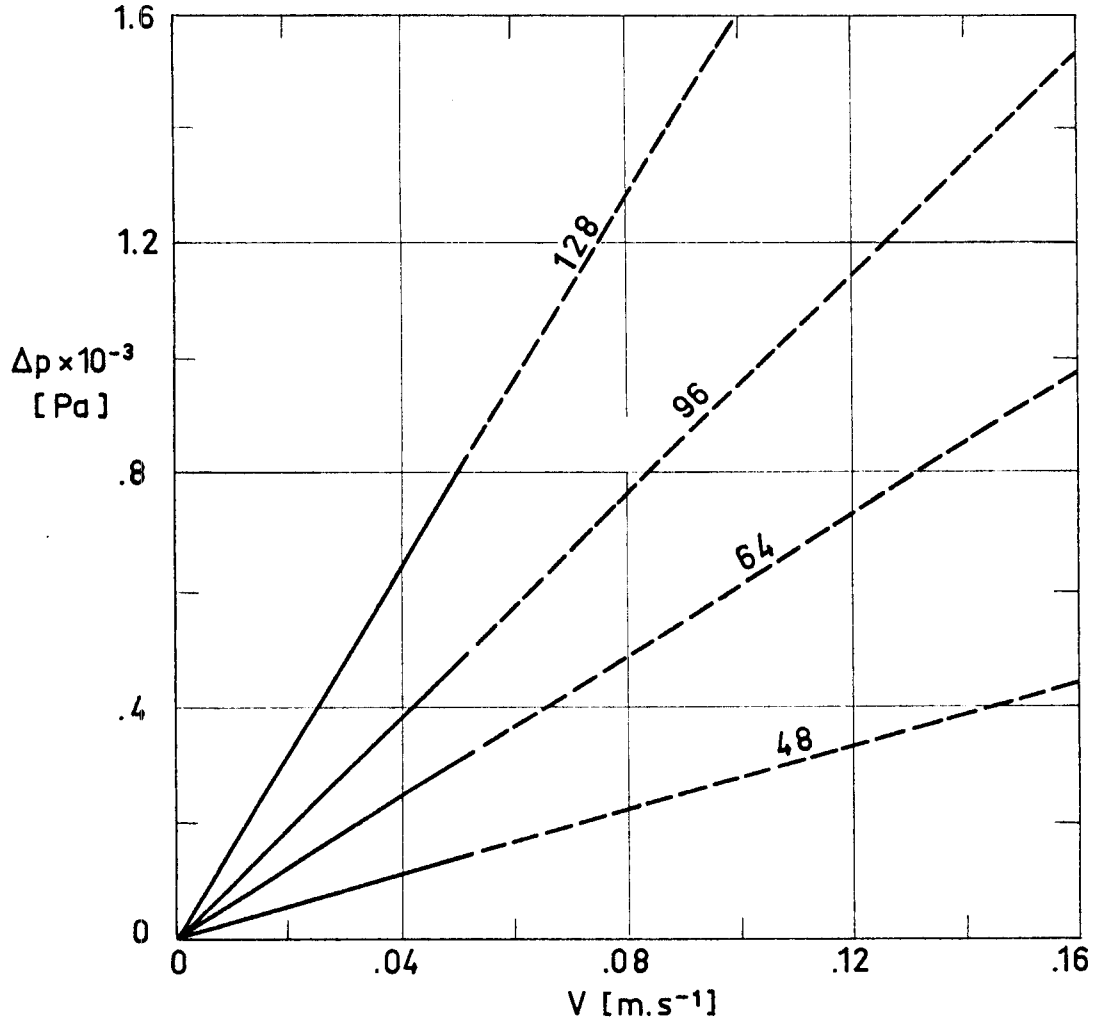

Fig 2-10. Air permeability across B & W Kaowool blankets, expressed as the variation of pressure drop, Δp, with the volume flow rate per unit area, V. Tests made under standard conditions of pressure and temperature. Numbers on curves indicate blanket densities in $kg.m^{-3}$.

FIBROUS INSULATIONS

Blankets and Felts

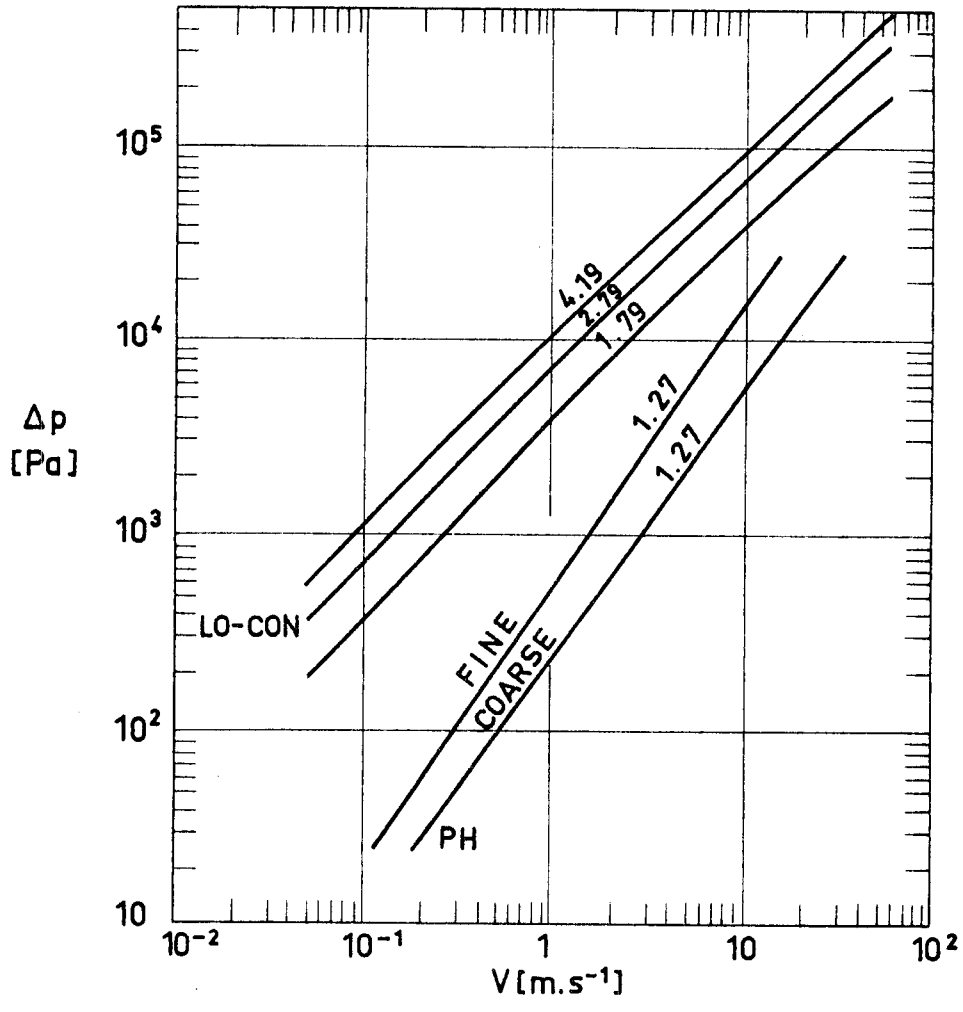

Fig 2-11. Air permeability across Carborundum Fiberfrax blankets expressed as the variation of pressure drop, Δp, with the volume flow rate per unit area, V. Tests made under standard conditions of pressure and temperature. The density of the blankets is, in any case, $\rho = 96\ kg.m^{-3}$. Numbers on curves give the thickness, $tx10^2$, measured in m.

FIBROUS INSULATIONS

Blankets and Felts

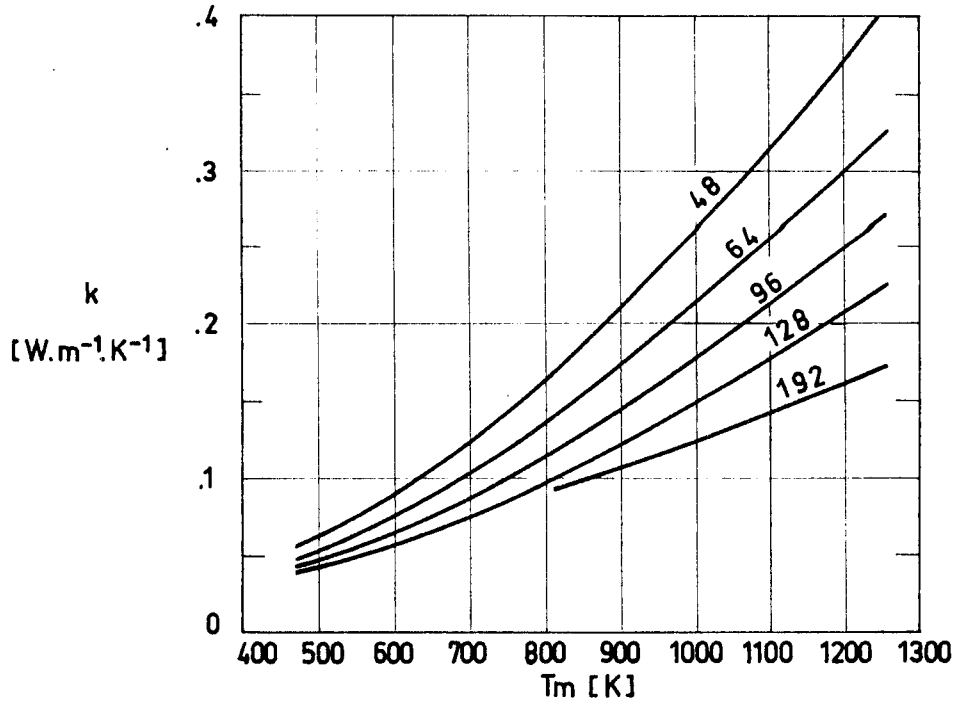

Fig 2-12. Thermal conductivity, k, of B & W Kaowool blankets vs. mean temperature, Tm. Numbers on curves indicate the blanket density in $kg.m^{-3}$.

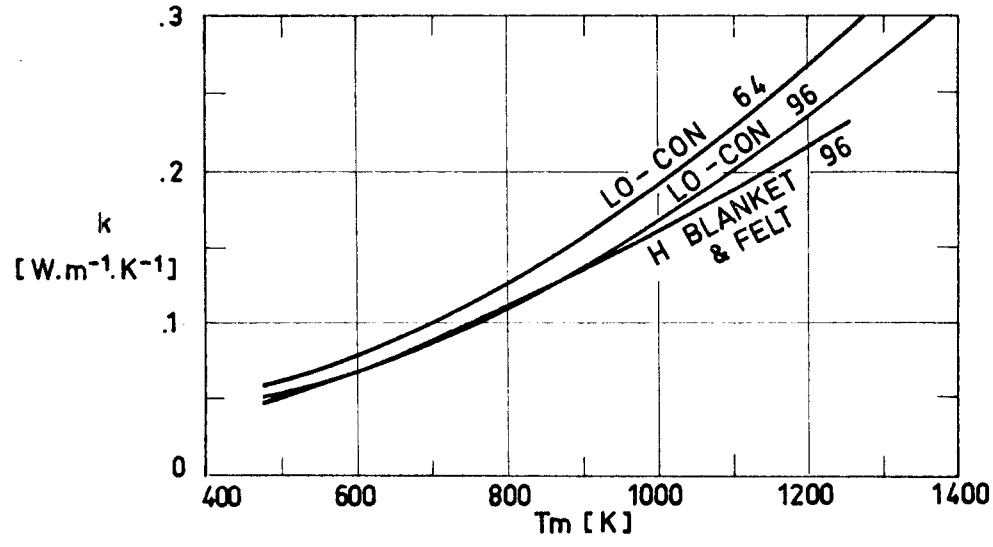

Fig 2-13. Thermal conductivity, k, of Fiberfrax blankets vs. mean temperature, Tm. Numbers on curves indicate the blanket density in $kg.m^{-3}$.

FIBROUS INSULATIONS

Blankets and Felts

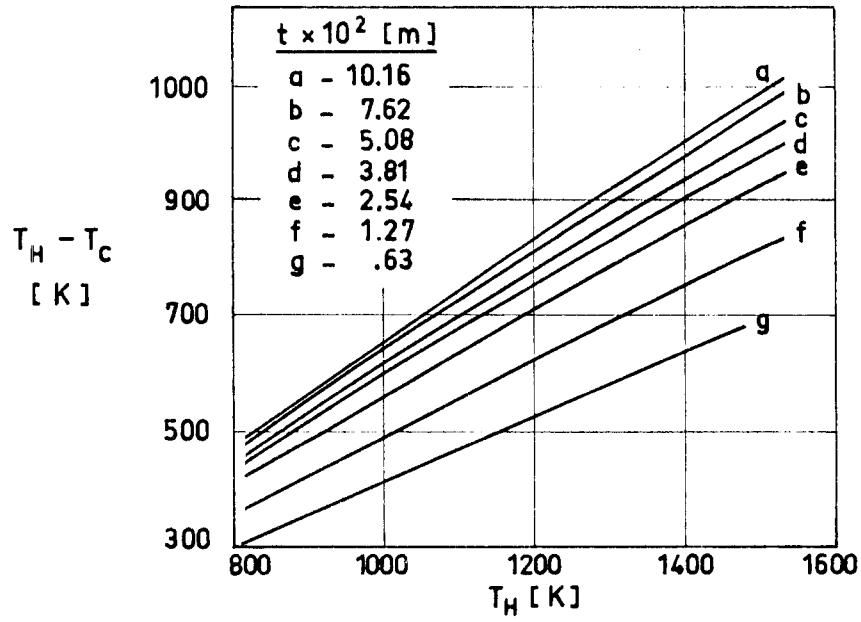

Fig 2-14. Temperature differential, T_H-T_C, vs. temperature of the hot face, T_H, for different values of the blanket thickness, t. Fiberfrax Lo-Con blanket & felt, $\rho = 64$ kg.m^{-3}.

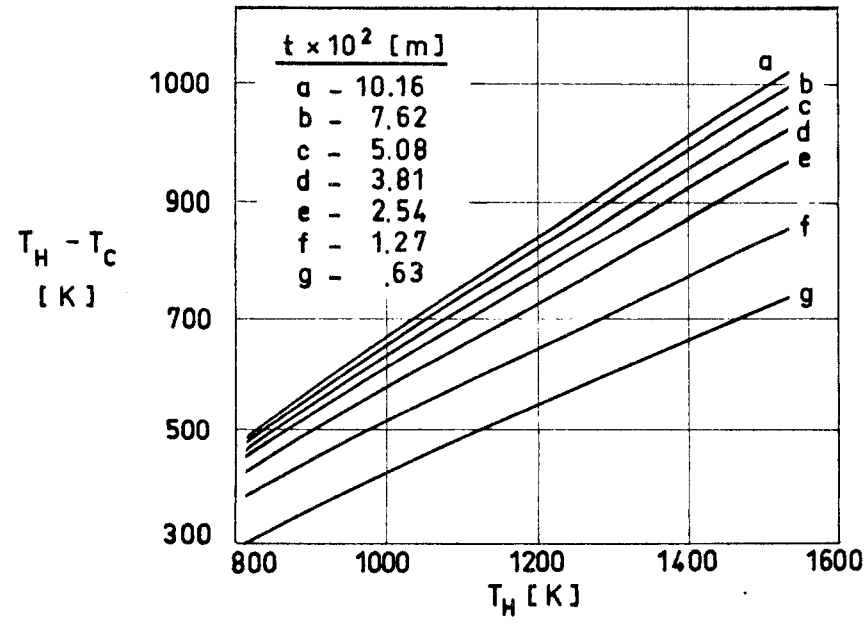

Fig 2-15. Temperature differential, T_H-T_C, vs. temperature of the hot face, T_H, for different values of the blanket thickness, t. Fiberfrax Lo-Con blanket & felt, $\rho = 96$ kg.m^{-3}.

FIBROUS INSULATIONS

Blankets and Felts

Table 2-1

Available Densities, ρ, and Thicknesses, t, of B & W Kaowool Blanket. O denotes available.

ρ [kg.m^{-3}]				$t \times 10^3$ [m]
48	64	96	128	
-	-	O	O	6.35
O	O	O	O	12.70
O	O	O	O	25.40
O	O	O	O	38.10
O	O	-	-	50.80

Table 2-2

Available Thicknesses, t, and Lengths, L, of Fiberfrax Lo-Con Blanket and Felt for densities of 64 kg.m^{-3} and 96 kg.m^{-3} and roll widths .3 m, .61 m, and 1.22 m.

$t \times 10^3$ [m]	6.35	9.56	12.70	19.12	25.40	31.75	38.10
L [m]	15.24	7.62	7.62	3.81	3.81	1.83	1.83

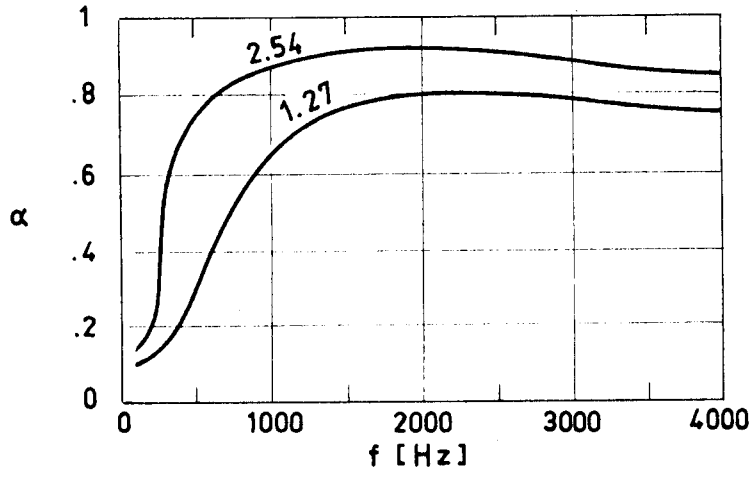

Fig 2-16. Sound absorption coefficient, α, as a function of frequency, f, for J-M Microlite Standard and Silicone Binder. Numbers on curves indicate the blanket thickness, $t \times 10^2$, measured in m.

FIBROUS INSULATIONS

Blankets and Felts

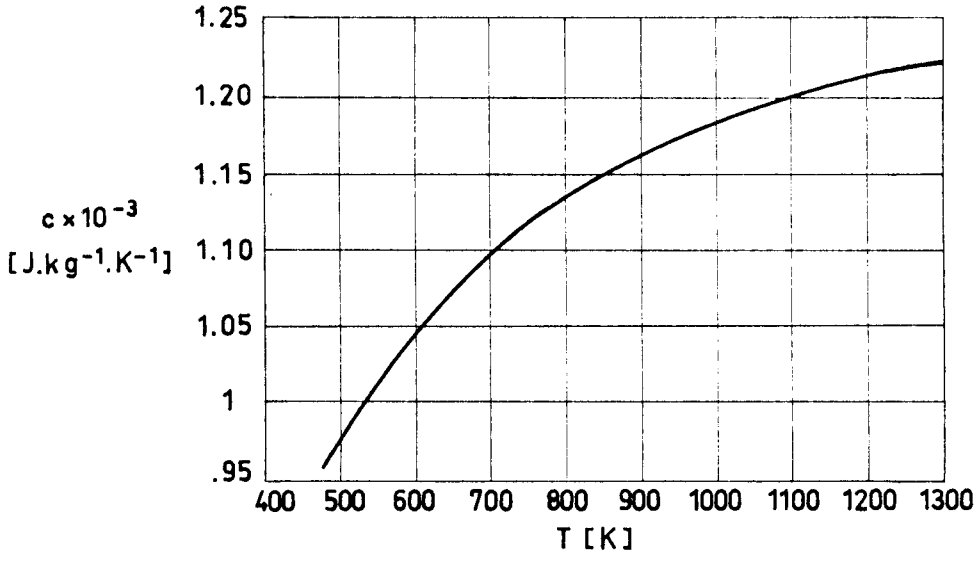

Fig 2-17. Calculated specific heat, c, as a function of temperature, T, for J-M Dyna-Quartz.

Table 2-3

Thermal Conductivity, k, $[W.m^{-1}.K^{-1}]$, of J-M Thermoflex Felt for different values of Density, ρ, $[kg.m^{-3}]$, and Mean Temperature, Tm, [K].

Tm \ ρ	48	64	96	128	160	192	224	256	288	320	352	384
422	.058	.055	.052	.049	.048	.050	.052	.053	.055	.056	.056	.056
477.5	.069	.063	.059	.056	.055	.055	.056	.056	.058	.059	.059	.061
533	.082	.075	.068	.065	.062	.061	.061	.061	.061	.062	.063	.065
588.5	.098	.088	.078	.073	.071	.066	.066	.065	.065	.066	.066	.069
644.5	.115	.102	.089	.082	.079	.071	.071	.071	.071	.071	.072	.073
700	.134	.118	.100	.092	.088	.078	.076	.076	.076	.076	.076	.078
755.5	.156	.135	.114	.104	.098	.085	.082	.082	.081	.081	.082	.082
811	.180	.154	.128	.117	.109	.094	.091	.089	.088	.088	.088	.088
866.5	-	-	.146	.130	.121	.102	.099	.097	.095	.095	.094	.094
922	-	-	.164	.146	.134	.112	.108	.105	.104	.102	.100	.100
977.5	-	-	-	-	-	.123	.117	.114	.111	.109	.108	.108
1033	-	-	-	-	-	.134	.128	.124	.121	.118	.117	.115
1088.5	-	-	-	-	-	.146	.138	.133	.128	.125	.124	.123
1144.5	-	-	-	-	-	.159	.151	.144	.138	.135	.133	.131
1200	-	-	-	-	-	.174	.163	.156	.148	.144	.141	.140
1255.5	-	-	-	-	-	.190	.177	.167	.159	.154	.151	.148

Accuracy: ±6% based on the precision of measurement and the variability of thickness.

Temperatures: T_H = Tm+366.5; T_C = Tm-366.5.

FIBROUS INSULATIONS

Blankets and Felts

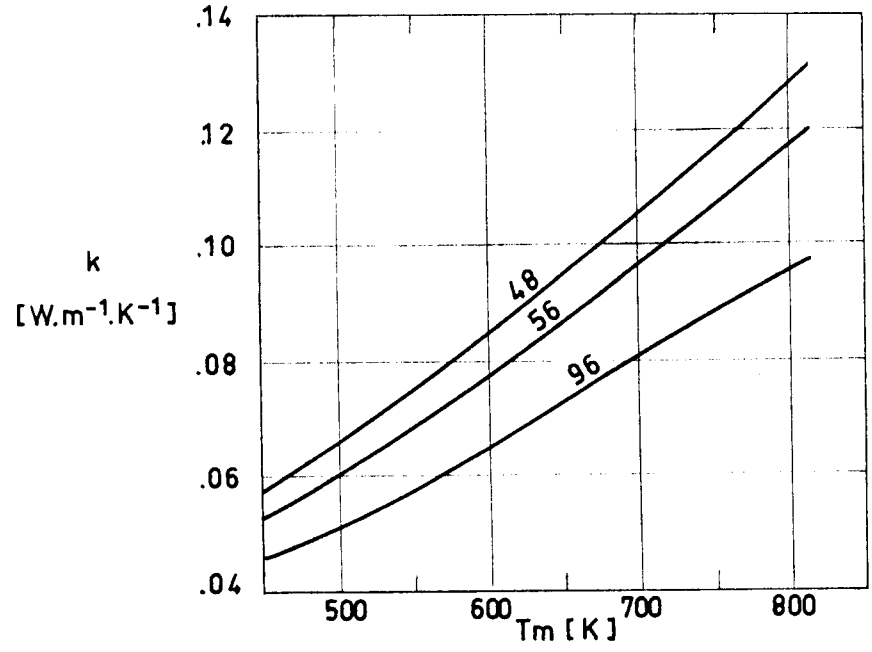

Fig 2-18. Thermal conductivity, k, of J-M Micro-Quartz felt vs. mean temperature, Tm. Numbers on curves indicate the felt density in $kg.m^{-3}$.

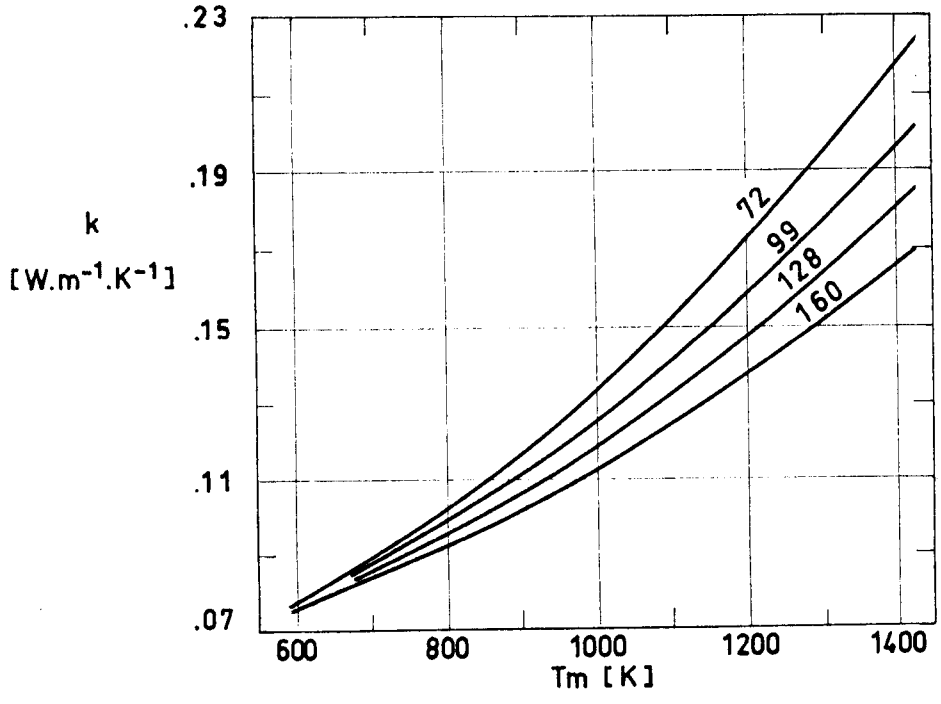

Fig 2-19. Thermal conductivity, k, of J-M Dyna-Quartz vs. mean temperature, Tm. Numbers on curves indicate the density in $kg.m^{-3}$.

FIBROUS INSULATIONS

Blankets and Felts

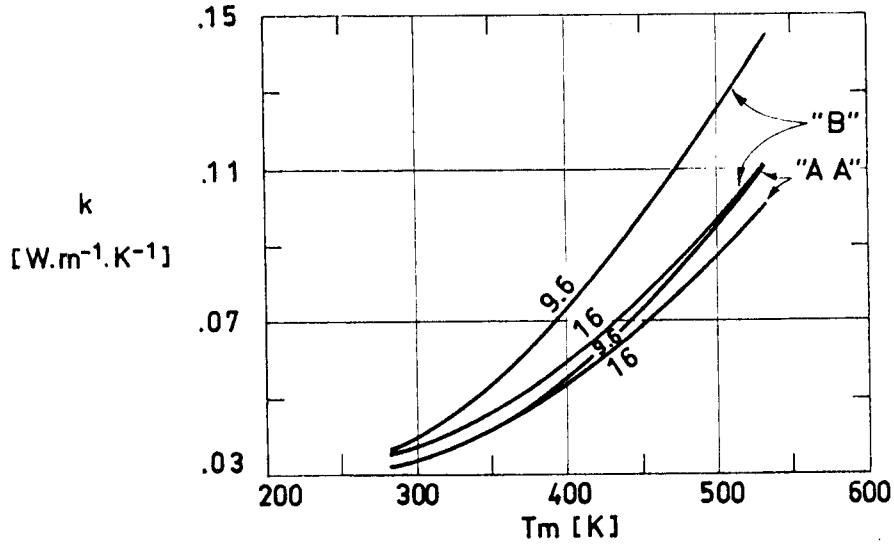

Fig 2-20. Thermal conductivity, k, of J-M Microlite "AA" and "B" vs. mean temperature, Tm. Numbers on curves indicate the density in $kg.m^{-3}$.

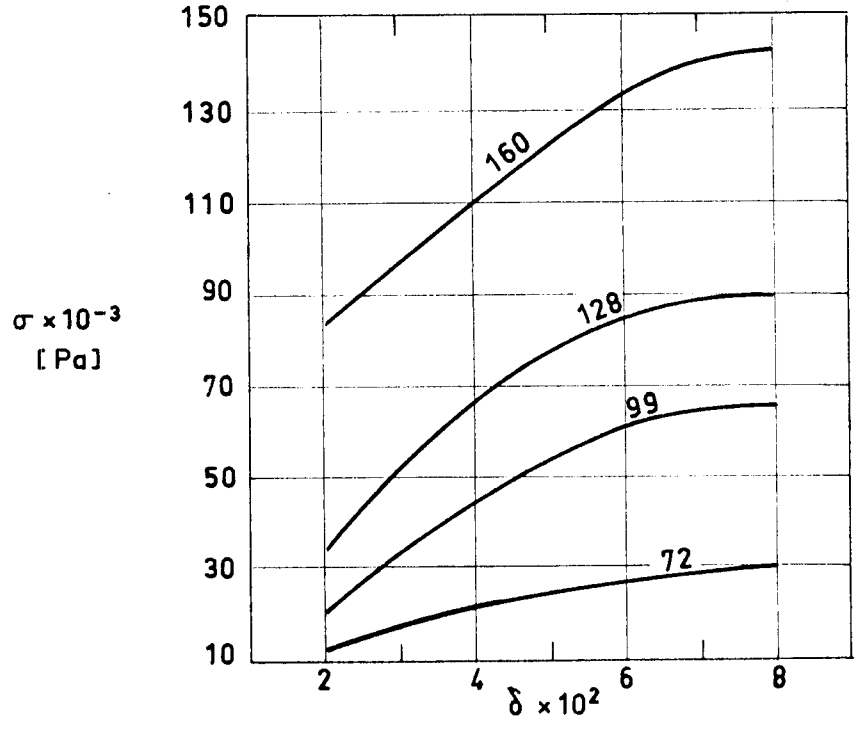

Fig 2-21. Compressive stress, σ, vs. compressive strain, δ, for J-M Dyna-Quartz. Numbers on curves indicate the density in $kg.m^{-3}$.

FIBROUS INSULATIONS

Blankets and Felts

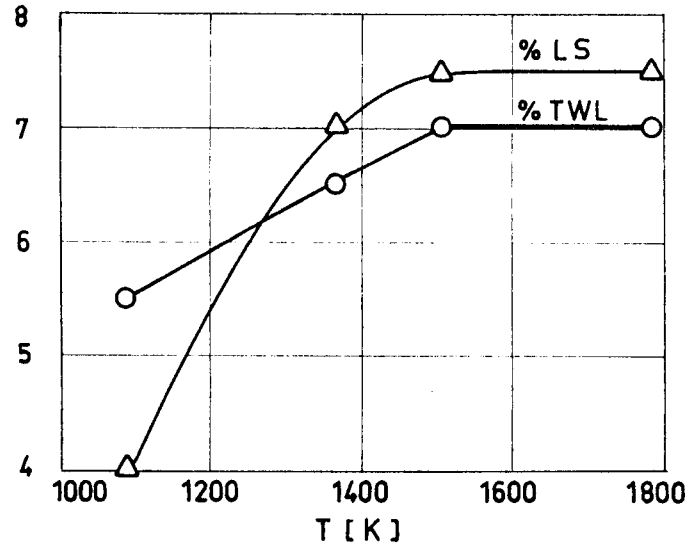

Fig 2-22. Linear Shrinkage, LS, and Total Weight Loss, TWL, of J-M Micro-Quartz Felt as a function of temperature, T.

Table 2-4

Available Densities, ρ, $[kg.m^{-3}]$, and Thicknesses, $tx10^3$ [m], of J-M Thermoflex.

ρ \ $tx10^3$	3.18	4.76	6.35	9.54	12.70	10.05	25.40	38.10	50.80
48	–	–	–	O	O	O	O	Δ	Δ
64	–	–	O	O	O	O	O	Δ	–
96	–	–	O	O	O	O	Δ	Δ	–
128	Δ	Δ	O	O	O	O	Δ	–	–
160	Δ	Δ	Δ	Δ	Δ	Δ	Δ	–	–
192	Δ	Δ	Δ	Δ	Δ	Δ	Δ	–	–
224	Δ	Δ	Δ	Δ	Δ	Δ	–	–	–
288	Δ	Δ	Δ	Δ	Δ	–	–	–	–
384	Δ	Δ	Δ	Δ	Δ	–	–	–	–

Explanation

O Sheets 1.22 m and 2.44 m length, or rolls 7.31 m length. Oven cured; can be recognized by the color and the imprint of the oven screen or conveyor flights on the surface.

Δ Sheets 1.22 m and 2.44 m length. Hot press cured; can be recognized by the gray-green color and the smooth surface resulting from the press platens.

FIBROUS INSULATIONS

Blankets and Felts

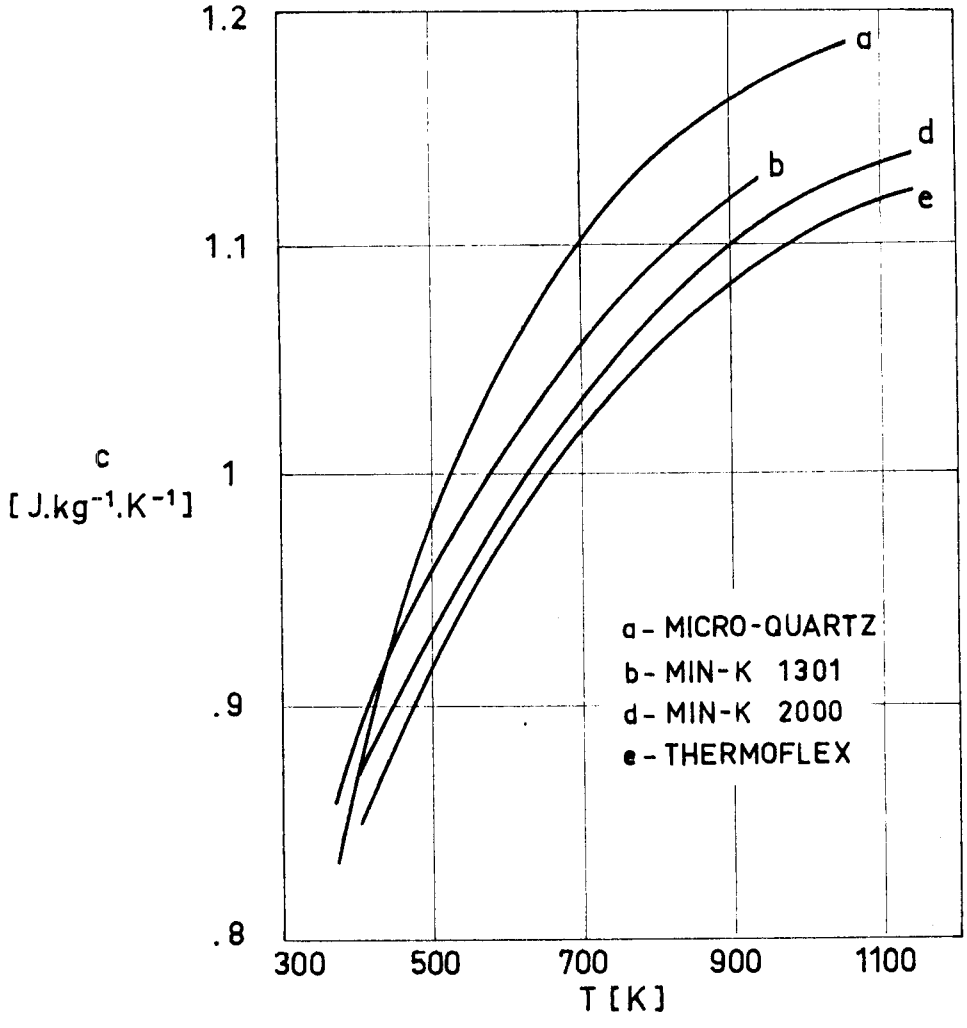

Fig 2-23. Calculated specific heat, c, as a function of temperature, T, for several J-M insulations.

FIBROUS INSULATIONS

Blankets and Felts

Table 2-5

Available Densities, ρ, and Thicknesses, t, of J-M Micro-Quartz

ρ $[kg.m^{-3}]$	$tx10^3$ [m]
48	4.76
56	12.70
96	4.76
96	12.70

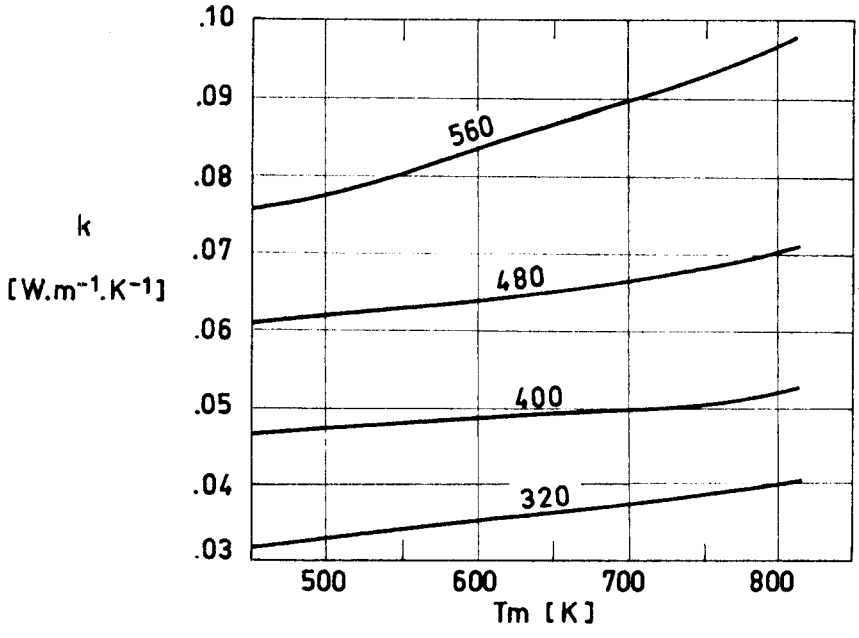

Fig 2-24. Thermal conductivity, k, of J-M Min-K 1301 vs. mean temperature, Tm. Numbers on curves indicate the density in $kg.m^{-3}$.

FIBROUS INSULATIONS

Blankets and Felts

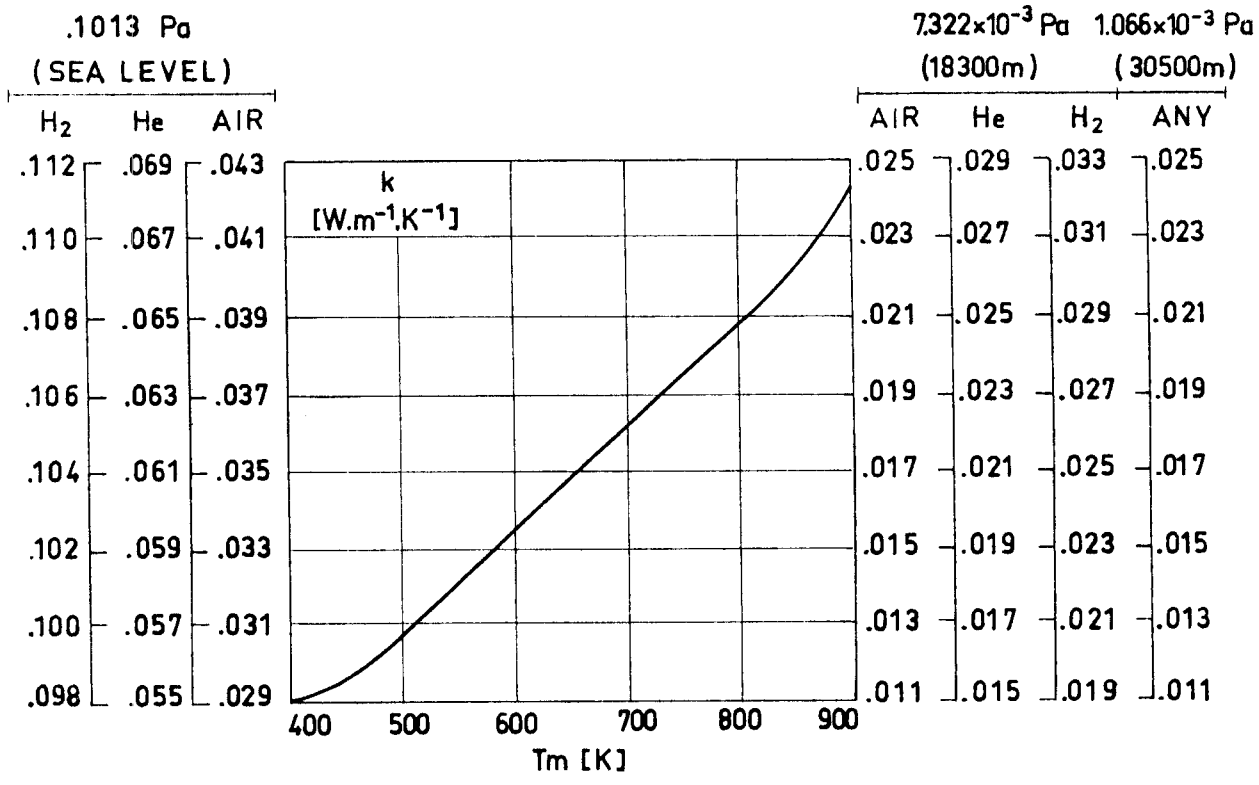

Fig 2-25. Influence of ambient pressure on the variation of thermal conductivity, k, of J-M Min-K 1301 vs. mean temperature, Tm, for several filling gases.

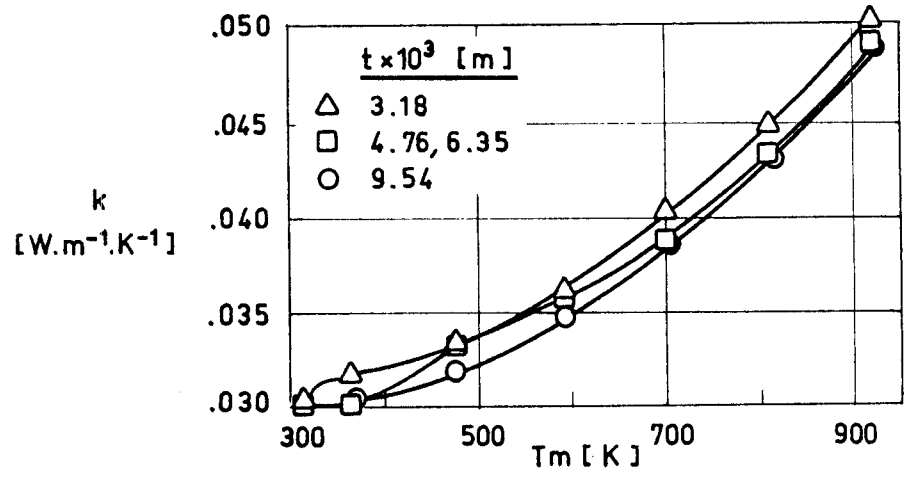

Fig 2-26. Thermal conductivity, k, of J-M Min-K 1301 vs. mean temperature, Tm, for different values of thickness, t.

FIBROUS INSULATIONS

Blankets and Felts

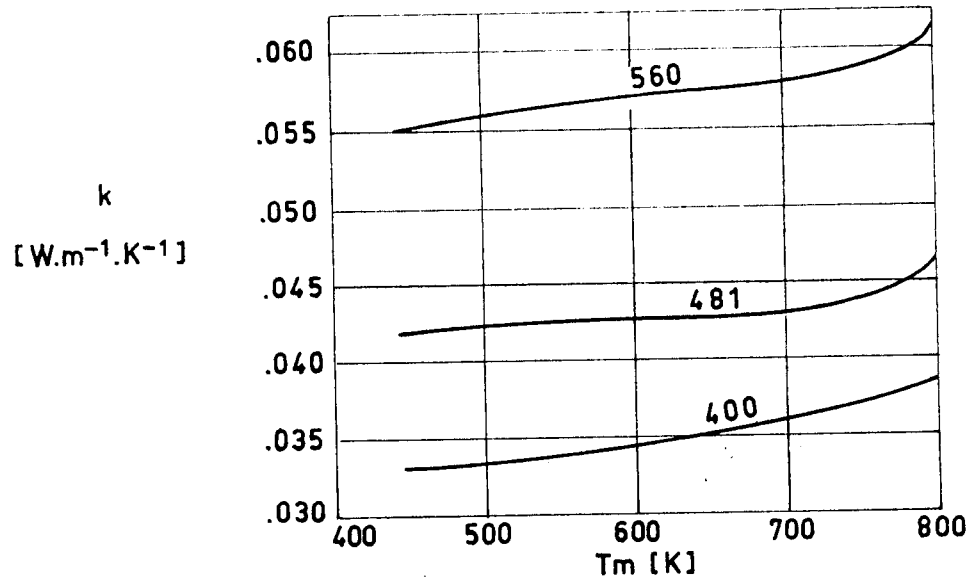

Fig 2-27. Thermal conductivity, k, of J-M Min-K 2000 vs. mean temperature, Tm. Numbers on curves indicate the density in $kg.m^{-3}$.

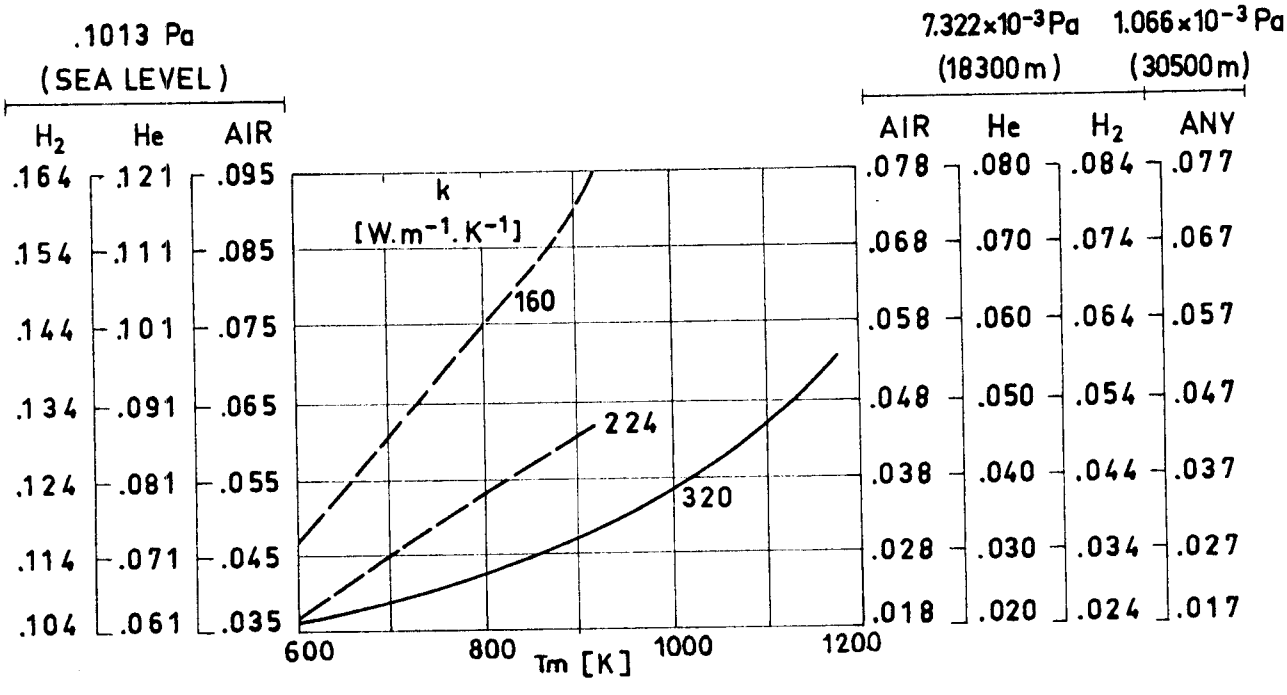

Fig 2-28. Influence of ambient pressure on the variation of thermal conductivity, k, of J-M Min-K 2000 vs. mean temperature, Tm, for several filling gases. Numbers on curves indicate the density in $kg.m^{-3}$.

FIBROUS INSULATIONS

Blankets and Felts

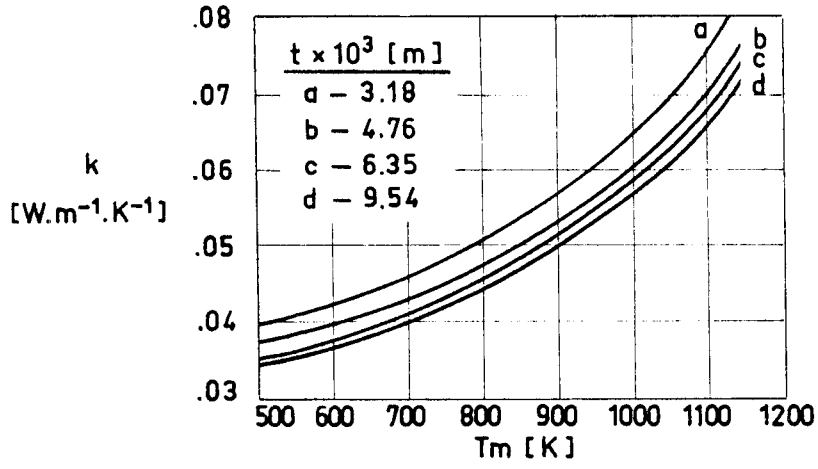

Fig 2-29. Thermal conductivity, k, of J-M Min-K 2000 vs. mean temperature, Tm, for different values of the thickness, t. The thermal conductivities are average values for the composite insulation.

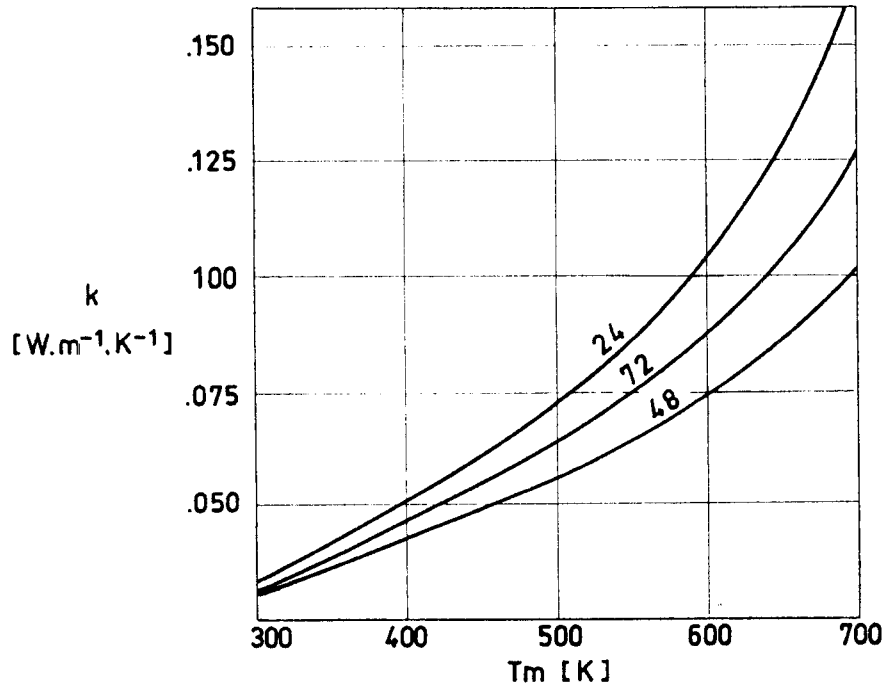

Fig 2-30. Thermal conductivity, k, of J-M unbounded B-Fiber batt vs. mean temperature, Tm. Numbers on curves indicate the density in $kg.m^{-3}$.

FIBROUS INSULATIONS

Blankets and Felts

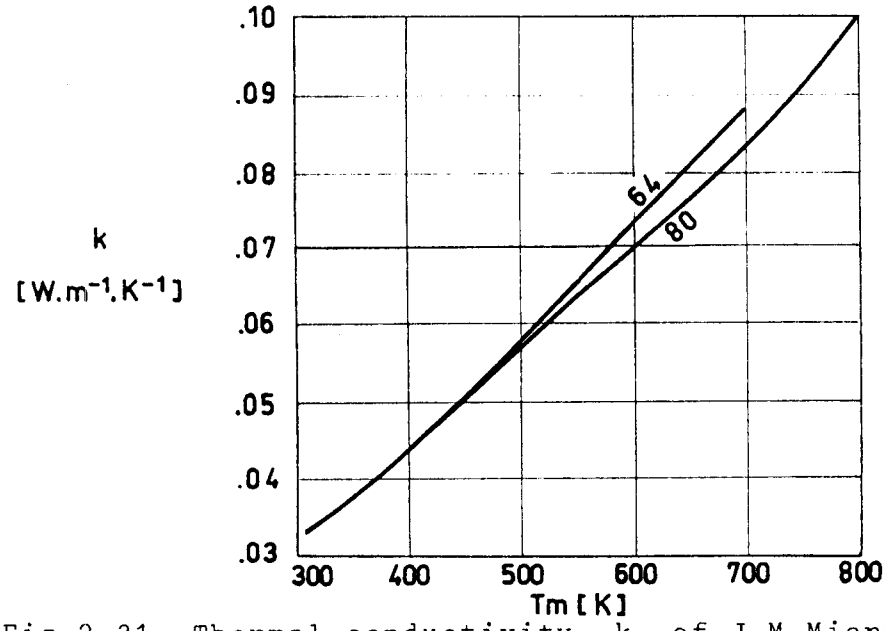

Fig 2-31. Thermal conductivity, k, of J-M Micro-Fibers felt Type "E" vs. mean temperature, Tm. Numbers on curves indicate the density in $kg.m^{-3}$.

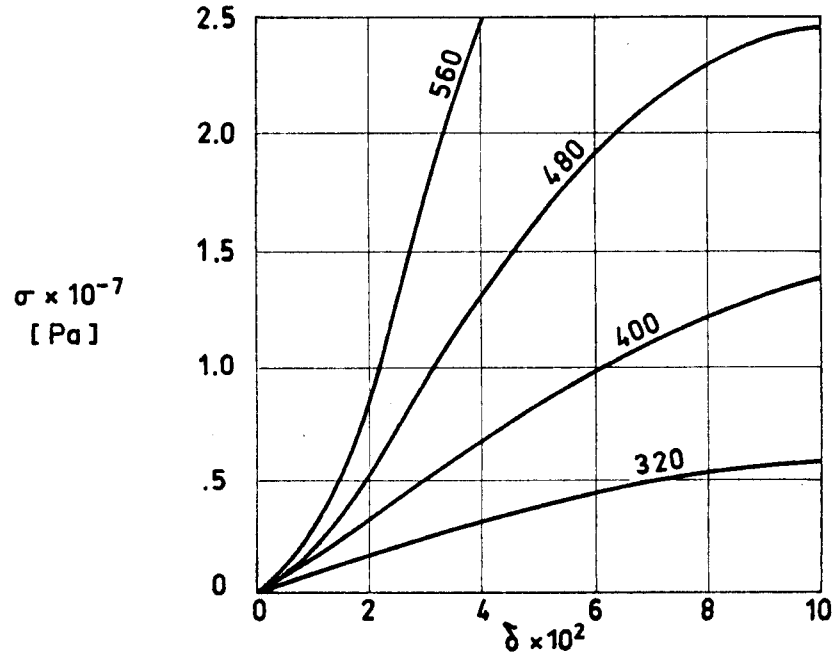

Fig 2-32. Compressive stress, σ, vs. compressive strain, δ, for J-M Min-K 1301. Numbers on curves indicate the density in $kg.m^{-3}$.

FIBROUS INSULATIONS

Blankets and Felts

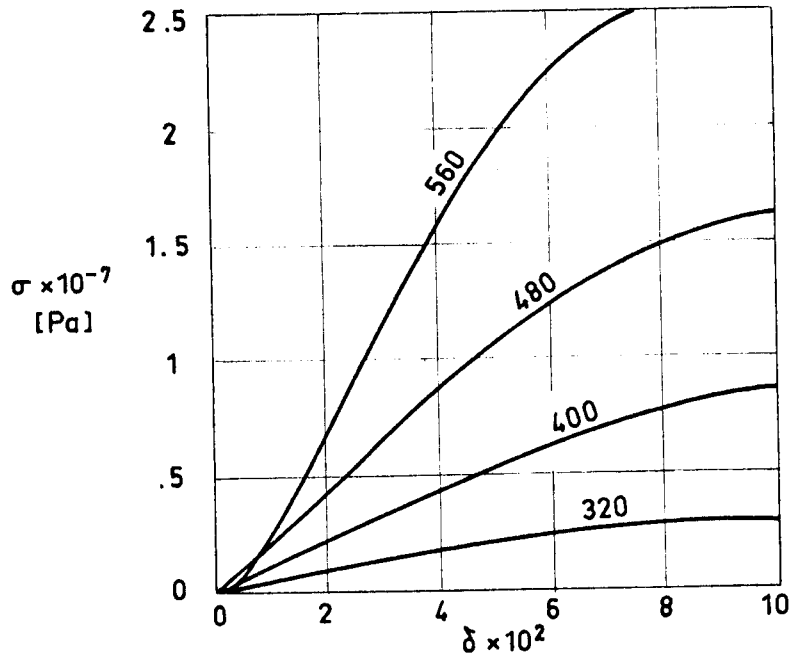

Fig 2-33. Compressive stress, σ, vs. compressive strain, δ, for J-M Min-K 2000. Numbers on curves indicate the density in $kg.m^{-3}$.

Table 2-6

Available Forms of J-M Min-K 1301

Type	Width [m]	Length [m]	tx10³ [m]	Mass/Area [kg.m⁻²]
SS	.914	.914	3.18	1.02
SS	.914	.914	4.76	1.42
SS	.914	.914	6.35	1.85
SS	.914	.914	9.54	2.64
SP	.914	1.828	4.76	1.42
SP	.914	1.828	6.35	1.81
SP	.914	1.828	9.54	2.64

Table 2-7

Available Forms of J-M Min-K 2000

Tipe	Width [m]	Length [m]	tx10³ [m]	Mass/Area [kg.m⁻²]
SS	.762	.762	3.18	1.61
SS	.762	.762	4.76	2.05
SS	.762	.762	6.35	2.44
SS	.762	.762	9.54	3.27
SP	.762	1.828	4.76	2.00
SP	.762	1.828	6.35	2.39
SP	.762	1.828	9.54	3.22

SS Stitched in 2.54×10^{-2} m square.
SP Stitched in 2.54×10^{-2} m parallel patterns.

FIBROUS INSULATIONS

Papers

2.4. PAPERS

MANUFACTURER	BABCOCK & WILCOX	CARBORUNDUM			
TRADE NAME	KAOWOOL PAPER	FIBERFRAX PAPER			
NATURE	ALUMINA-SILICA	ALUMINA-SILICA			
FORM	Paper, made from B&W Kaowool Ceramic Fibers	970 Paper, made from Fiberfrax Washed Fibers	H880 Paper, made from Fiberfrax H Washed Fibers	Hi-Fi 660 Paper made from Fiberfrax Hi-Fi Fibers	550 Paper
PHYSICAL PROPERTIES					
Color	White	White	White	White	Light Blue [a]
Binder Content	Amount not given	Table 2-9		Table 2-11	5% approx.
Density, ρ $[kg.m^{-3}]$	192 - 208	160 - 192	192	192	192 - 224
OPERATING TEMPERATURE					
Continuous [K]	Up to 1533	1533	1700	1533	1533
MELTING POINT [K]	Above 1972	2066.5	Above 2200	Above 2033	2033
THERMAL PROPERTIES					
Specific Heat, c $[J.kg^{-1}.K^{-1}]$					
Thermal Conductivity, k $[W.m^{-1}.K^{-1}]$	Fig 2-34	Fig 2-34	Same as 970 Paper	Fig 2-34	20% higher than 970 Paper
Temperature Differential [K]		Fig 2-35		Fig 2-36	
Thermal Reflectance, ρ		Fig 2-37			
MECHANICAL PROPERTIES					
CHEMICAL COMPOSITION	Same as B&W Kaowool Ceramic Fibers	Same as Fiberfrax Washed Fibers	Al_2O_3 62% SiO_2 38%	Same as Fiberfrax Washed Fibers	Al_2O_3 51.7% SiO_2 47.6%
CHEMICAL DEGRADATION	Papers exhibit good chemical stability with resistance to most chemicals, with the exception of hydrofluoric and phosphoric acids and strong alkalies. No water of combination.				
MOISTURE ABSORPTION	Unaffected by water				
OUTGASSING					
AVAILABILITY	Table 2-8	Tables 2-9,2-10	Width: .305 and .61 m. Roll weight: 4.53 and 11.34 kg. Thickness: Table 2-11	Width: .305 and .61 m. Roll weight: 4.53 and 11.34 kg. Thickness: Table 2-11	Width: .305, .61 and 1.22 m. Roll weight: 4.53 and 11.34 kg. Thickness: Table 2-11
APPROXIMATE COST					
APPLICATIONS	KAOWOOL PAPER: Aluminium & zinc launder and trough linings. Gasketing between aluminium & zinc trough sections. Aluminium furnace tap-out plug cover and parting agent. Aluminium distributor pan linings. Super Alloy Ingot mold and hot tops. FIBERFRAX 970 PAPER: High temperature gaskets. Thermal and electrical insulation. Combustion chamber liners. Back-up linings for metal troughs. Hot top linings. Tape hole plug covers. Ingot mold linings for high purity metals and glass.Etc. FIBERFRAX HI-FI 660 PAPER: Finer filtration and thermal insulation. FIBERFRAX 550 PAPER: For applications were high temperature protection is more critical than specific heat retention. Typical applications are: Industrial gasketing. Liquid metal back-up insulation. Brazing furnace insulation.				
[a]	White upon firing to approximately 811 K.				

From manufacturer's bulletins.

FIBROUS INSULATIONS

Papers

Table 2-8

Available Thicknesses of B & W Kaowool Paper

Code	20 Mil	40 Mil	80 Mil
Rated thickness, $t \times 10^3$ [m] [a]	.508	1.016	2.032
Uncompressed thickness, $t_u \times 10^3$ [m]	.795	1.59	3.18

[a] Thickness measured at 54800 Pa compression, per Tappi Method T-411m44.

Table 2-9

Available Thicknesses of Fiberfrax 970 Paper

Code [a]	970-A	970-AH	970-F	970-FH	970-J	970-JH
Rated thickness, $t \times 10^3$ [m] [b]	.508	.508	1.016	1.016	2.032	2.032
Uncompressed thickness, $t_u \times 10^3$[m]	.795	.795	1.59	1.59	3.18	3.18
Mass/Area [kg.m^{-2}]	.155	.155	.259	.244	.512	.488

[a] Series 970 may contain up to 5% organic binder. H indicates completely inorganic paper.

[b] Thickness measured at 54800 Pa compression, per Tappi Method T-411m44.

Table 2-10

Available Roll Sizes of Fiberfrax 970 Paper

Width [m]	Length [m]								
	.305			.610			1.22		
Weight kg / Thick. $t \times 10^3$[m]	1.13	4.53	11.32	1.13	4.53	11.32	1.13	4.53	11.32
.508	24.40	97.60	244.0	12.20	48.80	122.0	6.10	24.40	61.0
1.016	15.25	61.00	152.5	7.62	30.50	76.2	3.66	15.25	38.1
2.032	7.62	30.50	76.2	3.66	15.25	38.1	1.83	7.62	18.3

Each roll has indicated length; weight, however, may vary slightly.
Also available in sheet sized .305 m × .305 m, .61 m × .61 m , and .61 m × 1.22 m.
"H" Series (no binder)is not available in 1.22 m width.

Table 2-11

Available Thicknesses and Corresponding Mass/Area of Fiberfrax Paper H880; Hi-Fi 660, and 550.

	H 880			Hi-Fi 660			550	
Code [a]				C	A,AH	F,FH	F	J
Compressed thickness $t \times 10^3$ [m]	.508	1.016	2.032					
Uncompressed thickness $t_u \times 10^3$[m]	.795	1.59	3.18	.387	.795	1.59	1.59	3.18
Mass/Area [kg.m^{-2}]	.155	.259	.517	.057	.155	.259	.327	.610

[a] Series 660 may contain up to 5% organic binder. H indicates completely inorganic paper.

FIBROUS INSULATIONS

Papers

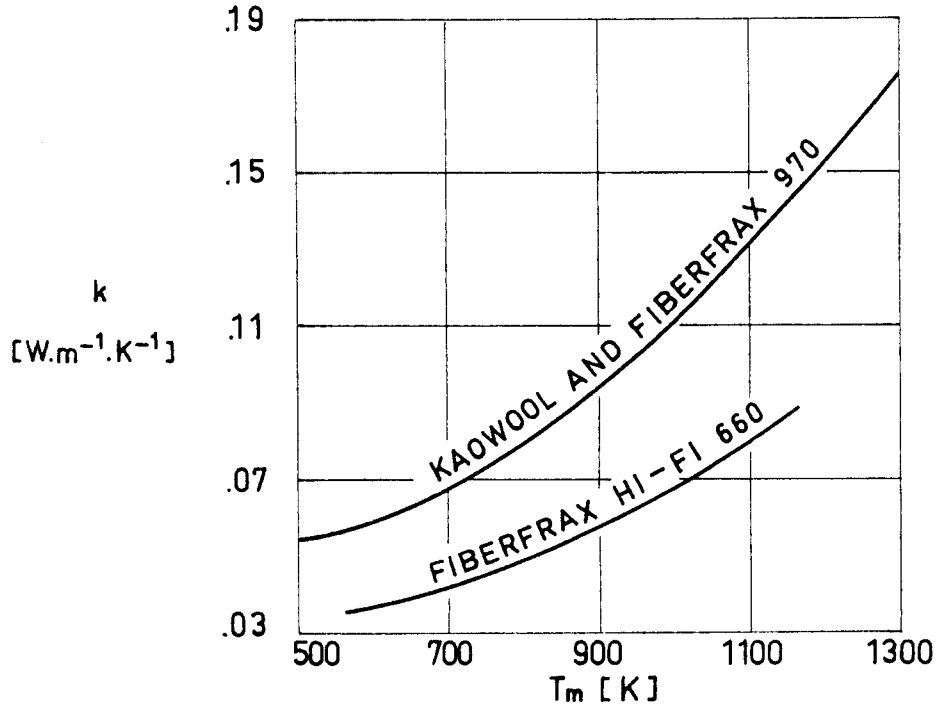

Fig 2-34. Thermal conductivity, k, of B & W Kaowool, Carborundum Fiberfrax 970 paper, and Fiberfrax Hi-Fi 660 paper vs. mean temperature, Tm.

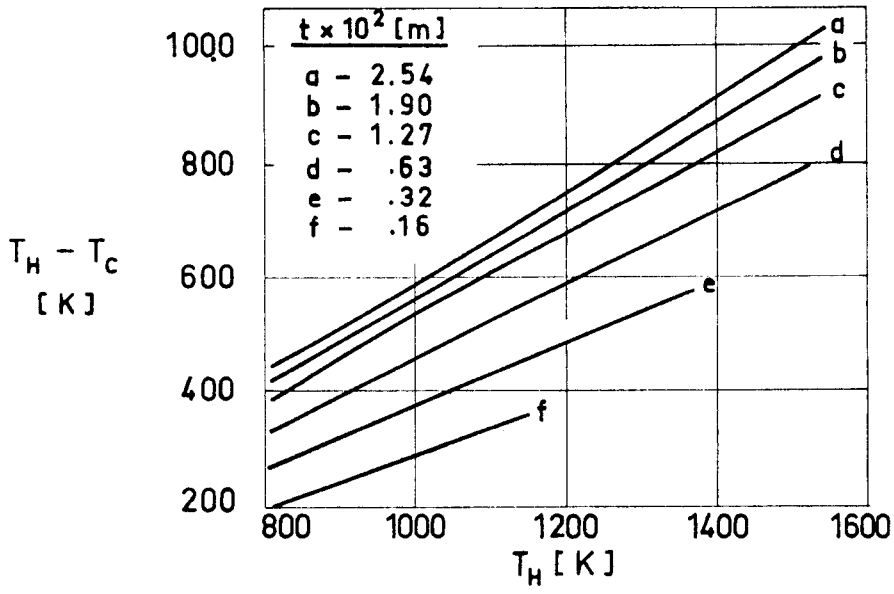

Fig 2-35. Temperature differential, T_H-T_C, vs. temperature of the hot face, T_H, for different values of the paper thickness, t. Fiberfrax 970 paper, ρ = 160 kg.m^{-3}.

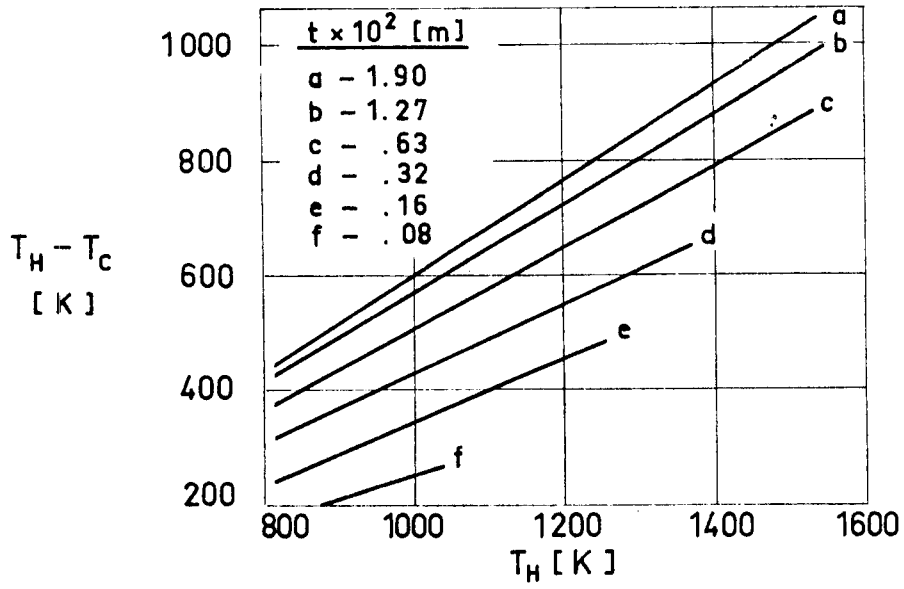

Fig 2-36 Temperature differential, T_H-T_C, vs. temperature of the hot face, T_H, for different values of the paper thickness, t. Fiberfrax Hi-Fi 660 paper.

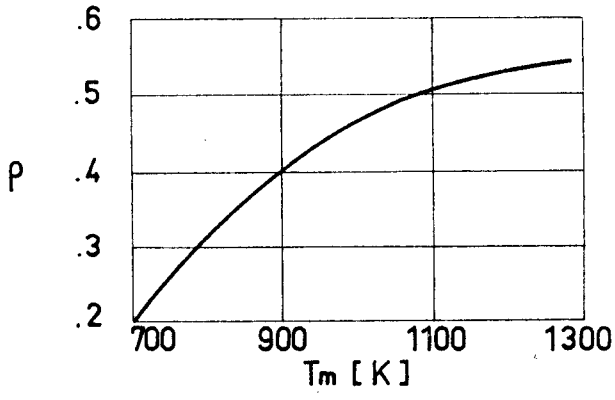

Fig 2-37. Thermal reflectance, ρ, of Fiberfrax 970-J paper vs. mean temperature, Tm.

INTENTIONALLY BLANK PAGE

3. MULTILAYER INSULATIONS

3.1. GENERAL

A multilayer insulation (MLI) consists of several layers of closely spaced radiation-reflecting shields which are placed perpendicular to the heat flow direction. These radiation shields aim at reflecting a large percentage of the radiation the layer receives from a warmer surface.

To avoid direct contact between shields, low-conductivity spacers may be used. Sometimes embossing or crinkling the shields produces small contact areas whose thermal joint conductance is low enough to keep conductive heat transfer between shields substantially below radiative heat transfer.

The space between shields is evacuated to decrease gas conduction. For space applications, proper venting of the insulation inner space should be provided to avoid undue pressure loads on the shields during ascent flight, to achieve an effective repressurization during re-entry, and to deliver outgassing from the insulation materials when long-term on-orbit missions are contemplated.

One-dimensional heat transfer testing has shown (Fig 3-1) that an evacuated MLI provides, for a given mass, insulation which is orders of magnitude greater than that furnished by more conventional materials such as foams and fiber-glass batting.

3.1.1. FUNDAMENTAL CONCEPTS CONCERNING MLI PERFORMANCE

The prediction of the thermal performance of multilayer

MULTILAYER INSULATIONS

General

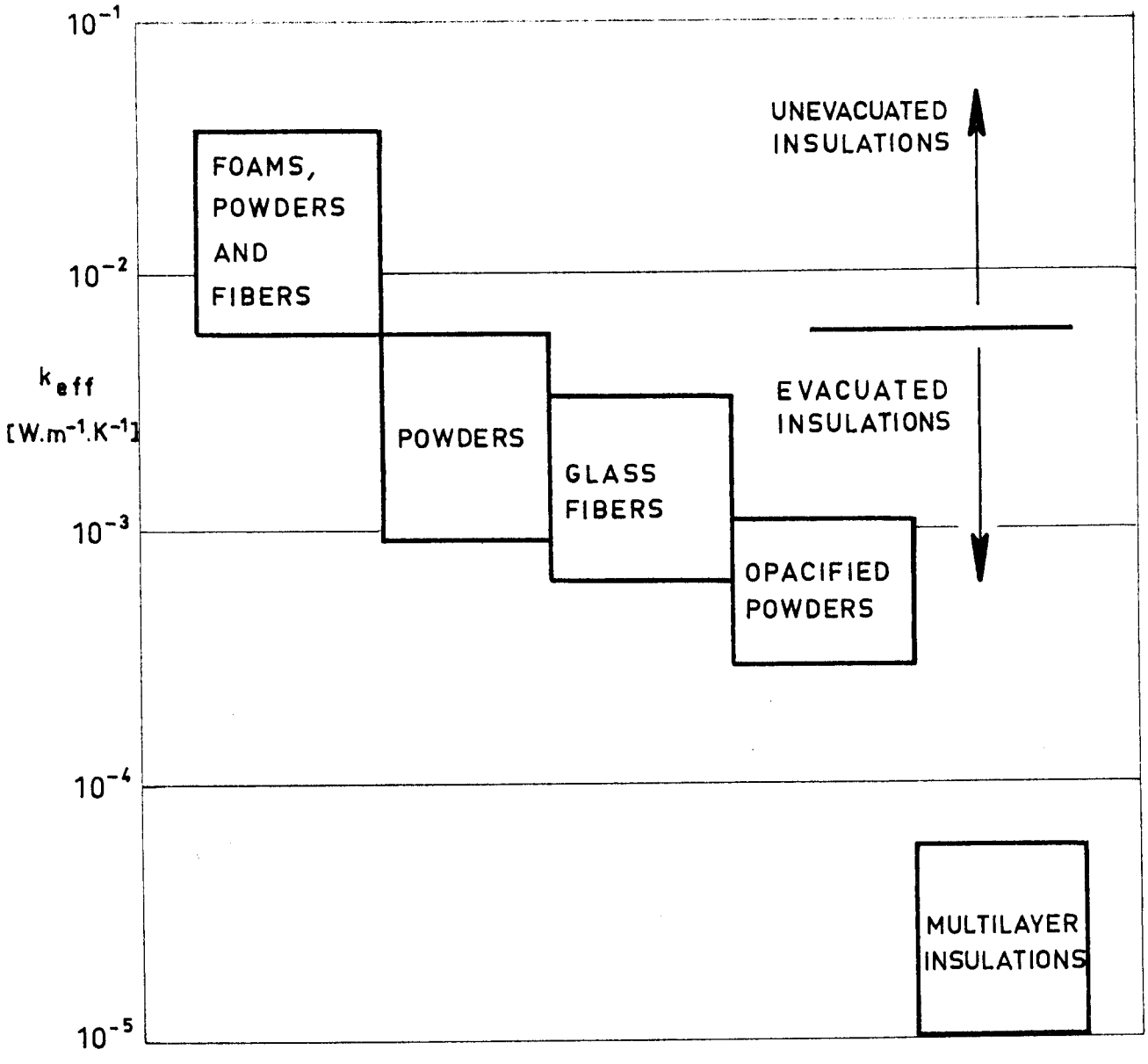

Fig 3-1. Thermal conductivity of multilayer insulations as compared with other insulation materials. From Glaser et al. (1967).

MULTILAYER INSULATIONS

General

insulations is difficult because its properties are anisotropic, discontinuous and subject to variations due to manufacture, handling and use. The variables which should be taken into account in an actual system are the following:

Number of shields, N, and total thickness, t.

Temperatures of the cold and warm boundaries, T_C and T_H respectively.

Applied compressive load, P.

Gas filling the insulation and its pressure, p.

Size and number of perforations to permit evacuation.

Most of the available data concerning heat transfer through multilayer insulations are based on a Fourier-Law type "effective conductivity", k_{eff}.

$$\frac{Q}{A} = k_{eff} \frac{T_H - T_C}{t}$$

where:

A , area normal to the temperature gradient. $[m^2]$.

Q , heat flow through the insulation. [W].

T_C , cold boundary temperature. [K].

T_H , warm boundary temperature. [K].

k_{eff} , effective thermal conductivity. $[W.m^{-1}.K^{-1}]$.

t , insulation thickness. [m].

It should be indicated that k_{eff} can be used only when comparing the qualities of various insulators, and should not be considered as an average property of the materials constituting the

MULTILAYER INSULATIONS

General

insulation.

Sometimes the performance of MLI systems is given in terms of a "heat transfer coefficient" or "effective thermal conductance", h_{eff}.

$$h_{eff} = \frac{k_{eff}}{t} \quad .$$

The use of the effective thermal conductance, h_{eff}, could be recommended in those cases where the thickness, t, cannot be measured with enough accuracy.

An alternative comparison between several MLI may be made on the basis of an "effective emittance", ε_{eff}.

$$\frac{Q}{A} = \sigma \varepsilon_{eff}(T_H^4 - T_C^4) \quad ,$$

where:

ε_{eff} , effective emittance.

σ , Stefan-Boltzmann Constant. $[W.m^{-2}.K^{-4}]$.

The following relations between the abovementioned magnitudes result:

$$k_{eff} = h_{eff}\, t = \sigma \varepsilon_{eff}\, t^4 T^3 \quad ,$$

where T is the characteristic temperature of the insulation, given by the expression:

$$T = \sqrt[3]{\frac{T_H^4 - T_C^4}{4(T_H - T_C)}} \quad .$$

The effective thermal conductivity of a multilayer insu-

lation is, loosely speaking, inversely proportional to the number of radiation shields per unit thickness, N/t, while the effective emittance is inversely proportional to N. The reason is that for an ideal system without radiation-absorbing spacers the radiative heat transfer decreases as 1/N. The measurements indicate that the real behavior of most MLI deviate from the ideal one when N/t increases, due to increased thermal conduction between adjacent layers.

Most of the heat transfer data presented in this compilation are based on k_{eff}, with the only exception of data giving the effect of surface perturbations on the characteristics of the blanket (such as overlaps, stitches, buttons,....), which are based on ε_{eff}.

3.1.2. FAILURE MODES

Failure of a multilayer insulation system can only occur by physical removal from the guarded surface. Performance can be degraded by compression, exposure to moisture and elevated temperatures, or improper handling techniques.

Blankets should be manufactured and manipulated in clean rooms, with a humidity range of 40-60% and a temperature range between 288 and 300 K. Persons handling the blankets and associated material must wear normal clean room clothing and flint-free gloves. For transportation purposes, the blankets should be welded in plastic bags containing silica gel packages.

The shieldings of aluminium foil or aluminized Mylar ig-

nite both in oxygen and air atmospheres. The inflammability and explosiveness of packs of multilayer insulation with glass-fiber spacing is reduced the lower is the content of organic additives in the spacer.

3.1.3. COST

Information on comparative costs of MLI systems is fairly scanty.

According to Knopf & Murray (1970), the material cost for a multilayer of 30 crinkled or embossed shields of single-aluminized Mylar is about 30 US $.m^{-2}. The combined cost of 22 Mylar shields and Tissuglas spacers is about 130 US $.m^{-2}.

Fairly recently, Klippel & Langer (1974), performing a selection among available European products, quoted the following prices:

1) Shields.

Single (or double)-aluminized Hostaphan (Polyester) 6×10^{-6}, 12×10^{-6}, 25×10^{-6} m thick: .60 to 1.50 DM.m^{-2}

Single (or double)-aluminized Melinex (Polyester) 12×10^{-6} to 25×10^{-5} m thick .....: 1 to 2 DM.m^{-2}

2) Spacers

Fibrex-Polyestervlies Type H 3002 4×10^{-5} to 5×10^{-5} m thick .....: .50 DM.m^{-2}

Polyester-Bobinet Tüll (Net) 1946: 2.50 DM.m^{-2}.

MULTILAYER INSULATIONS

General

It has been estimated (Kropschot et al. (1960)) that the material cost of an MLI is 10 to 20 times the cost of perlite, installation cost excluded.

In any case the material cost is small relative to the cost of fabricating the total system, and special attention should be devoted to the improvement of the manufacturing processes involved such as crinkling, cutting, sewing, hole-drilling and the like. For example, Maccalous (1968) reports that a reduction in cost of approximately 80% may be achieved in the cutting process by using appropriate techniques as compared with single layer cutting.

In order to give an order of magnitude idea of the cost of an MLI system it should be mentioned that Hale (1969) evaluates in US $ 400 per insulation the cost of preparation of multilayer specimens, of fairly simple shape, used to measure k_{eff} with a cylindrical calorimeter, .76 m in diameter, 1 m length.

INTENTIONALLY BLANK PAGE

MULTILAYER INSULATIONS
Radiation Shields

3.2. RADIATION SHIELDS

Radiation shields are low emittance foils used to attenuate the incoming radiation. Aluminium, gold and silver are the most commonly used materials either for coatings or to form thin metallic foils.

3.2.1. ALUMINIUM FOILS AND ALUMINIUM COATED PLASTIC FILMS

These materials are frequently used as radiation shields owing to the following reasons:

1) Aluminium is inexpensive and readily available in various thicknesses of foil and as a coating on a variety of metallic and non-metallic surfaces.

Aluminium vaporizes at a lower temperature than gold, making the aluminium deposition process easier to control. In addition, plastic films with an aluminium deposit have been used for decorative purposes for many years. As a result aluminium-coated films are less expensive and of better average quality than gold or silver--coated films.

2) The emittance of aluminium is only slightly higher than that of clear silver, but, whereas silver tarnishes in air, aluminium forms a very thin layer of oxide which prevents further degradation of the surface.

On the opposite side, moisture has a pernicious effect on aluminized plastic, as has been observed several times when Mylar and Kapton coated films have been used (ADL (1964), Leonhard & Hyde

MULTILAYER INSULATIONS

Radiation Shields

(1971)). Aluminium films tend to discolor and separate from the substrate.

For some applications, such as space suit thermal garments, abrasion resistance may be of concern. As has been indicated by Richardson, Ruccia & French (1970), the abrasion resistance of aluminized radiation shields can be substantially improved, without degrading the low emittance surfaces, by overcoating with a 5×10^{-8} m thick layer of vapor deposited germanium.

For comparable MLI systems, the aluminized polyester film is less effective than the aluminium shields by a factor of 1 to 2.5 based on the measured heat flux (Kropschot et al. (1960)). In applications where lightness is important, 6×10^{-6} to 12×10^{-6} m thick aluminium foils can be used for radiation shields even though these foils have very little tensile strength and are difficult to handle. Heavier foils (25×10^{-6} to 125×10^{-6} m thick) find only limited application where the weight is of secondary importance. According to Glaser et al. (1967), the main advantages of these thicker foils are the following:

1) Ease of handling.

2) Stiffness. They do not exhibit a tendency to bridge between the supports and maintain a given structural shape.

Plastic films are approximately one-half the weight of aluminium foils of equivalent thickness. In addition a 6.35×10^{-6} m thick Mylar film offers a tear strength much larger than that of an 1.27×10^{-5} m thick aluminium foil (Glaser et al. (1967)).

MULTILAYER INSULATIONS
Radiation Shields

3.2.2. GOLD FOILS AND GOLD COATED PLASTIC FILMS

The use of gold foils has been suggested several times. The cost of such systems would be several orders of magnitude higher than those of systems based on more conventional materials. In addition gold foils are only available in narrow widths and short lengths which would make the installation of such systems impractical.

Vapor-deposited gold appears more attractive for reusable vehicle radiation shields because of the lower emittance and no degradation effects after exposure to moisture.

Although gold-coated surfaces exhibit excellent thermal properties, their use is not so widely extended owing to problems of cost and manufacturing process control. The increased cost is due to the manufacture and not to the cost of the metal itself, which is deposited in very thin layers.

3.2.3. SILVER COATED PLASTIC FILMS

Since silver tarnishes in air, it is normally overcoated with SiO_x. Although silver-coated plastic films with SiO_x overcoating are commercially available, they are very sensitive to structural changes and are expensive owing to problems presented by some evaporation techniques.

3.2.4. OPERATING TEMPERATURE RANGES

The use of most polyester films is limited to operating

temperatures below 420 K, the point at which the film begins to deteriorate. Kapton polyimide retains 70% of its room temperature strength up to 480 K (Leonhard & Hyde (1971)).

Larger operating temperatures can be achieved using metallic foils. Aluminium foils can be used for temperatures up to 800 K, copper foils for temperatures between 720 and 1250 K, and nickel foils for temperatures up to 1470 K (Kaganer (1969)).

Emittances of copper and nickel are very sensitive to the degree of surface oxidation. There is the possibility of using gold to replace copper, and platinum to replace nickel, but the cost of such systems would be fairly large.

For some specific applications, when a refractory metal is necessary to prevent long term evaporation and metallurgical changes, molybdenum foil can be used (Dixon & Musgrove (1973)). Molybdenum has a particularly low emittance and is readily available commercially.

3.2.5. NORMALLY USED PLASTIC FILMS

Although Mylar polyester film is currently used in most MLI shields, other candidate film materials are Melinex and Hostaphan (polyesters), Kinfol and Lexan (polycarbonates), and Kapton H (polyimide).

The polycarbonates, although not very widely used, are attractive primarily due to their comparatively low density, and Kinfol is available in thicknesses down to 2×10^{-6} m. Kapton, while

slightly heavier and thicker than Mylar, and much more expensive, has the same room temperature tensile strength, higher maximum operating temperature and is non-flammable. Although Kapton has a higher moisture regain than the other materials, surface coating minimizes the importance of this factor.

In addition to Kapton H film, there is a commercially available Type F film which is coated with Teflon to impart heat sealability and enhance chemical resistance.

A significant advantage of most plastic films is the fact that the plastic itself has a low thermal conductivity, which enables the film to be used without spacers between the shields. In this case the film is coated on one side only, and is crinkled or embossed in order to reduce the area of contact between sheets. Since emittance of an uncoated side is higher than that of a coated side, more radiation shields are required to reduce the heat transfer to the level that can be achieved by coating both sides.

Embossment of Kapton is fairly troublesome. As a general rule long cycles are required to produce molded shapes from this high temperature polymer. Schroeder (1973) reports some difficulties connected with the fact that embossment of Kapton is not permanent, and suggests that more development effort should be spent in the near future on this problem.

In addition to the advantages mentioned above, metallized plastic films have a low thermal conductivity in a direction parallel to the film. This is because the metal layer (the highly ther-

MULTILAYER INSULATIONS
Radiation Shields

mal conducting component of the system) is extremely thin (approximately 5×10^{-8} m). The longitudinal conductivity of aluminized films is several hundred times lower than that of aluminium foils. This may be useful to increase the net efficiency of the insulation, whose ideally one-dimensional behavior is hampered by the end effects which are normally due to multidimensional heat transfer.

In some instances, when electromagnetic radiation must pass through the shield, uncoated plastic films can be used. Obviously, the insulating characteristics of the MLI are grossly degradated.

3.2.6. ONE-DIMENSIONAL HEAT FLOW THROUGH AN MLI. RELEVANCE OF SHIELD EMITTANCE.

The heat transfer rate between two infinitely parallel gray planes, 1 and 2, separated by a non-absorbing medium can be expressed (McAdams (1954)) as:

$$Q = \sigma A \left(T_2^4 - T_1^4\right) \frac{1}{\frac{1}{\varepsilon_1} + \frac{1}{\varepsilon_2} - 1}$$

where:

A , surface area. [m].

Q , heat flow between both surfaces, through area A. [W].

T_i, temperature of surfaces i. [K]. $i = 1,2$.

ε_i, emittance of surface i.

σ , Stefan-Boltzmann Constant. $[W.m^{-2}.K^{-4}]$.

MULTILAYER INSULATIONS

Radiation Shields

If N parallel shields are inserted between two boundaries C and H, the above expression, particularized to shields i and i+1, can be written as follows:

$$\frac{1}{\varepsilon_{i,1}} + \frac{1}{\varepsilon_{i+1,2}} - 1 = \frac{\sigma A(T_{i+1}^4 - T_i^4)}{Q}$$

The second subscript, either 1 or 2, is introduced to take into account the fact that when single-metallized plastic films are used, the emittances of both faces of a given shield are unequal.

Summing the N+1 equations which give the heat transfer rate between the consecutive couples of parallel plates, one can express the heat transfer rate between the boundaries H and C in terms of the boundary temperatures and the emittances of the shields. The resulting expression is:

$$Q = \sigma A(T_H^4 - T_C^4) \frac{1}{\frac{1}{\varepsilon_C} + \frac{1}{\varepsilon_H} + \sum_{i=1}^{N}\left(\frac{1}{\varepsilon_{i,1}} + \frac{1}{\varepsilon_{i,2}}\right) - (N+1)} .$$

Assuming that all the shields are made from exactly the same material, and neglecting the dependence of ε on temperature, so that $\varepsilon_{i1}=\varepsilon_1$, $\varepsilon_{i2}=\varepsilon_2$, the above equation becomes

$$Q = \sigma A(T_H^4 - T_C^4) \frac{1}{\frac{1}{\varepsilon_C} + \frac{1}{\varepsilon_H} + N\left(\frac{1}{\varepsilon_1} + \frac{1}{\varepsilon_2}\right) - (N+1)} .$$

In most space simulation tests, where a tank calorimeter is used, the boundary emittances, ε_C and ε_H, approach unity.

Sometimes the cold and warm plates are the two shields

MULTILAYER INSULATIONS
Radiation Shields

bounding the blanket. If the total number of shields is N, the heat transfer rate through surface area A is:

$$Q = \frac{\sigma A (T_H^4 - T_C^4)}{(N-1)\left[\frac{1}{\varepsilon_1} + \frac{1}{\varepsilon_2} - 1\right]} \quad .$$

Data concerning the hemispherical total emittance of metallic foils and metallized plastic films will be presented later.

3.2.7. SHADOW SHIELDS. RELEVANCE OF SHIELD ABSORPTANCE

Shield absorptance has not been mentioned before in this data item since it has been assumed to be equal to emittance. This assumption is only valid when the radiative source and the receiver are approximately at the same temperature, as is the case with neighboring shields of an MLI system. However, when metallic foils are used to shield a cryogenic surface from an outer source, such as the Sun, the above assumption is no longer valid.

The net rate of heat absorption for a surface, C, exposed, in a vacuum environment, to direct and reflected thermal radiation from an adjacent surface, H, may be written, according to Smolak, Knoll and Wallner (1962), as:

$$Q = \sigma A \left[\frac{\varepsilon_H F_{HC} \alpha_C T_H^4}{1 - F_{HC} F_{CH} (1-\alpha_H)(1-\alpha_C)} + \frac{\varepsilon_C F_{HC} F_{CH} (1-\alpha_H) \alpha_C T_C^4}{1 - F_{HC} F_{CH} (1-\alpha_H)(1-\alpha_C)} - \varepsilon_H T_C^4\right] \quad ,$$

where F_{HC} is the view factor giving the fraction of the total radiation that arrives at C coming from H; $F_{HC}=F_{CH}=1$ for closely spaced

MULTILAYER INSULATIONS

Radiation Shields

parallel foils of the same surface area. α is the absorptance, while the other symbols have been used previously.

When N parallel closely spaced shields are placed between surfaces H and C, the net rate of heat absorption for surface C is given (Smolak et al (1962)) by:

$$Q = \sigma A \frac{\varepsilon_C \left[\left(\frac{\alpha}{\varepsilon}\right)_C \left(\frac{\varepsilon}{\alpha}\right)_H \right]^{N+1} T_H^4 - \varepsilon_C T_C^4}{\left(1-\alpha_C + \frac{\alpha_C}{\alpha_H}\right) \left[\frac{1-\left[\left(\frac{\alpha}{\varepsilon}\right)_C \left(\frac{\varepsilon}{\alpha}\right)_H\right]^{N+1}}{1-\left(\frac{\alpha}{\varepsilon}\right)_C \left(\frac{\varepsilon}{\alpha}\right)_H} \right]} .$$

To obtain the above expression it has been assumed that all the shields have the same thermal radiation properties, namely: α_H and ε_H for the face looking to the cold surface and α_C and ε_C for the opposed face.

When $(\alpha/\varepsilon)_C(\varepsilon/\alpha)_H=1$ the denominator in the last equation becomes equal to $(N+1)(1-\alpha_C+(\alpha_C/\alpha_H))$. If, in addition, it is assumed that $\alpha=\varepsilon$, one obtains the expression already given in § 3.2.6 to calculate the radiative heat transfer through an MLI separated by a non-absorbing medium.

Data concerning spectral absorptance, α'_λ, and solar absorptance, α_s, of metallic foils will be found later.

INTENTIONALLY BLANK PAGE

MULTILAYER INSULATIONS
Emittance of Metallic Foils

3.3. EMITTANCE OF METALLIC FOILS

Data regarding the hemispherical total emittance of metallic foils are presented in Figs 3-2 to 3-14. These data have been arranged as is indicated in the following table.

Metal	Total Emittance Modifier	Variable	Fig	Comments
Aluminium	Hemispherical	T	3-2	Summary of available data
Copper	Hemispherical	T	3-3	Summary of available data
Copper	Hemispherical	T	3-4	Surface lapped, oxidated
Copper	Hemispherical	T	3-5	Surface grinded, oxidated
Gold	Hemispherical	T	3-6	
Molybdenum	Hemispherical	T	3-7	
Nickel	Hemispherical	T	3-8	
Nickel	Hemispherical	T	3-9	Influence of oxygen on the surface.
Nickel	Normal	T	3-10	
Ni Alloy (Inconel)	Normal	T	3-11	
Ni Alloy (Inconel X)	Normal	T	3-12	
Platinum	Hemispherical	T	3-13	
Silver	Hemispherical	T	3-14	

INTENTIONALLY BLANK PAGE

MULTILAYER INSULATIONS

Emittance of Metallic Foils

Emittance of Aluminium.

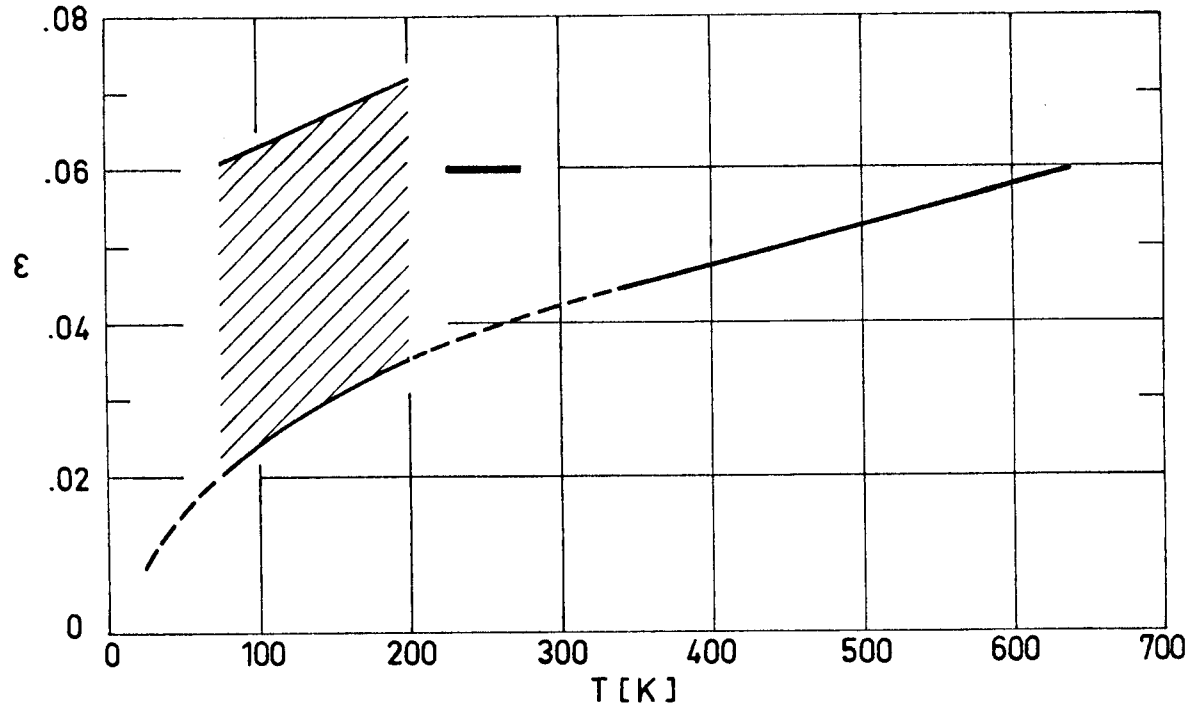

Fig 3-2. Summary of data concerning hemispherical total emittance, ε, of Aluminium foils and thin sheets as a function of temperature, T. From Touloukian & DeWitt (1970).

Explanation

Key	Description	Test Method	Comments
	Foils, Sheets.		Measured in vacuum ($<2.7\times10^{-2}$ Pa)
	Plate, 5.08×10^{-3} m thick. Hand polished.		Measured in vacuum (1.33×10^{-2} Pa). Reported error ±3%.
	Hollow sphere; polished to approx. 5×10^{-6} m, then rinsed with distilled water and alcohol, dried in a stream of nitrogen.		Measured in vacuum. Data from smooth curve. Reported error ±5%.

MULTILAYER INSULATIONS

Emittance of Metallic Foils

Emittance of Copper.

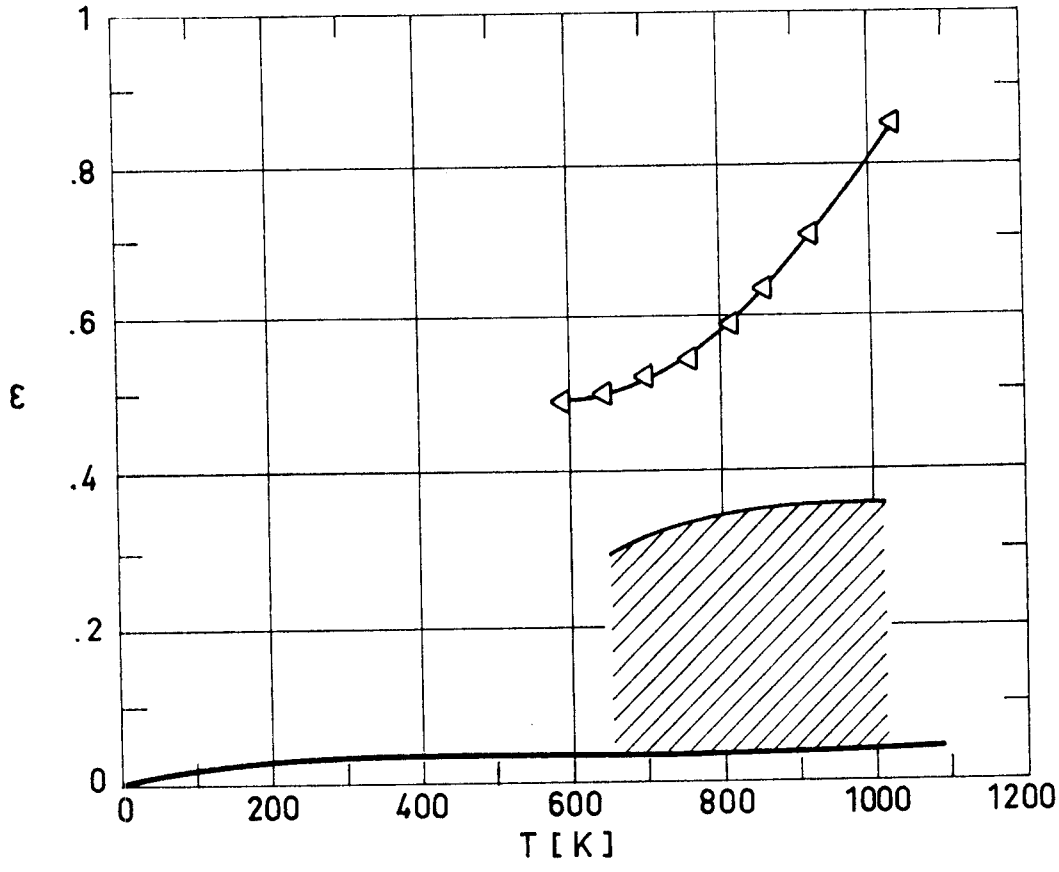

Fig 3-3. Summary of data concerning hemispherical total emittance, ε, of Copper as a function of temperature, T. Curves are from Touloukian & DeWitt (1970), while the shadowed zone is from Reid & Coon (1971).

Explanation

Key	Description	Test Method	Comments
———	Polished or electro-polished.		Average of data from several sources.
◁	Stably oxidized at 1 033 K in quiescent air.	From normal total emittance.	Reported error <2%.
▨	Electrolytic tough pitch Copper. 99.9% pure. Oxidized.	Calorimetric. T measured with thermocouples.	Measured in vacuum ($<4\times10^{-2}$ Pa). Additional details in Figs 3-4 and 3-5.

MULTILAYER INSULATIONS

Emittance of Metallic Foils

Emittance of Copper.

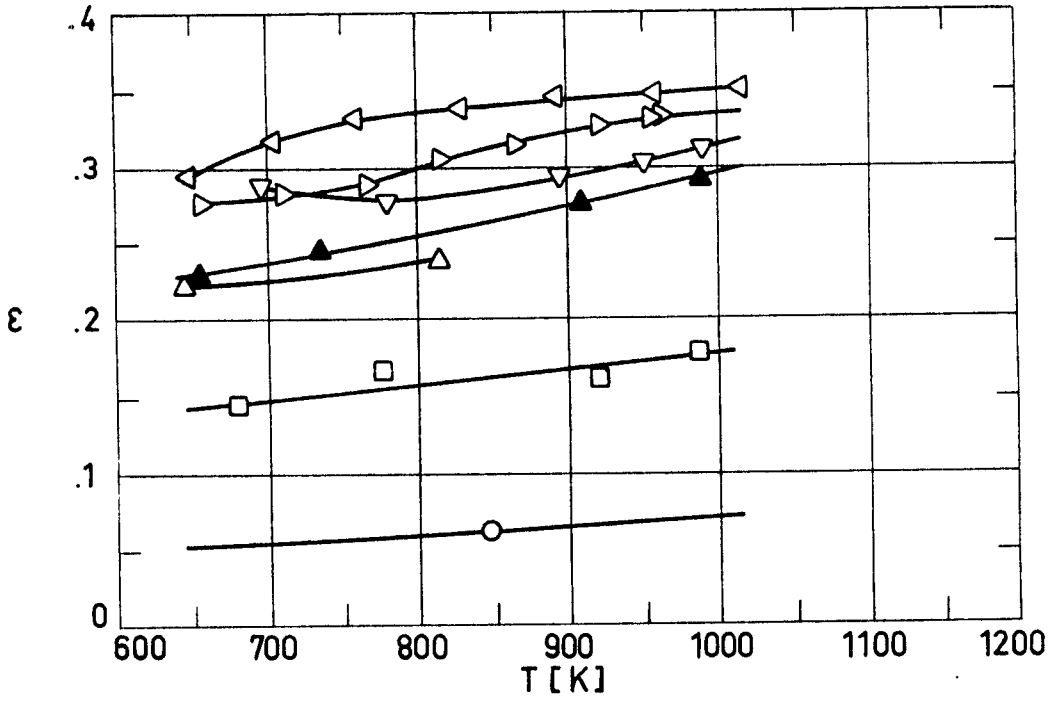

Fig 3-4. Hemispherical total emittance, ε, of Copper as a function of temperature, T. From Reid & Coon (1971).

Explanation

Key	Description	Test Method	Comments
○	Electrolytic tough pitch Copper 99.9% pure. Lapped, wiped lightly just before use, unoxidized.	Calorimetric. T measured with thermocouples. Electrical heater into the box-like specimen.	Measured in vacuum, ($<4\times10^{-2}$ Pa).
□	Oxidized, 15 min at 529 K.		
△	Oxidized, 3.3 h at 531.4 K.		
▲	Oxidized, 3.2 h at 532.5 K.		
▽	Oxidized, 47.2 h at 530 K.		
▷	Oxidized, 15.6 h at 527.5 K.		
◁	Oxidized, 13.25 h at 533 K.		

MULTILAYER INSULATIONS

Emittance of Metallic Foils

Emittance of Copper.

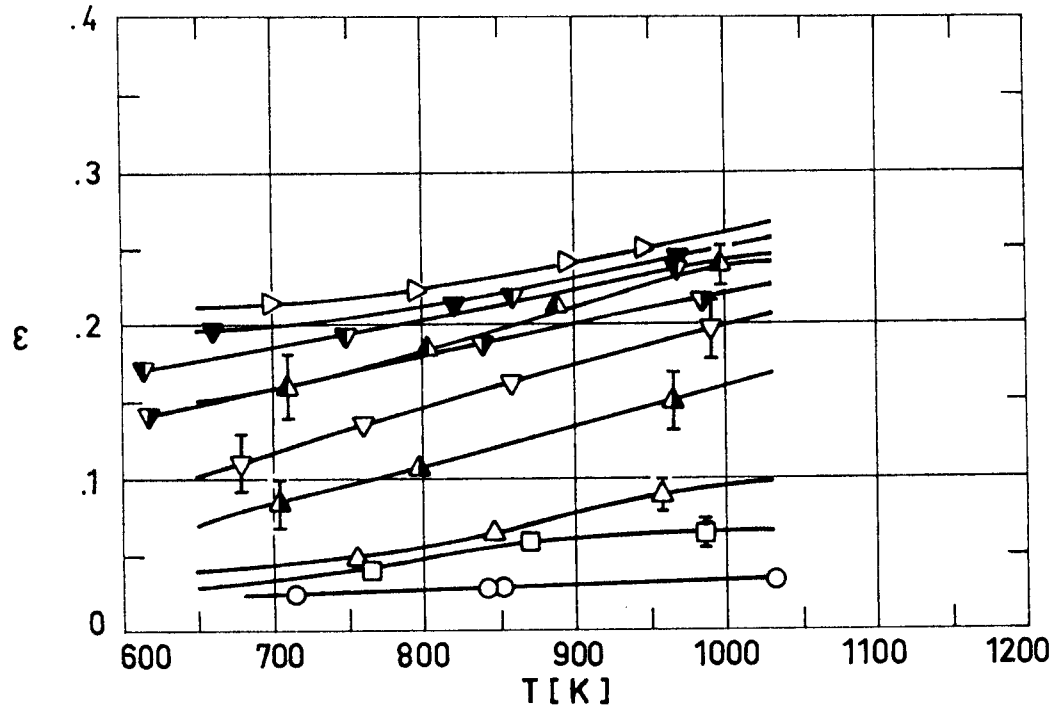

Fig 3-5. Hemispherical total emittance, ε, of Copper as a function of temperature, T. From Reid & Coon (1971).

Explanation

Key	Description	Test Method	Comments
○	Electrolytic tough pitch Copper 99.9% pure. Surface grinded, wiped lightly just before use, unoxidized.	Calorimetric. T measured with thermocouples. Electrical heater into the box-like specimen.	Measured in vacuum ($<4\times10^{-2}$ Pa).
□	Oxidized, 19 h at 417.8 K.		
△	Oxidized, 45 min at 480.3 K.		
◭	Oxidized, 4.42 h at 477.2 K.		
◭	Oxidized, 17.5 h at 475.7 K.		
▽	Oxidized, 15 min at 539.2 K.		
▼	Oxidized, 15 min at 550.6 K.		
▽	Oxidized, 43 min at 532.8 K.		
▼	Oxidized, 3.03 h at 534.4 K.		
▷	Oxidized, 8.38 h at 535.3 K.		

MULTILAYER INSULATIONS

Emittance of Metallic Foils

Emittance of Gold.

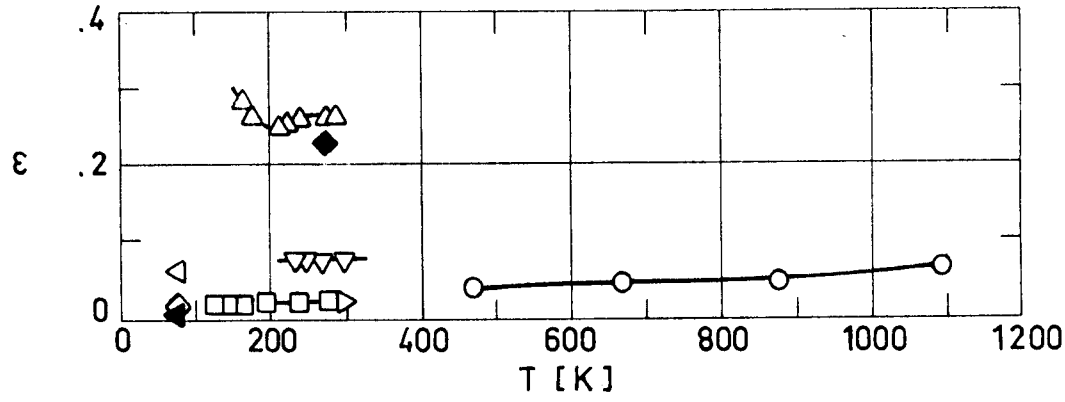

Fig 3-6. Hemispherical total emittance, ε, of Gold vs. temperature, T. From Touloukian & DeWitt (1970).

Explanation

Key	Description	Test Method	Comments
○	Ground with 600 grit carborundum and polished on a wet cloth lap.		Measured in vacuum (1.33×10^{-3} Pa). Reported error ≤10%
□	Polished.		Measured in vacuum (6.67×10^{-3} Pa). Reported error ±10%
△	Foil 3.81×10^{-5} m thick.		Measured in vacuum (1.33×10^{-4} Pa). Contaminated? Reported error <5%
▽	Commercial foil 2.54×10^{-4} m thick cleaned in both sodium dichromate and dilute nitric acid solutions, buffed, cleaned with carbon tetrachloride and acetone.		Measured in vacuum (1.33×10^{-4} Pa). Data from smooth curve. Reported error 3%.
▷	Gold plating 7.62×10^{-6} m thick. Polished, kerosene buff.		Measured in vacuum (4×10^{-4} Pa). Reported error ±20%
◁	Leaf 2.54×10^{-7} m thick.	Calorimetric absorptance. Source: 300 K blackbody. Absorbed heat related to boil-off rate of LN_2. Authors assumed α=ε.	Measured in vacuum (1.33×10^{-4} to 1.33×10^{-5} Pa). Reported error 5%.
◀	Foil 1.27×10^{-5} m thick. Solvent cleaned.		
◇	Foil 1.02×10^{-6} m thick. Solvent cleaned.		
◆	Bright foil. Typical of adhesive backed metals.		Reported error 10%.

MULTILAYER INSULATIONS

Emittance of Metallic Foils

Emittance of Molybdenum.

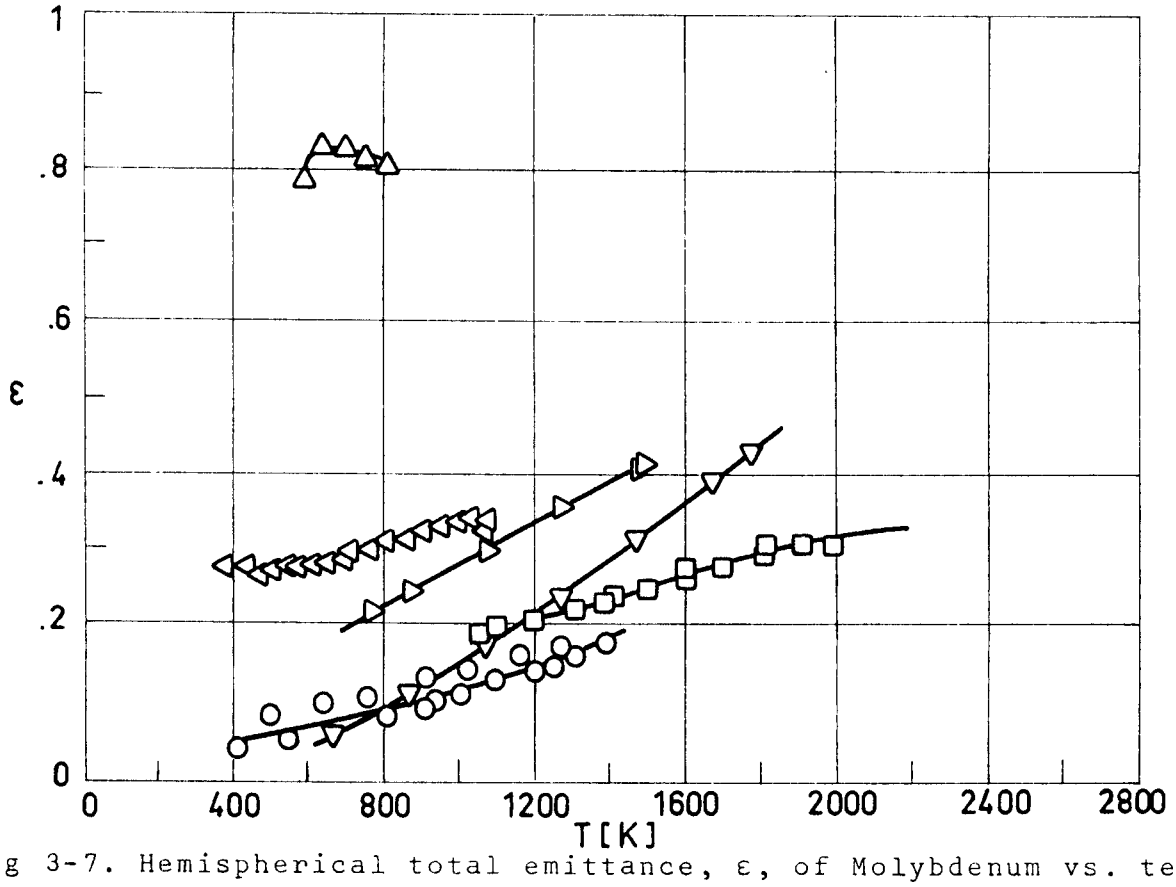

Fig 3-7. Hemispherical total emittance, ε, of Molybdenum vs. temperature, T. From Touloukian & DeWitt (1970).

Explanation

Key	Description	Test Method	Comments
○	Vapor-blasted with Techline Liquabrasive, PMC-3067, grit No. 325.		Measured in vacuum ($<6.7\times10^{-4}$ Pa). Reported error ±2.7%.
□	Degreased with acetone, cleaned with a rubber eraser, wiped with acetone		Measured in vacuum (1.33×10^{-2} to 1.33×10^{-4} Pa). Reported error ±4%.
△	Stably oxidized at 811 K in quiescent air.		Reported error <2%.
▽	Lightly etched and flashed in vacuum at 2 073 K for 10 min.		Measured in vacuum ($<6.7\times10^{-4}$ Pa). Data from smooth curve. Reported error ±2.5%.
▷	Shot-blasted and picled in hydrochloric acid.		
◁	Grit blasted with aluminium oxide No. 90 (PMC-3043A).		Measured in vacuum ($<3.9\times10^{-4}$ Pa). Reported error ±2.7%.

MULTILAYER INSULATIONS

Emittance of Metallic Foils

Emittance of Nickel.

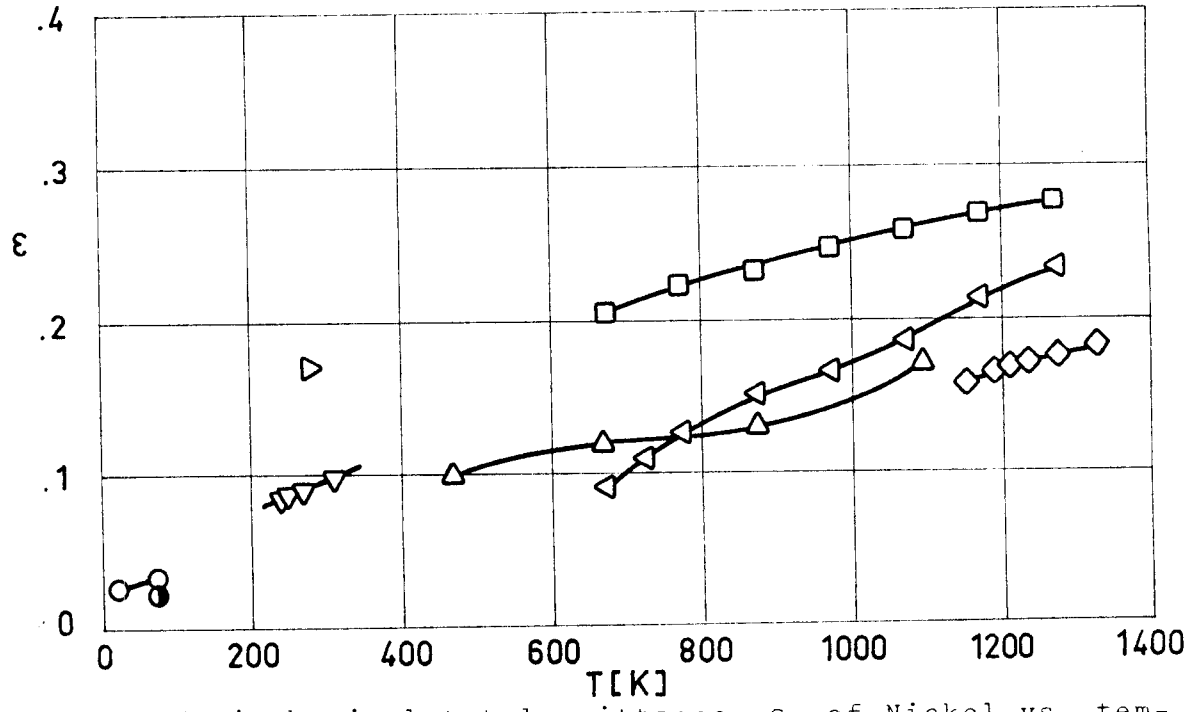

Fig 3-8. Hemispherical total emittance, ε, of Nickel vs. temperature, T. Data from Touloukian & DeWitt (1970), except O which are from Wood, Deem & Lucks (1961).

Explanation

Key	Description	Test Method	Comments
O	Commercially pure. As received, cleaned.	Calorimetric absorptance. Source: 300 K blackbody. Absorbed heat related to boil-off rate of LN_2. Authors assumed $\alpha=\varepsilon$.	Measured in vacuum (1.33×10^{-4} to 1.33×10^{-5} Pa). Reported error 5%.
◑	Foil 1.02×10^{-4} m thick. Solvent cleaned.		
□	Sandblasted.		Measured in vacuum ($<6.65\times10^{-4}$ Pa). Reported error ±2.5%
△	Commercially pure. Ground with 600 grit carborundum, polished		Measured in vacuum (1.33×10^{-3} Pa). Reported error <10%
▽	Commercial sheet. Cleaned, buffed, cleaned.		Measured in vacuum (1.33×10^{-4} Pa). Reported error 3%.
▷	Electroless nickel.		Reported error 10%.
◁	Commercially pure. Vacuum heated at 1 473 K for 15 min.		Measured in vacuum ($<6.65\times10^{-4}$ Pa). Reported error ±2.5%
◇	99.95 Ni.		

MULTILAYER INSULATIONS

Emittance of Metallic Foils

Emittance of Nickel.

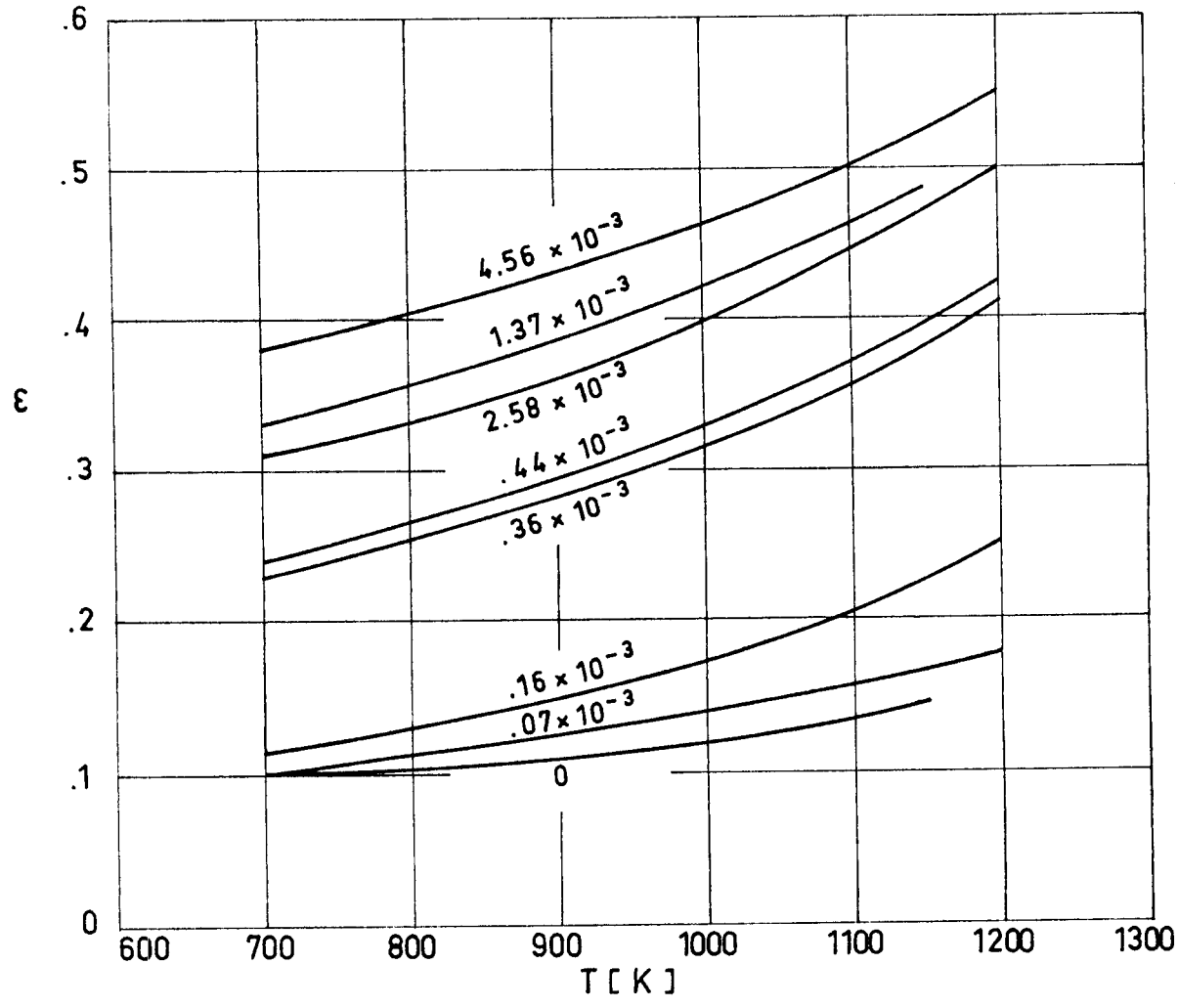

Fig 3-9. Hemispherical total emittance, ε, of oxidized Nickel as a function of temperature, T. Numbers near curves give the amount of oxygen on the surface in $kg.m^{-2}$. The emittance has been measured calorimetrically by the filament-in-vacuum method. The amount of oxygen has been deduced from the weight loss on reduction in hydrogen. Chamber pressure 1.33×10^{-5} Pa. From Shelton & Akers (1961).

MULTILAYER INSULATIONS

Emittance of Metallic Foils

Emittance of Nickel.

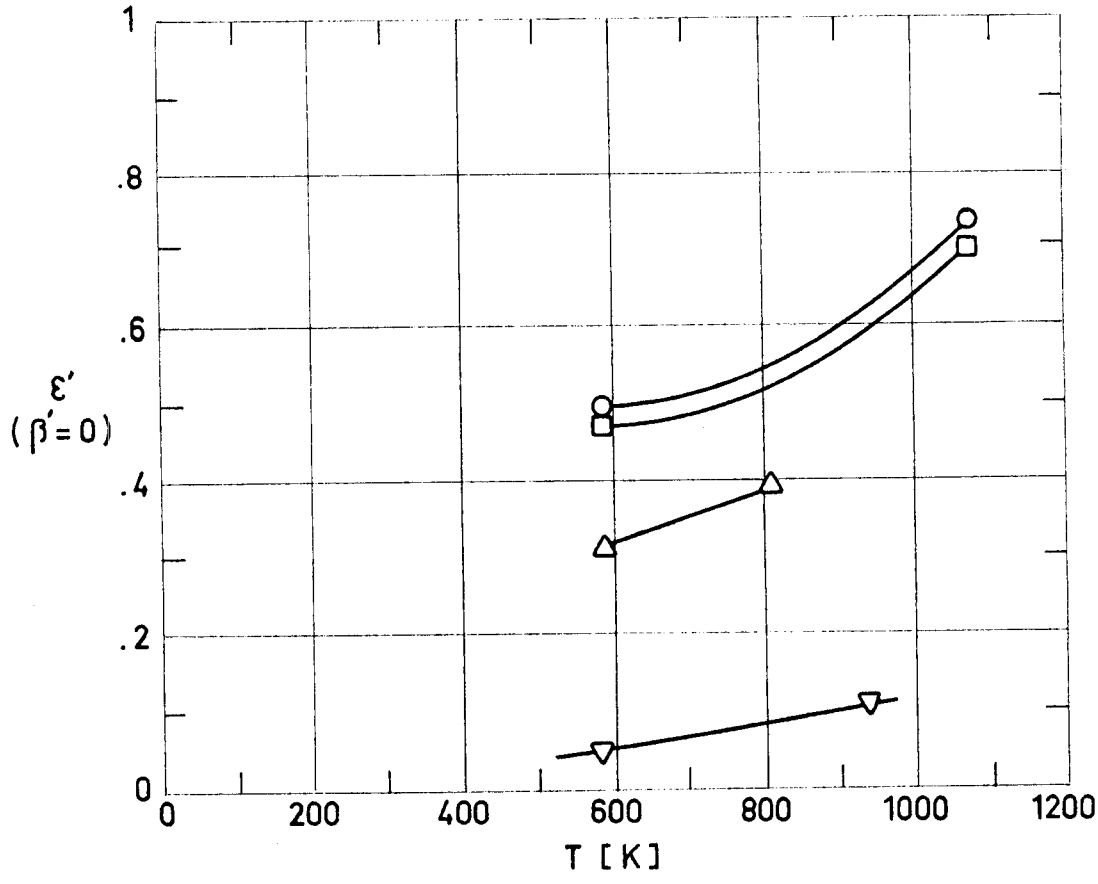

Fig 3-10. Normal total emittance, ε', of Nickel as a function of temperature, T. From Wood, Deem & Lucks (1961).

Explanation

Key	Description	Test Method	Comments
○	Oxidized at 1 015 K, shot blasted.	Thermopile detector. Comparison black-body. T measured with thermocouples. Self-resistance-heated specimen.	Measured in air. Data from smooth curves.
□	Oxidized, buffed.		
△	Unoxidized, shot blasted.		
▽	Unoxidized, buffed.		

MULTILAYER INSULATIONS

Emittance of Metallic Foils

Emittance of Nickel Alloys (INCONEL).

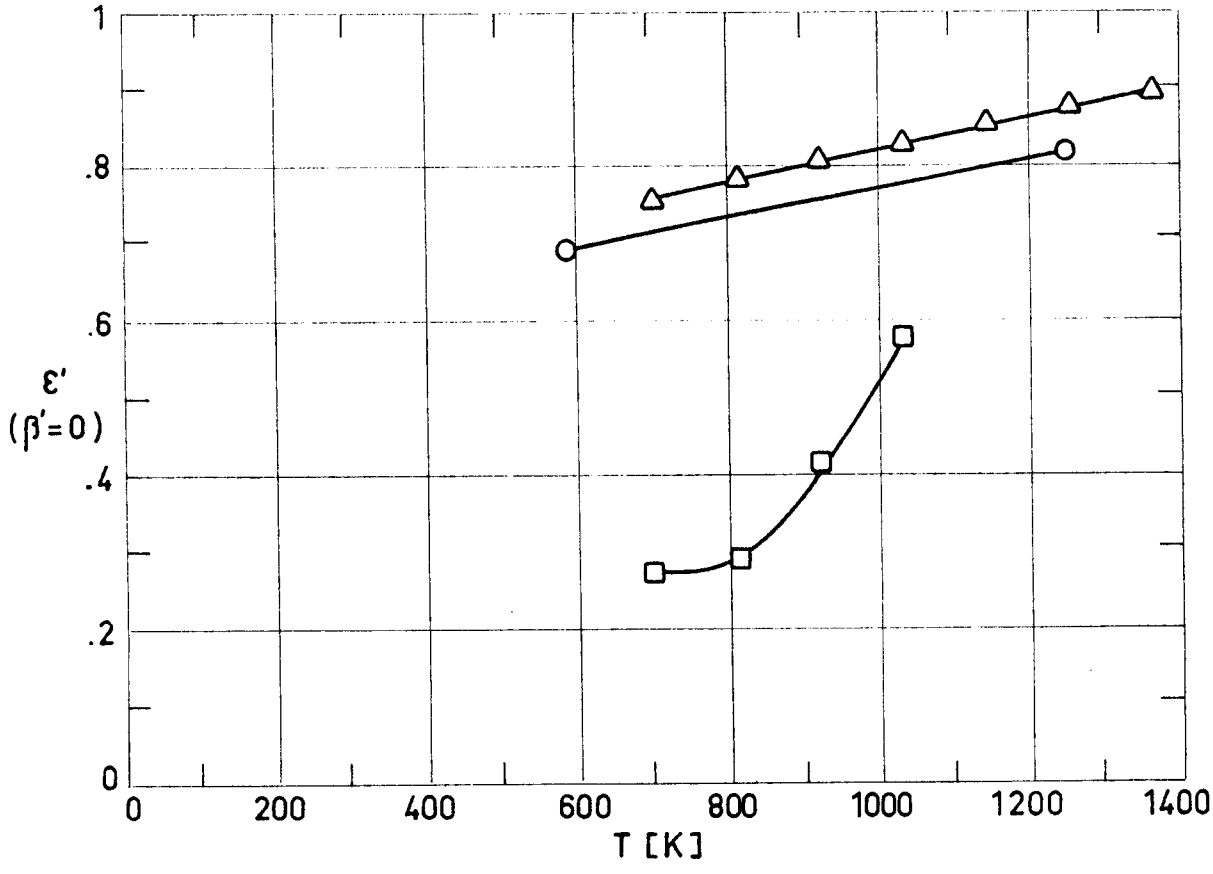

Fig 3-11. Normal total emittance, ε', of Inconel as a function of temperature, T. From Wood, Deem & Lucks (1961).

Explanation

Key	Description	Test Method	Comments
○	Stably oxidized at 1 370 K.	Thermopile detector. Comparison blackbody. T measured with thermocouples. Resistance-heated specimens.	Measured in air. Data from smooth curves.
□	As rolled.		
△	Heated in air for 15 min at 1 420 K.		

MULTILAYER INSULATIONS

Emittance of Metallic Foils

Emittance of Nickel Alloys (INCONEL X).

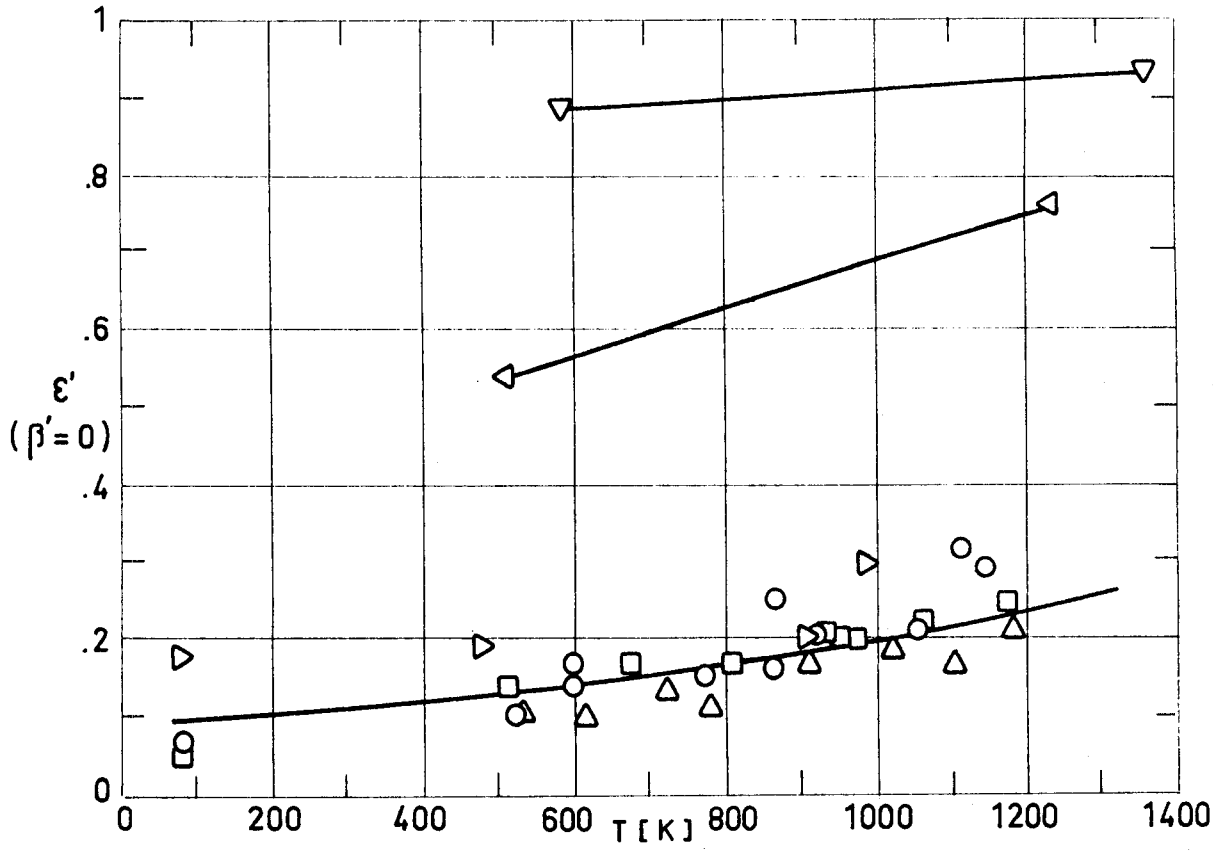

Fig 3-12. Normal total emittance, ε', of Inconel X as a function of temperature, T. From Wood, Deem & Lucks (1961).

Explanation

Key	Description	Test Method	Comments
○	Oxidized.	Resistance-heated specimens. Thermistor-bolometer detector. Comparison blackbody. T measured with thermocouples.	Measured in vacuum. Data from smooth curves.
□	As received or wiped clean.		
△	Polished.		
▽	Stably oxidized at 1 370 K.	Thermopile detector. Comparison blackbody. T measured with thermocouples.	Measured in air. Data from smooth curves.
▷	Polished.	Total-radiation detector. Comparison blackbody. T measured with thermocouples.	Measured in helium at 1.33×10^{-3} Pa.
◁	After prolonged heating and cycling above 1 370 K. (Some oxide indicated).		

MULTILAYER INSULATIONS

Emittance of Metallic Foils

Emittance of Platinum.

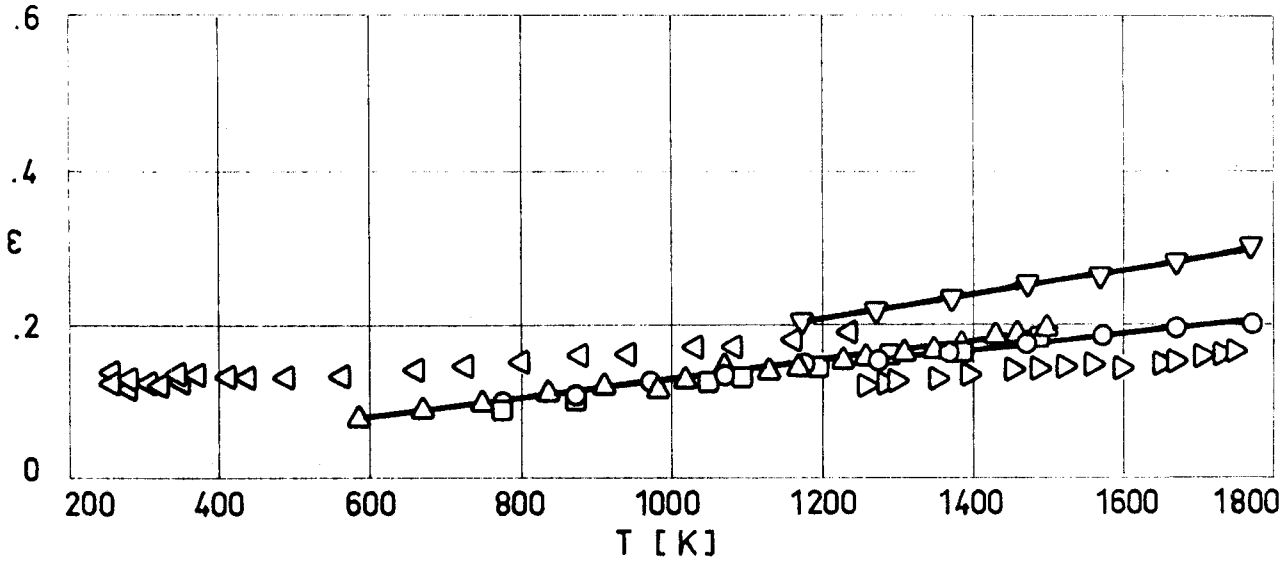

Fig 3-13. Hemispherical total emittance, ε, of Platinum as a function of temperature, T. From Touloukian & DeWitt (1970).

Explanation

Key	Description	Test Method	Comments
○	Clean polished surface.		Measured in vacuum (1.33×10^{-2} to 1.33×10^{-4} Pa). Reported error ±4%.
□	Clean rolled.		
△			Measured in vacuum.
▽	Flashed in vacuum at 2 023 K.		Measured in vacuum ($<6.6\times10^{-4}$ Pa). Data from smooth curve. Reported error ±2.5%
▷	Thin strip.		Reported error <8%.
◁	Disc. Polished on a cloth lap saturated with water and alumina.		Measured in vacuum (6.65×10^{-3} Pa).

MULTILAYER INSULATIONS

Emittance of Metallic Foils

Emittance of Silver.

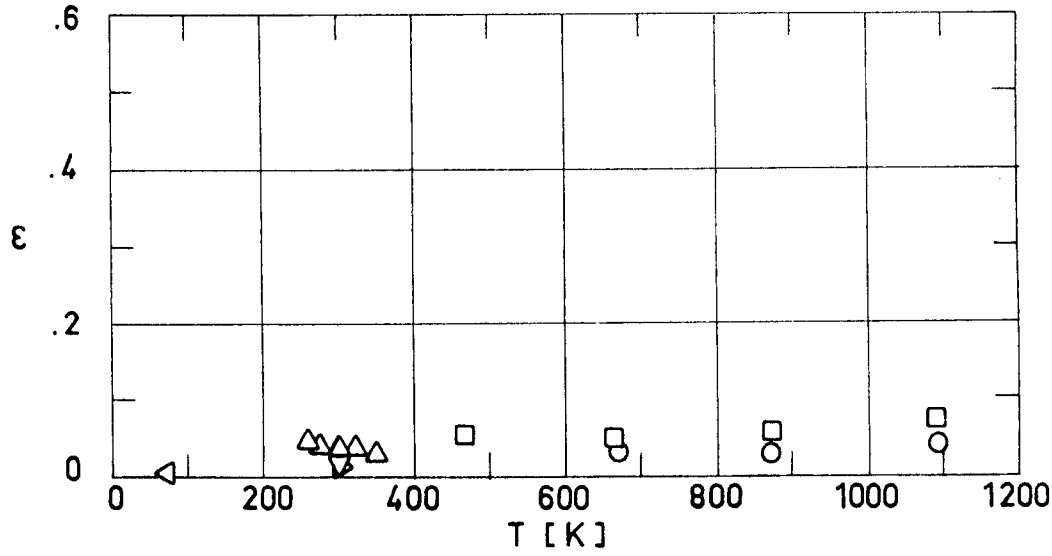

Fig 3-14. Hemispherical total emittance, ε, of Silver as a function of temperature, T. From Touloukian & DeWitt (1970).

Explanation

Key	Description	Test Method	Comments
○	Commercial rolled plate, 99.9 pure. Ground with 600 grit carborundum and polished on a wet cloth lap with unlevigated jewelers rouge.		Measured in vacuum (1.33×10^{-3} Pa). Reported error <10%.
□	Same as ○ after thermal etching.		
△	Commercial sheet. Cleaned with sodium dichromate and dilute nitric acid solutions. Buffed on a felt wheel, cleaned with carbon tetrachloride and acetone.		Measured in vacuum (1.33×10^{-4} Pa). Data from smooth curve. Reported error 3%.
▽	Silver plating (7.62×10^{-6} m thick). Matte surface.		Measured in vacuum ($<4\times10^{-4}$ Pa). Reported error ±20%.
▷	Same as ▽ except lume surface.		
◁	Solvent cleaned.	Calorimetric absorptance. From 300 K blackbody. LN_2 boil-off rate measured. Authors assumed $\alpha=\varepsilon$.	Measured in vacuum (1.33×10^{-4} to 1.33×10^{-5} Pa). Reported error 5%.

INTENTIONALLY BLANK PAGE

MULTILAYER INSULATIONS

Emittance of Metallized Films

3.4. EMITTANCE OF METALLIZED FILMS

Data regarding the hemispherical total emittance of metallized plastic films are presented in Figs 3-15 to 3-25. These data have been arranged as is indicated in the following table.

Metallized Plastic Film		Total Emittance Modifier	Variable	Fig	Comments
Metal	Plastic				
Aluminium	Mylar	Hemispherical	t_c [a]	3-15	T = 307 K.
Copper	Mylar	Hemispherical	t_c	3-16	T = 307 K.
Gold	Mylar	Hemispherical	t_c	3-17	T = 307 K.
Gold-Aluminium	Mylar	Hemispherical	t_c	3-18	T = 307 K.
Silver	Mylar	Hemispherical	t_c	3-19	T = 307 K.
SiO-Silver	Mylar	Hemispherical	t_c	3-20	T = 307 K.
Aluminium	Kapton	Hemispherical	T	3-21	For several values of t_c.
Aluminium	Kapton	Hemispherical	t_c	3-22	T = 300 K.
Aluminium	Kapton	Hemispherical	t_c	3-23	T = 400 K.
Gold	Kapton	Hemispherical	T	3-24	For several values of t_c.
Silver	Kapton	Hemispherical	T	3-25	For several values of t_c.

[a] t_c is the metallic coating thickness.

INTENTIONALLY BLANK PAGE

MULTILAYER INSULATIONS

Emittance of Metallized Films

Emittance of Aluminium Coated Mylar.

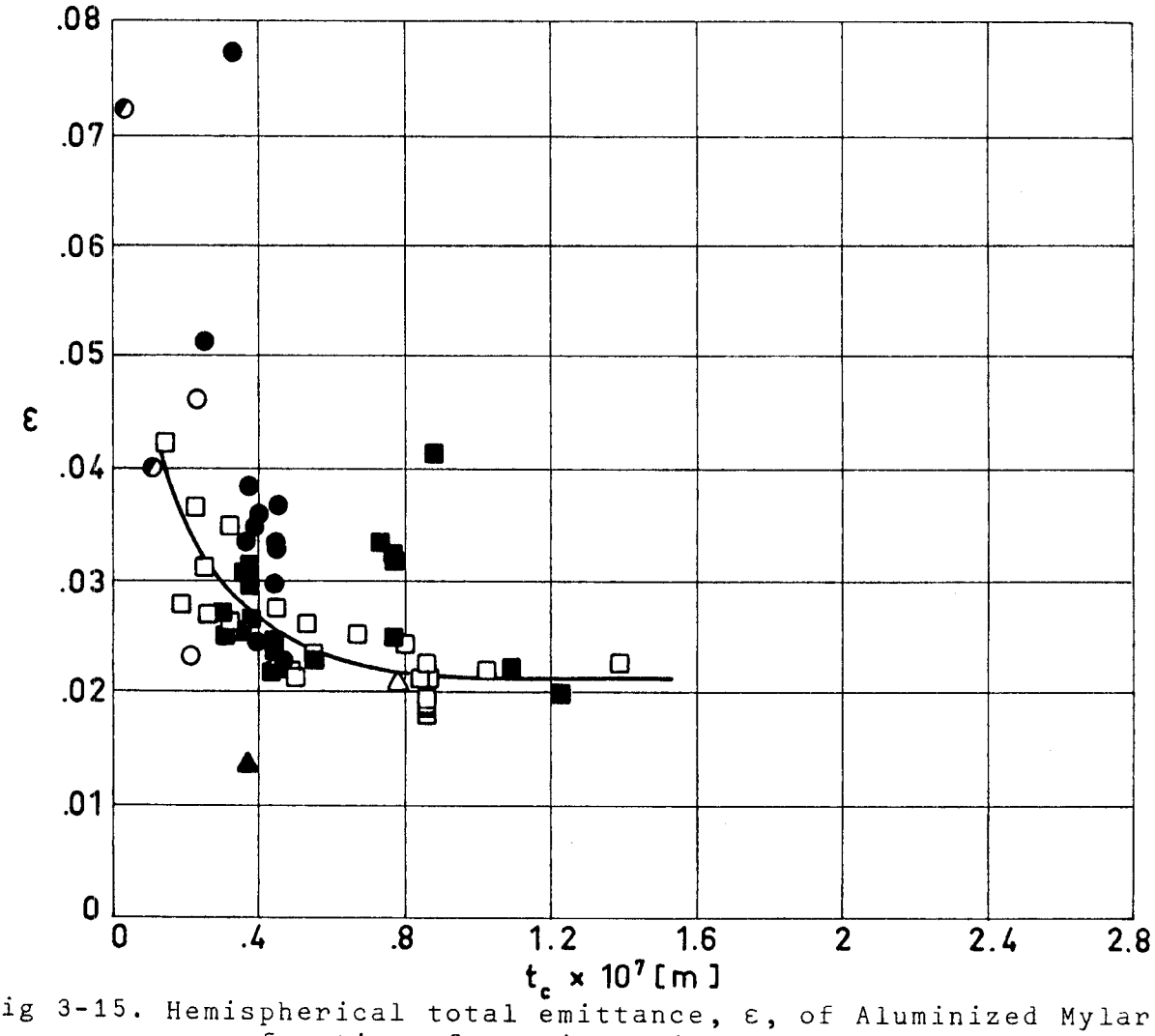

Fig 3-15. Hemispherical total emittance, ε, of Aluminized Mylar as a function of coating thickness, t_c. The emitting surface is coated. Solid data points represent two sided coating, while open data points are for one sided coating. ◐ indicates that no details are given in the source to decide whether the specimen was single or double coated.

Explanation

Film Thickness, $t \times 10^6$ [m]	Test Method	References
6.35	t_c: Electrical Resistance. Parallel bar electrode. ε: Receiver Disc exchanging heat with a closely spaced parallel sample. Sample Temperature: 307 K. Chamber Pressure: 1.33×10^{-4} Pa.	○ ◐ ADL (1964). □ ■ ADL (1966). △ ▲ Ruccia & Hinckley (1967). —— Coston (1967).

MULTILAYER INSULATIONS

Emittance of Metallized Films

Emittance of Copper Coated Mylar.

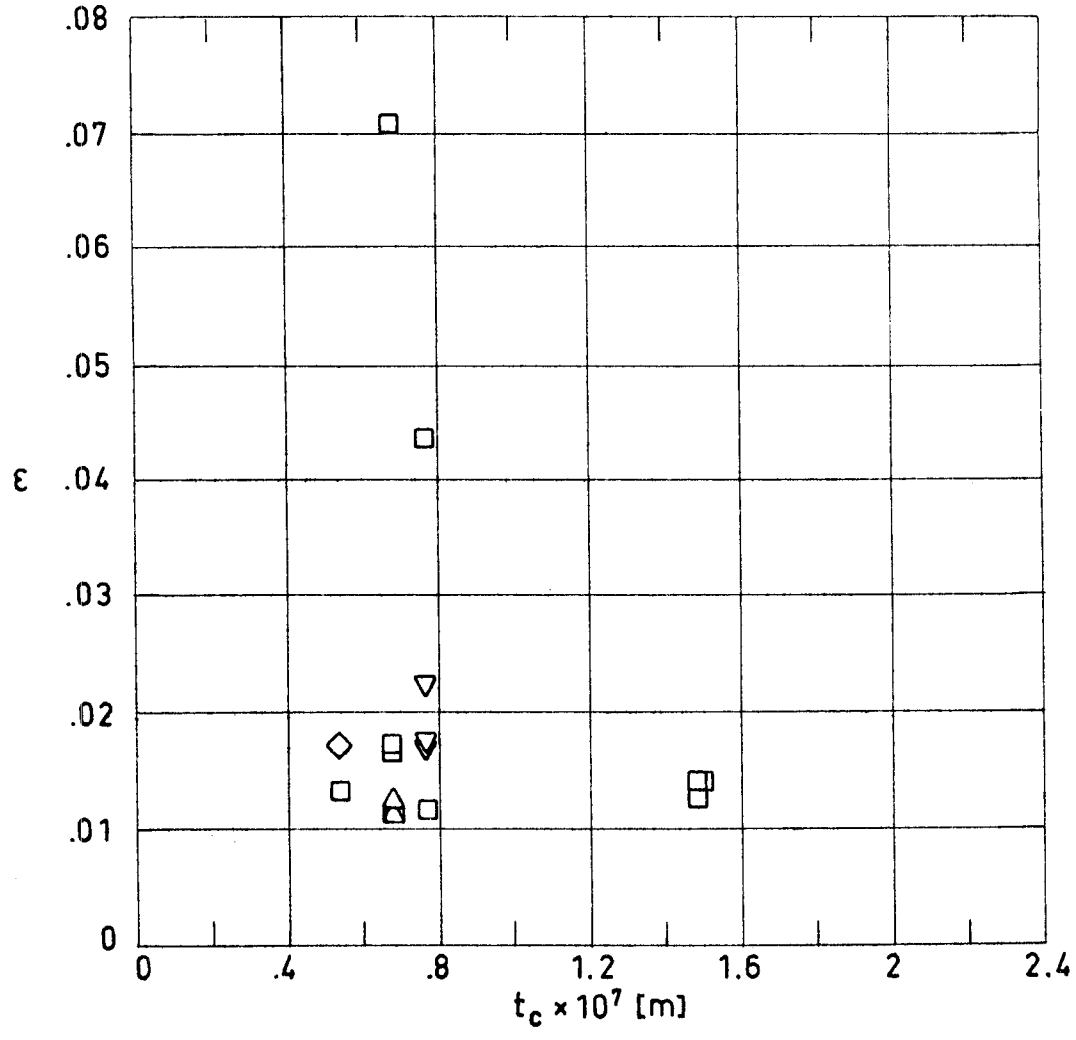

Fig 3-16. Hemispherical total emittance, ε, of Copper on Mylar as a function of coating thickness, t_c. The emitting surface is coated. One sided coating in all cases. ◇ and ▽ are overcoated with SiO.

Explanation

Film Thickness, $t \times 10^6$ [m]	Test Method	References
6.35	t_c: Electrical Resistance. Parallel bar electrode. ε: Receiver Disc exchanging heat with a closely spaced parallel sample. Sample Temperature: 307 K. Chamber Pressure: 1.33×10^{-4} Pa.	□ ◇ ADL (1966). △ ▽ Ruccia & Hinckley (1967).

MULTILAYER INSULATIONS

Emittance of Metallized Films

Emittance of Gold Coated Mylar.

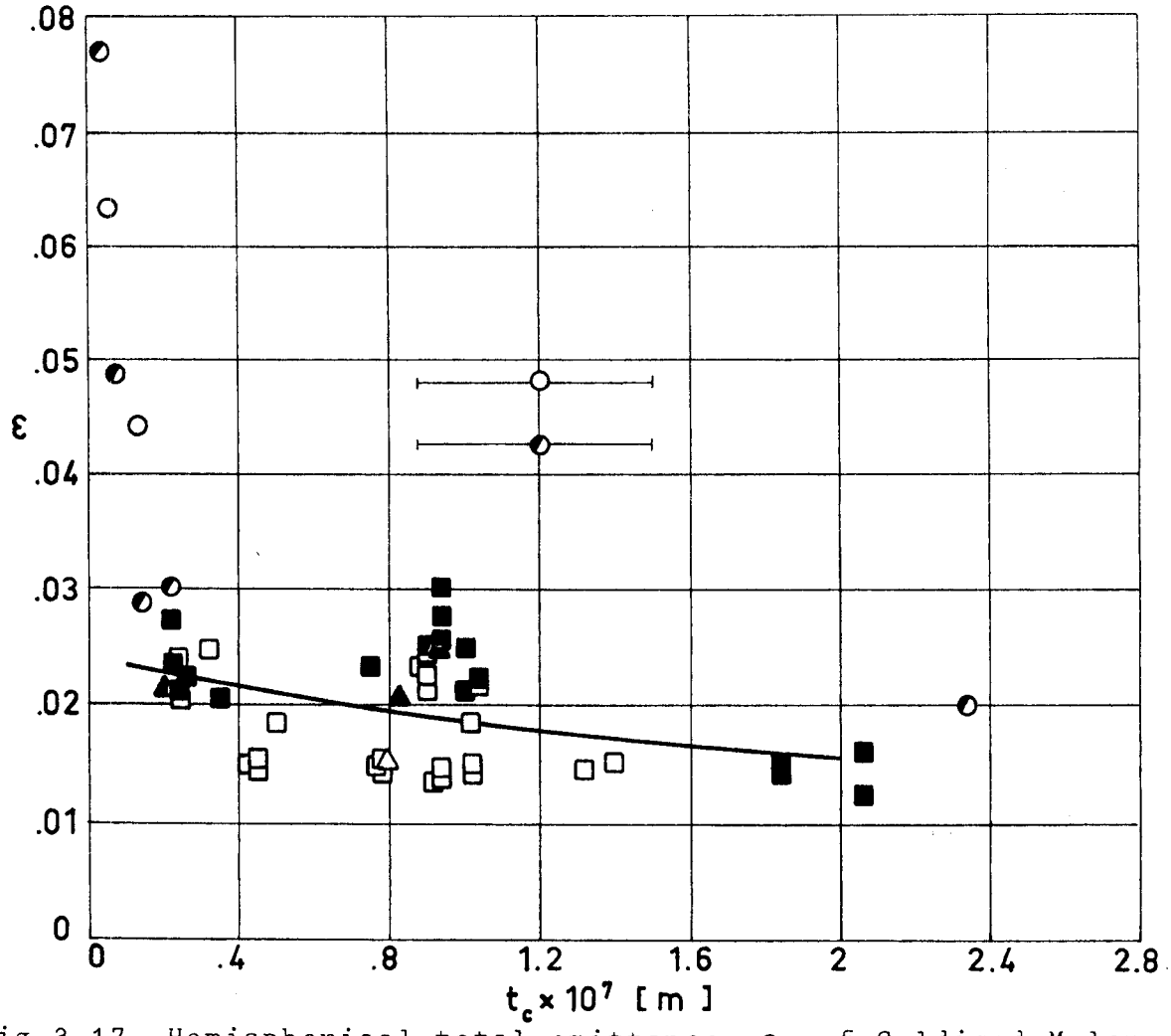

Fig 3-17. Hemispherical total emittance, ε, of Goldized Mylar as a function of coating thickness, t_c. The emitting surface is coated. Solid data points represent two sided coating, while open data points are for one sided coating. ◐ indicates that no details are given in the source to decide whether the specimen was single or double coated.

Explanation

Film Thickness, $t \times 10^6$ [m]	Test Method	References
6.35	t_c: Electrical Resistance. Parallel bar electrode. ε: Receiver Disc exchanging heat with a closely spaced parallel sample. Sample Temperature: 307 K. Chamber Pressure: 1.33×10^{-4} Pa.	○ ◐ ADL (1964). □ ■ ADL (1966). △ Ruccia & Hinckley (1967). —— Coston (1967).

MULTILAYER INSULATIONS

Emittance of Metallized Films

Emittance of Gold on Aluminized Mylar.

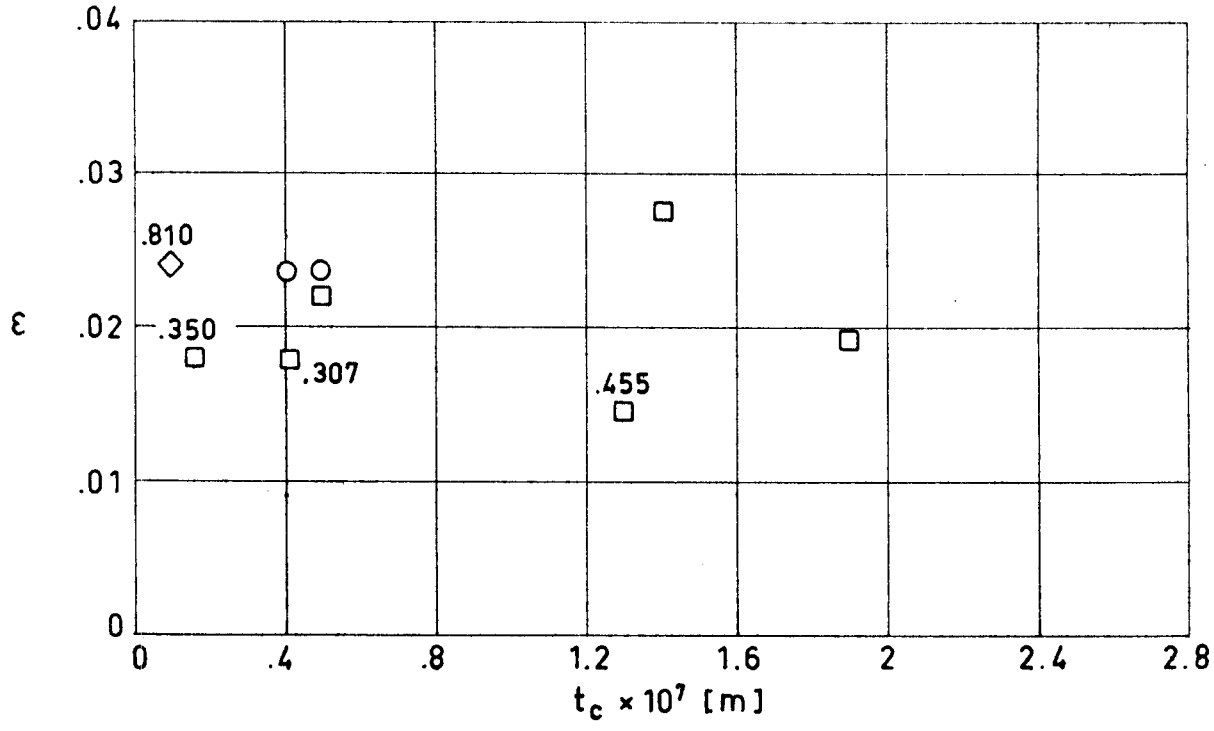

Fig 3-18. Hemispherical total emittance, ε, of Gold on Double Aluminized Mylar as a function of Gold thickness, t_c. The emitting surface is the goldized one. Numbers give the Aluminium layer thickness measured in the same units as t_c. ◇ Silver instead of Aluminium.

Explanation

Film Thickness, $t \times 10^6$ [m]	Test Method	References
6.35	t_c: Electrical Resistance. Parallel bar electrode. ε: Receiver Disc exchanging heat with a closely spaced parallel sample. Sample Temperature: 307 K. Chamber Pressure: 1.33×10^{-4} Pa.	○ ADL (1964). □ ◇ ADL (1966).

MULTILAYER INSULATIONS

Emittance of Metallized Films

Emittance of Silver Coated Mylar.

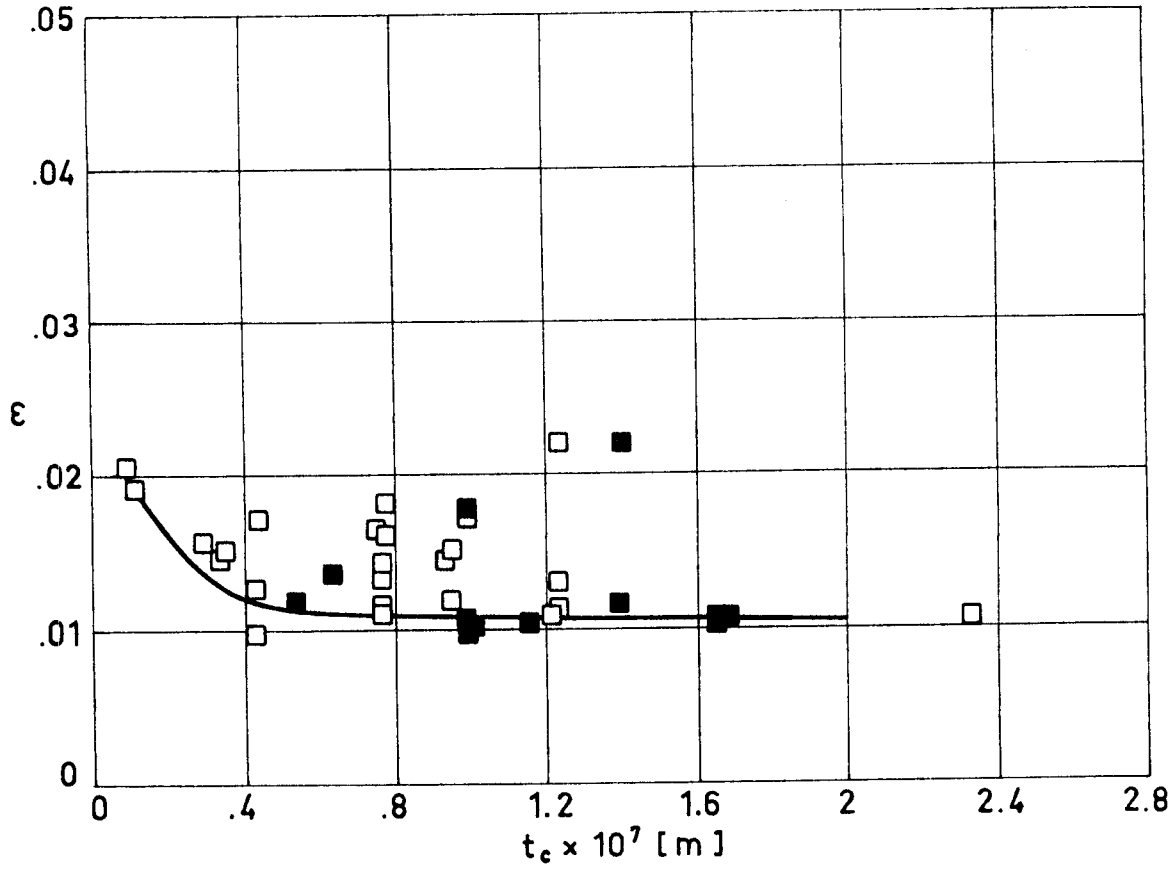

Fig 3-19. Hemispherical total emittance, ε, of Silvered Mylar as a function of coating thickness, t_c. The emitting surface is coated. Solid data points represent two sided coating, while open data points are for one sided coating.

Explanation

Film Thickness, $t \times 10^6$ [m]	Test Method	References
6.35	t_c: Electrical Resistance. Parallel bar electrode. ε: Receiver Disc exchanging heat with a closely spaced parallel sample. Sample Temperature: 307 K. Chamber Pressure: 1.33×10^{-4} Pa.	□ ■ ADL (1966). —— Coston (1967).

MULTILAYER INSULATIONS

Emittance of Metallized Films

Emittance of Silver Coated Mylar with SiO Overcoating.

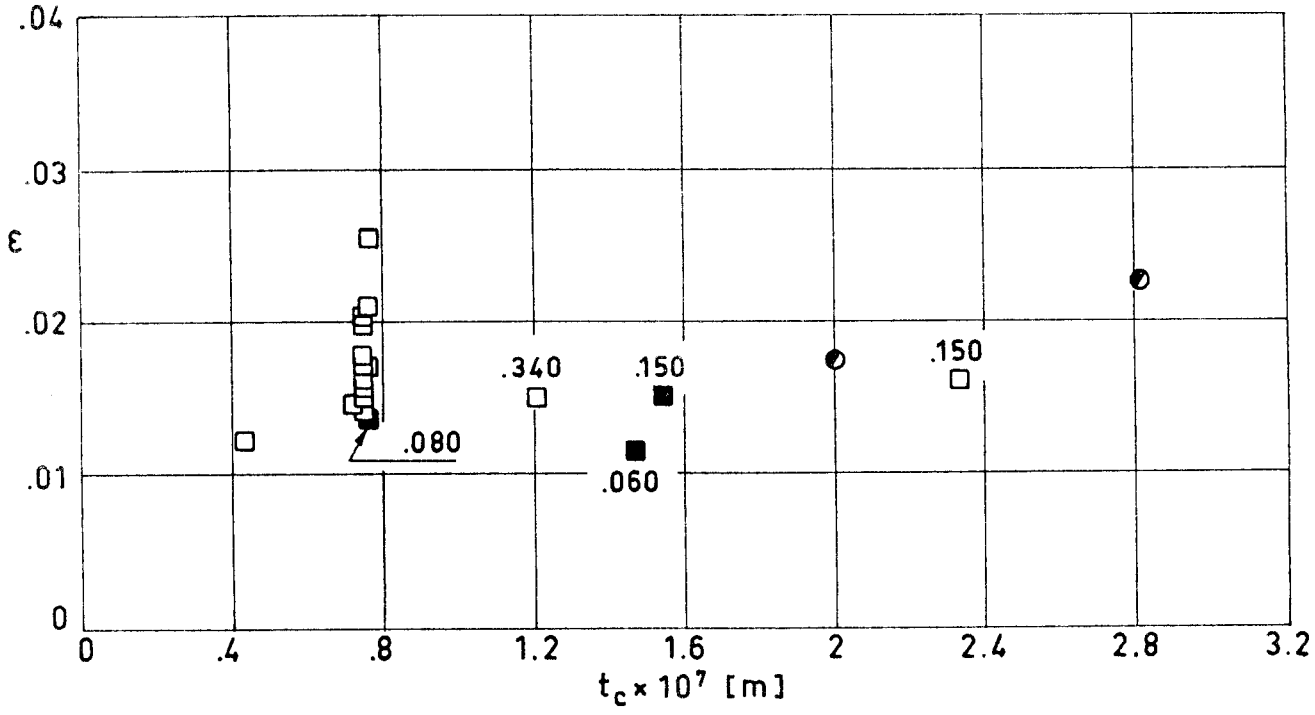

Fig 3-20. Hemispherical total emittance, ε, of Silvered Mylar overcoated with Silicon Monoxide as a function of Silver thickness, t_c. The emitting surface is overcoated. Solid data points represent two sided coating plus overcoating, while open data points are for one sided coating plus overcoating. ◐ indicates that no details are given in the source to decide whether the specimen was single or double coated. Numbers give the overcoating thickness measured in the same units as t_c. Overcoating thickness of □ is $.075 \times 10^{-7}$ m unless otherwise indicated in the figure.

Explanation

Film Thickness, $t \times 10^6$ [m]	Test Method	References
6.35	t_c: Electrical Resistance. Parallel bar electrode. ε: Receiver Disc exchanging heat with a closely spaced parallel sample. Sample Temperature: 307 K. Chamber Pressure: 1.33×10^{-4} Pa.	◐ ADL (1964). □ ■ ADL (1966).

MULTILAYER INSULATIONS

Emittance of Metallized Films

Emittance of Aluminium Coated Kapton.

The hemispherical total emittance as a function of temperature, for several values of the coating thickness, is given in Fig 3-21. The influence of thickness, for representative temperatures, is shown in Figs 3-22 and 3-23.

The table below concerns these three figures.

Explanation

Key	Film Thickness $\times 10^6$ [m]	Coating Thickness $\times 10^7$ [m]	Test Method	References
○		.3		Coston (1967).
□	12.7	∿.4	Calorimetrically. Specimens attached to a 2.54×10^{-2} m diameter cylinder internally heated. Optical flat monitor-Interferometry	Cunnington, Zierman, Funai & Lindahn (1967).
△	12.7	∿.6		
▲	12.7	∿.6		
◭	25.4	.65		
◭		.7		Coston (1967).
▽		.8		
▼	25.4	.8	Same as □.	Cunnington et al. (1967).
▽		.85		Coston (1967).
▼	25.4	.85	Same as □.	Cunnington et al. (1967).
▷	25.4	1.		
▶		1.05	Same as □.	Coston (1967).
◁		2.2		
◀	25.4	2.2	Same as □.	Cunnington et al. (1967).

All the data from Cunnington et al (1967) are for single-aluminized specimens radiating from the coated side. No details are given by Coston (1967) to decide whether the samples were single or double-coated.

MULTILAYER INSULATIONS

Emittance of Metallized Films

Emittance of Aluminium Coated Kapton.

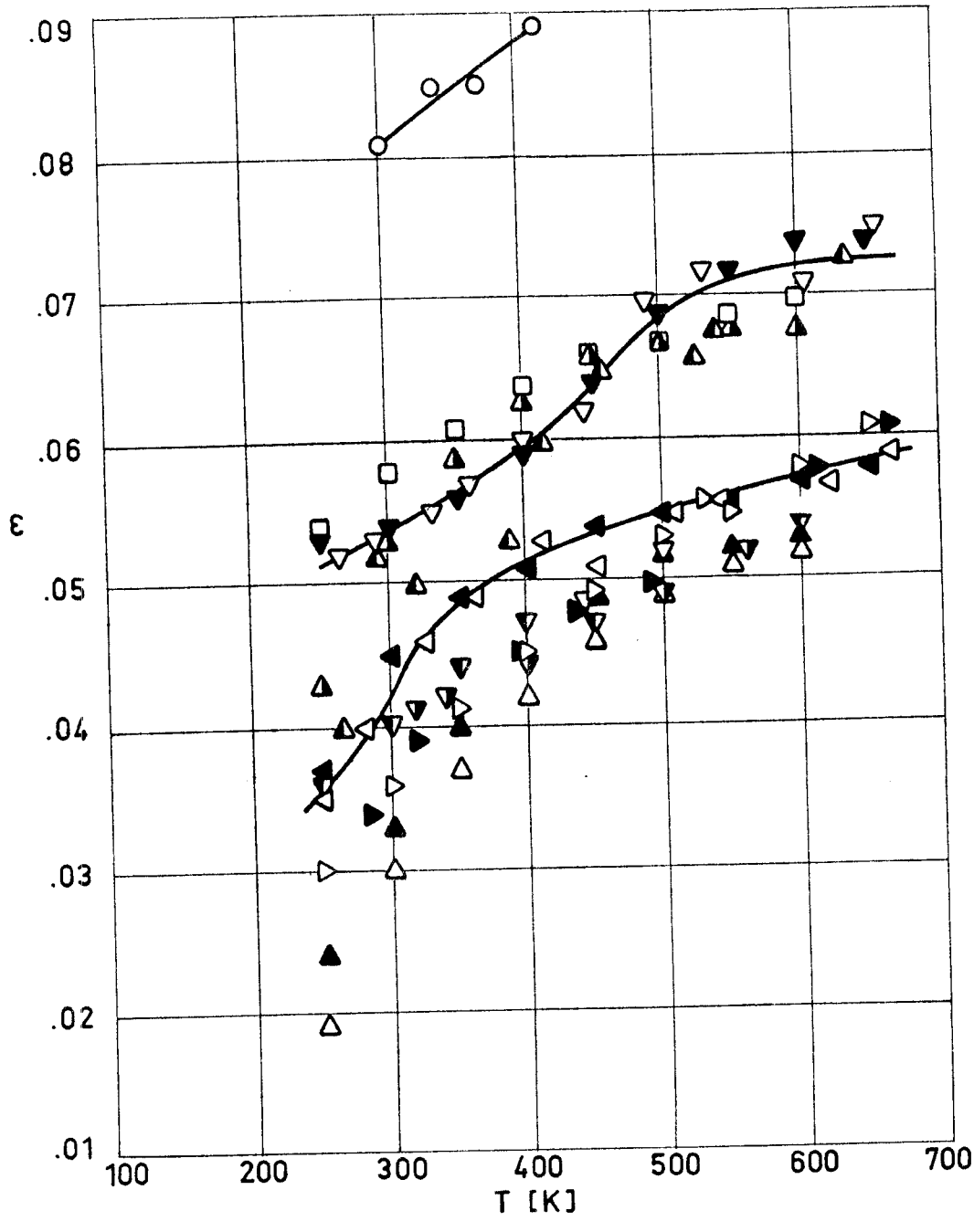

Fig 3-21. Hemispherical total emittance, ε, of Aluminized Kapton as a function of temperature, T.

MULTILAYER INSULATIONS

Emittance of Metallized Films

Emittance of Aluminium Coated Kapton.

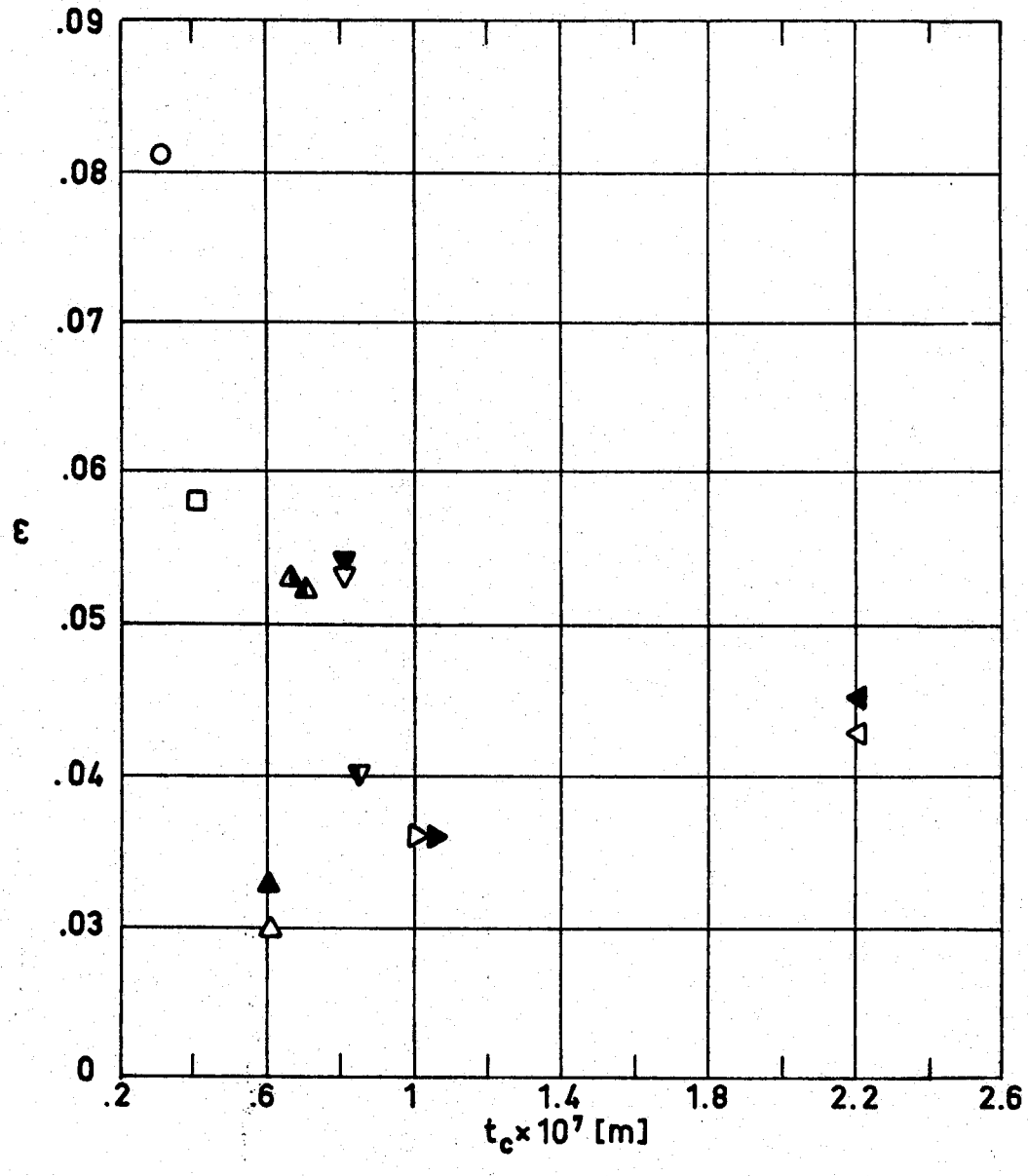

Fig 3-22. Hemispherical total emittance, ε, of Aluminized Kapton as a function of coating thickness, t_c, for T = 300 K.

MULTILAYER INSULATIONS

Emittance of Metallized Films

Emittance of Aluminium Coated Kapton.

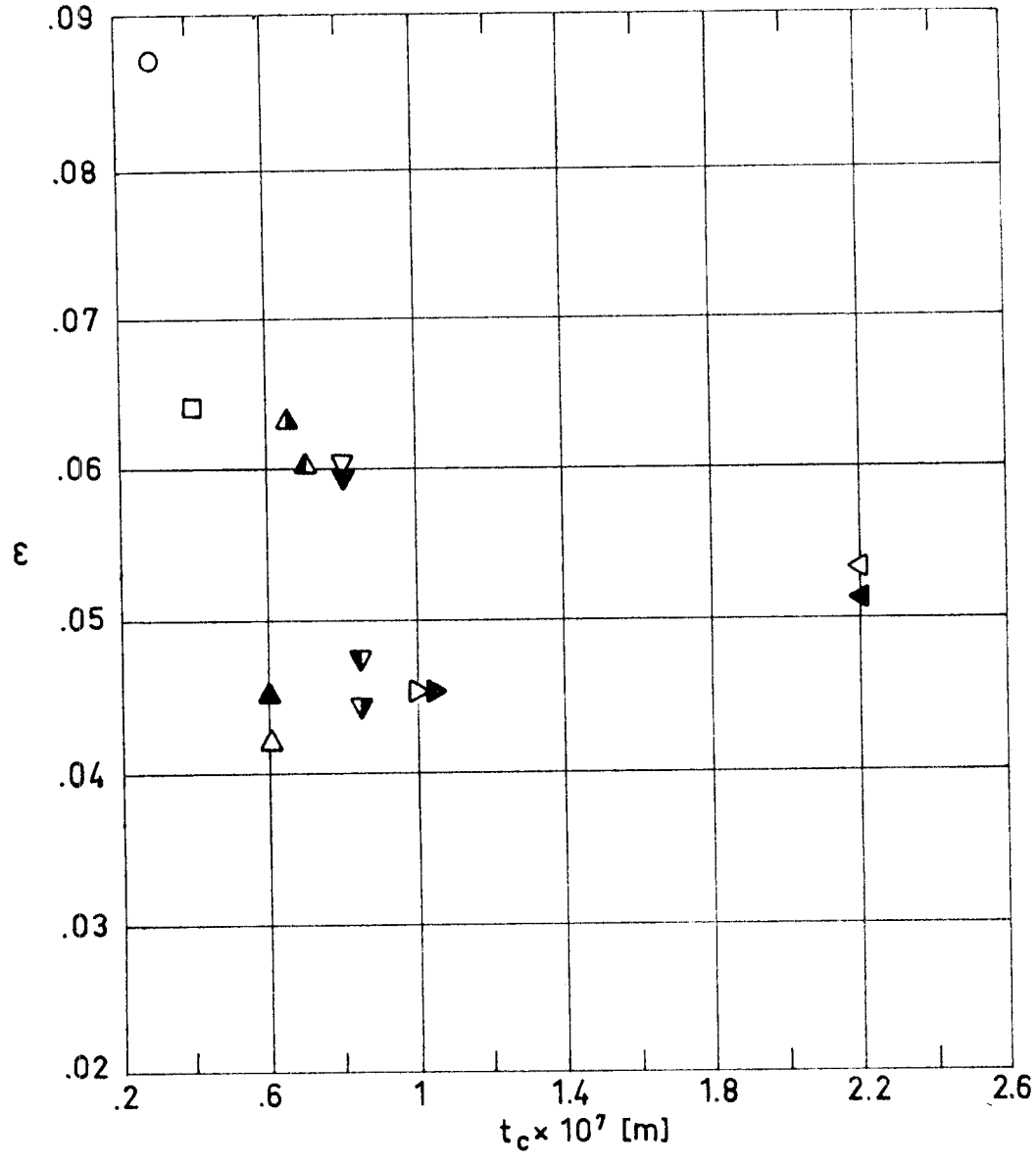

Fig 3-23. Hemispherical total emittance, ε, of Aluminized Kapton as a function of coating thickness, t_c, for T = 400 K.

MULTILAYER INSULATIONS

Emittance of Metallized Films

Emittance of Gold Coated Kapton.

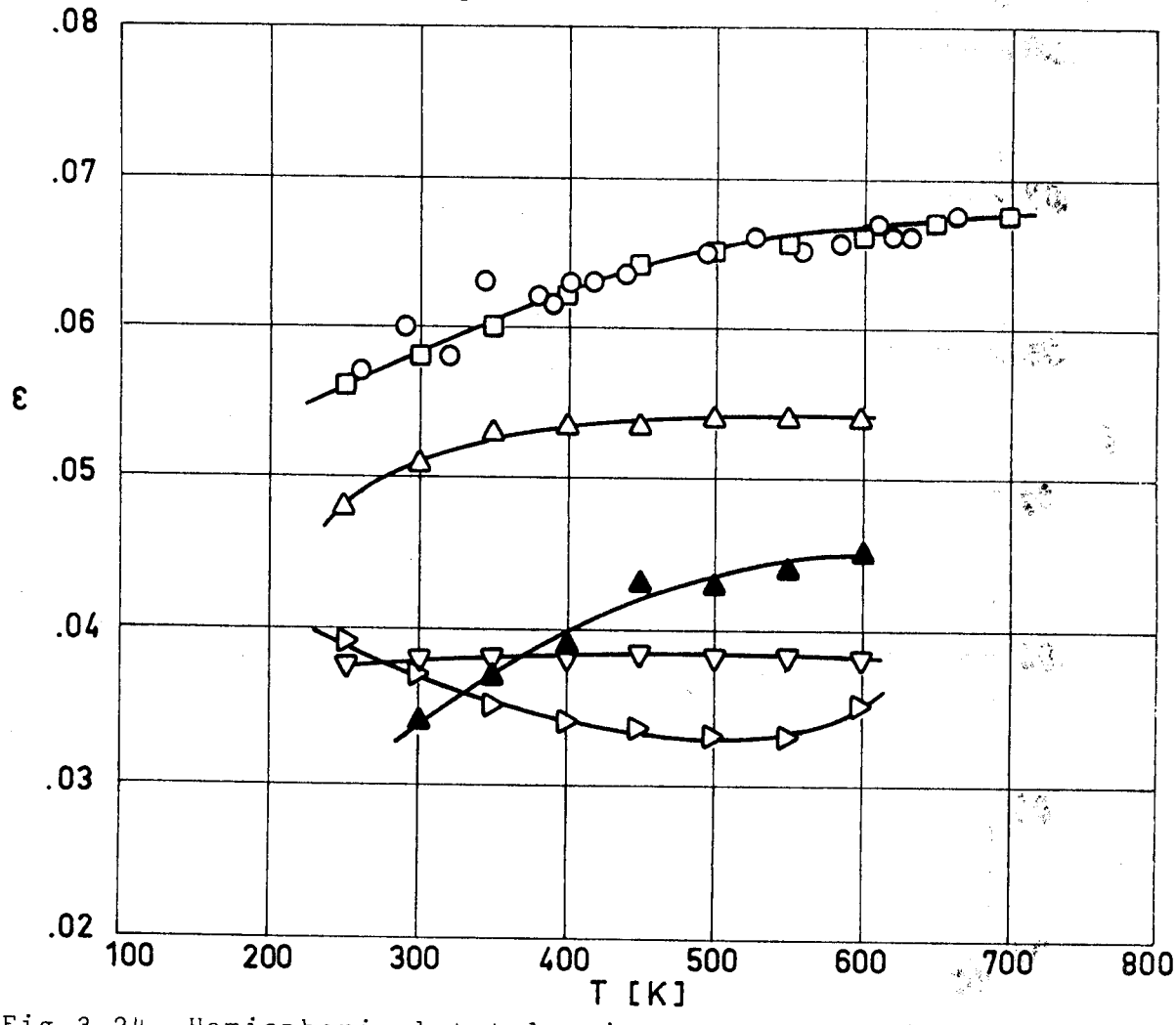

Fig 3-24. Hemispherical total emittance, ε, of Single-Goldized Kapton as a function of temperature, T.

Explanation

Key	Film Thickness $\times 10^6$ [m]	Coating Thickness $\times 10^7$ [m]	Test Method	References
○				Coston (1967)
□			ε: Calorimetrically. Specimens were attached to a 2.54×10^{-2} m diameter cylinder heated internally.	Cunnington, Zierman, Funai & Lindahn (1967).
△	12.7			
▲	12.7			
▽	25.4	.6	t_c: Optical flat monitor-interferometer. ε: Calorimetrically as above.	
▷	25.4	1.		

MULTILAYER INSULATIONS

Emittance of Metallized Films

Emittance of Silver Coated Kapton.

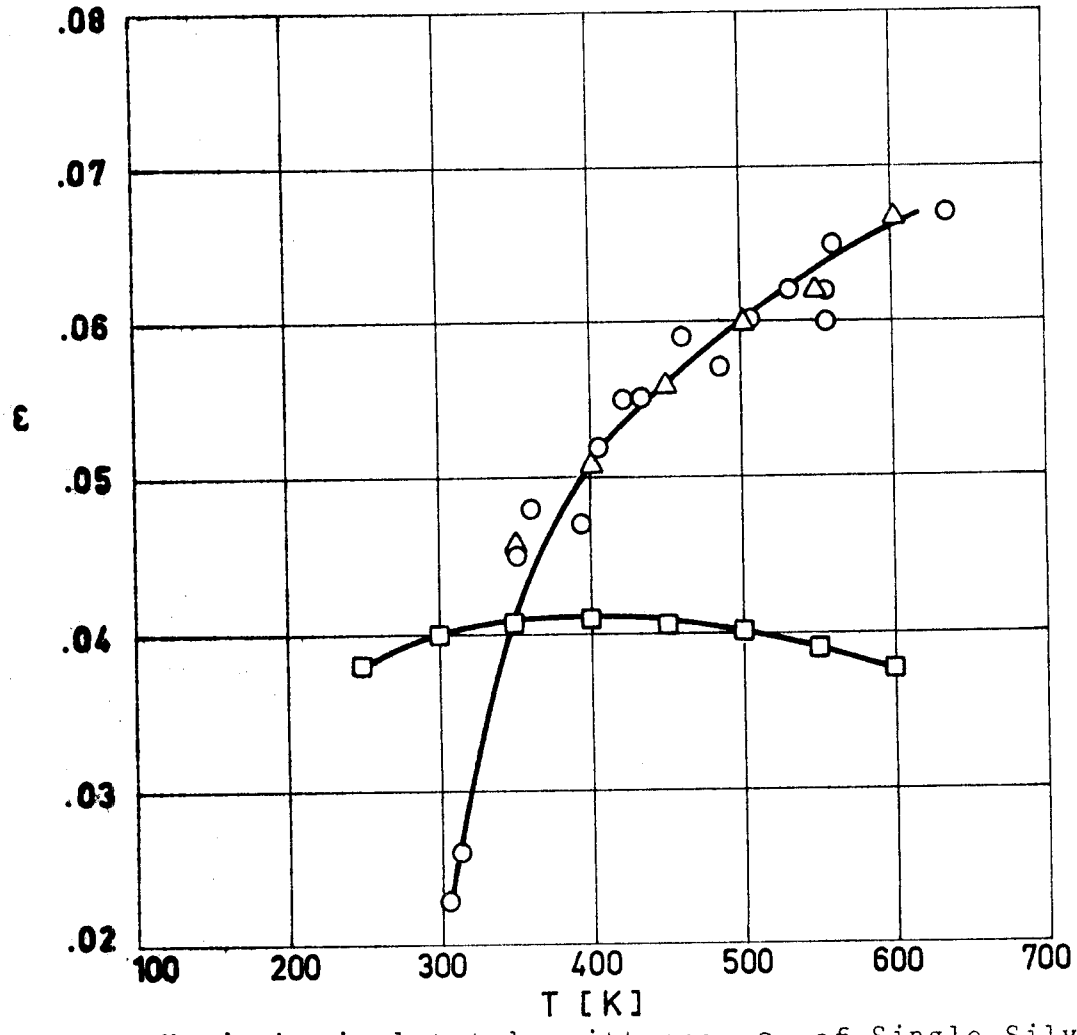

Fig 3-25. Hemispherical total emittance, ε, of Single-Silvered Kapton as a function of temperature, T.

Explanation

Key	Film Thickness $\times 10^6$ [m]	Coating Thickness $\times 10^7$ [m]	Test Method	References
○				Coston (1967).
□	25.4	.7	t_c: Optical flat monitor-interferometry. ε: Calorimetrically.	Cunnington, Zierman, Funai & Lindahn (1967).
△	12.7		ε: Calorimetrically. Specimens were attached to a 2.54×10^{-2} m diameter cylinder heated internally	

MULTILAYER INSULATIONS
Absorptance of Metallic Foils

3.5. ABSORPTANCE OF METALLIC FOILS

Data regarding spectral absorptance, α'_λ, and solar absorptance, α_s, of metallic foils are given in the following pages. These data have been arranged as is indicated below.

Metal	$\alpha'_\lambda(\lambda)$ Figure	$\alpha_s(T)$ Figure
Aluminium	3-26	3-27
Copper	3-28	3-29
Gold	3-30	3-31
Molybdenum	3-32	3-33
Nickel	3-34	3-35
Inconel	3-36	3-37
Platinum	3-38	3-39
Silver	3-40	3-41

In these figures β is the angle between the surface normal and the direction of the incident flux, λ is the wavelength of incoming radiation, and T the temperature of the sample.

INTENTIONALLY BLANK PAGE

MULTILAYER INSULATIONS

Absorptance of Metallic Foils

Absorptance of Aluminium.

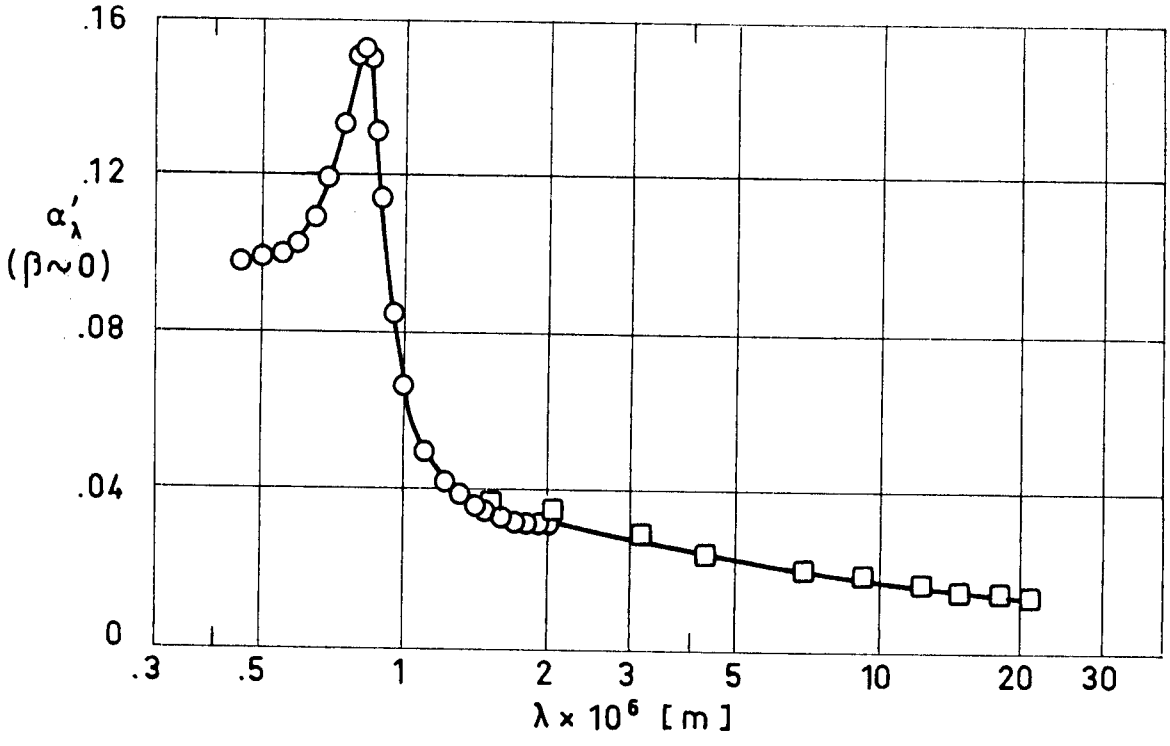

Fig 3-26. Normal spectral absorptance, α'_λ, of Aluminium as a function of wavelength, λ. From Touloukian & DeWitt (1970).

Explanation

Key	Description	Test Method	Comments
○	Evaporated film; evaporation rate 3×10^{-8} m.s^{-1} at 2.67×10^{-3} Pa. Aged 8 days before measurement.		β~10°. Measured in vacuum. Reported error ±1.4%. T=298 K.
□	Aluminium Foil.	Heated cavity at approx. 1 056 K with platinum reference. Authors assumed α=1-R(2π,25°).	β=25°. Measured in dry nitrogen. T=306 K.

MULTILAYER INSULATIONS

Absorptance of Metallic Foils

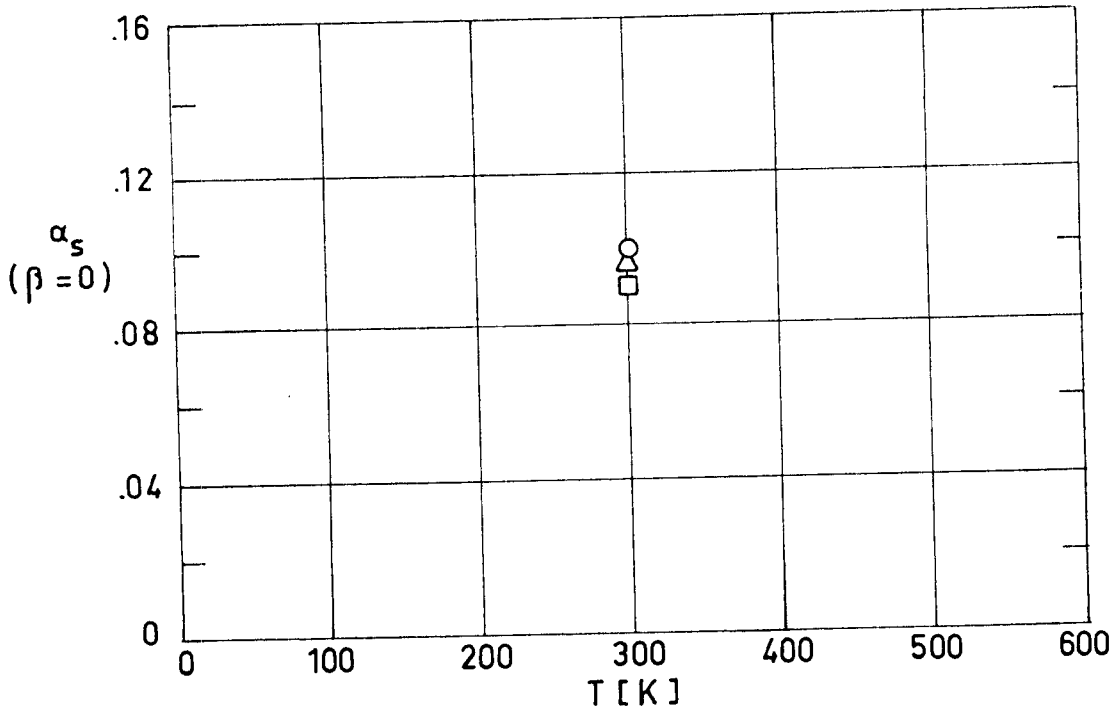

Fig 3-27. Normal solar absorptance, α_s, of Aluminium as a function of temperature, T. From Touloukian & DeWitt (1970).

Explanation

Key	Description	Test Method	Comments
○	Pure. 3×10^{-7} m thick opaque layer on glass. Freshly prepared.	Calculated from 1-ρ.	
□	Different sample. Same specimen and conditions as ○ .		
△	99.99 pure. Electropolished.	Calculated from spectral reflectance.	

MULTILAYER INSULATIONS

Absorptance of Metallic Foils

Absorptance of Copper.

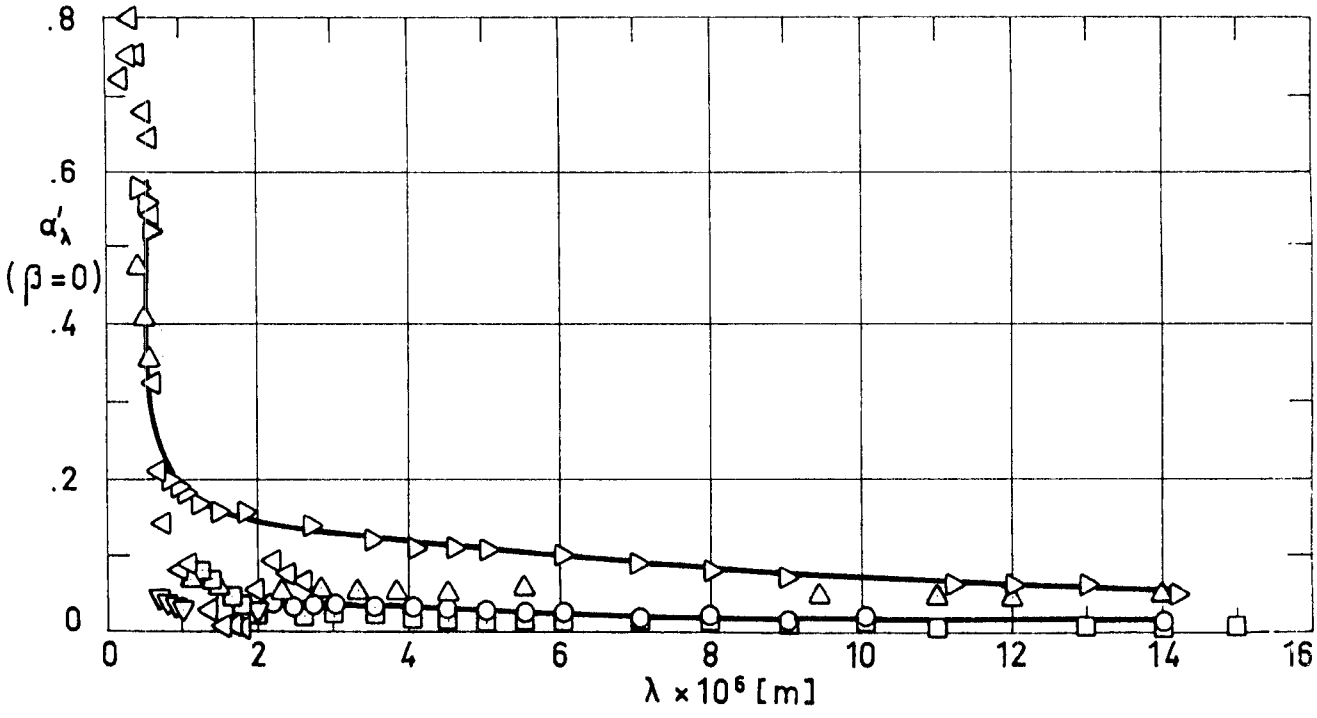

Fig 3-28. Normal spectral absorptance, α'_λ, of Copper as a function of wavelength, λ. From Touloukian & DeWitt (1970).

Explanation

Key	Description	Test Method	Comments
○	Mechanically polished (surface roughness 2×10^{-8} m peak to peak, 5×10^{-6} m lateral).		Measured in air. Data from smooth curve. T=294 K.
□	Same as ○ except heated at 922 K for 3 h.		
△	Same as ○ except heated at 1 222 K for 102 h.		
▽	Electropolished.	Calculated from 1-ρ	T=294 K.
▷	Roughened with sand paper, surface roughness $1.25\times\times10^{-6}$ m.		
◁			Data from smooth curve. T∿298 K.

MULTILAYER INSULATIONS

Absorptance of Metallic Foils

Absorptance of Copper.

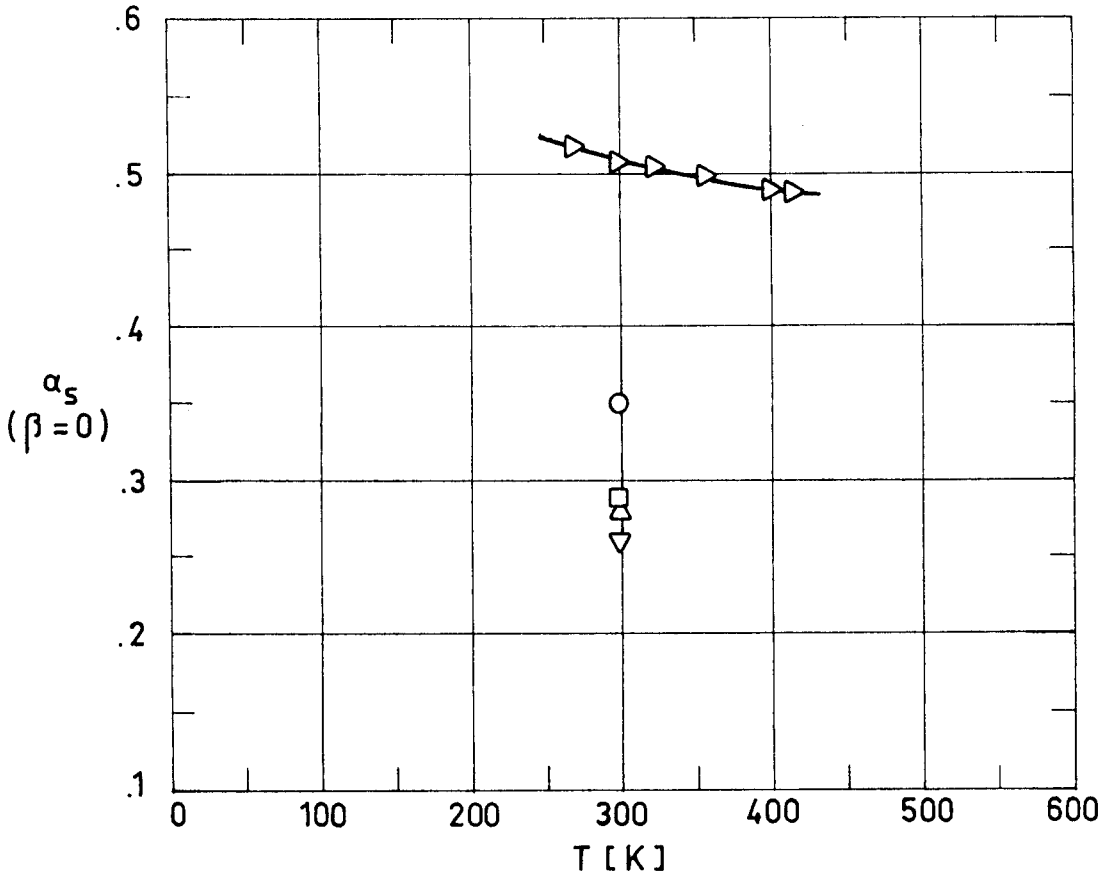

Fig 3-29. Normal solar absorptance, α_s, of Copper as a function of temperature, T. From Touloukian & DeWitt (1970).

Explanation

Key	Description	Test Method	Comments
○	99.9 min. Cu. Turned; freshly prepared.	Calculated from 1-ρ.	
□	Same as ○ except machine polished. Freshly prepared.		
△	Different sample. Same specimen and conditions as □ .		
▽	Different sample. Same specimen and conditions as □ .		
▷	Commercially pure. Cleaned, buffed, cleaned with carbon tetrachloride and acetone.		Measured in vacuum (1.33×10^{-4} Pa). Data from smooth curve.

MULTILAYER INSULATIONS

Absorptance of Metallic Foils

Absorptance of Gold.

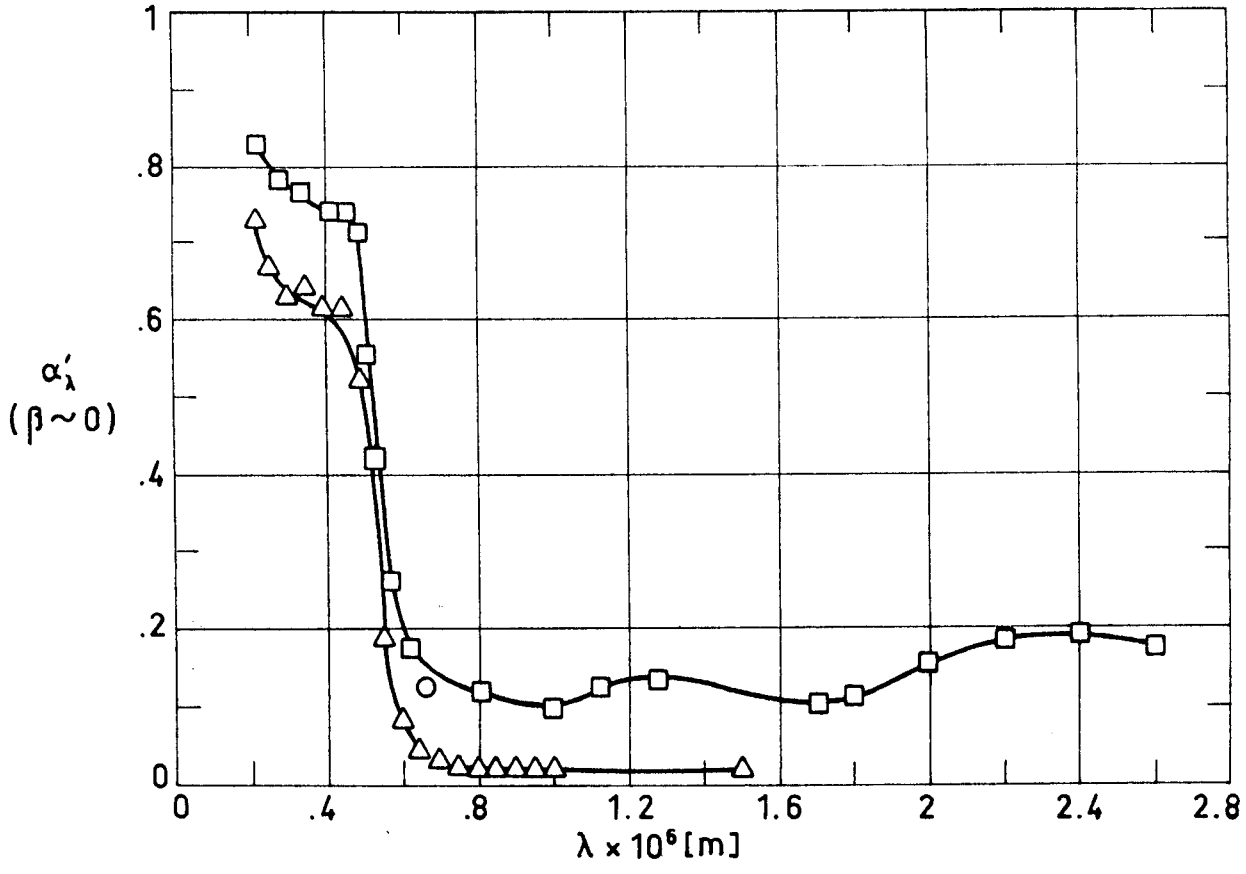

Fig 3-30. Normal spectral absorptance, α'_λ, of Gold as a function of wavelength, λ. O and □ from Touloukian & DeWitt (1970). △ from Fussell, Triolo & Jerozal (1963).

Explanation

Key	Description	Test Method	Comments
O			Measured in burning hydrogen. Temperature range 873 K - 2 073 K.
□			Data from curve. T ∿ 298 K.
△			

MULTILAYER INSULATIONS

Absorptance of Metallic Foils

Absorptance of Gold.

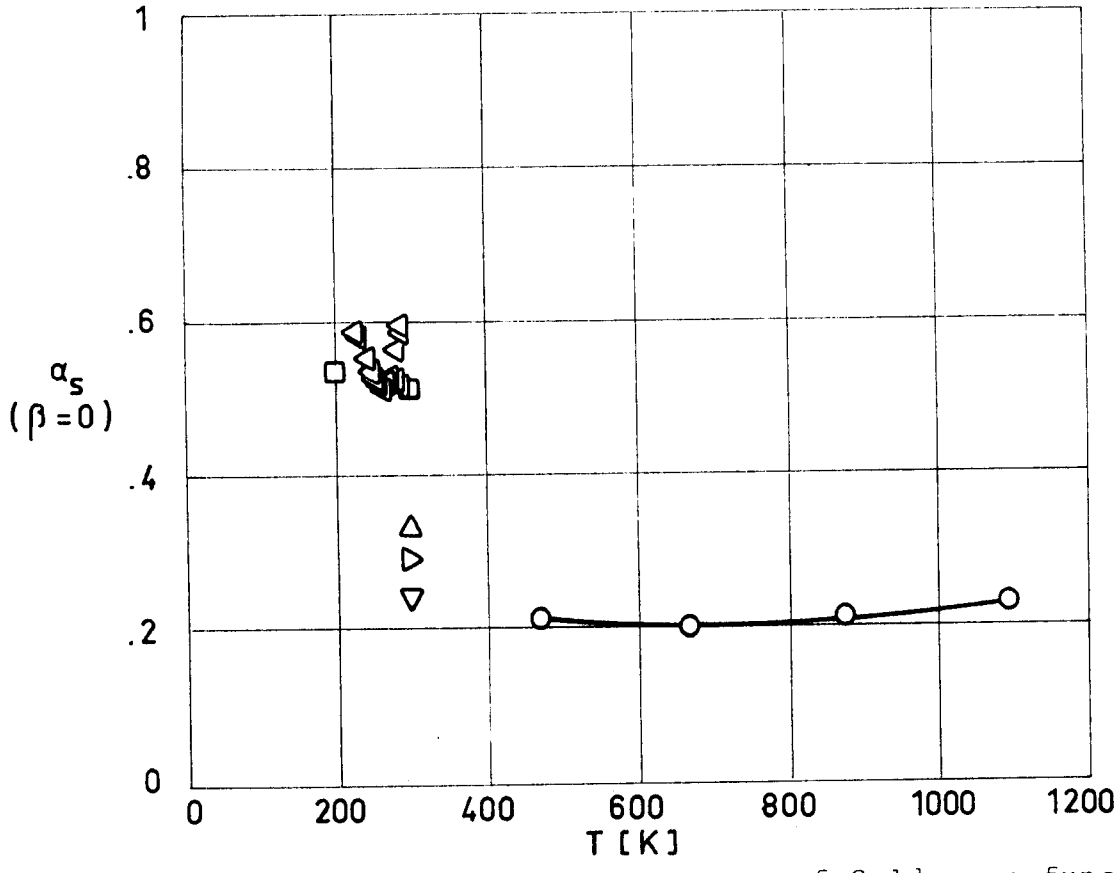

Fig 3-31. Normal solar absorptance, α_s, of Gold as a function of temperature, T. From Touloukian & DeWitt (1970).

Explanation

Key	Description	Test Method	Comments
○	99.95 Gold. Ground with 600 grit carborundum and polished on a wet cloth lap.		Measured in vacuum (1.33×10^{-3} Pa). Reported error ≤10%
□	Cleaned in sodium dichromate and dilute nitric acid solutions, buffed, cleaned with carbon tetrachloride and acetone.		Measured in vacuum (1.33×10^{-4} Pa). Data from smooth curve. Reported error 4%.
△	Vacuum deposit on buffed titanium.		Reported error 10%.
▽	Vacuum deposit on aluminium.		
▷	Bright foil.		
◁	Commercially pure. Cleaned, buffed, cleaned with carbon tetrachloride and acetone.		Measured in vacuum (1.33×10^{-4} Pa). Data from smooth curve.

MULTILAYER INSULATIONS

Absorptance of Metallic Foils

Absorptance of Molybdenum.

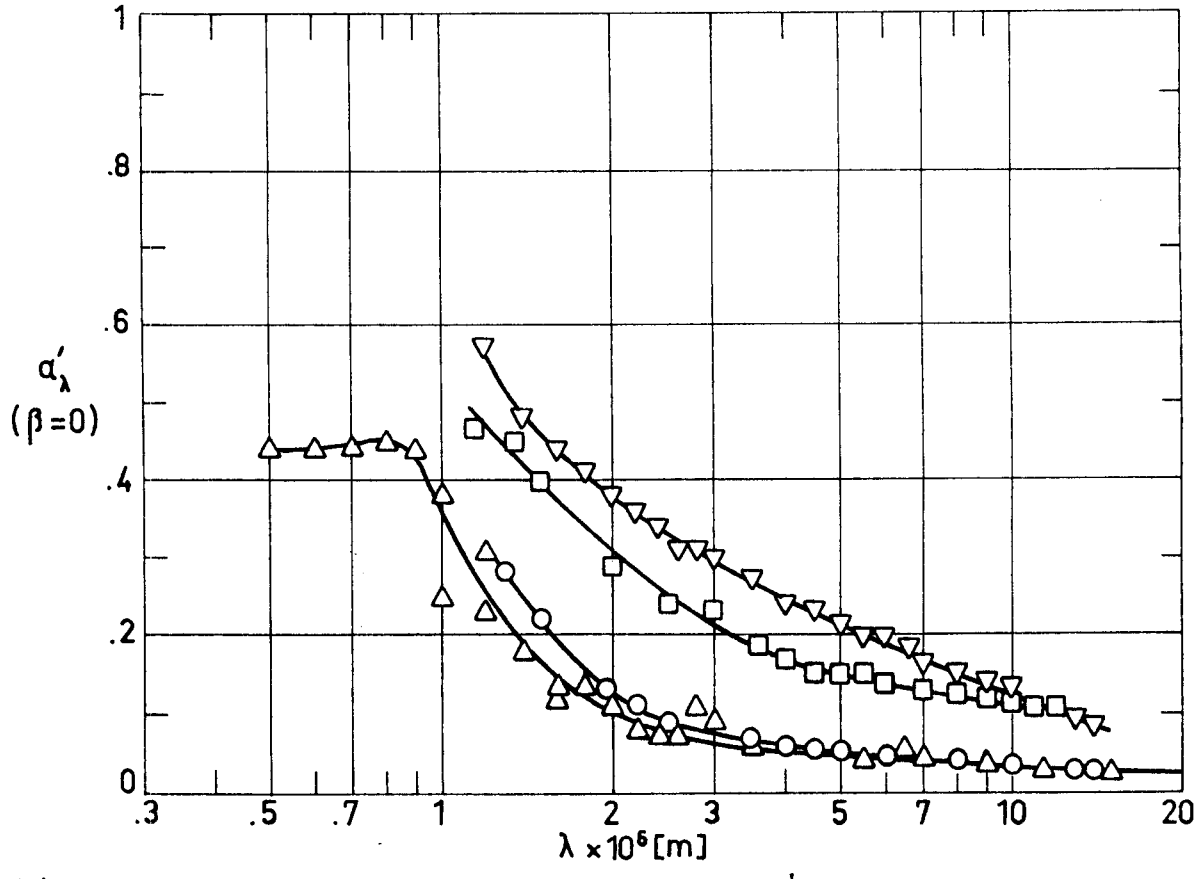

Fig 3-32. Normal spectral absorptance, α'_λ, of Molybdenum as a function of wavelength, λ. From Touloukian & DeWitt (1970).

Explanation

Key	Description	Test Method	Comments
○	Foil, 1.27×10^{-4} m thick. Cleaned with acetone.		Measured in air. Data from smooth curve. T = 294 K.
□	Foil, 1.27×10^{-4} m thick. Cleaned with acetone, heated in vacuum (1.33×10^{-3} Pa) 1 h at 1273 K.		
△	Polished.	Reflectance technique.	
▽	Machined smooth.	Reflectance technique.	

MULTILAYER INSULATIONS

Absorptance of Metallic Foils

Absorptance of Molybdenum.

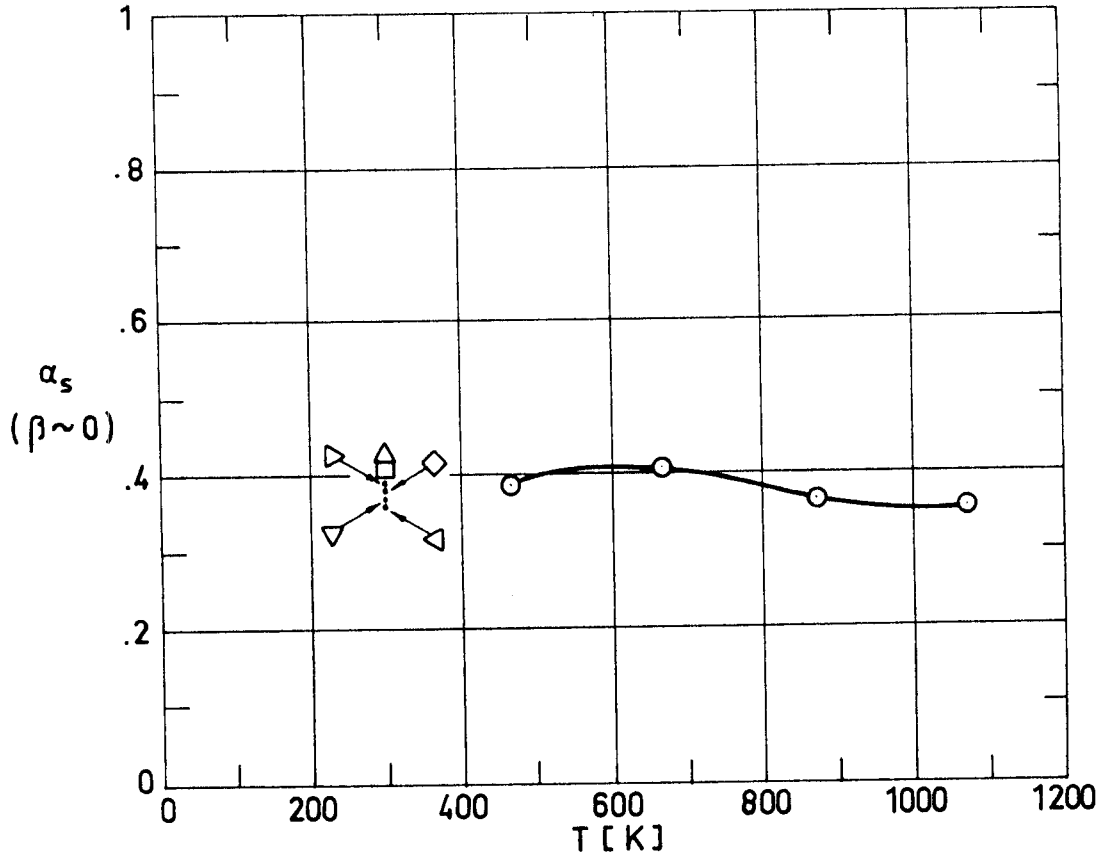

Fig 3-33. Normal solar absorptance, α_s, of Molybdenum as a function of temperature, T. From Touloukian & DeWitt (1970).

Explanation

Key	Description	Test Method	Comments
○	Vacuum arc cast, machined, extruded, recristallized, rolled. Disk 10^{-3} m thick, ground and polished.		$\beta=0°$ Measured in vacuum (1.33×10^{-3} Pa).
□	Arc melted, unalloyed, as received.	From spectral reflectance.	$\beta=9°$ Calculated for above atmosphere conditions.
△	Same as □		$\beta=0°$ Calculated for sea level conditions.
▽	Same as □ except cleaned with liquid detergent.		Same as □
▷	Same as ▽		Same as △
◁	Same as □ except polished.		Same as □
◇	Same as ◁		Same as △

MULTILAYER INSULATIONS

Absorptance of Metallic Foils

Absorptance of Nickel.

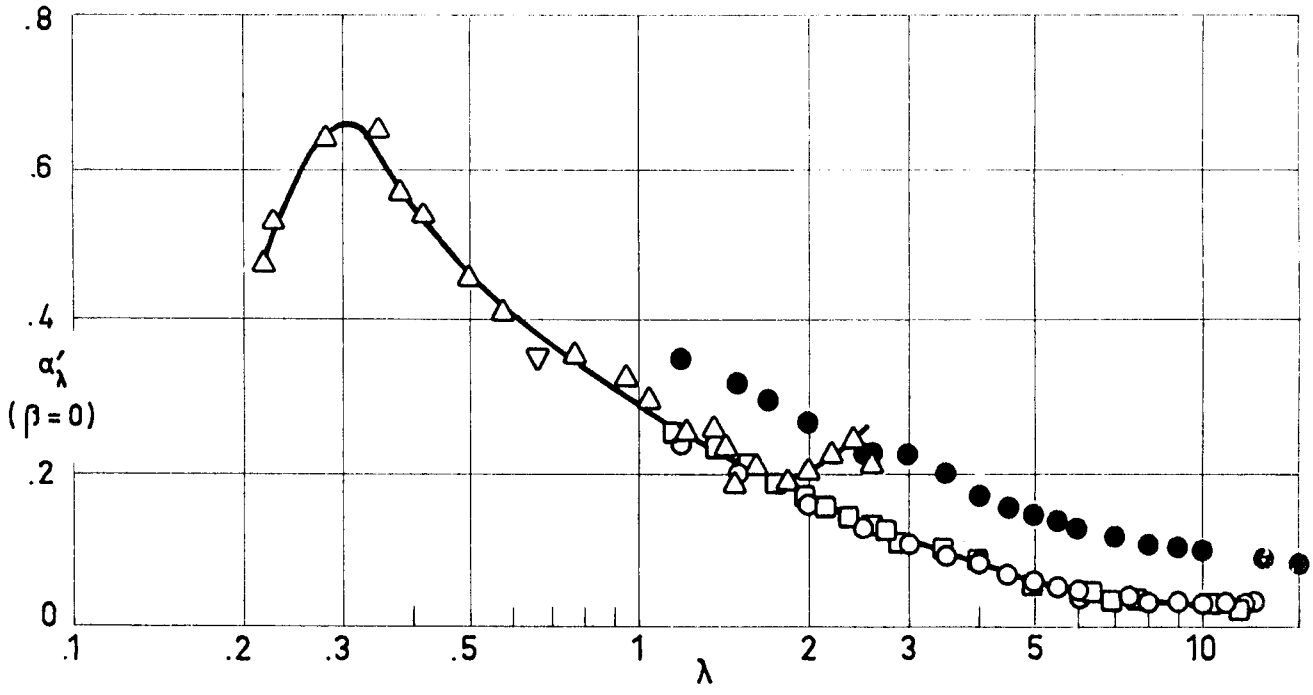

Fig 3-34. Normal spectral absorptance, α'_λ, of Nickel as a function of wavelength, λ. From Touloukian & DeWitt (1970).

Explanation

Key	Description	Test Method	Comments
○	Mechanically polished with aluminium oxide and cleaned with water (surface roughness 2.5×10^{-8} m peak to peak and 2.5×10^{-5} m lateral).		Measured in air. Data from smooth curve. T=298 K.
●	Polished and cleaned as above. Heated in vacuum: 3 h, 588 K; 3 h, 1 089 K; 4 h, 1 267 K; and 48 h above 1 256 K. Surface roughness (measured after 120 d) 7.5×10^{-6} m peak to peak and 2.5×10^{-5} m lateral		Data from smooth curve. T=298 K.
□		Hohlraum.	T=294 K. Reported error <5%.
△	Foil 7.62×10^{-5} m thick.		Data from smooth curve. T∿298 K.
▽			Measured in burning hydrogen. Authors assumed $\alpha=\varepsilon$. T=873 K.

MULTILAYER INSULATIONS

Absorptance of Metallic Foils

Absorptance of Nickel.

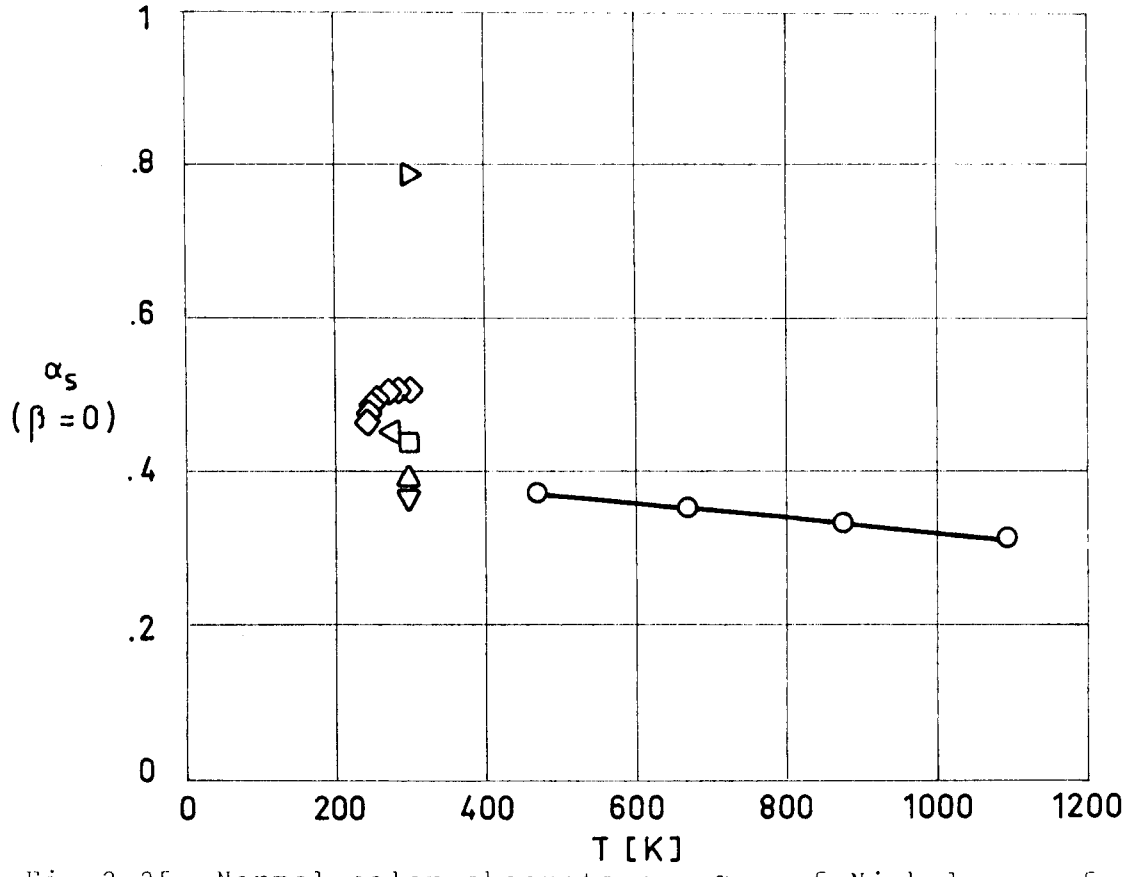

Fig 3-35. Normal solar absorptance, α_s, of Nickel as a function of temperature, T. From Touloukian & DeWitt (1970).

Explanation

Key	Description	Test Method	Comments
○	Commercially pure. Ground with 600 grit carborundum and polished.		Measured in vacuum (1.33×10^{-3} Pa).
□	Commercial grade A. As received	Spectral reflectance	Computed for sea level conditions.
△	Same as □ except cleaned with liquid detergent.		
▽	Same as □ except polished.		
▷	Same as □ except oxidized in air at red heat for 30 min.		
◁	Electroless nickel. Extraterrestrial.		Reported error 10%
◇	Commercially pure. Cleaned with carbon tetrachloride and acetone.		Measured in vacuum (1.33×10^{-4} Pa). Data from smooth curve.

MULTILAYER INSULATIONS

Absorptance of Metallic Foils

Absorptance of Nickel Alloys (INCONEL).

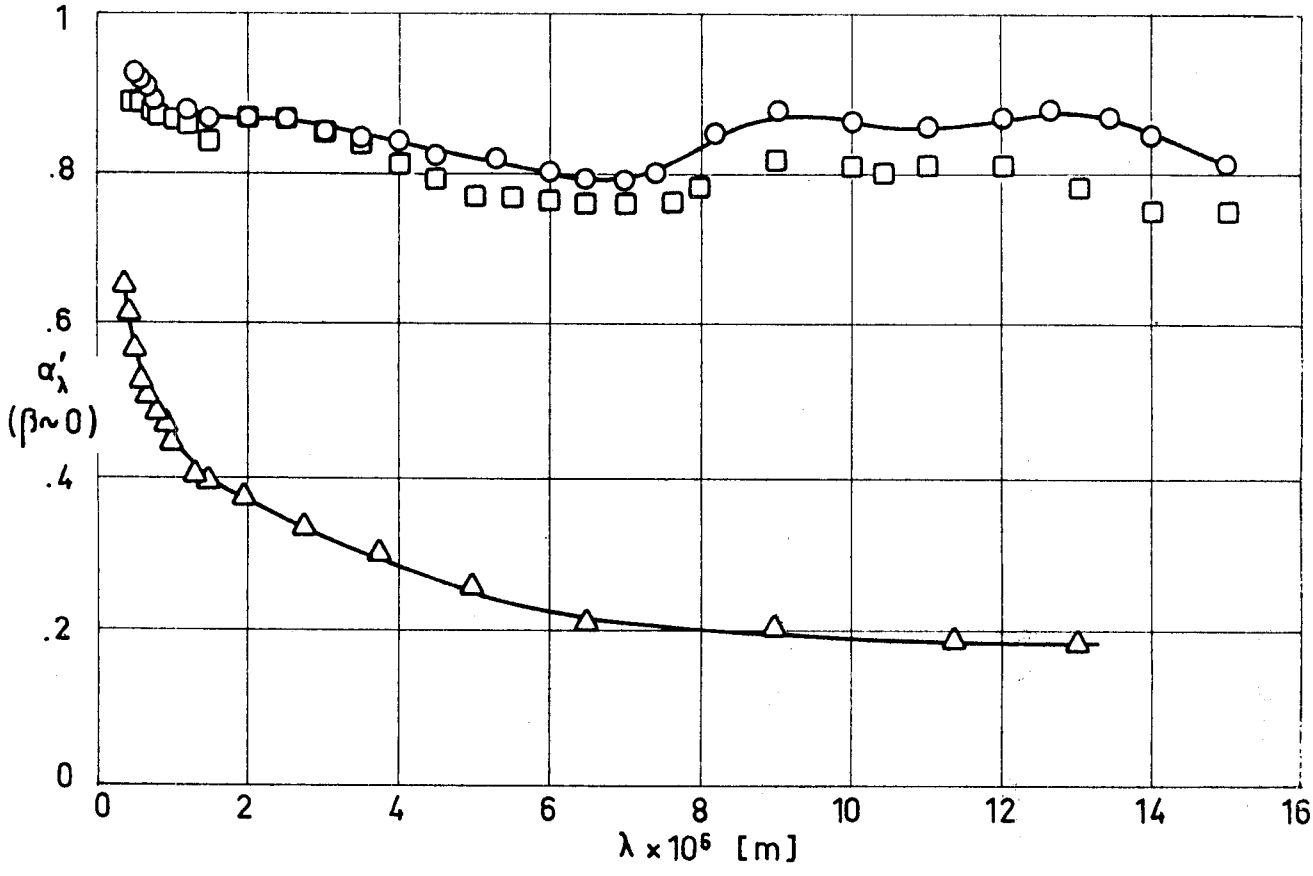

Fig 3-36. Normal spectral absorptance, α'_λ, of Inconel as a function of wavelength, λ. From Touloukian & DeWitt (1970).

Explanation

Key	Description	Test Method	Comments
○	Inconel. Nominal composition.		Measured in air. Data from smooth curve. T=294 K.
□	Same as ○. Heated at 1 250 K for 2 h and at 1 467 K for 2 h.		
△	Inconel X. Nominal composition. Rolled plate.	Heated cavity at approx. 1 056 K with platinum reference. Authors assumed $\alpha=1-R(2\pi,25°)$.	$\beta=25°$. Measured in dry nitrogen. T=306 K.

MULTILAYER INSULATIONS

Absorptance of Metallic Foils

Solar Absorptance of Nickel Alloys (INCONEL).

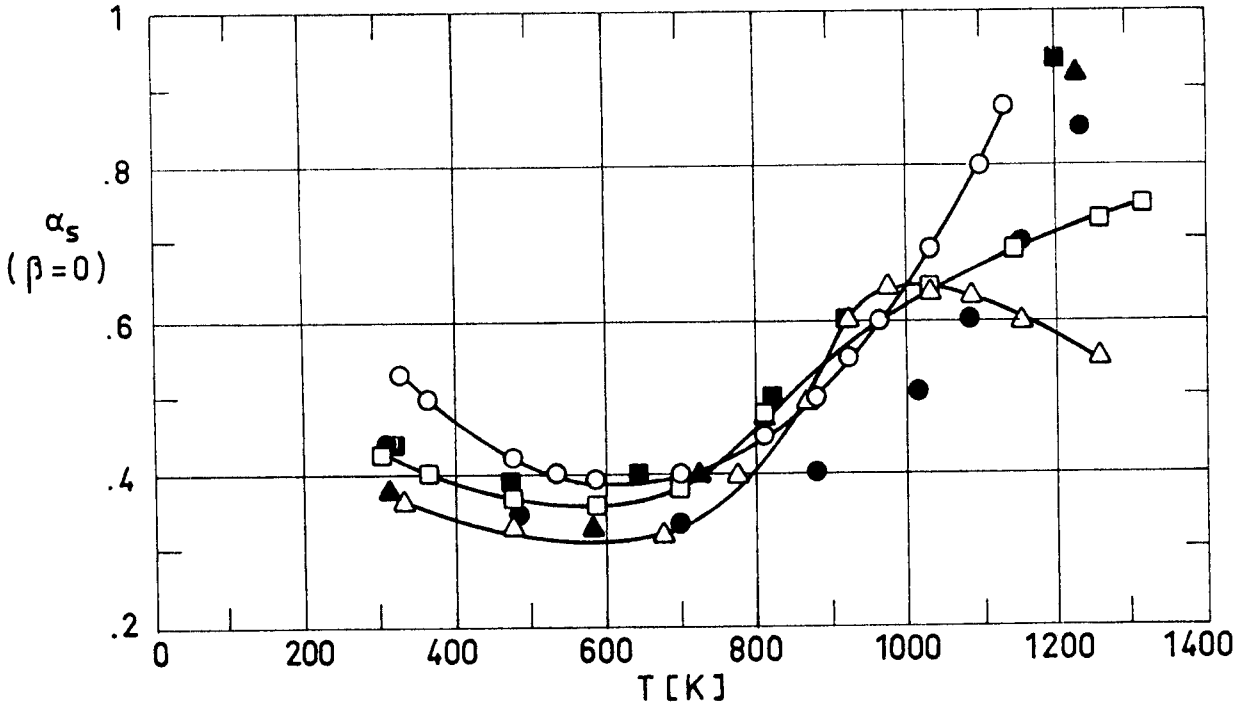

Fig 3-37. Normal solar absorptance, α_s, of Inconel as a function of the temperature, T, to which samples had been previously heated. From Wood, Deem & Lucks (1961).

Explanation

Key	Description	Test Method	Comments
○	Inconel B. As received.	Comparison standards. Comparison pyroheliometer. Temperature measured with thermocouples.	Measured in air at 311 K.
□	Inconel B. Clean and smooth.		
△	Inconel B. Polished.		
●	Inconel X. As received.		
■	Inconel X. Clean and smooth.		
▲	Inconel X. Polished.		

MULTILAYER INSULATIONS

Absorptance of Metallic Foils

Absorptance of Platinum.

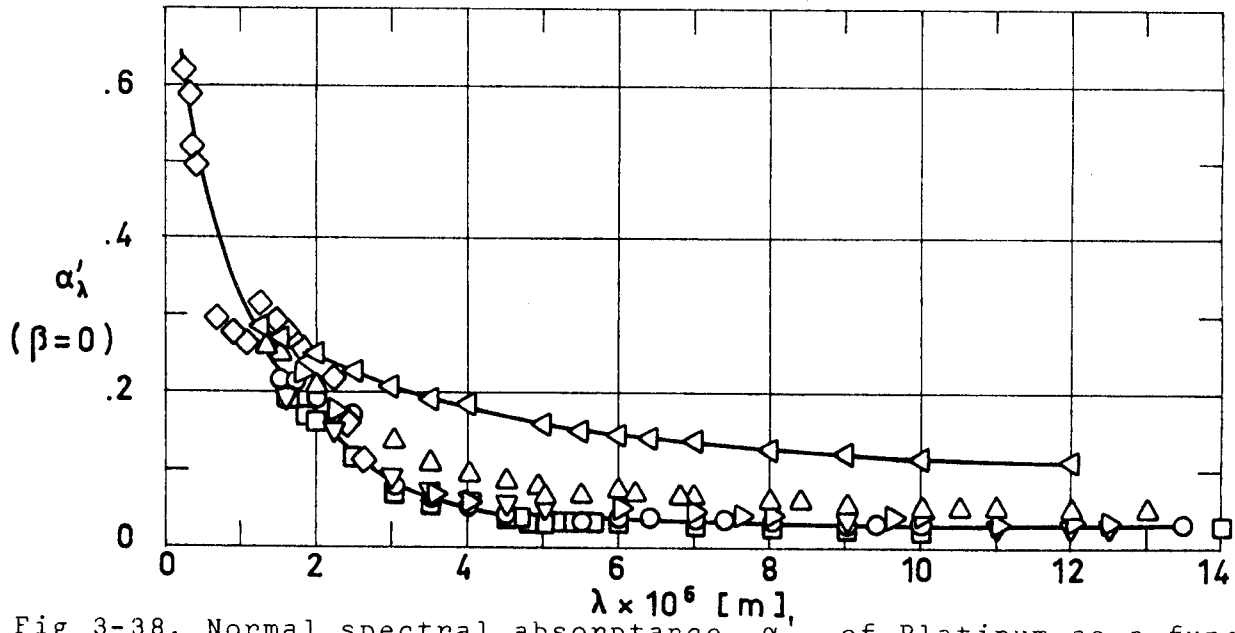

Fig 3-38. Normal spectral absorptance, α_λ, of Platinum as a function of wavelength, λ. From Touloukian & DeWitt (1970).

Explanation

Key	Description	Test Method	Comments
○	NBS platinum. Heated in air at 1523 K for 1 h, cooled for 12 h.		Measured in air. Data from smooth curve. T=294 K.
□	NBS platinum. Heated in air at 1523 K for 1 h, cooled for 12 h, heated at T>1088 K for 24 h and at 1523 K for 1 h.		
△	Same as □ except after 180 d heated at T>1083 K for 11 h and at T>1277 K for 1 h.		Measured after a total of 240 d. T=294 K.
▽	Mechanically polished with aluminium oxide and cleaned with water. Heated at 1088 K for 3 h.		Measured in vacuum (6.65×10^{-4} Pa). Data from smooth curve. T=294 K.
▷	Polished with aluminium oxide, cleaned with water. Heated at 672 K for 3 h, 1088 K for 6 h, T>1111 K for 53 h, and 1460 K for 30 h.		Measured in air. Data from smooth curve. T=294 K.
◁	Same as ▷ except heated for 58 additional hours at 1477 K.		
◇			Data from smooth curve. T≈294 K.

MULTILAYER INSULATIONS

Absorptance of Metallic Foils

Absorptance of Platinum.

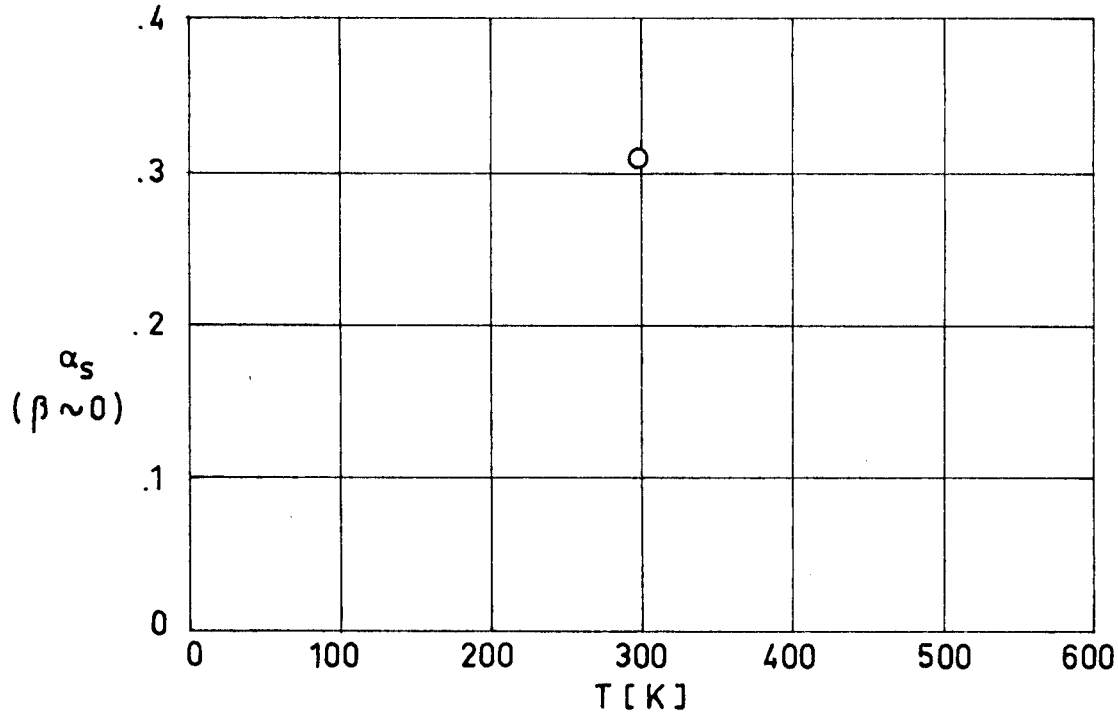

Fig 3-39. Normal solar absorptance, α_s, of Platinum as a function of temperature, T. From Touloukian & DeWitt (1970).

Explanation

Key	Description	Test Method	Comments
O	Pure metal. As received, bright.	Calculated from spectral reflectance data either for sea level or for above atmosphere conditions.	β=9°.

MULTILAYER INSULATIONS

Absorptance of Metallic Foils

Absorptance of Silver.

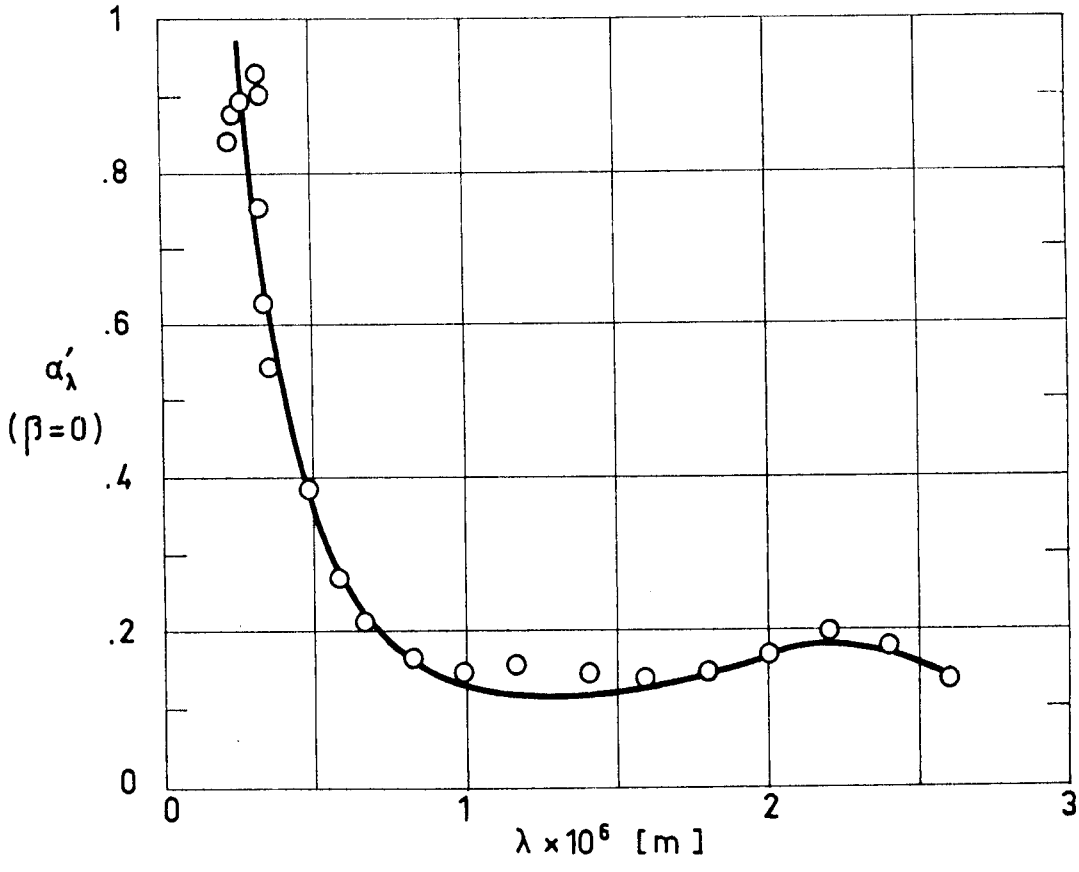

Fig 3-40. Normal spectral absorptance, α'_λ, of Silver as a function of wavelength, λ. From Touloukian & DeWitt (1970).

Explanation

Key	Description	Test Method	Comments
O	1.27×10^{-4} m thick.		Data from smooth curve. T∿298 K.

MULTILAYER INSULATIONS

Absorptance of Metallic Foils

Absorptance of Silver.

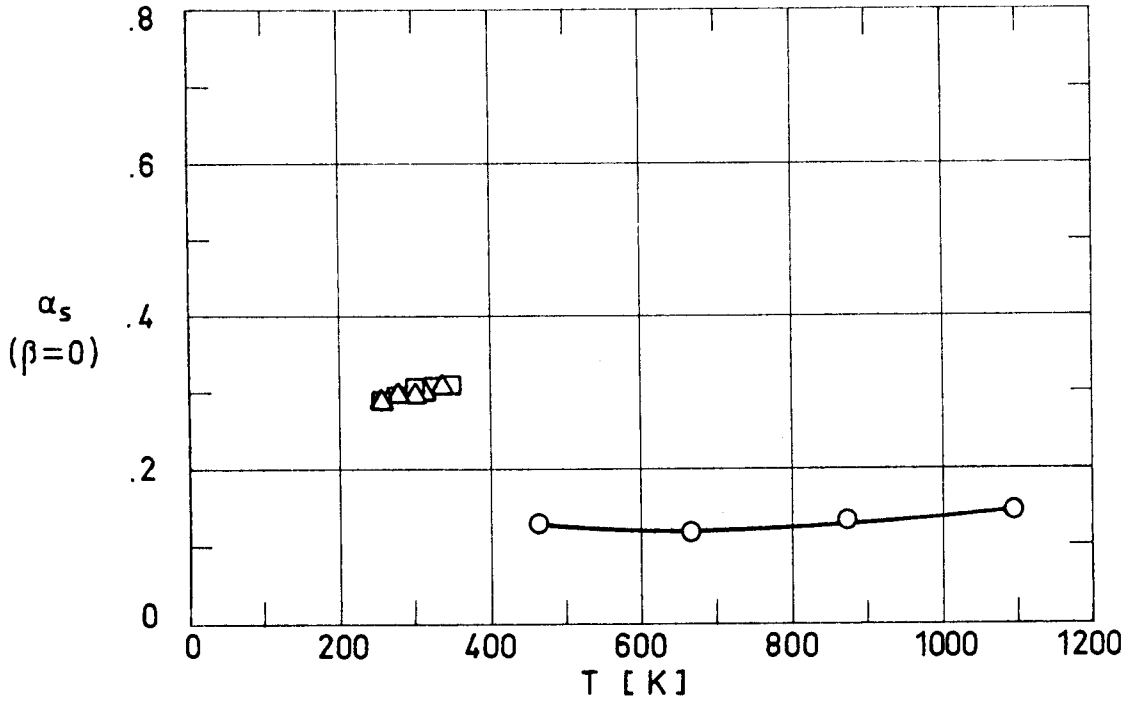

Fig 3-41. Normal solar absorptance, α_s, of Silver as a function of temperature, T. From Touloukian & DeWitt (1970).

Explanation

Key	Description	Test Method	Comments
○	Commercial rolled plate, 99.9 pure. Ground with 600 grit Carborundum, and polished on a wet cloth lap with unlevigated jewelers rouge.		Measured in vacuum. Reported error <10%.
□	Commercial sheet. Cleaned with both sodium dichromate and dilute nitric acid. Buffed on a felt buffing wheel and cleaned with carbon tetrachloride and acetone.		Measured in vacuum (1.33×10^{-4} Pa). Data from smooth curve. Reported error 5%.
△	Commercially pure. Cleaned; buffed; cleaned with carbon tetrachloride and acetone.		Measured in vacuum (1.33×10^{-4} Pa). Data from smooth curve.

MULTILAYER INSULATIONS

Radiations Shields. Miscellaneous Properties

3.6. RADIATION SHIELDS. MISCELLANEOUS PROPERTIES

Relevant properties of radiation shields are given in the next pages. The enclosed data have been arranged as follows:

Content	Table	Figure
Properties of Metallic Foils	3-1	
Properties of Polymeric Films	3-2	
Properties of Several Marketed Polycarbonate Resins	3-3	
Tensile Strength of Mylar and Kapton H for Different Values of the Temperature	3-4	
Properties of Coated Plastic Films	3-5	
Linear Thermal Expansion of Goldized Mylar as a Function of Temperature		3-42
Linear Thermal Expansion of Goldized Kapton as a Function of Temperature		3-43
Flammability of Several Radiation Shields in Oxygen and in Air	3-6	
Outgassing Characteristics of Non-Metallized and Metallized Plastic Films	3-7	
Procurement Data	3-8	

INTENTIONALLY BLANK PAGE

MULTILAYER INSULATIONS

Radiation Shields. Miscellaneous Properties

Table 3-1

Properties of Metallic Foils

Property	Aluminium	Copper	Gold	Molybdenum	Nickel	Inconel	Inconel X	Platinum	Silver
Melting Point [K]	933.2	1356	1336	2883	1726	1668-1695		2042	1233.8
Maximum Recommended Service Temperature [K]	723 [a] 772 [b]	723-1273 [a] 811 [b]	613 [c]	811 [b] 1200 [d]	811 [b] 1473 [a]	1477 [b]	1089 [b]		755 [b]
Density, $\rho \times 10^{-3}$ [$kg.m^{-3}$]	2.702	8.92	19.32	10.2	8.90	8.51	8.30 [e]	21.45	10.49
Tensile Strength $\sigma \times 10^{-7}$ [Pa]	4.7	19.3 [e] (σ_{ult})	12.4-22.1	79.3 [e]	28.3 [e] (σ_{ult})	55.2-103.4		13.8-16.6	12.6
Modulus of Elasticity, $E \times 10^{-10}$ [Pa]	6.8	12.4	7.86	29.	20.7	21.4			
Specific Heat, $c \times 10^{-2}$ [$J.kg^{-1}.K^{-1}$]	9.00 [e]	3.86	1.30	2.76	4.71	4.56	4.60 [e]	.131	2.34
Thermal Conductivity, $k \times 10^{-2}$ [$W.m^{-1}.K^{-1}$]	2.39	3.94	2.97	1.42	.92	.151	.159 [e]	.690	4.18
Linear Thermal Expansion Coefficient, $\beta \times 10^{6}$ [K^{-1}]	26.4	16.5	14.2	5.1 [e]	13.3	11.5		8.9	20.61
Minimum Thickness Available, $t \times 10^{6}$ [m]	5	6	1 [f]	5 [f]	25	25	25	1 [f]	1 [f]

All data in this table, unless otherwise stated, are from ASM (1961).

[a] From Kaganer (1969).

[b] From Rittenhouse & Singletary (1969).

[c] From Chapman & Porter (1910). Leaf becomes granular upon contraction.

[d] From Dixon & Musgrove (1973).

[e] From Smithells (1962).

[f] Foils of the quoted thicknesses have normally small surface areas. See Table 3-8 for additional details.

MULTILAYER INSULATIONS

Radiation Shields. Miscellaneous Properties

Table 3-2

Properties of Polymeric Films

PROPERTY	Mylar "A" Polyester (DuPont)	Kimfol [a] Polycarbonate (Kimberley Clark)	Lexan [a] Polycarbonate (General Electric)	Kapton "H" Polyimide (DuPont)
Maximum Recommended Service Temperature [K]	422	408	405	672
Density, $\rho \times 10^{-3}$ [$kg.m^{-3}$]	1.395	1.21	1.20	1.42
Moisture Regain [percent]	.37 at 297 K in a 50% relative humidity atmosphere	.4 after 24 h immersion	.15 at 296 K in a 50% relative humidity atmosphere	1.3 at 296 K in a 50% relative humidity atmosphere
Tensile Strength, $\sigma \times 10^{-8}$ [Pa]	1.72 [b]	2.14 .76	.55	1.72 [b]
Thermal Conductivity, k at 298 K, [$W.m^{-1}.K^{-1}$]	.152	.19	.19	.156
Flammability [e]	Slow rate of burning	Moderate. Can be made flame resistant	Slow rate of burning	Self-extinguishing
Minimum Thickness Available, $t \times 10^{6}$ [m]	3.81	2.03	12.70	6.35

From Leonhard & Hyde (1971)

[a] Comparative data concerning several commercially available polycarbonates are given in Table 3-3.

[b] For the influence of temperature see Table 3-4.

[c] Machine direction.

[d] Cross direction.

[e] Additional data on the flammability of several shields are given in Table 3-6.

MULTILAYER INSULATIONS

Radiation Shields. Miscellaneous Properties

Table 3-3

Properties of Several Marketed Polycarbonate Resins

PROPERTY	Lexan (General Electric)	Merlon (Mobay Chemical)	Makrolon (Bayer AG)
Color	Light amber	Light straw	Light yellow
Density, $\rho \times 10^{-3}$ [$kg.m^{-3}$]	1.20	1.20	1.20
Tensile yield strength, $\sigma_o \times 10^{-8}$ [Pa]	.55 - .62	.62	.61 - .66
Tensile ultimate strength, $\sigma_{ult} \times 10^{-8}$ [Pa]	.62 - .72		.78 - .88
Tensile Modulus $E \times 10^{-9}$ [Pa]	2.21	2.07	
Shear yield strength, $\tau_o \times 10^{-8}$ [Pa]	.37		
Shear ultimate strength, $\tau_{ult} \times 10^{-8}$ [Pa]	.63		
Specific heat, $c \times 10^{-3}$ [$J.kg^{-1}.K^{-1}$]		1.17	1.17
Thermal conductivity, k [$W.m^{-1}.K^{-1}$]	.19		.20
Thermal linear expansion coefficient, $\beta \times 10^{5}$ [K^{-1}]	7	7	6
Heat distortion temperature [K]	411 - 416 (1.82×10^6 Pa)	413.5 (1.82×10^6 Pa)	408 - 419
	412.5 - 418 ($.46 \times 10^6$ Pa)	416.5 ($.46 \times 10^6$ Pa)	
Brittle temperature [K]	138		133
Melting point [K]	541 Crystalline		533-538 Crystalline 495-503 Amorphous
Flammability	Self-extinguishing	Self-extinguishing	Self-extinguishing
Water absorption [percent]	.3 after 24 h immersion		.36 after 16 d

From Kazanjian (1974).

MULTILAYER INSULATIONS

Radiation Shields. Miscellaneous Properties

Table 3-4

Tensile Strength of Mylar and Kapton H for Different Values of the Temperature

T [K]	Tensile Strength, $\sigma \times 10^{-8}$, [Pa]	
	Mylar	Kapton H
77.5	2.70	1.72
298	1.60	1.47
472	.34	.83

From Rosato (1968).

Table 3-5

Properties of Coated Plastic Films

Sample Description / Useful Temperature Range [K]	Tensile Strength, $\sigma \times 10^{-8}$ [Pa]	Propagating Tear Strength, $F \times 10^{2}$ [N]	Flexure Endurance Cycles / Load, [N]	Abrasion Resistance Cycles / Load, $P \times 10^{-3}$, [Pa]	Hemispherical total emittance Before	Hemispherical total emittance After
Mylar 6.35×10^{-6} m thick with vapor deposited Aluminium on both sides / 213.5 to 422	4.1	1.3	27000 / 5	500 / 1.4	.023	destroyed
Kapton 12.7×10^{-6} m thick with vapor deposited Aluminium on both sides / 5 to 672	4.8	2.7	11000 / 15	1000 / 1.4	.025	.20
Kapton 12.7×10^{-6} m thick with vapor deposited Aluminium and Germanium on both sides / 5 to 672	4.8	2.7	26000 / 15	5000 / 1.4 to 12	.026	.028
Kapton 25.4×10^{-6} m thick with liquid bright Gold on both sides / 5 to 672	5.2	7.8	16000 / 15	5000 / 1.4 to 12	.018	.025
Kapton 25.4×10^{-6} m thick with liquid bright Gold and vapor deposited Germanium on both sides / 5 to 672	5.2	$\geq$ 7.8 (estimated)	$\geq$16000 / 15 (both estimated)	1500 / 1.4 to 12	.020	.020

From Richardson, Ruccia & French (1970).

MULTILAYER INSULATIONS

Radiation Shields. Miscellaneous Properties

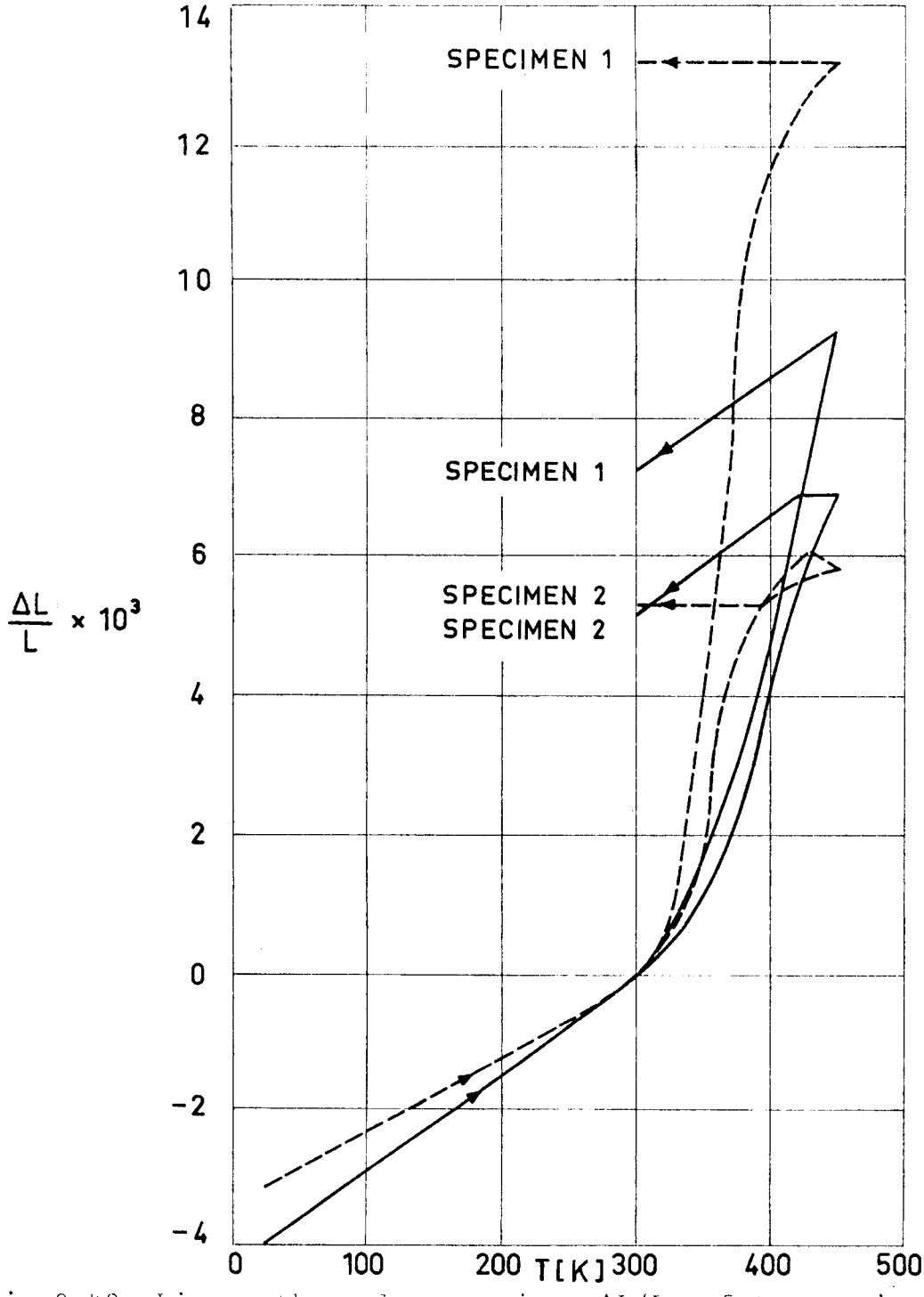

Fig 3-42. Linear thermal expansion, $\Delta L/L$, of two nominally identical specimens of 6.35×10^{-6} m thick Mylar Double-Goldized as a function of temperature, T. ——— Longitudinal direction, – – – – Transverse direction. From Leonhard & Hyde (1971).

MULTILAYER INSULATIONS

Radiation Shields. Miscellaneous Properties

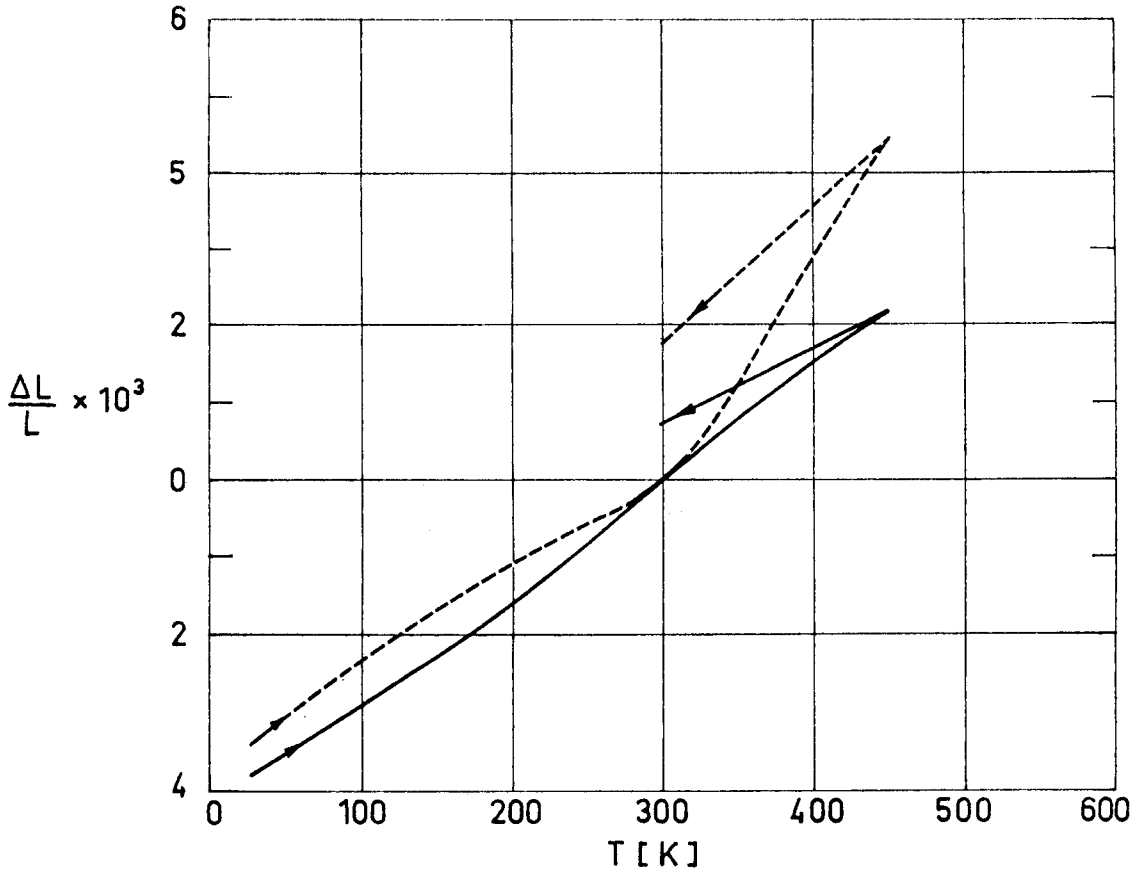

Fig 3-43. Linear thermal expansion, $\Delta L/L$, of 6.35×10^{-6} - - 7.62×10^{-6} m thick Kapton Double-Goldized, with Dacron flocking, as a function of temperature, T. ——— Longitudinal direction, ---- Transverse direction. From Leonhard & Hyde (1971).

MULTILAYER INSULATIONS

Radiation Shields. Miscellaneous Properties

Table 3-6

Flammability of Several Radiation Shields in Oxygen and in Air

Shield Description	Oxygen		Air
	1.14×10^{5} Pa	$.43\times10^{5}$ Pa	10^{5} Pa
Mylar 6.35×10^{-6} m thick with vapor deposited Aluminium on both sides	F	F	F
Kapton 12.7×10^{-6} m thick with vapor deposited Aluminium on both sides	F	F	SE
Kapton 12.7×10^{-6} m thick with vapor deposited Aluminium and vapor deposited Germanium on both sides	F	F	SE
Kapton 25.4×10^{-6} m thick with liquid bright Gold on both sides	F	F	F
Kapton 25.4×10^{-6} m thick with liquid bright Gold and vapor deposited Germanium on both sides	F	F	SE

From Richardson, Ruccia & French (1970).

F : Flammable

SE: Self-extinguishing

MULTILAYER INSULATIONS

Radiation Shields. Miscellaneous Properties

Table 3-7

Outgassing Characteristics of Non-Metallized and Metallized Plastic Films

Material (Manufacturer)	%TWL[a]	%VCM[b]	Cure Time [h]	Cure Temp [K]	Vacuum Conditions	Reference
Mylar 100S (DuPont)	.220	.120				Campbell, Marriot & Park (1973)
Mylar 100T (DuPont)	.200	.120				
Mylar 500A (DuPont)	.240	.060				
Mylar LA616-1.77×10^{-6} m thick film (DuPont)	.156	.004				
Kapton 200XH667 (DuPont)	.140	.090				
Kapton 200XHF929A Fluorocarbon Coated (DuPont)	.540	.050				
Kapton FEP film 400F022 (DuPont)	.310	.180				
Kapton FEP film 400F022 (DuPont)	.250	.010	1.5	575	Air	
Kapton H film 1.27×10^{-6} m thick film (DuPont)	.771	.027				
Teflon FEP 100A (DuPont)	.060	.060				
Teflon FEP 500A (DuPont)	.050	.050				
Teflon FEP 500C (DuPont)	.020	.010				
Hostaflon PTFE (Hoechst)	0	0			1.33×10^{-4} Pa	Zwaal, Dauphin & Alonso (1971)
Makrofol E (Bayer)	.04	.01			1.33×10^{-4} Pa	
Mylar Aluminized (Int. Research G.B.)	.16	.0			1.33×10^{-4} Pa	
Kapton Double-Aluminized (ADL)	1.1					Richardson, Ruccia & French (1970)
Kapton Double-Aluminized with Germanium Overcoating (ADL)	.9					
Kapton Double-Goldized (ADL)	.5					
Kapton Double-Goldized with Germanium Overcoating	.8					

[a] TWL: Total Weight Loss.

[b] VCM: Volatile Condensable Materials (by weight)

Outgassing rates of several shield materials are given in § 3.17.2.1. in connection with evacuation under outgas controlled conditions.

MULTILAYER INSULATIONS

Radiation Shields. Miscellaneous Properties

Table 3-8

Procurement Data

Material	Minimum Thickness, t×10^6 [m]	Width, w [m]	Length, L [m]	Purity [percent]	Approximate Cost [US $]	Suppliers	Alternative Applications
Aluminium	5 8	.5 1	roll roll	99 99	2.7 per kg 2.7 per kg	a a b, c, d, e, f	Thin film circuitry, electrical capacitors, fornitures, packing.
Copper	6	.27	roll	99.9	8.83 per kg	g c	Car radiators, electrical components, heaters.
Gold	1	.2	.45	99.9	2520 per piece	c h	Accelerator targets, alpha counter windous, electrical components, jewellery.
Molybdenum	5 15	.2 .3	.45 roll	99.9 99.93	3160 per piece 560 per kg	c i h, j, k	Accelerator targets, furnaces.
Nickel	25 80	.1 .2	roll roll	99.5 99.5	7.95 per kg 7.95 per kg	l, m l, m c, h	Electronic equipment transducers.
Inconel	25 80	.1 .2	roll roll		10.3 per kg 10.3 per kg	l, m l, m	Afterburner components, jet insulation blankets, combustion cans.
Inconel X	25 80	.1 .2	roll roll		8.23 per kg 8.23 per kg	l, m l, m	Thrust chamber walls, turbine housings, engine seals, support bands.
Platinum	1	.2	.45	99.9	4220 per piece	c h	Heat flux sensors, electrical components, jewellery.
Silver	1	.2	.45	99.99	4500 per piece	c h	Electrical components, jewellery.
Polyester	6 9 12 12	 1.2	 roll	Single or Double-Aluminized Single or Double-Aluminized Single-Aluminized	.25 to .61 per m^2 .41 to .82 per m^2 .15 per m^2	n o p q	Electrical capacitors, furnitures.
Polyimide	25	.4	roll			r	

Key to Suppliers:

a Empresa Nacional del Aluminio, S.A., General Sanjurjo, 4, Madrid-3, Spain.
b Alcan Wire Ltd., Windsor Ave., Merton Abbey, London SW 19, England.
c Goodfellow Metals Ltd., Ruxley Towers, Claygate-Esher, Surrey KT 10 OTS, England.
d Pechiney, 23 Rue Balzac, 65360 Paris, France.
e Star Aluminium Co., Ltd., 97 Penn Road, Wolverhampton, Staffs WV 3 ODM, England.
f Vereingte Aluminium-Werke Aktiengesellschaft, 5300 Bonn, Germany.
g Gränges Metallverken, S-721 88 Västerås, Sweden.
h Reactor Experiments, Inc., 963 Terminal Way, San Carlos, California 94070, USA.
i Metallwerk Plansee AG & Co. KG., A-6600 Reutte, Tirol, Austria.
j Climax Molybdenum Company (American Metal Climax), 1 Greenwich Plaza, Greenwich, Connecticut 06830, USA.
k Metals Research Ltd., Melbourn Royston, Hestfordshire, England.
l Henry Wiggin & Company Ltd., Holmer Road, Hereford-HR4 9SL, England.
m Huntington Alloy Products Division, The Internacional Nickel Company, Inc., Huntington, West Virginia 25720, USA.
n Verolme Vacuumtechnik AG, 6228 Eltville, Sudetenstr. 3, Germany.
o Imperial Chemical Industries Ltd., Millbank, London SWIP 3JF, England.
p Westfälische Metallindustrie KG, Hueck & Co., 4780 Lippstadt, Germany.
q Sarrió, Compañía Papelera de Leiza, S.A., Leiza, Navarra, Spain.
r Carl Huth & Söhne, 712 Bietigheim, Postfach 114, Germany.

INTENTIONALLY BLANK PAGE

3.7. RADIATION SHIELDS. MEASUREMENT OF THE COATING THICKNESS

The thermal performance of an evacuated multilayer insulation system depends upon the emittance of its radiation shields. When shields are formed by metal coating on substrate films, the coating thickness affects the emittance and controls the portion of incident radiation which is transmitted through the shield material.

Among the different existing methods to measure the coating thickness, the Resistance Method is the most widely used by commercial metal depositors. According to Ohm's law, the electrical resistance, R, between the ends of a right prism of length, L, and cross-sectional area, wt_c, is given by

$$R = \rho \frac{L}{w t_c} \quad ,$$

ρ being the electrical resistivity of the metal. When L=w, the resistance (measured in ohms per square) is proportional to $1/t_c$.

In the practical application of the above idea two different types of electrodes may be used: the parallel bar and the two-point electrode. The reader is referred to ADL (1966) for details concerning the operating methods.

When the coating thickness is comparable to the mean free path of the electrons through the metal lattice, which loosely speaking is of the order of 2×10^{-8} m, Ohm's law must be modified as we shall see below.

Fig 3-44 compares the coating thickness, t_c, measured by

MULTILAYER INSULATIONS

Radiation Shields. Measurement of the Coating Thickness

several methods with that measured by use of the Resistance Method, $t_{c\Omega}$. It may be seen that the last one gives reasonably accurate values of the coating thickness for the copper, gold, and silver coatings examined. For several of the aluminium coatings, large discrepancies arise between the resistance and the other methods.

The values of t_c which are plotted in Fig 3-44 have been measured by means of some of the following methods.

C. Vibrating Crystal Method. The coating is being deposited on a vibrating crystal. The shift of the natural frequency of the crystal relates to the coating thickness.

L. Light Transmission. When the sample is transparent the characteristics of the light transmitted through it, which can be analyzed with a spectrophotometer, are related to the coating thickness.

M. Melt Method. The coating is produced as in the bell-jar vacuum deposition method, from weighted amounts of metal.

O. Optical Method. Optical flats are placed adjacent to the film during the deposition process. The film coating thickness on the flats is determined by interferometry.

W. Weight-by-Difference Method. A coated film is weighted before and after removal of the coating thickness. It is important to realize that the removing solvent does not change the substrate.

To deduce the coating thickness from the electrical resistance, the following expression can be used (Maissel (1970)).

MULTILAYER INSULATIONS

Radiation Shields. Measurement of the Coating Thickness

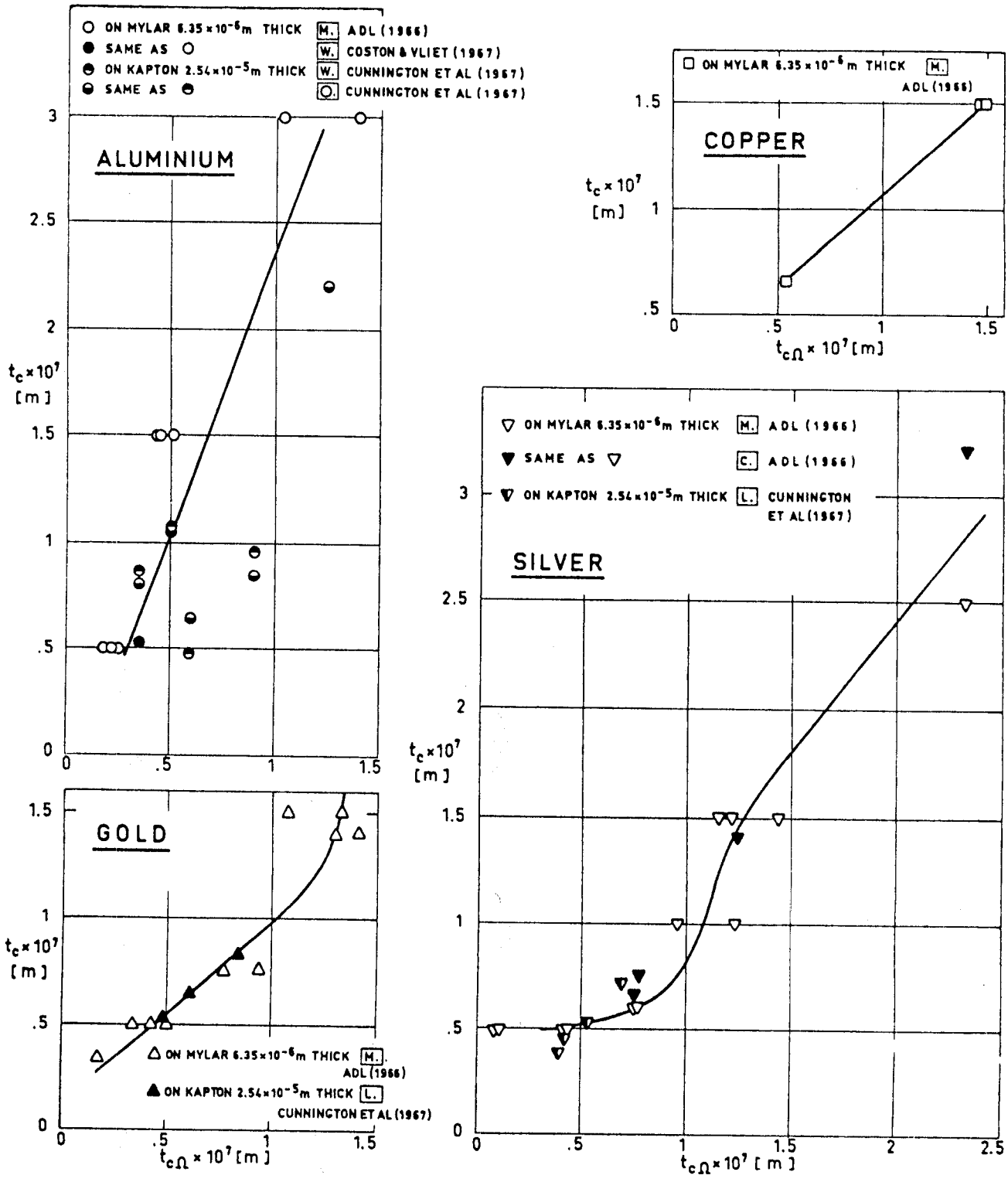

Fig 3-44. Coating thickness, t_c, given by several methods, compared with that given by the electrical resistance method, $t_{c\Omega}$. All coatings are vacuum deposited. Capital letters refer to the measuring method according to the following key: C, Crystal; L, Light transmission; M, Melt; O, Optical; W, Weight difference.

MULTILAYER INSULATIONS

Radiation Shields. Measurement of the Coating Thickness

$$R = \frac{\rho}{t_{c\Omega}} + \frac{3}{8}\,\frac{\lambda(1-p)}{t_{c\Omega}^{2}}\,\rho \quad ,$$

where:

R, Resistance. [Ω per square].

p, Fraction of the electrons suffering specular reflection at the surfaces of the metallic film. In the following it is assumed that p=0, although such an assumption may not be appropriate for Gold.

$t_{c\Omega}$, Coating Thickness. [m].

λ, Mean Free Path of the electrons in the metal lattice. [m].

ρ, Bulk Resistivity of the metal. [Ω.m].

Table 3-9 gives ρ and 3λρ/8 for the four metals considered.

Table 3-9

ρ and 3λρ/8 for Aluminium, Copper, Gold and Silver

Metal	$\rho\times10^{8}$ [Ω.m]	$\frac{3}{8}\lambda\rho\times10^{16}$ [Ω.m²]
Aluminium	2.65[a]	3.14[a]
Copper	1.55[b]	2.44[c]
Gold	2.35[b]	3.61[d]
Silver	1.59[a]	3.38[a]

[a] From Cunnington et al. (1967).

[b] From Bardeen (1958).

[c] Calculated by the compiler ($\lambda=4.2\times10^{-8}$ m at T=273 K. From Kittel (1966)).

[d] Calculated by the compiler ($\lambda=4.1\times10^{-8}$ m at T=273 K. From Kittel (1966)). The value quoted by Cunnington et al. (1967) seems to be a misprint.

The variation of R with $t_{c\Omega}$ is shown in Fig 3-45.

MULTILAYER INSULATIONS

Radiation Shields. Measurement of the Coating Thickness

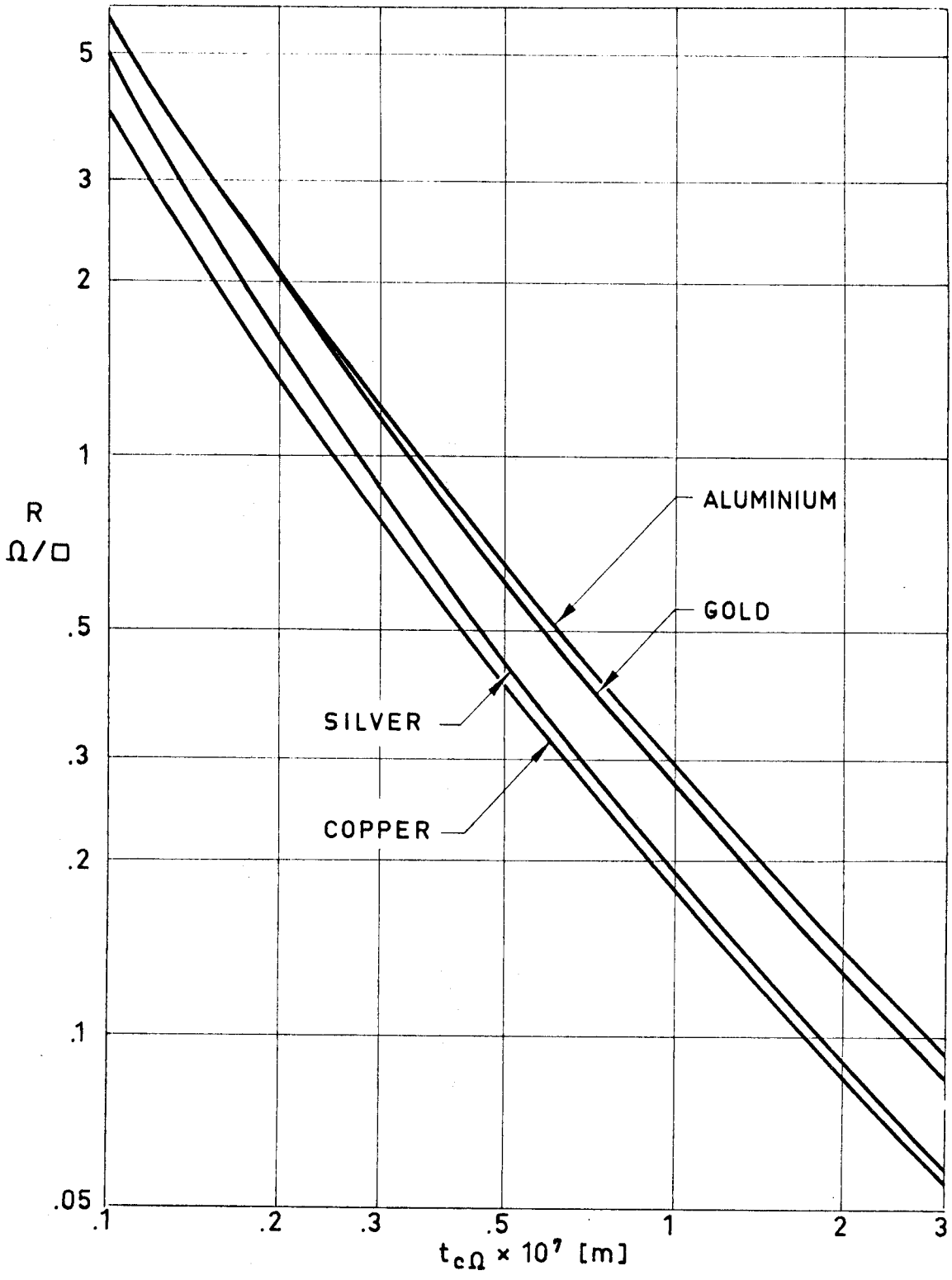

Fig 3-45. Thickness, $t_{c\Omega}$, of metallic coatings as a function of film electrical resistance, R. Calculated by the compiler.

INTENTIONALLY BLANK PAGE

3.8. SPACERS

Spacers are low thermal conductivity materials whose aim is to decrease the solid conductivity between parallel neighboring radiation shields. Spacers can be classified in four groups (Glaser et al. (1967)): multiple resistance, point contact, single component, and composite. "Superfloc"(*) has several characteristics in common with the first two groups and will be classified separately.

3.8.1. MULTIPLE-RESISTANCE SPACERS

Contacting particles exchange heat through their points of contact. Therefore, a mat of fibers arranged in a parallel array, in which the heat must pass from each fiber to another nearly-parallel fiber to reach the next radiation shield, can be used as an effective spacer.

The contact thermal conductance grows with the force pressing the particles against each other, so that solid heat conduction through fibrous systems depends not only on the temperature gradient, fiber thermal conductivity, volume fraction of fibers, and packing geometry, but also depends upon the contacting load and mechanical properties of the fibers. For a given bulk material, the finer the fibers, the greater the resistance per unit thickness the mat presents to the heat flow.

(*) "Superfloc" is a trade name of Convair Division of General Dynamics.

MULTILAYER INSULATIONS

Spacers

The prediction of the thermal conductivity of a fibrous system is fairly complicated because of the random orientation of the fibers, and local variations in loading and thermal resistance at each contact area. Semiempirical correlations have been often attempted in terms of the solid fraction, thermal conductivity of the bulk material, and fiber diameter. The reader is referred to the monography by Kaganer (1969) for further details concerning theoretical models of heat transfer through fibrous materials.

Glass fibers, quartz fibers, and plastic fibers are used as spacers in MLI systems. Fibrous mats are produced in thicknesses ranging from 7.5×10^{-5} to 7.5×10^{-4} m. Fiber diameters as small as 5×10^{-7} m are commercially available.

Problems in connection with the use of these spacers arise from their very poor dimensional stability. Bonding together the fibers could be detrimental to the performance of the MLI because of the heat flow across the bonded contact areas. In addition, bonding materials contribute to the outgassing of the spacer.

Stitching is often used to increase the stability of the MLI system without greatly decreasing its thermal performance.

3.8.2. POINT-CONTACT SPACERS

The dimensional stability of the MLI system can be improved by using silk, nylon or fiber-glass screens, whose knots, which can be assimilated to isolated spheres, do space neighboring radiation shields.

MULTILAYER INSULATIONS

Spacers

The mesh size of the screen, or distance between spheres, should be as large as possible, but an upper limit exists determined by the requirements that direct contact between radiation shields, produced by their sagging, must be avoided.

The thickness of the screens used as spacers in MLI systems ranges from 7.5×10^{-5} to 6×10^{-4} m; the mesh size ranging from 1.53×10^{-3} to 6.35×10^{-3} m.

In addition to their dimensional stability, screen spacers allow an easy evacuation of the gas contained in the MLI.

3.8.3. SUPERFLOC

Superfloc spacer consists of small tufts of a synthetic fiber bonded with a suitable adhesive to one side of each radiation shield.

The current configuration consists of tufts, made of 10^{-3} m long Dacron needles, arranged in a triangular pattern of approximately 10^{-2} m side, and bonded to one face of the shield with Crest 7343 polyurethane adhesive.

The method of manufacturing Superfloc, described by Leonhard & Hyde (1971), is as follows:

1) A silk screen printing device is placed on the radiation shield material to which dots of adhesive are transferred by using a squilgee.

2) The shield is vibrated by being pulled across hexagonal bars that are rotating at 150 rpm.

MULTILAYER INSULATIONS

Spacers

3) The fiber tufts, arranged in the triangular pattern, "stand" about 10^{-2} m above the radiation shield base.

4) The vibration forces the needles into the adhesive while being held in an orderly vertical position.

5) Curing, whose peculiarities depend on the adhesive used, is performed.

The thickness of a typical Mylar-Superfloc MLI system having 22 shielding layers is of the order of 2.5×10^{-2} m (Scollon & Carpitella (1970)).

The main advantages of this system are that it provides low thermal conduction paths between shields; reasonable structural strength; ease purging, venting, and repressurization; density control, and simple insulation application.

3.8.4. SINGLE-COMPONENT MLI

Embossed or crinkled neighboring shields exhibit randomly distributed small contact areas having heat transfer rates which are of the same order of magnitude as those corresponding to radiative transfer.

This system can only be used with single-metallized plastic films of low thermal conductivity, such as Mylar.

Embossment pattern should be deep enough to allow for material memory, otherwise its geometrical characteristics would change with time. The problem is particularly acute when Kapton films are used.

MULTILAYER INSULATIONS

Spacers

A typical geometric component of the embossment pattern is approximately 1.5×10^{-3} m deep, 3×10^{-3} m long and 1.5×10^{-3} m wide, and is located on 10^{-2} m centers (Cunnington et al. (1967)).

Surface emittance increases because embossment. The available information on this point is not precise enough and sometimes both the effect of embossment and of perforations are reported together. For simple geometric patterns the effect of embossment on emittance could be estimated by using the information concerning groove cavities. Unfortunately, since the aim of such cavities is to increase further the absorptance of absorptive surfaces, most of the available data concern medium and high values of the surface absorptance. Fig 3-46 gives the apparent emittance of a V-groove cavity for a range of surface absorptances which is well below that taken to calculate the data shown in D.

3.8.5. COMPOSITE SPACERS

As mentioned above in connection with bonded against non-bonded fibrous mat spacers, several materials which are very attractive from the insulating point of view show very poor dimensional stability. The consideration of this and similar situations leads to the concept of a spacer consisting of two or more materials: a very light, dimensionally stable one whose thermal properties are of no concern, plus a second material whose selection is guided exclusively by its thermal properties.

This concept permits a designer to select the materials

MULTILAYER INSULATIONS

Spacers

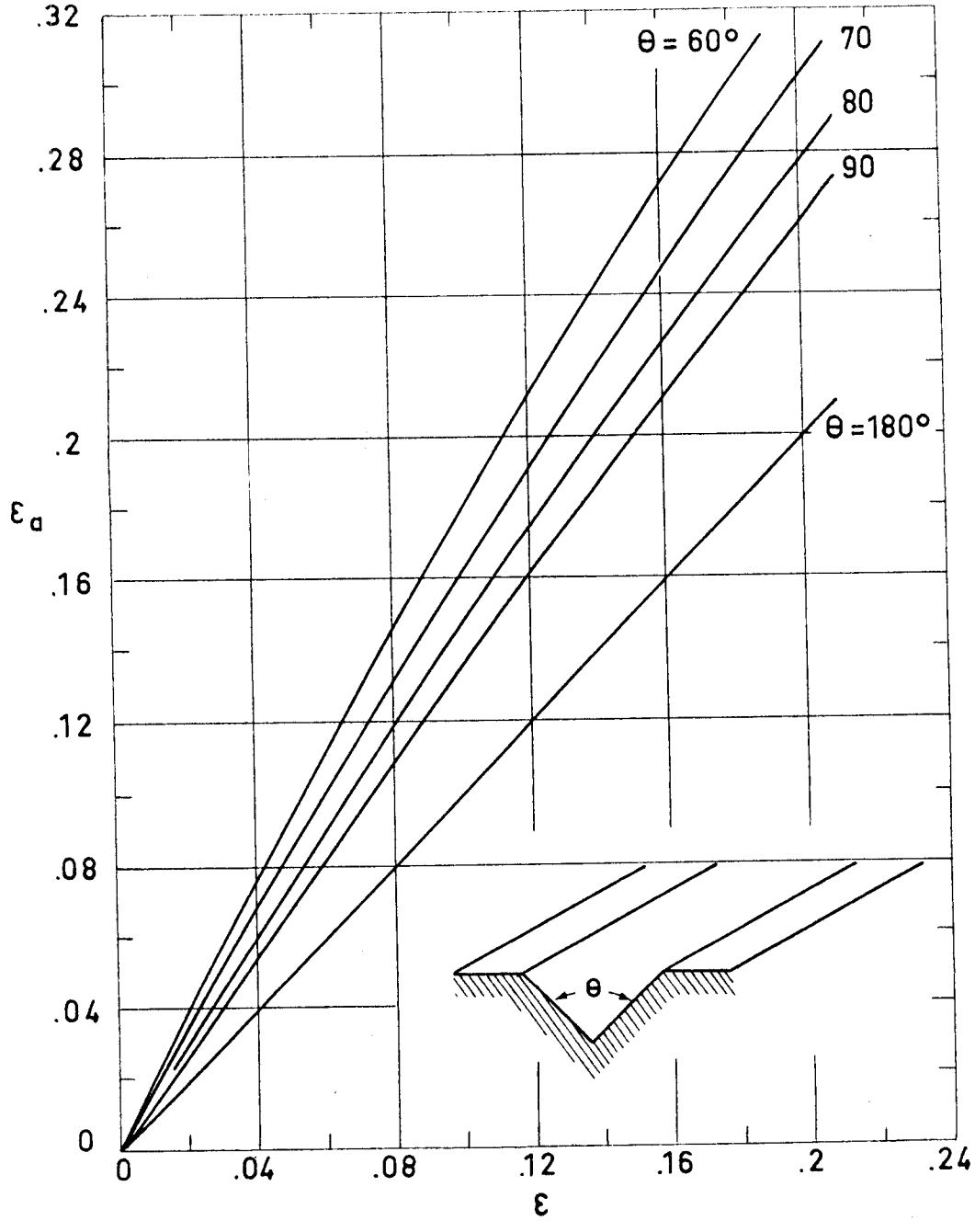

Fig 3-46. Apparent emittance, ε_a, of a gray V-Groove as a function of surface emittance, ε, illustrating the effect of embossing or crinkling on the optical properties of the shield. Calculated by the compiler.

best suited to the specific function and the desired performance of the complete assembly.

3.8.6. ONE-DIMENSIONAL HEAT FLOW THROUGH AN MLI WITH ABSORBING AND SCATTERING SPACERS

The heat transfer rate through an MLI formed by N shields, having the same emittance on both faces, and by N-1 thin spacers, is given, according to Cunnington et al. (1969) by the following expression:

$$Q = \frac{n^2 \sigma A (T_N^4 - T_1^4)}{(N-1)\left(\frac{2}{\varepsilon} - 1\right) + (a+2s)\frac{t'}{2}} \quad ,$$

where:

A, area normal to the temperature gradient. $[m^2]$.

N, number of radiation shields.

Q, heat flow through the insulation. $[W]$.

T_i, temperature of shield i. $[K]$. $i=1,N$

a, absorption coefficient of the spacer. $[m^{-1}]$.

s, scattering coefficient of the spacer. $[m^{-1}]$.

t', total spacer thickness. $[m]$.

n, index of refraction of the spacer.

ε, emittance of shields, assumed to be the same for all of them.

σ, Stefan-Boltzmann Constant. $[W.m^{-2}.K^{-4}]$.

It should be mentioned that a, n, and s depend on the

MULTILAYER INSULATIONS

Spacers

spacer material, volume fraction of spacer, packing geometry and optical characteristics of the gas filling the space between shields, if any. Normally n can be assumed to be equal to unity. A limited amount of data concerning absorption and scattering coefficients is given in Table 3-10. The values presented in that table were deduced from total transmission data. The measurements were performed with the specimens at room temperature. Uncertainties of thicknees measurement and spatial distribution of transmitted energy, and the errors associated with measurement of very low values of transmission, result in an estimated maximum uncertainty of 50% for the reported coefficients.

The effect of absorption and scattering by the spacers can be neglected in most cases, especially when the emittance of the shields is small.

MULTILAYER INSULATIONS

Spacers

Table 3-10

Absorption and Scattering Coefficients for Spacer Materials

Material	Nominal Density, ρ [$kg.m^{-3}$]	Thickness, $t \times 10^5$ [m]	Fiber Diameter, $d \times 10^6$ [m]	Source Temp., [K]	Absorption Coefficient, $a \times 10^{-4}$ [m^{-1}]	Scattering Coefficient, $s \times 10^{-4}$ [m^{-1}]
Dexiglas	200	7.62	< 1	500	.13	2.6
				650	.11	2.7
				800	.11	2.8
				1000	.07	3.1
				1700	.06	2.5
Tissuglas	220	1.52	< 1	500	.03	2.65
				650	.11	2.8
				800	.11	3.0
Refrasil A-100	50	4.83	1.3	500	<.02	.38
				650		.57
				800		.73
				1000		.76
Refrasil B-100	50	4.83	10	500	<.02	.33
				650		.50
				800		.71
				1000		.74
Carbon Fiber Paper			10	775	.04	3.85
				923	.02	2.60
				1123	.02	1.85
				1273	.04	2.00

From Cunnington, Zierman, Funai & Lindahn (1967).

INTENTIONALLY BLANK PAGE

MULTILAYER INSULATIONS

Spacers. Miscellaneous Properties

3.9. SPACERS. MISCELLANEOUS PROPERTIES

Relevant properties of spacer materials are given in the following pages. Because of the countless variety of both candidate materials and testing procedures it seems to be advisable to present the data using the same layout as in the different sources, without trying to unify them.

The table below guides in the search for these data.

Property	Table	Figure
Effect of Heat	3-11, 3-12	
Moisture Regain	3-11, 3-13	
Density	3-11, 3-17	
Breaking Strength	3-11	
Effect of Temperature on Breaking Strength	3-14, 3-15, 3-16	
Elastic Recovery	3-11	
Average Stiffness	3-11	
Thermal Conductivity	3-11, 3-17	3-47 to 3-52
Specific Heat	3-11, 3-17	3-53
Thermal Diffusivity	3-17	
Flammability	3-11, 3-18, 3-19	
Outgassing	3-20	

INTENTIONALLY BLANK PAGE

MULTILAYER INSULATIONS

Spacers. Miscellaneous Properties

Table 3-11

Properties of Staple Fibers

Property	Dacron Polyester (DuPont)	Kodel Polyester (Eastman)	Nomex Polyamide (DuPont)	Nylon 6 Polyamide (DuPont)	PBI [a] (Celanese)	Silk	Teflon Fluorocarbon (DuPont)	"E" Glass
Effect of Heat [b]	Melts at 522 K	Melts at 561 K	Does not melt. Degrades above 640 K. At 520 K has 60% of at room temperature strength.	Melts at 488.5 K. Yellows after 5 h at 422 K.	Shrinks at 1088 K.	Desintegrates at 444 K.	Melts at 600 K. Non-degraded at 477.5 K. Sublimes .0002% per h at 560 K.	Softens at 1110 K. At 640 K has 50% of at room temperature strength.
Moisture Regain [Percent] [c]	.4	.4	5	4	13	11	0	0
Density, $\rho \times 10^{-3}$ [$kg.m^{-3}$]	1.38	1.22	1.38	1.14	-	1.25-1.35	2.3	2.54
Breaking Strength [gpd] [d]	3.8-4.3	2.5-3	5.3	3.8-5.5.	4.9	2.8-5.2	1.6	6.0-7.3
Elastic Recovery [percent]	80 at 8%	90-97 at 2%	100 at 4%	100 at 2%	-	-	-	100 at 2%
Average Stiffness [gpd] [d]	12	11	24 (Calculated)	17 - 20	105	18	12	322
Thermal Conductivity, k [$W.m^{-1}.K^{-1}$] [e]	.171	.17	.13	.247	-	-	.24	1
Specific Heat, $c \times 10^{-3}$ [$J.kg^{-1}.K^{-1}$] [f]	2.1-2.5	2.1-2.5	1.21	2.5	-	-	1.05	.80
Flammability [g]	Slow burning rate	Slow burning rate	Self-extinguishing	Self-extinguishing	Non-flammable	Moderate burning rate	Non-flammable	Non-flammable

From Leonhard & Hyde (1971).

[a] PBI: polybenzimidazole (Polyimide).

[b] Additional data are given in Table 3-12.

[c] Additional data are given in Table 3-13.

[d] gpd: grams per denier. The fineness of a fiber is expressed in units of denier, which is the weight in grams of a 9000 m length. Physically the tenacity is that length of fiber or yarn which will just cause rupture due to its own weight.

Additional data concerning the influence of thermal exposure on tenacity are given in Tables 3-14, 3-15 and 3-16.

[e] Thermal properties of fabrics woven of several fibers are given in Table 3-17. Effective thermal conductivities of fibrous spacers are given in Figs 3-47 to 3-52.

[f] Additional data are given in Fig 3-53.

[g] Additional data are given in Tables 3-18 and 3-19.

MULTILAYER INSULATIONS

Spacers. Miscellaneous Properties

Table 3-12

Effect of Heat on Several Fibers

Fiber	Sticks or softens T [K]	Melts T [K]	Decomposes T [K]	Chars T [K]
Acrilan	508			
Nomex				722
Orlon	508			
PBI				811
Rayon			450 - 477	
Teflon		600 (Gel temp.)		

From Ross (1968).

Table 3-13

Moisture Regain of Several Fibers

Fiber	Moisture Regain [percent]
Nomex	7
Nylon 6	4
Nylon 6 - 6	4
PBI	13
Polyester	>1
Rayon	13
Silk	11

From Ross (1968).

Table 3-14

Effect of Exposure Temperature, Pressure and Time on the Strength of Fabrics

T = 450 K

Material	Breaking Strength, $F \times 10^{-5}$ [$N.m^{-1}$]					
	0 h	2 h		6 h		24 h
		1.7×10^6 Pa	0 Pa	$.34 \times 10^6$ Pa	1.7×10^6 Pa	1.7×10^6 Pa
Nylon 6 - 6 .12 $kg.m^{-2}$	.277	.247	.156	.140	.152	-
Nylon 6 - 6 .24 $kg.m^{-2}$	.587	.515	.177	.229	.240	-
Nylon 6 - 6 .48 $kg.m^{-2}$	1.26	.963	.672	.692	.660	-
Dacron .12 $kg.m^{-2}$	.256	-	.250	.247	.247	-
Nomex .13 $kg.m^{-2}$	.242	.236	.236	.235	.233	.243
Glass .31 $kg.m^{-2}$	.678	-	.753	.683	.753	-
Glass .64 $kg.m^{-2}$	1.16	-	1.10	1.19	1.11	-

From Ross (1968).

MULTILAYER INSULATIONS

Spacers. Miscellaneous Properties

Table 3-15

Fiber Strength after 10 min Exposure to Temperature

T [K]	Breaking Strength [gpd]				
	Nomex	Nylon 6-6	PBI	"E" Glass	Fusel Silica
Room	6.6	6.5	4	13.8	15
399.5	6.5	4.6	-	-	15.6
422	-	-	4.4	-	-
455	4.8	3.8	-	-	-
505	-	No strength	3.2	-	-
511	3.8	-	-	13.7	16.3
566.5	2.8	-	-	-	-
588.5	-	-	2.6	-	-
622	1.1	-	-	9.9	9.3
672	-	-	1	-	-
677.5	-	No strength	-	-	-
699.5	-	-	.4	-	-
733	-	-	-	8.6	8.9
811	-	-	-	7.6	8.8
866.5	-	-	-	6.5	8.2
922	-	-	-	4.2	6.3
1033	-	-	-	No strength	5.2

From Ross (1968).

Table 3-16

Effect of Cycling vs. Continuous Exposure to Temperature of Two Fibers in Woven Forms

Material	Strength Change [percent]			
	394 K		422 K	
	Cycling, 2 h soaks, 3 soaks	Continuous 6h	Cycling, 2 h soaks, 3 soaks	Continuous 6h
Dacron Sewing thread size E, natural	.3	0	- 1.3	- .9
Sewing thread size E, sage green	1.3	1.	3.5	-2.1
Nylon 6-6 Fabric 5.42×10^{-2} kg.m^{-2} 3/1 twill, warp	- 6.7	1.4	-21	-20.7
Fabric 7.63×10^{-2} kg.m^{-2} dobby weave, warp	- .5	.6	-21.9	-14.7
Fabric 16.1×10^{-2} kg.m^{-2} 2/2 twill, warp	5.6	4.4	-24.3	-14.5
Webbing, untreated 38700 N min. strength	- 1.5	- 2.7	-33.4	-36.8
Webbing, treated 38700 N min. strength	-23.5	- 2.5	-52.2	-52.4

From Ross (1968).

MULTILAYER INSULATIONS

Spacers. Miscellaneous Properties

Table 3-17

Thermal Properties of Fabrics Woven of Several Fibers

Fiber and Fabric	Pressure $p \times 10^{-4}$ [Pa]	Temperature T [K]	Density $\rho \times 10^{-2}$ [kg.m^{-3}]	Thickness under load $t \times 10^{4}$ [m]	Mass/Area $\rho t \times 10^{2}$ [kg.m^{-2}]	Avg. Thermal Conductivity $k \times 10^{2}$ [W.m^{-1}.K^{-1}]	Specific Heat $c \times 10^{-3}$ [J.kg^{-1}.K^{-1}]	Thermal Diffusivity $\alpha \times 10^{7}$ [m^{2}.s^{-1}]
Nomex 6.61×10^{-2} kg.m^{-2} Dobby Weave	11.7	477.5	4.53	1.45	6.59	3.63	1.47	.981
	.204	477.5	4.53	1.45	6.59	1.38	1.47	.361
	11.7	588.5	4.53	1.45	6.59	4.33	1.47	1.16
	.204	588.5	4.53	1.45	6.59	1.73	1.47	.465
Nylon 7.63×10^{2} kg.m^{-2} 2/1 Twill	11.7	477.5	6.12	1.17	7.13	3.81	2.39	.310
	.204	477.5	6.12	1.17	7.13	2.60	2.39	.178
Glass fiber 30.2×10^{-2} kg.m^{-2} Satin weave	11.7	588.5	9.02	3.34	30.17	6.58	1.09	.671
	.204	588.5	9.27	3.34	30.17	3.81	1.09	.387
Fused Silica 30.2×10^{-2} kg.m^{-2} Satin weave	11.7	588.5	8.25	3.93	32.42	7.27	1.05	.852
	.056	588.5	8.25	3.93	32.42	4.33	1.05	.516
	12.1	922	8.25	3.93	32.42	10.38	1.09	1.16
	.056	922	8.25	3.93	32.42	5.71	1.09	.645
Graphite	12	922	4.95	5.23	25.88	28.73	1.67	.877
	.216	922	5.06	5.11	25.88	20.77	1.67	2.45

From Ross (1968).

MULTILAYER INSULATIONS

Spacers. Miscellaneous Properties

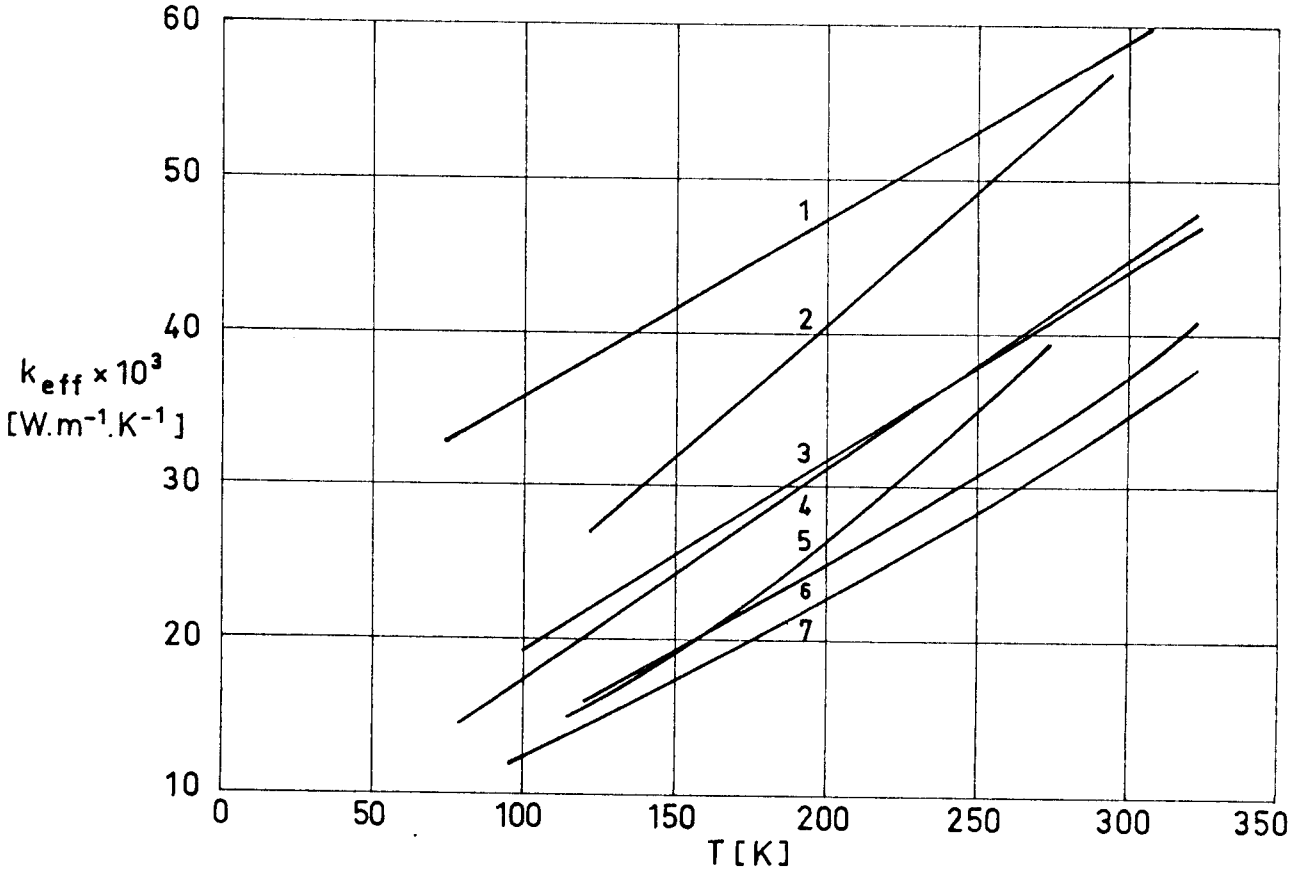

Fig 3-47. Effective thermal conductivity, k_{eff}, of several fibrous spacers as a function of mean temperature, T. From Kaganer (1969).

Explanation

Key	Description	Test Method	Comments
1	Cotton wool ρ = 81 kg.m^{-3}		Measured in air at normal pressure.
2	Rock wool 400		
3	Rock wool 260		
4	Glass wool 50		
5	Cotton wool 42		
6	Floss silk 58		
7	Rock wool 95		

MULTILAYER INSULATIONS

Spacers. Miscellaneous Properties

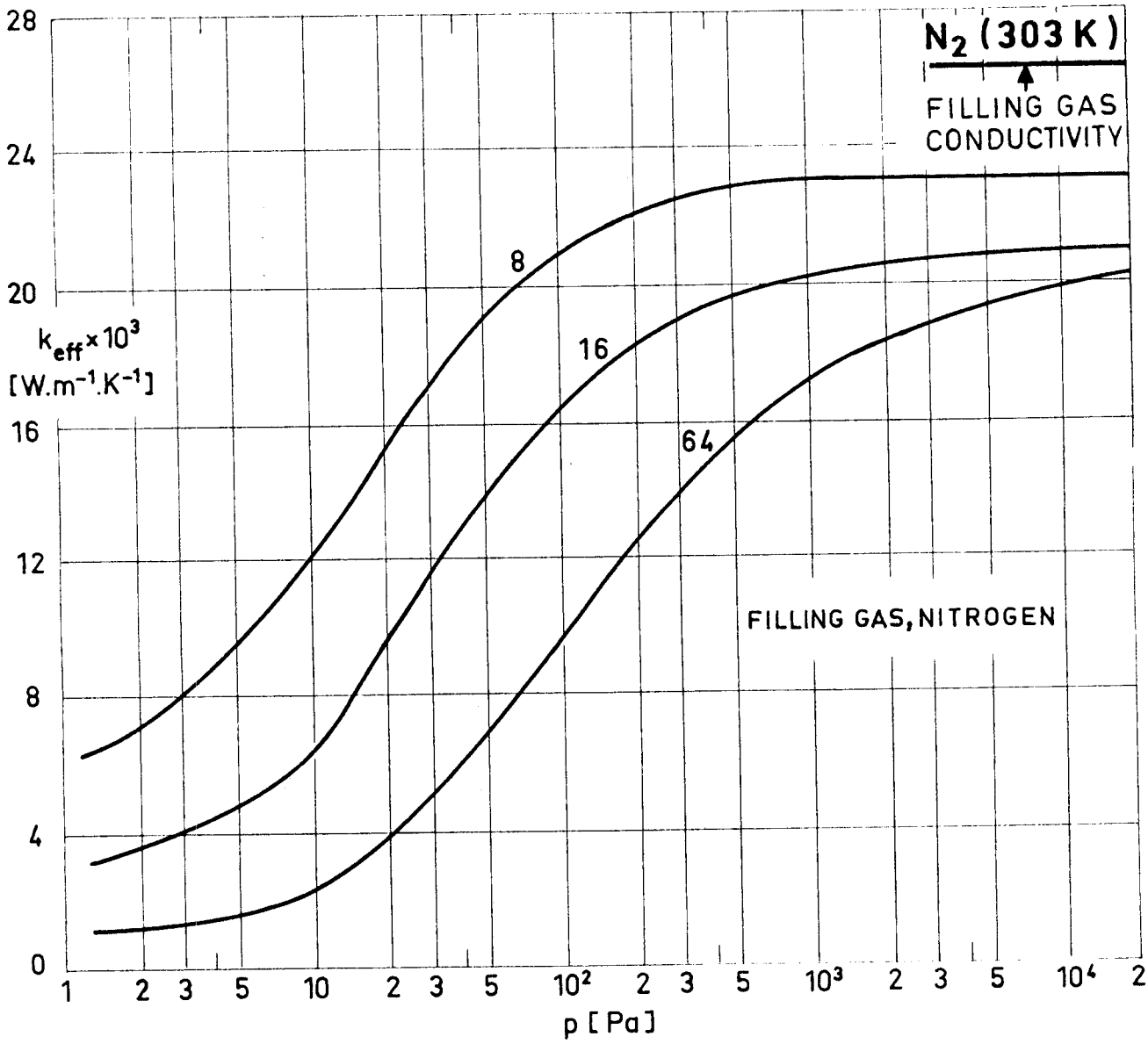

Fig 3-48. Effective thermal conductivity, k_{eff}, of Fiber-glass batting as a function of Nitrogen gas pressure, p. Numbers on curves indicate batting densities in kg.m^{-3}. T_H=303 K, T_C=80.5 K. Thermal conductivity of Nitrogen at 303 K is indicated for comparison. From Coston (1967).

MULTILAYER INSULATIONS

Spacers. Miscellaneous Properties

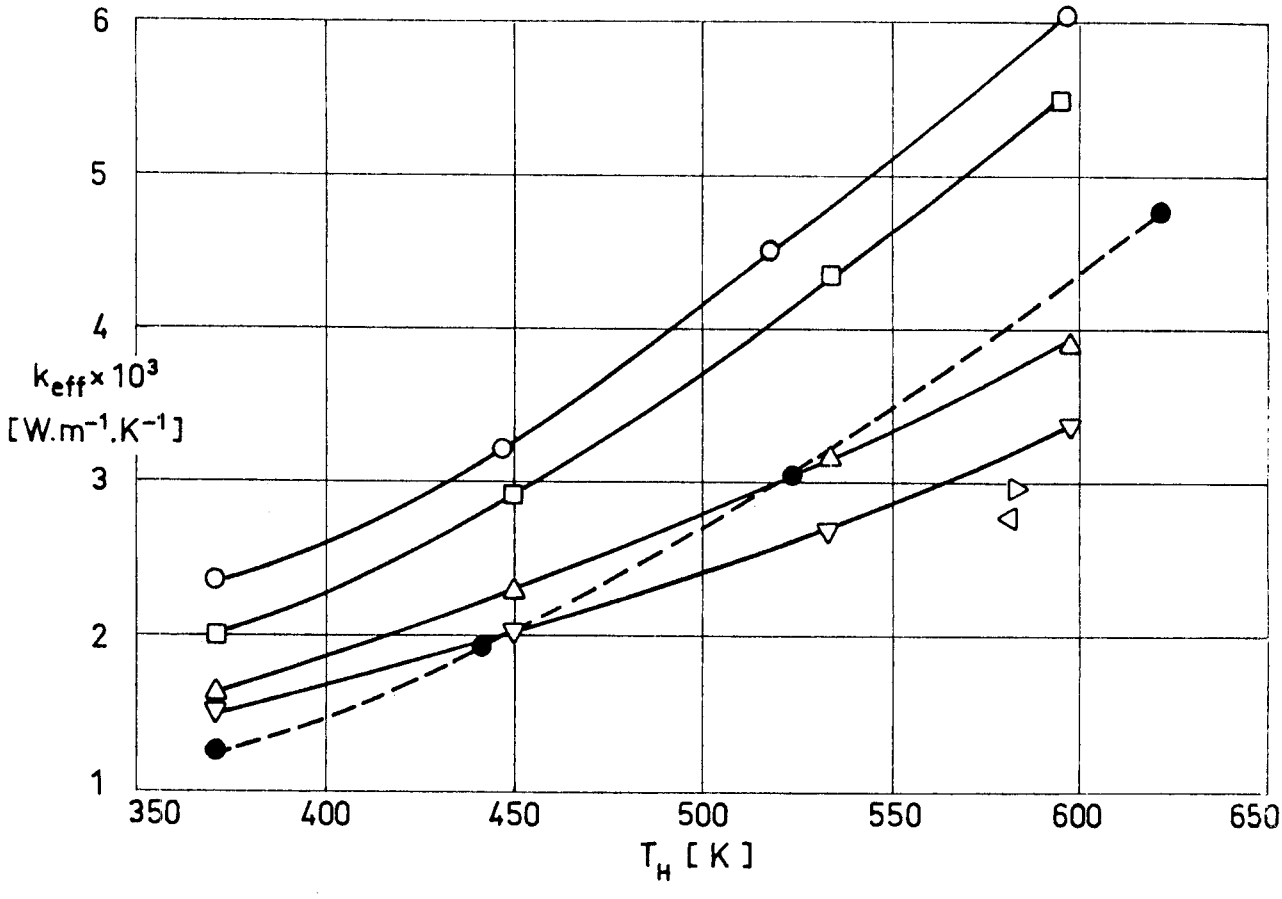

Fig 3-49. Effective thermal conductivity, k_{eff}, of Dexiglas as a function of warm-boundary temperature, T_H. From Cunnington, Zierman, Funai & Lindahn (1967).

Explanation

Key	ρ_{bulk} [kg.m^{-3}]	Layers.m^{-1}	Test Method	Comments
○	69.5	4 650	Flat-Plate Calorimeter. Heat flux related to boil-off rate of liquid butane.	T_C = 273.5 K. Measured in vacuum (<1.33×10^{-2} Pa).
□	74	4 920		
△	118	7 870		
▽	147	9 840		
▷	197	13 110		
◁	236	15 750		
●	69.5	4 650	Flat-Plate Calorimeter. Heat flux related to boil-off rate of liquid nitrogen.	T_C = 77.5 K. Measured in vacuum (<1.33×10^{-2} Pa).

MULTILAYER INSULATIONS

Spacers. Miscellaneous Properties

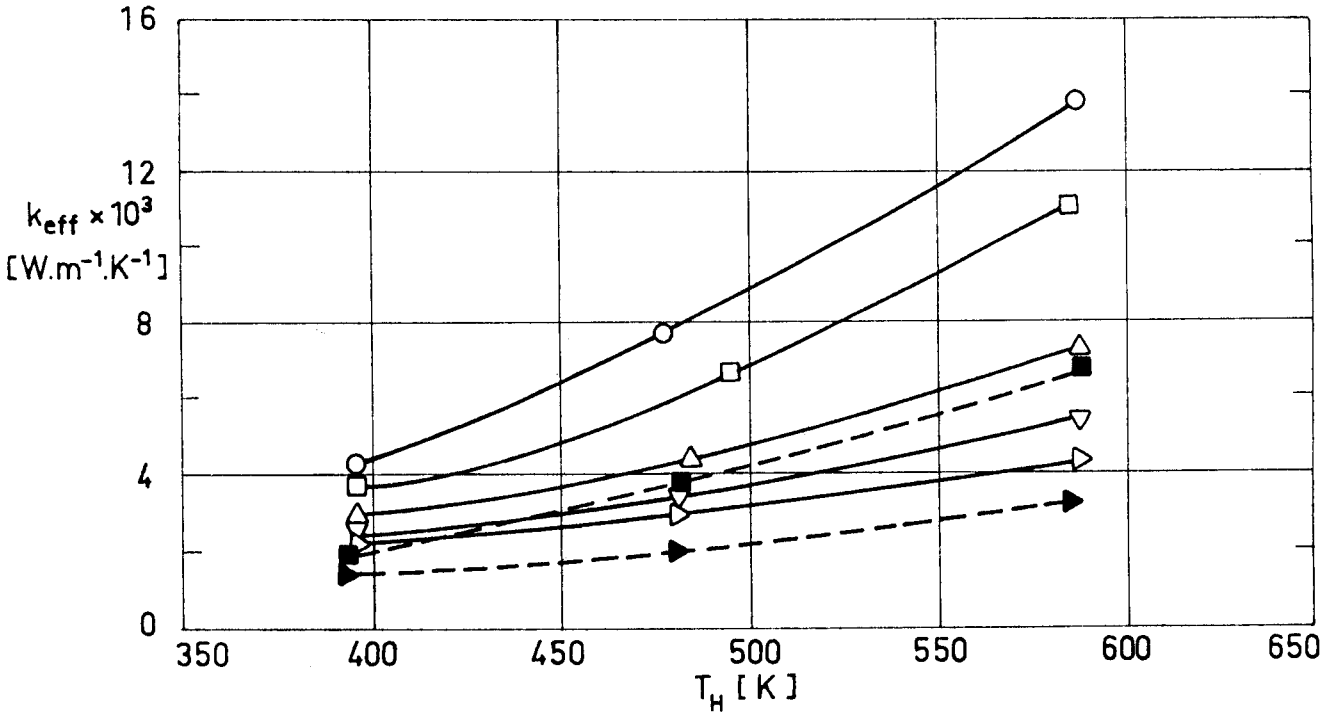

Fig 3-50. Effective thermal conductivity, k_{eff}, of Tissuglas as a function of warm-boundary temperature, T_H. From Cunnington, Zierman, Funai & Lindahn (1967).

Explanation

Key	ρ_{bulk} [kg.m^{-3}]	Layers.m^{-1}	Test Method	Comments
○	26.6	6 570	Flat-Plate Calorimeter. Heat flux related to boil-off rate of liquid butane.	T_C = 273.5 K. Measured in vacuum (<1.33×10^{-2} Pa).
□	40	9 840		
△	53.2	13 110		
▽	80.2	19 720		
▷	107	26 380		
■	40	9 840	Flat-Plate Calorimeter. Heat flux related to boil-off rate of liquid nitrogen.	T_C = 77.5 K. Measured in vacuum (<1.33×10^{-2} Pa).
▶	107	26 380		

MULTILAYER INSULATIONS

Spacers. Miscellaneous Properties

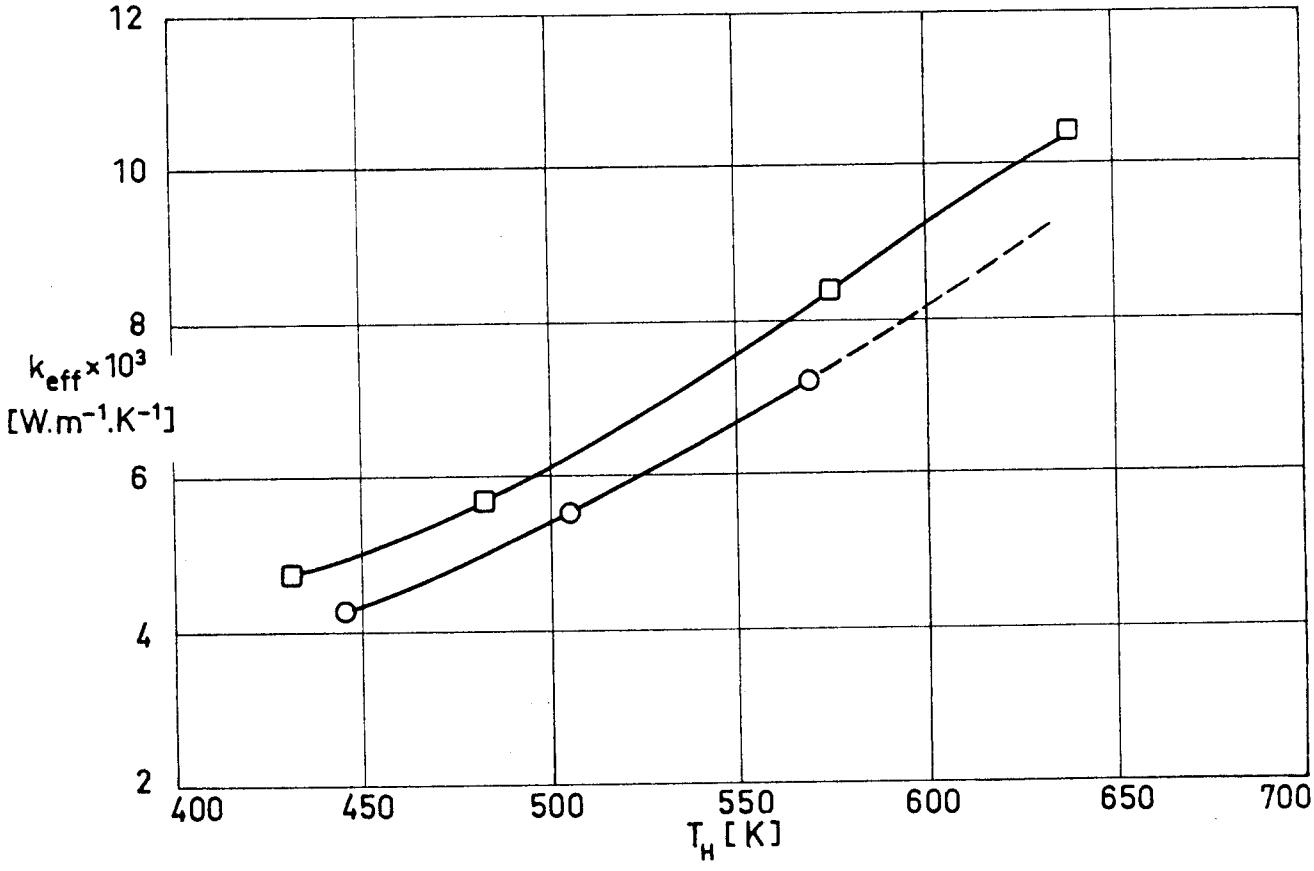

Fig 3-51. Effective thermal conductivity, k_{eff}, of Refrasil as a function of warm-boundary temperature, T_H. From Cunnington, Zierman, Funai & Lindahn (1967).

Explanation

Key	Description	Test Method	Comments
○	Refrasil A-100 Fiber Batt. Nominal fiber diameter, 10^{-6} - 2×10^{-6} m. ρ_{bulk} = 128.5 kg.m^{-3}	Flat-Plate Calorimeter. Heat flux related to boil-off rate of liquid butane.	T_C = 273.5 K. Measured in vacuum (<1.33×10^{-3} Pa).
□	Refrasil B-100 Fiber Batt. Nominal fiber diameter, 10.2×10^{-6} m. ρ_{bulk} = 125 kg.m^{-3}		

MULTILAYER INSULATIONS

Spacers. Miscellaneous Properties

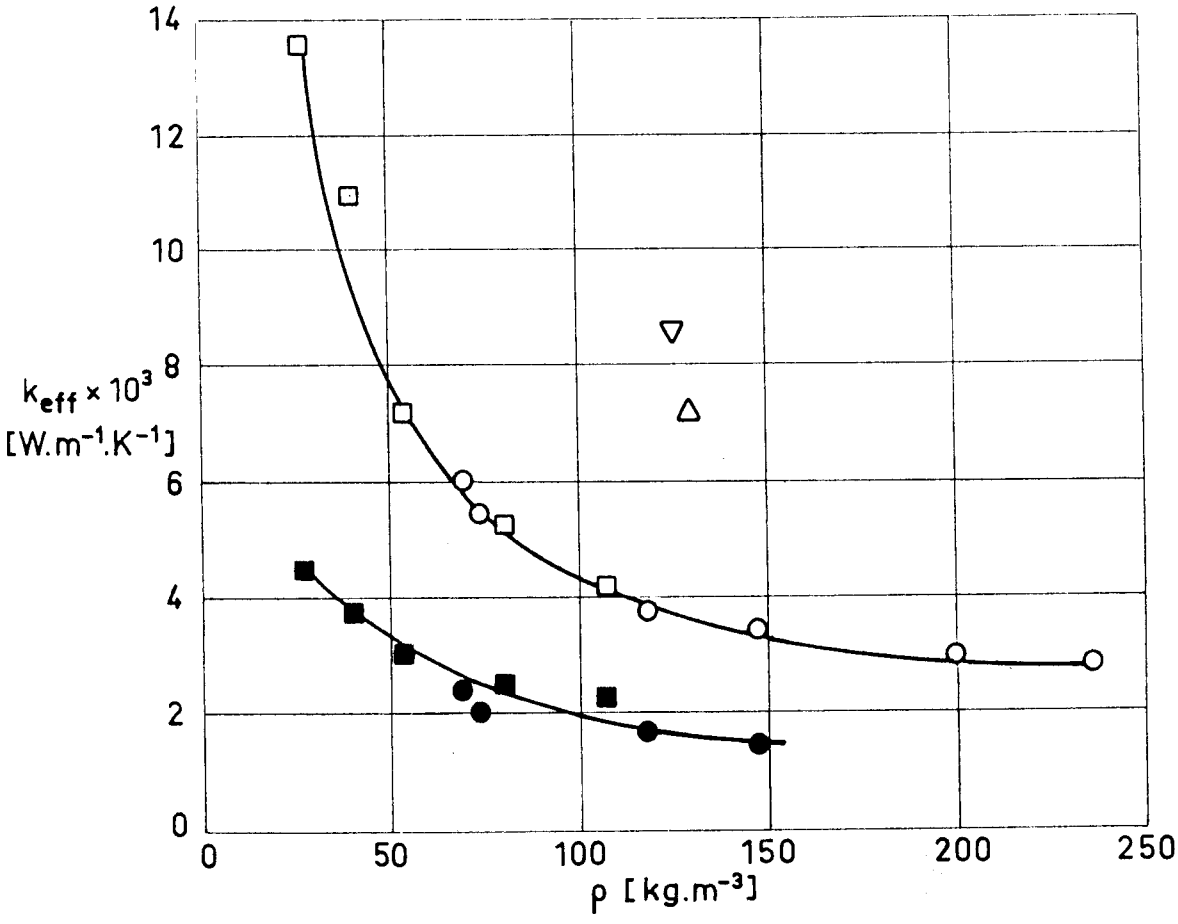

Fig 3-52. Effective thermal conductivity, k_{eff}, of several spacer materials as a function of bulk density, ρ. From Cunnington, Zierman, Funai & Lindahn (1967).

Explanation

Key	Description	Test Method	Comments
○	Dexiglas.	Flat-Plate Calorimeter. Heat flux related to boil-off rate of liquid butane.	T_H = 580 K. T_C = 273.5 K. Measured in vacuum (<1.33×10^{-2} Pa).
□	Tissuglas.		
△	Refrasil A-100.		
▽	Refrasil B-100.		
●	Dexiglas.	Same as ○ .	T_H = 400 K. T_C = 273.5 K. Measured in vacuum (<1.33×10^{-2} Pa).
■	Tissuglas.		

MULTILAYER INSULATIONS

Spacers. Miscellaneous Properties

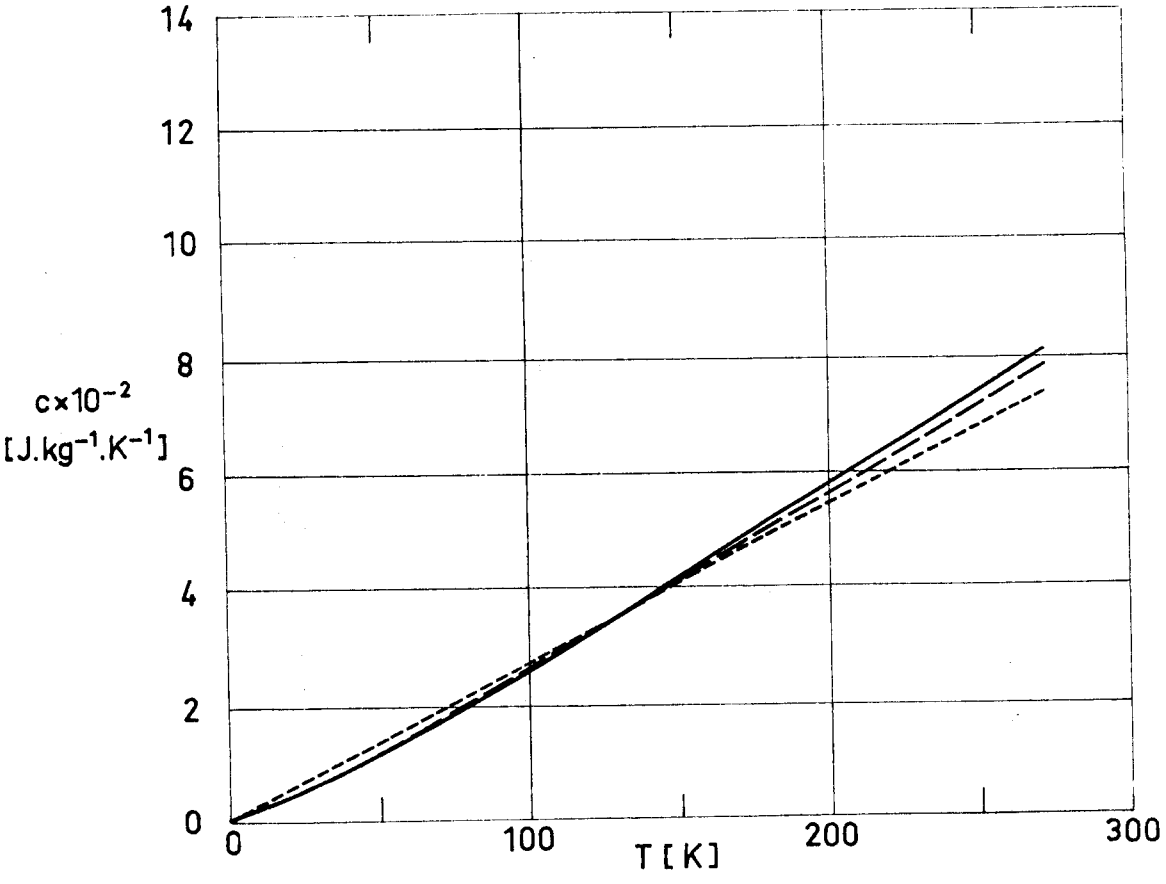

Fig 3-53. Specific Heat, c, of several spacer materials as a function of temperature, T. From Coston (1967).

Explanation

Key	Description	Comments
———	Dexiglas.	Deduced from the specific heat of Aluminium foil with Dexiglas paper spacers.
— — —	Glass Fibers.	
-----	Quartz.	

MULTILAYER INSULATIONS

Spacers. Miscellaneous Properties

Table 3-18

Flammability per Vertical Flame Test

Material	Flame Time [s]	Glow Time [s]	Char Length [m]
Nomex OG. .11 kg.m^{-2}	0	12.8	.081
Nomex OG. .17 kg.m^{-2}	0	15.2	.086
PBI, Gold .10 kg.m^{-2}	0	0	.058
PBI, Gold .17 kg.m^{-2}	0	0	.015
Kynol [a] .20 kg.m^{-2}	0	2.8	.003

From Ross & Stanton (1973).

[a] Kynol is a phenol formaldehyde from The Carborundum Company.

Table 3-19

Flammability of Several Spacers in Oxygen and in Air

Material	Oxygen		Air
	1.14×10^5 Pa	.43×10^5 Pa	10^5 Pa
Dacron batt-nonwoven, 18×10^{-3} kg.m^{-2}, 3.81×10^{-5} m thick	F	F	F
Fiber-glass Beta Marquisette, Style 2530	NF	NF	NF
Fiber-glass Plainweave Style 104 (unstabilized)	NF	NF	NF
Fiber-glass Plainweave Style 104, stabilized with 5 to 8 percent (by weight) of L-3306 Fluorel	SE	SE	NF
Polyurethane foam 4×10^3 pores per m, 7.62×10^{-4} m thick	F	F	F

From Richardson, Ruccia & French (1970).

F : Flammable
NF : Non-flammable
SE : Self-extinguishing

MULTILAYER INSULATIONS

Spacers. Miscellaneous Properties

Table 3-20

Outgassing Characteristics of Several Spacers

Material (Manufacturer)	% TWL [a]	% VCM [b]	Cure Time [h]	Cure Temp. [K]	Vacuum Conditions	References
Dacron Cloth 302 Caprollon	.050	.040				Campbell, Marriot & Park (1973)
Dacron Netting 70886-10 (Berkshire Hathaway)	.190	.060				
Dacron Polyester Mesh Style 15320 (Stern & Stern Textiles)	.127	.016				
Silk Netting Style 5517 (Jordan Marsh)	2.533	.077				
Silk Netting Style 5517 (Jordan Marsh)	2.452	.115	24 [c] 5 3	298[c] 363 298	1.33×10^{-4} Pa 1.33×10^{-4} Pa 1.33×10^{-4} Pa	
Silk Netting Style 5517 (Jordan Marsh)	2.342	.125	24 [c] 5 3	298[c] 398 298	1.33×10^{-4} Pa 1.33×10^{-4} Pa 1.33×10^{-4} Pa	
Fiberil-Oberflächenvlies Typ T 1751 (Viledon-Werk Carl Freudenberg)	1.44	.03			1.33×10^{-4} Pa	Klippel & Langer (1974)
Fibrex-Polyestervlies Typ H 3002 (Viledon-Werk Carl Freudenberg)	.36	.03			1.33×10^{-4} Pa	
Perlon-Wirktüll Net F 134 (Textilwerk Schauenstein)	1.23	.031			1.33×10^{-4} Pa	
Perlon-Wirktüll Net F 152 (Textilwerk Schauenstein)	1.70	.04			1.33×10^{-4} Pa	
Polyester-Bobinet-Tüll Net 1946 (Textilwerk Schauenstein)	.12	.038			1.33×10^{-4} Pa	
Fiberglass Beta Marquisette Stevens Style 2530	.9					Richardson, Ruccia & French (1971)

[a] TWL : Total Weight Loss.

[b] VCM : Volatile Condensable Materials (by weight).

[c] Each one of these cures was used in the order given.

Outgassing rates of spacer materials are given in § 3.17.2.1. in connection with evacuation under outgas controlled conditions.

INTENTIONALLY BLANK PAGE

MULTILAYER INSULATIONS
Complete Systems

3.10. COMPLETE SYSTEMS

As it has been emphasized repeatedly, the calculation of the insulation characteristics of an MLI is a difficult task. Hence it seems useful to collect as many experimental data as possible on the performance of existing systems. This collection is the objective of Sections 3.11 to 3.17.

Ideally an MLI system is supposed to be placed normally to the temperature gradient, so that most of the data presented regard the performance of ideal systems as measured on normal calorimeters (Section 3.11). However, thermal conductivities obtained on spacecraft can be considerably higher than those obtained in an idealized system, because of the discontinuities which are necessarily introduced in real configurations. Information on non-normal heat transfer is given in Section 3.12. The effect of singularities such as overlaps, stitches and patches appears in Section 3.13. In addition to these discontinuities, which are introduced during the assembling process, holes may be made in the shields to ease evacuation. These holes increase the shield transmittance, and consequently the thermal conductivity of the system. Data on the degrading effect of these holes are presented in Section 3.14.

A limited amount of information on the effect of other type of holes, those introduced because of mechanical damage, is given in Section 3.15.

An important point concerns the effect of the inner gas on the blanket thermal conductivity. This gas may be either air, a

purge gas, or species absorbed or adsorbed in the system. Since MLI systems exhibit low thermal conductivity when evacuated, two questions arise: 1) How the inner gas degrades the thermal performance of the system (Section 3.16), and 2) how such gases are to be evacuated (Section 3.17).

The interaction of the evacuation system with the heat transfer processes is also worth being considered since holes made in the shields degrade the performance of the system. This point has been already discussed in connection with Section 3.14.

MULTILAYER INSULATIONS
Normal Heat Transfer

3.11. NORMAL HEAT TRANSFER

Effective thermal conductances of MLI systems under temperature gradients normal to the insulation surface are given in this Section. In particular, the effects of layer density and boundary temperatures on the thermal conductance are considered.

For each MLI system at least three among the following four plots have been drawn.

1) The effective thermal conductance, k_{eff}, as a function of the layer density measured by the number of radiation shields per unit thickness, N/t.

2) The product of apparent density and effective thermal conductivity, $\rho\, k_{eff}$, as a function of N/t. This product provides a measure of the MLI usefulness in space applications and a basis for comparing it with other systems.

3) The compressive mechanical load, P, versus the resulting layer density, N/t. Since compression increases solid conduction, degrading the insulating characteristics of the system, some feeling on how sensitive the system is to mechanical loads is required.

4) The variation of the effective thermal conductance with temperature for a given layer density.

It has been common practice the plotting of apparent thermal conductivity of a given system versus the warm-boundary temperature, T_H. It can be shown that for large temperature differentials the effective thermal conductivity is approximately proportional to T_H^3. When the cold-boundary temperature, T_C, is not constant, T_H is not

MULTILAYER INSULATIONS

Normal Heat Transfer

the most appropriate parameter. The experimental evidence indicates that, when T_H is held constant, a higher thermal conductivity results from increasing T_C. The following options are now open to the compiler:

1) For results corresponding to the same MLI with the same value of T_C, the plotting of k_{eff} vs. T_H seems to be the best choice.

2) When neither the maximum nor the minimum temperatures are constant a combination of both values -the characteristic temperature T- is used.

$$T = \sqrt[3]{\frac{T_H^4 - T_C^4}{4(T_H - T_C)}} \quad .$$

The data presented are arranged as follows. The MLI systems are grouped according to their shields, and for each shield, according to their spacers. The first page dealing with a given system shows k_{eff} and $\rho\, k_{eff}$ as functions of N/t. The second page gives P vs. N/t and k_{eff} vs. T. A fairly detailed description of the samples involved is given in the third page. This description includes the conditions under which the tests have been performed, such as chamber pressure, boundary temperatures and type of calorimeter used. Appropriate references are precisely identified.

In those cases where the available information has allowed the drawing of only three figures among the four abovementioned, the explanatory table is enclosed in the second of the pages corresponding to the system involved.

An index of the compiled data is given in the next page.

MULTILAYER INSULATIONS

Normal Heat Transfer

System			Data		
Shield	Spacer	Fig	$k_{eff}(N/t)$, $\rho k_{eff}(N/t)$	P(N/t)	$k_{eff}(T)$
Aluminium	Fiber-Glass	3-54	O	O	
Single-Aluminized Mylar Crinkled		3-55	O		O
Aluminized Mylar Dimpled		3-56	O		O
Double-Aluminized Mylar	Glass Fabric	3-57	O	O	
	Foam	3-58	O	O	O
	Silk Net	3-59	O	O	O
	Silk+Foam	3-60	O	O	
	Silk+Paper	3-61	O	O	
Single-Aluminized Kapton	Dexiglas	3-62	O		O
	Tissuglas	3-63	O		O
Double-Goldized Kapton	Dacron	3-64	O	O	
	Nomex	3-65	O	O	
Superfloc		3-66	O	O	O

INTENTIONALLY BLANK PAGE

MULTILAYER INSULATIONS

Normal Heat Transfer

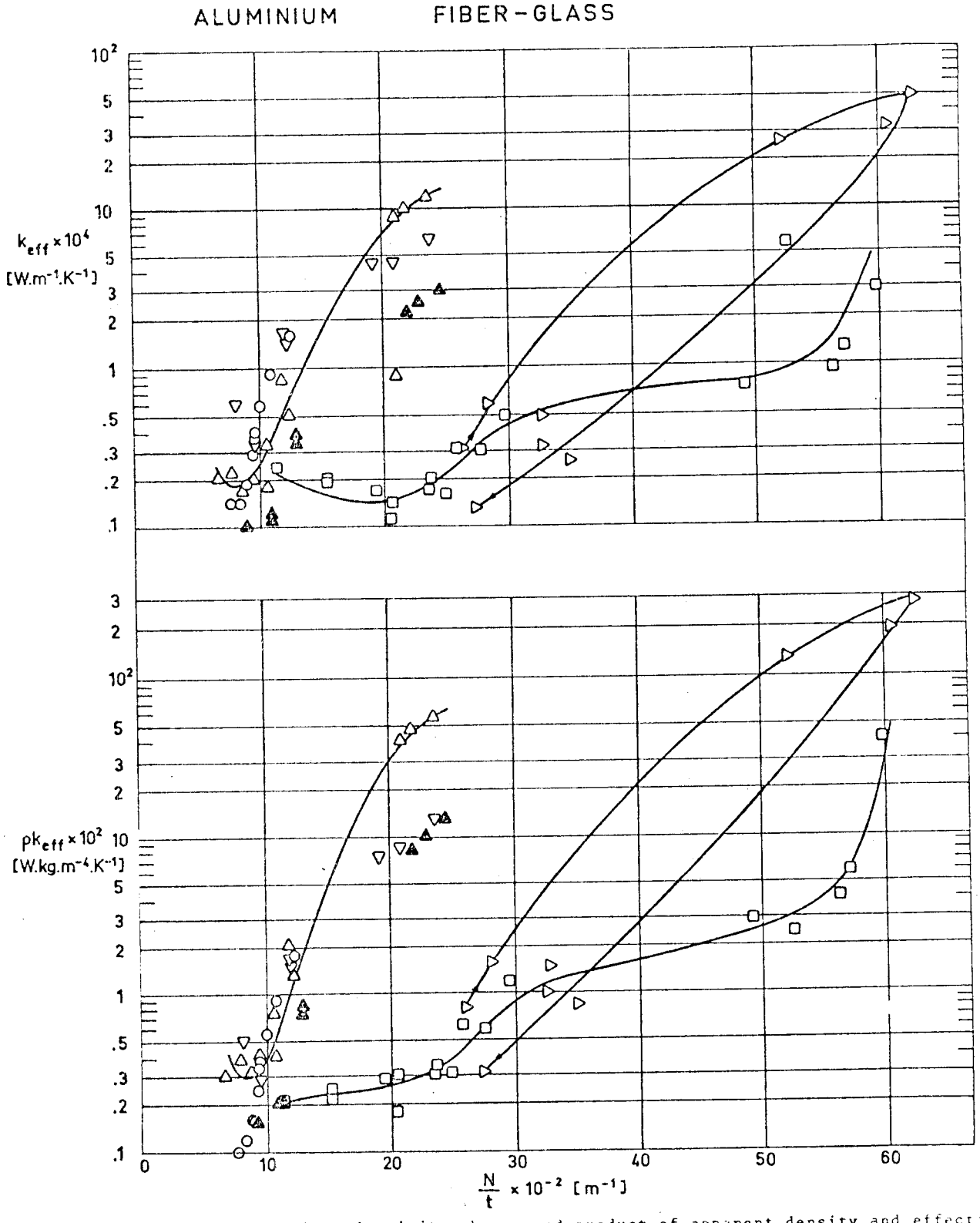

Fig 3-54a. Effective thermal conductivity, k_{eff}, and product of apparent density and effective thermal conductivity, ρk_{eff}, vs. the number of radiation shields per unit thickness, N/t. Arrows in curves indicate whether the system is being loaded or unloaded.

MULTILAYER INSULATIONS

Normal Heat Transfer

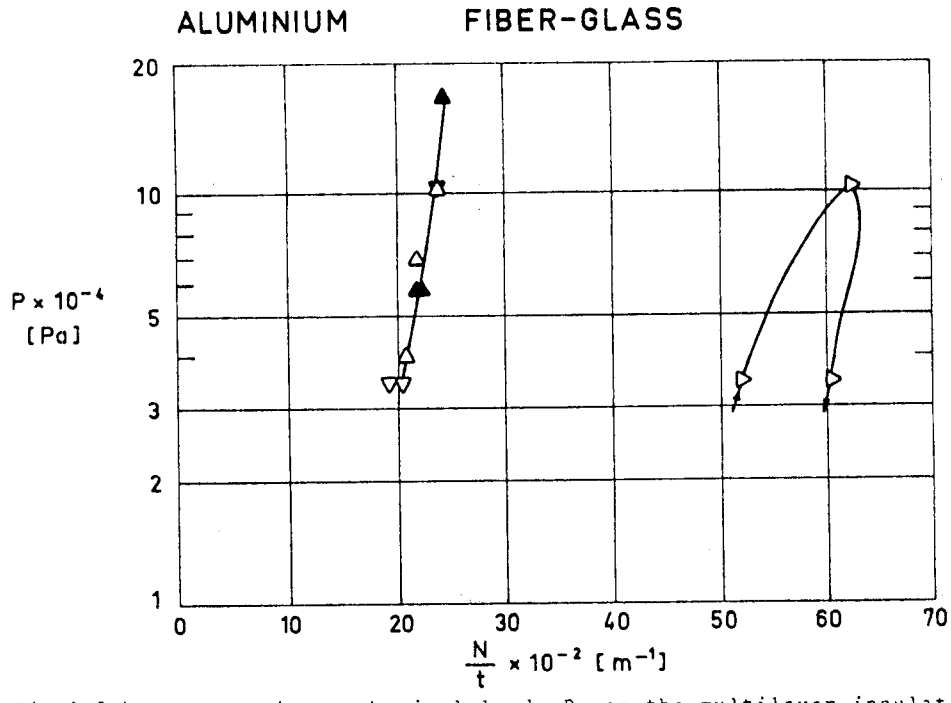

Fig 3-54b. Compressive mechanical load, P, on the multilayer insulation vs. the number of radiation shields per unit thickness, N/t.

Explanation

Key	Sample Description	$t \times 10^2$ [m] Uncompressed	$p \times 10^3$ [Pa]	T_H [K]	T_C [K]	Calorimeter Type	References
○	N=10 Shields. 12.7×10^{-6} m thick smooth Aluminium. 11 Spacers. 3.56×10^{-4} m thick Fiber-glass mat.	1.28	<1.33	293.5±5	77.5	ADL Model 12. Flat-Plate (double-guarded cold-plate).	ADL (1964) p. II-17.
□ ◨ ■	N=10 Shields. 12.7×10^{-6} m thick smooth Aluminium. 11 Spacers. Each consisting of 3 layers of 25.4×10^{-6} m thick glass fiber cloth (genin). Spacers thickness 10^{-4} m.	.88	<1.33	□ 288±2.5 ◨ 284±1.5 ■ 293±.5	77.5 20.5 20.5	Same as ○.	ADL (1964) p. II-18.
△	N=10 Shields. 5.08×10^{-5} m thick Al alloy 1145-H19 bright both sides. 11 Spacers. 5.08×10^{-4} m thick and 144 Kg.m^{-3} CTL-449 Fiber-glass mat. CTL Div of Studebaker Corp.	1.49 [a]		282±2	20.5	Same as ○.	ADL (1964) p. II-33.
▲	Same as △. Slots cut in the spacer to produce 11% support area.	1.11 [a]	<.67	291.5±1	20.5	Same as ○.	ADL (1964) p. II-36.
▽	N=10 Shields. 12.7 10^{-6} m thick Aluminium Embossed. 11 Spacers. 3.56×10^{-4} m thick Fiber-glass mat.	1.22	<1.33	281±1.5	20.5	Same as ○.	ADL (1964) p. II-19.
▷	Same as □ except Aluminium Embossed, wave-like pattern.	.38	<.13	280.5±1.5	20.5	Same as ○.	ADL (1964) p. II-20.

[a] Largest quoted value.

MULTILAYER INSULATIONS

Normal Heat Transfer

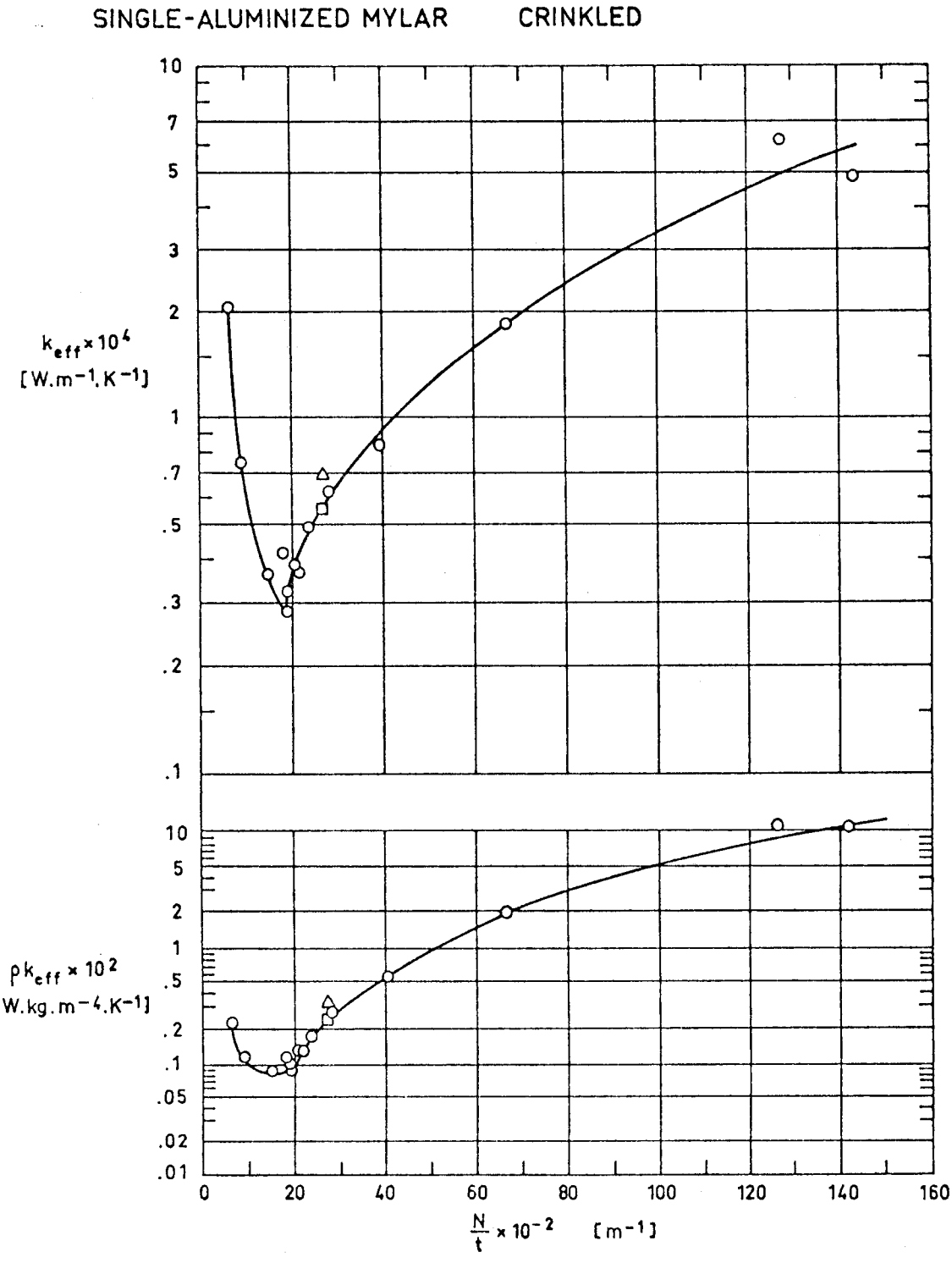

Fig 3-55a. Effective thermal conductivity, k_{eff}, and product of apparent density and effective thermal conductivity, ρk_{eff}, vs. the number of radiation shields per unit thickness, N/t.

MULTILAYER INSULATIONS

Normal Heat Transfer

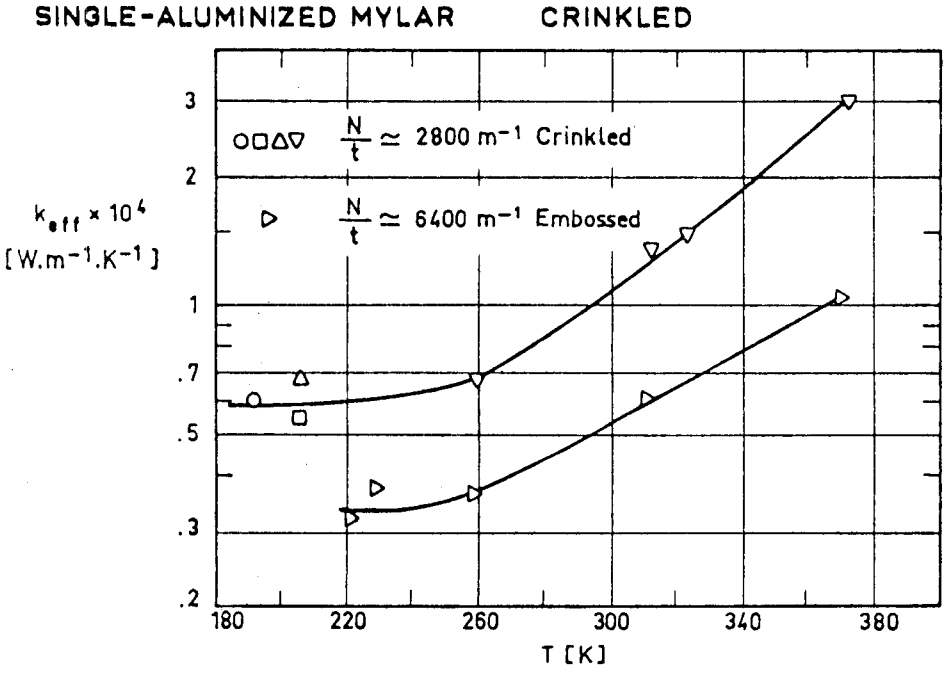

Fig 3-55c. Effective thermal conductivity, k_{eff}, as a function of the characteristic temperature, T.

Explanation

Key	Sample Description	$t \times 10^2$ [m] Uncompressed	$p \times 10^3$ [Pa]	T_H [K]	T_C [K]	Calorimeter Type	References
○	N=20 Shields 6.35×10^{-6} m thick Mylar Single-Aluminized Crinkled	3.29[a]	<1.33	294.5	20.5	ADL Model 12 Flat-Plate (double-guarded cold-plate)	ADL (1964) p. II-24
□	N=35 Shields 6.35×10^{-6} m thick Mylar Single-Aluminized Crinkled	1.27		296	76.5		Scollon & Carpitella (1970) p. B-6
△	N=35 Shields 33 layers of 6.35×10^{-6} m thick Mylar Single-Aluminized Crinkled 2 layer of 12.7×10^{-6} m thick Kapton Single-Aluminized Crinkled and installed next to cold plates	1.27		295.5	76		Same as □
▽	N=70 Shields 6.35×10^{-6} m thick Mylar Single-Aluminized Crinkled	2.54		313.5 335.5 262 375	308 308 255 366	Lockheed/Huntsville Cylindrical	Scollon & Carpitella (1970) p. B-11 after Hale et al. (1967)
▷	N=81 Shields 6.35×10^{-6} m thick Mylar Single-Aluminized Embossed	1.27	.373 .613 .453 .373 .307	238 273 321.5 384 295.5	204.5 244 300 355.5 147.5	Lockheed/Huntsville Cylindrical	Hale (1969) p. 41

[a] Largest quoted value.

MULTILAYER INSULATIONS

Normal Heat Transfer

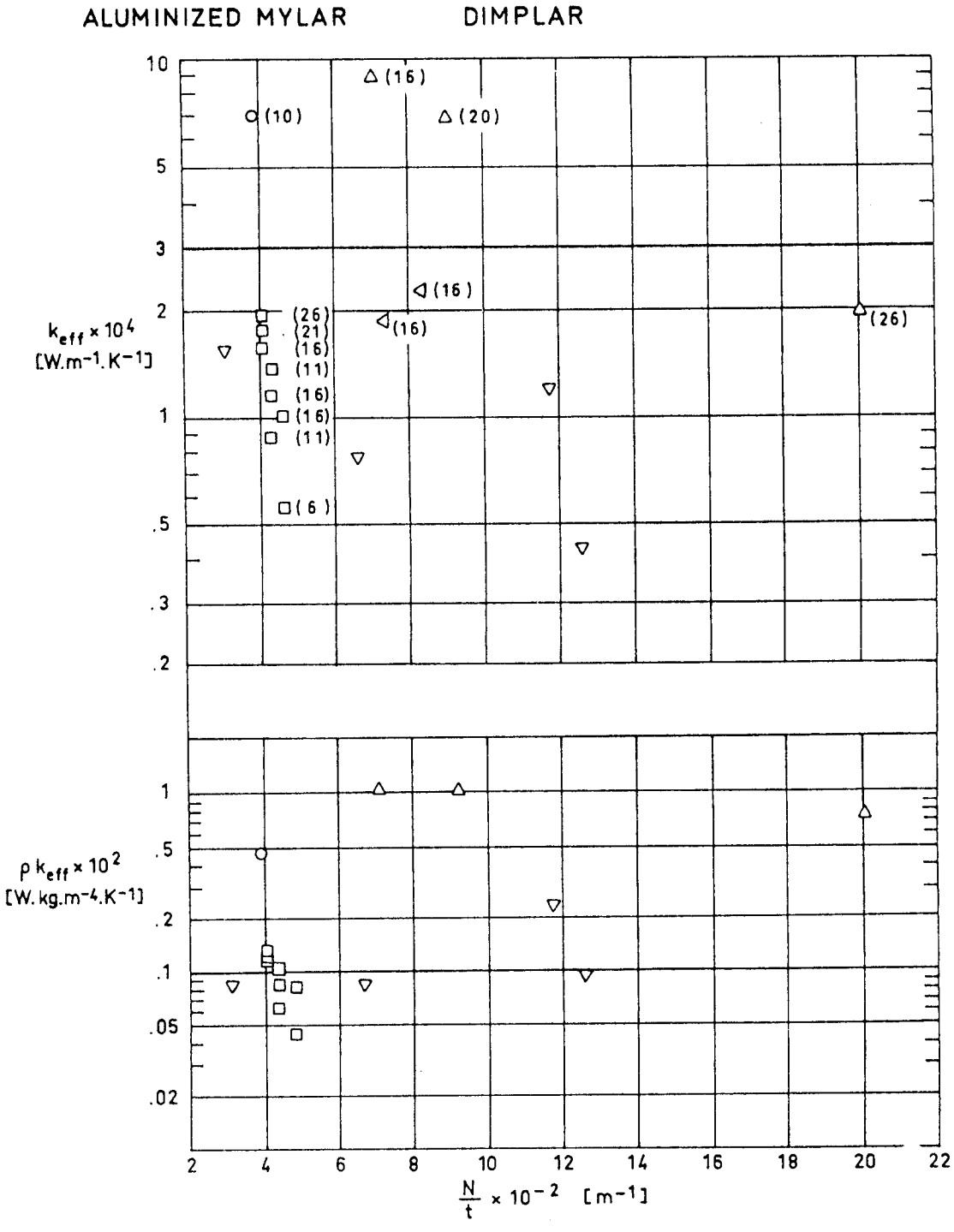

Fig 3-56a. Effective thermal conductivity, k_{eff}, and product of apparent density and effective thermal conductivity, ρk_{eff}, vs. the number of radiation shields per unit thickness, N/t. Values of N are given in parenthesis.

MULTILAYER INSULATIONS

Normal Heat Transfer

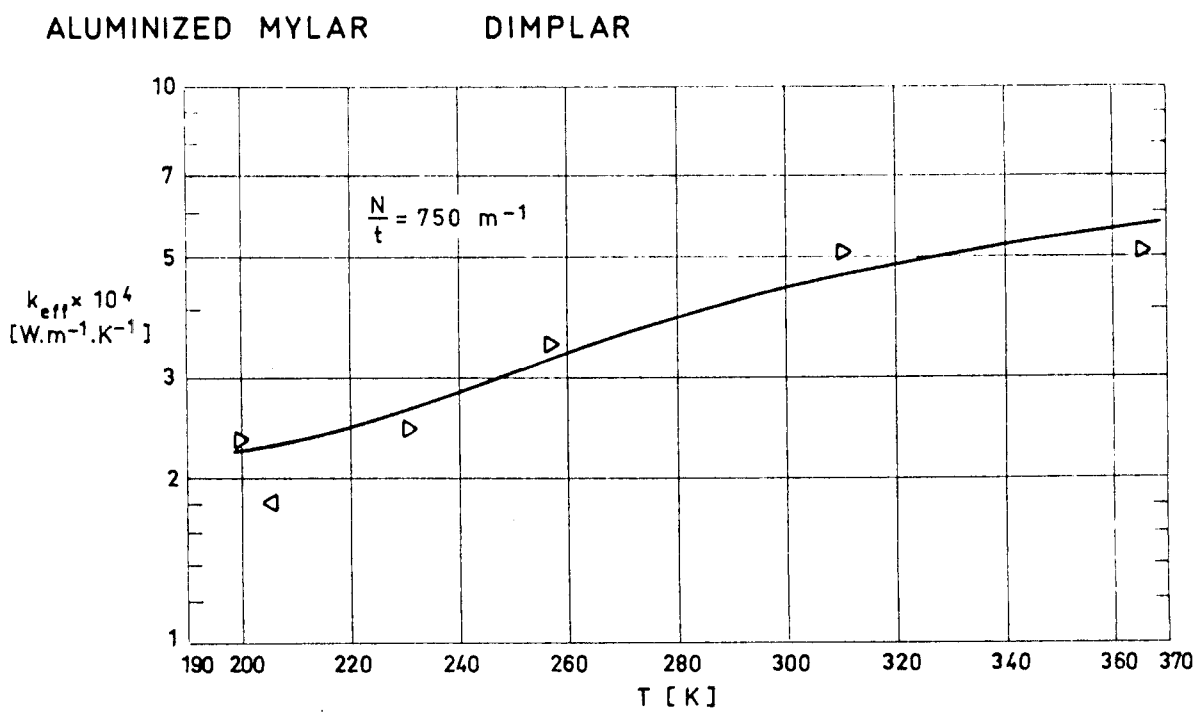

Fig 3-56c. Effective thermal conductivity, k_{eff}, as a function of the characteristic temperature, T.

Explanation

Key	Sample Description	$t \times 10^2$ [m] Uncompressed	$p \times 10^3$ [Pa]	T_H [K]	T_C [K]	Calorimeter Type	References
○	N=10 10 Layers 12.7×10^{-6} m thick Mylar Double-Aluminized 10 Layers 12.7×10^{-6} m thick Mylar Double-Aluminized Dimpled	2.54		294.5	78	NBS - Cryostat Cylindrical	Coston (1967) pp. 4.3-5, 4.3-11
□	Variable number of layers Same components as ○			303	78	Same as ○	Same as ○
△	Same as □			296	20.5	Flat-Plate	Same as ○
▽	Same as △					Same as △	Same as ○
▷	N=22 22 Layers 6.35×10^{-6} m thick Mylar Single-Aluminized Dimpled 22 Layers 6.35×10^{-6} m thick Mylar Single-Aluminized Embossed	2.92	.333 .133 .506 .506 .440	210 267 290 319.5 376.5	189 245.5 159 301.5 356	Lockheed/Huntsville Cylindrical	Hale (1969) p. 42
◁	N=8 8 Layers 12.7×10^{-6} m thick Mylar Single-Aluminized Deeply Corrugated 8 Layers 12.7×10^{-6} m thick Mylar Smooth Reflector	1.90 2.16		295 295.5	77 76		Scollon & Carpitella (1970) p. B-7.

MULTILAYER INSULATIONS

Normal Heat Transfer

DOUBLE-ALUMINIZED MYLAR GLASS FABRIC

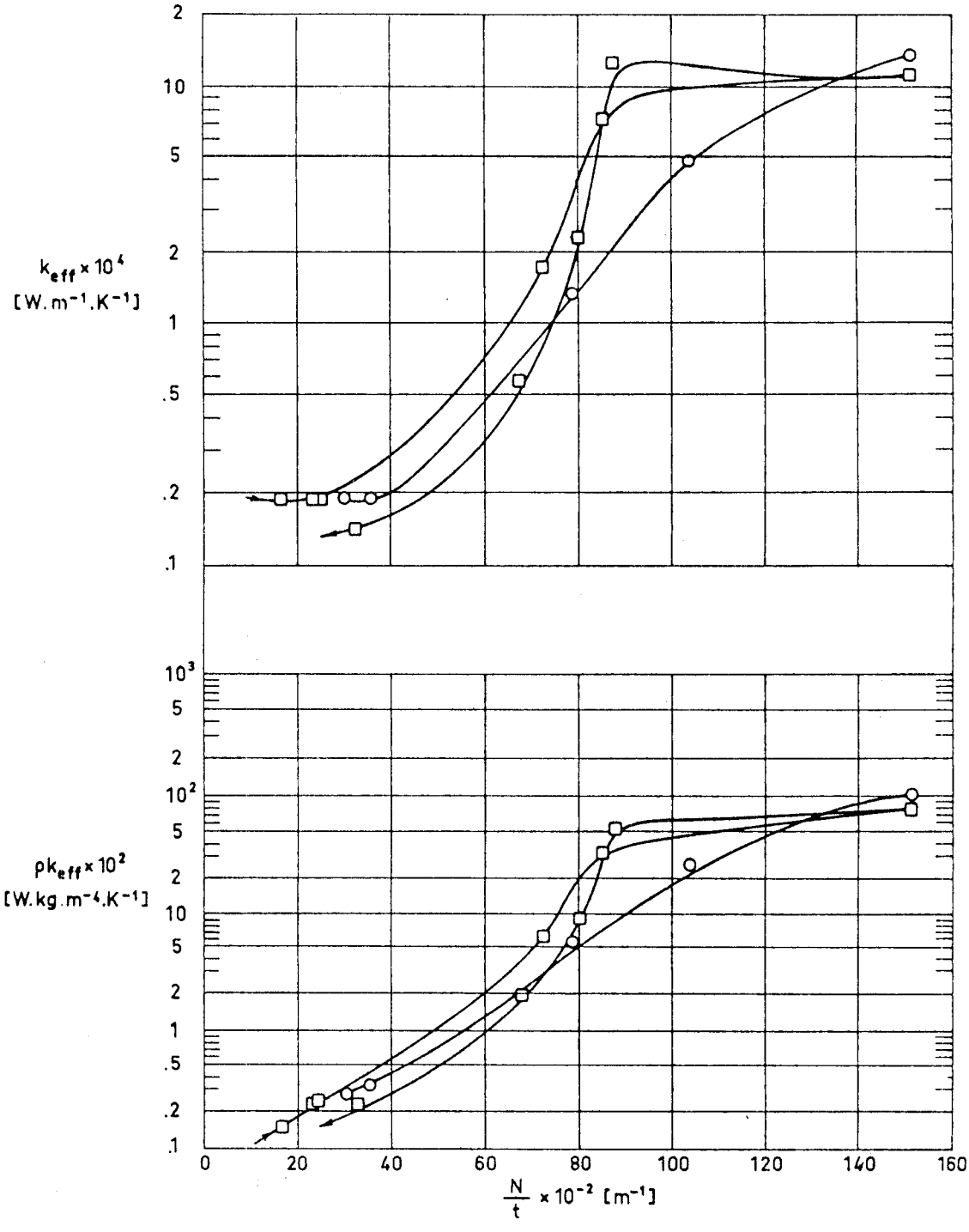

Fig 3-57a. Effective thermal conductivity, k_{eff}, and product of apparent density and effective thermal conductivity, pk_{eff}, vs. the number of radiation shields per unit thickness, N/t. Arrows in curves indicate whether the system is being loaded or unloaded.

MULTILAYER INSULATIONS

Normal Heat Transfer

DOUBLE-ALUMINIZED MYLAR GLASS FABRIC

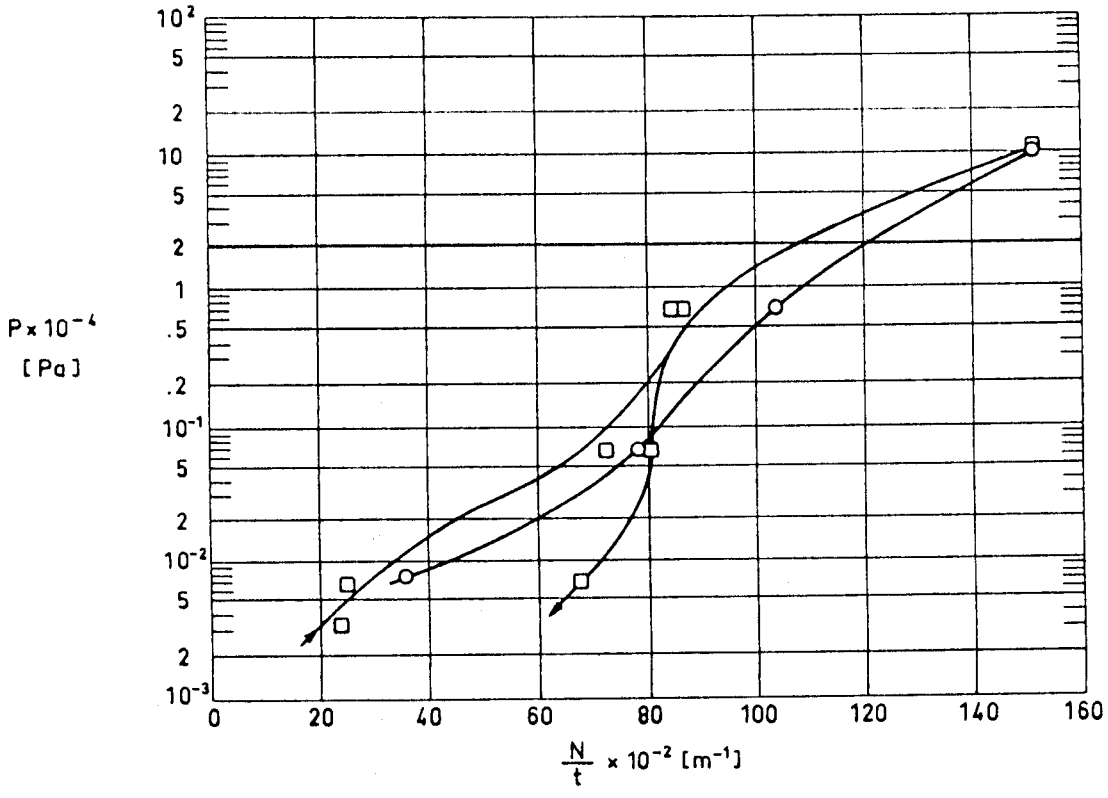

Fig 3-57b. Compressive mechanical load, P, on the multilayer insulation vs. the number of radiation shields per unit thickness, N/t.

Explanation

Key	Sample Description	t×10² [m] Uncompressed	p×10³ [Pa]	T_H [K]	T_C [K]	Calorimeter Type	References
○	N=10 Shields. 6.35×10⁻⁶ m thick × .279 m diameter Mylar. Double-Aluminized. 21 Spacers. 25.4×10⁻⁶ m thick × .305 m diameter Glass fabric.	.330	<6.67	277.5±1	77.5	ADL Model 12 Flat-Plate (double-guarded cold-plate)	ADL (1966) p. II-33.
□	N=10 Shields. 6.35×10⁻⁶ m thick × .279 m diameter Mylar. Double-Aluminized. 22 Spacers. 25.4×10⁻⁶ m thick × .305 m diameter Glass fabric.	.599	<.67	294±3	77.5	Same as ○.	ADL (1966) p. II-87.

MULTILAYER INSULATIONS

Normal Heat Transfer

DOUBLE-ALUMINIZED MYLAR FOAM

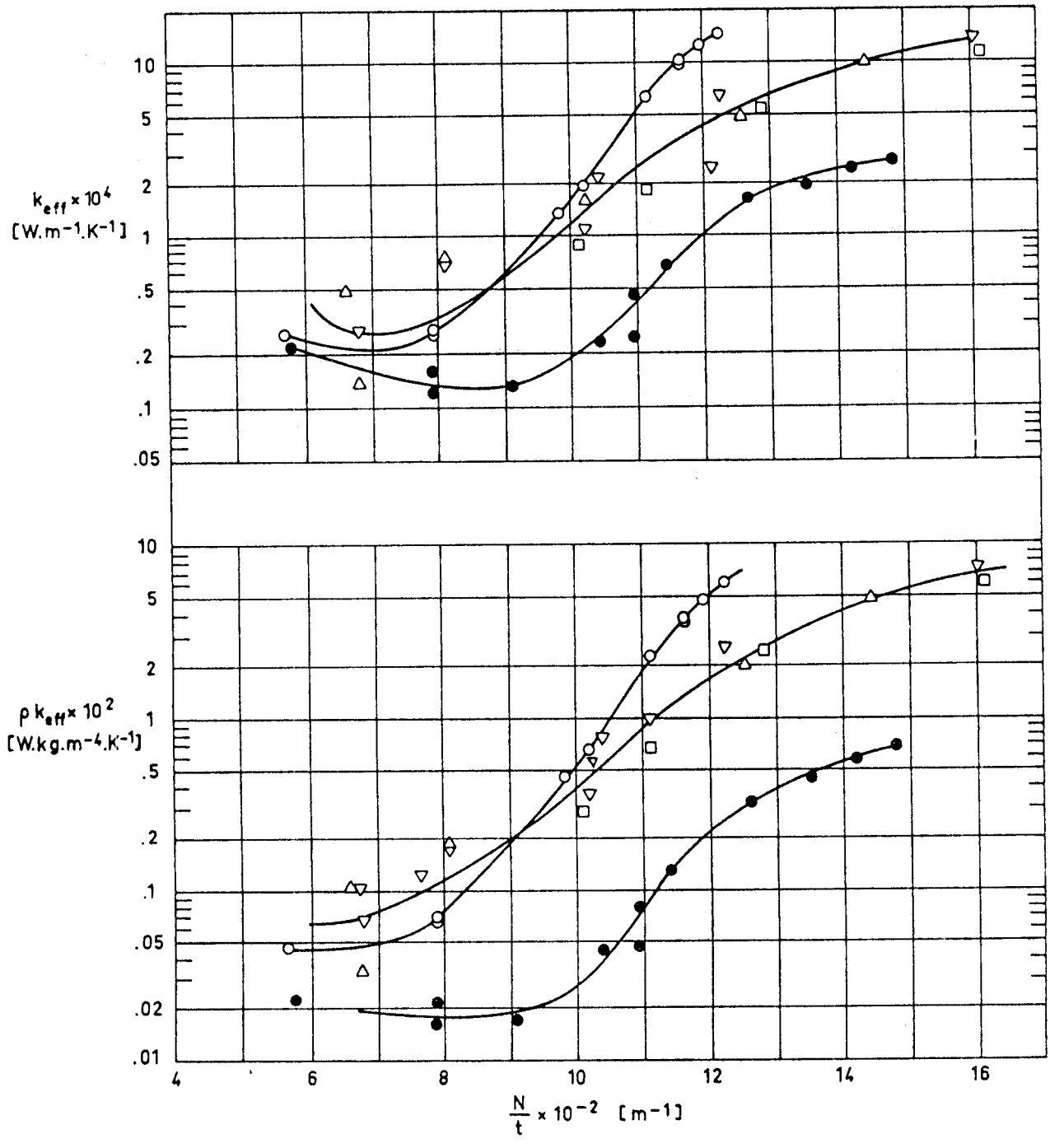

Fig 3-58a. Effective thermal conductivity, k_{eff}, and product of apparent density and effective thermal conductivity, ρk_{eff}, vs. number of radiation shields per unit thickness, N/t.

MULTILAYER INSULATIONS

Normal Heat Transfer

DOUBLE-ALUMINIZED MYLAR FOAM

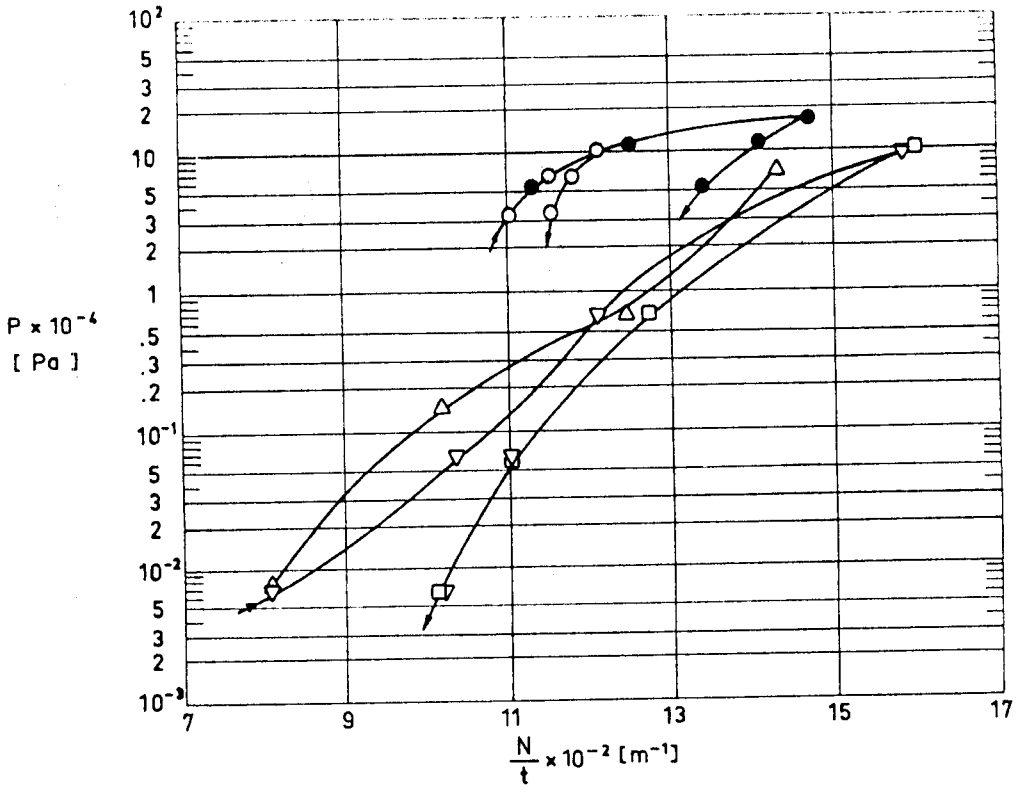

Fig 3-58b. Compressive mechanical load, P, on the multilayer insulation vs. the number of radiation shields per unit thickness, N/t. Arrows in curves indicate whether the system is being loaded or unloaded.

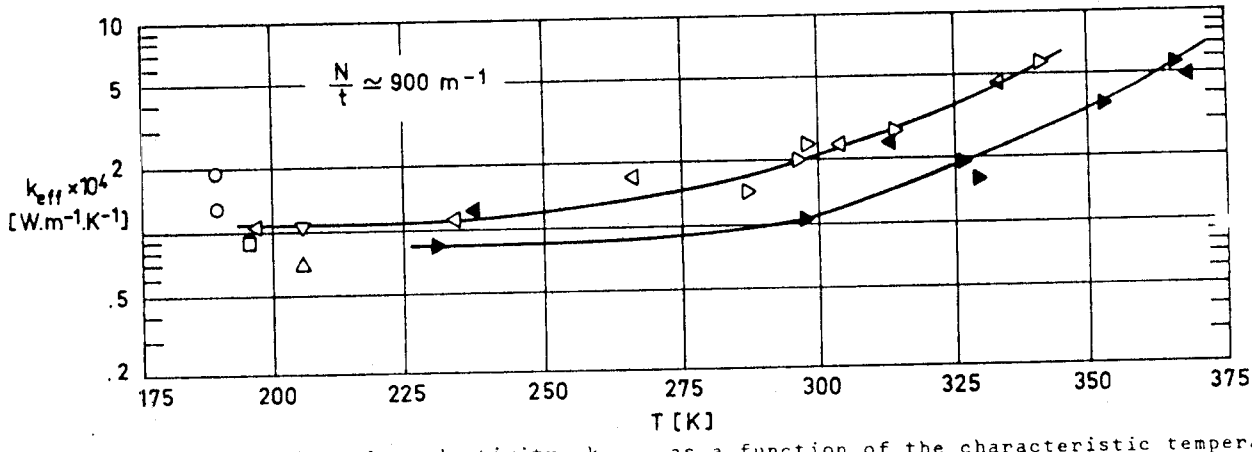

Fig 3-58c. Effective thermal conductivity, k_{eff}, as a function of the characteristic temperature, T.

MULTILAYER INSULATIONS

Normal Heat Transfer

DOUBLE-ALUMINIZED MYLAR FOAM

Explanation

All Shields are 6.35×10^{-6} m thick Mylar Double-Aluminized.

Key	Sample Description	$t\times10^{2}$ [m]	$p\times10^{3}$ [Pa]	T_H [K]	T_C [K]	Calorimeter Type	References
○	N=10 Shields 11 Spacers 32 Kg.m^{-3} Freon blown polyurethane foam. 5×10^{-4} m thick. The spacers were formed by placing two semicircles together and cementing them only near the outer edge.	1.74[a]	<6.7	293±.5	20.5	ADL Model 12 Flat-Plate (double--guarded cold-plate)	ADL (1964) p. II-34
●	Same as ○ Slots were cut in the spacers to produce 11% support area.	1.71[a]	<6.7	293.5±1	20.5	Same as ○	ADL (1964) p. II-35
□	N=10 Shields 11 Spacers 32 Kg.m^{-3} Freon blown polyurethane foam. 5×10^{-4} m thick ×.305 m diameter.	.99[a]	<4.0	277.5	77.5	Same as ○	ADL (1966) p. II-72
△	Same as □	1.51[a]	<6.7	279±1	77.5	Same as ○	ADL (1966) p. II-32
▽	Same as □	1.52[a]	<4.0	295±1	77.5	Same as ○	Same as □
▷	N=22 Shields 21 Spacers 7.62×10^{-4} m thick Goodyear foam (before outgassing of foam at 366.5 K)	2.54	<1.1	300.5 316.5 344 289.5 299	295 311 338 283.5 292.5	Lockheed/ /Huntsville Cylindrical	Scollon & Carpitella (1970). pp. B-11, B-12
▶	Same as ▷ (after outgassing of foam at 366.5 K)	2.54	<1.1	369 298 356 332.5 300 232	362.5 148 349 325.5 294 227	Same as ▷	Same as ▷
◁	N=24 Shields 23 Spacers 7.11×10^{-4} m thick Goodyear foam (before outgassing of foam at 366.5 K)	2.54	.400 .533 .533 .987	210 246.5 278 311.5	184 219 254.5 297.5	Same as ▷	Hale (1969) p. 39
◀	Same as ◁ (during outgassing of foam at 366.5 K)	2.54	2.67	344	322.5	Same as ▷	Same as ◁
◀	Same as ◁ (after outgassing of foam at 366.5 K)	2.54	1.87 .480 .200	379 325.5 299	357 301.5 166	Same as ▷	Same as ◁

[a] Largest quoted value.

INTENTIONALLY BLANK PAGE

MULTILAYER INSULATIONS

Normal Heat Transfer

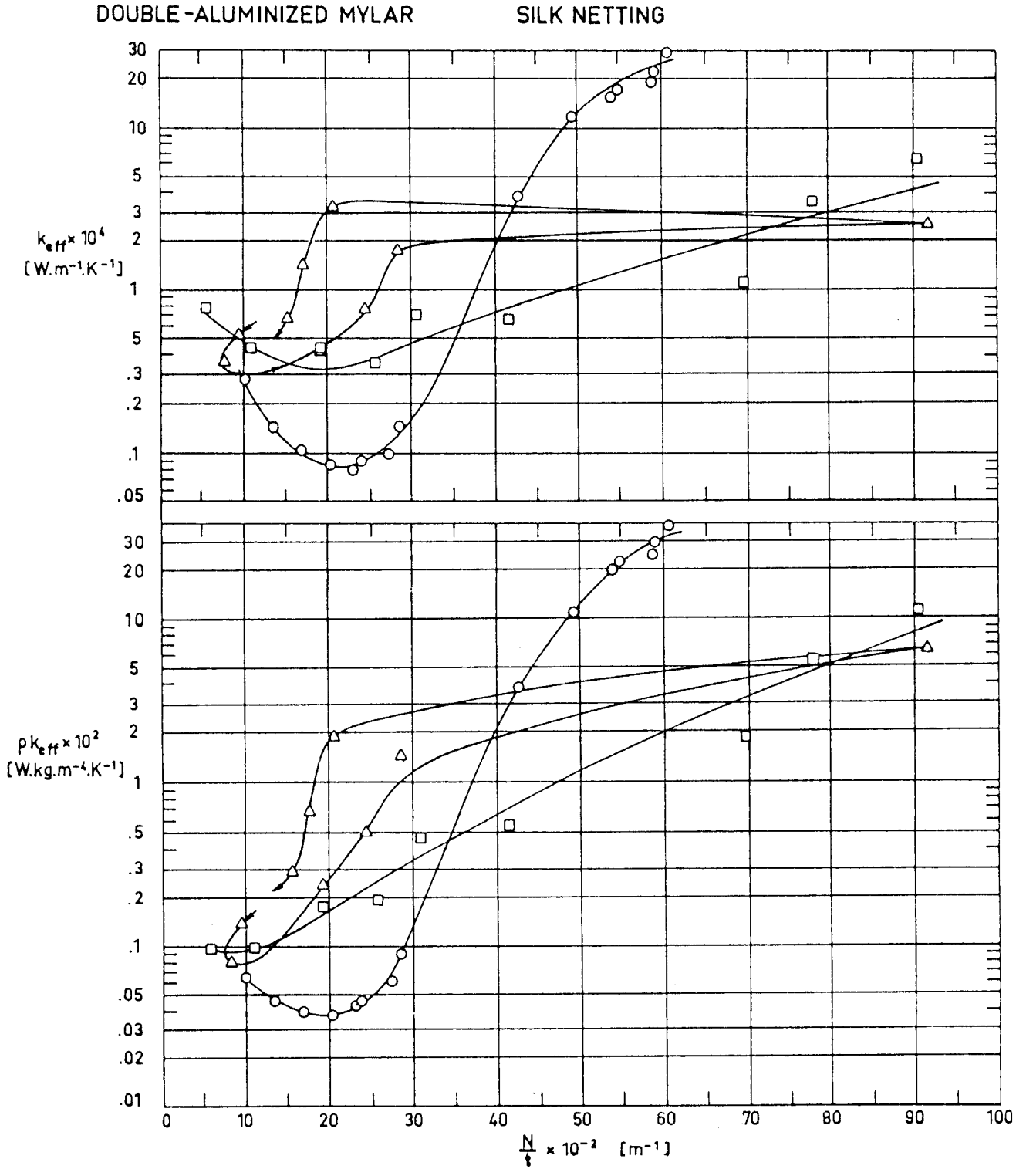

Fig 3-59a. Effective thermal conductivity, k_{eff}, and product of apparent density and effective thermal conductivity, ρk_{eff}, vs. the number of radiation shields per unit thickness, N/t. Arrows in curves indicate whether the system is being loaded or unloaded.

MULTILAYER INSULATIONS

Normal Heat Transfer

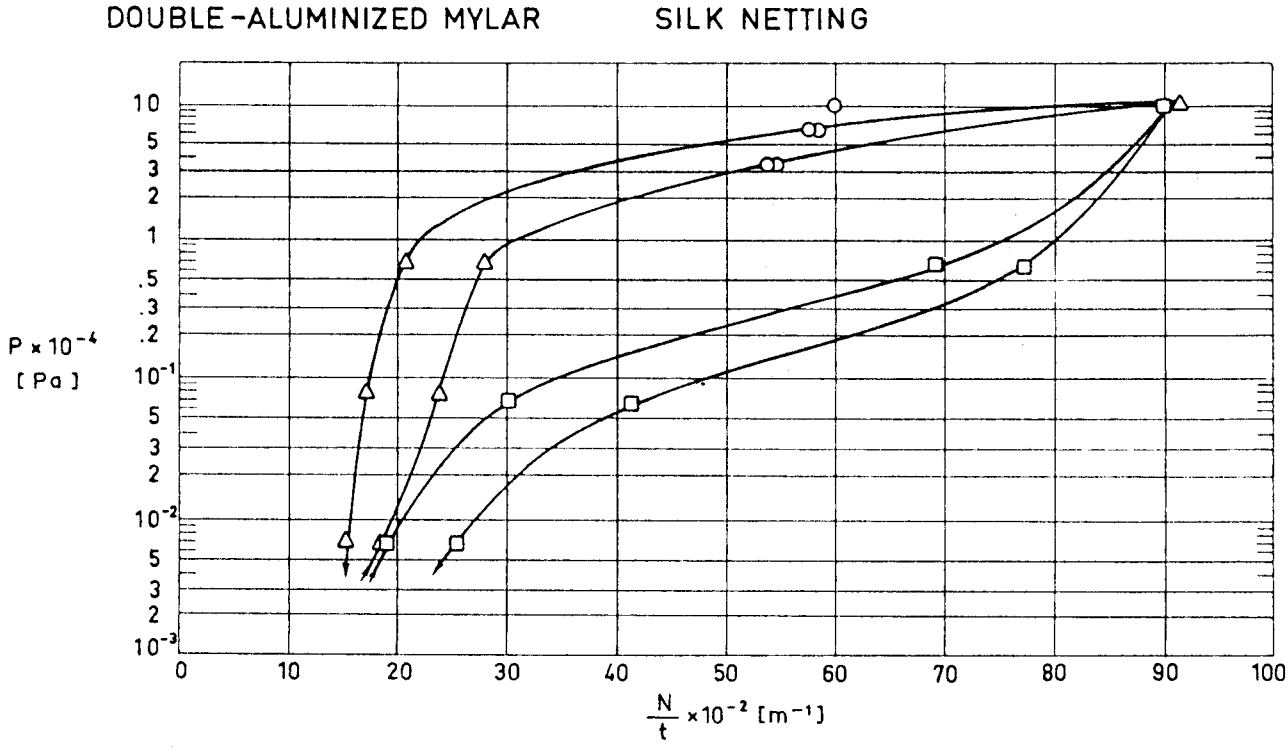

Fig 3-59b. Compressive mechanical load, P, on the multilayer insulation vs. the number of radiation shields per unit thickness, N/t.

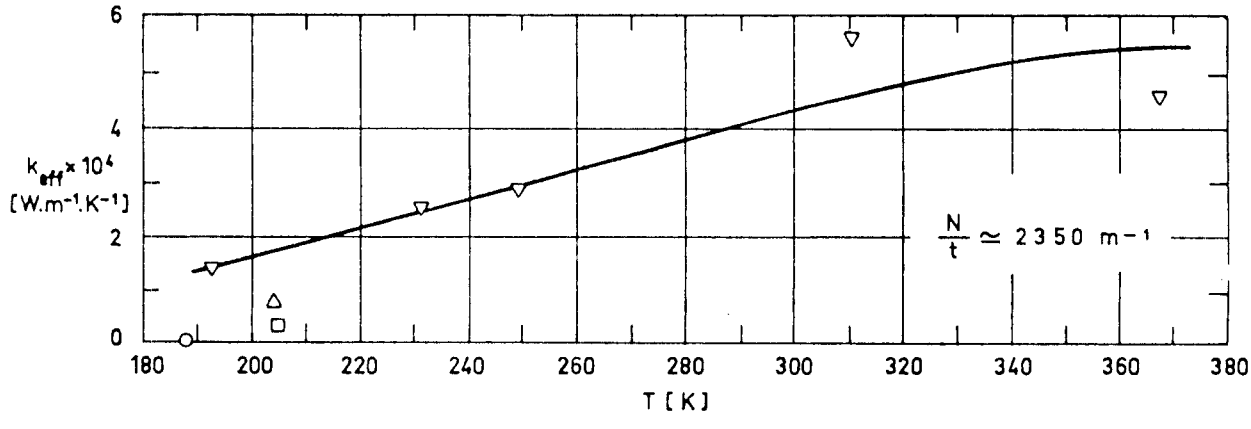

Fig 3-59c. Effective thermal conductivity, k_{eff}, as a function of the characteristic temperature, T.

MULTILAYER INSULATIONS

Normal Heat Transfer

DOUBLE-ALUMINIZED MYLAR SILK NETTING

Explanation:

Key	Sample Description	$t \times 10^2$ [m] Uncompressed	$p \times 10^3$ [Pa]	T_H [K]	T_C [K]	Calorimeter Type	References
O	N=10 Shields 6.35×10^{-6} m thick Mylar Double-Aluminized 11 Spacers 1.78×10^{-4} m thick Nylon Netting	1[a]	<.53	292±1	20.5	ADL Model 12 Flat-Plate (double-guarded cold-plate)	ADL (1964) p. II-37
□	N=10 Shields 6.35×10^{-6} m thick × × 2.79×10^{-1} m diameter Mylar Double-Aluminized 22 Spacers 7.62×10^{-5} m thick × × 3.05×10^{-1} m diameter Silk Netting	1.73[a]	<6.67	295±1.5	77.5	Same as O	ADL (1966) p. II-35
△	N=10 Shields 6.35×10^{-6} m thick × × 2.79×10^{-1} m diameter Mylar Double-Aluminized 33 Spacers 7.62×10^{-5} m thick × × 2.79×10^{-1} m diameter Silk Netting	1.24	<6.67	294±3	77.5	Same as O	ADL (1966) p. II-34
▽	N=60 Shields 6.35×10^{-6} m thick Mylar Single-Aluminized Embossed 60 Spacers White Nylon Netting	2.54	<.96	209 261.5 296 320 378	176 236.5 152.5 301.5 357	Lockheed/Huntsville Cylindrical	Hale (1969) p. 43

[a] Largest quoted value.

INTENTIONALLY BLANK PAGE

MULTILAYER INSULATIONS

Normal Heat Transfer

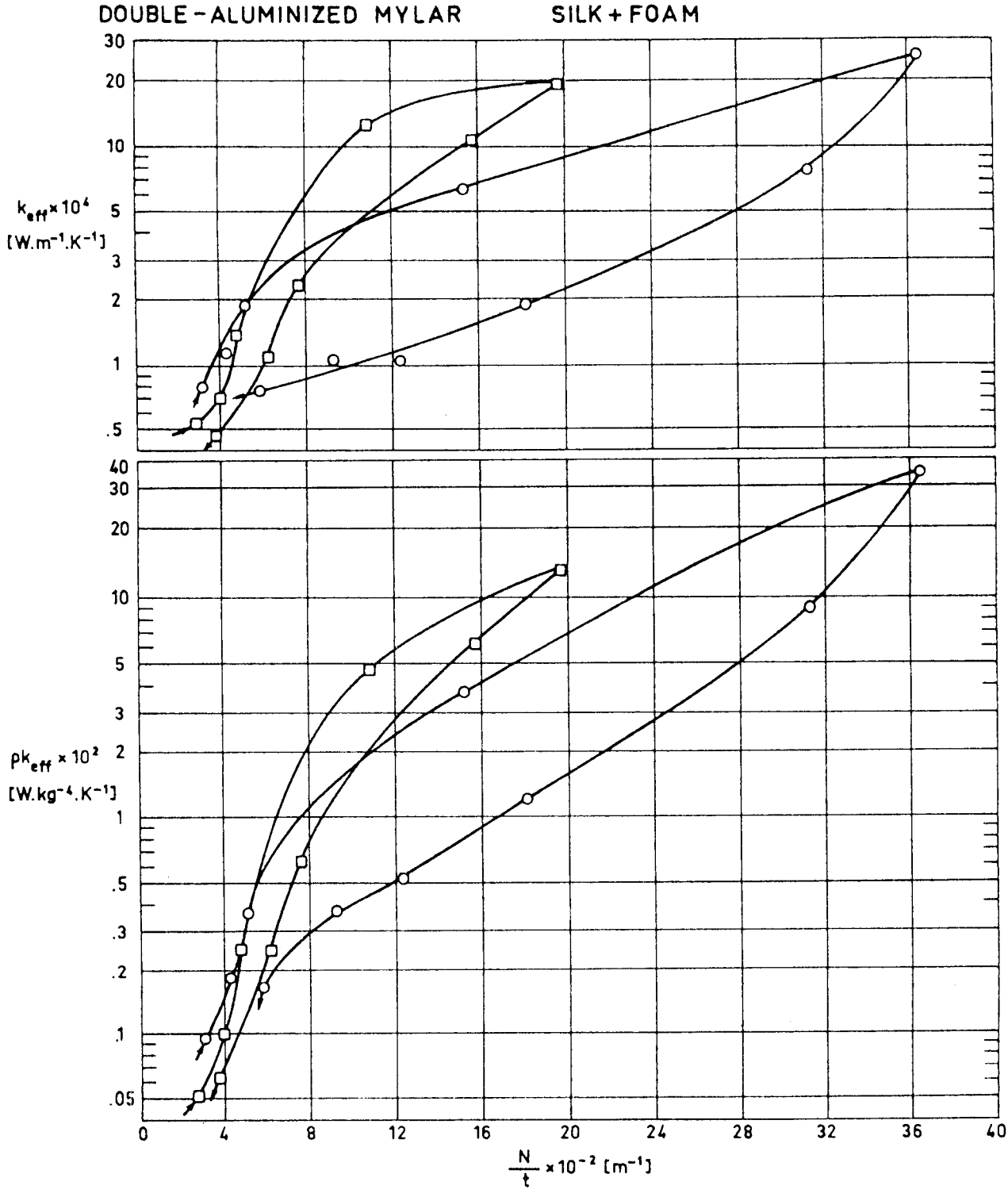

Fig 3-60a. Effective thermal conductivity, k_{eff}, and product of apparent density and effective thermal conductivity, ρk_{eff}, vs. the number of radiation shields per unit thickness, N/t. Arrows in curves indicated whether the system is being loaded or unloaded.

MULTILAYER INSULATIONS

Normal Heat Transfer

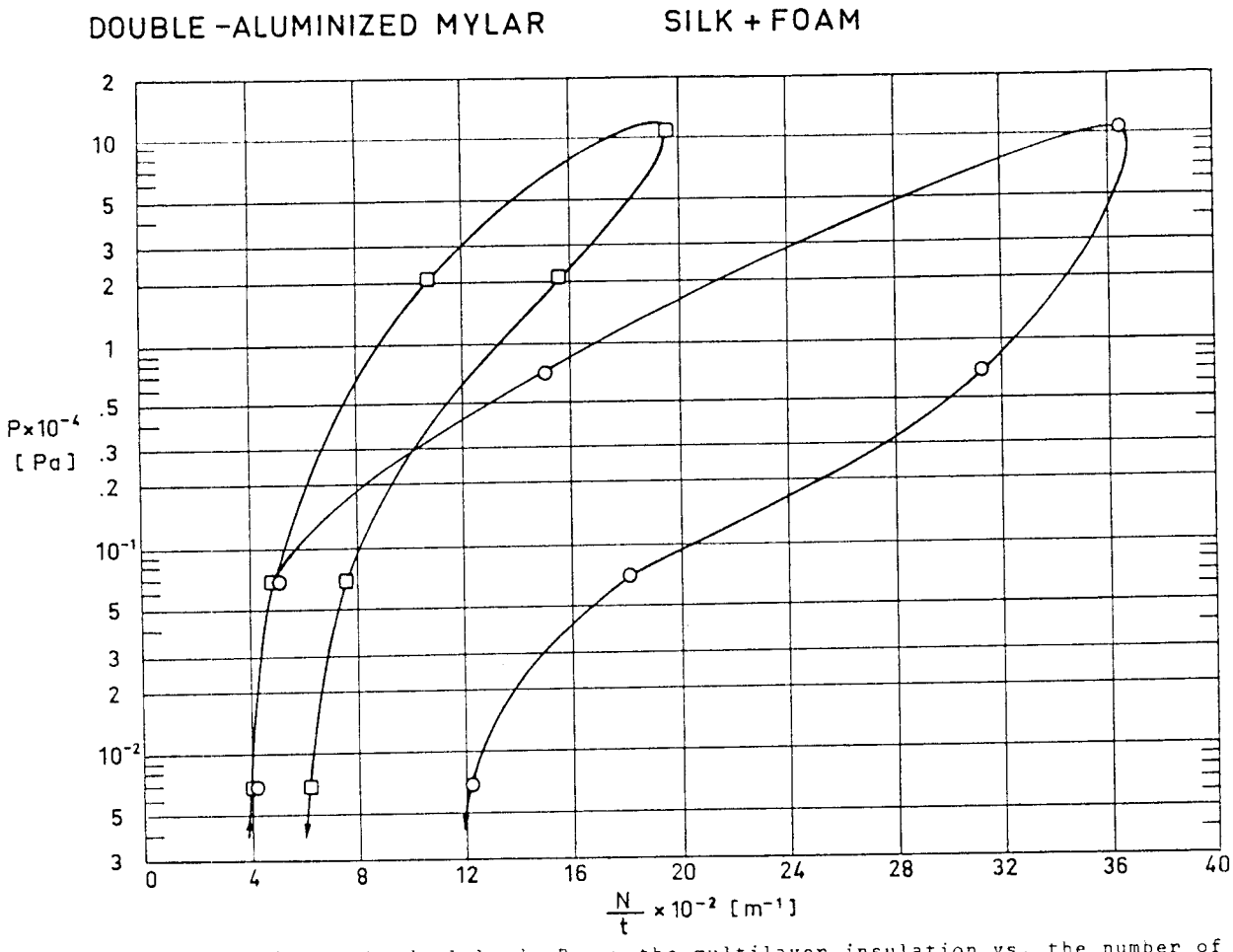

Fig 3-60b. Compressive mechanical load, P, on the multilayer insulation vs. the number of radiation shields per unit thickness, N/t.

Explanation

Key	Sample Description	$t \times 10^2$ [m] Uncompressed	$p \times 10^3$ [Pa]	T_H [K]	T_C [K]	Calorimeter Type	References
○	N=10 Shields. 6.35×10^{-6} m thick × .279 m diameter Mylar Double-Aluminized. 11 Spacers. 7.62×10^{-5} m thick × .305 m diameter Silk Netting having 2.54×10^{-3} m thick × 6.35×10^{-3} m wide × 5.72×10^{-2} m long flexible polyurethane foam (Scott Paper Co) strips heat sealed by a polyester film strip.	3.20 a	<6.67	294±3	77.5	ADL Model 12. Flat-Plate (double-guarded cold-plate).	ADL (1964) p. II-61.
□	Same as ○ except polyurethane foam rigid. A soft cusnion consisting of 3 layers of 1.78×10^{-3} m thick flexible polyurethane foam was placed between the test sample and the warm plate. The temperature of the face toward the sample of the cushion was monitored at 294 K.	3.60 a	<6.67	294±3	77.5	ADL Model 12. Flat-Plate (double-guarded cold-plate).	ADL (1966) p. II-62.

[a] Largest quoted value.

MULTILAYER INSULATIONS

Normal Heat Transfer

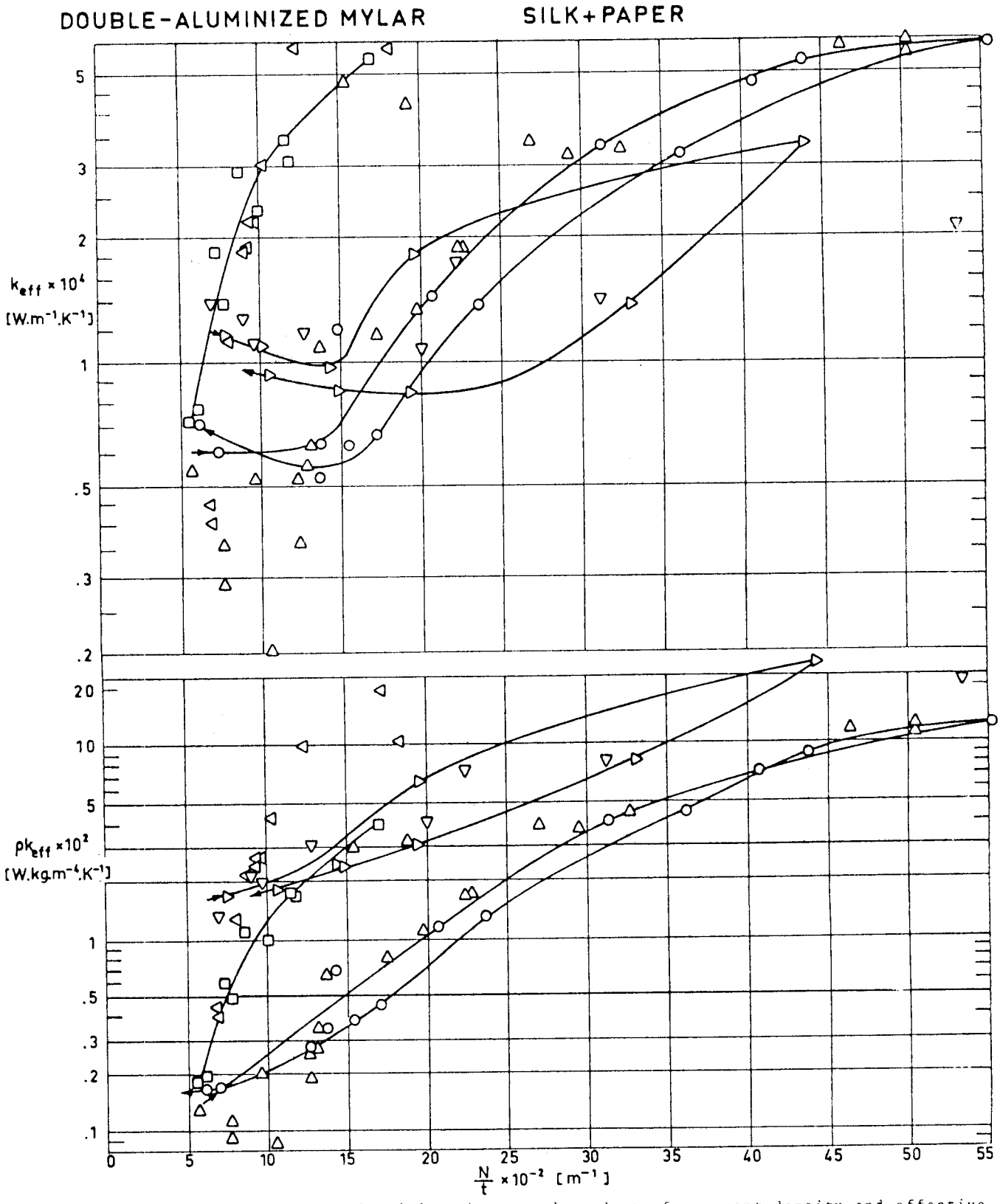

Fig 3-61a1. Effective thermal conductivity, k_{eff}, and product of apparent density and effective thermal conductivity, ρk_{eff}, vs. the number of radiation shields per unit thickness, N/t. Arrows in curves indicate whether the system is being loaded or unloaded.

MULTILAYER INSULATIONS

Normal Heat Transfer

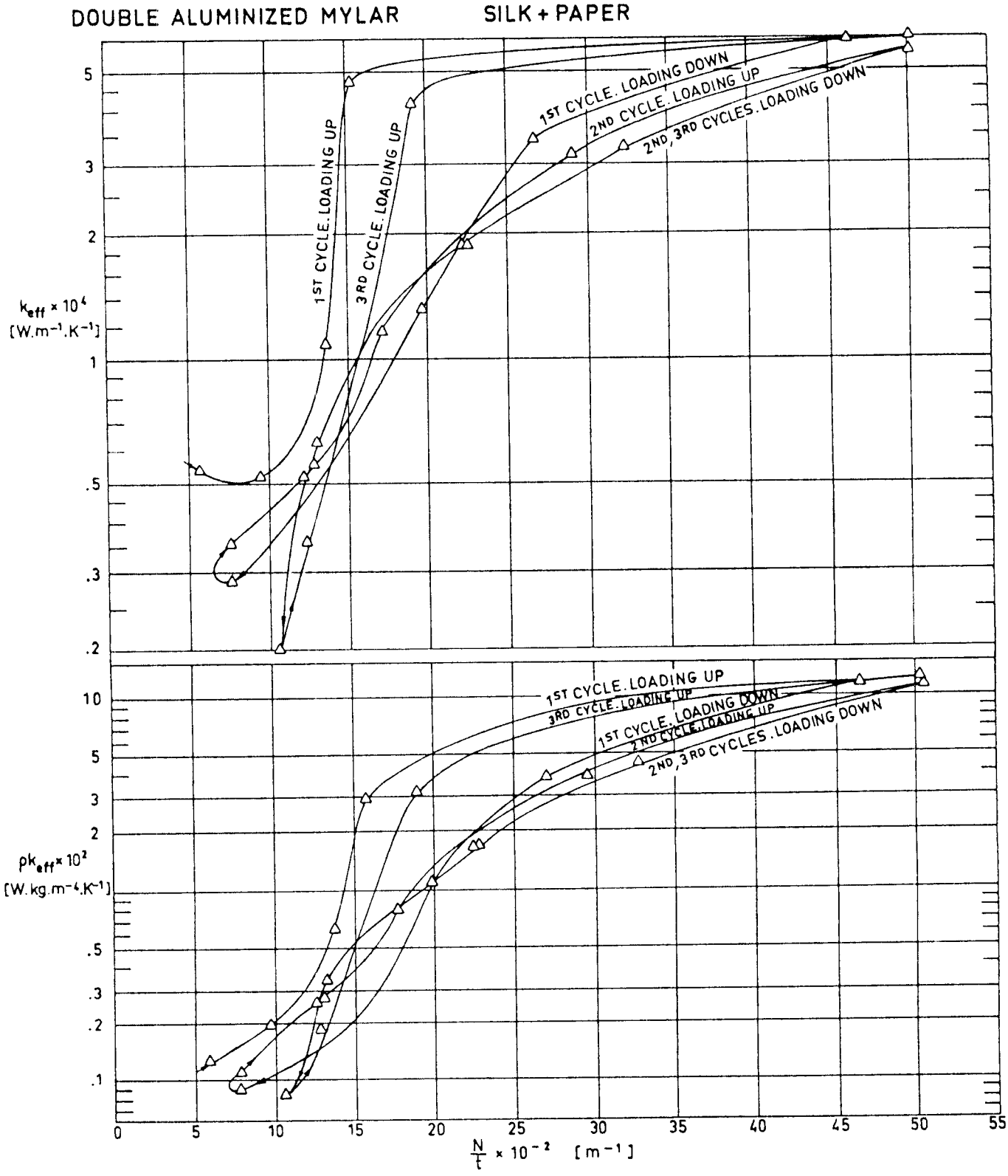

Fig 3-61a2. Effective thermal conductivity, k_{eff}, and product of apparent density and effective thermal conductivity, ρk_{eff}, vs. the number of radiation shields per unit thickness, N/t. Complete loading-unloading history of system Δ .

MULTILAYER INSULATIONS

Normal Heat Transfer

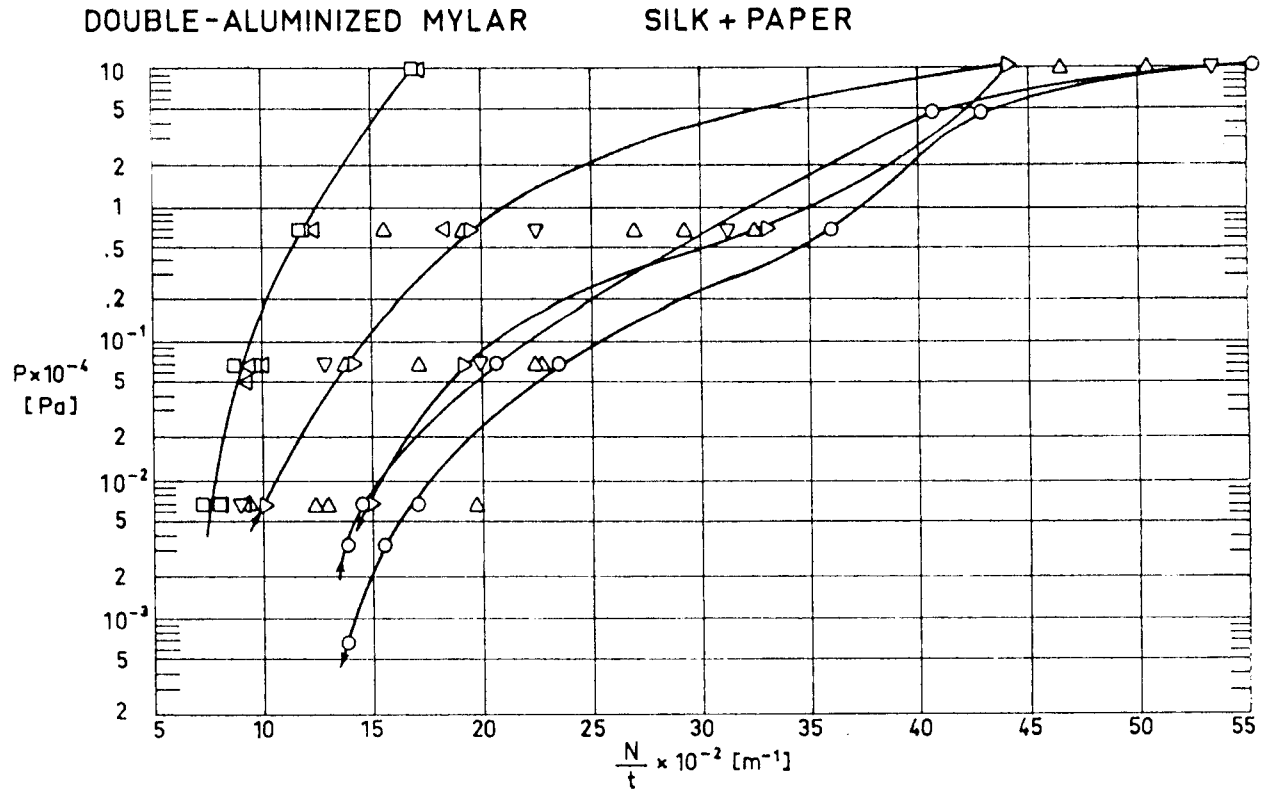

Fig 3-61b1. Compressive mechanical load, P, on the multilayer insulation vs. the number of radiation shields per unit thickness, N/t.

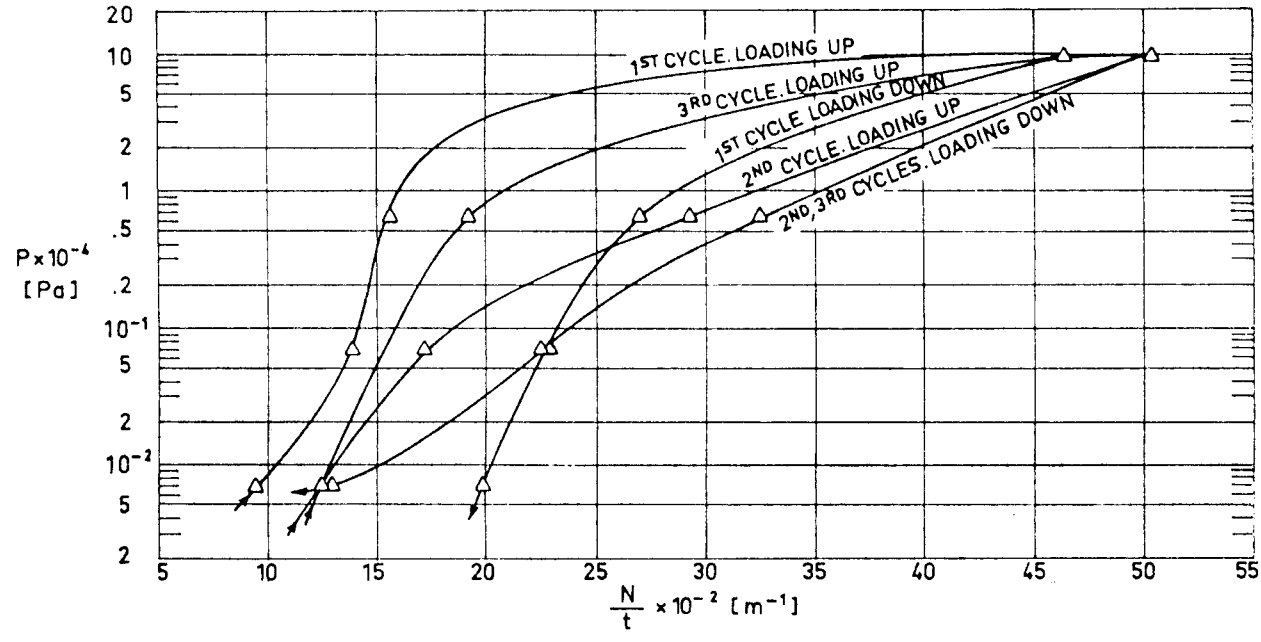

Fig 3-61b2. Compressive mechanical load, P, on the multilayer insulation vs. the number of radiation shields per unit thickness, N/t. Complete loading-unloading history of system Δ .

MULTILAYER INSULATIONS

Normal Heat Transfer

DOUBLE-ALUMINIZED MYLAR SILK + PAPER

Explanation

Key	Sample Description	$t \times 10^2$ [m] Uncompressed	$p \times 10^3$ [Pa]	T_H [K]	T_C [K]	Calorimeter Type	References
○	N=10 Shields 6.35×10^{-6} m thick × × 2.79×10^{-1} m diameter Mylar Double-Aluminized 11 Spacers 7.62×10^{-5} m thick × × 3.05×10^{-1} m diameter Silk Netting plus 1.02×10^{-4} m thick Glass Paper strips 1.27×10^{-2} m wide sewed on both sides of silk netting 2.54×10^{-2} m apart	1.36[a]	<2.67	294± ±1.5	77.5	ADL Model 12 Flat-Plate (double-guarded cold-plate)	ADL (1966) p. II-45
□	N=10 Shields 6.35×10^{-6} m thick × × 2.79×10^{-1} m diameter Mylar Double-Aluminized 11 Spacers 7.62×10^{-5} m thick × × 3.05×10^{-1} m diameter Silk Netting plus 2.54×10^{-4} m thick Glass Paper sewed on both sides of silk netting	1.72[a]	<2.67	295±2	77.5	Same as ○	ADL (1966) p. II-46
△	N=10 Shields 6.35×10^{-6} m thick × × 2.79×10^{-1} m diameter Mylar Double-Aluminized 11 Spacers 7.62×10^{-5} m thick × × 3.05×10^{-1} m diameter Silk Netting plus 2.03×10^{-4} m thick Glass Paper strips 6.35×10^{-3} m wide sewed on both sides of silk netting 3.18×10^{-2} m apart	1.71[a]	<1.33	294±1	77.5	Same as ○	ADL (1966) pp. II-48, II-49
▽	N=10 Shields 6.35×10^{-6} m thick × × 2.79×10^{-1} m diameter Mylar Double-Aluminized 11 Spacers 7.62×10^{-5} m thick × × 3.05×10^{-1} m diameter Silk Netting plus 2.03×10^{-4} m thick Glass Paper disks 6.35×10^{-3} m diameter sewed on both sides of silk netting on 3.81×10^{-2} m centers with 1.52×10^{-4} m diameter thread	1.40[a]	<1.33	294±2	77.5	Same as ○	ADL (1966) p. II-52
▷	Same as ▽ although threads were removed	1.31[a]	<5.33	296±3	77.5	Same as ○	ADL (1966) p. II-55
◁	N=10 Shields 6.35×10^{-6} m thick × × 2.79×10^{-1} m diameter Mylar Double-Aluminized 11 Spacers 7.62×10^{-5} m thick × × 3.05×10^{-1} m diameter Silk Netting plus 22 disks 2.03×10^{-4} m thick Glass Paper .305 m diameter placed on both sides of silk netting	1.43[a]	<9.33	296±3	77.5	Same as ○	ADL (1966) p. II-56

[a] Initial Value.

MULTILAYER INSULATIONS

Normal Heat Transfer

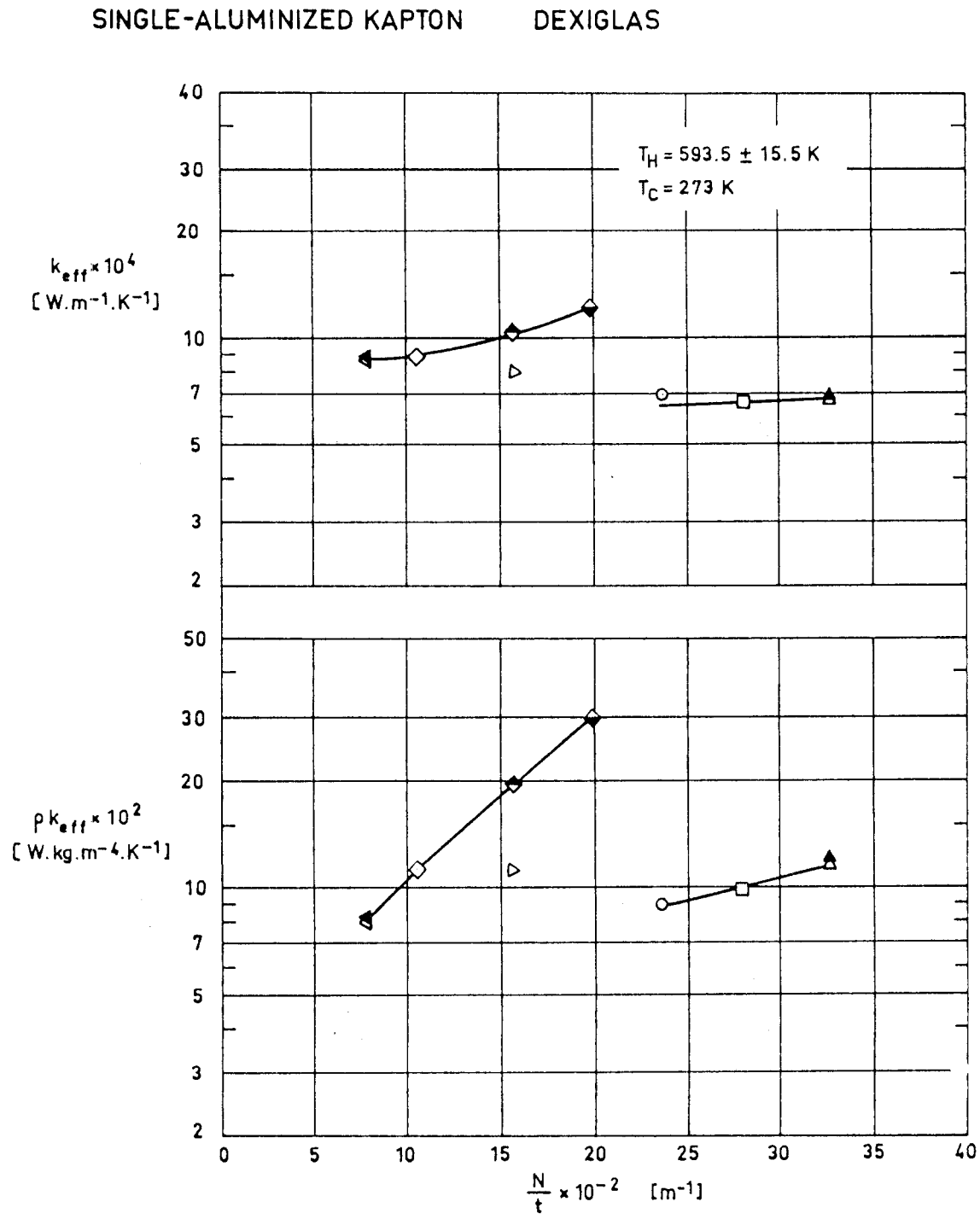

Fig 3-62a. Effective thermal conductivity, k_{eff}, and product of apparent density and effective thermal conductivity, ρk_{eff}, vs. the number of radiation shields per unit thickness, N/t.

MULTILAYER INSULATIONS

Normal Heat Transfer

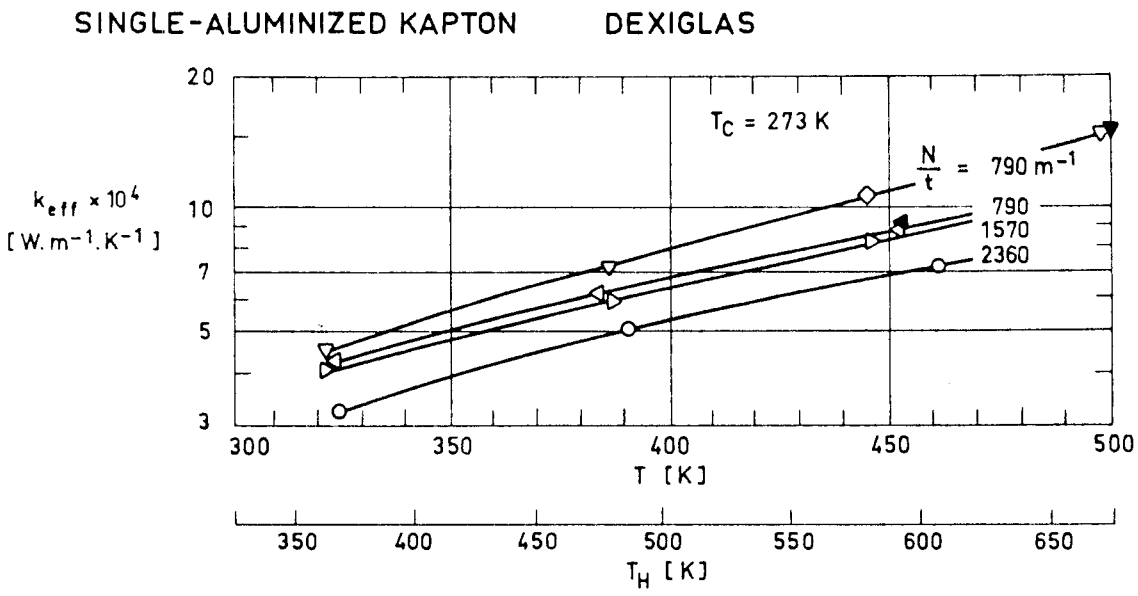

Fig 3-62c. Effective thermal conductivity, k_{eff}, as a function of the characteristic temperature, T.

Explanation

Key	Sample Description	$t \times 10^2$ [m] Uncompressed	$p \times 10^3$ [Pa]	T_H [K]	T_C [K]	T_E[a] [K]	Calorimeter Type	References
○	N=30 Shields 25.4×10^{-6} m thick Kapton Single-Aluminized 31 Spacers 76.2×10^{-6} m thick Dexiglas paper	1.27	<6.7	371 489 609	273 273 273		LMSC/Sunnyvale Flat-Plate	Cunnington et al. (1967) p. 66
□	Same as ○	1.07	<6.7	602	273		Same as ○	Same as ○
△	Same as ○	0.92	<6.7	582	273		Same as ○	Same as ○
▲	Same as ○	0.92	<6.7	602	273		Same as ○	Same as ○
▽	N=10 Shields 25.4×10^{-6} m thick Kapton Single-Aluminized 11 Spacers 230×10^{-6} m thick Dexiglas paper	1.27	<6.7	365 482 670	273 273 273	300 300 300	Same as ○	Cunnington et al. (1967) p. 68
▼	Same as ▽	1.27	<6.7	675	273	420	Same as ○	Same as ▽
▷	Same as ▽	.635	<6.7	365 482 584	273 273 273		Same as ○	Same as ▽
◁	N=10 Shields 25.4×10^{-6} m thick Kapton Single-Aluminized 11 Spacers 380×10^{-6} m thick Dexiglas paper	1.27	<6.7	368 478 595	273 273 273	300 300 300	Same as ○	Cunnington et al. (1967) p. 69
◀	Same as ◁	1.27	<6.7	596	273	420	Same as ○	Same as ◁
◇	Same as ◁	.950	<6.7	586	273		Same as ○	Same as ◁
◈	Same as ◁	.635	<6.7	582	273		Same as ○	Same as ◁
◆	Same as ◁	.508	<6.7	578	273		Same as ○	Same as ◁

[a] Edge boundary heat exchangers have been used in some experiments to evaluate the two-dimensional effects. T_E is the resulting edge temperature.

MULTILAYER INSULATIONS

Normal Heat Transfer

SINGLE-ALUMINIZED KAPTON TISSUGLAS

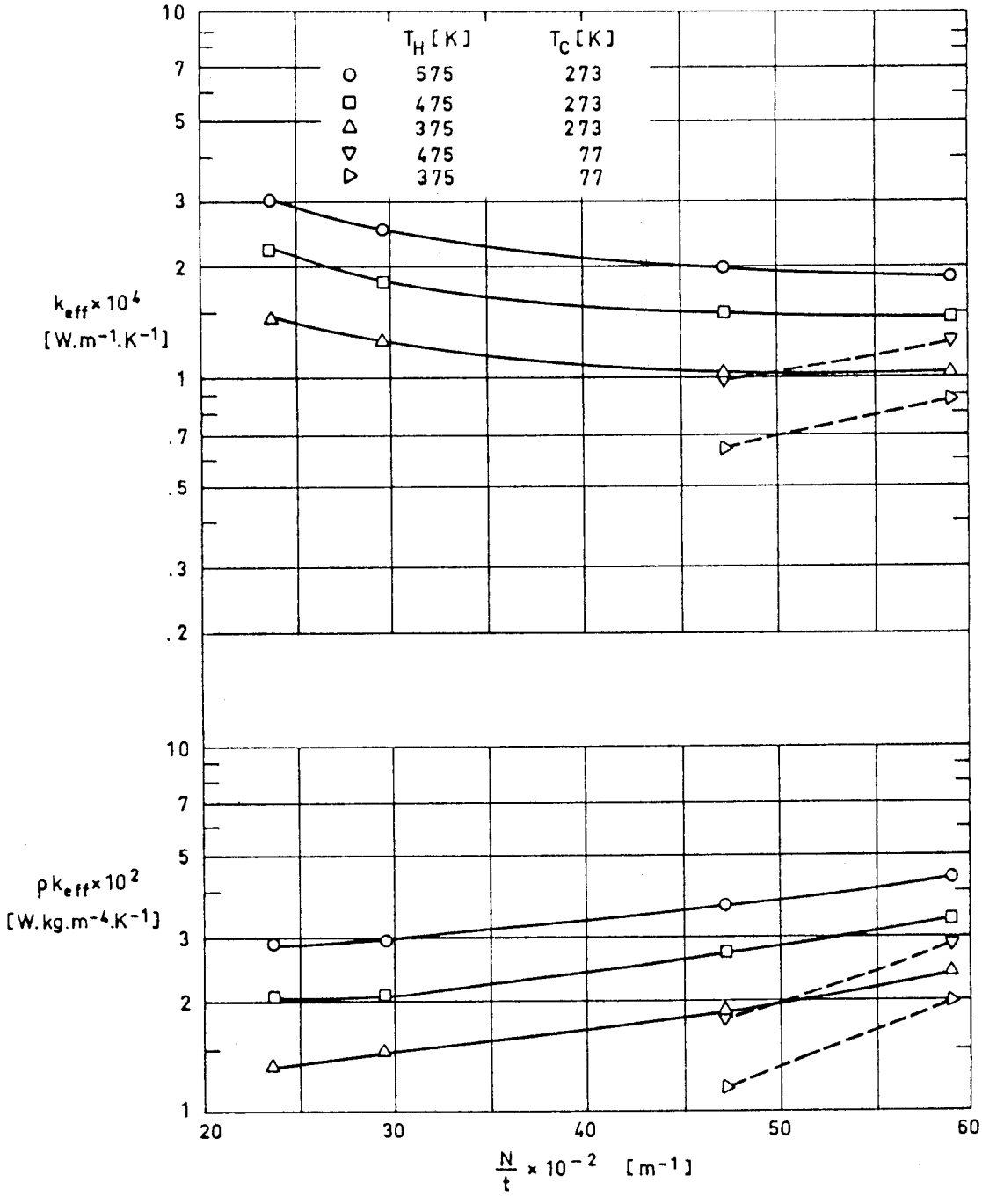

Fig 3-63a. Effective thermal conductivity, k_{eff}, and product of apparent density and effective thermal conductivity, ρk_{eff}, vs. the number of radiation shields per unit thickness, N/t.

MULTILAYER INSULATIONS

Normal Heat Transfer

SINGLE-ALUMINIZED KAPTON TISSUGLAS

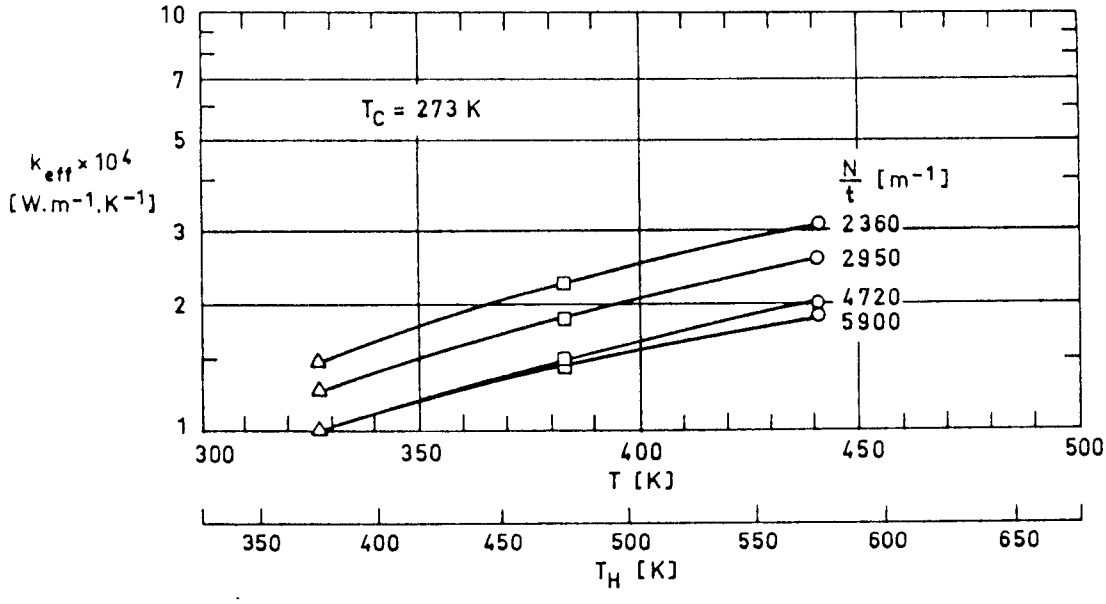

Fig 3-63c. Effective thermal conductivity, k_{eff}, as a function of the characteristic temperature, T.

Explanation

Key	Sample Description	$t \times 10^2$ [m] Uncompressed	$p \times 10^3$ [Pa]	T_H [K]	T_C [K]	Calorimeter Type	References
O	N=15 Shields 25.4×10^{-6} m thick Kapton Single-Aluminized 16 Spacers 15.2×10^{-6} m thick Tissuglas A single layer of Tissuglas for each spacer	0.64[a]	<6.7	575	273	LMSC/Sunnyvale Flat-Plate	Cunnington et al. (1967) p. 72
□	Same as O	0.64[a]	<6.7	475	273	Same as O	Same as O
△	Same as O	0.64[a]	<6.7	375	273	Same as O	Same as O
▽	Same as O	0.64[a]	<6.7	475	77	Same as O	Same as O
▷	Same as O	0.64[a]	<6.7	375	77	Same as O	Same as O

[a] Deduced from layer density.

Comments: To calculate ρ the following values have been used:
Aluminized Kapton: 3.58×10^{-2} Kg/m^2 (Cunnington et al. (1967), p. 47)
Tissuglas : 3.4×10^{-3} Kg/m^2 (Cunnington et al. (1967), p. 65)

MULTILAYER INSULATIONS

Normal Heat Transfer

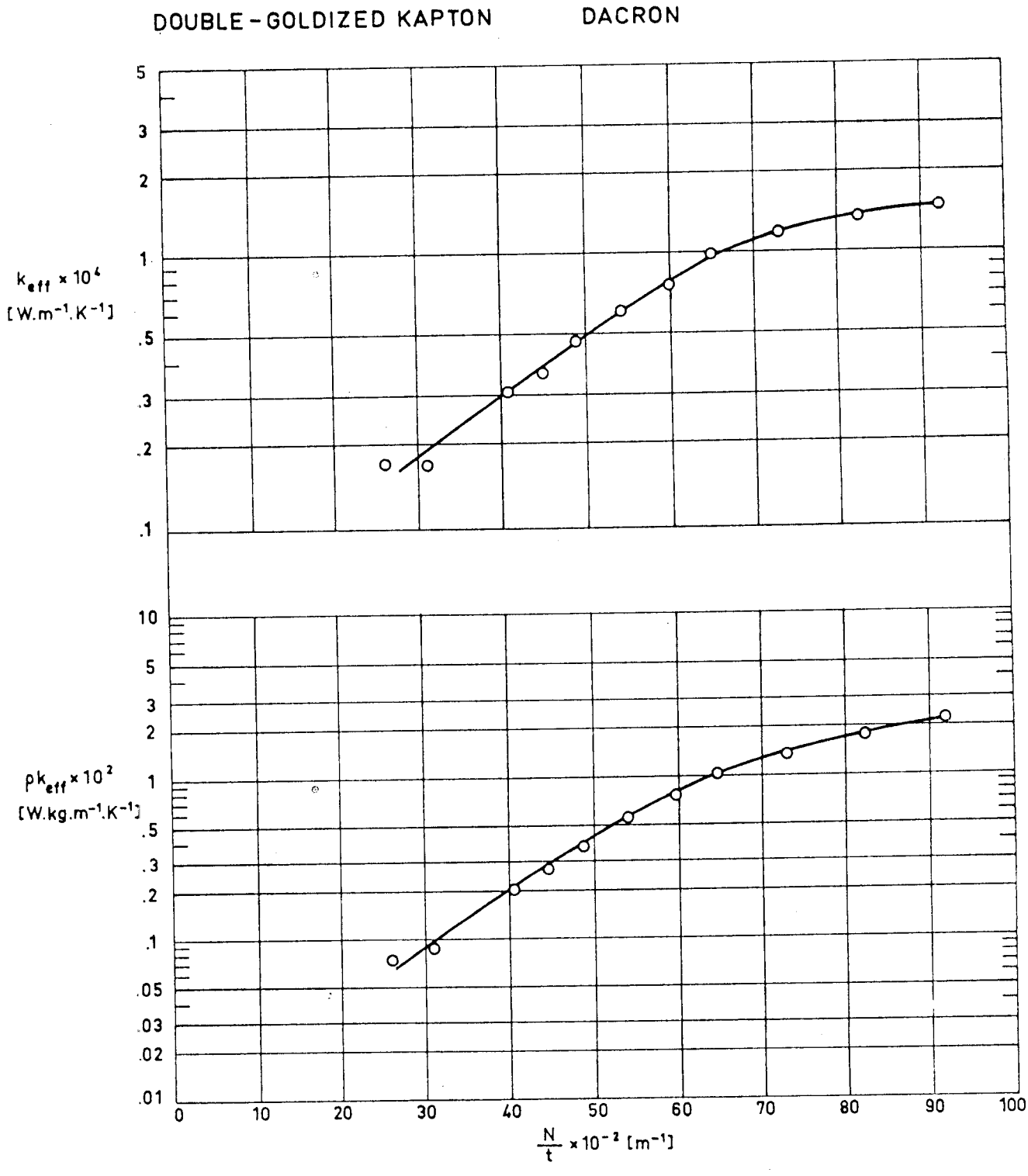

Fig 3-64a. Effective thermal conductivity, k_{eff}, and product of apparent density and effective thermal conductivity, ρk_{eff}, vs. the number of radiation shields per unit thickness, N/t.

MULTILAYER INSULATIONS

Normal Heat Transfer

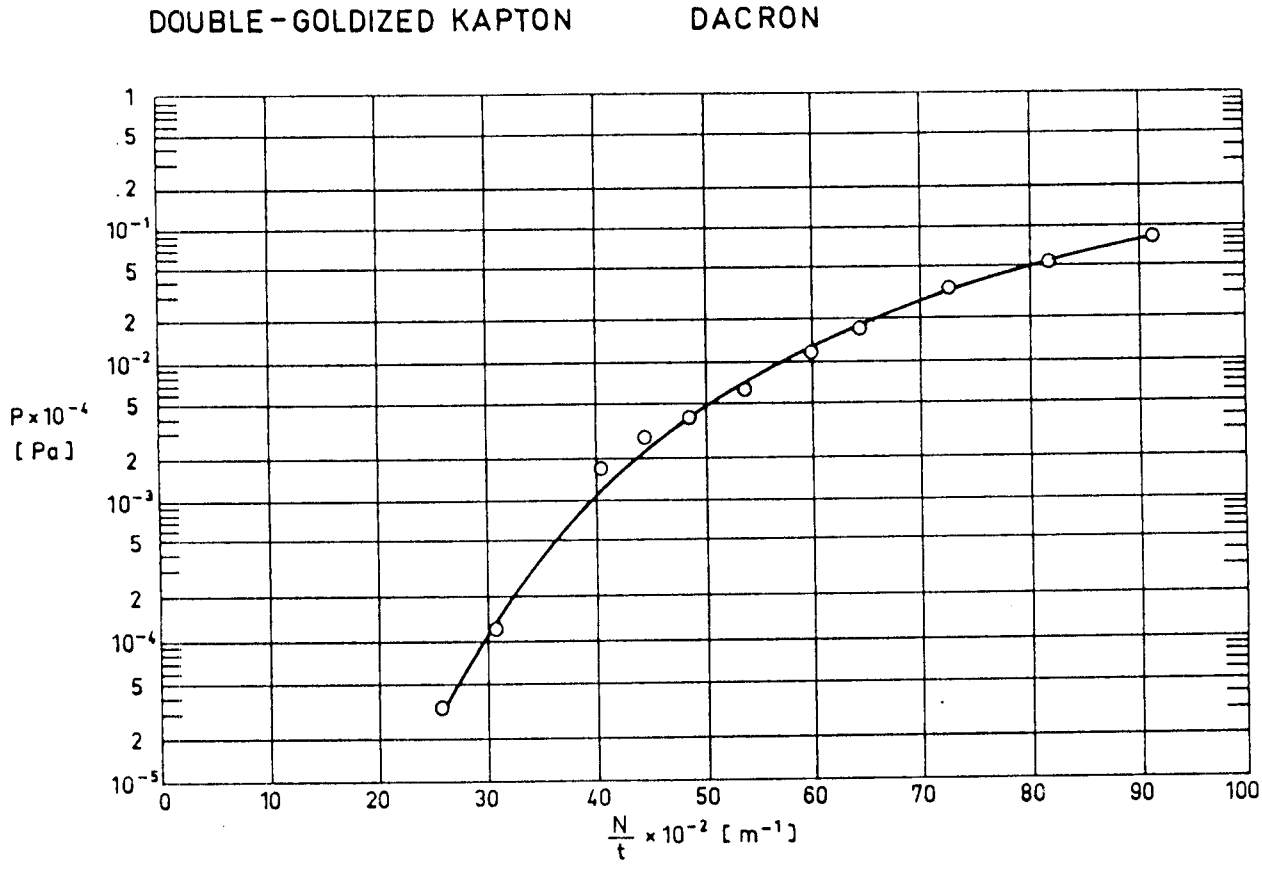

Fig 3-64b. Compressive mechanical load, P, on the multilayer insulation vs. the number of radiation shields per unit thickness, N/t.

Explanation

Key	Sample Description	$t \times 10^2$ [m] Uncompressed	$p \times 10^3$ [Pa]	T_H [K]	T_C [K]	Calorimeter Type	References
O	N=10 Shields. 6.35×10^{-6} - 8.13×10^{-6} m thick Kapton. Double-Goldized. 10 Spacers. 16.7×10^{-5} m thick Dacron b4A.	.386 [a]	<.13	~288	77.5	Double-guarded cold-plate.	Holmes, McCrary & Krause (1972) p. 794. Krause (1974).

[a] Largest quoted value.

MULTILAYER INSULATIONS

Normal Heat Transfer

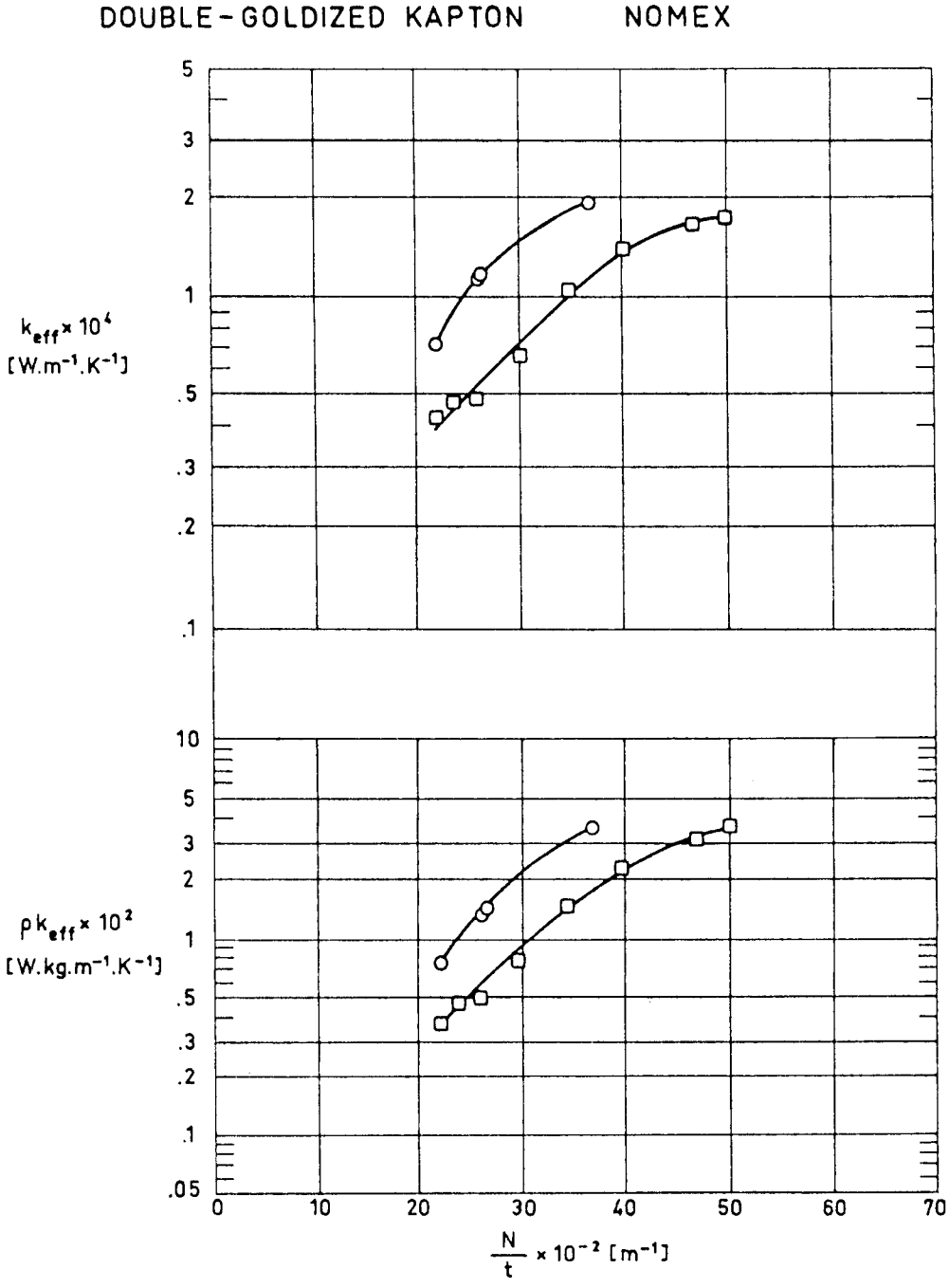

Fig 3-65a. Effective thermal conductivity, k_{eff}, and product of apparent density and effective thermal conductivity, ρk_{eff}, vs. the number of radiation shields per unit thickness, N/t.

MULTILAYER INSULATIONS

Normal Heat Transfer

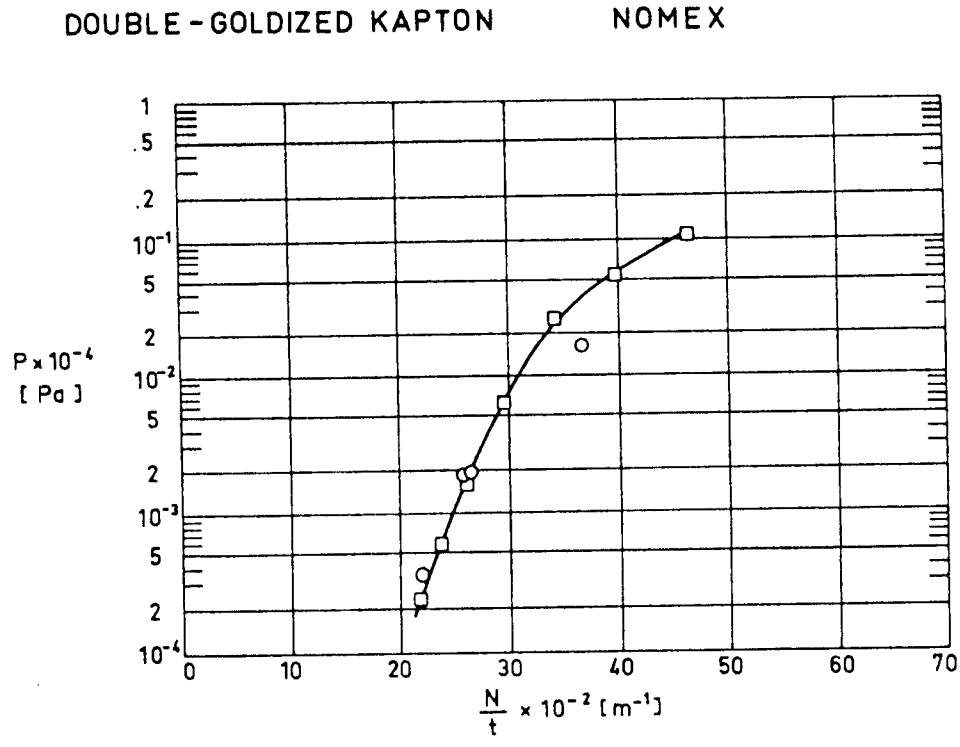

Fig 3-65b. Compressive mechanical load, P, on the multilayer insulation vs. the number of radiation shields per unit thickness, N/t.

Explanation

Key	Sample Description	$t \times 10^2$ [m] Uncompressed	$p \times 10^3$ [Pa]	T_H [K]	T_C [K]	Calorimeter Type	References
○	N=10 Shields. 6.35×10^{-6} - 8.13×10^{-6} m thick Kapton. Double-Goldized. 10 Spacers. 17.8×10^{-5} m thick Nomex HT-287.	.459 [a]	<.13	~288	77.5	Double-guarded cold-plate.	Holmes, McCrary & Krause (1972) p. 794. Krause (1974).
□	N=10 Shields. 6.35×10^{-6} - 8.13×10^{-6} m thick Kapton. Double-Goldized. 10 Spacers. 31.8×10^{-5} m thick Nomex HT-96.	.462 [a]	<.13	~288	77.5	Same as ○.	Same as ○.

[a] Largest quoted value.

MULTILAYER INSULATIONS

Normal Heat Transfer

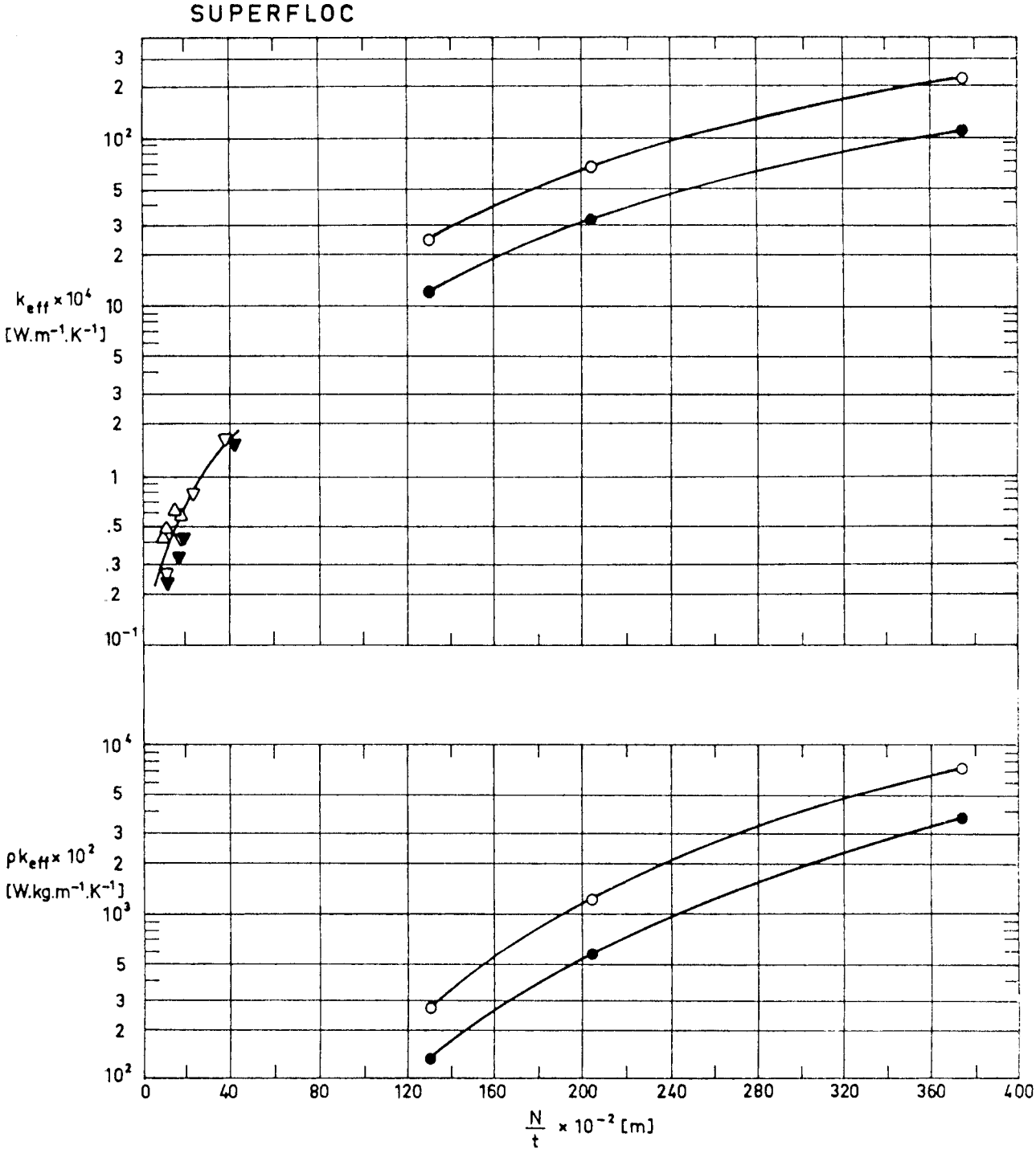

Fig 3-66a. Effective thermal conductivity, k_{eff}, and product of apparent density and effective thermal conductivity, ρk_{eff}, vs. the number of radiation shields per unit thickness, N/t.

MULTILAYER INSULATIONS

Normal Heat Transfer

SUPERFLOC

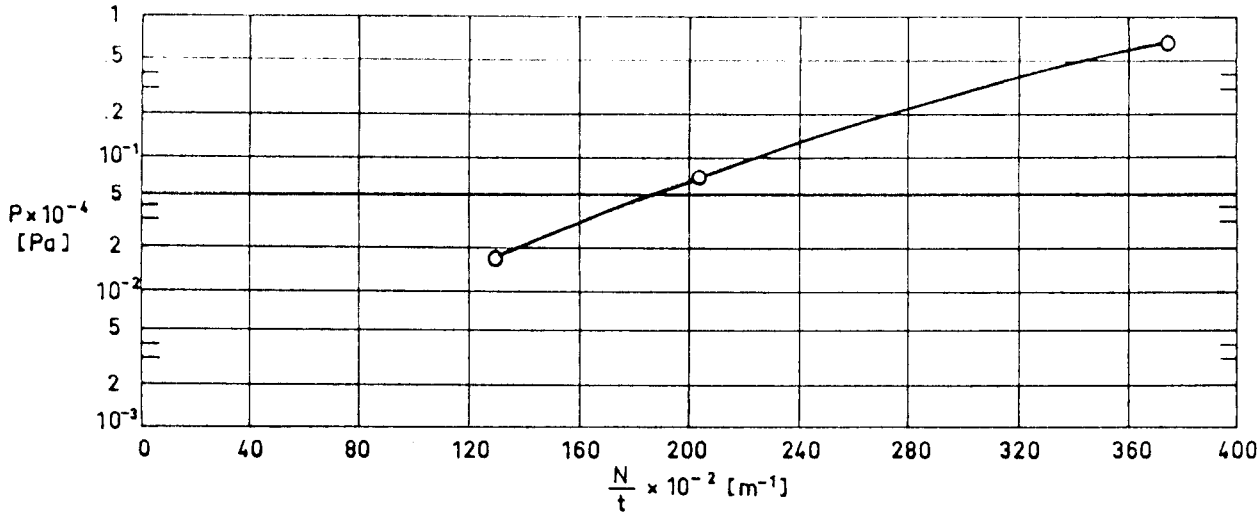

Fig 3-66b. Compressive mechanical load, P, on the multilayer insulation vs. the number of radiation shields per unit thickness, N/t.

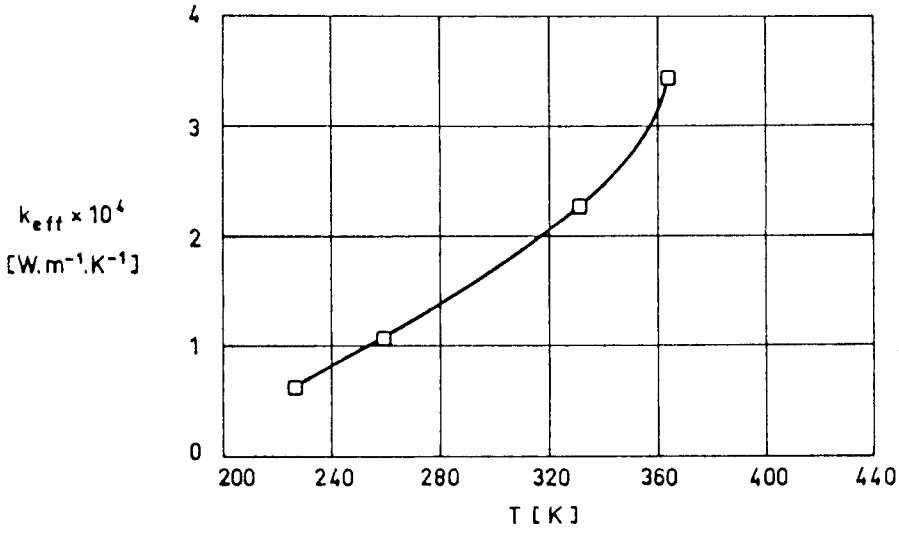

Fig 3-66c. Effective thermal conductivity, k_{eff}, as a function of the characteristic temperature, T.

MULTILAYER INSULATIONS

Normal Heat Transfer

SUPERFLOC

Explanation

Key	Sample Description	$t \times 10^2$ [m] Uncompressed	$p \times 10^3$ [Pa]	T_H [K]	T_C [K]	Calorimeter Type	References
○	Superfloc.			255	255		Hale (1969) p. 46.
●	Same as ○ .			222	22.2		Same as ○ .
□	N=22 Shields. 6.35×10^{-6} m thick Mylar Double-Aluminized Separated by flocking of glass fibers 1.27×10^{-4} m long on 1.27×10^{-2} m centers.	2.54		230 262.5 335.5 368	225 257 330 361	Lockheed/Huntsville Cylindrical	Scollon & Carpitella (1970) p. B-13. After Hale et al. (1967).
△	Mylar Double-Aluminized Superfloc $.95 \times 10^{-2}$ m spacing.			300	77.5		Leonhard & Hyde (1971). p. 655.
▽	N=15 Shields. 6.35×10^{-6} m thick Kapton. Double-Goldized Separated by flocking of Dacron tufts $1.57 \times \times 10^{-3}$ m diameter, 1.02×10^{-3} m length on 1.27×10^{-2} m centers. Adhesive Crest 7343 Silane modified.	1.27 [a]	<1.33	300	77.5	ADL Model 12 Flat-Plate (double-guarded cold-plate).	Same as △ .
▼	Same as ▽ except tufts placed on $.95 \times 10^{-2}$ m centers.	1.27 [a]	<1.33	300	77.5	Same as ▽ .	Same as △ .

[a] Largest quoted value.

INTENTIONALLY BLANK PAGE

MULTILAYER INSULATIONS
Lateral Heat Transfer

3.12. LATERAL HEAT TRANSFER

Multilayer insulations are usually designed to reduce the heat transfer normal to the surface of the insulation. However, these systems have thermal conductivities parallel to the layers which are 10^3 to 10^6 times greater than those perpendicular to them. As a consecuence, the efficiency of the system may be impaired by three-dimensional effects, as occurs in the cases of edges, joints and penetrations.

Data concerning the effective lateral thermal conductivity, $k_{eff\parallel}$, of typical multilayer systems are plotted against the characteristic temperature, T, in the following sheets.

The effective thermal conductivity is given by

$$k_{eff\parallel} = \frac{Q}{A} \frac{L}{T_H - T_C}$$

where: A, Cross-sectional area. $[m^2]$.

L, Specimen length. $[m]$.

Q, Heat transfer rate along the insulation. $[W]$.

T_C, Cold boundary temperature. $[K]$.

T_H, Hot boundary temperature. $[K]$.

The cross-sectional area, A, may be defined either as the bulk cross-sectional area, A_b, or the metallic cross-sectional area, A_m. The relationship between $k_{eff\parallel,b}$ (based on A_b), and $k_{eff\parallel,m}$ is:

$$k_{eff\parallel,b} = k_{eff\parallel,m} \, j \, t_c \frac{N}{t}$$

where: N, Number of radiation shields.

MULTILAYER INSULATIONS

Lateral Heat Transfer

j, Numerical factor. j=1 for single-coated layers, and j=2 for double-coated layers.

t, Total thickness of the insulation. [m].

t_c, Metallic-coating thickness. [m].

Throughout this compilation only the form $k_{eff\parallel,m}$ of $k_{eff\parallel}$ will be used, although the subscript $\parallel,m$ will be deleted to simplify the notation. This choice is advantageous when trying to correlate the experimental data with the results of existing theoretical models (Tien, Jagannathan & Chan (1972)).

Based on similar considerations, the characteristic temperature used to plot the data is defined as

$$T = \sqrt[3]{\frac{T_H^4 - T_C^4}{4(T_H - T_C)}}$$

The theory predicts that in the optically thick case ($aL>>h$) k_{eff} is a linear function of T^3. In the parenthetic inequality, a is the transmission constant depending on the shield surface reflectance and the spacer scattering coefficient, and h is the spacing between neighboring shields. This optically thick condition is fulfilled in many actual situations of interest to MLI systems.

MULTILAYER INSULATIONS

Lateral Heat Transfer

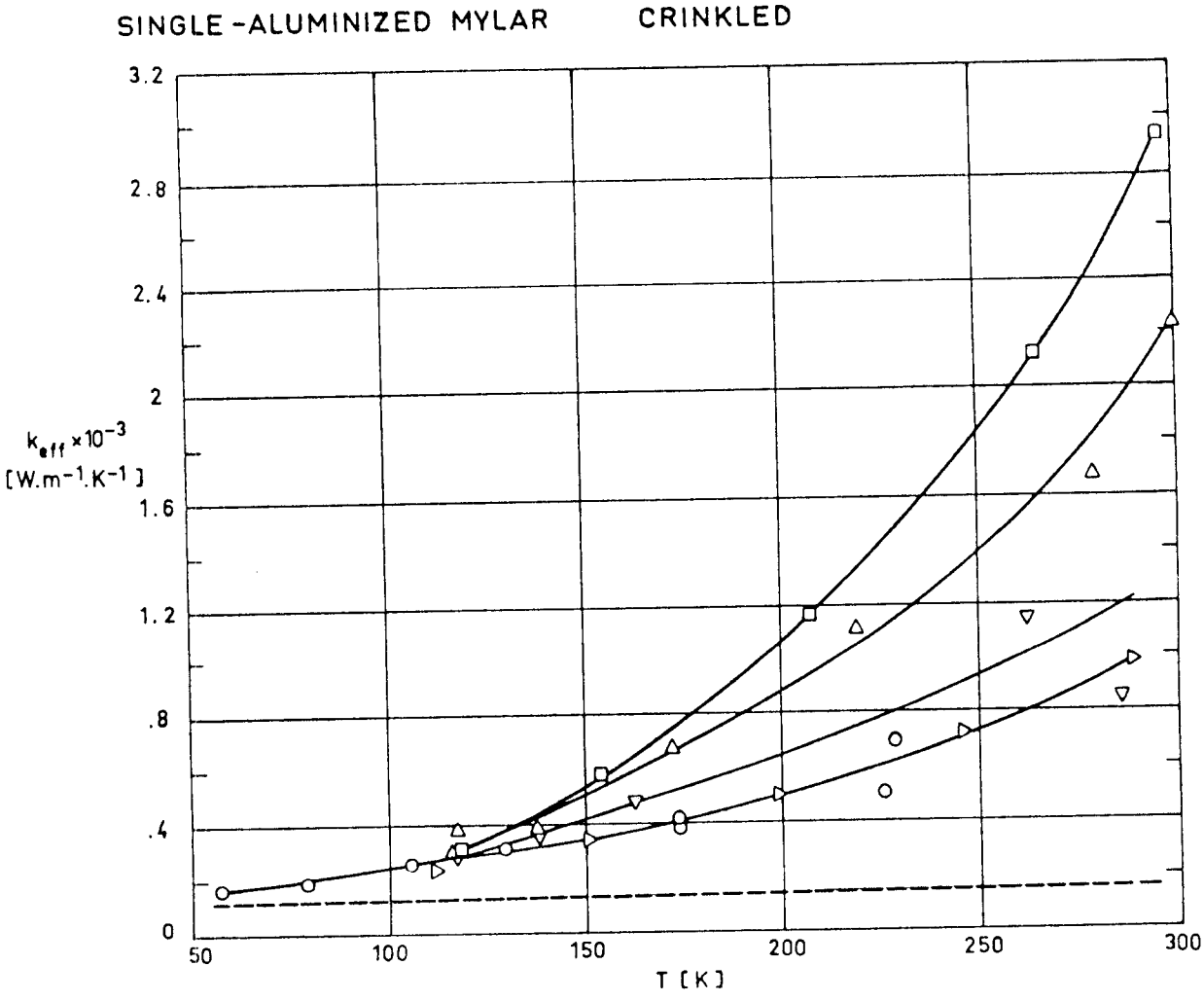

Fig 3-67. Lateral effective thermal conductivity, k_{eff}, as a function of characteristic temperature, T.

Explanation

All shields, unless otherwise stated, are 6.35×10^{-6} m thick Mylar Single-Aluminized, Crinkled.

Key	n_s	N/t [m^{-1}]	L [m]	$t_c \times 10^{10}$ [m]	Method used to measure t_c	$p \times 10^3$ [Pa]	Apparatus	References
○		2050	.101 and .280	300	Electrical Resistance	<1.33	Cylindrical	Vliet & Coston (1968) p. 674
□		1380	.0762 and .152	256	Electrical Resistance	1.33×10^{-3}	Cylindrical	And oulakis (1970) p. 4
△		1850	.0762 and .152	256	Electrical Resistance	1.33×10^{-3}	Cylindrical	Androulakis (1970) p. 4
▽		3230	.0762 and .152	256	Electrical Resistance	1.33×10^{-3}	Cylindrical	Androulakis (1970) p. 4
▷		4530	.0762 and .152	256	Electrical Resistance	1.33×10^{-3}	Cylindrical	Androulakis (1970) p. 4
---- Thermal conductivity of the metallic coating estimated by Tien et al. (1972), p. 120.								

MULTILAYER INSULATIONS

Lateral Heat Transfer

DOUBLE-ALUMINIZED MYLAR DEXIGLAS

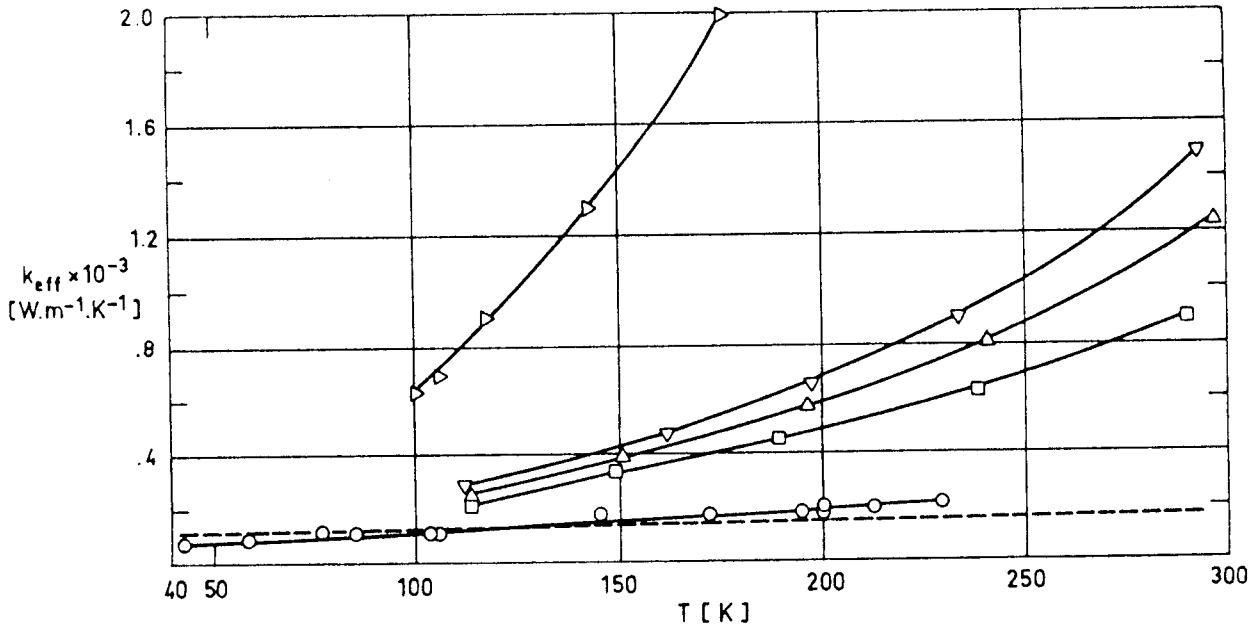

Fig 3-68. Lateral effective thermal conductivity, k_{eff}, as a function of characteristic temperature, T.

Explanation

All shields, unless otherwise stated, are 6.35×10^{-6} m thick Mylar Double-Aluminized. The spacers are Dexiglas 71×10^{-6} m thick, unless otherwise stated. The number, n_s, of spacer layers per shield is given below.

Key	n_s	N/t [m^{-1}]	L [m]	$t_c \times 10^{10}$ [m]	Method used to measure t_c	$p \times 10^3$ [Pa]	Apparatus	References
○	1	3230	.0864 to .28	378 525[a]	Electrical Resistance Chemical Reduction	<1.33	Cylindrical	Coston & Vliet (1967) p. 914
□	1	3350	.0762 and .152	194	Electrical Resistance	1.33×10^{-3}	Cylindrical	Androulakis (1970) p. 4
△	2	2080	.0762 and .152	194	Electrical Resistance	1.33×10^{-3}	Cylindrical	Androulakis (1970) p. 4
▽	3	1380	.0762 and .152	194	Electrical Resistance	1.33×10^{-3}	Cylindrical	Androulakis (1970) p. 4
▷[b]	1	1000	.371	400±3	Electrical Resistance	$<1.33 \times 10^{-3}$	Plane (transient conduction)[c]	Tien et al. (1972) p. 120
----Thermal Conductivity of the metallic coating, measured by Tien et al. (1972), p. 120.								

[a] A value of $t_c = 400 \times 10^{-10}$ m has been assumed by Tien et al. (1972).

[b] Mylar thickness: 76.2×10^{-6} m. Dexiglas thickness 600×10^{-6} m.

[c] See Jagannathan & Tien (1971).

MULTILAYER INSULATIONS

Lateral Heat Transfer

DOUBLE-ALUMINIZED MYLAR NYLON NET

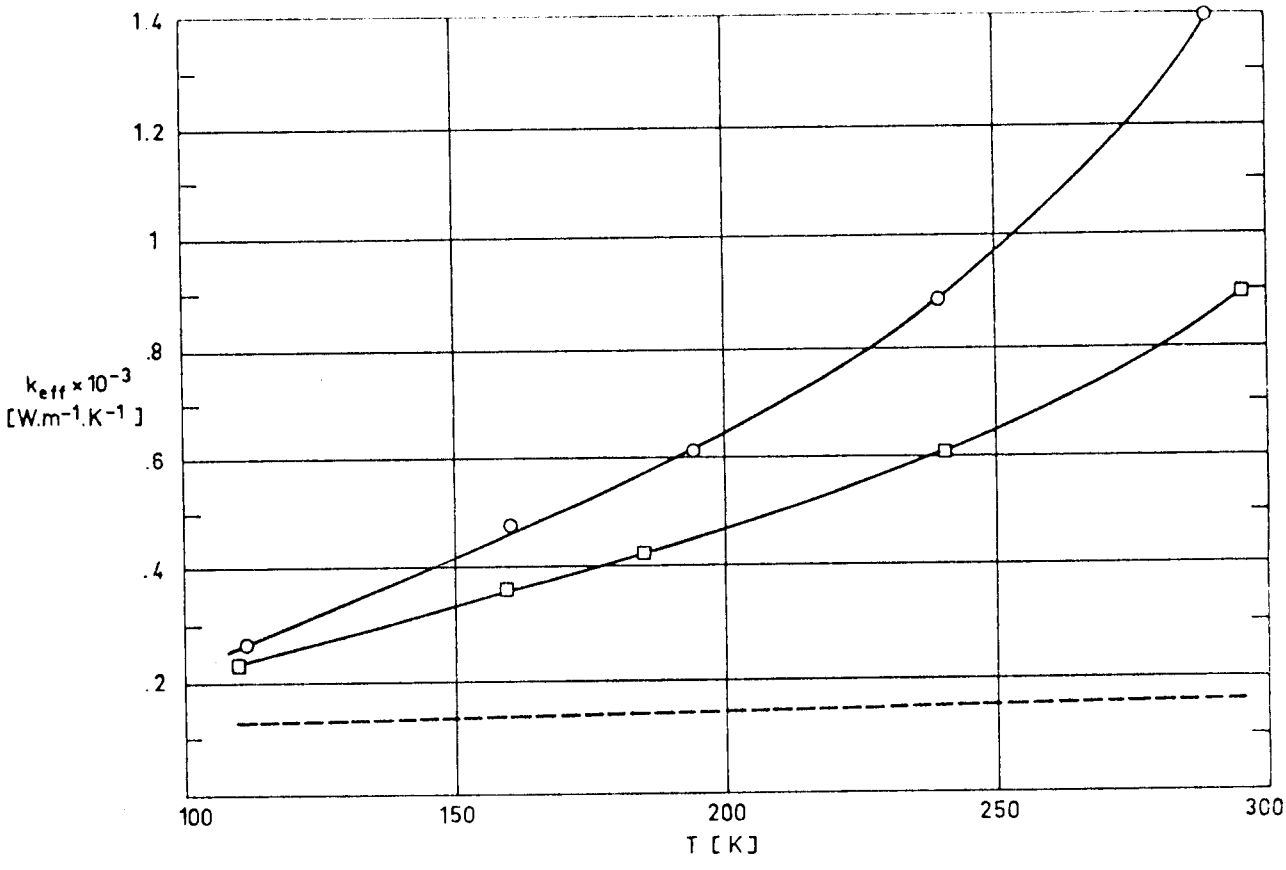

Fig 3-69. Lateral effective thermal conductivity, k_{eff}, as a function of characteristic temperature, T.

Explanation

All shields, unless otherwise stated, are 6.35×10^{-6} m thick Mylar Double-Aluminized, with perforations having an open area of 0.5% and a hole size of 1.17×10^{-3} m diameter. The spacers are 127×10^{-6} m thick Nylon net, unless otherwise stated. The number, n_s, of layers per shield is given below.

Key	n_s	N/t [m^{-1}]	L [m]	$t_c \times 10^{10}$ [m]	Method used to measure t_c	$p \times 10^3$ [Pa]	Apparatus	References
○	2	2080	.0762 and .152	194	Electrical Resistance	1.33×10^{-3}	Cylindrical	Androulakis (1970) p. 4
□	2	3310	.0762 and .152	194	Electrical Resistance	1.33×10^{-3}	Cylindrical	Androulakis (1970) p. 4
---- Thermal conductivity of the metallic coating, estimated by Tien et al. (1972), p. 121.								

MULTILAYER INSULATIONS

Lateral Heat Transfer

DOUBLE-ALUMINIZED MYLAR STRETCHED [a]

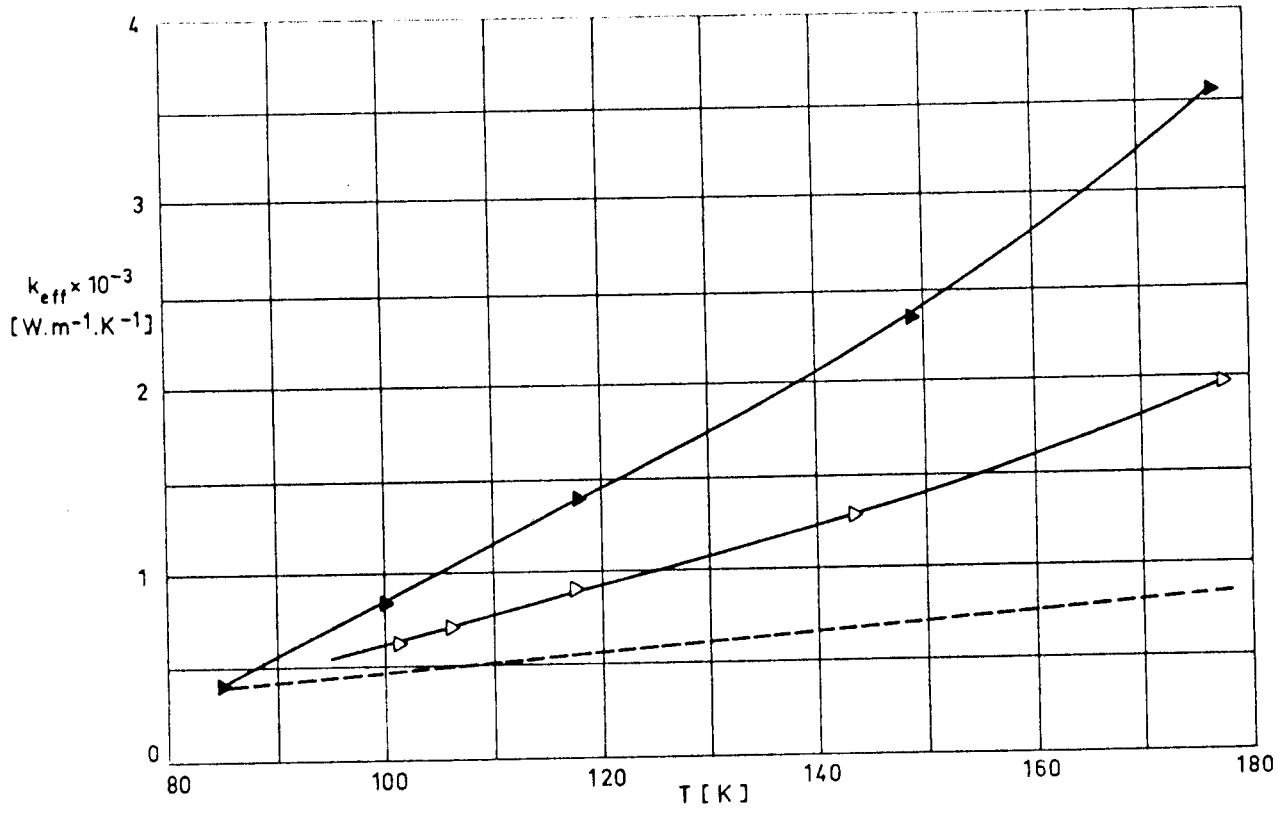

Fig 3-70. Lateral effective thermal conductivity, k_{eff}, as a function of characteristic temperature, T.

Explanation

The performance of a system of 32 parallel films, 76.2×10^{-6} m thick Mylar Double-Aluminized, Uncrinkled, is compared with that of a similar system of shields separated by layers of 600× $\times 10^{-6}$ m thick Dexiglas blotting paper. The number, n_s, of spacer layers per shields is given below.

Key	n_s	N/t [m^{-1}]	L [m]	$t_c \times 10^{10}$ [m]	Method used to measure t_c	$p \times 10^3$ [Pa]	Apparatus	References
▷	1	1000	.371	400±3	Electrical Resistance	$<1.33 \times 10^{-3}$	Plane (transient conduction)[a]	Tien et al. (1972) p. 120
▶	0	1000	.371	400±3	Electrical Resistance	$<1.33\ 10^{-3}$	Plane (transient conduction)[a]	Tien et al. (1972) p. 120
---- Thermal conductivity of the metallic coating, measured by Tien et al. (1972), p. 120.								

[a] See Jagannathan & Tien (1971).

3.13. EFFECT OF SINGULARITIES

The performance of an idealized MLI is normally degraded because of the discontinuities introduced in the insulation by securing devices, penetrations, overlaps, stitches, and by many other artifices used to contour flat layers onto complicated surfaces.

The aim of this item is to present data which can be used to evaluate the effect of these singularities on the heat transfer characteristics of an MLI system.

3.13.1. JOINTS

Although attempts have been made to numerically analyze the thermal degradation of high-performance MLI systems in the vicinity of a joint, the results obtained are too limited in scope. Hence, it is more straightforward to collect as many experimental data as possible in order to quantify the heat losses through MLI discontinuities and thus enable the designer to predict the blanket performance.

Experimental studies have been undertaken by several investigators with the aim of relating the heat transfer through an MLI blanket in which well defined discontinuities have been introduced, to the heat transfer characteristics of the same blanket without these discontinuities.

The total heat flow rate through the blanket can be expressed as:

$$Q_{total} = Q_{ideal} + \Delta Q \qquad (1)$$

MULTILAYER INSULATIONS
Effect of Singularities

where Q_{ideal} is the heat flow rate of an ideal blanket having the same surface area as the real one, while ΔQ accounts for the effect of the discontinuities. This effect is normally related to the boundary temperatures, T_H and T_C, and to the surface area of the blanket, A, by means of an effective emittance, $\Delta\varepsilon_{eff}$, such that

$$\frac{\Delta Q}{A} = \sigma \Delta \varepsilon_{eff}(T_H^4 - T_C^4) \qquad (2)$$

According to Knopf & Murray (1970), the influence of additional joints can be taken into account by means of the following linear relationship

$$\Delta\varepsilon_{eff} = \frac{1}{A} \sum_i C_i(T_H)L_i \qquad (3)$$

where:

C_i, joint coefficient for joint i. [m].

L_i, length of joint i. [m].

A limited amount of the data presented is based on an effective thermal conductivity, Δk_{eff},

$$\frac{\Delta Q}{A} = \Delta k_{eff} \frac{T_H - T_C}{t} \qquad (4)$$

t being the blanket thickness. These data have been obtained numerically. The geometrical model used for the computation is an infinitely long slab of width L. The singularity, an overlap, underlap or whatever could be, spans along the whole length of the slab. The presence of the singularity changes the heat flow through the blanket. If the width of an ideal slab transfering one-dimensionally the

MULTILAYER INSULATIONS
Effect of Singularities

same heat flow rate as the blanket considered is $L+L^*$, the effective thermal conductivity increment, Δk_{eff}, will be:

$$\Delta k_{eff} = \frac{L^*}{L} k_{eff\perp}$$

where $k_{eff\perp}$ is the normal effective thermal conductivity of the ideal blanket.

The length L^* is negative in the case of an edge rejecting heat to the space, because the slab transfers less heat, normally to its surface, than an equal slab having an adiabatic edge.

Experimental data regarding several types of joints are given in the following pages. Source data are based either on C_i, on $\Delta\varepsilon_{eff_i}$, or on $\Delta Q_i/A$; nevertheless, provided that sufficient details are available, it is not difficult to relate the different functions involved. Heavily bounded boxes in Table 3-21 indicate that the enclosed data have been taken from the quoted reference, while data in the lightly bounded boxes have been calculated by the compiler.

MULTILAYER INSULATIONS

Effect of Singularities

Table 3-21

Thermal Effects of Joints

Description	Sketch	$C_j \times 10^3$ [m]	$\Delta\varepsilon_{eff} \times 10^3$	$\Delta Q/A$ [W/m^2]	Comments
1 N = 15 Shields 3.17×10^{-5} m thick Mylar Double-Aluminized 1.58×10^{-3} m diam holes on 1.4×10^{-2} m centers 14 Spacers Nylon Net --- 7.62×10^{-2} m Simple Overlap	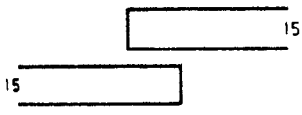	3.34 (T_H = 300 K)	1.80	1.70	From Crosby (1970). See Comments concerning configurations 21-26. The variation of effective emittance vs. overlap is given in Fig. 3-71.
2 N = 15 Shields 6.35×10^{-6} m thick Mylar Double-Aluminized 6.35×10^{-3} m diam holes on .15 m centers 14 Spacers 2.30×10^{-4}m honeycomb Nylon Net 2 Outer Layers 2.54×10^{-5} m thick Teflon 7.62×10^{-2} m Simple Overlap		2.20 (300 K)	2.51	1.12	From Crosby (1970), Stimpson & Jaworski(1972). See Comments concerning configurations 21-26. The variation of effective emittance vs. overlap is given in Fig. 3-71.
3 Two semi-infinite blankets having the following effective conductivities: $k_{eff\perp}$ =8.6×10^{-4} W.m^{-1}.K^{-1} (normal) $k_{eff\parallel}$ =1.7×10^{-2} W.m^{-1}.K^{-1} (lateral) --- 2.5×10^{-2} m Overlapping of alternate layers		.0938 (700 K)	.0469	.618	From Cunnington, Zierman, Funai & Lindahn (1967). Authors give their results in terms of the length, $L+L^*$, of an ideal blanket transfering one-dimensionally the same amount of heat that the real blanket of length L. Calculated values of L^* are given in the following figures: Overlapping effect: Fig 3-72. Underlapping effect: Fig 3-73. Edge effects: Fig 3-74. Values of $\Delta Q/A$ have been deduced from Eqs. (4) and (5) with: $k_{eff\perp}$=8.6×10^{-4} W.m^{-1}.K^{-1}. L = 1 m T_H= 700 K T_C= 295 K t = 2×10^{-2} m $\Delta\varepsilon_{eff}$ deduced from Eq. (2) with: σ=5.6697×10^{-8} W.m^{-2}.K^{-1}. $C_j(T_H)$ from Eq.(3) with L_j/A = .9 m^{-1}.
4 Two semi-infinite blankets having the following effective conductivities: $k_{eff\perp}$ = 8.6×10^{-4} W.m^{-1}.K^{-1} (normal) $k_{eff\parallel}$ = 1.7×10^{-2} W.m^{-1}.K^{-1} (lateral) --- 2.5×10^{-2} m Underlapping	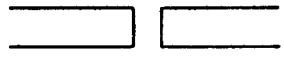	.660 (700 K)	.330	4.35	
5 A semi-infinite blanket having the following effective conductivities: $k_{eff\perp}$ = 8.6×10^{-4} W.m^{-1}.K^{-1} (normal) $k_{eff\parallel}$ = 1.7×10^{-2} W.m^{-1}.K^{-1} (lateral) --- Edge rejecting heat.	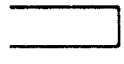	-.264 (700 K)	-.132	-1.74	
6 N = 30 Shields 6.35×10^{-6} m thick Mylar Single-Aluminized Crinkled --- Butt, laced buttons on 5.08×10^{-2} m spacing.	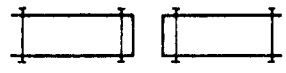	3.20 (366 K) --- 3.81 (389 K)	3.11 --- 3.70	1.68 --- 3.04	From Knopf & Murray (1970). See Comments in the next page.

(Continued onto next page)

MULTILAYER INSULATIONS

Effect of Singularities

Table 3-21 (Continued)

Thermal Effects of Joints

Description	Sketch	$C_i \times 10^3$ [m]	$\Delta\varepsilon_{effi} \times 10^3$	$\Delta Q_i/A$ [W/m^2]	Comments
7 N = 30 Shields 6.35×10^{-6} m thick Mylar Single-Aluminized Crinkled. ——— 7.62×10^{-2} m Shiplap, laced buttons on 5.08×10^{-2} m spacing.		.610 (T_H = 366 K) ——— .732 (389 K)	.593 ——— .711	.320 ——— .583	From Knopf & Murray (1970). Effective emittance of a blanket with joints was measured by using an internally heated cylinder over which the insulation was wrapped. The dimensions of the cilinder were .61 m in diameter, 1.52 to 1.83 m in length. The area of the test frame varied between 3.16 and 3.62 m^2. Length of a typical axial joint: 1.22 to 1.52 m. Length of a circumferential joint: 1.92 m. Temperatures were measured by eight internal and eleven external thermocouples. ε_{eff} is deduced from the heating power required to stabilize the temperature. One-dimensional flat-plate data concerning effective emittances of undisturbed specimens were obtained from different sources. $\Delta\varepsilon_{ieff}$ has been deduced by the compiler from the reported values of C_i, by using Eq.(3) with L_i=3.4 m, A = 3.5 m^2. $\Delta Q/A$ deduced from Eq.(2) with σ=5.6697x10^{-8} W.m^{-2}.K^{-4}. T_C = 303 K.
8 N = 30 Shields 6.35×10^{-6} m thick Mylar Double-Aluminized Embossed (Tile Geometric Square). ——— 7.62×10^{-2} m Shiplap, laced buttons on 5.08×10^{-2} m spacing.		.610 (366 K) ——— .732 (389 K)	.593 ——— .711	.320 ——— .583	
9 N = 22 Shields 6.35×10^{-6} m thick Mylar Double-Aluminized 21 Spacers Tissuglas. ——— 7.62×10^{-2} m Shiplap, laced buttons on 5.08×10^{-2} m spacing.		.335 (366 K) ———	.325 ———	.175 ———	
10 N = 30 Shields 6.35×10^{-6} m thick Mylar Double-Aluminized Embossed (Tile Geometric Square). ——— 15.2×10^{-2} m Overlap, stitched Velcro.		.640 (366 K) ——— .762 (389 K)	.622 ——— .740	.336 ——— .607	
11 N = 30 Shields 6.35×10^{-6} m thick Mylar Single-Aluminized Crinkled. ——— Butt, Stitched Velcro.		8.99 (366 K) ——— 9.97 (389 K)	8.73 ——— 9.69	4.71 ——— 7.95	
12 N = 30 Shields 6.35×10^{-6} m thick Mylar Single-Aluminized Crinkled. ——— 7.62×10^{-2} m Shiplap, stitched Velcro base, laced exterior.		3.44 (366 K) ———	3.34 ———	1.80 ———	

(Continued onto next page)

MULTILAYER INSULATIONS

Effect of Singularities

Table 3-21 (Continued)

Thermal Effects of Joints

Description	Sketch	$C_i \times 10^3$ [m]	$\Delta\varepsilon_{effi} \times 10^3$	$\Delta Q_i/A$ [W/m^2]	Comments
13 N = 30 Shields 6.35x10^{-6} m thick Mylar Double-Aluminized Embossed (Tile Geometric Square) Exposed edge, corner buttoned on 15.2x10^{-2} m spacing	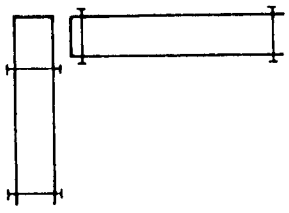	.945 (T$_H$ = 366 K) 1.25 (389 K)	.918 1.21	.495 .933	From Knopf & Murray (1970). Effective emittance of a blanket with joints was measured by using an internally heated cylinder over which the insulation was wrapped. The dimensions of the cylinder were .61 m in diameter, 1.52 to 1.83 m in length. The area of the test frame varied between 3.16 and 3.62 m^2 Length of a typical axial joint: 1.22 to 1.52 m. Length of a circumferential joint: 1.92 m. Temperatures were measured by eight internal and eleven external thermocouples. ε_{eff} is deduced from the heating power required to stabilize the temperature. One-dimensional flat-plate data concerning effective emittances of undisturbed specimens were obtained from different sources. $\Delta\varepsilon_{ieff}$ has been deduced by the compiler from the reported values of C_i, by using Eq.(3) with L_i=3.4 m, A = 3.5 m^2. $\Delta Q/A$ deduced from Eq.(2) with σ=5.6697x10^{-8} W.m^{-2}.K^{-4} T_C = 303 K.
14 N = 30 Shields 6.35x10^{-6} m thick Mylar Double-Aluminized Embossed (Tile Geometric Square) Exposed edge, corner buttoned on 15.2x10^{-2} m spacing, with Dexiglas		.945 (366 K) 1.097 (389 K)	.918 1.066	.495 .875	
15 N = 30 Shields 6.35x10^{-6} m thick Mylar Single-Aluminized Crinkled Exposed edge, corner buttoned on 5.08x10^{-2} m spacing, with reflective tape		1.34 (366 K) 1.71 (389 K)	1.30 1.66	.701 1.36	
16 N = 22 Shields 6.35x10^{-6} m thick Mylar Double-Aluminized 21 Spacers Tissuglas Exposed edge, corner buttoned on 5.08x10^{-2} m spacing, with reflective tape		.732 (366 K)	.711	.384	
17 N = 30 Shields 6.35x10^{-6} m thick Mylar Single-Aluminized Crinkled 7.62x10^{-2} m Shiplap, laced buttons with compound corner	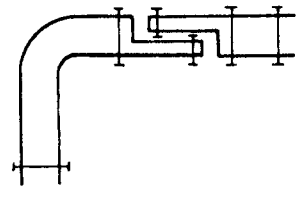	1.16 (366 K) 1.46 (389 K)	1.13 1.42	.610 1.16	
18 N = 22 Shields 6.35x10^{-6} m thick Mylar Double-Aluminized 21 Spacers Tissuglas 7.62x10^{-2} m Shiplap, laced buttons with compound corner		.640 (366 K)	.622	.336	
19 N = 30 Shields 6.35x10^{-6} m thick Mylar Double-Aluminized Embossed (Tile Geometric Square) Exposed edge, corner single line stitching	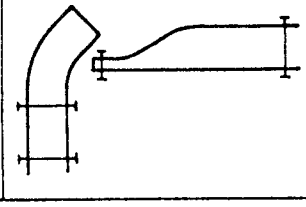	2.47 (366 K) 2.71 (389 K)	2.40 2.63	1.29 2.16	

(Continued onto next page)

MULTILAYER INSULATIONS

Effect of Singularities

Table 3-21 (Continued)
Thermal Effects of Joints

Description	Sketch	$C_i \times 10^3$ [m]	$\Delta\varepsilon_{effi} \times 10^3$	$\Delta Q_i/A$ [W/m^2]	Comments
20 N = 30 Shields 6.35×10^{-6} m thick Mylar Double-Aluminized Embossed (Tile Geometric Square) Exposed edge, corner double line stitching		5.27 (T_H = 366 K) 5.49 (389 K)	5.12 5.33	2.76 4.37	From Knopf & Murray (1970). Same comments as for the other data from this source.
21 N = 15 Shields 6.35×10^{-6} m thick Mylar Double-Aluminized. Holes 6.35×10^{-3}m diam.,.15m centers 14 Spacers 2.30×10^{-4}m thick Nylon Net 2 Outer Layers 2.54×10^{-5}m thick Teflon 7.62×10^{-2}m Overlap, stitched	15 15	3.31 (300 K)	3.77	1.69	From Stimpson & Jaworski (1972). Effective emittance of a blanket with joints was measured by using an electrically heated cylindrical calorimeter. The dimensions of the cylinder were .254 m in diameter, .711 m in length. Since the actual test section length is .406 m, the effective area of the shield in the test section is approximately .325 m^2. Temperatures were measured with thermocouples. Heat losses were estimated by means of the electrical power required to maintain a desired equilibrium temperature inside the blanket. The heat losses through the undisturbed blanket were calculated as a function of the number of layers, shield emittance and percentage of holes. C_i has been deduced by the compiler from the reported values of $\Delta\varepsilon_{eff}$, by using Eq.(3) with L_i = .37 m and A = .325 m^2. $\Delta Q/A$ has been deduced from Eq.(2) with $\sigma = 5.6697\times10^{-8}$ W.m^{-2}.K^{-4}, T_H = 300 K T_C = 120 K
22 N = 15 Shields 6.35×10^{-6} m thick Mylar Double-Aluminized. Holes 6.35×10^{-3}m diam.,.15m centers 14 Spacers 2.30×10^{-4}m thick Nylon Net 2 Outer Layers 2.54×10^{-5}m thick Teflon 7.62×10^{-2}m Overlap. Interleaved. Number of layers indicated in the sketch	15 NYLON NET 7 8	2.14 (300 K)	2.44	1.092	
23 N = 15 Shields 6.35×10^{-6} m thick Mylar Double-Aluminized. Holes 6.35×10^{-3}m diam., .15m centers 14 Spacers 2.30×10^{-4}m thick Nylon Net 2 Outer Layers 2.54×10^{-5}m thick Teflon 7.62×10^{-2}m Overlap. Interleaved. Number of layers indicated in the sketch	7 NYLON NET 7 8 8	1.88 (300 K)	2.14	.958	
24 N = 15 Shields 6.35×10^{-6} m thick Mylar Double-Aluminized. Holes 6.35×10^{-3}m diam., .15m centers 14 Spacers 2.30×10^{-4}m thick Nylon Net 2 Outer Layers 2.54×10^{-5}m thick Teflon 7.62×10^{-2}m Overlap. Interleaved. Number of layers indicated in the sketch	7 NYLON NET 5 5 8 5	1.70 (300 K)	1.94	.869	
25 N = 15 Shields 6.35×10^{-6}m thick Mylar Double-Aluminized. Holes 6.35×10^{-3}m diam., .15m centers 14 Spacers 2.30×10^{-4}m thick Nylon Net 2 Outer Layers 2.54×10^{-5}m thick Teflon 7.62×10^{-2}m Overlap. Interleaved. Number of layers indicated in the sketch	5 NYLON NET 3 5 4 5 4 5 4	1.70 (300 K)	1.94	.869	
26 N = 15 Shields 6.35×10^{-6} m thick Mylar Double-Aluminized. Holes 6.35×10^{-3}m diam., .15m centers 14 Spacers 2.30×10^{4}m thick Nylon Net 2 Outer Layers 2.54×10^{-5}m thick Teflon 7.62×10^{-2}m Overlap. Interleaved. Number of layers indicated in the sketch	TAPE NYLON NET 7 8 5 5 5 TAPE	1.62	1.84	.822	

MULTILAYER INSULATIONS

Effect of Singularities

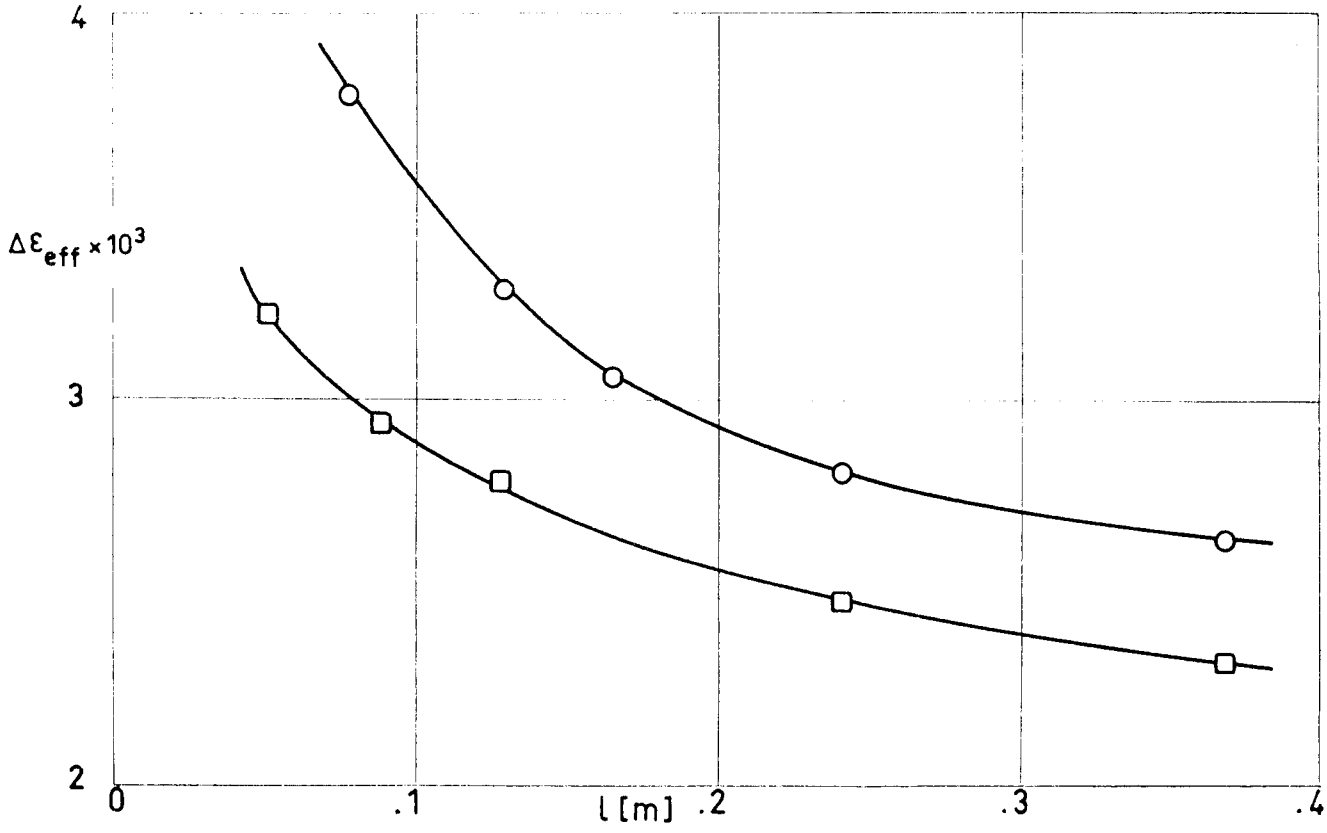

Fig 3-71. Effective emittance, $\Delta\varepsilon_{eff}$, vs. overlap, l. O Configuration 1 of Table 3-21. □ Configuration 2. From Crosby (1970).

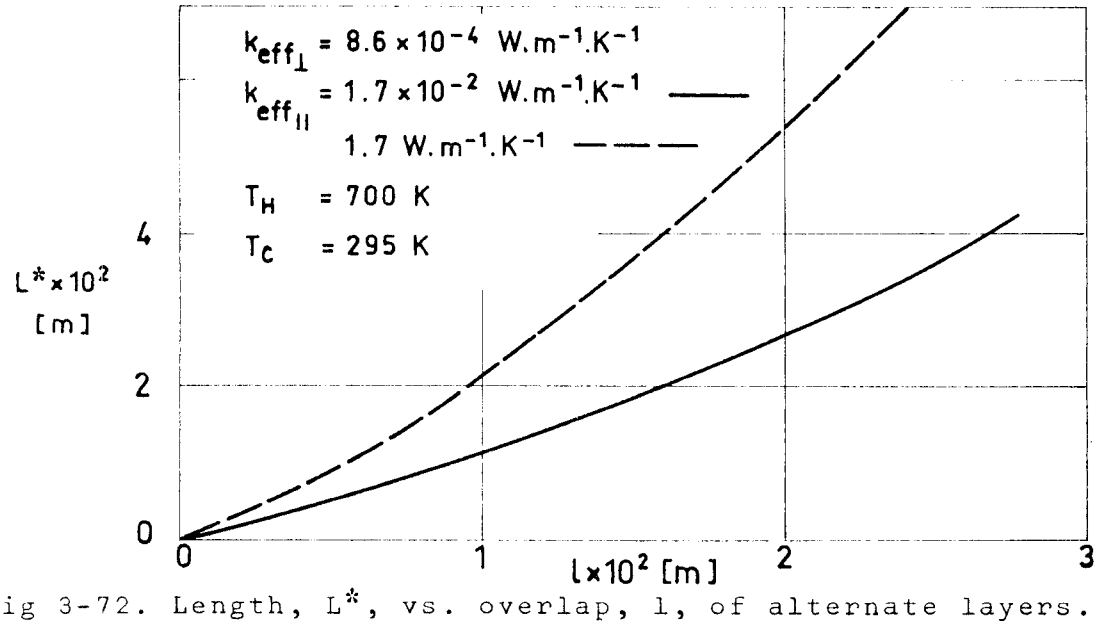

Fig 3-72. Length, L^*, vs. overlap, l, of alternate layers. From Cunnington et al. (1967).

MULTILAYER INSULATIONS

Effect of Singularities

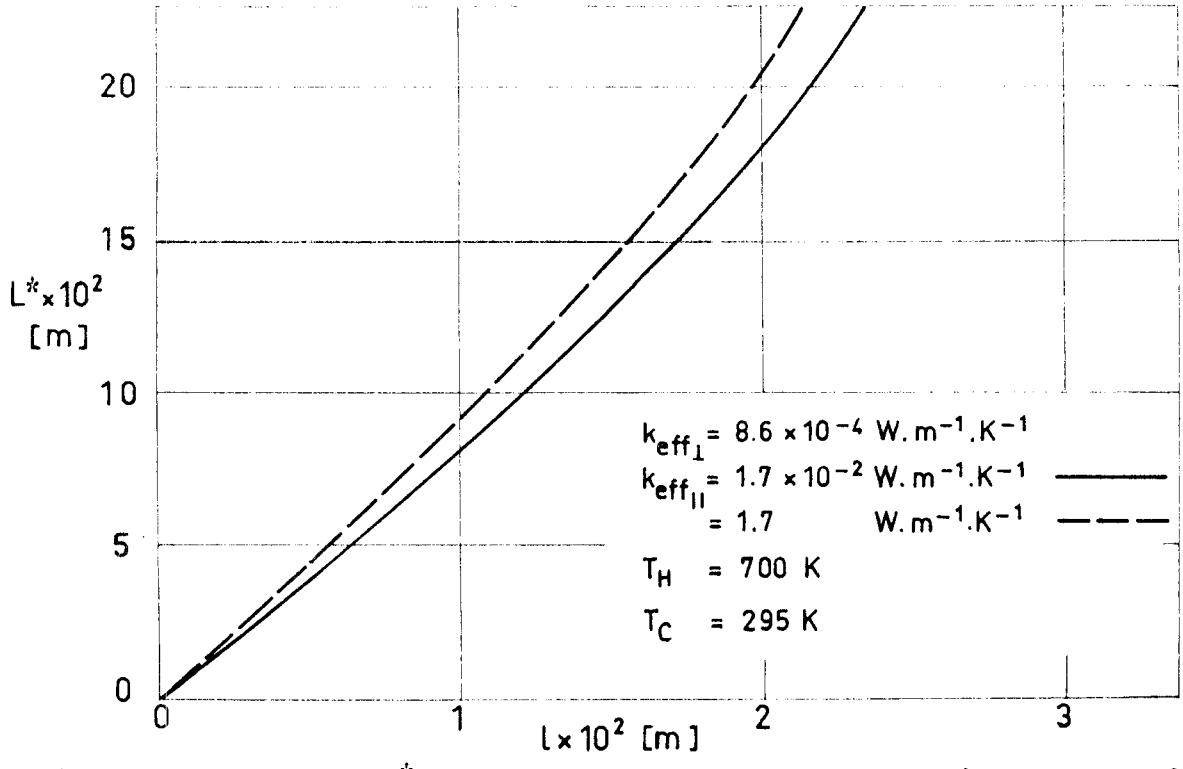

Fig 3-73. Length, L^*, vs. underlap, l. From Cunnington et al. (1967).

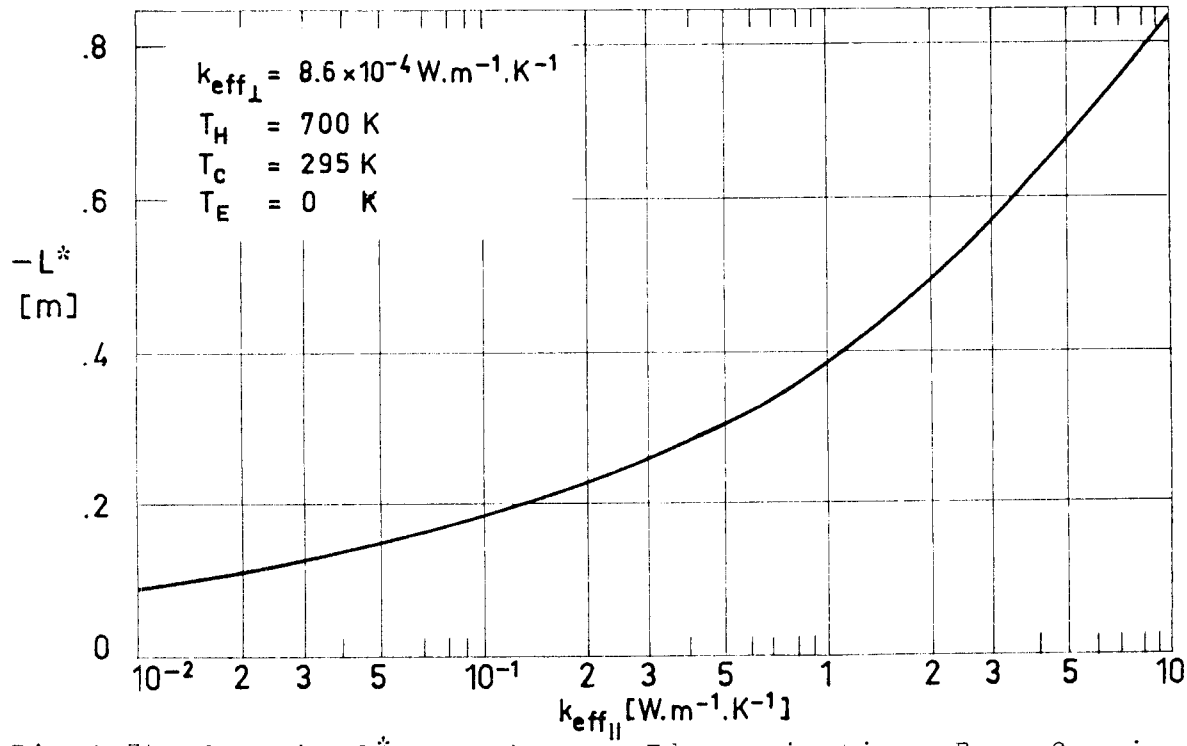

Fig 3-74. Length, L^*, vs. k_{eff}. Edge rejection. From Cunnington et al. (1967).

MULTILAYER INSULATIONS
Effect of Singularities

3.13.2. STITCHES AND PATCHES

Stitches are extensively used in spacecraft MLI systems to contain cutting debris and to improve the dimensional stability of the blanket enabling ease of handling during extensive testing and repeated use.

Stitching increases locally the layer density and subsequently the blanket thermal conductivity.

According to Stimpson & Jaworski (1972), the heat loss caused by stitching may be approximated by the following straight-line relationship based upon the length, L, of the stitch

$$\Delta Q = .0335 + .88\,L$$

where:

ΔQ, heat loss due to stitching. [W].

L, length of stitch. [m].

This relationship is represented in Fig 3-75, where several experimental data points have been also plotted.

For shorter stitch lengths ($L<.07$ m) the above relationship is no longer valid. Tests on individual button ties resulted in an average heat loss of .012 W, which is about a third of the sum of two stitch indent losses from a longer stitch.

Patches have been used to reduce the heat loss caused by stitches. Patching shields locally the blanket, reducing the temperature differential across it. The influence of the patches on the heat loss is given in Fig 3-76. As a general rule it can be said that patches on the hot side are more effective than on the cold side, and on both sides only slightly better.

MULTILAYER INSULATIONS

Effect of Singularities

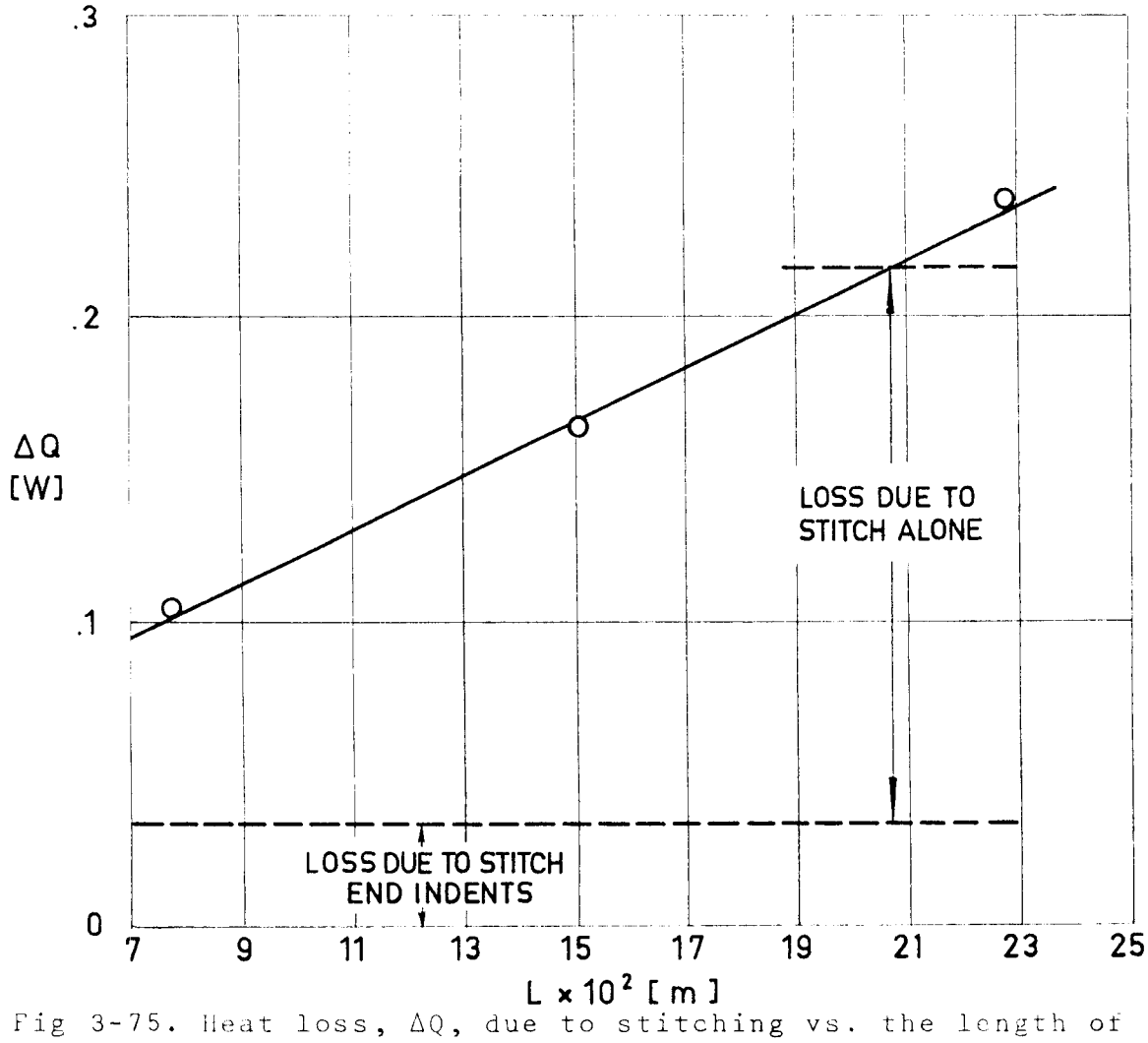

Fig 3-75. Heat loss, ΔQ, due to stitching vs. the length of stitch, L. From Stimpson & Jaworski (1972).

Explanation

Undisturbed System	Stitching	Test Method
15 Shields 6.35×10^{-6} m thick Mylar Double-Aluminized; holes $6.35\times\times10^{-3}$ m diameter on .15 m centers. 14 Spacers 2.30×10^{-4} m thick Nylon Net. 2 Outer Layers $2.54\times\times10^{-5}$ m thick Teflon Single aluminized. Wrapped around the heated cylinder.	3 axial .228 m in length stitches. The stitch was shortened to .152 m and then to .076 m by removing threads. A circumferential stitch was then installed and tested for the same lengths.	Effective emittance of the system was measured by using an electrically heated cylindrical calorimeter. The dimensions of the cylinder were .254 m in diameter, .711 m in length. The heat losses through the undisturbed blanket were calculated.

MULTILAYER INSULATIONS

Effect of Singularities

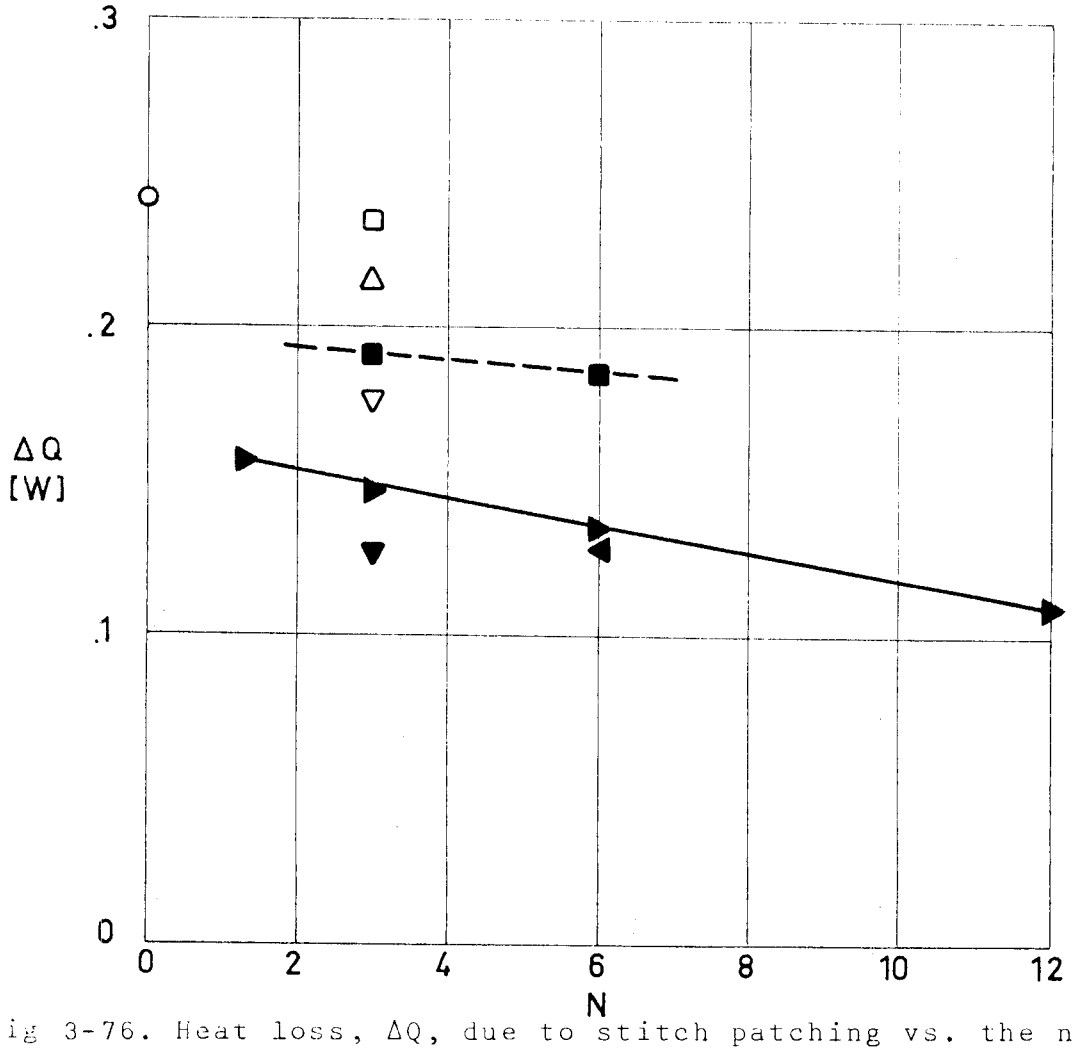

Fig 3-76. Heat loss, ΔQ, due to stitch patching vs. the number of patch layers, N. Undisturbed system and test method as in Fig 3-75. From Stimpson & Jaworski (1972).

Explanation

Patch Layer Description	Key	Patching
3 Layers of Mylar Double-Aluminized. 3 Nylon Net spacers. 1 Layer of Teflon Single-Aluminized.	○	Stitch .228 m length. Unpatched.
	□	.1×.33 m. Type B. Cold Side.
	■	.1×.33 m. Type A. Cold Side.
	△	.2×.4 m. Type B. Cold Side.
In Type A the Teflon layer was extended 4×10^{-3} m beyond the patch borders. Type B had no Teflon extension.	▽	.1×.33 m. Type B. Both Sides.
	▼	.1×.33 m. Type A. Both Sides.
	▶	.1×.33 m. Type A. Hot Side.
	◀	.15×.38 m. Type A. Hot Side.

3.14. EFFECT OF EVACUATING HOLES

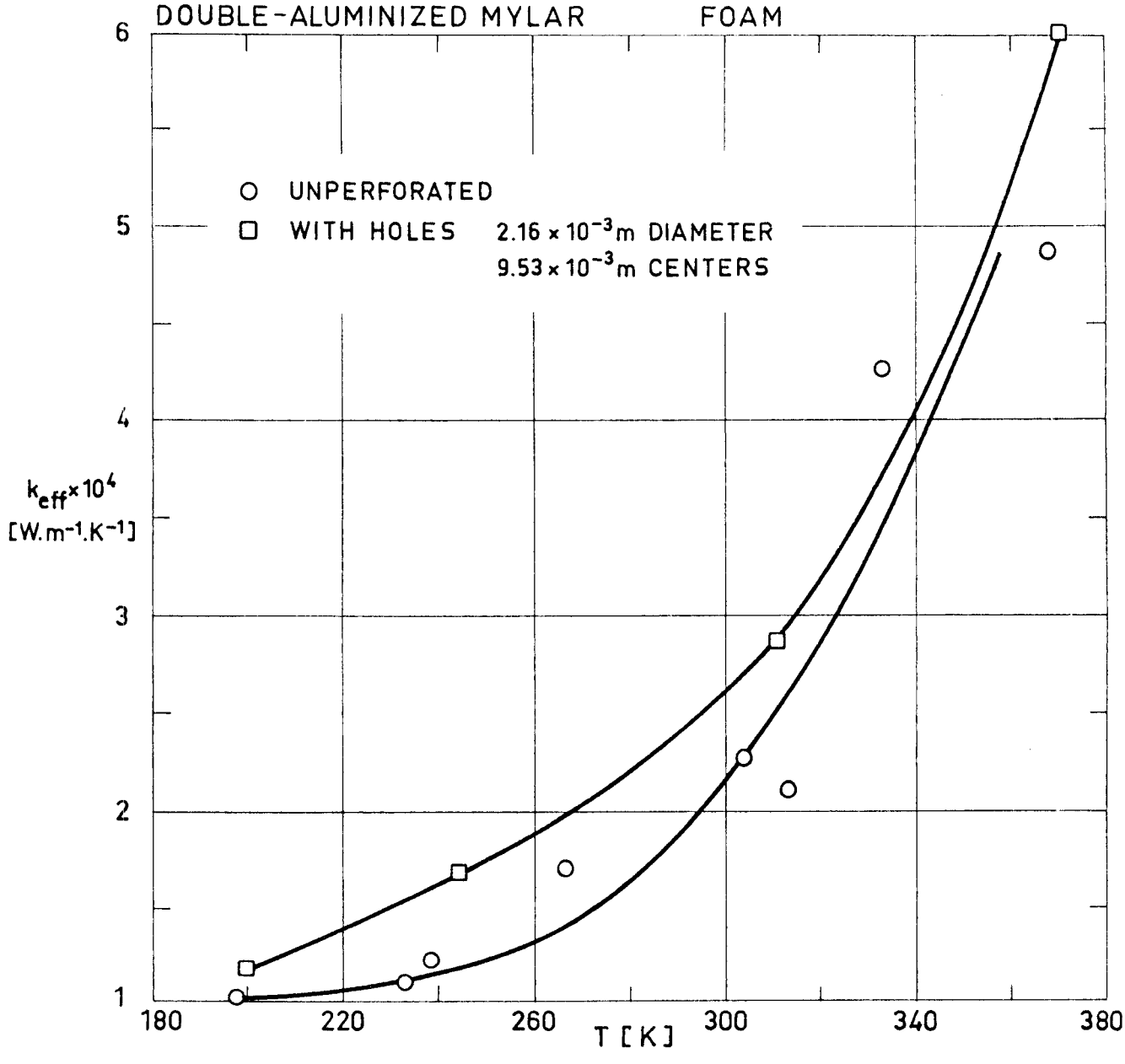

Fig 3-77. Effect of perforations on the effective thermal conductivity of a multilayer insulation formed by 24 Radiation Shields 6.35×10^{-6} m thick Mylar Double-Aluminized, and 23 Spacers 7.11×10^{-4} m thick Polyurethane Foam. From Hale (1969).

MULTILAYER INSULATIONS

Effect of Evacuating Holes

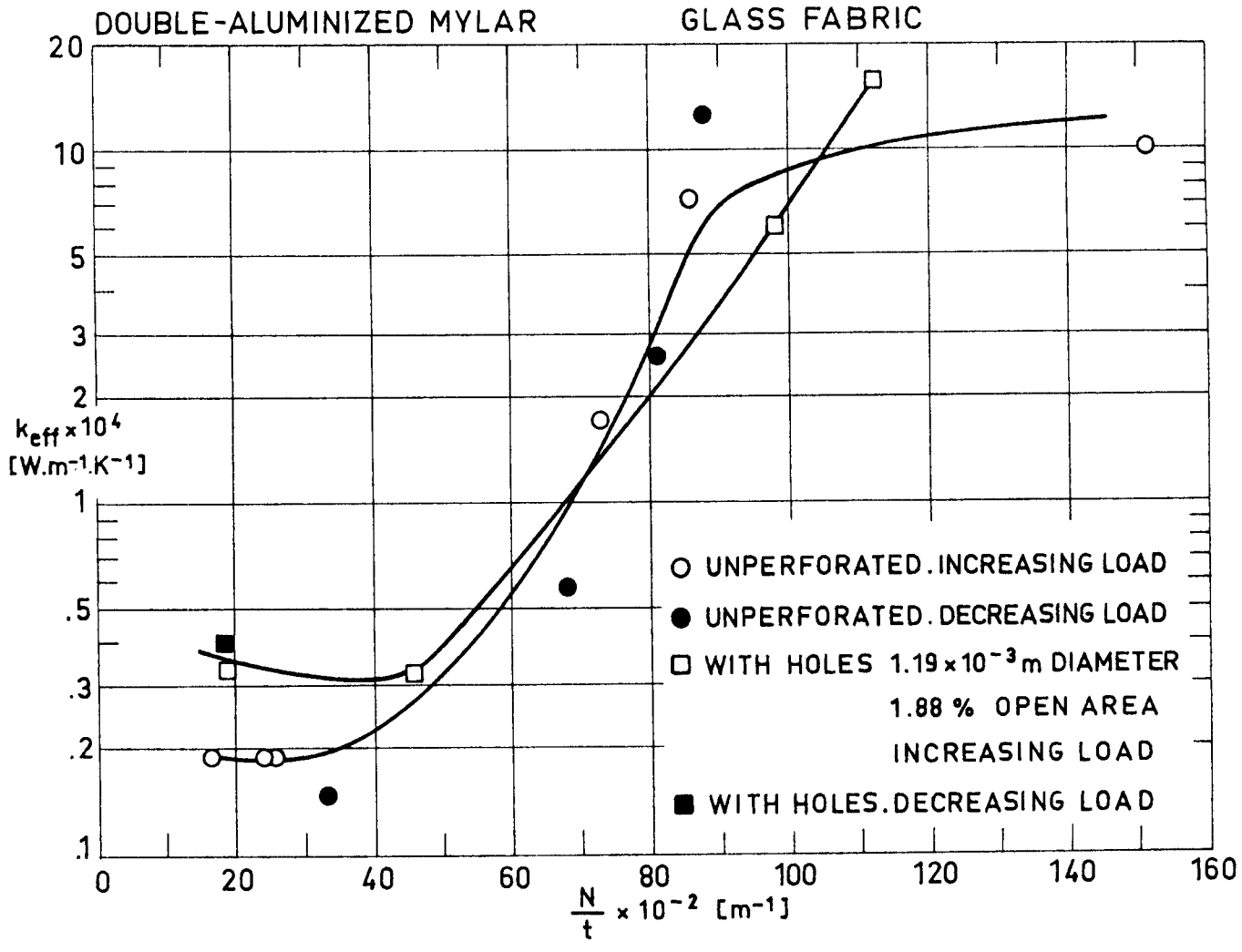

Fig 3-78. Effect of perforations on the effective thermal conductivity of a multilayer insulation formed by 10 Radiation Shields 6.35×10^{-6} m thick by .279 m diameter Mylar Double-Aluminized, and 22 Spacers 2.54×10^{-5} m thick by .305 m diameter Glass Fabric. From ADL (1966).

MULTILAYER INSULATIONS

Effect of Evacuating Holes

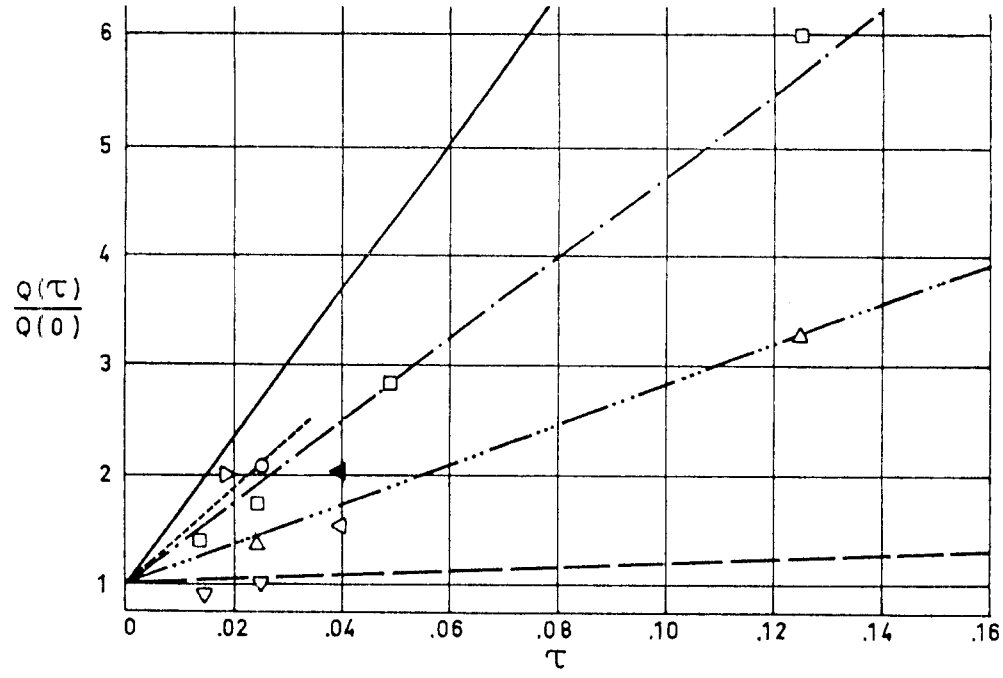

Fig 3-79. Effect of percentage of perforations, τ, on the heat flux through a multilayer insulation.

Explanation

Key	Description	Hole diameter $\times 10^3$ [m]	T [K]	References
———	$\frac{Q(\tau)}{Q(0)} = \frac{(2-\varepsilon)\tau+\varepsilon}{\varepsilon(1-\tau)}$. Boundary for small holes ε=.033			Tien & Cunnington (1973).
— — —	$\frac{Q(\tau)}{Q(0)} = 1+2\tau$. Boundary for large holes.			
O	10 Shields. Tempered Aluminium 11 Spacers. 3.18×10^{-3} m by 3.18×10^{-3} m thick Vinyl-Coated Fiber-Glass Screen	1.59	T_C=77	Glaser et al. (1967) pp. 58-59
-------	Straight-line through O points			
□	Same as O	3.18		
—·—·—	Straight-line through □ points			
△	Same as O	6.35		
—···—	Straight-line through △ points			
▽	20 Shields. Mylar Single-Aluminized Crinkled	3.18	T_C=20	
▷	10 Shields. 6.35×10^{-6} m thick Mylar Double-Aluminized 22 Spacers. 2.54×10^{-5} m thick by 30.48×10^{-2} m diameter Glass Fabric	1.85	T_H=294 T_C=77	ADL (1966) pp. II-87; II-91.
◁	24 Shields. 6.35×10^{-6} m thick Mylar Double-Aluminized 23 Spacers. 7.11×10^{-4} m thick. Polyurethane Foam	9.53	T=200[a]	Hale (1969) p. 39
◁	Same as ◁	9.53	T=240[a]	

[a] T is the characteristic temperature.

INTENTIONALLY BLANK PAGE

MULTILAYER INSULATIONS

Effect of Mechanical Damage

3.15. EFFECT OF MECHANICAL DAMAGE

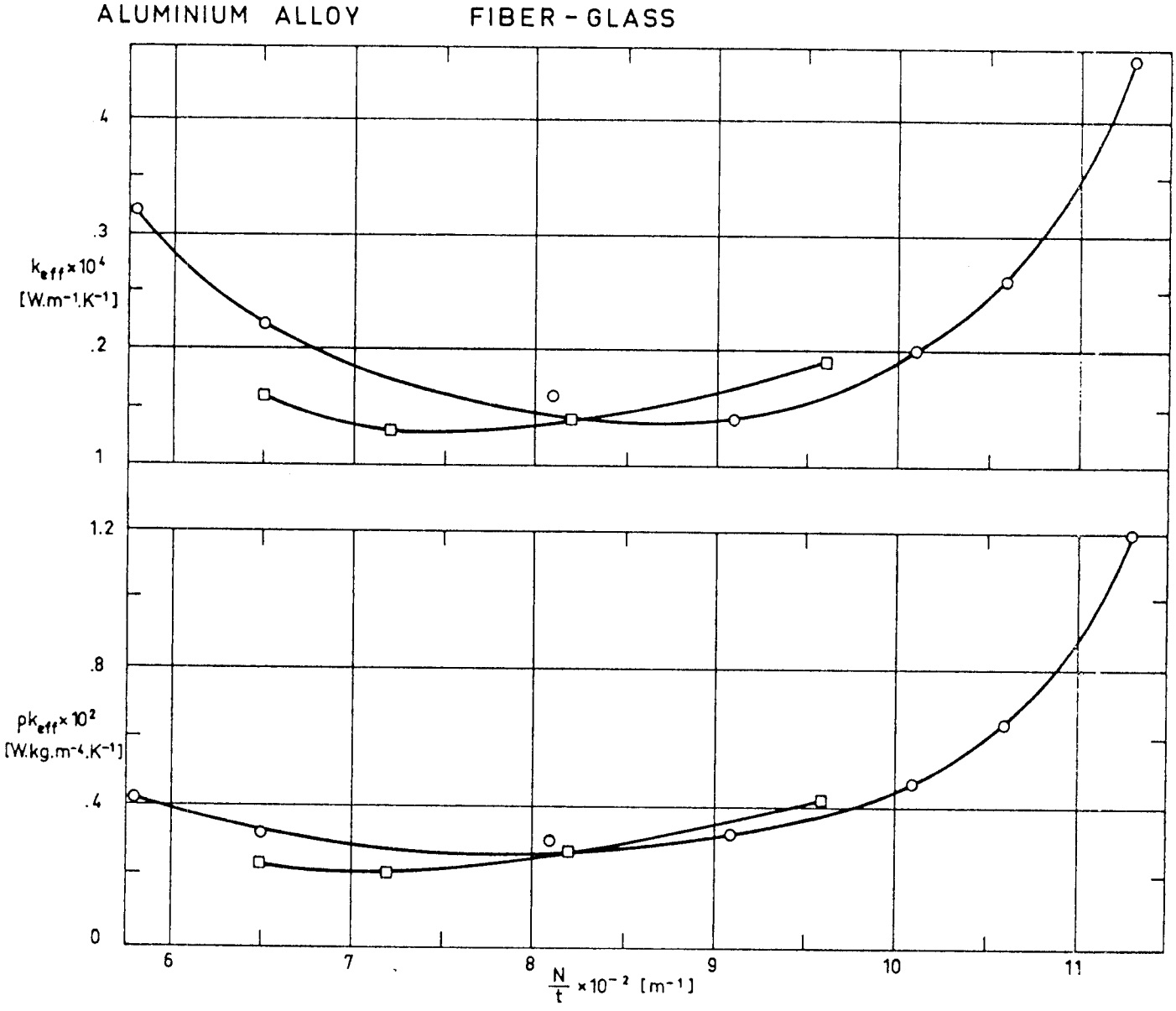

Fig 3-80. Effect of Meteoroid-Bumper debris damage on the effective thermal conductivity, k_{eff}, and product of apparent density and effective thermal conductivity, ρk_{eff}. Both functions are plotted vs. the number of radiation shields per unit thickness. N/t. Sample O was damaged by being fired upon by hypervelocity pellets. Sample □ was not damaged.

Explanation

Key	Sample Description	$t \times 10^2$ [m] Uncompressed	$P \times 10^3$ [Pa]	T_H [K]	T_C [K]	Calorimeter Type	References
O	N=5 Shields 5.08×10^{-5} m thick Al. Alloy 1145-0 6 Spacers 5.08×10^{-4} m thick Vinyl-Coated Glass-Fiber screen $3.18 \times 10^{-3} \times 3.18 \times 10^{-3}$ m mesh. Damaged	.86[a]	<.93	293±1	20.5	ADL Model 12 Flat-Plate (double-guarded cold-plate)	ADL (1964) p. II-63
□	Same as O Undamaged	.77[a]	<.93	293±1	20.5	Same as O	Same as O

[a] Largest quoted value.

INTENTIONALLY BLANK PAGE

3.16. EFFECT OF INNER GAS PRESSURE

Evacuated MLI exhibit low thermal conductivity, since the effect of gas conduction decreases when pressure decreases.

According to kinetic theory, the thermal conductivity, k_g, of a gas is a function of the product of the density, ρ, times the mean free path, λ, of the gas molecules

$$k_g \propto \rho \lambda c_p \bar{c}$$

where neither the specific heat at constant pressure, c_p, nor the mean molecular speed, $\bar{c}$, depend upon the pressure.(*).

In the continuous region, where the pressure goes from an atmosphere to a few hundred pascals, the molecular mean free path of the gas is much smaller than the characteristic length of the spacer voids. Under these conditions, the gas conduction is independent of pressure, as the decrease in density is compensated for by the increase in the mean free path.

On the other hand, if the pressure is low enough the characteristic length of the spacer voids may become much smaller than the gaseous mean free path. Thence, the thermal conductivity decreases in proportion to pressure because the characteristic length, d, is now that of the void rather than the mean free path of the gas (free molecular region).

It is obvious that the transition from one region to the other depends upon the dimensions of the individual components of the insulation. The larger the voids, the lower the pressure required to approach the free molecular region.

At atmospheric pressure the thermal conductivity of a complete multilayer insulation system approaches that of the inner gas,

---

(*) Strictly speaking c_p is a slowly varying function of pressure.

MULTILAYER INSULATIONS

Effect of Inner Gas Pressure

and is independent of the thermal conductivity of the evacuated system. At very low pressure the gaseous conduction is negligible compared to solid and radiative conduction, and the thermal conductivity of the system becomes again independent of pressure. Because of these reasons, the thermal conductivity of the multilayer insulation relates to gas pressure by an S-like curve.

Concerning the type of gas, it should be said that gases of high thermal conductivity (e.g., helium or hydrogen) cause more drastic degradation of the performance of the system than gases with low conductivity (e.g., nitrogen or air). At low temperatures, the condensations of the inner gases reduces the insulation effectiveness, in addition to damaging the blanket (upon pressurization due to subsequent heating), and constituting a fire and explosion hazard when the condensates come in contact with the organic components of the spacer.

Gas within the insulation may be evacuated with a vacuum system connected to a cryogenic storage tank. As an alternative, cryopumping may be achieved by using carbon dioxide, which is a gas at room temperature but freezes on a surface cooled below 190 K, thus reducing the gas pressure in a sealed space. A third technique for preventing condensation of air is to purge the insulation with helium gas, which does not condense at liquid hydrogen temperatures. Purging with warm helium is often used to improve outgassing of organic materials. The principal advantage of purging is that it greatly reduces the need for leak reliability in a protective enclosure, however, failure to provide venting may result in a rupture of the enclosure and degradation of the insulation.

Thermal conductivities of several multilayer insulation systems containing different gases are plotted versus gas pressure in the following data sheets.

MULTILAYER INSULATIONS

Effect of Inner Gas Pressure

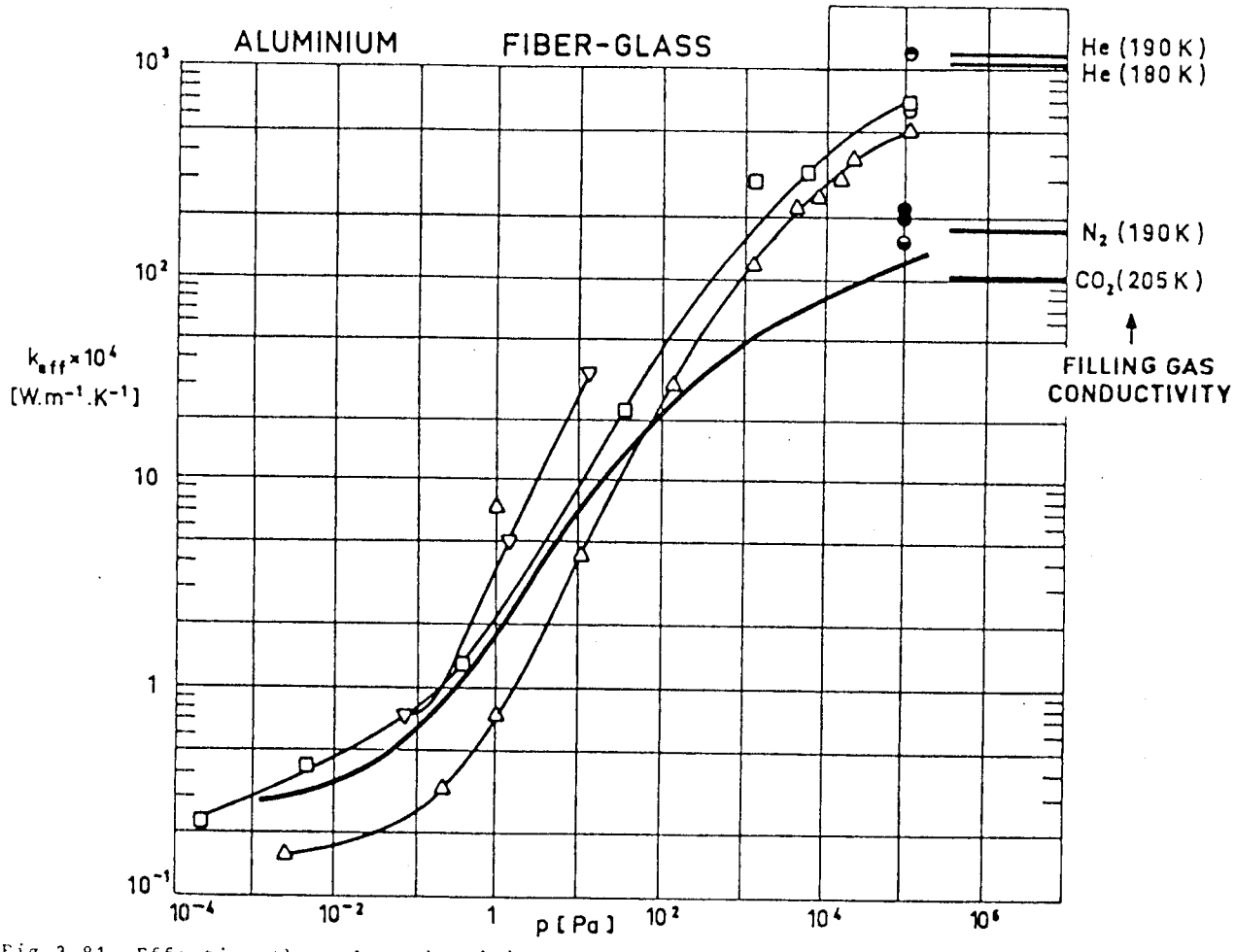

Fig 3-81. Effective thermal conductivity, k_{eff}, as a function of gas pressure, p. The thermal conductivities of the filling gases at the characteristic temperatures are indicated for comparison.

Explanation

Key	Sample Description	$t \times 10^2$ [m] Uncompressed	Filling Gas	T_H [K]	T_C [K]	Calorimeter Type	References
○	N=10 Shields 5.08×10^{-5} m thick Al. Alloy 1145-H19 bright both sides 11 Spacers 5.08×10^{-4} m thick Glass Fiber screen 3.175×10^{-3} by 3.175×10^{-3} m mesh [a]	.94	He	273	20.5	ADL Model 12 Flat-Plate (double-guarded cold-plate)	ADL (1964) p. II-48
○	Same as ○	.89	N_2	264.5±6	77.5	Same as ○	Same as ○
◓	Same as ○	.94	N_2	265.5	20.5	Same as ○	Same as ○
◒	Same as ○	.91	CO_2	293.5	77.5	Same as ○	Same as ○
□	Shields: Tempered Aluminium Spacers: Vinyl-Coated Fiber Glass Screen		He		77		Glaser et al. (1967) p. 56
△	Shields N not quoted. $N/t = 1417$ m^{-1} Aluminium Spacers: Fiber Glass		N_2 N_2	294 294	20.7 20.7		Coston (1967) p. 4.3-25
—	Shields: Aluminium Spacers: Fiber Glass		N_2	294	20.7		Same as △
▽	Shields: Aluminium Spacers: Glass Wool		Air				Same as □

[a] The sample was enclosed in a polyester film container for purging.

MULTILAYER INSULATIONS

Effect of Inner Gas Pressure

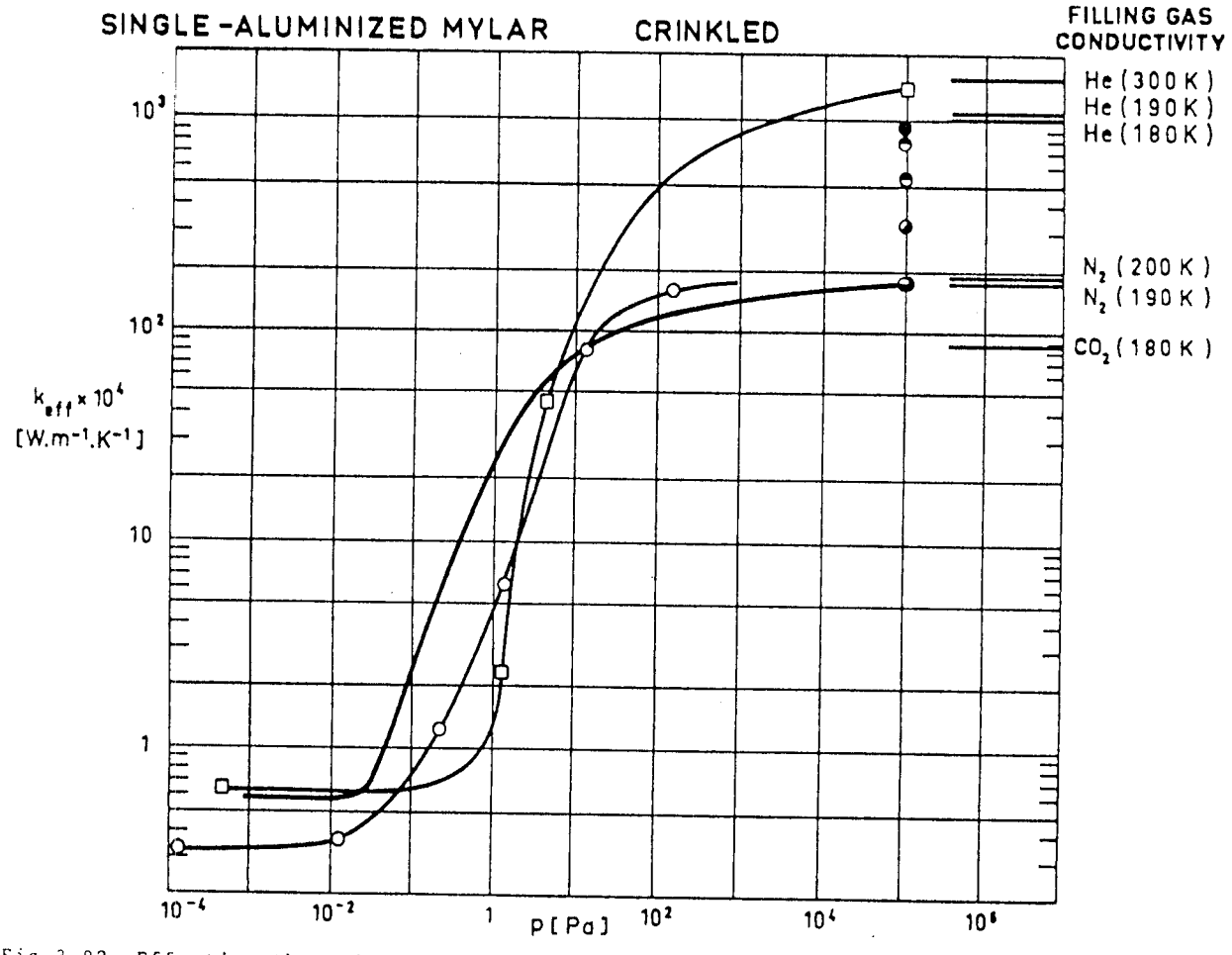

Fig 3-82. Effective thermal conductivity, k_{eff}, as a function of gas pressure, p. The thermal conductivities of the filling gases at the characteristic temperatures are indicated for comparison.

Explanation

Key	Sample Description	$t \times 10^2$ [m] Uncompressed	Filling Gas	T_H [K]	T_C [K]	Calorimeter Type	References
○	Mylar Single-Aluminized Crinkled		Air				Glaser et al. (1967) p. 56
●	N=20 Shields 6.35×10^{-6} m thick Mylar Single-Aluminized Crinkled	.94[a]	He	274	77.5	ADL Model 12 Flat-Plate (double-guarded cold-plate)	ADL (1964) p. II-49
◓	Same as ●	.94[a]	He	274	20.5	Same as ●	Same as ●
◒	Same as ●	.94[a]	CO_2	261	77.5	Same as ●	Same as ●
◑	Same as ●	.94[a]	N_2	275.5	77.5	Same as ●	Same as ●
◐	Same as ●		N_2	268.5	20.5	Same as ●	Same as ●
—	Shields N not quoted. N/t=1575 m^{-1} 6.35×10^{-6} m thick Mylar Single-Aluminized Crinkled		N_2	294	79.4		Coston (1967) p. 4.3-25
□	N=81 Shields 6.35×10^{-6} m thick Mylar Single-Aluminized Embossed	1.27	He	312± ±9.5	300.5± ±1	Lockheed/Huntsville Cylindrical	Hale (1969) p. 41

[a] Largest quoted value.

MULTILAYER INSULATIONS

Effect of Inner Gas Pressure

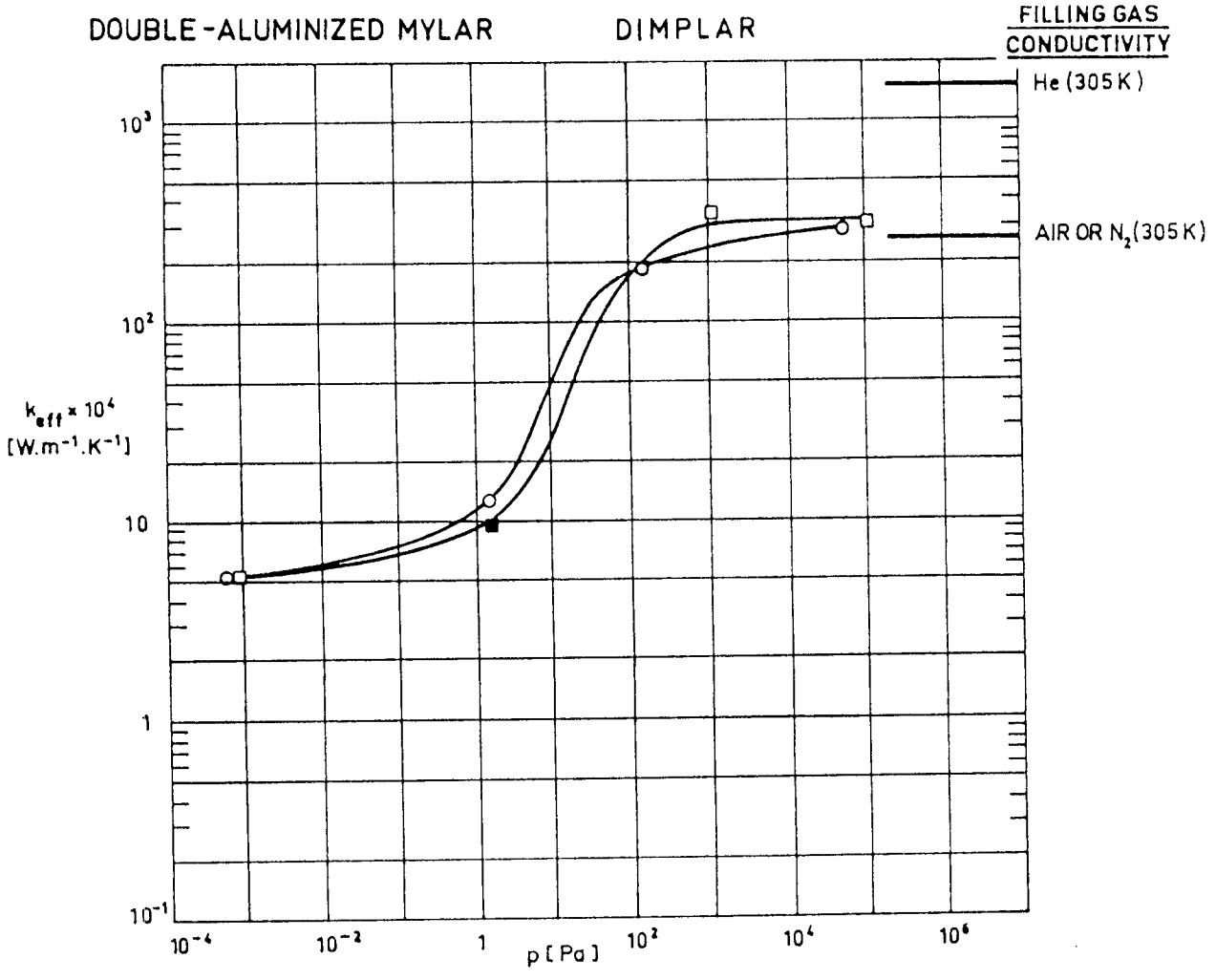

Fig 3-83. Effective thermal conductivity, k_{eff}, as a function of gas pressure, p. The thermal conductivities of the filling gases at the characteristic temperatures are indicated for comparison.

Explanation

Key	Sample Description	$t \times 10^2$ [m] Uncompressed	Filling Gas	T_H [K]	T_C [K]	Calorimeter Type	References
○	N=22 22 Layers 6.35×10^{-6} m thick Mylar Single-Aluminized Dimpled 22 Layers 6.35×10^{-6} m thick Mylar Single-Aluminized Embossed	2.92	He ?	311.5± ±8	301.5± ±1.5	Lockheed/Huntsville Cylindrical	Hale (1969) p. 42
□	N=60 Shields 6.35×10^{-6} m thick Mylar Single-Aluminized Embossed 60 Spacers White Nylon Net	2.54	He ?	316± ±4.5	304± ±2.5	Same as ○	Hale (1969) p. 43
■	Same as □	2.54	He ?	266	255	Same as ○	Same as □

Comment:

Although the author claims that the system has been purged with helium preheated to 394 K, it seems obvious that the filling gas is either nitrogen or air.

MULTILAYER INSULATIONS

Effect of Inner Gas Pressure

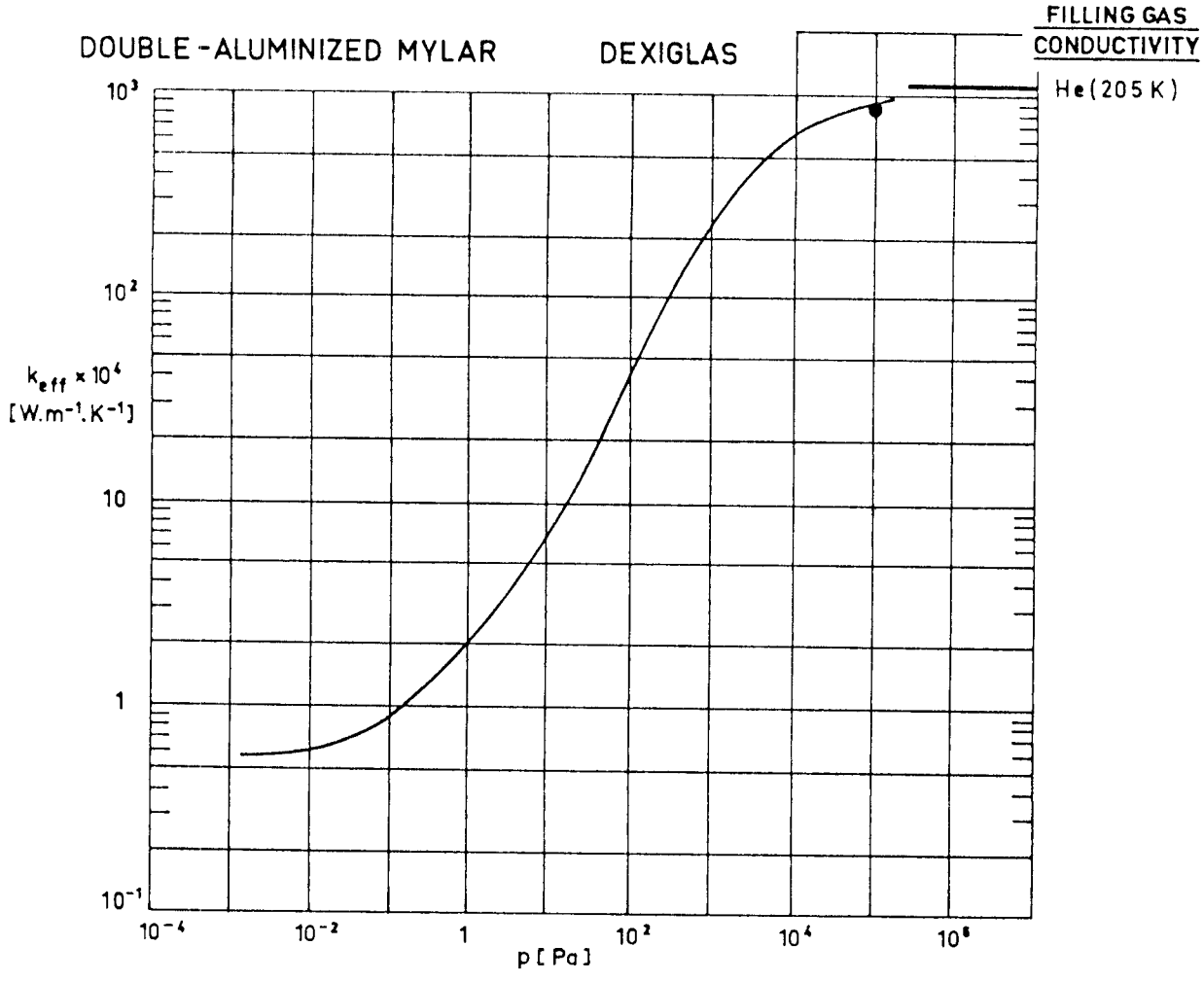

Fig 3-84. Effective thermal conductivity, k_{eff}, as a function of gas pressure, p. The thermal conductivity of the filling gas at the characteristic temperature is indicated for comparison.

Explanation

Key	Sample Description	t×10^2 [m] Uncompressed	Filling Gas	T_H [K]	T_C [K]	Calorimeter Type	References
—	Shields N not quoted, N/t=2677 m^{-1} 6.35×10^{-6} m thick Mylar Double-Aluminized Spacers 7.11×10^{-6} m thick Dexiglas buttons on 0.1 m centers		He	294	77.2		Coston (1967) p. 4.3-25
●	N=20 Shields 6.35×10^{-6} m thick Mylar Single-Aluminized Crinkled	.94[a]	He	274	77.5	ADL Model 12 Flat-Plate (double-guarded cold-plate)	ADL (1964) p. II-49

[a] Largest quoted value.

MULTILAYER INSULATIONS

Effect of Inner Gas Pressure

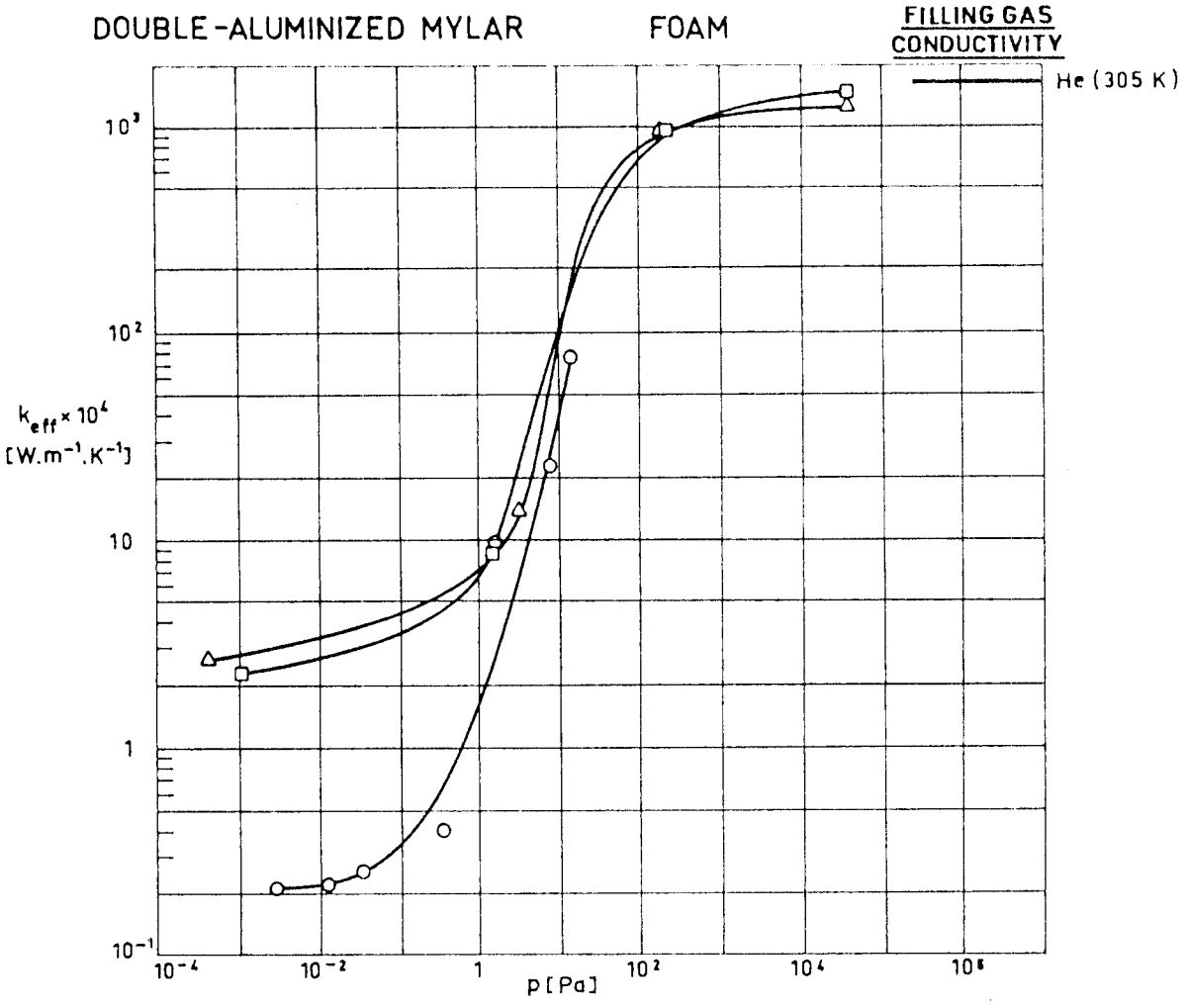

Fig 3-85. Effective thermal conductivity, k_{eff}, as a function of gas pressure, p. The thermal conductivity of the filling gas at the characteristic temperature is indicated for comparison.

Explanation

Key	Sample Description	$t \times 10^2$ [m] Uncompressed	Filling Gas	T_H [K]	T_C [K]	Calorimeter Type	References
○	Shields Mylar Spacers Foam		He				Glaser et al. (1967) p. 56
□	N=24 Shields 6.35×10^{-6} m thick Mylar Double-Aluminized 23 Spacers 7.11×10^{-6} m thick Red Polyurethane Goodyear Foam	2.54	He	307± ±4.5	301± ±4	Lockheed/Huntsville Cylindrical	Hale (1969) p. 39
△	Same as □ . Perforated-Shields having holes of 2.16×10^{-3} m diameter 9.53×10^{-3} m between centers	2.54	He	312± ±9.5	301± ±1	Same as □	Same as □

INTENTIONALLY BLANK PAGE

MULTILAYER INSULATIONS

Evacuation

3.17. EVACUATION

The thermal conductivity of an MLI system can be reduced to a very low level provided that the interstitial pressure is kept below roughly 10^{-3} Pa so that gaseous conduction is practically eliminated. This pressure level can be achieved, before or after launch, by certain pumping processes.

During ascent flight the inner gas pressure should be reduced rapidly enough to prevent high stresses on the shields, and to decrease the transient heating and associated propellant boil-off. As the gas pressure is reduced, outgassing from the insulation materials becomes important, seriously prolonging the evacuation period.

There have been two pumping procedures in practice, namely the edge pumping, which causes the gas to flow parallel to the shield layers, and the broadside pumping in which the gas flows, normally to the layers, through small holes made in the shields.

To study the evacuation -and repressurization- processes the MLI system is assimilated to a porous medium. The motion of a gas through a porous medium is fairly well understood, at least for engineering purposes. The characteristics of the gas flow depend on the ratio of the molecular mean free path, λ, to the pore diameter, d. λ/d is often called the Knudsen number.

At the outset of evacuation, when the pressure is of the order of one atmosphere (10^5 Pa), $\lambda/d \ll 1$, the intermolecular collisions are dominant, and the gas behaves as a continuum medium.

For very low pressures, when outgassing from the material

MULTILAYER INSULATIONS

Evacuation

controls the fluid motion, $\lambda/d>>1$, collisions with the walls dominate, and the so called free molecular flow prevails.

In the intermediate range of pressures the problem is extremely complicated, however, useful semiempirical correlations exist which can be used for the present purposes.

3.17.1. INTERSTITIAL PRESSURE DURING RAPID EVACUATION

Although the gas flow through an MLI can be three-dimensional, a conservative estimate of the pressure variation may be achieved by use of the results of one-dimensional theory wherein the minimum linear flow path is used as the half-length of the equivalent one-dimensional configuration.

In the case of edge pumping the minimum linear flow path, L, is the distance from center of blanket to the nearest open edge. This case has been considered by Kneisel & Bennet (1970).

For broadside pumping L would be equal to the blanket thickness, t.

In order to analyze the flow of the gas through the MLI system it will be assumed that the gas is perfect, and that the temperature and the gas properties are constant.

3.17.1.1. CONTINUUM REGIME

Near the atmospheric pressure, the mass flow rate per unit cross-sectional area, m, is given by Darcy's law

MULTILAYER INSULATIONS

Evacuation

$$m = \frac{\kappa}{\mu} \rho \frac{\partial p}{\partial x} \qquad (1)$$

where:

p, Gas pressure, depending on coordinate, x, and time, t. [Pa].

x, Coordinate parallel to flow direction. [m].

κ, Permeability of the porous medium. [m^2].

μ, Gas viscosity at the average blanket temperature. [Pa.s].

ρ, Mean density of the gas. [$kg.m^{-3}$].

Taking into account the mass preservation condition in a differential control element

$$\frac{\partial \rho}{\partial t} = \frac{\partial m}{\partial x} \quad ,$$

the following equation results:

$$\frac{\mu}{\kappa} \frac{\partial p}{\partial t} = \frac{\partial}{\partial x} \left(p \frac{\partial p}{\partial x} \right) \qquad (2)$$

The initial and boundary conditions are:

Initial condition: $p(x,o) = p_o(o)$

Boundary conditions:

Blanket Center (x=o): $\frac{\partial p}{\partial x} = o$ for any t

Blanket Edge (x=L): $p(L,t) = p_o(t)$

$p_o(t)$ being the outer pressure at instant t.

In the case of edge pumping, once this model of fluid flow has been postulated, κ can be estimated from data giving the variation of pressure with time. Conversely, from the value of κ it

MULTILAYER INSULATIONS

Evacuation

can be deduced the pressure time relationship in an MLI system of given evacuation length, L.

Values of κ for several MLI systems are shown in Fig 3-86.

In the case of broadside pumping the fitting of the one-dimensional model is not so obvious if the hole diameter is smaller than the diameter of the pores in the spacer. This small hole limiting case has some technical interest since the shield emittance would be degraded because increased transmittance produced by large holes.

When the hole diameter is of the same order or smaller than the pore diameter, the resistance to fluid flow is localized in the holes. Hence, it can be assumed that the pressure in each one of the spaces between two neighboring shields is uniform although different from a space to the other. The pressure difference between two consecutive spaces is equal to the pressure loss experimented by the fluid when flowing through the hole.

For Reynolds numbers, defined in terms of the hole diameter and the mean fluid velocity through the hole, smaller than one, the mass flow rate per unit cross-sectional area, m_h, of an isolated, circular, hole is given (Happel & Brenner (1965)) by the following expression:

$$m_h = \frac{d^2}{6 \pi \mu} \rho \frac{\Delta p}{d}$$

where:

d, Hole diameter. [m].

Δp, Pressure loss through the hole. [Pa].

MULTILAYER INSULATIONS

Evacuation

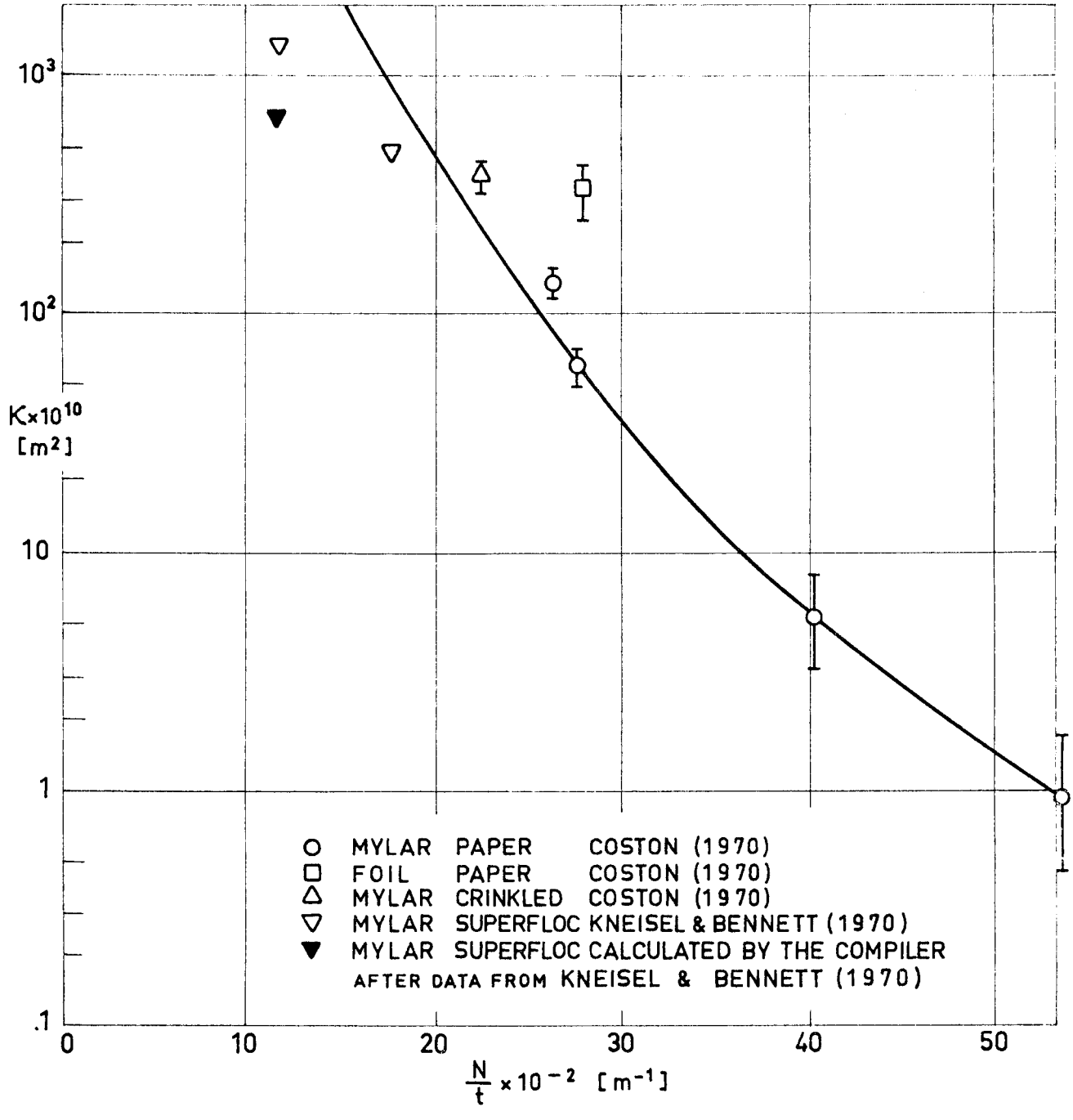

Fig 3-86. Permeability, κ, of several multilayer insulation configurations as a function of the layer density, N/t.

MULTILAYER INSULATIONS

Evacuation

Since the number of shields per unit blanket thickness, N/t, is normally large, the multiple-step-like pressure distribution across the blanket can be substituted by a continuous one, so that the mass flow rate, m, per unit area of the shield becomes

$$m = \frac{\tau d}{6\pi(N/t)\mu} \rho \frac{\partial p}{\partial x} \quad , \qquad (3)$$

τ being the fractional open area or transmittance of the perforated shields.

By comparing Eq. (3) to Eq. (1) it is deduced that the above one-dimensional approach can be applied to the hole-controlled broadside pumping provided that the following value of the permeability is used

$$K_h = \frac{\tau d}{6\pi(N/t)} \quad .$$

3.17.1.1.1. EDGE PUMPING VS. BROADSIDE PUMPING

A simple dimensional reasoning, based on Eq. (2), indicates that the characteristic edge-evacuation time, t_e, will obey the following order of magnitude relationship

$$t_e \sim \frac{\mu}{p} \frac{L^2}{K} \qquad (4)$$

Likewise, for the hole-controlled broadside pumping case

$$t_h \sim \frac{\mu}{p} \frac{6\pi t^2 (N/t)}{\tau d} \qquad (5)$$

Expressions (4) and (5) supply a criterion for guiding in the selection of the evacuation procedure, which could be useful,

MULTILAYER INSULATIONS

Evacuation

at least for the pressure range considered. When

$$\frac{L^2}{\kappa} < 6\pi \frac{Nt}{\tau d} \quad ,$$

the edge pumping should be preferred, otherwise broadside evacuation would allow a faster outgoing of the inner gas.

At very low pressures, when the main problem is to manage the outgassing products, broadside evacuation is normally preferred.

3.17.1.1.2. MATHEMATICAL SOLUTION OF THE PROBLEM

Although Eq. (2), with the appropriate initial and boundary conditions, has been numerically integrated by Kneisel & Bennet (1970) in several particular cases, it is possible to obtain very simple results of more general usefulness.

Owing to obvious structural reasons, the maximum to minimum pressure difference should be small compared to the outer pressure, thence one can write.

$$p(x,t) = p_o(t) + \pi(x,t) \quad ,, \quad |\pi(x,t)| << p_o(t)$$

The differential equation giving $\pi(x,t)$ is, to a first approximation:

$$\frac{\partial^2 \pi}{\partial x^2} = \frac{\mu}{\kappa p_o} \frac{dp_o}{dt} \quad ,$$

which can be easily integrated, leading to the following expression:

$$p(x,t) = p_o(t) + \frac{\mu}{2\kappa} \frac{1}{p_o} \frac{dp_o}{dt} (x^2 - L^2) \quad . \qquad (6)$$

MULTILAYER INSULATIONS

Evacuation

It has been assumed that, for a typical booster pressure profile

$$\left.\frac{dp_o}{dt}\right|_{t=o} = o \quad ,$$

otherwise slight changes should be made in this mathematical treatment in order to fulfill the initial condition.

Values of $p(o,t) - p_o(t)$ deduced from Eq. (6) have been compared to those given by Kneisel & Bennett (1970), both calculated and measured, in Fig 3-87. It can be seen that the results of the present calculation agree fairly closely with those obtained by Kneisel & Bennett using similar values of κ, μ and $p_o(t)$, and that the fitness of the present analytical prediction to experimental results is excellent when the value of the blanket permeability, κ, is appropriately choosen.

3.17.1.2. INTERMEDIATE REGIME

When the pressure is low, rarefection effects must be taken into account, so that the equation giving the mass flow rate, m, through unit cross-sectional area of a porous body, becomes

$$m = \left(\frac{\kappa p}{\mu} + D_K\right) \rho \frac{\partial}{\partial x} \ln p \qquad (7)$$

where:

D_K, Knudsen Diffusion Coefficient. $[m.s^{-1}]$.

$$D_K = \frac{4}{3} \bar{c} K_o$$

MULTILAYER INSULATIONS

Evacuation

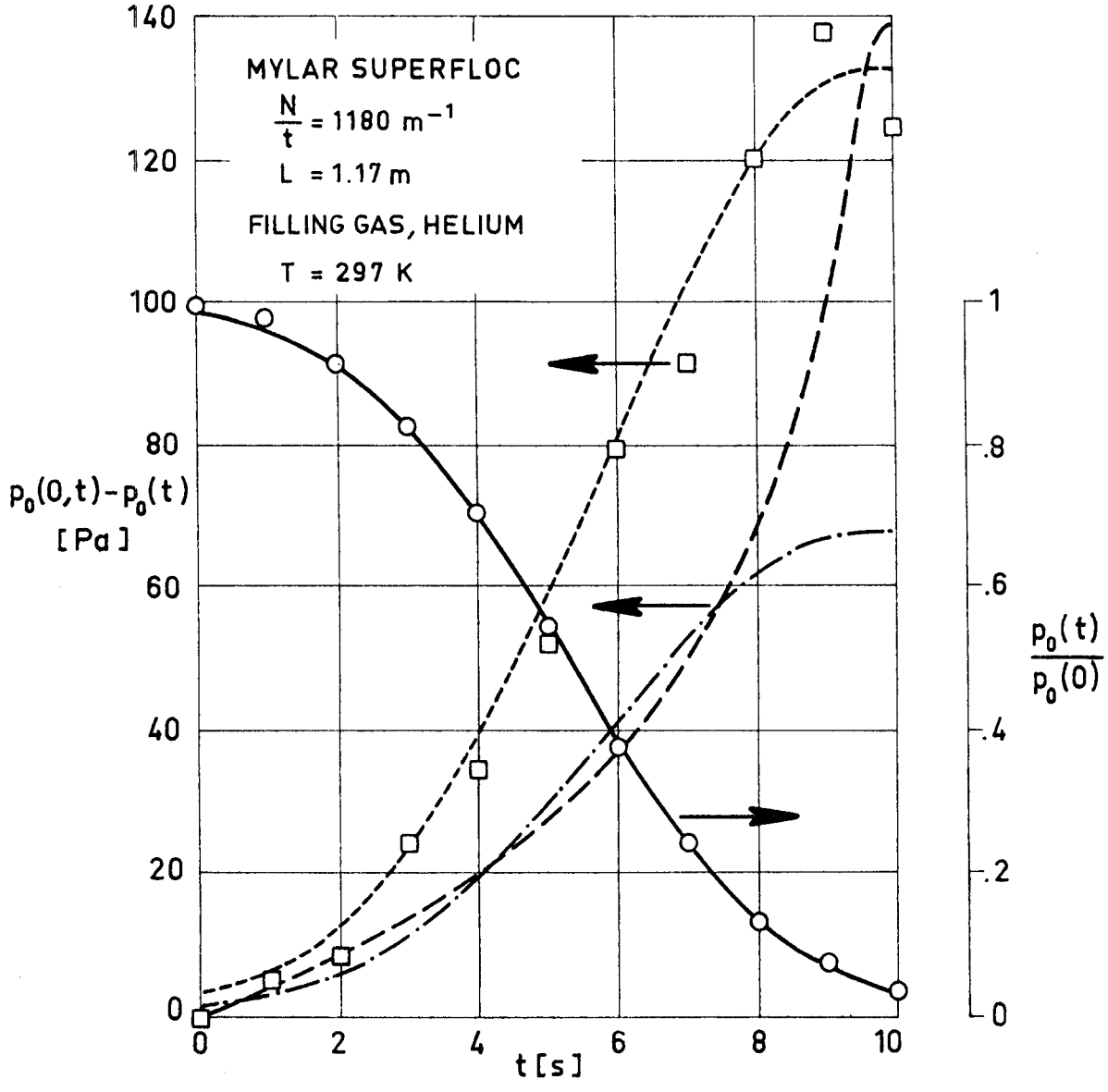

Fig 3-87. Pressure differential, $p(o,t) - p_o(t)$, vs. time, t.

□ Experimental (Kneisel & Bennett (1970)).

— — — Computed by the same authors.

—·—·— Eq. (6). $\kappa = 1.37\times10^{-7}$ m^2.

- - - - - Eq. (6). $\kappa = .70\times10^{-7}$ m^2.

○ Vacuum chamber pressure as measured by Kneisel & Bennett.

——— Curve given by the expression

$$\frac{p_o(t)}{p_o(o)} = \frac{1}{2}\left[1-\text{erf}\{.3(t-5.28)-.0012(t-5.28)^3\}\right]$$

which has been used to calculate dp_o/dt.

MULTILAYER INSULATIONS

Evacuation

$\bar{c}$, Average Molecular Speed. $[m.s^{-1}]$.

$$\bar{c} = \sqrt{\frac{8\,R\,T}{\pi m}}$$

R, Boltzmann Constant,

$$R = 1.38054 \times 10^{-23}\ J.K^{-1}.$$

T, Temperature. [K].

m, Mass of one molecule. [kg].

$$m = M.N_A^{-1}$$

M, Gas molecular mass. $[kg.mol^{-1}]$.

N_A, Avogadro Constant,

$$N_A = 6.02252 \times 10^{23}\ mol^{-1}.$$

K_o, Constant dependent on the interaction between the gas and the porous medium. [m].

From Eq. (7), following the same procedure as above, it is obtained:

$$\frac{\mu}{\kappa}\frac{\partial p}{\partial t} = \frac{\partial}{\partial x}\left(p\frac{\partial p}{\partial x}\right) + \frac{D_K \mu}{\kappa}\frac{\partial^2 p}{\partial x^2} \qquad (8)$$

When the pressure is so low that $\kappa p/D_K\mu << 1$, the first term in the right hand side can be neglected, and the following equation results

$$\frac{\partial p}{\partial t} = D_K \frac{\partial^2 p}{\partial x^2} \qquad (9)$$

Values of D_K, obtained under different conditions, have been represented in Fig 3-88. The curve, which appears in that figure, has been plotted assuming that D_K depends only on M regardless

MULTILAYER INSULATIONS

Evacuation

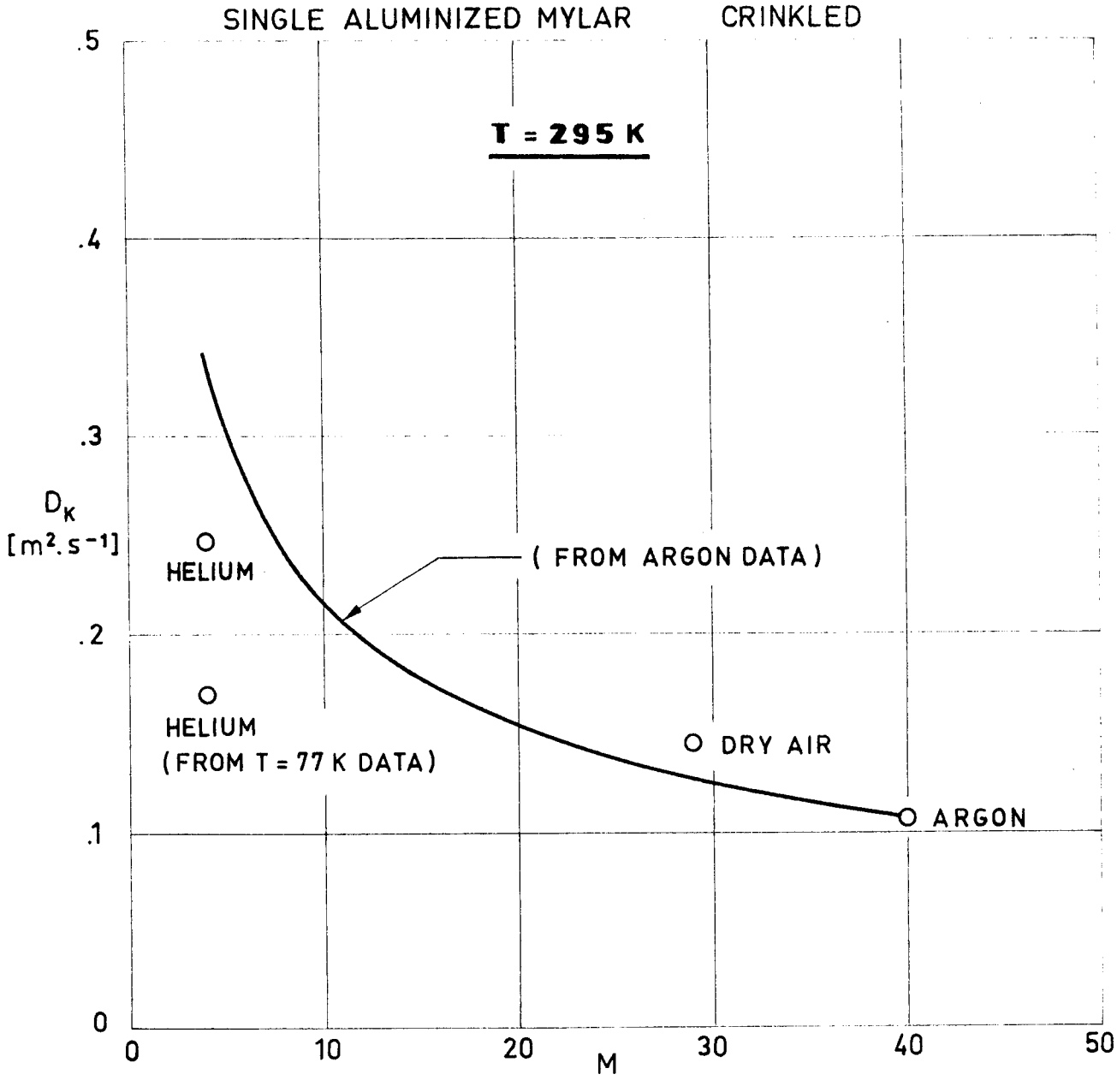

Fig 3-88. Knudsen Diffusion Coefficient, D_K, as a function of gas molecular mass, M. From Coston (1967), p. 4.3-31.

MULTILAYER INSULATIONS
Evacuation

of the interaction of the gas molecules with the porous medium; and this interaction is assumed to be always that corresponding to Argon flowing through a Mylar-Crinkled blanket at 295 K.

The pressure evolution is given by the following equation:

$$p(x,t) = p_o(t) + \frac{1}{2D_K} \frac{dp_o(t)}{dt} (x^2-L^2) \qquad (10)$$

3.17.2. INTERSTITIAL PRESSURE IN OUTGAS CONTROLLED SITUATIONS

When the pressure in the MLI has been reduced, outgassing from the insulation surfaces becomes dominant.

For normal satellite temperatures there is not outgassing at atmospheric or higher pressures. The outgassing rate increases as the pressure decreases, reaching appreciable values at very low pressures. In the very low-pressure ranges, such as those considered presently, the outgassing rate is almost independent of pressure.

Outgassing data for several shields and spacers, and one complete MLI system are given in Figs 3-89 to 3-94. The influence of purging, prepumping and ambient temperature on the outgassing rate can be deduced from these figures. Outgassing rates are usually given in units of pressure times volume per unit time per unit apparent surface area as a function of time, for constant experimental temperature and negligible ambient pressure.

Broadside pumping is normally used for evacuating outgassing products, which come from sources homogeneously distributed throughout the different layers of the insulation material.

MULTILAYER INSULATIONS

Evacuation

3.17.2.1. ANALYSIS OF GAS FLOW IN AN MLI WITH OUTGASSING

Broadside pumping of an MLI at very low pressures has been considered by Lin (1973, 1974). His approach can be outlined as follows:

1) The gas properties are uniform in each space between adjacent shields. This assumption is satisfied when the percentage area of perforations, τ, is small, and the number of shields per unit thickness, N/t, is large.

2) The fluid motion is slow, and the relevant properties, namely: temperature and partial pressures of the species, can be calculated by use of the equations of conservation of mass and energy. Notice that there are as many mass conservation equations as outgassing species. However, for most MLI systems the outgassing products are mainly constituted by water vapor originally absorbed or adsorbed in the system.

3) At very low pressures, such as those existing in an outgas dominated situation, the heat transfer is controlled by thermal radiation between insulation layers. Assuming that shield emittances are constant, and that absorption and scattering of radiation by the spacers is negligible, the energy equation will be replaced by:

$$T(x) = \sqrt[4]{T_C^4 + (T_H^4 - T_C^4)\frac{x}{t}} \quad , \qquad (11)$$

where:

T_C, cold boundary temperature. [K].

T_H, warm boundary temperature. [K].

MULTILAYER INSULATIONS

Evacuation

t, insulation thickness. [m].

x, distance to the cold boundary. [m].

4) The mass conservation equation for the species j in the interstice i may be written as:

$$t_i \frac{\partial p_i^{(j)}/T_i}{\partial t} = \frac{\tau_{i-1}}{4}\left[\frac{p_{i-1}^{(j)}}{T_{i-1}} c_{i-1}^{(j)} - \frac{p_i^{(j)}}{T_i} c_i^{(j)}\right] - \frac{\tau_i}{4}\left[\frac{p_i^{(j)}}{T_i} c_i^{(j)} - \frac{p_{i+1}^{(j)}}{T_{i+1}} c_{i+1}^{(j)}\right] + (2 - \tau_{i-1} - \tau_i)\frac{Q_i^{(j)}}{T_i} \qquad (12)$$

where:

$Q_i^{(j)}$, outgassing rate of species j in space i. [Pa.m.s^{-1}].

$c_i^{(j)}$, molecular speed for species j in space i. [m.s^{-1}].

$p_i^{(j)}$, partial pressure of species j in space i. [Pa].

t, time. [s].

t_i, thickness of interstitial space i. [m].

τ_i, percentage area of perforations for the shield placed between spaces i and i+1.

Since the gas in any interstitial space is in thermal equilibrium, the expression of the molecular speed $c_i^{(j)}$ is that given in connection with Eq. (7) above, with $T=T_i$ and $m=m^{(j)}$.

The outgassing rates are supposed to be known functions of temperature; the effect of pressure is negligible in the pressure range under consideration.

5) By taking into account the initial and boundary conditions, the system of simultaneous first order differential equations (12) for the partial pressures $p_i^{(j)}$ can be numerically solved.

MULTILAYER INSULATIONS

Evacuation

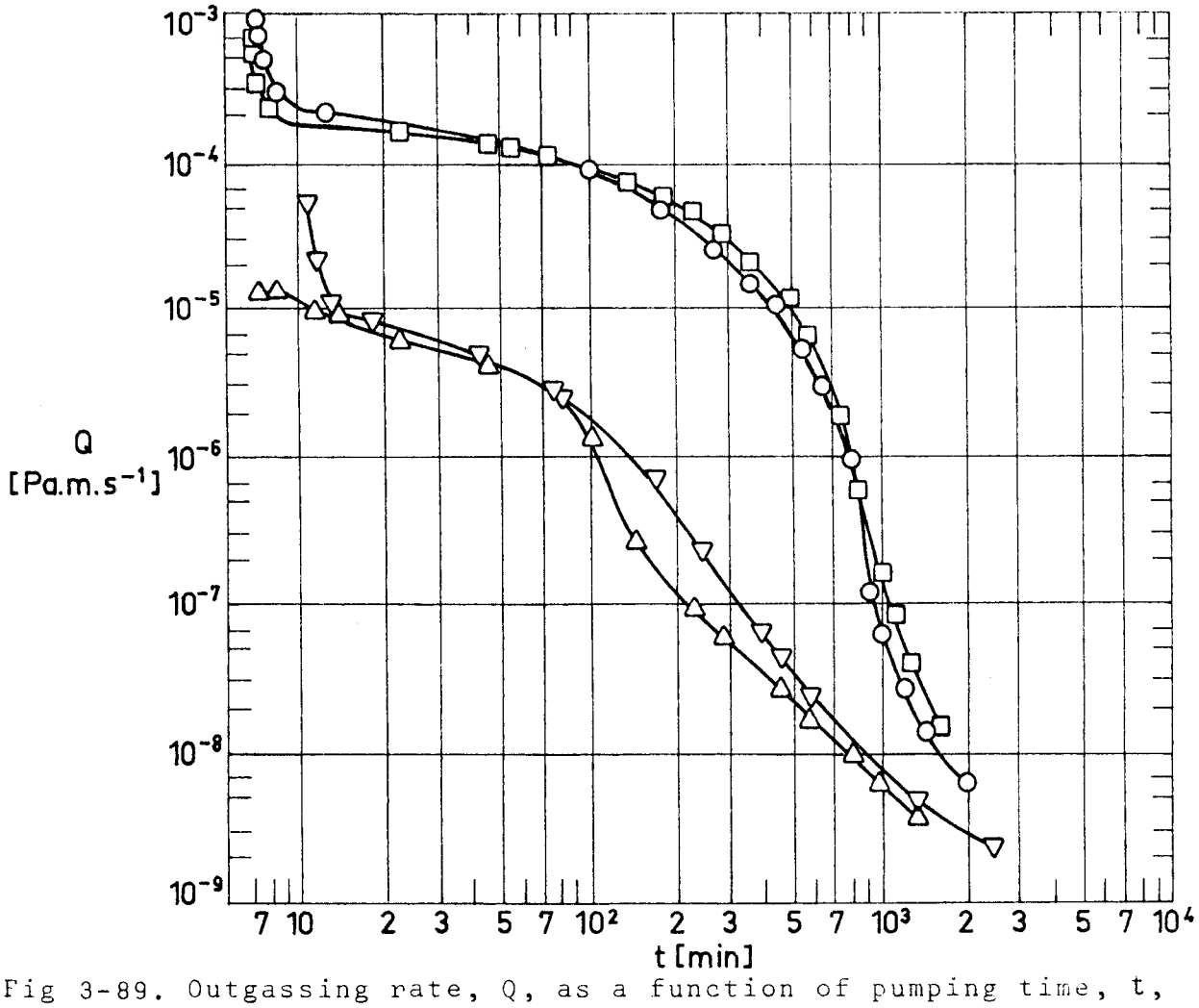

Fig 3-89. Outgassing rate, Q, as a function of pumping time, t, for Mylar Double-Aluminized. Effect of preconditioning. From Glassford (1970).

Explanation

Sample Description	Test Method	Key	Preconditioning
Film thickness, $t = 6.35\times10^{-6}$ m. Coating thickness, $t_c = .5\times10^{-7}$ m.	Q found from the difference in slopes of the pressure histories for the chamber plus sample and the empty chamber. Slopes deduced from graphically smoothed pressure vs. time data. Reproducibility of pressure data: 2%. Chamber temperature: 297 K. Chamber pressure below $1.33\times\times10^{-2}$ Pa.	O	As received.
		□	Purged at ambient temperature with Helium (4.2×10^{-3} $m^3.min^{-1}$ for 30 min).
		△	Purged at 373 K with Helium. (Same flow rate and purging time).
		▽	Purged at 373 K with Nitrogen. (Same flow rate and purging time).

MULTILAYER INSULATIONS

Evacuation

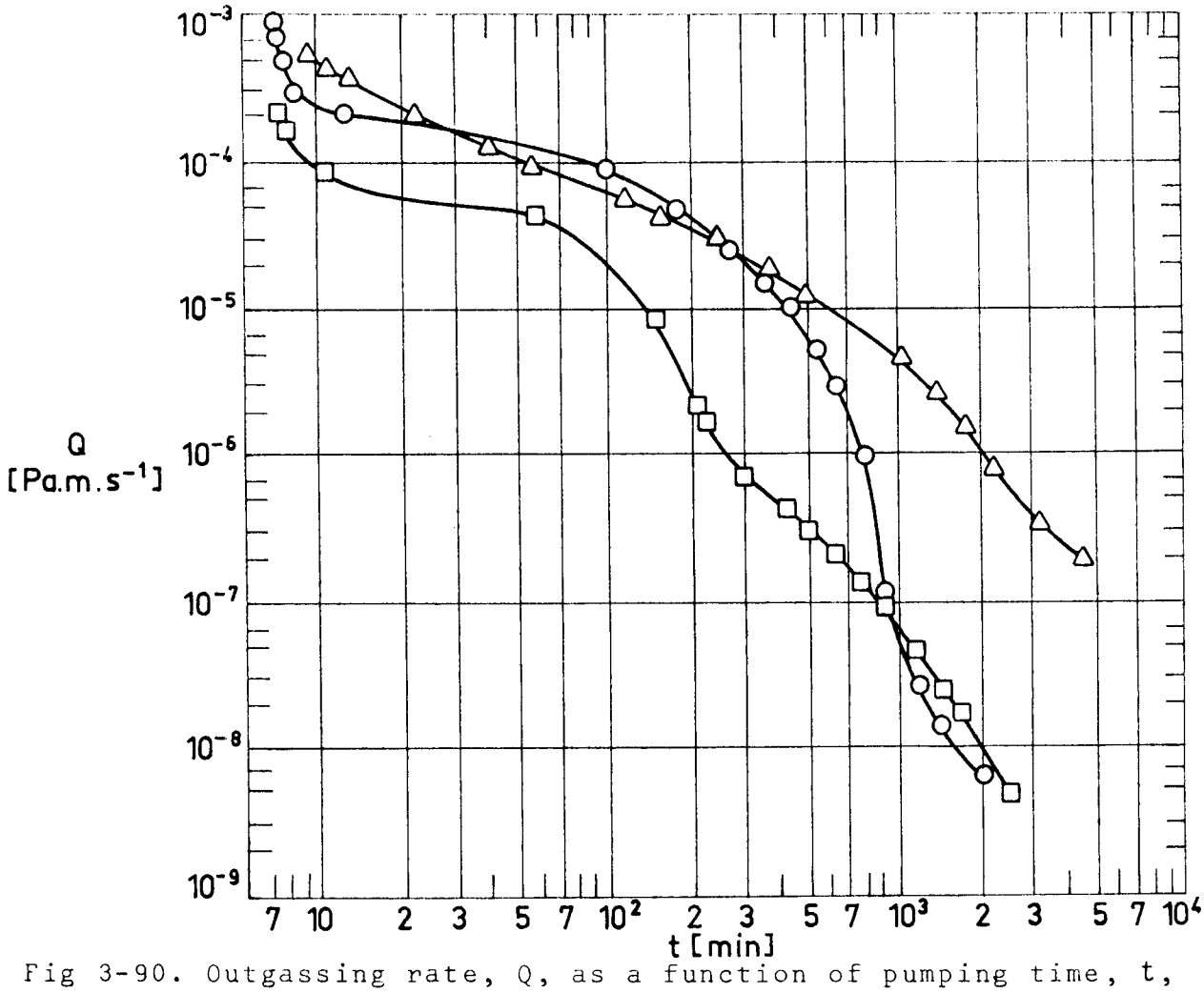

Fig 3-90. Outgassing rate, Q, as a function of pumping time, t, for Mylar Double-Aluminized. Effect of prepumping. From Glassford (1970).

Explanation

Sample Description	Test Method	Key	Prepumping
Film thickness, $t=6.35\times10^{-6}$ m. Coating thickness, $t_c=.5\times10^{-7}$ m.	Q found from the difference in slopes of the pressure histories for the chamber plus sample and the empty chamber. Slopes deduced from graphically smoothed pressure vs. time data. Reproducibility of pressure data: 2%. Chamber temperature: 297 K. Chamber pressure below 1.33×10^{-2} Pa.	O	As received.
		□	Prepumped as in a normal test and pressurized back to atmospheric pressure with He. Exposed to atmosphere (35% humidity) for 5 d and 31 d (identical curves). Then tested.
		△	Prepumped as in a normal test and pressurized back to atmospheric pressure with Air. Exposed to atmosphere for 1 d. Then tested.

MULTILAYER INSULATIONS

Evacuation

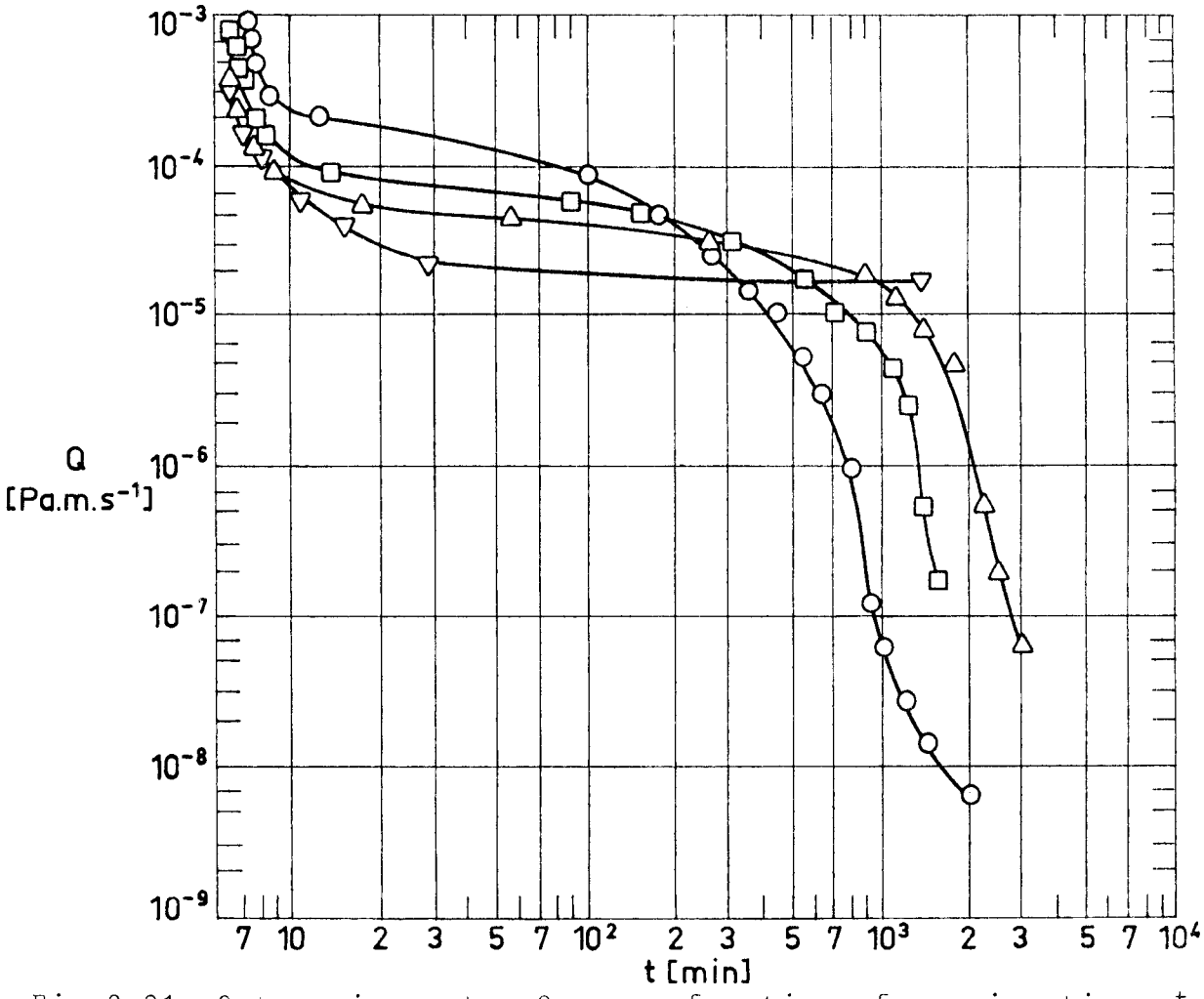

Fig 3-91. Outgassing rate, Q, as a function of pumping time, t, for Mylar Double-Aluminized, as received. Effect of test temperature. From Glassford (1970).

Explanation

Sample Description	Test Method	Key	Test Temperature
Film thickness, $t = 6.35\times10^{-6}$ m. Coating thickness, $t_c = .5\times10^{-7}$ m.	Q found from the difference in slopes of the pressure histories of the chamber plus sample and the empty chamber. Slopes deduced from graphically smoothed pressure vs. time data. Reproducibility of pressure data: 2%. Chamber pressure below 1.33×10^{-2} Pa.	○	T = 297 K.
		□	T = 282 K. Coolant: Melting water-glycerine solution.
		△	T = 273 K. Coolant: Melting ice.
		▽	T = 262 K. Coolant: Melting water-ethylene glycol solution.

MULTILAYER INSULATIONS

Evacuation

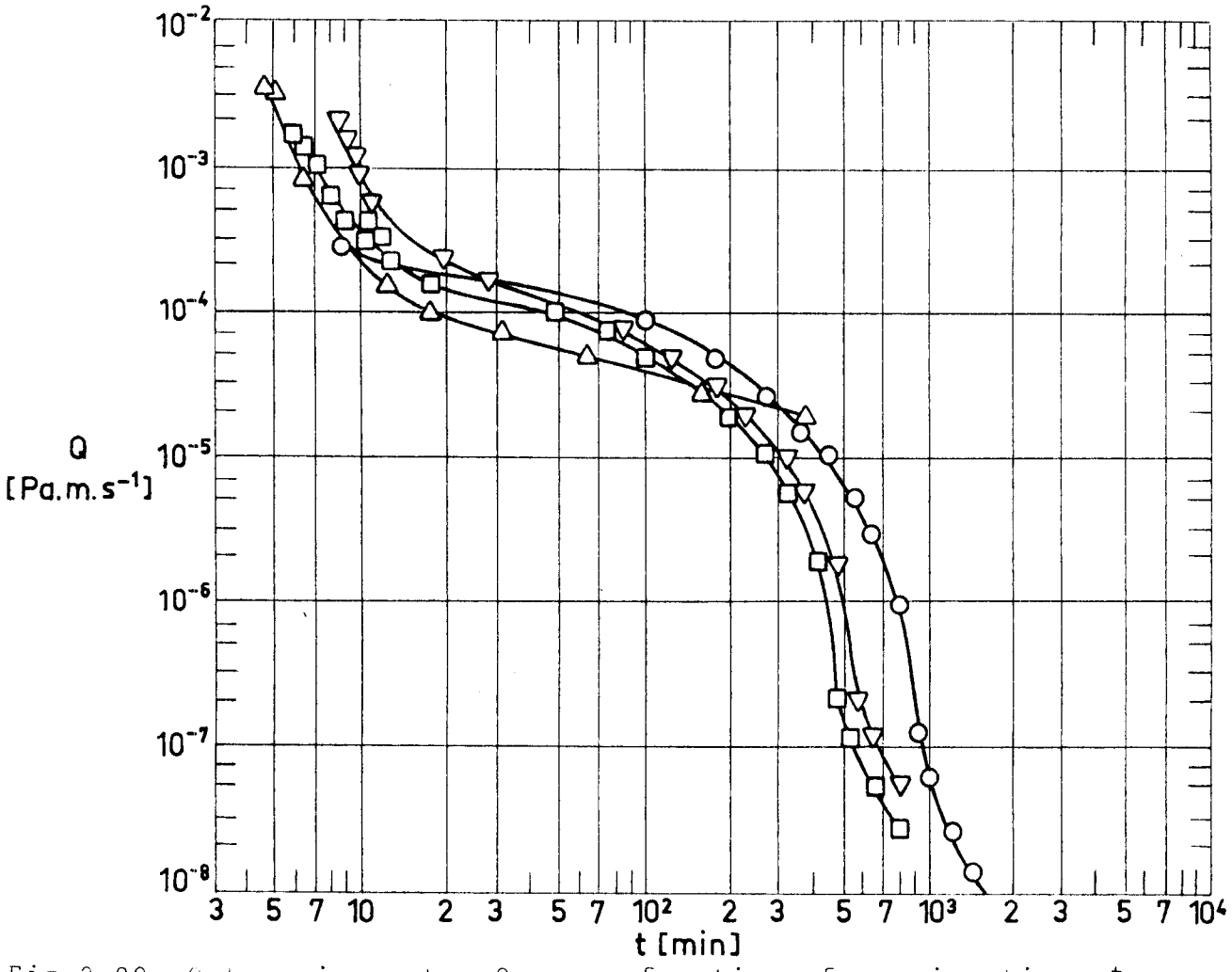

Fig 3-92. Outgassing rate, Q, as a function of pumping time, t, for several shielding materials, as received. From Glassford (1970).

Explanation

Key	Sample Description	T [K]	Test Method
○	6.35×10^{-6} m thick Mylar Double-Aluminized. Coating thickness, $t_c=.5\times\times10^{-7}$ m.	297	Q found from the difference in slopes of the pressure histories for the chamber plus sample and the empty chamber. Slopes deduced from graphically smoothed pressure vs. time data. Reproducibility of pressure data: 2%. Chamber pressure below 1.33×10^{-2} Pa.
□	3.81×10^{-6} m thick Mylar Double-Aluminized Crinkled. $t_c=.5\times10^{-7}$ m.	297	
△	Same as □ .	273	
▽	6.35×10^{-6} m thick Mylar Double-Aluminized flocked with Dacron tufts on 1.27×10^{-2} m centers. $t_c=.5\times10^{-7}$ m.	297	

MULTILAYER INSULATIONS

Evacuation

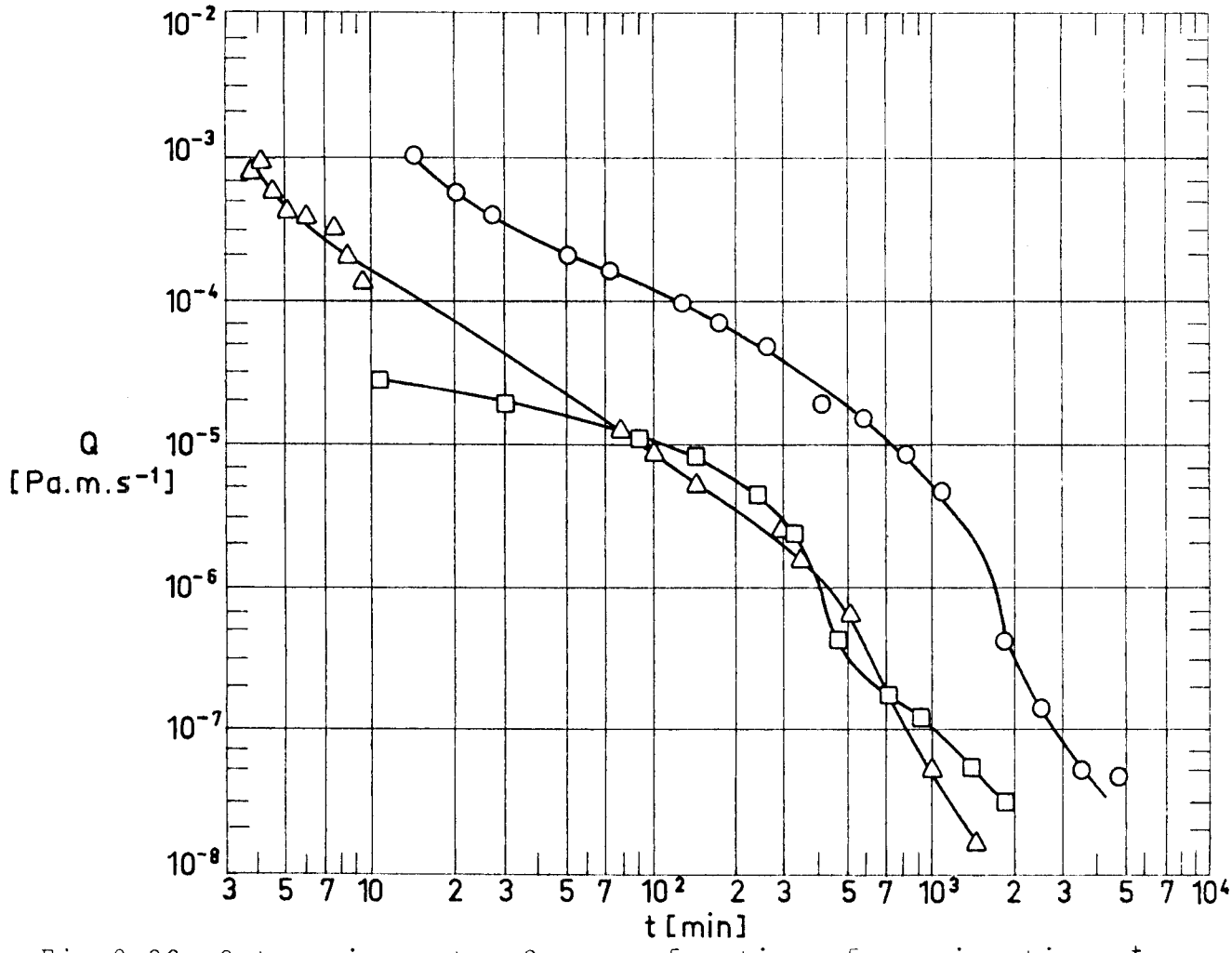

Fig 3-93. Outgassing rate, Q, as a function of pumping time, t, for several spacing materials. From Glassford (1970).

Explanation

Key	Sample Description	Test Method
○	15.2×10^{-6} m thick Tissuglas. Nominal density, ρ=224 kg.m^{-3}. As received.	Q found from the difference in slopes of the pressure histories for the chamber plus sample and the empty chamber. Slopes deduced from graphically smoothed pressure vs. time data. Reproducibility of pressure data: 2%. Chamber temperature: 297 K. Chamber pressure below 1.33× ×10^{-2} Pa.
□	Same as ○ Purged with Helium at 373 K.	
△	6.35×10^{-6} m thick Mylar Uncoated. Density, ρ=1.41×10^3 kg.m^{-3}.	

MULTILAYER INSULATIONS

Evacuation

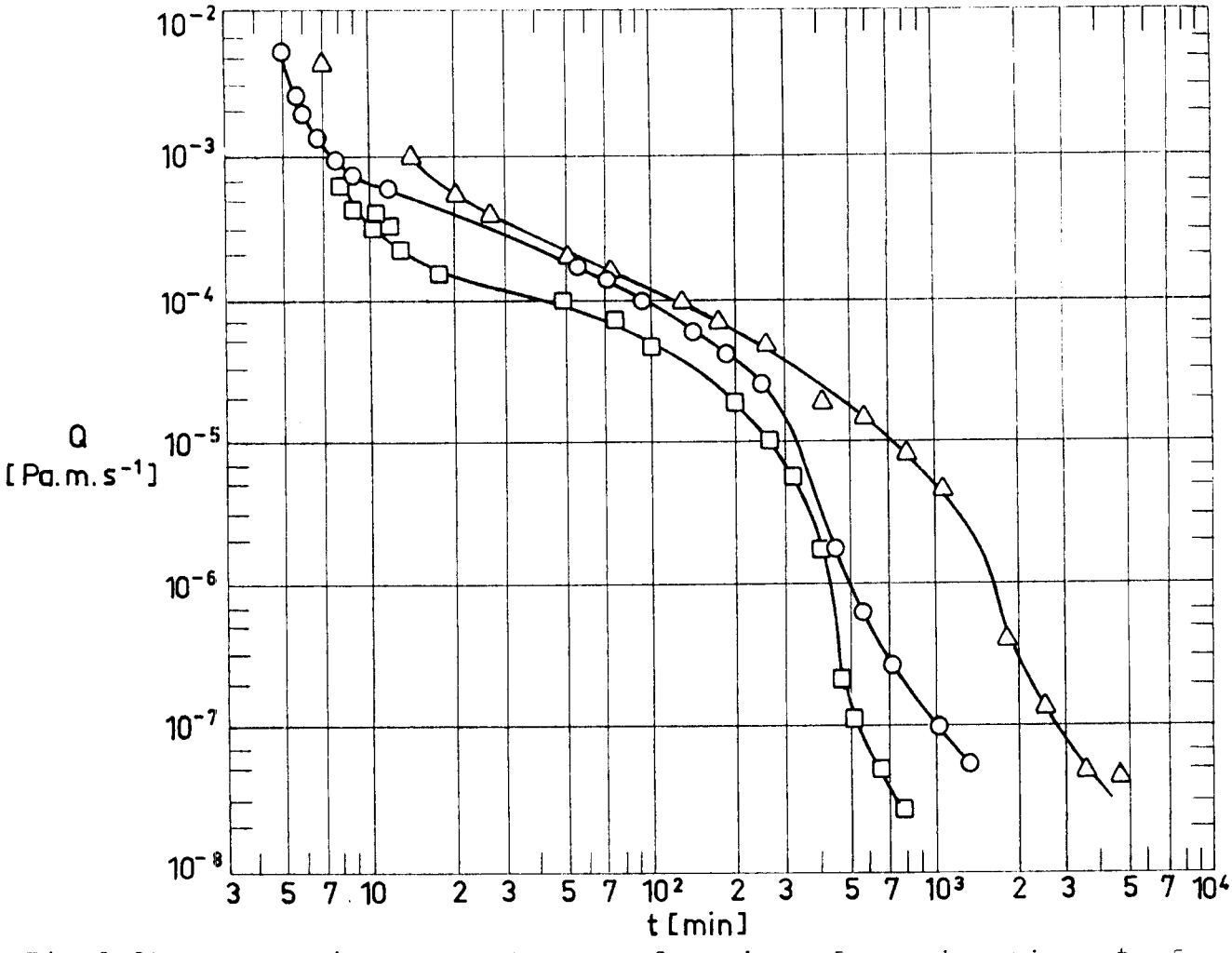

Fig 3-94. Outgassing rate, Q, as a function of pumping time, t, for an MLI system and for its components. No preconditioning. From Glassford (1970).

Explanation

Key	Sample Description	Test Method
○	Two layers of 3.81×10^{-6} m thick Mylar Double-Aluminized Crinkled. Coating thickness, $t = .5\times10^{-7}$ m. One layer of 15.2×10^{-6} m thick Tissuglas. Nominal density, $\rho = 224$ kg.m^{-3}.	Q found from the difference in slopes of the pressure histories for the chamber plus sample and the empty chamber. Slopes deduced from graphically smoothed pressure vs. time data. Reproducibility of pressure data: 2%. Chamber temperature: 297 K. Chamber pressure below $1.33\times\times10^{-2}$ Pa.
□	3.81×10^{-6} m thick Mylar Double-Aluminized Crinkled. Coating thickness, $t_c = .5\times10^{-7}$ m.	
△	15.2×10^{-6} m thick Tissuglas. Nominal density, $\rho = 224$ kg.m^{-3}.	

INSULATIONS

References

Chapman, J.C., Porter, H.L. 1910 "On the Physical Properties of Gold Leaf at High Temperatures", Proceedings Royal Society of London, Ser. A, Vol. 83, pp. 65-68, 1910.

McAdams, W.H. 1954 "Heat Transmission", 3rd Edition, McGraw-Hill Book Company, Inc., New York, 1954, p. 63.

Bardeen, J. 1958 "Conduction: Metals and Semiconductors", in "Handbook of Physics", E.U. Condon and H. Odishaw, Eds., McGraw-Hill Book Company, Inc., New York, 1958, pp. 4-74.

Kropschot, R.H., Schrodt, J.E., Fulk, M.M., Hunter, B.J. 1960 "Multiple-Layer Insulation", in "Advances in Cryogenic Engineering", Vol. 5, K.D. Timmerhaus, Ed., Plenum Publishing Corporation, New York, 1960, pp. 189-197.

ASM 1961 "Metals Handbook", Vol. 1, "Properties and Selection of Metals", 8th Edition, T. Lyman, Ed., American Society for Metals (ASM), Metals Park, Cleveland, Ohio, 1961.

Smolak, G.R., Knoll, R.H., Wallner, L.E. 1961 "Analysis of Thermal-Protection Systems for Space-Vehicle Cryogenic-Propellant Tanks", NASA TR R-130, Aug. 3, 1961.

Wood, W.D., Deem, H.W., Lucks, C.F. 1961 "The Emittance of Iron, Nickel, and Cobalt and their Alloys", Defense Metals Information Center, DMIC Memorandum 119, Battelle Memorial Institute, Columbus 1, Ohio, July 25, 1961.

INSULATIONS

References

Smithells, C.J. 1962 "Metals Reference Books", Vol. II, 3rd Edition, Butterworth & Co (Publishers) Ltd., London, 1962, pp. 695--827.

Fussel, W.B., Triolo, J.J., Jerozal, F.A. 1963 "Portable Integrating Sphere for Monitoring Reflectance of Spacecraft Coatings", in "Measurement of Thermal Radiation Properties of Solids", J.C. Richmond, Ed., NASA SP-31, 1963.

ADL 1964 "Basic Investigation of Multi-Layer Insulation Systems", NASA CR-54191, ADL 65958-00-04 (NAS3-4181), Arthur D. Little, Inc., Cambridge, Massachusetts, Oct. 30, 1964.

Happel, J., Brenner, H. 1965 "Low Reynolds Number Hydrodynamics with Special Applications to Particulate Media", Prentice-Hall, Inc., Englewood Cliffs, N. J., 1965, Chap. 4, pp. 153-154.

ADL 1966 "Advanced Studies on Multi-Layer Insulation Systems", NASA CR-54929, ADL 67180-00-04 (NAS3-6283), Arthur D. Little, Inc., Cambridge, Massachusetts, June 1, 1966.

Kittel, Ch. 1966 "Introduction to Solid State Physics", 3rd Edition, John Wiley & Sons, Inc., New York, 1966, pp. 208-218.

Shelton, J.L., Akers, W.W. 1966 "Total Hemispherical Thermal Emittance of Nickel as a Function of Oxide Thickness in the Temperature Range 400°-900°C",

INSULATIONS

References

in "Progress in Astronautics and Aeronautics", Vol. 18, G.B. Heller, Ed., Academic Press, New York, 1966, pp. 151-165.

Coston, R.M. 1967 "Handbook of Thermal Design Data for Multilayer Insulation Systems", LMSC-A847882, Vol. II, (NAS8-20353), Lockheed Missiles & Space Company, Sunnyvale, California, June 1967.

Coston, R.M., Vliet, G.C. 1967 "Thermal Energy Transport Characteristics along the Laminations of Multilayer Insulations", in "Progress in Astronautics and Aeronautics", Vol. 20, G.B. Heller, Ed., Academic Press, New York, 1967, pp. 909-923.

Cunnington, G.R., Zierman, C.A., Funai, A.I., Lindahn, A. 1967 "Performance of Multilayer Insulation Systems for Temperatures to 700°K", NASA CR-907 (NAS2-2441), Lockheed Aircraft Corporation, Palo Alto, California, Oct. 1967.

Glaser, P.E., Black, I.A., Lindstrom, R.S., Ruccia, F.E., Wechsler, A.E. 1967 "Thermal Insulation Systems - A Survey", NASA SP-5027, 1967.

Ruccia, F.E., Hinckley, R.B. 1967 "The Surface Emittance of Vacuum-Metallized Polyester Film", in "Advances in Cryogenic Engineering", Vol. 12, K.D. Timmerhaus, Ed., Plenum Publishing Corporation, New York, 1967, pp. 300-307.

INSULATIONS

References

Touloukian, Y.S. 1967a "Thermophysical Properties of High Temperature Solid Materials", Vol. 4: "Oxides and Their Solutions and Mixtures", Part I: "Simple Oxygen Compounds and Their Mixtures", The MacMillan Company, New York, 1967.

Touloukian, Y.S. 1967b "Thermophysical Properties of High Temperature Solid Materials", Vol. 5: "Nonoxides and Their Solutions and Mixtures Including Miscellaneous Ceramic Materials", The MacMillan Company, New York, 1967.

Maccalous, J.W. 1968 "Methods of Fabricating Super-Insulation Blankets", in "Advanced Techniques for Material Investigation and Fabrication", Vol. 14, SAMPE, Florida Press, Inc., Orlando, Florida, Nov. 1968, II-1A-4.

Rosato, D.V. 1968 "Other Properties and Characteristics (Corrosive, Thermal, Space, Biological, Ocean, Fire)", in "Environmental Effects on Polymeric Materials, Vol. I: Environments", D.V. Rosaro and R.T. Schwartz, Eds., Interscience Publishers, New York, 1968, pp. 755-991.

Ross, J.H. 1968 "Fibers", in "Environmental Effects on Polymeric Materials, Vol. II: Materials", D.V. Rosato and R.T. Schwartz, Eds., Interscience Publishers, New York, 1968, pp. 1282-1302.

INSULATIONS

References

Vliet, G.C., Coston, R.M. 1968 "Thermal Energy Transport Parallel to the Laminations in Multilayer Insulation", in "Advances in Cryogenic Engineering", Vol. 13, K.D. Timmerhaus, Ed., Plenum Publishing Corporation, New York, 1968, pp. 671-679.

Hale, D.V. 1969 "Study of Thermal Conductivity Requirements", "High Performance Insulation Thermal Conductivity Test Program", NASA CR-61279 (NAS8-21347), Lockheed Missiles and Space Company, Huntsville, Alabama, Jan. 1969.

Hammond, Jr., M.B. 1969 "An Analytical Model for Determining the Thermal Conductivity of Closed-Cell Foam Insulation", in "Advances in Cryogenic Engineering", Vol. 15, K.D. Timmerhaus, Ed., Plenum Publishing Corporation, New York, 1970, pp. 332-342.

Kaganer, M.G. 1969 "Thermal Insulation in Cryogenic Engineering", Israel Program for Scientific Translations, Jerusalem, 1969.

Rittenhouse, J.B., Singletary, J.B. 1969 "Space Materials Handbook", 3rd Edition, NASA SP-3051, 1969, p. 647.

Androulakis, J.G. 1970 "Effective Thermal Conductivity Parallel to the Laminations of Multilayer Insulation", AIAA Paper No. 70-846, 1970.

INSULATIONS

References

Bustard, T.S., Princiotta, F.T., Barr, H.N. 1970 "Reentry Protection for Radioisotope Heat Sources", Nuclear Applications & Technology, Vol. 9, No. 10, Oct. 1970, pp. 572-583.

Crosby, J.R. 1970 "Multilayer Insulation Testing", JPL Space Programs Summary 37-64, Vol. III, 1970, pp. 79-80.

Glassford, A.P.M. 1970 "Outgassing Behavior of Multilayer Insulation Materials", Journal of Spacecraft and Rockets, Vol. 7, No. 12, Dec. 1970, pp. 1464-1468.

Kneisel, K.M., Bennett, F.O. 1970 "Prediction of Interstitial Gas Pressure in Multilayer Insulation During Rapid Evacuation", Journal of Spacecraft and Rockets, Vol. 7, No. 10, Oct. 1970, pp. 1259-1261.

Knopf, P.W., Murray, D.O. 1970 "Empirical Thermal Performance of Embossed/ /Crinkled Aluminized Film Multilayer Insulation with Joints", in "Proceedings of the Symposium in Thermodynamics and Thermophysics of Space Flight", Palo Alto, California, 1970, pp. 211-219.

Maissel, L.I. 1970 "Electrical Properties of Metallic Thin Films", in "Handbook of Thin Film Technology", L.I. Maissel and R. Glang, Eds., McGraw-Hill Book Co., New York, 1970, pp. 13-7 - 13-10.

INSULATIONS

References

Reid, R.L., Coon, C.W. 1970 "Hemispherical Thermal Emittance of Copper as a Function of Oxidation Conditions", in "Progress in Astronautics and Aeronautics", Vol. 24, J.W. Lucas, Ed., The MIT Press, Cambridge, Massachusetts, 1971, pp. 184-204.

Richardson, D.L., Ruccia, F.E., French, B. 1970 "Extravehicular Space Suit Thermal Insulations", in "Progress in Astronautics and Aeronautics", Vol. 24, J.W. Lucas, Ed., The MIT Press, Cambridge, Massachusetts, 1971, pp. 519-544.

Scollon, T.R., Carpitella, M.J. 1970 "Long Life High Reliability Thermal Control Systems Study Data Handbook", Prepared under Contract NAS 8-26252 by Space Systems Organization, General Electric Company, Valley Forge Space Technology Center, Pennsylvania, 1970.

Touloukian, Y.S., DeWitt, D.P. 1970 "Thermal Radiative Properties. Metallic Elements and Alloys", Thermophysical Properties of Matter, Vol. 7, IFI/Plenum, New York, 1970.

Jagannathan, P.S., Tien, C.L. 1971 "Experimental Investigation of Lateral Heat Transfer in Cryogenic Multilayer Insulation", in "Advances in Cryogenic Engineering", Vol. 16, K.D. Timmerhaus, Ed., Plenum Publishing Corporation, New York, 1971, pp. 138-142.

INSULATIONS

References

Leonhard, K.E., Hyde, E.H. 1971 "Multilayer Insulation Materials for Reusable Space Vehicles", in "Space Shuttle Materials", Vol. 3, SAMPE, Azusa, California, Oct. 1971, pp. 645-658.

Zwaal, A., Dauphin, J., Alonso, A. 1971 "Screening of Space Materials with Micro-VCM Weight-Loss Test", ESTEC TN-110, European Research Organisation, Feb. 1971.

Arvidson, J.M., Durcholz, R.L., Reed, R.P. 1972 "Compressive Properties of Polyurethane and Polystyrene Foams from 76 to 300 K", in "Advances in Cryogenic Engineering", Vol. 18, K.D. Timmerhaus, Ed., Plenum Publishing Corporation, New York, 1973, pp. 194-201.

Holmes, V.L., McCrary, L.E., Krause, D.R. 1972 "Measurement of Apparent Thermal Conductivity of Multilayer Insulations at Low-Compressive Loads", Journal of Spacecraft and Rockets, Vol. 9, No. 11, Nov. 1972, pp. 791-795.

Reed, R.P., Arvidson, J.M., Durcholz, R.L. 1972 "Tensile Properties of Polyurethane and Polystyrene Foams from 76 to 300 K", in "Advances in Cryogenic Engineering", Vol. 18, K.D. Timmerhaus, Ed., Plenum Publishing Corporation, New York, 1973, pp. 184-193.

Stimpson, L.D., Jaworski, W. 1972 "Effects of Overlaps, Stitches, and Patches on Multilayer Insulation", in "Progress in Astronautics and Aeronautics", Vol. 31, C.L. Tien, Ed., The MIT

INSULATIONS

References

Press, Cambridge, Massachusetts, 1972, pp. 247-266.

Tien, C.L., Jagannathan, P.S., Chan, C.K. 1972 "Lateral Heat Transfer in Cryogenic Multilayer Insulation", in "Advances in Cryogenic Engineering", Vol. 18, K.D. Timmerhaus, Ed., Plenum Publishing Corporation, New York, 1972, pp. 118-123.

Campbell, W.A., Marriott, R.S., Park, J.J. 1973 "A Compilation of Outgassing Data for Spacecraft Materials", NASA TN D-7362, Sept. 1973.

Dixon, J.C., Musgrove, P.J. 1973 "Thermal Insulation for Electrothermal Thrusters", in "Conference on Electric Propulsion of Space Vehicles", The Institution of Electrical Engineers I.S.B.N. 0852961197, 1973, pp. 166-170.

Lin, J.T. 1973 "Analysis of Gas Flow through a Multilayer Insulation System", AIAA Journal, Vol. 11, No. 7, July 1973, pp. 995-1000.

Ross, J.H., Stanton, R.M. 1973 "Relationship of Fabric Flammability to Fabric Structure", in "Applied Polymer Symposia No. 21", J. Preston and J. Economy, Eds., John Wiley & Sons, 1973, pp. 109-119.

Schroeder, C.J. 1973a "Insulation Commonality Assessment", (Phase I), Vol. 1, Section 1.0 through 6.0, NASA CR-124471, SD72-SA-0157-1 (NAS7-200),

INSULATIONS

References

Space Division, North American Rockwell Corp., Feb. 1, 1973, pp. 6-151.

Schroeder, C.J. 1973b "Insulation Commonality Assessment", (Phase I), Vol. 2, Section 7.0 through 16.0, NASA CR-12447B, SD72-SA-0157-2, (NAS 7-200), Space Division, North American Rockwell Corp., Feb. 1, 1973.

Tien, C.L. Cunnington, G.R. 1973 "Radiation Heat Transfer in Multilayer Insulation Having Perforated Shields", AIAA Paper No. 73-718, July 1973.

Kazanjian, A.R. 1974 "Review of Properties of Polycarbonate Resins", in "Polymer-Plastics Technology and Engineering", L. Naturman, Ed., Marcel Dekker, Inc., New York, 1974, pp. 123-160.

Klippel, E., Langer, H. 1974 "Multilayer Superinsulation Development and Testing", UR-258-74, ESTEC/Contract 2042/73 SK, Messerschmitt-Bölkow-Blohm GmbH, Ottobrunn bei München, Nov. 30, 1974, pp. 26-28.

Krause, D.R. 1974 Private Communication. Sept. 30, 1974.

Petajan, J.H., Voorhees, K.J., Packham, S.C., Baldwin, R.C., Einhorn, I.N., Grunnet, M.L., Dinger, B.G., Birky, M.M. 1975 "Extreme Toxicity from Combustion Products of a Fire-Retarded Polyurethane Foam", Science, Vol. 187, No. 4178, Feb. 28, 1975, pp. 742-744.

BABCOCK & WILCOX Data Sheets No. 110-1, 120-1, 5 14-4, Babcock & Wilcox, Refractories Division, Augusta, Georgia 30903 USA.

INSULATIONS
References

CARBORUNDUM Co. "Fiberfrax Ceramic Fiber Technical Information",
The Carborundum Company, Refractories and Electronics Division, Niagara Falls, New York 14302 USA.

DOW CORNING Bulletin 61-041; Date 3/71,
Dow Corning International Ltd., Chaussée de la Hulpe, 177. B-1170 Brussels, Belgium.

EMERSON & CUMING INC. Technical Bulletins: 3-2-2A, 6-2-1B, 6-2-2B, 7-2-9,
Emerson & Cuming Europe NV, Nijverheidsstraat 24, B-2431 Oevel, Belgium.

FIBERFIL "Ready-to-mold Fiberglass Reinforced Structural Foams",
Fiberfil Division, Dart Industries Inc., 1701 N, Heidelbach Avenue, Evansville, Indiana 47717, U.S.A..

JOHNS-MANVILLE "Thermophysical Data". Data Sheets No. IN--526A, IN-554A, IN-560A, IN-563A, IN-568A, IN-569A, IN-570A, IN-571A, IN-575A, IN--576A, IN-577A, IN-578A.
Johns-Manville International Corporation, Denver, Colorado 80217 USA.

MOSITES Data Sheet of Mosites 1062 Fluorel,
Mosites Rubber Company, Inc., P.O. Box 2115, Fort Worth, Texas 76101, U.S.A..

INTENTIONALLY BLANK PAGE